21 February 2014 | $10

Science

Gordon Research Conferences

AAAS

CONTENTS continued >>

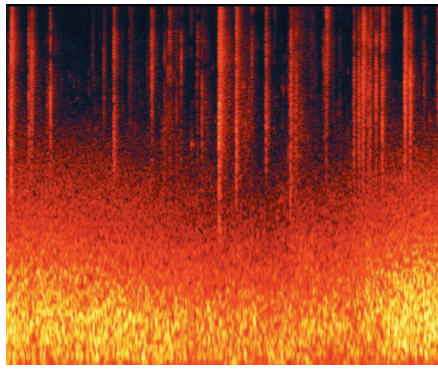

page 834

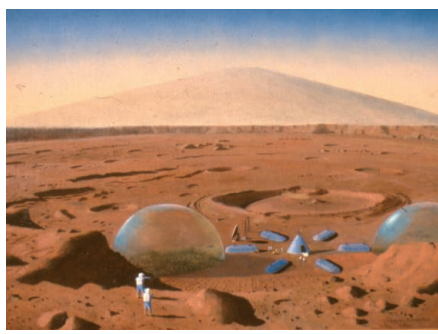

page 841

ON THE WEB THIS WEEK

>> *Science* Podcast
This week's show features a segment on the science of soundscapes and a roundup of shorts from our daily news site.

>> Find More Online
Check out the latest in a series of Perspectives on Challenges in Climate Science at **www.sciencemag.org/extra/climate**.

COVER

Composite image from a molecular animation of how endocytic clathrin-coated vesicles ~100 nanometers in diameter form. Clathrin is the principal molecular scaffold for many cellular membrane trafficking processes. The Gordon Research Conference on Lysosomes and Endocytosis will be held 15 to 20 June 2014 in Andover, New Hampshire. See page 902 for the conference schedule and preliminary programs.

Image: Janet Iwasa (University of Utah) and Tom Kirchhausen (Harvard Medical School)

DEPARTMENTS

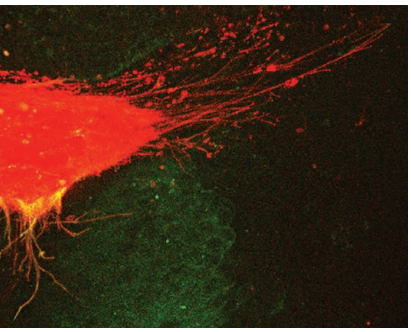

pages 848 & 852

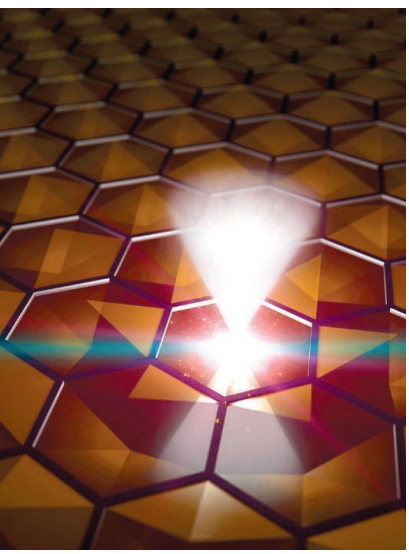

page 864

RESEARCH ARTICLES

REPORTS

CREDIT: (BOTTOM) G. STEWART/Z. K. LIU/Z. X. SHEN/Y. L. CHEN

SCIENCE (ISSN 0036-8075) is published weekly on Friday, except the last week in December, by the American Association for the Advancement of Science, 1200 New York Avenue, NW, Washington, DC 20005. Periodicals Mail postage (publication No. 484460) paid at Washington, DC, and additional mailing offices. Domestic individual membership and subscription (51 issues): $149 ($74 allocated to subscription). Domestic institutional subscription (51 issues): $990; Foreign postage extra: Mexico, Caribbean (surface mail) $55; other countries (air assist delivery) $85. First class, airmail, student, and emeritus rates on request. Canadian rates with GST available upon request, GST #1254 88122. Publications Mail Agreement Number 1069624. **Printed in the U.S.A.**

Change of address: Allow 4 weeks, giving old and new addresses and 8-digit account number. **Postmaster:** Send change of address to AAAS, P.O. Box 96178, Washington, DC 20090–6178. **Single-copy sales:** $10.00 current issue, $15.00 back issue prepaid includes surface postage; bulk rates on request. **Authorization to photocopy** material for internal or personal use under circumstances not falling within the fair use provisions of the Copyright Act is granted by AAAS to libraries and other users registered with the Copyright Clearance Center (CCC) Transactional Reporting Service, provided that $30.00 per article is paid directly to CCC, 222 Rosewood Drive, Danvers, MA 01923. The identification code for *Science* is 0036-8075. *Science* is indexed in the *Reader's Guide to Periodical Literature* and in several specialized indexes.

Toward an Artificial Muscle >>

In designing materials for artificial muscles, the goals are to find those that will combine high strokes, high efficiency, long cycle life, low hysteresis, and low cost. Now, **Haines *et al.*** (p. 868; see the Perspective by **Yuan and Poulin**) show that this is possible. Twisting high-strength, readily available polymer fibers, such as those used for fishing lines or sewing thread, to the point where they coil up, allowed construction of highly efficient actuators that could be triggered by a number of stimuli.

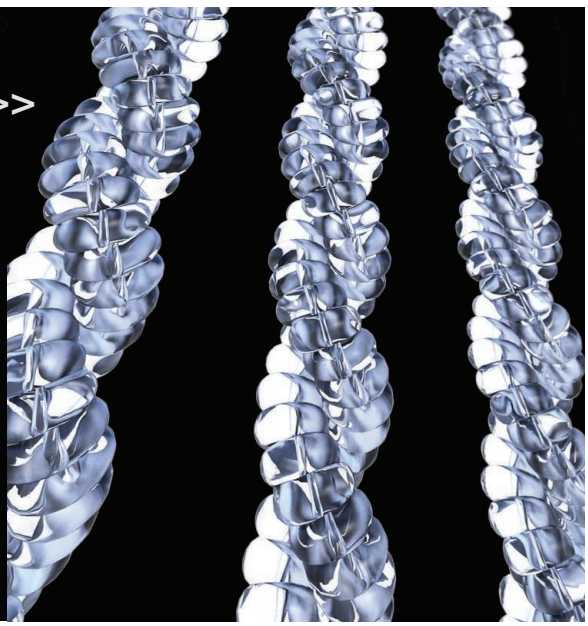

Silicon Siting

The synthesis of many pharmaceutical and agrochemical compounds requires selective functionalization of multiple different sites on aromatic ring frameworks. The size and electronic properties of the first substituent added can influence where the next one is likely to end up. **Cheng and Hartwig** (p. 853, see the Perspective by **Tobisu and Chatani**) discovered a rhodium-catalyzed reaction that is particularly sensitive to size that places a silicon substituent as far away as possible from the largest group already on the ring. The silicon group can then be replaced with carbon, oxygen, nitrogen, or halide substituents as needed.

Fear, Memory, and Place

Contextual fear conditioning (CFC) is widely used as a hippocampal-dependent classical conditioning task to model human episodic memory. **Lovett-Barron *et al.*** (p. 857) combined in vivo imaging with pharmacology, pharmacogenetics, and optogenetics and they found that somatostatin-expressing, dendrite-targeting γ-aminobutyric acid–releasing interneurons in hippocampal area CA1 are required for CFC. During CFC, sensory features of the aversive event reach hippocampal output neurons through excitatory cortical afferents and require active inhibitory filtering to ensure that the hippocampus exclusively encodes the conditioned stimulus.

A 3D Graphene?

Discoveries of materials with exciting electronic properties have propelled condensed matter physics over the past decade. Two of the best-known examples, graphene and topological insulators, have something in common: a linear energy-momentum relationship—the Dirac dispersion—in their two-dimensional (2D) electronic states. Topological insulators also have a more mundane aspect of their electronic structure, characterized by a band gap. Another class of materials, topological Dirac semimetals, has been proposed that has a linear dispersion along all three momentum directions—a bulk Dirac cone; these materials are predicted to have intriguing electronic properties and to be related to other exotic states through quantum phase transitions. **Liu *et al.*** (p. 864, published online 16 January) detected such a state in the compound Na_3Bi by using photoemission spectroscopy.

Optimizing Injectable Hydrogels

Injectable hydrogels are showing promise as scaffolds in regenerative medicine because they can be injected in liquid form and transform in situ into the gel state. However, when exposed to ionic solutions, such as those found in the body, hydrogels can increase in volume by a factor of 2, which can weaken the material. **Kamata *et al.*** (p. 873) added a thermoresponsive component to a hydrogel so that the thermoresponsive component would tend to collapse in shape when heated and counteract the hydrogel's tendency to swell. Indeed, the resulting gel retained its unswollen volume following immersion in a physiological solution and retained its mechanical strength during repeated stretching or compression.

Toward Successful Tissue Repair

The therapeutic use of growth factors in tissue regeneration has suffered from safety and efficacy issues. Reasoning that the unmet potential may be because of nonphysiological delivery, **Martino *et al.*** (p. 885) engineered growth factors to bind strongly to extracellular matrix proteins. These variants were able to induce superior tissue repair, compared to the wild-type proteins. Furthermore, unwanted side effects were decreased: For example, the engineered angiogenic growth factor VEGF showed reduced vascular permeability, a concern that has limited the therapeutic efficacy of wild-type VEGF.

Two-Faced Viral Protein

Flaviviruses cause human diseases such as West Nile fever and dengue fever. The flavivirus nonstructural protein 1 (NS1) has multiple functions in flavivirus biology and is a target for vaccine development. Dimeric NS1 is essential for replication of the viral genome inside host cells, while hexameric NS1 is secreted and plays a role in evasion of the immune system. **Akey *et al.*** (p. 881, published online 6 February; see the Perspective by **Shi**) report crystal structures for full-length glycosylated NS1 from West Nile and dengue viruses. The structures show a hexamer comprised of three dimers. The structural analysis together with liposome and mutational studies identify a membrane interacting surface on one face of the dimer and an immune evasion surface on the other.

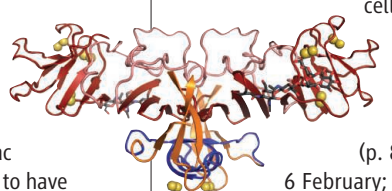

Oops, That's Not Right…

Evaluating our actions, and detecting our errors, is crucial for adaptive behavior. These fundamental executive functions are intensively studied in cognitive and social neuroscience, but their anatomical basis remains poorly characterized. Using intracerebral electroencephalography in patients being prepared for epilepsy surgery, **Bonini *et al.*** (p. 888) found that, contrary to what is widely assumed, the supplementary motor area, and not the anterior cingulate cortex, plays a leading role in these processes. The data provide a precise spatio-temporal description of the cortical network underlying action monitoring and error processing.

CREDITS (TOP TO BOTTOM): UNIVERSITY OF TEXAS AT DALLAS NANOTECH INSTITUTE; AKEY *ET AL.*

Additional summaries

Robust to Change

The variation in genetic sequences determining the binding of transcription factors is believed to be an important facet of evolution. However, the degree to which a genome is robust, that is, able to withstand changes and how robustness affects evolution is unclear. **Payne and Wagner** (p. 875) investigated the empirical support for mutational robustness by examining transcription factor (TF) binding in the mouse and yeast genomes. A network analysis of the degree of variation revealed that the sites with the highest affinity for TF binding exhibit the greatest tolerance for nucleotide substitutions, whereas low-affinity sites exhibit greater sensitivity to mutation. Thus, while mutational robustness and evolvability are antagonistic at the genotypic level, they are synergistic at the phenotypic level.

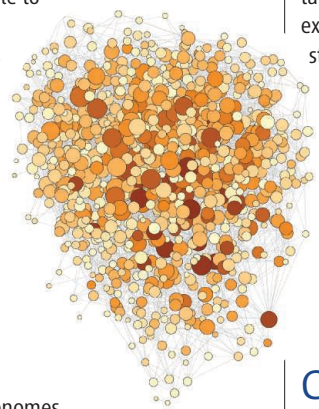

Morphogen Pipeline

Developmental effects of morphogens are often thought to result from release of such signaling proteins from a cell, which then diffuse away to act by binding to receptors on distant target cells. But evidence is accumulating that another mechanism exists for such communication. Endothelial cells in the fruit fly have long, skinny extensions that reach away from cells for long distances, and these "cytonemes" can take up morphogens from adjacent cells. A key experiment to support a signaling role of such structures would be to show that disruption of cytonemes disrupts signal transduction. **Roy *et al.*** (p. 852, published online 2 January; see the Perspective by **Rørth**) provide such evidence and conclude that the fly morphogen known as decapentaplegic (a relative of transforming growth factor–β) must be transported through cytonemes to promote proper development of the trachea.

Catalysis in the Membrane

Enzymes in the UbiA superfamily of integral membrane proteins synthesize lipid-soluble aromatics such as ubiquinones and chlorophylls that function in energy storage and energy transfer in mitochondrial and chloroplast membranes. **Cheng and Li** (p. 878) report structures of an archaeal UbiA protein in both apo and substrate-bound states. The structures show a large active site with a lateral portal that is likely to give access to the long-chain isoprenoid substrates. The findings suggest a mechanism for substrate recognition and catalysis and can explain disease-related mutants in eukaryotic homologs.

Entorhinal Cell Clusters

There is considerable interest in understanding the function of neurons in layer 2 of the medial entorhinal cortex and how they generate their unique firing patterns, which are important in the recall of facts and past events (see the Perspective by **Blair**). **Ray *et al.*** (p. 891, published online 23 January) investigated principal cells in layer 2 by immunoreactivity, projection patterns, microcircuit analysis, and assessment of temporal discharge properties in awake, freely moving animals. In tangential sections, pyramidal neurons were clustered into patches arranged in a hexagonal grid—very similar to the patterns observed in grid cell spatial firing. These patches received selective cholinergic innervation, which is critical for sustaining grid cell activity. **Kitamura *et al.*** (p. 896, published online 23 January) found that these cells drive a hippocampal circuit by projecting directly to the hippocampal CA1 area and synapsing with a distinct class of inhibitory neurons. This circuit provides feed-forward inhibition in combination with excitatory inputs from layer 3 cells of the medial entorhinal cortex, projecting to CA1 pyramidal cells to determine the strength and time window of temporal associative inputs.

CREDIT: PAYNE AND WAGNER

Marcia McNutt is Editor-in-Chief of *Science*.

Keystone XL

I DRIVE A HYBRID CAR AND SET MY THERMOSTAT AT 80°F IN THE WASHINGTON, DC, SUMMER. I USE public transportation to commute to my office, located in a building given "platinum" design status by the U.S. Green Building Council. The electric meter on my house runs backward most months of the year, thanks to a large installation of solar panels. I am committed to doing my part to cut greenhouse gas (GHG) emissions and minimize global warming. At the same time, I believe it is time to move forward on the Keystone XL pipeline to transport crude oil from the tar sands deposits of Alberta, Canada, and from the Williston Basin in Montana and North Dakota to refineries on the U.S. Gulf Coast.

This position may seem incongruous with my personal crusade to minimize fossil fuel use, a desire rooted in scientific understanding that climate change is a real threat and that tar sands oil produces higher GHG emissions than many alternatives. Prominent environmentalists oppose Keystone XL. When the extension was originally proposed, I, too, was opposed, believing that it would hasten development of the petroleum resource. Certainly, some fossil fuel deposits remain untouched because there is no pipeline to transport the resource; a good example is natural gas on the Alaskan North Slope. However, the absence of Keystone XL has not stopped development of the Canadian oil sands; unlike the situation on the Alaskan North Slope, truck and rail are viable alternatives to a pipeline between Canada and the United States.

Even after accepting that Keystone XL would not accelerate extraction of the Canadian oil sands, I still opposed the project because the pipeline would cross environmentally sensitive regions, such as the Sandhills of Nebraska, a natural wetland that supports many species, including migratory birds, and the Ogallala Aquifer, one of the world's largest groundwater resources. The project's developers, the TransCanada Corporation, modified the pipeline to avoid sensitive areas and have promised comprehensive monitoring and state-of-the-art shutoff valves to reduce risk to the environment. No method for moving hydrocarbons can be considered completely fail-safe. At least the current permitting process can, and should, be used to ensure that Keystone XL sets new standards for environmental safety. There is no similar leverage on the truck and rail transportation options, which produce higher GHG emissions and have a greater risk of spills, at a higher cost for transport.*

I remain very concerned by the slow rate at which the United States, one of the larger per-capita consumers of total energy globally,† is moving to develop renewable sources of energy. Unfortunately, blocking Keystone XL will not reduce GHG emissions nor will it increase investment in renewable forms of energy. But allowing Keystone XL to move forward could advance both goals. For example, President Obama, who has yet to decide on the pipeline, could put conditions on approval that require Canadian authorities to reduce the carbon intensity of extracting the tar from the oil sands and processing it into a liquid petroleum product.‡ As part of a compromise to allow the project to move forward, let's now insist on an income stream from Keystone XL revenues to support investment in renewable energy sources to secure our energy future.

Opponents of Keystone XL have been right to contest construction of the pipeline without reasonable assurance that the plan is environmentally acceptable. It should now be possible to determine this, with the release in January 2014 of a thorough Environmental Impact Statement. It is also time to insist on concessions so that building the pipeline ultimately reduces GHG emissions and speeds progress toward renewable energy.

– Marcia McNutt

10.1126/science.1251932

*www.fas.org/sgp/crs/misc/R43390.pdf. †http://data.worldbank.org/indicator/EG.USE.PCAP.KG.OE. ‡http://harvardmag.com/pdf/2013/11-pdfs/1113-37.pdf

Published by AAAS

GENETICS

Origins of Sparrow Speciation

Homoploid hybrid speciation is the result of hybridization between two parental species without a change in chromosome number. Such speciation is relatively rare, however, because it requires the rapid establishment of reproductive isolation of the new species from that of its parents. Trier *et al*. examine the origins of the Italian sparrow, which originated as a result of hybridization between the house and Spanish sparrows. Transcriptome analysis of the parental sparrows identified 86 species-specific SNPs. This allowed tracing of the genetic ancestry within the Italian sparrow and identified some ongoing, but limited, gene flow between the parental species and the Italian sparrows. Mosaic ancestry of the Italian sparrow sex chromosomes was evidenced by a cline analysis framework. This identified ancestry of both house and Spanish sparrow sex chromosome–linked loci that exhibited allele frequency shifts. Mitochondrial and nuclear encoded mitochondrial genes exhibited similar divergences. These results suggest that mito–nuclear interactions may also be a factor in isolating the Italian sparrows from their parental species and that reproductive isolation may be evolving as a result of mito–sex chromosome interactions. — LMZ

PLOS Genet. **10**, e1004075 (2014).

CREDITS (TOP TO BOTTOM): © DANIELE OCCHIATO/BUITEN-BEELD/ALAMY; XI CHEN/COLUMBIA UNIVERSITY

BIOMEDICINE

Orchestrating an Attack

Urinary tract infections (UTIs) persist if the innate immune system fails to clear the bacteria. Immune defense against UTIs requires neutrophils, macrophages, and the cytokines they secrete; however, how they all work together is unclear. Using a murine model of UTI, Schiwon *et al*. found that neutrophils are the key antibacterial effectors in UTI but that neutrophil migration was regulated by two functionally distinct macrophage subsets: sentinel macrophages resident in the bladder and helper macrophages that need to be recruited from the circulation. The sentinel macrophages sensed the infection and produced chemokines to recruit neutrophils and helper macrophages. Helper macrophages did not directly combat bacteria like neutrophils, but did produce the cytokine tumor necrosis factor as a "helper signal," which allowed the sentinel macrophages to produce the chemokine CXCL2. CXCL2 in turn induced the secretion of matrix metalloproteinase-9, which allowed neutrophils to enter the uroepithelium to combat the bacteria. Thus, the antibacterial phagocyte response is not simply a disorganized tissue invasion of neutrophils and macrophages that clear the bacteria by eating them, but instead a highly coordinated process involving the exchange of information between three phagocyte subsets with distinct immunological tasks. — SMH

Cell **156**, 456 (2014).

BIOMATERIALS

The Heart of the Matter

A common problem after a serious wound or injury is the formation of scar tissue that prevents the full restoration of functionality. Scarring can occur rapidly, so there is a need for a quick and easy way to deliver protective materials to damaged tissues. After myocardial infarction (MI), otherwise known as a heart attack, there is an expansion of the infarct site in the left ventricle (LV) that is caused by the healing process. A key component of this adverse LV remodeling is the family of extracellular proteases known as the matrix metalloproteinases (MMPs), which are regulated by the presence of tissue inhibitors of MMPs (TIMPs). In an effort to modulate the balance of MMPs and TIMPs to prevent LV expansion after MI, Eckhouse *et al*. developed an injectable degradable hydrogel based on hyaluronic acid that was loaded with recombinant TIMP-3. Using a porcine model, which has a similar coronary anatomy to humans, the hydrogel was locally injected into the heart after MI. After 7 days, TIMP-3 was specifically localized to the injection sites. More importantly, in comparison to the control animals, the gel-injected pigs showed a reduction in the infarct size, improved remodeling of the LV, and increased cardiac function. — MSL

Sci. Transl. Med. **6**, 223ra21 (2014).

ENGINEERING

Spore Work Pays Off

The presence or absence of water on a surface or surrounding a cell can have a strong influence on its mechanical properties. This response to water gradients is useful in applications such as microfluidics or for transpiration in plants, but in principle can also generate work that might be harvested as electrical power. Chen *et al.* show

Continued on page 818

Continued from page 817

that dormant spores of *Bacillus subtilis* and *Bacillus thuringiensis* are actually much more effective at converting energy from water gradients—in this case, changes in relative humidity—than are synthetic materials designed for this purpose. Furthermore, a mutation in *B. subtilis* causing a loss of most of its coating layers also confers an increase in energy density. Monolayers of assembled spores induced large deformations as a response to water potential on microcantilevers and latex sheets, and even when integrated into an energy-harvesting device. — NW

Nat. Nanotechnol. **9**, 137 (2014).

PLANT SCIENCE

Sneaky Smut

When the fungus *Ustilago maydis* colonizes a maize plant, causing corn smut, its hyphae wind their way through to the vascular tissue, which is rich in resources that sustain fungal growth. The fungus also secretes an effector protein called Tin2, which causes the plant to produce

anthocyanins, flavonoid pigments that lend a reddish color. Tanaka *et al.* now show that Tin2 contributes to the virulence of *U. maydis* and also induces the expression of genes that encode the plant's anthocyanin biosynthetic pathway. This results in more anthocyanin. Not so coincidentally, it also results in less lignin, the complex polymer that lends sturdiness to cell walls. This is because the biosynthetic pathways for anthocyanins and lignins share a common precursor. Plants with reduced lignin content were overly susceptible to fungal infection, which suggests that Tin2 promotes anthocyanin production at the expense of lignin production, reducing the plant's barriers to fungal growth. — PJH

eLife **3**, e01355 (2014).

CHEMISTRY

Waves of NO

Diffraction is perhaps the best evidence that light acts as a wave. The peaks and valleys in overlapping beams can either reinforce or suppress each other, leading to visible intensity oscillations on a detection screen. Quantum mechanics dictates that atoms manifest this type of behavior also, although the experimental conditions necessary to observe it can be as challenging to achieve as the mental agility needed to reconcile it with human-scale experience. von Zastrow *et al.* have detected remarkably clear interference fringes in the distribution of nitric oxide (NO) scattering angles from inelastic collisions with noble gas atoms. Close agreement between the experimental results and quantum-mechanical calculations confirmed a type of matter diffraction as the underlying cause of the striking oscillatory pattern in the angular distribution. — JSY

Nat. Chem. 10.1038/nchem.1860 (2014).

MATERIALS SCIENCE

A Coat To Fit Many

Applying a coating is a useful way to change the surface properties of a material. Common examples include antiglare coatings on lenses or anticorrosion coating on metals. Flat surfaces can be uniformly coated relatively easily, but uniformly coating a complex, porous three-dimensional (3D) shape can be much more challenging. Nguyen *et al.* develop a method to coat such structures conformally by using membrane precursors dissolved in a mixed solvent that includes a component that will selectively swell the object that needs to be coated. Initial experiments used polydimethylsiloxane (PDMS) as the membrane precursor and poly(lactic acid) (PLA) fibers as the material to be coated in and explored the role of solvent composition, precursor concentration, and exposure time on the thickness of the coating that formed. The precursor infiltrates the thin swollen surface region of the PLA fibers, becomes trapped there upon unswelling, and can be cured into a solid conformal coating on heating. The PLA can be removed through selective vaporization, leaving behind the PDMS membrane that retains the geometry of the original PLA fiber or more complicated initial shapes generated using 3D printing. This technique works for a wide range of precursor materials, including acrylic, epoxy, and polyurethane. — MSL

ACS Appl. Mater. Interfaces 10.1021/am4053943 (2014).

Published by AAAS

AROUND THE WORLD

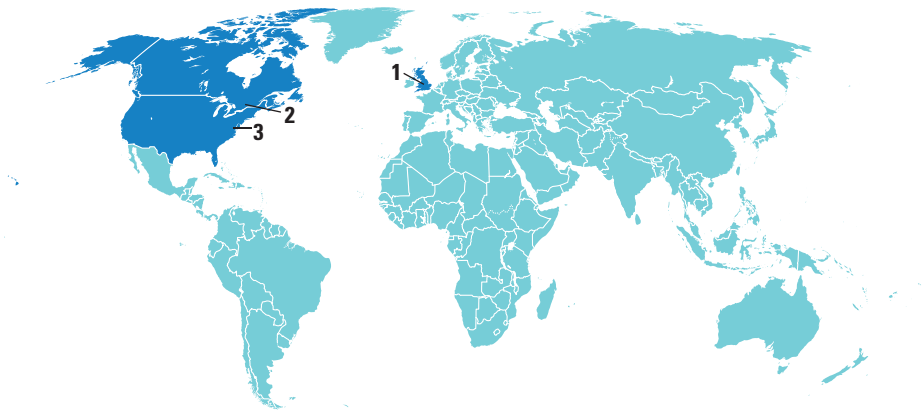

Leicester, U.K. **1**

A Royal's Genome

What color were Richard III's eyes and hair? Was he lactose intolerant? Did he have a high risk of diabetes or heart disease? All these questions and more may be answered after researchers at the University of Leicester sequence the entire genome of the deceased king of England, whose skeleton was unearthed last year. If successful, Richard III—who reigned during the 15th century—will become the first famous historical figure whose remains have undergone a complete genetic analysis. The study is expected to last about a year and a half and cost more than $160,000.

Ottawa **2**

Canada to Set Up Billion-Dollar Research Fund

The Canadian government plans to shell out $1.36 billion over 10 years to create a Canada First Research Excellence Fund. Its goal is to "position Canada's post-secondary institutions to compete with the best in the world for talent and breakthrough discoveries," according to budget documents. Finance Minister Jim Flaherty said the fund would "help [institutions] excel globally in research areas that create long-term economic advantages for Canada."

The new fund is the latest example of a large research program to serve national goals set up outside the regular channel of competitive grants to individual scientists. The Canada Foundation for Innovation has supported research infrastructure since 1997, and in 2000 the Canada Research Chairs program was launched to enable leading universities to snare talent. Exactly where the new fund fits won't be known until the government provides more details.

Funding won't begin to flow until 2015, and the first tranche will be a modest $45 million. That amount is expected to ramp up to $182 million in the 2018 to 2019 budget. **http://scim.ag/Canada_funds**

Washington, D.C. **3**

U.S. Cracks Down on Sales Of Ivory, Rhino Horn

The U.S. government has a new national strategy to combat the surging trade in elephant ivory, rhino horn, and other wildlife products. Such trade is decimating elephant and rhino populations: Some 35,000 elephants are slaughtered each year, while 1000 rhinoceros were poached in South Africa alone last year.

Threatened. The black rhinoceros.

THEY SAID IT

"This seems like a very light penalty for a doctor who purposely tampered with a research trial and directly caused millions of taxpayer dollars to be wasted on fraudulent studies."

—Senator Charles "Chuck" Grassley, in a letter to the Department of Health and Human Services last week, questioning whether a 3-year ban from participating in federally funded research was adequate punishment for a former Iowa State University researcher, Dong-Pyou Han, who admitted to committing fraud in an HIV vaccine study.

As part of the strategy unveiled last week, the U.S. Fish and Wildlife Service will ban commercial trade of elephant ivory in the United States, including resale and exports. Commercial elephant ivory in any form, including antiquities, can no longer be imported. Only items documented to be more than 100 years old will be allowed to be sold in the United States.

New regulations will also be enacted to stop the illicit shipments of fish, birds, reptiles, snakes, and coral through the United States. **http://scim.ag/ivorysales**

NEWSMAKERS

Three Q's

Russia's scientific community is in the throes of upheaval. The powerful Russian Academy of Sciences (RAS) has merged with two sister academies that serve medical and agricultural research under a reform law that also created a new agency to oversee the combined academies and their assets. *Science* last week caught up with RAS president and plasma physicist **Vladimir Fortov**.

Q: Why is the government reforming RAS?

V.F.: Reforms were happening in the Russian Academy of Sciences, but they were not so conspicuous to society and to the leaders of the country. That is why the lead-

CREDITS (TOP TO BOTTOM): © GL ARCHIVE/ALAMY; COURTESY OF VLADIMIR FORTOV; GETTY IMAGES/ISTOCKPHOTO

Published by AAAS

Fossil Trove Discovered in Canada

Paleontologists have unearthed a colossal cache of fossilized arthropods—a group of invertebrates that includes insects, crustaceans, and arachnids—in the Canadian Rockies' Marble Canyon. The fossil trove, described last week in *Nature Communications*, may surpass the nearby Burgess Shale—one of the world's most famous fossil repositories, home to more than 60,000 fossils of creatures that lived 500 million years ago. During a mere 15 days of collecting in Marble Canyon, scientists say they documented a whopping 50 species from that period.

CREDITS: (TOP LEFT TO RIGHT) © ROYAL ONTARIO MUSEUM, IMAGE JEAN-BERNARD CARON; JONATHAN EISEN; PROJECT MERCCURI/SPACEMICROBES/UC DAVIS; (BOTTOM) D. ANDERSON/NIST

ership introduced its own plan of action. It was the plan for more rapid and more radical reforms, without appropriate consultations with scientists.

Q: Has RAS ceased to exist?

V.F.: On 8 February, the Russian Academy of Sciences celebrated its 290th anniversary. Will it be able to celebrate its 300th anniversary 10 years from now? Much depends on the interpretation and implementation of the law on reform.

Random Sample

Microbial Super Bowl In Space

In 2012, Darlene Cavalier approached Jonathan Eisen, a microbiologist at the University of California, Davis, about applying to do research on the International Space Station. At first Eisen wanted to compare microbes from the space station with bugs from indoor spaces on Earth. But at Cavalier's urging—and with the help of professional cheerleaders—Project MERCCURI now includes a microbial Super Bowl, to begin next month.

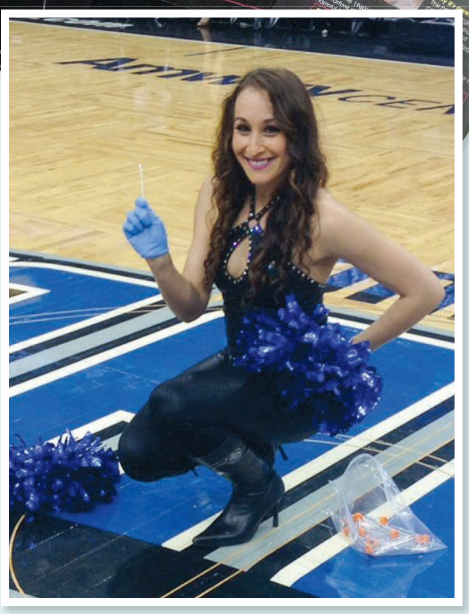

Cavalier is the founder of Science Cheerleader—a group of current and former professional cheerleaders pursuing science and technology careers. For the past year, she and her fellow cheerleaders have collected or helped fans and students collect microbes from football stadiums, basketball courts, and baseball fields around the United States. One microbe from each arena is heading to space in March, where they will compete to see which one grows the fastest. Project MERCCURI has come out with baseball cards featuring pictures and statistics for each microbial contestant.

"I had my skepticism" about collaborating with cheerleaders, Eisen recalls. But at the sports events where the samples were collected, thousands of people have gotten acquainted with the microbial world. "And the passion the cheerleaders have for outreach is unlike anything I have ever seen."

Q: To what extent will research directions continue to be decided by the researchers?

V.F.: It's one of the most complicated and pressing questions. We'll see how it'll work in practice. But according to the general health of the economy, the financial support of science is hardly likely to trend upward. So some directions will suffer.

Extended interview at http://scim.ag/VFortov.

NIST Director Heading To Steel Country

Patrick Gallagher, director of the National Institute of Standards and Technology (NIST) since 2009, is leaving for academia. Gallagher, 50, will become chancellor of the University of Pittsburgh (Pitt) starting 1 August.


Gallagher

After earning a Ph.D. in physics from Pitt in 1991, Gallagher joined NIST in 1993 as a research physicist. As NIST director, Gallagher oversees some 3000 scientists, engineers, and support staff at two main labs in Gaithersburg, Maryland, and Boulder, Colorado. NIST has a budget of more than $850 million for fiscal year 2014. **http://scim.ag/PGallagher**

Science LIVE

Join us on Thursday, 27 February, at 3 p.m. EST for a live chat with experts on a hot topic in science. **http://scim.ag/science-live**

Published by AAAS

AAAS | 2014 ANNUAL MEETING

The AAAS annual meeting, held in Chicago, Illinois, from 13 to 17 February, attracted roughly 7600 participants, including scientists, journalists, and visitors to Family Science Days activities. Here are some highlights from the meeting. You can find more AAAS coverage, including reports from sessions, live chats, and responses to "What's the Coolest Science Fact You Know?" at **http://scim.ag/AAAS2014**.

FINDINGS

Shrinking Arctic Ice Exposes Seals to Deadly Parasite

In March 2012, wildlife pathologists arriving at Hay Island off Nova Scotia met an eerie sight: Roughly a fifth of the gray seals laying on the rocky outcrop were dead. Michael Grigg of the National Institute of Allergy and Infectious Diseases in Bethesda, Maryland, and colleagues discovered that they were infested with a moon-shaped parasite, a new strain of the genus *Sarcocystis*, which "completely destroys the architecture" of their livers, Grigg says. The parasite is known to be harmless to ring seals, historically isolated from gray seals, which inhabit warmer waters. But as ice covering the Arctic disappears, gray seals have entered the ring seals' territory. The new mixing of species exposes them to new diseases, says biological oceanographer Sue Moore of the U.S. National Oceanic and Atmospheric Administration. More research linking climate change to marine mammal health is critical, she adds, as some estimate all Arctic ice will be gone in 20 years. **http://scim.ag/_seal**

New menace. The parasite *Sarcocystis pinnipedi* (*inset*) causes liver failure in gray seals.

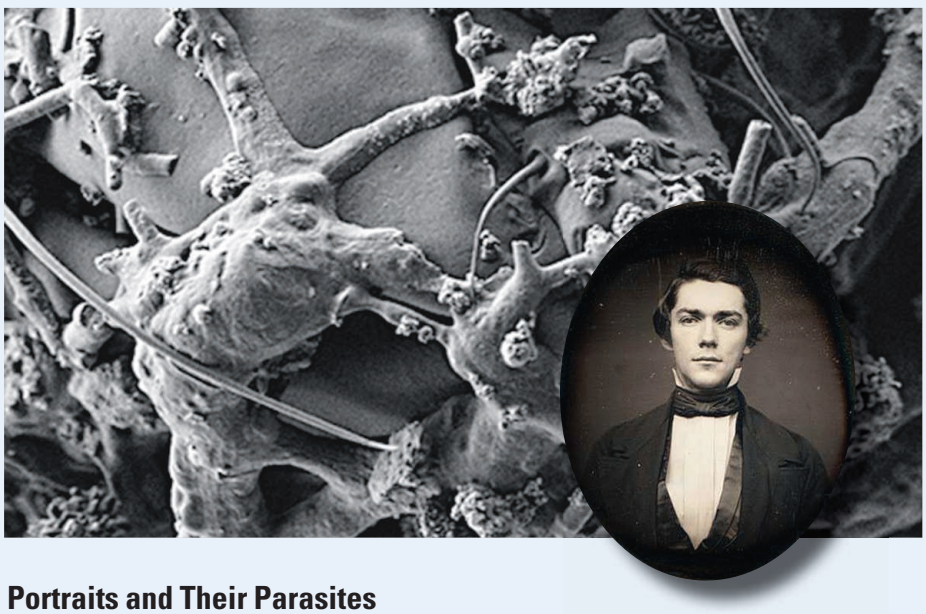

Portraits and Their Parasites

Daguerreotypes may seem frozen in time, but their surfaces are living landscapes. Popular in the mid-19th century, daguerreotypes were a precursor to photography created by layering silver on a copper plate and exposing it to light and various chemicals, often including gold. Many have become fuzzy or faded with time, and now researchers have discovered one reason why: Their surfaces are teeming with life. Fungi and various unidentified life forms eat and digest the metals, then excrete gold and silver nanoparticles that disfigure the image. The good news is that the precise mixture of life forms on an unidentified daguerreotype may offer clues to where it was made. And the parasites may even suggest new ways to manufacture nanoparticles through biological processes. http://scim.ag/daguerr

CREDITS (LEFT TO RIGHT): AMANDA BOYD/USFWS; (INSET) DR. PIERRE YVES-DAOUST; THE COLLABORATION OF WEIGANDT AND BIGELOW (2)

The Benefits of Baby Banter

Infants aren't known for being skilled conversationalists, but that doesn't mean that they don't benefit from early conversations. According to new research from Stanford University's Anne Fernald, differences in how parents talk to their babies—linked to the family's socioeconomic status (SES)—may help explain differences in school performance and career success.

Babies who are spoken to frequently in an engaging way, generally from a higher SES, tend to develop faster word-processing skills, which directly relate to the development of vocabulary and language, memory, and even nonverbal cognitive abilities. Fernald and colleagues measured parent-baby banter from round-the-clock recordings in babies' homes, then used an eye-tracking test to see how well they followed a prompt to look at a picture.

By 2 years of age, high SES children were 6 months ahead of low SES counterparts; by age 3, differences in processing abilities were predictive of later performance in and out of school. The group hopes this research will lead to interventions that shrink the language gap between kids on either side of the income gap. **http://scim.ag/_babytalk**

A Science-Religion Detente? Survey Suggests It's Possible

The science-religion wars are as old as science itself, but an ambitious new survey suggests that the rift can be bridged. In collaboration with the AAAS Dialogue on Science, Ethics, and Religion, sociologist Elaine Howard Ecklund of Rice University in Houston, Texas, surveyed more than 10,000 Americans, including 574 scientists, on their views of science and religion. The early results confirm that scientists—including engineers,

Published by AAAS

doctors, and others with technical training—have more unbelievers in their ranks than the general population. But almost 75% of these scientists professed some religion, and 17% identified as evangelical Christians. And while large fractions of both scientists and evangelicals see science and religion as in conflict (about 25% and 30%, respectively), even larger fractions say there is room for collaboration. On some issues, common ground will be hard to reach: Forty-three percent of evangelicals surveyed believe God created the universe and all of life within the last 10,000 years. But as Ecklund put it, what you make of the results "depends on whether you feel the cup is half empty or half full."

A Retro View of the Cosmos

Telescopes have come a long way since Galileo Galilei confirmed the heliocentric worldview using a tube and two pieces of glass. But studying these crude gadgets may allow us to experience the skies through his eyes. A group of science historians has compiled the most extensive database of early refracting telescopes to date—an online collection called Dioptrice. It contains about 1300 telescopes—both physical artifacts from museums and private collections and images from books and art.

Early observers. A 1692 depiction of Galileo (*left*) with refracting telescopes.

CREDIT: COURTESY OF DIOPTRICE

Now, they plan to test how well some of these devices transmitted distant light. Using adaptive optics, the technology behind today's large telescopes, they will feed a light source, such as an image of a planet, into a telescope and observe how it gets distorted after passing through 400-year-old glass. Such tests could reveal precisely what Galileo—and the stargazing naysayers of his time—saw when they peered at the rings of Saturn, the moons of Jupiter, and the phases of Venus. **http://scim.ag/dioptrice**

Thwarting Genome Hackers

Ever cheaper genetic sequencing technology could help detect diseases and save lives, but not everyone is comfortable with releasing their biological blueprints to the world. Now, cryptologists are perfecting a privacy tool that puts genetic information in a secure yet functional format.

Today, most genetic sequences are simply anonymized before being sent out for analysis. But a little genetic sleuthing can link data to its owner. In the new technique, called homomorphic encryption, computers can perform addition and multiplication on encrypted data. By approximating genetic testing algorithms with these basic operations, a computer can return encrypted results without ever decoding the information. At first, the method seemed too time-consuming to be practical, but a variation geared toward faster performance promises to be "a huge tool in our toolbox," says cryptologist Kristin Lauter of Microsoft Research in Redmond, Washington. She predicts it will begin to see wide-scale adoption within 10 years. **http://scim.ag/_encrypt**

Virtual Bodies Come to Life

The motion capture technology that brought Na'vi to life in the film *Avatar* has another use in the lab: creating fine-scale, highly personalized models of how a body moves. Using professional ballerinas as test subjects, computer scientist Nadia Magnenat Thalmann of the University of Geneva in Switzerland and colleagues have created virtual models of bodies in motion—not just their external shape but also dynamics hidden in their joints.

They used MRI to generate a model of the muscles, cartilage, and bone in each dancer's hip. Then, by adding data from a motion sensor suit, they watched how stress was distributed within the tissues as she performed. Many ballerinas need hip replacement surgery in their early teens, Thalmann says, and the model can show them which movements put them at risk of damage. Analyzing the data takes about a month, she adds, but it may someday be used for quick clinical assessments. **http://scim.ag/_dancer**

WHAT'S THE COOLEST SCIENCE FACT YOU KNOW?

Science asked meeting attendees to share their favorite science fact. Here are a few of the responses. To see the whole collection of videos and tweets, visit **http://scim.ag/scienceWOW**.

"The summit of Mt. Everest is marine limestone."

—Monterey Bay Aquarium Communications Director Ken Peterson

"There are bacteria that expand or contract depending on if they're wet or dry. … One pound of these bacteria, when they're made wet, can lift a car 3 feet. These can help you change your tire!"

—Actor and science communicator Alan Alda

"The actual brain takes about 20 watts of power in order to do all the fancy things it does. If we want to simulate that on a computer these days, it's going to take something like a full power plant in order to power that computer."

—University of Waterloo neuroscientist Terrence Stewart

"My fave science fact is that science is not just cool facts, its how we know anything is a fact."

—Science enthusiast Eric Lawton (@Eric0Lawton)

Published by AAAS

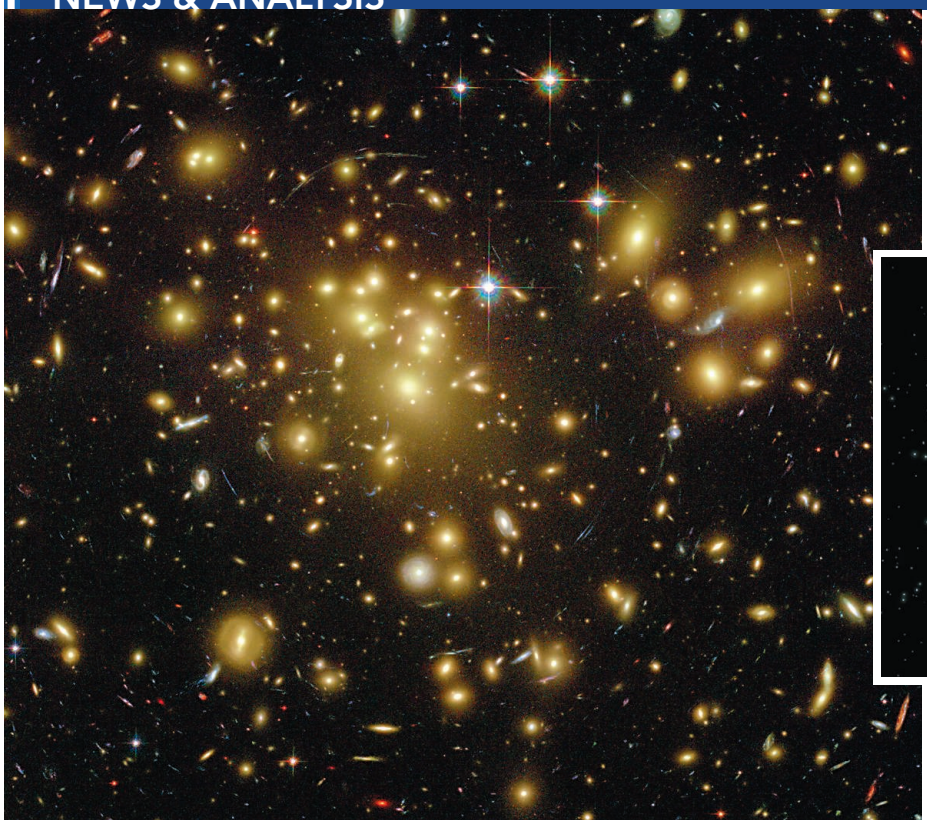

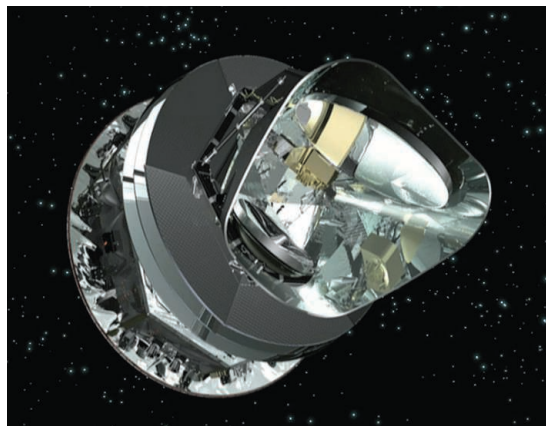

Short supply. A supposed deficit of galaxy clusters like Abell 1689 (*left*) may hint at a new particle that data from the Planck spacecraft (*below*) did not show.

ASTROPHYSICS

New Neutrino May Have Heated Baby Universe

Last March, when cosmologists working with the Planck spacecraft released the most detailed study yet of the afterglow of the big bang—the cosmic microwave background (CMB)—many researchers were disappointed that the European Space Agency mission merely confirmed the standard cosmological theory and found nothing new (*Science*, 29 March 2013, p. 1513). Or did it? In separate papers, three groups of theorists now argue that when combined with other data, the Planck data show evidence of a new particle called a sterile neutrino, something that the Planck team had dismissed.

"At second glance, the universe might turn out to be less boring than initially thought," says Jasper Hasenkamp, a cosmologist at New York University (NYU) in New York City and co-author of one of the papers.

According to the standard model of cosmology, the universe consists of 5% ordinary matter, 27% mysterious dark matter whose gravity binds the galaxies, and 68% weird space-stretching dark energy. Some 13.8 billion years ago it sprang into existence and instantly underwent a faster-than-light growth spurt called inflation, which magnified tiny density fluctuations in the primordial soup of matter and radiation. Afterward, dark matter gathered in the denser spots and eventually drew in ordinary matter to form the galaxies. That history is recorded in part-in-100,000 variations in the temperature of the CMB across the sky, which reflect the primordial density fluctuations.

Many researchers had hoped that Planck, which took data from 2009 until last year, would sniff out something novel in the statistical distribution of those temperature variations. Some hoped the data would require a new neutrino in addition to the three known now, which might help explain oddities in some experiments with particle accelerators and nuclear reactors (*Science*, 21 October 2011, p. 304). The neutrino would have to be sterile, meaning that it could not be created in ordinary particle interactions but only when a normal neutrino morphs into a sterile one. Sterile neutrinos would act like extra radiation in the infant universe.

But the Planck data didn't cry out for an extra neutrino or other major changes to the standard theory. They did suggest that the universe is expanding a bit more slowly than researchers had measured directly by studying distant beacons including supernova explosions and variable stars. Some researchers thought that slight discrepancy in the expansion rate, or Hubble constant, might hint that dark energy is not, as the standard theory assumes, a property of space itself but is something more complicated (*Science*, 6 September 2013, p. 1056).

Now, the three teams argue that, taken all together, cosmological data point to a sterile neutrino. Hasenkamp and Jan Hamann of CERN, the European laboratory for particle physics near Geneva, Switzerland, spelled out the argument last October in the *Journal of Cosmology and Astroparticle Physics*. In separate papers published on 6 February in *Physical Review Letters*, two teams—Mark Wyman, a cosmologist now at NYU, and colleagues at the University of Chicago in Illinois, and Richard Battye of the University of Manchester in the United Kingdom and Adam Moss of the University of Nottingham in the United Kingdom—make similar arguments.

The three papers all start with the same basic observation: With its parameters set by the Planck data, the standard cosmology predicts more clusters of galaxies than astronomers see. "All the cluster counting technologies agree with each other, and they all have a profound disagreement with Planck," Wyman says.

But clusters would be less abundant in a universe containing sterile neutrinos about a millionth as massive as an electron. That's

CREDITS (LEFT TO RIGHT): NASA, ESA, L. BRADLEY/JHU, R. BOUWENS/UCSC, H. FORD/JHU, AND G. ILLINGWORT/UCSC; ESA

Published by AAAS

because in the standard model, dark matter consists of cold, massive, slow-moving particles that tend to clump. But if some dark matter consisted of hot, fast-moving particles such as neutrinos, then clumping would occur more slowly, producing fewer clusters. A sterile neutrino would also add a dollop of radiation to the early universe and bump up Planck's estimate of the Hubble constant, solving that puzzle as well.

The case for the sterile neutrinos is tricky. To avoid adding too much radiation and running afoul of Planck's previous results, the new neutrino would have to be out of so-called thermal equilibrium with other particles in the early universe, says John Beacom, a physicist at Ohio State University, Columbus, who doubts the new claim. "That's possible, but not natural," he says.

Some cosmologists say the cluster deficit may be illusory. Astronomers must count clusters in a given mass range, and they estimate a cluster's mass by methods such as measuring its x-ray emissions or how its gravity distorts images of galaxies beyond it. Underestimate those masses and the count would appear artificially low, says Anthony Challinor, a Planck team member from the University of Cambridge in the United Kingdom. "Trying to do cosmology from cluster counts is very, very difficult," he says. Unpublished analyses suggest clusters may indeed be more massive than assumed.

The issue could come to a head quickly, says David Spergel, a cosmologist at Princeton University. This year, the Planck team should release new results based on more data. And other researchers may improve their cluster-mass calibrations by comparing methods. Whether or not the discrepancy is real, Spergel says, "we should know soon." **–ADRIAN CHO**

ASSISTED REPRODUCTION

FDA Considers Trials of 'Three-Parent Embryos'

An experimental technique that manipulates a woman's DNA could spare her from passing on a potentially deadly disease to her children. But the technique breaks new and ethically fraught ground: It would create a child that has DNA from "three parents"—the mother, the father, and an egg donor. And any daughter could in turn pass on the new DNA mix to future generations. Until now, procedures that produce inheritable gene alterations have been ethically taboo.

Now, regulators on both sides of the Atlantic are grappling with whether to allow the first human trials of the technique, called mitochondrial DNA replacement therapy, to go forward. In the United Kingdom, the government has given the technique a cautious endorsement. And at a meeting on 25 and 26 February, an advisory committee to the U.S. Food and Drug Administration (FDA) will consider the topic. It is expected to draft its recommendations in the coming months, which the agency will draw on to develop regulations.

FDA's Cellular, Tissue, and Gene Therapies Advisory Committee, which includes doctors, researchers, and representatives from industry and patient groups, will weigh whether the technique is effective and safe enough to try in humans. Animal models are imperfect, and cell-based studies give only limited clues about possible long-term side effects.

Next week's meeting will focus on safety, but there are equally knotty ethical issues for regulators to consider: whether the benefit of averting severe disease overrides societal objections to changing the human germ line. Another is how the ethical calculus is affected by another potential use of mitochondrial DNA replacement: to treat age-related infertility, which would widen the potential pool of patients to include millions of women. "Once it's used, it will be used in all sorts of ways for all sorts of people. That's the reality of this kind of medicine," says bioethicist Jeffrey Kahn of Johns Hopkins University in Baltimore, Maryland.

Pushing to go forward are patients with mitochondrial diseases and the doctors who care for them. "I have nothing to offer these people, and that's heartbreaking," says Douglas Wallace, an expert in mitochondrial genetics at the University of Pennsylvania. The diseases arise when something goes wrong in the mitochondria, the organelles that provide energy to cells. Mitochondria carry their own set of genes, called mitochondrial DNA (mtDNA), and mutations in those genes cause many of the syndromes. But because each cell contains many mitochondria, and each mitochondrion has up to 10 copies of its genome, some cells and tissues can acquire more faulty genes than others. This randomness means that apparently healthy women can be carriers of mitochondrial disease, not discovering the problem until

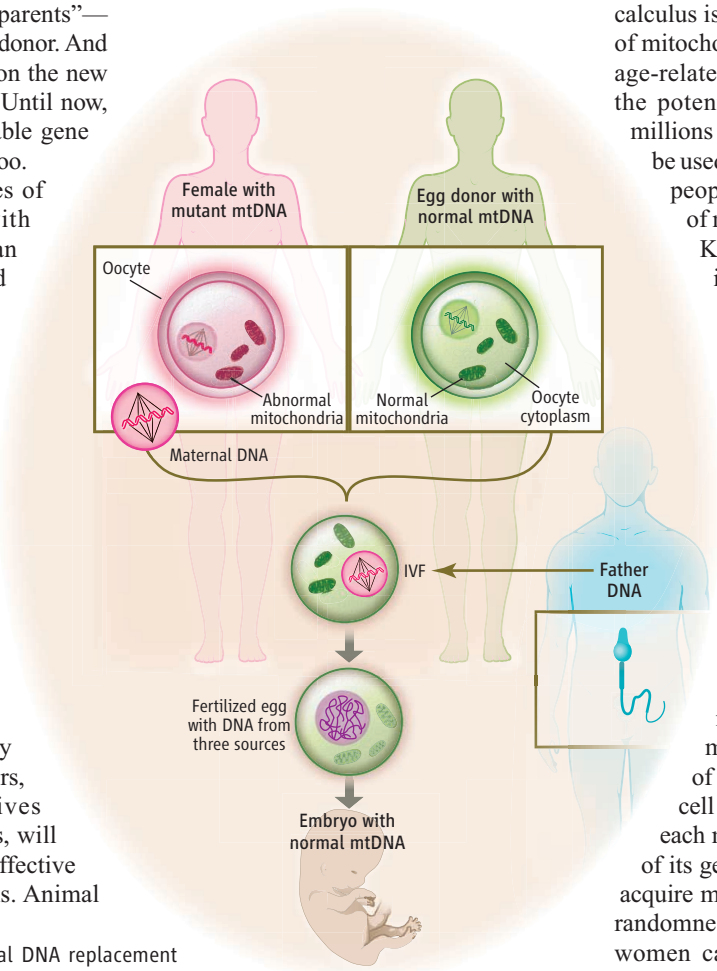

CREDIT: K. SUTLIFF/*SCIENCE*

Controversial therapy. Mitochondrial DNA replacement could help carriers of severe disease have healthy children.

Published by AAAS

they give birth to children who are very ill.

Because brain, muscles, and heart require so much energy, symptoms often appear in those tissues first. Some cases are diagnosed at birth and are soon fatal. Others don't appear until adulthood. There are no treatments; doctors attempt to alleviate symptoms with antiseizure medications or physical therapy.

Although sperm carry mitochondria, they are usually degraded shortly after fertilization, so mitochondrial diseases are passed down through the mother. To avoid having a desperately ill child, women who carry severe mitochondrial mutations can adopt, undergo in vitro fertilization (IVF) with a donor egg cell, or allow embryos or fetuses to be tested for mitochondrial defects—although such tests aren't very accurate. Several research groups say the best way for carriers to have a healthy, genetically related child could be to remove the nuclear genes from an egg with mutated mitochondria and place them into a donor egg with healthy mitochondria (see diagram, p. 827). Using different approaches, these groups have made enough progress in animals and with human cells that they would like to have permission to try the techniques in patients. In the United Kingdom, current law prohibits IVF techniques that alter the DNA of an embryo. But since 2011, both ethical and scientific review panels have said mtDNA replacement research should be allowed to proceed for women who are carriers of severe disease, and the government has agreed. The Department of Health is expected to release a proposed law this spring, and Parliament could vote on a final version later this year.

In the United States, FDA has said it has the power to regulate any transfer of mitochondrial DNA in embryos, because it is a form of gene therapy. At least one researcher, Shoukhrat Mitalipov of Oregon Health & Science University in Beaverton, has asked the agency for guidance on what a clinical trial would require. (Mitalipov's lab has produced seven monkeys born after mtDNA replacement.)

Kahn, the ethicist, puts the key issue facing the panel this way. By mixing new DNA into the germ line, "we're not treating humans. We're creating humans. There's not a model for that." Then there is the thorny issue of whether the technique should be used to treat infertility. Some reproductive biologists think that faulty mitochondria—or perhaps other factors in the egg cytoplasm that are exchanged in mtDNA replacement techniques—might be one of the key reasons fertility falls in women in their late 30s. They say that the procedure could help such women conceive, but critics say there is little animal data to support the idea.

So far so good. Mito and Tracker, the first rhesus monkeys born after mtDNA replacement, seem healthy so far. They will reach adulthood, and breeding age, when they turn 5 later this year.

"No studies clearly indicate the efficacy of treatment" with the technique, Mitalipov says. But clinical trials "would be the way to test it." He would like to go forward with trials in both disease carriers and infertile women. "Mitochondrial diseases are rare, but age-related infertility is a huge problem."

Others say existing safety data are insufficient to green light any clinical trial. One worry is that a mismatch between nuclear and mtDNA could cause health problems in children conceived with the technique (*Science*, 20 September 2013, p. 1345). Many nuclear and mitochondrial genes work together and depend on each other. In some animal studies, says Klaus Reinhardt of the University of Tübingen in Germany, mismatched nuclear and mtDNA caused a range of problems, including infertility, especially in male offspring.

Wallace thinks there is "some possibility of incompatibility." To minimize the risk, he would recommend finding egg donors who have a similar mitochondrial DNA type as the potential mother.

But Robin Lovell-Badge, a developmental biologist at the MRC National Institute for Medical Research in London who led a U.K. scientific review of the technique, says the studies that found developmental and health problems were in inbred strains of animals and are unlikely to apply to humans. Other studies have produced apparently healthy animals, he says.

Mitalipov says no problems have appeared in the rhesus monkeys his lab produced, even though the egg donor and the nuclear donor were from different macaque subspecies. "We monitor them very closely, but so far the monkeys were pretty normal," he says. Whether relatively subtle effects like cognitive defects would show up in monkeys is unclear, however. Nor would fertility problems be apparent in the monkeys so far.

Some children have in fact been born with mitochondria from unrelated donors. In the late 1990s, a fertility clinic in New Jersey treated the unfertilized eggs of infertile women by injecting them with cell cytoplasm from eggs from fertile donors. Along with proteins and other cellular material, mitochondria from the donor were injected, resulting in children who carried a mix of mitochondria from their mother and from the egg donor.

More than a dozen children were born after the procedure, but several had developmental problems. One was missing one copy of the X chromosome, and another developed pervasive development disorder, a spectrum of conditions that includes autism. The treatments were not part of a controlled trial, however, so it is impossible to say whether the cytoplasm injection actually helped the women become pregnant or whether it was the cause of the developmental problems. The clinic stopped the practice in 2001 when FDA said it had the authority to regulate the practice as germline gene therapy.

Many mtDNA disease carriers, who otherwise face a virtual certainty of having a severely ill child, would be eager to accept a low risk of more minor problems, Wallace says. But, he adds, the risk-benefit ratio for society at large is different. "It's going to be hard to find what a fair balance is."

–GRETCHEN VOGEL

CREDIT: OREGON HEALTH & SCIENCE UNIVERSITY

GENOMICS

DNA Sequencers Still Waiting for The Nanopore Revolution

Plug and play. Soon researchers will have a chance to put a new hand-held DNA sequencer through its paces.

Marco Island, Florida, is mecca for genome sequencers, who for more than a decade have made an annual pilgrimage there for a conference* where companies roll out their latest technological advances, some with revolutionary potential. In one of the most dramatic recent claims, a British-based firm called Oxford Nanopore Technologies announced 2 years ago that it had succeeded with a sequencing technique many thought would not work: sequencing unprecedentedly long stretches of DNA in real time, by threading the molecule through a nano-sized pore in a membrane (*Science*, 4 May 2012, p. 534). The company promised to quickly make available cheap prototype devices for outside researchers to confirm its claims.

After 2 years of silence, it has finally produced more tantalizing evidence of progress. Although the company didn't send anyone to the Florida meeting, an academic researcher collaborating with the company reported that he had used data from the first bacteria sequenced using this new technology to help piece together the microbes' genomes. And the firm began to make good on its earlier promise, notifying scientists newly accepted into a program to test out the new instruments. Still, not everyone was impressed at the firm's second act, as its DNA sequence data was not good enough to put together these genomes without help.

Meanwhile, conventional sequencers are racing ahead, trying to push the costs of sequencing ever further down (see table). Illumina, the largest maker of sequencing machines, grabbed the latest headlines in January with the promise of a system that could produce a genome for $1000—a long-discussed threshold that some believe will begin to make sequencing a routine part of medical care (*Science*, 17 March 2006, p. 1544).

Illumina's machine, like other so-called next-gen sequencers, identifies the bases making up the DNA as they are added to a chain matching the DNA being sequenced. The bases must be chemically tagged so that they can be identified, and the technique yields many short stretches of sequence that have to be pieced together. Oxford Nanopore's approach is radically different: Its devices pull a single strand of DNA through a tiny pore. As bases go through, they interrupt an ionic current in a way that reveals each base's identity. In theory, the technique allows DNA strands thousands of bases long to be decoded in a single pass, without the delay and effort needed to piece together many short reads. The idea is almost 20 years old, and it finally seemed to be a reality in 2012, when Oxford Nanopore showed a viral genome they claimed had been determined with nanopore technology.

So why did progress stall?

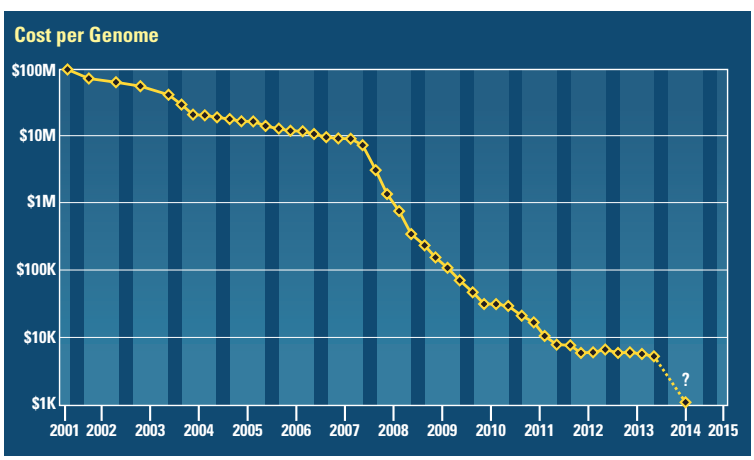

Long fall. After many years of decline, the cost of sequencing a genome had leveled off, but may dive again (dashed line) if Illumina's promise of a $1000 genome holds up.

Over the past 2 years, the company says, it had to find a new membrane to support the pore, because its original choice could not be manufactured on a large scale. The firm also shifted from focusing on a large sequencing machine to developing a hand-held, disposable sequencer first, because there was such overwhelming interest in it.

This year, however, David Jaffe of the Broad Institute in Cambridge, Massachusetts, offered some evidence of progress. His group provided DNA samples from two bacterial genomes, the common *Escherichia coli* and *Scardovia wiggsiae*, a microbe involved in tooth decay, and the firm sequenced them. With genomes 4.6 million and 1.55 million bases long, respectively, these organisms represent a step up from the viral genome Oxford Nanopore said it sequenced 2 years ago.

But Jaffe's talk showed the company still has a long way to go. The company-provided data indicated its device sequenced as large a piece of DNA as was in the samples, in this case, up to 10,000 bases at a time. While there were stretches of perfect data, systematic errors prevented Jaffe from assembling the genomes with just that data, one of the great hopes for nanopore technology. Instead, he showed how these data could be used to refine a genome assembled from short DNA fragments generated by Illumina technology. "Already at this very early stage, it's very useful for certain things," says Jeffery Schloss of the National Human Genome Research Institute in Bethesda, Maryland. But others were less enthused. "What is the point of a hand-held transportable device if it can only be used in tandem with existing technologies?" notes Ken Dewar, a genomicist at McGill University in Montreal, Canada.

Oxford Nanopore is now inviting researchers to try for themselves. On the same day as Jaffe's talk, the firm sent out e-mails asking several hundred applicants to deposit $1000 in exchange for a chance to try its new portable sequencer, called MinION. As a first pass, participants will run DNA provided by Oxford Nanopore to learn how to use the MinION, but thereafter, they can try any DNA they like.

David Deamer, a nanopore pioneer at the University of California (UC), Santa Cruz, can't wait. "People are going to have a lot of things that they are going to try it out with,"

*Advances in Genome Biology & Technology, Marco Island, Florida, 12–15 February.

CREDITS (TOP TO BOTTOM): OXFORD NANOPORE TECHNOLOGIES LTD.; ADAPTED FROM THE NATIONAL HUMAN GENOME RESEARCH INSTITUTE

Published by AAAS

he says. Some might try real-time analysis of microbes in food, as a precursor to food safety tests, or see how well MinION can read ancient DNA. Deamer wants to see if the device can process a single strand of DNA 16,000 bases long in one pass. "We are really going to challenge the instrument."

While Oxford Nanopore offers individual researchers a chance to experiment with a cheap, hand-held device, Illumina is about to sell high-end technology designed for just the biggest genome sequencing organizations. Last month, it introduced the HiSeq X, a million-dollar machine capable of sequencing 1800 human genomes a year, saying that this new technology would push the cost of a human genome below $1000, including labor, depreciation, and reagents. "We saw an emerging demand for population scale sequencing," says Joel Fellis, a senior marketing manager at Illumina in San Francisco, California, such as the British plan to sequence 100,000 participants in its national health plan by 2017.

There is a catch, however. Any buyer must order at least 10 machines and agree to use them only for sequencing human genomes. "That prices out a lot of general researchers," says Zak Wescoe, a UC Santa Cruz bioengineer. And the $1000 cost requires that all these machines run pretty much at full capacity. Not many places have a demand for 18,000 genomes a year, or the capacity to analyze that many sequences, says Elaine Mardis, co-director of The Genome Institute at Washington University in St. Louis. "I don't know how you could sustain it."

Deanna Church, a genomicist with Personalis in Menlo Park, California, welcomes the advances at both ends of the cost scale. "There's going to be room for multiple players, and some technologies are going to lend themselves better to some applications over others."

–ELIZABETH PENNISI

U.S. SCIENCE POLICY

Antarctic Scientists Continue to Reel From Shutdown

The 16-day shutdown of the U.S. government this past October is a distant memory for most Americans. But scientists working in Antarctica continue to feel its negative effects. The shutdown triggered a logistics nightmare in a field season that ends this month, forcing the National Science Foundation (NSF) to scale back some projects and defer others. That move, in turn, will aggravate an already tight budget situation.

Heading home. The cargo ship *Maersk Illinois* left Antarctica this month after enduring an intense storm that wrecked the ice dock at McMurdo Station.

"We lost a good month of our normal season," estimates Scott Borg, head of NSF's Antarctic science program. "It's an opportunity cost that you can't put a figure on." The weather isn't helping either: Storm damage to an ice dock this month prevented some scientists whose projects did go forward from shipping their samples.

The shutdown, which began on 1 October after Congress failed to pass a 2014 budget, occurred just as NSF was preparing for the annual onslaught of scientists during the short austral summer. Without the authority to spend money, NSF had to reverse direction and begin winterizing all its facilities—including labs, balloon launch sites, and field stations—so they could be shut down for an indefinite period.

The agency was already coping with the impact of sequestration, the 5% spending cut that took effect last March. NSF's budget for Antarctic research grants shrank from $68 million in 2012 to $64 million in 2013, and it remained frozen at that level under the temporary budget agreement that ended the shutdown and allowed NSF to get back to business in Antarctica. But the delay and the budget squeeze forced NSF to scale back a dozen projects and move an additional 17 projects into next season.

Program managers will have to tap some of the money they had planned to spend on the next round of grant proposals to support the deferred projects. And that means even stiffer competition for those with new ideas. Earlier this month, Borg tried to squelch rumors that the funding well was dry with a "Dear Colleague" letter that encourages scientists to submit proposals before the 15 April deadline.

"The point of the letter was to say, 'Hey, things aren't that bad,' " Borg explains. "Yes, we are facing some tough fiscal realities … and we'll have fewer new starts next year. But we haven't gotten to the point of not being able to do anything new."

This year has been a real test for a team of meteorite collectors coordinated by Ralph Harvey of Case Western Reserve University in Cleveland, Ohio. Sequestration trimmed the size of this season's team by one-third. And in the wake of the shutdown, Harvey adds, "NSF's desire to support people exceeded its grasp."

His team also felt the wrath of Mother Nature. Although good weather allowed them to make the most of a shorter collecting season, the 330 rock samples they amassed won't be making it to a NASA lab in Houston, Texas, for at least a year. A storm last week took out the ice pier at NSF's McMurdo Station, preventing workers from loading freezers holding the extraterrestrial cargo onto a ship. "I hate to use the term 'perfect storm,' but this was the last in a series of extraordinary events this season," Harvey says.

The shutdown also put a big crimp in the expected finale of a multiyear effort to drill into the subglacial Lake Whillans, which lies under 800 meters of continental ice and flows into the Ross Sea. NSF decided to delay the WISSARD project because of its need for heavy logistical support: The team must travel by ice tractor on a 2000-kilometer round trip to the drilling site.

Last month, NSF approved what Ross Powell, WISSARD's chief scientist, calls a "cut-down version" of the project for next January with a smaller team and only one borehole instead of three. Powell, a geologist at Northern Illinois University, DeKalb, says he's also lost a promising graduate student who was so "demoralized" by this year's cancellation that he's leaving school to find a job.

–JEFFREY MERVIS

Published by AAAS

Tattletale. Deep Atlantic water leaves its isotopic mark in the sand-size foram *Cibicidoides wuellerstorfi.*

CREDITS (TOP TO BOTTOM): A. HOLBOURN AND A. HENDERSON, *PALAEONTOLOGIA ELECTRONICA* **4** (31 JANUARY 2002); E. GALAASEN *ET AL.*, *SCIENCE* (ADVANCED ONLINE EDITION)

CLIMATE CHANGE

Atlantic Current Can Shut Down For Centuries, Disrupting Climate

For decades, climate scientists have cast a worried eye at the grand ocean circulation that draws warm southern waters into the North Atlantic. A shutdown due to global warming—a possibility hinted at by some climate models—would not bury Manhattan under a tsunami of ice, as one Hollywood disaster movie had it. But it would unsettle climate around the North Atlantic and beyond.

Now, researchers have hard evidence that the real Atlantic circulation did indeed abruptly slow or perhaps even stop for centuries at a time more than 100,000 years ago, when the world was only a bit warmer than today. "That's really, really dramatic," says paleoceanographer Jerry F. McManus of the Lamont-Doherty Earth Observatory in Palisades, New York, who was not involved in the work, which was reported online this week in *Science* (http://scim.ag/EVGalaasen). "It's exciting and potentially important." The clues, from a sediment core recovered in 2003 from the sea floor just beyond the southern tip of Greenland, show that the Atlantic circulation recovered each time. But the vulnerability of the Atlantic's circulation is sobering news for today's greenhouse world.

A key driver of the currents is the formation of North Atlantic Deep Water (NADW), which starts out as cold, dense surface water in the Nordic Seas between Greenland and Scandinavia. Being heavier, it sinks to the bottom and begins wending its way southward. Sand-sized single-celled protozoa called Foraminifera, or forams, that lived on the bottom beneath the current millennia ago incorporated the water's distinctive isotopic signature—a particularly high ratio of carbon-13 to carbon-12—into their shells, which were buried as the sediment built up. By analyzing the carbon isotopes in fossil forams from different parts of a sediment core, scientists can find out how much, if any, NADW was passing by at a particular time.

Paleoceanographer Eirik Galaasen of the University of Bergen in Norway and his colleagues thought they might get an exceptionally sharp look at the state of the NADW more than 100,000 years ago from a low ridge of sediment off Greenland called the Eirik Drift (named after Eirik the Red, not Galaasen). That's because the drift, which lies beneath the flowing NADW, was deposited five or 10 times as fast as other records used to piece together the history of the NADW. So it holds a "large print" record that is much easier to read than phyllolike "fine print" layers of sediment that piled up more slowly.

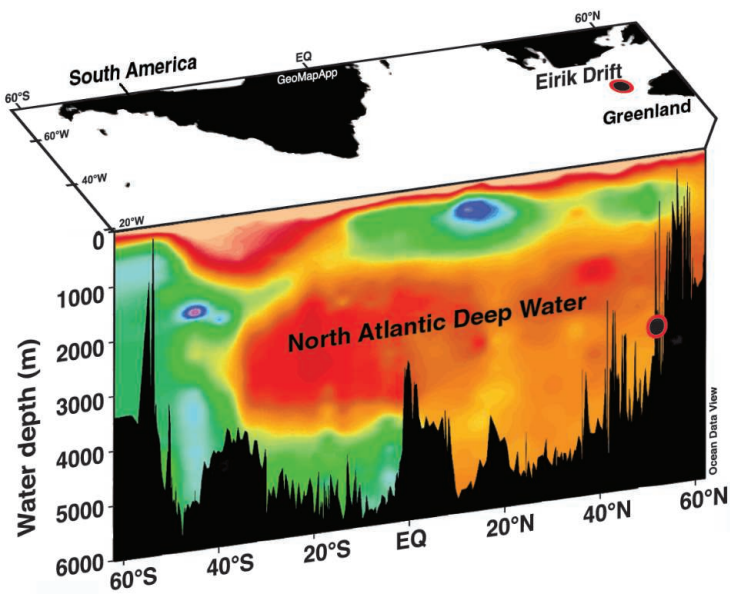

Fragile flow. Isotopically distinctive North Atlantic Deep Water (orange) hugs the bottom of the North Atlantic as it spreads into the Southern Hemisphere.

And it revealed new detail during the warm period between the two previous ice ages 115,000 to 130,000 years ago—that had seemed to be a tranquil enough time for North Atlantic circulation. Instead, the fossils analyzed by Galaasen and colleagues testified to three episodes in which the flow of NADW had slowed, stopped, or risen toward the surface. Each of the two more recent reductions in NADW flow lasted a few hundred years, but the earlier one consisted of several centuries-long drop-offs chockablock over about 2500 years.

If the far North Atlantic were to respond that way during the present interglacial period, change would be the order of the day, Galaasen says. As the sinking of NADW slowed, the northward flow of warm surface water would also slow, and the far North Atlantic would cool. That would alter atmospheric circulation patterns and thus change far-flung regional climates; Sahel droughts in West Africa, for example, could become more severe as a result. Less carbon dioxide absorbed from the atmosphere would be carried into the deep sea by the NADW, aggravating global warming. And in a complete NADW shutdown, the loss of the southward bottom flow could send the North Atlantic sloshing onto North America, increasing sea level by a meter on top of the rise due to melting ice.

Whether this happens depends on whether today's North Atlantic responds to global warming the way the last interglacial period's Atlantic responded to its warmer climate. Galaasen and colleagues do see signs in the core and in others plucked from the length of the Atlantic that melting of high-latitude ice 120,000 years ago sent icebergs and fresh water pouring into the Nordic Seas. The influx would have freshened surface waters and made them less dense and therefore less prone to sink—though only temporarily.

Global warming today is already freshening the far North Atlantic by melting Greenland ice, a trend expected to accelerate in the decades ahead. So NADW's southward flow will be watched even more closely now.

–RICHARD A. KERR

Published by AAAS

Vantage point. Europe's Very Large Telescope will host the SPHERE planet imager.

ASTRONOMY

Rival Detectors Prepare to Take Snapshots of Distant Worlds

In the coming months on two mountaintops in Chile, two new state-of-the-art instruments will start scanning the skies for planets around other stars. The vast majority of the roughly 1000 exoplanets identified so far have been found using indirect methods because starlight swamps their faint optical signals. But the new instruments, one North American and one European, will see planets directly. Fixed to two of the world's biggest telescopes, they push optical technology to the limit. "After 10 years building it, to see it on the sky is fantastic," says Bruce Macintosh of the Lawrence Livermore National Laboratory in California, principal investigator for the Gemini Planet Imager (GPI).

GPI, built by a consortium of U.S. and Canadian institutions, is already mounted on the 8-meter Gemini South telescope on Chile's Cerro Pachón. "The integration went very smoothly, which was a pleasant surprise," says Macintosh, who will soon be moving to Stanford University. "It worked on the first star we pointed it at." On 7 January, the GPI team published its first image of an exoplanet: Beta Pictoris b, a young planet several times the size of Jupiter that an indirect detection strategy had previously spotted. Commissioning of GPI will continue for a few months.

Meanwhile, the SPHERE instrument, built by the Institute of Planetology and Astrophysics of Grenoble in France and a group of other European institutions, is in transit to Chile. Once it arrives at Cerro Paranal later this month, it will be mounted on one of the four 8.2-meter scopes of the European Southern Observatory's (ESO's) Very Large Telescope. Co–principal investigator Markus Feldt of the Max Planck Institute for Astronomy in Heidelberg, Germany, acknowledges that there is a friendly rivalry between the two teams. "GPI is way ahead now," he says. SPHERE is not expected to see its first light until 12 May.

Trying to see an exoplanet is often likened to trying to spot a firefly while staring into a billion-times-brighter searchlight. Astronomers use a mask called a coronagraph to block out the star's light, but it takes sophisticated optics to stop glare that can hide the planet and to correct for various optical imperfections.

Using these techniques, astronomers have directly imaged seven exoplanets, all supergiants both larger and farther from their parent star than Jupiter. About 10 years ago, researchers began working on instruments optimized for detecting exoplanets; GPI and SPHERE are the first to be completed. To remove the distorting effect of Earth's atmosphere, both teams have added another technology: extreme adaptive optics, in which deformable mirrors are reshaped in real time to correct for atmospheric distortion. GPI and SPHERE both boast more than a thousand actuators able to make adjustments a thousand times a second. GPI's system is built on a microchip 3 centimeters across sporting 4000 microelectromechanical actuators spaced 0.4 millimeters apart.

Both instruments use multistage systems to eliminate stray light and correct the light path. GPI cuts out diffracted light by passing the beam through a small circular window fringed with a pattern of 10-micrometer dots carefully designed to prevent scattering. In SPHERE, after the coronagraph blocks a star's light, other instruments split the remaining beam into two, shift one of them by half a wavelength, and then recombine them so that any remaining starlight is removed by destructive interference. SPHERE also has multiple detectors at different wavelengths so that starlight can be removed electronically.

Despite these efforts, the new instruments will see only a few of the hordes of undiscovered exoplanets thought to lurk in space. Reflected light is just too dim, so they will focus on young planets still glowing from the heat of their formation. They won't be able to see planets much smaller than Jupiter, and they work best for planets orbiting far from their star. (The other main exoplanet detection methods—picking up a star's wobble as an orbiting planet pulls on it or the star's dimming as it passes in front—favor close-in planets.)

Later this year, each instrument will embark on a large-scale survey of about 500 nearby young stars to spot orbiting planets and analyze their light to measure their temperatures, the composition of their atmospheres, and even the structure of their cloud cover.

GPI and SPHERE will likely be the prime instruments for exoplanet imaging until the next generation of 30- to 40-meter extremely large telescopes start observing next decade. To see rocky planets the size of Earth, however, will require a telescope in space. Last decade, researchers at NASA and the European Space Agency drew up plans for ambitious planet imaging missions, but neither got off the drawing board. "It's a very costly endeavor. None of the proposed concepts were funded," says ESO instrument scientist Markus Kasper. There is, however, a more modest proposal on the table: adding a coronagraph instrument to WFIRST, a NASA astronomy mission that may fly around 2024 (*Science*, 15 February 2013, p. 748).

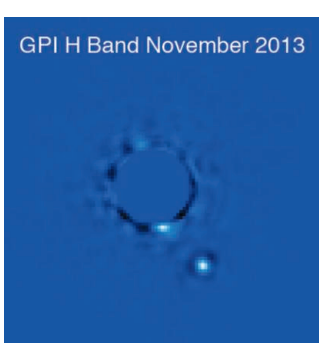

First light. Beta Pictoris b (bright dot), the first extrasolar planet snapped by the Gemini Planet Imager.

–DANIEL CLERY

CREDITS (TOP TO BOTTOM): G.HUEDEPOHL/EUROPEAN SOUTHERN OBSERVATORY; GEMINI OBSERVATORY

Published by AAAS

CREDIT: KRISTOFFER AHLM

Eavesdropping on Ecosystems

Researchers are collecting terabytes of recordings, from bird chirps to chainsaw roars. The emerging field of soundscape ecology has a lot to offer … and a lot to prove

MICHAEL SCHERER-LORENZEN WAS ONE of 80 scientists appealing for funding from the German Science Foundation at a review meeting in Potsdam, Germany, last November. But his pitch was the only one that began with the harsh, throaty sounds of barking roe deer.

The midnight recording lasted just a few seconds, but it demonstrated exactly the kind of data the University of Freiburg researcher proposed to collect with a network of 300 microphones scattered across Germany. Each would record 1 minute of sound every hour for a year, he explained, capturing nearly 44,000 hours in all. The payoff: detailed "soundscapes" that could help researchers relate bird, insect, and other animal populations to patterns of land management in Germany's forests and grasslands. "It would be really cool," he says, to use sound as a convenient proxy for measuring biodiversity.

Scheren-Lorenzen isn't the only researcher enticed by the emerging field of soundscape ecology. Advances in cheap, tough automated recorders and powerful sound-analysis software are inspiring scientists to launch increasingly ambitious efforts that use sound to document and analyze ecosystems. Rather than focus on the calls of one or a few species at a time—as in many traditional bioacoustics projects—soundscape ecologists are trying to describe the cacophony of entire landscapes, including nonbiological sounds such as rushing water, thunderclaps, and even the drone of cars and airplanes.

They hope to find more efficient ways to characterize an ecosystem than spending countless hours tromping through, and potentially disturbing, the landscape. Instead, they aim to find unique patterns hidden in the acoustic realm—and then track how they change in response to disruptions, such as increasing air traffic or construction projects, the arrival of invasive species, or the gradual effects of climate change.

Online

sciencemag.org

Sound clips and podcast interview with author Kelly Servick (http://scim.ag/pod_6173).

Published by AAAS

Ears in the sky. Soundscape ecologist Bryan Pijanowski installs a fuzzy microphone on a research tower in Borneo earlier this year.

Researchers want to quantify "what we experience ourselves as we go through the day and listen," says soundscape ecologist Bryan Pijanowski of Purdue University in West Lafayette, Indiana.

But studying whole soundscapes poses major technical and conceptual challenges. Researchers are struggling to find practical ways to boil down huge collections of digital recordings into something they can use. Converting complex soundscapes into relatively simple numerical indices of biodiversity is proving difficult. And soundscape ecologists have sometimes strained to persuade their colleagues, who may see little original in the approach, that large-scale networks of microphones can tell a meaningful story. Not that long ago, "there were many in the bioacoustics community that just said 'No, no, no! This is not a new idea at all,' " Pijanowski says.

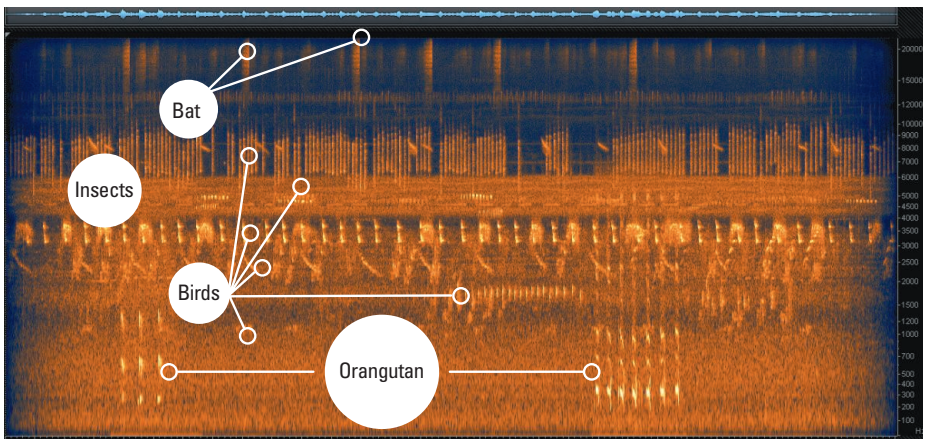

Everything in its place. A recording from the Sumatran rainforest illustrates the acoustic niche hypothesis, in which different kinds of animals utilize different parts of the sound spectrum. Bats, for instance, call at higher frequencies while orangutans use lower frequency sound.

Sound foundations

Scientists have long observed how animals produce and perceive sound, and analyzed their communication patterns. The first field recordings of birdsong date back nearly a century. But for the most part, bioacoustics studies focused on individual species, mining a recording for particular calls of interest.

That species-level approach misses the forest for the trees, says Bernie Krause, a studio musician-turned-natural sound recordist who is often credited with developing the concepts behind modern soundscape ecology. "This reductionist, detached, and fragmented way of looking at the world is really incoherent," he says.

Instead, Krause has proposed a theory of "acoustic partitioning," which he first published in the magazine *Whole Earth Review* in 1987. Inspired by the complex soundscapes he heard in Kenya while collecting sound for a science museum exhibit, he suggested that natural sound be viewed as a resource shared among vocal organisms, like a nesting habitat or a food supply. An animal must carve out its own aural niche, he wrote, for example by using a signature frequency or by signaling at a particular time of day, to avoid interference from other sounds.

In Krause's view, a healthy ecosystem would be clearly partitioned into niches by frequency or time. In contrast, a disrupted area would have gaps at some frequencies, where species had been lost. And when invasive newcomers or human-generated sounds intrude on a niche, the existing patterns might shift.

Many scientists were skeptical, seeing only anecdotal evidence for the theory. "It was completely rejected as a nice, aesthetic idea," Krause recalls. "But then, to be fair, I really didn't have, at the time, a way to express what I was finding … in the language of [scientific] publications."

But the idea intrigued some researchers, including Stuart Gage, a soundscape ecologist and professor emeritus at Michigan State University in East Lansing and one of the field's earliest champions. In the early 2000s, he worked with Krause to develop what he calls "a taxonomy of sound." By analyzing the distribution of frequencies in their recordings, the pair broke the soundscape into three components: "biophony," or wild animal sounds (usually found at high frequencies); "geophony," or geophysical sounds like wind, rain, and rushing water (which stretch across a wide frequency range); and "anthrophony," or human-produced sounds (generally lower frequency).

Gage developed computer programs that quantified the amount of acoustic energy within certain frequency ranges; then he and Krause set out to compare natural and human-created sounds in a landscape. The effort was labor intensive. The pair gathered their soundscapes in California's Sequoia National Park using nearly 5 kilograms of recording equipment, which they had to babysit in the field. Its drawbacks became abundantly clear one evening, Gage recalls, when he found himself standing alone in a meadow waiting for a curious black bear to finish molesting the recorder he'd placed on a nearby rock. "He smelled it, he licked it, he slobbered all over it," Gage says. "Then he whacked it."

> "This is a science that's plagued by the big data challenges that you see in, say, genetics."
>
> —Bryan Pijanowski, Purdue University

Luckily, the bear didn't break it; his muffled snorts and loud smack were immortalized in the recording. But Gage and others were already dreaming of systems that would be less likely to draw a bear's attention: small recorders that could be hidden in the field for weeks or months at a time, collecting hours of high-fidelity sound with almost no human supervision. He began experimenting

CREDIT: BERNIE KRAUSE

with automated setups, connecting recording gear to laptop computers, but these were prohibitively bulky, power-hungry, and fragile.

Such problems caught the attention of Ian Agranat, an entrepreneur and technologist with an interest in birdsong. In 2003, Agranat had founded a company called Wildlife Acoustics, planning to make hand-held recorders for amateur bird enthusiasts. But he soon spotted a more promising market: scientists. Field recording equipment was "cobbled together by biologists who … knew a little bit about technology," he recalls. In 2007, he offered something better: the Song Meter, a $600 weatherproof recorder in a lunchbox-sized metal case. When Gage first saw one, he decided he could "stop being an engineer and go back to being an ecologist." Agranat has since sold more than 12,000 of the devices to researchers in some 60 countries.

The Song Meter now has plenty of company. Researchers can deploy a variety of powerful yet affordable sensors, some emphasizing portability, others designed for specific frequency ranges or extreme environments. Such technologies mark "the start of the story" for soundscape science, says Jérôme Sueur, an ecologist at the National Museum of Natural History in Paris.

Planting ears. Engineer Philippe Gaucher uses a crossbow to hang a microphone from the forest canopy in Guinea. A recorder (blue box, *right*) is mounted on a tree.

A magic number?

Sueur was among the first researchers to seize on the new recorders to scale up his studies, hoping to show that sound could be a proxy for biodiversity. Sueur and his colleagues weren't interested in exactly which species were calling. Instead, he says they wanted "to take a global measure of the acoustic output of the community." Their goal was an algorithm that could boil hours of acoustic data down to a single number describing how an ecosystem's acoustic energy is distributed across the frequency spectrum and over time.

Sueur's team named their measure the Acoustic Entropy Index. It is based on what's called a Shannon index, which turns an inventory of the animals sighted in an area into an estimate of species diversity. In Sueur's index, sounds at various frequencies take the place of animal species. A single, pure tone, for example, scores close to zero, representing low acoustic diversity. A noisy, chaotic, and more diverse soundscape should approach the highest possible score of 1.

In 2007, Sueur's team ran their first real-world test of the index in Tanzania, recording dawn and dusk sounds over several days in two coastal forests that are separated by 50 kilometers—and a lot of history. Loggers had exploited one for decades, but had been cutting trees in the other for just a few years. Sure enough, in a 2008 paper the team reported that the less disturbed forest had significantly higher acoustic entropy scores than the logged forest.

Since then, soundscape ecologists have developed a bouquet of indices based on different properties of the soundscape. At the University of Urbino in Italy, Almo Farina has developed an Acoustic Complexity Index based on sound qualities that can distinguish animal vocalizations from human-generated noise: Many animal sounds exhibit quick spikes in intensity (think of the abrupt crescendo of a bird's song) while many human-generated sounds, such as a droning engine, remain flat.

From Sueur's group came an Acoustic Dissimilarity Index, which compares two ecosystems based on differences in the timing and frequency of their sounds. In field tests, the index provided a ready way to estimate the number of species found in one community but not in the other.

The acoustic arsenal

Such acoustic measures can be powerful tools, but have their pitfalls, says Aaron Rice, director of the Bioacoustics Research Program at Cornell University. Many indices assume that biological sounds have shorter durations than humanmade ones. But in Rice's own marine acoustics research, the punctuated bursts of seismic air guns used for oil and gas exploration were a problematic exception. His conclusion: Indices are most useful when researchers have a good sense of the sources of sound they are likely to encounter. "Going into a place where you're recording somewhat blindly may not work," he warns.

Similar limitations plague Sueur's Acoustic Entropy Index, which turned out to be highly sensitive to humanmade background noise. In fact, Sueur no longer believes he can create a single

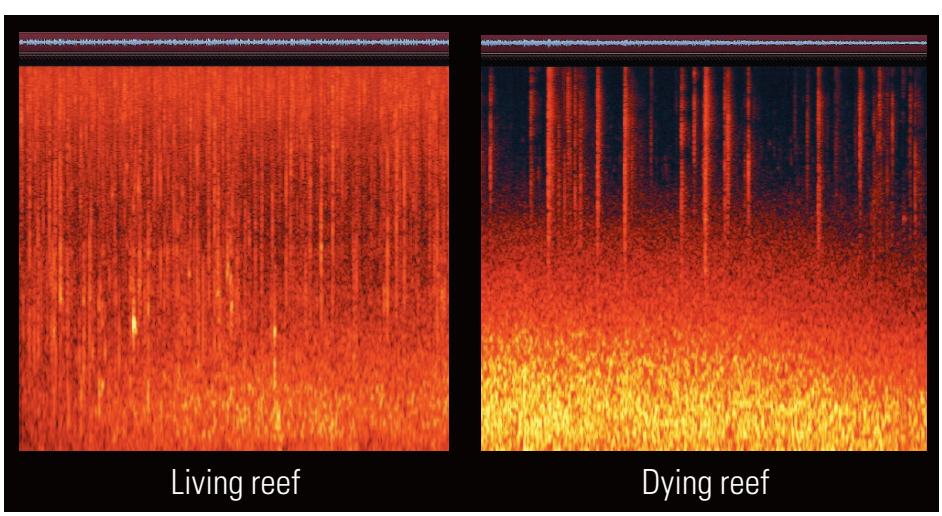

Visible decline. In visualizations of underwater recordings from Fiji, the spectrum from a healthy reef includes fish activity in the top half of the image. A nearby dying reef features mostly low-frequency ocean waves.

CREDITS (TOP TO BOTTOM): JÉRÔME SUEUR AND AMANDINE GAS; BERNIE KRAUSE (2)

Published by AAAS

acoustic measure that is a reliable proxy for biodiversity. The "index is not a miracle," he says. "It would be stupid to try to summarize everything with a single value."

Sueur does believe, however, that acoustic indices could become a useful element of a complete ecosystem portrait, especially when they are correlated with other indicators. For instance, Purdue's Pijanowski—once a graduate student under Gage—has discovered a relationship between acoustic diversity and vegetation structure. His team planted sound recorders at 14 sites in the Costa Rican rainforest and compared features of the soundscape with vegetation data from light detection and ranging (LiDAR) surveys. Hot spots for vocal species turned out to correlate with patches of forest with large gaps in the upper canopy and dense foliage in the lower canopy, the researchers reported in a 2012 paper.

Such results make Pijanowski optimistic that sound recordings could someday shape management decisions by highlighting especially rich habitats or helping explain which features of a landscape support particular animal communities. In the last year, he says, there's been an "explosion of people who are willing to think like this—more holistically." One recent convert, Anne Axel of Marshall University, Huntington, in West Virginia, is using sound recordings to predict whether abandoned coal mines on Appalachian mountaintops still have potential value as habitats. She hopes to find out how the acoustic signatures of these pseudograsslands compare with their state "prior to people chopping off the tops of the mountains."

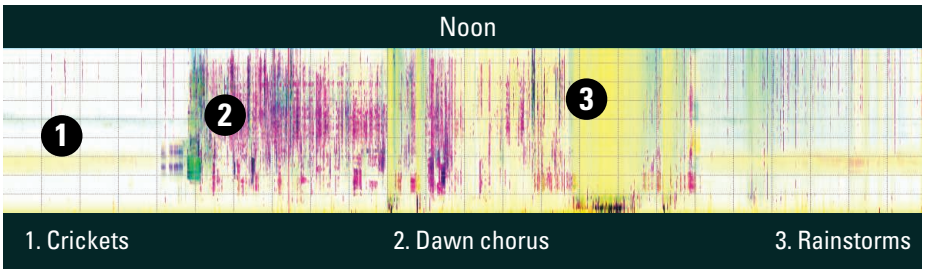

Day in the life. A false-color spectrogram made from a recording in the Australian bushland highlights the daily variation in the soundscape. Colors indicate values drawn from three acoustic indices, each sensitive to different types of sound. The chirps of crickets dominate between dusk and dawn. As the sun rises, a bird call chorus fills the air. Rainstorms strike in the afternoon; the black, low-frequency marks at the bottom of the image are produced by waterdrops hitting the recorder.

Perils of the long view

The boom in sound-recording studies poses a challenge familiar in other fields: a glut of data. Pijanowsky's lab alone has amassed about 85 terabytes of sound—more than 100,000 hours—in just 5 years. "This is a science that's plagued by the big data challenges that you see in, say, genetics," he says. Many researchers already have libraries of field recordings that, if played in real time, would be longer than their careers.

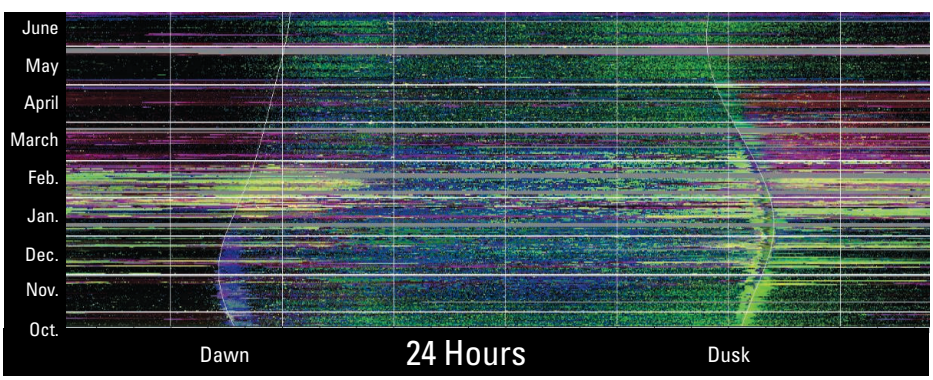

Zoom out. Computer scientist Michael Towsey combines 8 months of continuous recordings at a research station in Brisbane, Australia, into a single image. Colors indicate different acoustic indices. At dawn (*left curve*), a morning bird chorus (blue) is obvious during the Australian spring and early summer (October through December), but fades later in the year. Horizontal green streaks indicate heavy rainfall in January and February. At dusk (*right curve*), cicada activity is evident in the spring and summer months (green); by winter, the night is increasingly silent.

"We know that we're not going to be able to listen to it all," says computer scientist Michael Towsey of the Queensland University of Technology in Brisbane, Australia.

To get around that problem, he's developing ways to navigate soundscapes by sight, creating color-coded spectrograms that trained eyes can interpret at a glance (see graphic). Towsey describes the visualizations as "acoustic weather" charts. Some show how the spectrum of sounds shifts over a single day, while others assemble daily records into long-term snapshots to capture changes between seasons or years. That's akin to studying the "acoustic climate," he notes. And "when we start thinking about the acoustic climate, then we can start thinking about acoustic climate change." Year-to-year comparisons could eventually highlight subtle and potentially problematic changes, he predicts, such as changing rain patterns or shifts in bird activity.

Proving grounds

To enable such long-term efforts, some soundscape researchers are eager to piggyback on existing ecological surveys, which can be large and relatively well funded. In the United States, biological oceanographer Susan Parks of Syracuse University in New York hopes to get acoustic sensors installed at the 106 sites planned for the National Ecological Observatory Network—an ambitious monitoring effort by the National Science Foundation that will fully launch in 2017. So far, however, Parks has the go-ahead to put her own recorders at just four sites. "The onus is upon me to show people that it would be a valuable research tool," Parks says. To do so, she will spend 2 years gathering and analyzing recordings to measure human-generated sound and find seasonal patterns in birdsong.

Meanwhile, in Germany, Scherer-Lorenzen is strategizing about his first acoustic project. Thirty years after Bernie Krause first advanced his niche hypothesis, many soundscape experiments remain isolated case studies. Scherer-Lorenzen plans to take a broader view. By recording at locations where researchers funded by Germany's Biodiversity Exploratories have already collected data on flora and fauna, he aims to see how well soundscape indices describe biodiversity across multiple landscapes. He expects the German Science Foundation to reach a verdict on his proposal in March. By April, he hopes to be out sprinkling microphones across the German countryside.

–KELLY SERVICK

CREDITS: COURTESY OF MICHAEL TOWSEY (2)

Published by AAAS

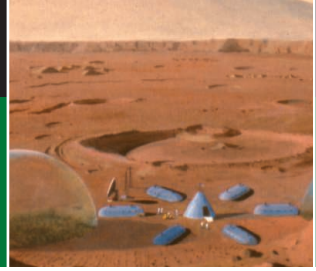

LETTERS

edited by Jennifer Sills

Taking a Bite Out of Biodiversity

IN THE REVIEW "STATUS AND ECOLOGICAL EFFECTS OF THE WORLD'S largest carnivores" (10 January, DOI: 10.1126/science.1241484), W. J. Ripple *et al*. claim that meat consumption by humans is one of many threats to carnivores and biodiversity. We argue that human carnivory is in fact the single greatest threat to overall biodiversity. Livestock production accounts for up to 75% of all agricultural lands and 30% of Earth's land surface, making it the single largest anthropogenic land use (*1*). Meat and feedstock production is rapidly rising in biodiversity-rich developing countries. For example, in China, animal products currently constitute ~20% of diets, but this amount is expected to increase to ~30% or higher over the next two decades (*2*). For China to attain a level of carnivory similar to the United States, its projected 1.5 billion inhabitants would increase consumption of animal products by almost 30% (*3*). Given current trends, 1 billion additional hectares of natural habitats—an area larger than the United States—will be converted to agriculture by 2050 (*4*).

Substituting meat with soy protein could reduce total human biomass appropriation in 2050 by 94% below 2000 baseline levels (*5*) and greatly reduce other environmental impacts related to use of water, fertilizer, fossil fuel, and biocides. Soy protein production for global livestock markets is the second leading cause of Amazonian deforestation after pasture creation. Eliminating livestock and instead growing crops, including soy protein, only for direct human consumption could negate future agricultural land expansion, while increasing the number of calories available for human consumption by as much as 70% (*6*)—enough to feed an additional 4 billion people, exceeding the projected global population growth of 2 to 3 billion (*6*). This savings in land and calories is due to eliminating the loss of ~90% of the energy available in plants during the conversion to livestock (*7*). We argue that reducing and maintaining animal products to even 10% of the global human diet would enable the future global population to be fed on just the current area of agricultural lands. Without a global decrease in per capita meat consumption by humans, the loss of natural habitats, large carnivores, and biodiversity is certain to continue.

BRIAN MACHOVINA* AND KENNETH J. FEELEY

Florida International University, Miami, FL 33199, USA.

*Corresponding author. E-mail: brianmachovina@gmail.com

References

1. Food and Agriculture Organization, "Livestock's long shadow: Environmental issues and options" (FAO, Rome, 2006); www.fao.org/docrep/010/a0701e/a0701e00.HTM.
2. M. A. Keyzer, M. D. Merbis, I. F. P. W. Pavel, C. F. A. van Wesenbeeck, *Ecol. Econ*. **55**, 187 (2005).
3. S. Bonhommeau *et al*., *Proc. Natl. Acad. Sci. U.S.A*. **110**, 20617 (2013).
4. D. Tilman *et al*., *Science* **292**, 281 (2001).
5. N. Pelletier, P. Tyedmers, *Proc. Natl. Acad. Sci. U.S.A*. **107**, 18371 (2010).
6. E. Cassidy, P. C. West, J. S. Gerber, J. A. Foley, *Environ. Res. Lett*. **8**, 8 (2013).
7. H. Charles *et al*., *Science* **327**, 812 (2010).

Curtailing Chimpanzee Exploitation

AS D. GRIMM POINTS OUT IN HIS NEWS & Analysis story "Lawsuits seek 'personhood' for chimpanzees" (6 December 2013, p. 1154), our hairy cousins are getting their day in court. Legally, in the United States, the word "person" includes corporations, companies, and even boats, but not chimpanzees, which without this legal construct are simply property without legal standing (*1*, *2*). Personhood is not the only legal issue emerging in the public domain for chimpanzees in the United States this year. Recent efforts by the director of the U.S. Fish and Wildlife Service, Daniel Ashe, may help curtail the exploitation of chimpanzees for entertainment. In May, Ashe proposed that "all chimpanzees, whether in the wild or in captivity, [be listed] as endangered under the Endangered Species Act of 1973, as amended (Act)" [(*3*), p. 35202]. The change in classification remains under review (*4*).

Across their natural range (spanning 21 African countries), chimpanzees have been classified on the International Union for Conservation of Nature (IUCN) Red List as "endangered" since 1996, and they are thus protected by international law (*5*, *6*). Accordingly, they cannot be kept as pets or used for entertainment purposes. Enforcement of these laws is difficult, as shown by the 1150 confiscated chimpanzees currently being cared for in sanctuaries in 12 African countries [(*7*), p. 43]. Meanwhile, in the United States, chimpanzees are kept as pets as well as used in commercials, mov-

CREDIT: JEFF VANUGA/USDA

Published by AAAS

Artificial muscles

845

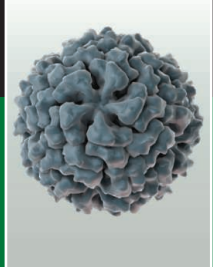

Flavivirus, structure and function

849

ies, and TV sitcoms, for which they are seen dressed in clothes, driving cars, or serving as caricatures of humans behaving badly (*8*). Chimpanzee "actors" have appeared in at least 59 television advertisements since 1986 in the United States alone (*9*). Social media and online access to images or videos of these chimpanzees can be viewed anywhere in the world, which has led to misperceptions that adult chimpanzees are small and cute, just like those seen in the movies. Since 1990, chimpanzees residing in the United States have only been listed as "threatened" (*3*), creating a confusing loophole in legislation, potentially hindering conservation of wild chimpanzees, and inadequately protecting the more than 2000 captive chimpanzees in the United States (*10*). Great Apes Survival Partnership of the United Nations has requested international support to "end the use of trained great apes in films, television shows, or advertising," as it fuels the illicit trade in chimpanzees [(*7*), p. 10].

Classifying chimpanzees in the United States as endangered is the right decision. It is up to scientists to embrace these changes in policy and lead the way in exploring how our research with chimpanzees contributes to their conservation in the wild and improves their welfare in captivity.

CARLA A. LITCHFIELD

School of Psychology, Social Work and Social Policy, University of South Australia, Adelaide, South Australia 5072, Australia. E-mail: carla.litchfield@unisa.edu.au

References

1. K. L. Schrengohst, *Western New Engl. Law Rev.* **33**, 855 (2011).
2. L. L. Fisher, *Hastings Commun. Entertainment Law J.* **2**, 405 (2005).
3. D. M. Ashe, *Federal Register* **78**, 35201 (2013).
4. Regulations.gov, Endangered Status for All Chimpanzees (www.regulations.gov/#!docketDetail;D=FWS-R9-ES-2010-0086-9647).
5. CITES Appendix 1 (www.cites.org/eng/app/appendices.php).
6. J. F. Oates *et al.*, in IUCN 2013. IUCN Red List of Threatened Species. Version 2013.2 (2008); www.iucnredlist.org.
7. D. Stiles, I. Redmond, D. Cress, C. Nellemann, R. K. Formo, Eds., *Stolen Apes—The Illicit Trade in Chimpanzees, Gorillas, Bonobos, and Orangutans: A Rapid Response Assessment* (United Nations Environment Programme, GRID-Arendal, Norway, 2013).
8. S. R. Ross *et al.*, *Science* **319**, 1487 (2008).
9. S. R. Ross, V. M. Vreeman, E. V. Lonsdorf, *PLOS ONE* **6**, e22050 (2011).
10. J. Cohen, "Captive chimpanzees in U.S. may get status bump to endangered, possibly affecting research," *ScienceInsider* (11 June 2013).

Letters to the Editor

Letters (~300 words) discuss material published in *Science* in the past 3 months or matters of general interest. Letters are not acknowledged upon receipt. Whether published in full or in part, Letters are subject to editing for clarity and space. Letters submitted, published, or posted elsewhere, in print or online, will be disqualified. To submit a Letter, go to www.submit2science.org.

A Defense of Eastern European Science

IN THE NEWS & ANALYSIS STORY "FRENCH mathematician tapped to head key funding agency" (M. Enserink, 1 November 2013, p. 545), European science policy followers say that one of the major challenges of the new European Research Council (ERC) president is "to resist pressure from countries in southern and eastern Europe that want a bigger slice of ERC's pie." Enserink explains that "[r]esearchers from those countries have often fared poorly with the ERC, which awards funding solely based on excellence."

In our opinion, this statement not only portrays the eastern and southern European countries as those that want to drain the money from the hard-working North and West but also sums up all of the stereotypes that some western scientists have about all nonwestern science.

Our researchers are awarded (sometimes leading) positions in good, and even excellent, research and academic institutions in many western European countries and further overseas, in the United States, Canada, and Australia.

Our manuscripts are published in high-ranking international journals. Despite this, even professional language editing does not spare us impertinent remarks about our English. Sometimes manuscripts are rejected without any objective critique. Prejudiced statements like those cited in your article do not contribute in the least to improving our situation.

Years ago a Belgian colleague said that he is always very proud of his eastern peers as he knows how difficult it is for us to succeed in science: "You have to prove yourself twice as much, you have to speak more languages, you have to be prepared to go through more rejections and more evaluations than almost any of your western colleagues."

Unfortunately, several years on, he could still say exactly the same.

ANA ROTTER* AND CENE GOSTINČAR

National Institute of Biology, Ljubljana, 1000, Slovenia.
*Corresponding author. E-mail: ana.rotter@nib.si

CORRECTIONS AND CLARIFICATIONS

Research Articles: "The petrochemistry of Jake_M: A martian mugearite" by E. M. Stolper *et al.* (27 September 2013; full text online only at http://dx.doi.org/10.1126/science.1239463). In Table 1, the value reported for Na_2O in JM2n was incorrect. The correct value is 6.59(14). Additionally, the Table 1 legend should have indicated that for Cr_2O_3, only the two long-duration analyses, JM1 and JM2n, were averaged. The HTML and PDF versions online have been corrected.

Reports: "N_2 reduction and hydrogenation to ammonia by a molecular iron-potassium complex" by M. M. Rodriguez *et al.* (11 November 2011, p. 780). This Report described, inter alia, the reaction of a $Fe_4(N)_2$ complex with H_2 to give a $Fe_2(H)_2$ complex and ammonia. Subsequent study has shown that ammonia is not actually produced in the reaction with H_2. In the reported experiments, we used nuclear magnetic resonance spectroscopy to monitor the reaction in benzene, which showed that the disappearance of the $Fe_4(N)_2$ species and appearance of the $Fe_2(H)_2$ were complete in 6 hours. Our test for ammonia formation was to repeat the reaction on a larger scale for the same amount of time and then add acid to generate NH_4^+. Unfortunately, the larger-scale reaction was done in toluene rather than benzene. We have now learned that the reaction with H_2 is significantly slower in toluene than in benzene. As a result, the reaction with H_2 in toluene was stopped before it was complete, and the ammonia observed was from the reaction of the $Fe_4(N)_2$ complex with acid in the ammonia detection protocol. When the H_2 reaction proceeds to completion in benzene, toluene, or other solvents, treatment with acid gives no ammonia. Thus, the claim of N_2 hydrogenation to ammonia in this Report is incorrect. We are currently quantifying the products of the H_2 reaction and will describe full details of these experiments in due course. The other claims in the Report (reduction of N_2 to give the bis-nitride complex, characterization of the bis-nitride complex, and the reaction of the bis-nitride complex with acids to give ammonia) have been reproduced many times.

Reports: "A topoisomerase IIβ–mediated dsDNA break required for regulated transcription," by B.-G. Ju *et al.* (23 June 2006, p. 1798). There were several errors in preparation of Fig. S5. The correct images for input and αTopoIIβ for *RAR*β promoter in panel A and *MMP12*, *GAPDH*, and *HPRT1* in the TPA+Mer set of *MMP12* mRNA; *HPRT1* in the DHT+3AB set of *PSA* mRNA; and *HPRT1* in the RA set and *HPRT1* in the RA+3AB set of *RAR*β mRNA in panel B have been substituted for incorrect data. A corrected version of the supplementary materials (SM) has been posted to reflect the corrections to Fig. S5. The SM remains unchanged in all other respects.

Published by AAAS

EARTH SCIENCES

Breathing Life into Oxygen

Woodward W. Fischer

If one could boil all of Earth's behavior down to a single number—a statistic that captured the rich intersection of geological, chemical, and biological processes operating on our planet's surface—a strong argument could be made for the atmosphere's O_2 content. That is presently 21% by volume, but a wide range of data extracted from the geologic record demonstrates that O_2 levels have varied considerably. To first order, Earth's history is written in O_2, and tangled in the story are plate tectonics, the rock cycle, the evolution of photosynthesis, and the appearance of animals. In *Oxygen*, Don Canfield lucidly unpacks this story through a careful mix of overview and detail, with a focus on the relevant biogeochemical mechanics.

Oxygen
A Four Billion Year History
by Donald E. Canfield
Princeton University Press, Princeton, NJ, 2014. 222 pp. $27.95, £19.95.
ISBN 9780691145020.

Although it's widely appreciated that molecular oxygen derives from photosynthesis, understanding the dynamics and history of O_2 encompasses a rich and complex multiscale problem. Canfield (a biogeochemist at the University of Southern Denmark) walks readers through a logical foundation of the processes connecting solid Earth with the chemistry and biology of oceans and atmosphere. Not a recondite history of O_2, the book explores how we reconstruct redox processes that operated in ancient environments and how to think about the behavior of biogeochemical cycles across geological time.

Much of the book proceeds chronologically, with the cadence set by critical redox and evolutionary phenomena such as anaerobic metabolisms before oxygen and the evolution of photosynthesis. Canfield takes full advantage of the process-history duality that underpins all good Earth science, presenting different geobiological processes that affect O_2 in the context of critical historical events.

The chapter on cyanobacteria, one of the highlights of the book, is presented with a spectacular blend of scientific discovery and evolutionary wonderment. By inventing oxygen-producing photosynthesis, this group changed the world in a fashion unmatched by any other evolutionary innovation (save perhaps the human brain). Canfield also does a wonderful job emphasizing the potential feedbacks between O_2 in the atmosphere and oceans and the rock cycle (which both buries and exposes organic matter and pyrite). Although these connections among tectonics, sedimentary geology, and biogeochemical cycles appear critically important, they remain understudied.

Given the book's scientific breadth, I found remarkably few points that I would dispute. In his discussion of the evolution of oxygenic photosynthesis, Canfield places too much emphasis on the pigments and not enough on the photochemistry. And he attributes the rise of oxygen circa 2.35 billion years ago to a change in the composition of volcanoes, an idea championed by Dick Holland. But there is little geological support for such a change, and at times during the past 100 million years volcanic outgassing changed manyfold while oxygen levels seem to have shifted little.

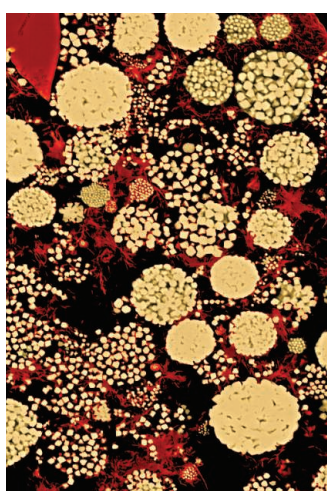

Locked away. Pyrite burial (here pyrite framboids in a thin section of a shale) "represents an oxygen source to the atmosphere."

Canfield's research has played a major role in shaping current knowledge of geobiological interactions among the iron, sulfur, carbon, and oxygen cycles. He is particularly adept at leveraging understanding of modern processes to study the past. In the book, he effectively uses autobiographical anecdotes to drive the narrative and connect related concepts. He also reveals how much impact geochemists from the previous generation (such as Bob Garrels, Bob Berner, and Dick Holland) have had on his thinking. Like his talks, Canfield's prose presents stories and concepts with a youthful enthusiasm that masks substantial wisdom.

Breakthroughs in analytical chemistry are improving our ability to read paleoenvironmental history from sedimentary rocks, and breakthroughs in molecular biology and genomics are providing stronger frameworks for interpreting the evolution of biota and metabolisms. Consequently, our understanding of Earth's O_2 history is remarkably dynamic. Canfield does a great job of acknowledging what we don't know and identifying areas that are in radical flux. He recognizes that the subject will likely require a very different book in 30 years. I suspect that might be closer to 10.

Compared with two other recent works on O_2 and early Earth history (*1*, *2*), Canfield's book is more focused on understanding the key biogeochemical processes. Not satisfied to simply present the history, he strives to make readers familiar with the relevant mechanics. He demands that we wrestle simultaneously with geochemical observations used to assess ancient O_2 levels, the processes that provide the sources and sinks for oxygen (including how these processes have changed with time), and the poorly understood phenomena that introduce uncertainty into our knowledge.

Concise and easily read, *Oxygen* provides an ideal starting block for those interested in learning about Earth's O_2 history and, more broadly, the function and history of biogeochemical cycles. It requires no substantial prior knowledge of Earth science, although readers with some exposure to that field (or prepared with Wikipedia at the ready) will gain a much deeper understanding of O_2 on Earth. The endnotes provide valuable entries for readers who wish to explore particular points in greater depth and, in other cases, enable brief digressions for interesting personal notes without disrupting the logical thread of a given concept. And the detailed bibliography captures a vast swath of the relevant primary literature. I highly recommend Canfield's book for anyone with even a remote interest in Earth history, as O_2 singularly encompasses much of what makes our planet special.

References

1. N. Lane, *Oxygen: The Molecule That Made the World* (Oxford Univ. Press, Oxford, 2002).
2. A. H. Knoll, *Life on a Young Planet: The First Three Billion Years of Evolution on Earth* (Princeton Univ. Press, Princeton, NJ, 2003); reviewed in (*3*).
3. G. M. Narbonne, *Science* **301**, 919 (2003).

The reviewer is at the Division of Geological and Planetary Sciences, California Institute of Technology, Pasadena, CA 91125, USA. E-mail: wfischer@caltech.edu

10.1126/science.1248669

HISTORY OF SCIENCE

The Significance of "Frontier"

Catherine L. Newell

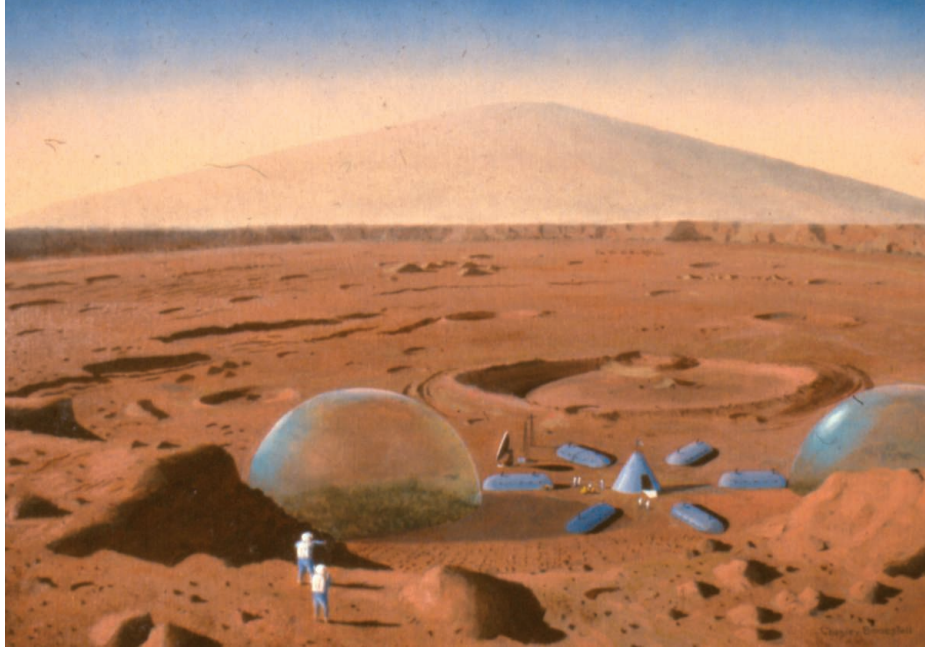

Space as new frontier. Chesley Bonestell's *Domed Colony on Mars* (1976).

On 17 November 1944, Franklin Delano Roosevelt requested that Vannevar Bush, director of the U.S. Office of Scientific Research and Development, put together a report with recommendations for postwar American science policy. Roosevelt closed the letter to Bush with the reminder "New frontiers of the mind are before us, and if they are pioneered with the same vision, boldness, and drive with which we have waged this war we can create … a fuller and more fruitful life." Bush responded to the president's exhortation with his 1945 report, *Science—The Endless Frontier*, which established not only the shape and scope of postwar scientific research in the United States but also a metaphor that endures in current American scientific rhetoric: the frontier.

This entrenched metaphor is the subject of Leah Ceccarelli's fascinating *On the Frontier of Science*. Ceccarelli (Department of Communication, University of Washington) explores how the metaphor of the frontier (with its close cousin, the pioneer) has become rooted in American scientific rhetoric. The metaphor evokes a certain kind of science and a certain kind of scientist—a rugged individualist who throws off the constraints of ordinary expectations and strikes out on his (and it's nearly always his) own to conquer the unexplored and unexplained. This fixed "belief that competition between rugged individualists is a constitutive feature of science," Ceccarelli dryly points out, "may come more from convention than necessity."

On the Frontier of Science
An American Rhetoric of Exploration and Exploitation

by Leah Ceccarelli
Michigan State University Press, East Lansing, MI, 2013. 218 pp. Paper, $44.95. ISBN 9781611861006.

Ceccarelli argues that the frontier metaphor in science changes "what is selected and what is deflected" in scientific practice—the type of science funded by the government or industry and the sort disdained as too safe. She also holds that scientists ensnared by the metaphor think of their practice as part of the larger sacred cause of the conquest of the unknown. These scientists buy into the belief that they are pioneers operating on a vast frontier and believe their work has more cultural value than unromanticized collaborative research or the deliberate plodding of the scientific method.

The book begins with the fascinating etymological and philosophical development of the concepts of pioneer and frontier. Interestingly, both terms were used to describe the importance of science not long after Frederick Jackson Turner's 1893 essay "The Significance of the Frontier in American History" (*1*). Science was quickly taken up as a replacement for the closed material frontier and a suitable field of conquest.

Ceccarelli then examines the use of the frontier metaphor by American scientists in speeches, a rhetorically important area of study that ironically, she points out, scholars of rhetoric now give little attention. She finds that scientists intentionally use the metaphor to put forward an agenda of "science on the edge": science that is innovative rather than instructive and features the archetype of "scientist as pioneer" on the verge of new discoveries.

The book's central chapters deal with the practical implications of the metaphor for scientists and society. Ceccarelli explores the public rhetoric of evolutionary biologist E. O. Wilson and genomics researcher Francis Collins. She believes both have internalized the metaphor of the frontier—in Wilson's case, to the extent that it has negatively shaped the legacy of his scientific work, casting him as a colonizer rather than an explorer.

Turning to how politicians have used the metaphor, Ceccarelli offers a close reading of George W. Bush's 9 August 2001 speech on stem cell research. The speech is a craftily employed double entendre of moral rhetoric that asked Americans to "restrain their frontier-crossing impulses without ever abandoning the frontier myth that endorses such behavior." This rhetorical high-wire act illustrates how the frontier metaphor is so entangled in "American history, politics, and science" that moving away from it will be a "challenging proposition."

The future of science, however, might depend on a lasting withdrawal from the frontier metaphor. One of the book's most powerful lessons is the possibility that the frontier metaphor creates a culture of science that "sees science as a contest for territory" rather than a global and collaborative effort. Additionally, one finds a growing rift between "pioneering scientists" and those who are not fortunate or brave enough to be scientists (who are implied to be "a weaker class of people"). These are, Ceccarelli believes, avoidable consequences of thinking of science as a vast frontier waiting to be conquered. While Ceccarelli limits the scope of her inquiry to the biological sciences, *On the Frontiers of Science* prompts questions of broader relevance. What would happen, for example, if the exploration of the real frontier of Mars was not cast in the same rhetoric as the American frontier and instead portrayed as the triumph of global scientific cooperation? Perhaps a fresh metaphor could unleash a new era in science, one where the victor is not a conqueror but a collaborator instead.

The reviewer is at the Department of Religious Studies, University of Miami, Post Office Box 248264, Coral Gables, FL 33124–4651, USA. E-mail: clnewell@miami.edu

References
1. F. J. Turner, *Annu. Rep. Am. Hist. Assoc.* **1893**, 199 (1894).

10.1126/science.1249876

Published by AAAS

CONSERVATION

Averting Lemur Extinctions amid Madagascar's Political Crisis

Community-based management, ecotourism, and researchers' presence are proposed to prevent lemur extinctions.

C. Schwitzer,[1]* R. A. Mittermeier,[2] S. E. Johnson,[3] G. Donati,[4] M. Irwin,[5] H. Peacock,[6] J. Ratsimbazafy,[7,8] J. Razafindramanana,[8] E. E. Louis Jr.,[9] L. Chikhi,[10,11] I. C. Colquhoun,[12] J. Tinsman,[13] R. Dolch,[14] M. LaFleur,[15] S. Nash,[2,16] E. Patel,[17] B. Randrianambinina,[18] T. Rasolofoharivelo,[8] P. C. Wright[16]

The most threatened mammal group on Earth, Madagascar's five endemic lemur families (lemurs are found nowhere else) (*1*), represent more than 20% of the world's primate species and 30% of family-level diversity. This combination of diversity and uniqueness is unmatched by any other country—remarkable considering that Madagascar is only 1.3 to 2.9% the size of the Neotropics, Africa, or Asia, the other three landmasses where nonhuman primates occur. But lemurs face extinction risks driven by human disturbance of forest habitats. We discuss these challenges and reasons for hope in light of site-specific, local actions proposed in an emergency conservation action plan (*2*).

Political Crisis, Remarkable Threat

An International Union for Conservation of Nature (IUCN) Species Survival Commission (SSC) Red List reassessment found that 94% of lemur species are threatened (*2*) (fig. S1 and table S1), up from 74% in 2008, which makes lemurs the most imperiled group of large vertebrates. Although other large mammals are also under pressure, for the vast majority of taxa in an entire infraorder (Lemuriformes) to be threatened is new, notable, and disturbing. This reevaluation has resulted from both the deterioration of habitat and the recent application of genetic data to phylogenetic analyses (increasing the number of extant lemur species from 43 to 101) (*3*), revealing more species with smaller ranges.

Male blue-eyed black lemur. *Eulemur flavifrons* in Sahamalaza–Iles Radama National Park.

This unique primate diversity relies on forest habitats that are shrinking under persistent anthropogenic destruction and disturbance. Remaining intact forest habitat was estimated to cover 92,200 km^2 in 2010, only 10 to 20% of Madagascar's original forest cover and down from 106,600 km^2 in 1990 (*4*); much of this habitat is inadequately or not at all protected. Habitat and lemur conservation are interdependent: Lemurs have important ecological roles and are essential to maintaining the island's unique forests. Their loss would likely trigger extinction cascades (*5*).

Challenges to in situ lemur conservation are immense. Madagascar is one of the poorest countries in the world; more than 92% of Malagasy live on less than U.S. $2/day (*6*). Although there is a paucity of published data compared to other lemur-related subjects, lemur poaching for bushmeat has drastically increased since the onset of the political crisis in 2009 (*7*, *8*). Illegal logging of rosewood and ebony, mining, and slash-and-burn agriculture are all causing lemur population declines, by habitat loss, fragmentation, and alteration. Protected areas have not been spared; for example, armed timber poachers extracting valuable hardwoods targeted Masoala and Marojejy National Parks in the northeast once local law enforcement broke down (*9*). Foreign demand, as well as political turmoil and corruption, drive these destructive, and often unlawful, activities (*8*).

Effective management of Madagascar's protected areas, as well as creation of more reserves, will be critical to future conservation of lemurs. In 2003, only ~3% (~17,000 km^2) of Madagascar's land area was designated as protected. During the administration of former President Ravalomanana, conservation became a national priority. In 2003, Ravalomanana announced that the government would triple its protected areas. Some 30,000 km^2 of community-based reserves were gazetted. As of January 2010, 47,000 km^2 are officially protected, ~8% of Madagascar's land area.

The creation of new protected areas has continued despite political instability brought on by the unconstitutional change of government in early 2009. However, this process has been slowed by a breakdown of government presence and control in many regions, exacerbated by suspension of funding for environmental programs by most international donors in the wake of the political crisis (*10*). The U.S. Agency for International Development shelved a comprehensive 25-year environmental program until the country returns to democratic government (although humanitarian assistance continues), and several European governments have responded similarly. Only the World Bank has maintained its commitment, but even its substantial support has not been utilized effectively by the transitional government for the management of protected areas (*11*). Presidential elections, held in two rounds on 25 October and 20 December 2013, resulted in a narrow victory for former Finance Minister Hery Rajaonarimampianina. There are encouraging signs that the new president will set the conditions for a return to effective governance and resumption of international aid.

Outside the official protected areas, the situation is worse, with illegal slash-and-burn agriculture, logging, mining, and bushmeat hunting on the rise. Commercial lemur hunting, a practice previously unreported from the country, has been noted in regions such as Foulpointe, Vatomandry, Daraina, and the forests south of Antsiranana (Diego Suarez).

[1]Bristol Zoological Society, Bristol BS8 3HA, UK. [2]Conservation International, Arlington, VA 22202, USA. [3]University of Calgary, Calgary, Alberta T2N 1N4, Canada. [4]Oxford Brookes University, Oxford OX3 0BP, UK. [5]Northern Illinois University, DeKalb, IL 60115, USA. [6]Golder Associates, Calgary, Alberta T2A 7W5, Canada. [7]Durrell Wildlife Conservation Trust, Antananarivo 101, Madagascar. [8]Groupe d'Etude et de Recherche sur les Primates de Madagascar, Antananarivo 101, Madagascar. [9]Omaha's Henry Doorly Zoo, Omaha, NE 68107, USA. [10]Instituto Gulbenkian de Ciência, 2781-901 Oeiras, Portugal. [11]Laboratoire Evolution et Diversité Biologique, CNRS, UMR 5174 Université Paul Sabatier, 31062 Toulouse cedex 9, France. [12]Western University, London, Ontario N6A 5C2, Canada. [13]American Museum of Natural History, New York, NY 10024, USA. [14]Association Mitsinjo, Andasibe 514, Madagascar. [15]University of Veterinary Medicine Vienna, 1210 Vienna, Austria. [16]Stony Brook University, Stony Brook, NY 11794, USA. [17]Duke Lemur Center, Durham, NC 27705, USA. [18]Université de Mahajanga, Mahajanga 401, Madagascar. *Corresponding author. cschwitzer@bcsf.org.uk

Published by AAAS

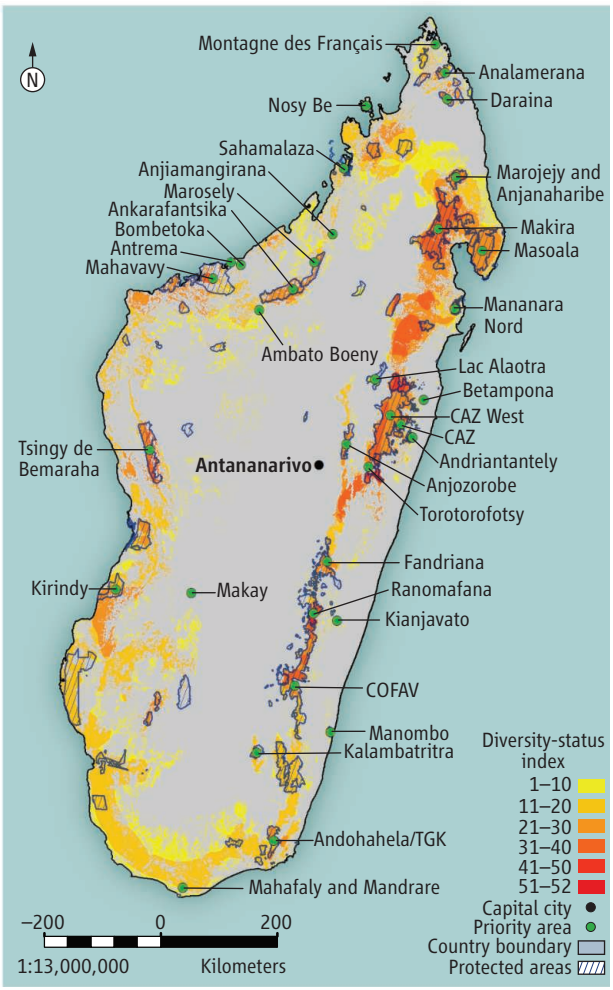

Lemur species richness-extinction risk index and priority conservation areas. Each species range was given a weighting according to its estimated extinction risk (the likelihood of a species becoming extinct in the near future, given current knowledge about population trends, range, and recent, current or projected threats, expressed by its 2012 IUCN Red List status (1, Least Concern; 2, Near Threatened; 3, Vulnerable or Data Deficient; 4, Endangered; 5, Critically Endangered). All lemur species' range weightings were summed to provide the richness-risk index, a composite measure of richness and estimated extinction risk. For example, where two Near Threatened species co-occur, there is a value of 4, and where two Critically Endangered species co-occur, the value is 10. The color spectrum represents the continuum from areas with low species richness and lower extinction risk to areas with high species richness and high extinction risk. Hatched areas indicate terrestrial protected areas. Green dots show locations of priority areas for lemur conservation digitized from the 2013 to 2016 conservation action plan (*2*).CAZ, Corridor Ankeniheny-Zahamena; COFAV, Corridor Fandriana-Vondrozo; TGK, Tsitongambarika. See supplementary materials for details.

In several parts of the northeastern rain forests, large-bodied indris (*Indri indri*) and diademed sifakas (*Propithecus diadema*) are in danger of being extirpated (*7*).

Tourism, Research, Local Management

Despite these profound problems, we believe there is still hope. Overall, lemur conservation must tie in with national conservation efforts in Madagascar, such as expanding the protected area network and enforcing environmental laws. However, there are specific site-based actions that can be carried out by conservationists, researchers, and local communities, which are less expensive than national initiatives (*2*). The emergency 3-year action plan takes such an approach, combining a broad framework with concrete steps modeled on past successes. It proposes conservation actions for 30 priority sites harboring endangered lemurs (see the chart), for a total budget of U.S. $7.6 million. This is a reasonable amount in terms of international aid, for an incalculable return. Major goals include stabilizing the immediate crisis in priority areas and laying the groundwork for longer-term actions in all habitats crucial for preventing lemur extinctions.

Promoting and expanding ecotourism is one important component of the action plan. Lemurs represent Madagascar's most distinctive "brand" for tourism. Ecotourism continues in spite of political problems and remains one of the country's most important foreign-exchange earners, providing livelihoods for the rural poor in environmentally sensitive regions and often fostering local valuation of primates and ecosystems. Examples of implementation already exist and could be replicated, provided resources are available and there is sufficient community engagement to ensure appropriate investment. An important element of this is the development of local tourist guide associations.

Another key mechanism is the creation of protected areas managed at the community level. Despite the fact that such reserves may take a long time to establish, empowering local communities to create reserves and training them in management through small grants is where we are likely to see the greatest growth in habitat protection over the next decade.

Another goal is to sustain and expand long-term research presence in critical lemur sites. Field stations that support a permanent presence of local and international field workers—such as those at Ranomafana, Marojejy, Kirindy, Tsinjoarivo and Sahamalaza—can serve as training grounds for Malagasy scientists while deterring illegal hunting and logging (*12*). Scientists are working with local communities, providing economic benefits and knowledge exchange for conservation at local levels.

Past successes highlighted in the plan, such as Anja Community Reserve and Kianjavato Classified Forest, demonstrate that collaboration between local communities, nongovernmental organizations and researchers can protect imperiled species. We urgently invite all stakeholders to join our efforts to meet the action plan's goals and to ensure the continued existence of lemurs and the considerable biological, cultural and economic richness they represent. Madagascar—and the world—will undoubtedly be much poorer without them.

References and Notes

1. Two species have been introduced to the neighboring Comoro Islands in the past few hundred years.
2. C. Schwitzer *et al.*, *Lemurs of Madagascar: A Strategy for Their Conservation 2013–2016* (IUCN SSC Primate Specialist Group, Bristol Conservation and Science Foundation, and Conservation International, Bristol, 2013); https://portals.iucn.org/library/node/10414.
3. R. A. Mittermeier *et al.*, *Lemurs of Madagascar* (Conservation International, Arlington, VA, ed. 3, 2010).
4. Office National pour l'Environnement (ONE) *et al., Evolution de la Couverture de forêts naturelles à Madagascar 2005-2010* (ONE, Antananarivo, 2013); www.pnae.mg/index.php/Autres/evolution-de-la-couverture-de-forets-naturelles-a-madagascar-2005-2010.html.
5. J. U. Ganzhorn *et al.*, *Conserv. Biol.* **13**, 794 (1999).
6. World Bank, "Madagascar: Measuring the impact of the political crisis" (World Bank, Washington, DC, 2013); www.worldbank.org/en/news/feature/2013/06/05/madagascar-measuring-the-impact-of-the-political-crisis.
7. R. K. B. Jenkins *et al.*, *PLoS ONE* **6**, e27570 (2011).
8. M. A. Barrett *et al.*, *Science* **328**, 1109 (2010).
9. Global Witness, Environmental Investigation Agency, *Investigation into the Illegal Felling, Transport and Export of Precious Wood in SAVA Region, Madagascar* (Global Witness, London, 2009); www.parcs-madagascar.com/doc/report_vsfinal.pdf.
10. World Bank, *The World Bank Adopts an Interim Strategy for Madagascar* [press release] (World Bank, Washington, DC, 2012); http://go.worldbank.org/5XTWG1TGG0.
11. J.-C. Carret, *Madagascar Country Environmental Analysis (CEA): Taking Stock and Moving Forward* (World Bank, Washington, DC, 2013).
12. W. F. Laurance, *Trends Ecol. Evol.* **28**, 261 (2013).

Acknowledgments: We thank organizers and participants of the International Prosimian Congress, held in Ranomafana, Madagascar, 5 to 9 August, 2013, as well as the three anonymous reviewers of this manuscript. This paper is dedicated to Alison Jolly (1937–2014) in recognition of her dedication to the conservation of Madagascar's lemurs.

Supplementary Material

www.sciencemag.org/content/343/6173/842/suppl/DC1

10.1126/science.1245783

ATMOSPHERIC SCIENCE

From Past to Future Warming

Analyses of past observations help to predict the human contribution to future climate change.

Gabi Hegerl[1] and Peter Stott[2]

In its Fifth Assessment Report, the Intergovernmental Panel on Climate Change concluded that it is "extremely likely that more than half of the observed increase in global average surface temperature from 1951 to 2010 was caused by the anthropogenic increase in greenhouse gas concentrations and other anthropogenic forcings together" (*1*). This conclusion was based on an expert assessment drawing on multiple analyses of observed temperature changes. However, substantial uncertainties remain, especially in estimating the human contribution to regional temperature change and extreme events.

The physics through which greenhouse gases warm the atmosphere is well understood. However, feedbacks within the atmosphere can enhance or reduce this warming, and the magnitudes of those feedbacks, particularly those associated with clouds, are much more uncertain.

One way to address these uncertainties is to use observations of past climate change and estimate from them the magnitude of "fingerprints" for human and natural influences. The fingerprints themselves are based on climate models and reflect physically robust features (*2*). For example, greenhouse gases cause steadily increasing warming that is stronger over land than ocean; cooling from aerosols is less widespread and has flattened recently in some regions while greenhouse gas levels continued to rise; volcanic eruptions cause short-term cooling; and the sun causes variations that include an 11-year cycle. Variability generated within the climate system also has distinct spatial patterns.

Because observations are used to estimate the magnitude of the fingerprint patterns, the resulting estimates of past temperature changes caused by greenhouse gas increases and other factors (see the first figure) do not depend strongly on models representing uncertain feedbacks correctly, provided that the fingerprint patterns derived from models are reasonably accurate (*2*). These estimates can be used to predict future warming, assuming that any errors in models through under- or overestimating past warming continue into the future. The uncertainty ranges of future warming so derived largely overlap with those directly based on climate models but suggest that a few models may predict too much future warming (*3*).

Despite substantial progress in determining observational constraints for future global-mean warming, the uncertainty range in the estimated contribution of greenhouse gases to the observed global-mean warming is still quite large at 0.5 to 1.3°C (*1*) (see the first figure). A large part of this uncertainty results from difficulties in distinguishing the effects of greenhouse gas-induced warming from other effects, particularly the cooling effect of tropospheric aerosols (*4*). The fingerprints for greenhouse gases and aerosols can be rather similar, and the observations could be explained either by large greenhouse warming counteracted by a large aerosol response, or by smaller greenhouse warming with a smaller aerosol effect. Furthermore, the pattern of aerosol emissions is uncertain (*4*) and cannot always be distinguished from climate variability, particularly regionally (*5*). As a result, uncertainty ranges for the separate contributions by greenhouse gases and other anthropogenic factors remain large (see the first figure) (*6*). In contrast, the pattern of temperature changes expected from all human influences combined is substantially different from that from the combination of volcanic eruptions and changes in the Sun and can thus be estimated more confidently.

Human influence can also be detected in temperature changes over individual continents and many regions (*1*). This is important because the effects of climate change will be felt through regional changes and extremes such as heat waves. Extreme temperatures are often associated with unusual weather patterns, such as blocking high pressure systems (*7*, *8*), but studies suggest that long-term warming from anthropogenic climate change has substantially increased the probability of extremely high temperatures being experienced in some regions (*9*–*11*).

Several factors limit the attribution of regional temperature change and extreme events to climate change. First, data gaps are a problem, particularly in tropical regions and high latitudes (see the second figure). Regional temperature changes caused by human activities are expected to emerge from the range of climate variability in the tropics first (*12*), because climate is least variable there. However, these regional changes can only be observed where long-term data exist. Arctic and Antarctic regions are important because feedbacks to warming are strong there and melting ice contributes to sea level rise. However, in those regions, climate variability is very large and data records are short. Better observational information, including from satellite data and further back in time from digitization of old weather records, will improve understanding of regional climate change and climate variability.

Second, local influences, such as changes in land cover and pollution reducing sunlight, are often poorly known and difficult to distinguish from large natural variability. This makes it difficult to estimate how much regional warming is due to greenhouse gases and how much is due to (or has been offset by) other factors.

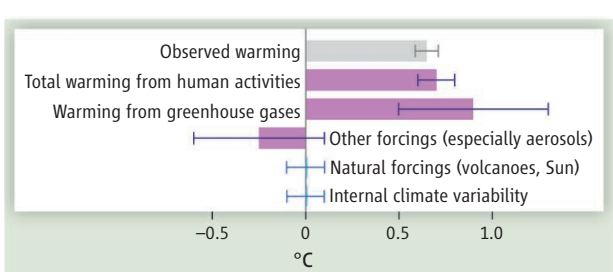

Getting warmer. The observed global temperature change between 1951 and 2010 (gray bar; whisker: observational uncertainty) is compared to the warming from human activities (purple bars), both combined and split into greenhouse gas and other forcings. The blue bars show the estimated contributions by natural forcings and by variability generated by the climate system. Bars give best estimates, and whiskers indicate the assessed uncertainty range within which the contribution is likely to lie (>66% probability). [Adapted from (*1*)]

[1]School of GeoSciences, University of Edinburgh, Edinburgh EH9 3JW, UK. [2]Hadley Centre, Met Office, Exeter EX1 3PB, UK. E-mail: gabi.hegerl@ed.ac.uk

Published by AAAS

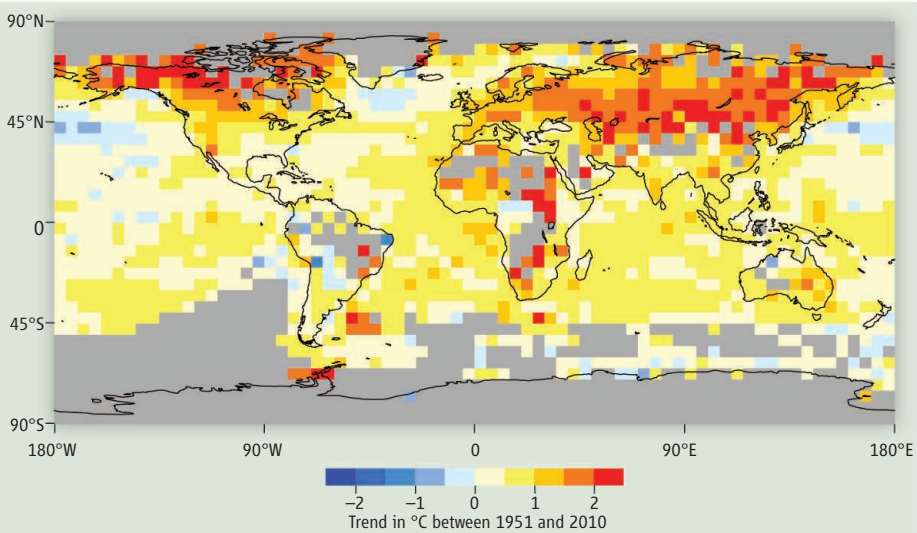

A mixed regional picture. In this map of observed local surface temperature changes from 1951 to 2010, areas without adequate observational coverage (shown in gray) are mostly found in the tropics and at high latitudes. [Adapted from (*1*)]

Third, systematic changes in weather systems would influence local weather and the incidence of extremes. Understanding and predicting such changes is much harder than predicting changes in mean temperatures. In observations, changes in circulation are difficult to identify among large random variability. Climate models struggle to simulate some circulation changes reliably (*8*). Increasingly, climate models have finer spatial resolution and better resolve processes relevant to regional climate variability. This will eventually improve confidence in attribution results on regional scales.

In the aftermath of damaging extreme events, it is important to be able to address the question to what extent human-induced climate change is to blame. Therefore, reliable information is needed to determine whether human influence has changed the risk of the occurrence of extreme climate events. Where regional changes appear to buck the long-term expected trend, scientists must determine whether this is because climate variability masks climate change or because observations and models disagree as a result of model deficiencies. This information can then be used to improve future climate models. There is little doubt that human activities were the main cause of global warming over the past 60 years, but work to better understand the causes of changes in regional climate, and thereby better understand our vulnerability to climate extremes, is far from done.

References

1. N. L. Bindoff *et al.*, in *Climate Change 2013: The Physical Science Basis*, T. F. Stocker *et al.*, Eds. (Cambridge Univ. Press, Cambridge, 2013), chap. 10.
2. G. Hegerl, F. Zwiers, *WIREs, Clim. Change* **2**, 570 (2011).
3. P. Stott, P. Good, G. Jonrs, N. Gillett, E. Hawkins, *Environ. Res. Lett.* **8**, 014024 (2013).
4. D. Rosenfeld, S. Sherwood, R. Wood, L. Donner, *Science* **343**, 379 (2014).
5. B. B. B. Booth, N. J. Dunstone, P. R. Halloran, T. Andrews, N. Bellouin, *Nature* **484**, 228 (2012).
6. A. Ribes, L. Terray, *Clim. Dyn.* 10.1007/s00382-013-1736-6 (2013).
7. R. Dole *et al.*, *Geophys. Res. Lett.* **38**, L06702 (2011).
8. G. Masato, B. Hoskins, T. Woollings, *J. Clim.* **26**, 7044 (2013).
9. P. A. Stott, D. A. Stone, M. R. Allen, *Nature* **432**, 610 (2004).
10. F. E. L. Otto *et al.*, *Geophys. Res. Lett.* **39**, L04702 (2012).
11. S. C. Lewis, D. J. Karoly, *Geophys. Res. Lett.* **40**, 3705 (2013).
12. I. Mahlstein, R. Knutti, S. Solomon, R. W. Portmann, *Environ. Res. Lett.* **6**, 034009 (2011).

10.1126/science.1249368

MATERIALS SCIENCE

Fibers Do the Twist

Twisted fibers provide a simple, low-cost route to high-energy artificial muscles.

Jinkai Yuan and Philippe Poulin

In a rubber band–powered airplane, a pretwisted band untwists when the hook used to initially balance its torque is released (see the figure). Such an actuation is based on the elastic recovery of the stretched polymer chains. The material has to be mechanically retwisted to operate but the method is simple and efficient, because the rubber band delivers almost as much energy as needed to twist it. Unfortunately, soft rubber cannot easily provide large stress and cannot be used in modern applications such as robotics, artificial muscles, smart textiles, and new medical devices. But as Haines *et al.* show on page 868 of this issue (*1*), the concept of twisted fibers can nevertheless be useful in demanding actuator applications.

Centre de Recherche Paul Pascal, CNRS, Université de Bordeaux, 115 Avenue Schweitzer, 33600 Pessac, France. E-mail: poulin@crpp-bordeaux.cnrs.fr

Twisted carbon nanotube yarns can act as highly efficient torsional and tensile actuators. Actuation in these yarns is not based on the entropic elasticity of polymer chains (as in a rubber band) but instead involves ionic swelling in a liquid electrolyte (*2*), electromagnetic effects (*3*), or the thermal expansion of an infiltrated paraffin wax (*4*). However, carbon nanotube yarns are expensive and difficult to make. Also, their energy density is low compared to that of competing materials such as shape memory alloys, considered to be the highest–energy density materials in the field of actuators (*5*).

Haines *et al.* now report artificial muscles made of twisted polymer fibers that deform in response to thermal expansion. Thermal expansion has long been used for thermal actuators—for example, in the "solar muscle," which converts solar heat into mechanical energy (*6*). These systems are simple, robust, and cheap, but have low thermal efficiency and provide lateral deformations of only a few percent. The strain can be amplified into large stroke by combining different materials, but this makes the actuators heavier and less efficient. By contrast, Haines *et al.* use a single material and a basic design. This single material can, for example, be commercial polyamide fibers used for fishing lines.

Polyamide is a semicrystalline polymer with a large stiffness over a wide temperature range. Its deformations involve not only entropic elasticity but also strong interac-

tions between the polymer chains, which are highly aligned along the axis of the fibers and contract with rising temperature. As a consequence of this contraction, the diameter of the fiber expands with temperature, whereas the fibers contract in length. As Haines *et al*. show, these effects induce untwisting of the fiber, providing torsional actuators with giant energy density because thermal expansion is directly converted into torsion. The achieved energy density is comparable to that of shape memory polymer fibers (*7*) and shape memory alloys (*8*).

Similar to the materials studied by Haines *et al*., shape memory polymers also deform through the stretching and contraction of polymer chains as a response to mechanical load and heating. In shape memory polymers, the chains are frozen in stretched conformations below a thermal transition temperature. They contract as they become mobile above this temperature. The deformed polymers remain stable at room temperature. Consequently, twisted fibers made from shape memory polymers could potentially serve as torsional actuators without being hooked or constrained. Furthermore, the transition temperature of polymers can be adjusted by changing the composition of the polymer (*9*). Development of such actuators could provide another route to high-energy artificial muscles made from twisted polymer fibers that respond to temperature changes. However, shape memory polymer fibers may not be suitable when the material is expected to operate reversibly in response to repeated decreases and increases of temperature.

Beyond the domain of torsional actuators, Haines *et al*. show that twist insertion allows the conversion of a small strain induced by thermal expansion into a giant tensile deformation along the coiled fiber axis. The highest tensile stroke achieved was 34% for a temperature variation of ~220°C, compared with 4% strain for the untwisted fiber. The level of stroke amplification is controlled by coiling of the fiber. Indeed, fibers form coils when highly twisted. The degree of coiling can be adjusted by changing the tensile load of the fiber during twisting and/or by varying the degree of twist. This concept is a notable advance because it allows the response of the actuator to be controlled at will. Compact coiling allows large stroke and low stress, whereas a less coiled structure generates a greater stress and a lower stroke. The energy density in tensile actuation is as high as in torsion, confirming that the same underlying mechanism operates in torsion and tension.

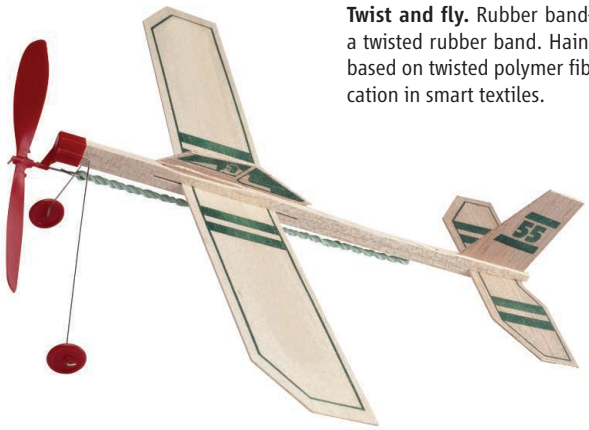

Twist and fly. Rubber band–powered airplanes are propelled by a twisted rubber band. Haines *et al*. now report artificial muscles based on twisted polymer fibers that may, for example, find application in smart textiles.

But record energy density, giant stroke, and versatility are not the sole impressive advantages of the technology reported by Haines *et al*. Polymer fibers are small in diameter and thus respond rapidly, resulting in high power density. Yet despite their small diameter, the fibers can be indefinitely long and used in large structures. Hence, the present concepts could find uses in miniaturized actuators, as well as in macroscopic structures. Haines *et al*. use twisted fibers to make macroscopic active textiles that deliver mechanical energy and exhibit reversible changes in porosity with temperature. Fiber materials are ideally suited to be integrated in smart textiles, gas or liquid filters that clog with temperature, and active cables that move objects or lever arms as natural muscles do. Finally, the robustness, commercial availability, and low cost of the materials used may allow the concept reported by Haines *et al*. to be integrated rapidly in modern applications.

References

1. C. S. Haines *et al*., *Science* **343**, 868 (2014).
2. J. Foroughi *et al*., *Science* **334**, 494 (2011).
3. W. H. Guo *et al*., *Adv. Mater.* **24**, 5379 (2012).
4. M. D. Lima *et al*., *Science* **338**, 928 (2012).
5. J. E. Huber, N. A. Fleck, M. F. Ashby, *Proc. R. Soc. Lond. A* **453**, 2185 (1997).
6. E. D. Ray, *Pop. Sci.* **216**, 126 (1980).
7. P. Miaudet *et al*., *Science* **318**, 1294 (2007).
8. J. Van Humbeeck, *Adv. Eng. Mater.* **3**, 837 (2001).
9. A. Lendlein, S. Kelch, *Angew. Chem. Int. Ed.* **41**, 2034 (2002).

10.1126/science.1250471

NEUROSCIENCE

Charting the Islands of Memory

A newly discovered population of neurons called island cells may be important signaling hubs within neural microcircuits for memory.

H. T. Blair

Exquisitely structured microcircuits in the hippocampus and entorhinal cortex (EC) were first sketched more than a century ago by the great Spanish neuroanatomist Ramon y Cajal. It has since become known that these circuits are components of a memory system that allows us to recall facts and past events from our lives. Two reports on pages 891 and 896 of this issue describe newly discovered circuits formed by a population of neurons in the EC, which congregate in distinctive clusters referred to as "patches" by Ray *et al*. (*1*) and as "islands" by Kitamura *et al*. (*2*). Both studies suggest that these island cells may play important roles in learning and memory.

Psychology Department and Brain Research Institute, University of California, Los Angeles, CA 90095, USA. E-mail: blairlab@gmail.com

Island cells belong to a common class of cortical neurons called pyramidal cells, and are distinguished by their expression of a protein called calbindin, which other EC neurons lack. The EC comprises six distinct layers, each with its own pattern of input and output connections. Patches of island cell bodies reside in the second layer (ECII), which sends a major excitatory projection—called the perforant path—to the dentate gyrus (DG) and CA3 subregions of the hippocampus (see the figure). However, the perforant path arises from ECII stellate cells that are interleaved between island cell patches, so island cell axons do not project to the DG or CA3.

Kitamura *et al*. show that island cell axons follow the temporoammonic path-

CREDIT: OCEAN/CORBIS

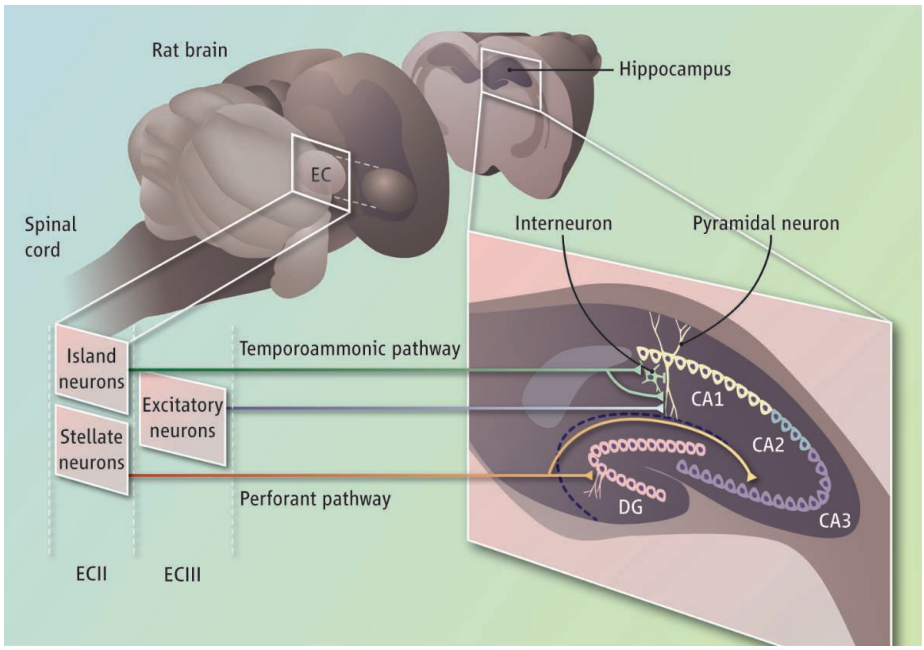

Memory microcircuits. Island cells in layer II of the entorhinal cortex (ECII) exert inhibitory control over the ability of ECIII neurons to excite CA1 neurons in the hippocampus. This network may operate to impair or enhance specific kinds of memories. A schematic of the rat brain is shown.

CREDIT: H. MCDONALD/*SCIENCE*

way from the EC to the CA1 subregion of the hippocampus. This pathway contains many axons from neurons in the third layer of the EC (ECIII), which excite the apical dendrites of CA1 pyramidal cells. By contrast, island cell axons preferentially excite CA1 interneurons, which inhibit the same apical dendrites of CA1 pyramidal cells that are excited by ECIII axons. Hence, island cells appear well positioned to exert inhibitory control over the ability of ECIII neurons to excite CA1.

To investigate how island cells influence memory, Kitamura *et al*. engineered island cells to express a light-sensitive ion channel. Island cells were then artificially stimulated by light while mice were trained to fear an auditory tone by pairing the tone with an electric shock that occurred 20 s after the tone had ended. Stimulation of the island cell pathway impaired memory for trace fear evoked by the tone (thus, mice could not remember that the tone predicted the shock) but spared context fear evoked by the experimental chamber (that is, mice could still remember that a shock had occurred in the chamber). Prior evidence indicates that trace fear requires activation of CA1 by inputs from ECIII (*3*), whereas context fear depends on other inputs to CA1 (*4*). Thus, artificial stimulation of island cells may have selectively switched off temporoammonic inputs to CA1 from ECIII, thereby inhibiting specific memory processes (such as trace fear) while sparing others (such as context fear).

By artificially manipulating island cells, it may thus be possible to selectively impair or enhance specific kinds of memories. However, the natural activity of island cells may serve functions more complex than simply acting as an "off switch" for ECIII inputs to CA1. CA1 contains spatially tuned neurons called place cells, each of which fires selectively when the animal visits a preferred location (*5*). The EC contains spatially tuned neurons called grid cells, each of which fires at multiple locations that form a hexagonal lattice on the floor of the environment (*6*), as well as border cells that fire along environmental boundaries (*7*). In rodents, firing patterns of neurons in CA1 and the EC are comodulated by 4- to 12-Hz theta oscillations (*8*), a prominent brain rhythm that becomes especially strong when the animal is moving through its environment. Ray *et al*. recorded island cells in freely behaving mice, and found that they were more strongly modulated by movement-related theta rhythm than neighboring stellate cells. This was unexpected because island cells are ECII pyramidal cells, which have been shown to exhibit less theta resonance of their intrinsic membrane currents than stellate cells (*9*). Theta rhythmicity of island cells may thus be driven by an external source of oscillatory input.

From where might island cells receive such inputs? Island cell patches are anatomically distributed to form a hexagonal lattice over the cortical surface, calling to mind the hexagonal geometry of grid cell firing rate maps (*1*). Rows of myelinated axons in EC layer I (ECI) trace a parallel path across the cortical surface, aligned along a principal axis of the island cell patch grid. The hexagonal geometry of island cell patches may permit them to receive input from patterned subsets of these ECI axons, and this may be a critically important feature of EC microcircuitry. Island cell patches also appear to be preferential targets of inputs to the EC that release the neurotransmitter acetylcholine, and many of these inputs come from the medial septum, a structure that generates the theta oscillations necessary for grid cell activity (*10*, *11*).

Is the hexagonal geometry of calbindin patches functionally related to the hexagonal geometry of grid cell firing fields? Unfortunately, Ray *et al*. were unable to assess spatial tuning properties of the island cells they recorded. Some island cells might be grid cells or border cells, and if so, then place cells in CA1 might derive some of their spatially selective tuning from island cell inputs, in accordance with theoretical models showing how place cells can be formed from grid cells (*12*) or border cells (*13*). But even if island cells lack any spatial tuning at all, their theta rhythmicity may shape the location-specific firing properties of CA1 place cells and EC grid cells, in accordance with "oscillatory interference" models that show how grid (*14*) and place (*15*) cells can derive their spatial tuning by detecting location-dependent synchrony among theta cells that lack spatial tuning of their own.

Further research will be needed to clarify the functional contributions of island cells to memory and spatial coding. But now that they have taken the stage, it appears likely that EC island cells will become a new focus for research on memory microcircuits.

References

1. S. Ray *et al*., *Science* **343**, 891 (2014); 10.1126/science.1243028.
2. T. Kitamura *et al., Science* **343**, 896 (2014); 10.1126/science.1244634.
3. J. Suh, A. J. Rivest, T. Nakashiba, T. Tominaga, S. Tonegawa, *Science* **334**, 1415 (2011).
4. T. Nakashiba, J. Z. Young, T. J. McHugh, D. L. Buhl, S. Tonegawa, *Science* **319**, 1260 (2008).
5. J. O'Keefe, J. Dostrovsky, *Brain Res.* **34**, 171 (1971).
6. T. Hafting, M. Fyhn, S. Molden, M.-B. Moser, E. I. Moser, *Nature* **436**, 801 (2005).
7. T. Solstad, C. N. Boccara, E. Kropff, M.-B. Moser, E. I. Moser, *Science* **322**, 1865 (2008).
8. K. Mizuseki, A. Sirota, E. Pastalkova, G. Buzsáki, *Neuron* **64**, 267 (2009).
9. A. Alonso, R. Klink, *J. Neurophysiol.* **70**, 128 (1993).
10. J. Koenig *et al*., *Science* **332**, 592 (2011).
11. M. P. Brandon *et al*., *Science* **332**, 595 (2011).
12. T. Solstad *et al*., *Hippocampus* **16**, 1026 (2006).
13. T. Hartley *et al*., *Hippocampus* **10**, 369 (2000).
14. N. Burgess *et al*., *Hippocampus* **17**, 801 (2007).
15. A. C. Weldaye*t al*. *J. Neurosci.* **31**, 16157 (2011).

10.1126/science.1251252

Published by AAAS

CELL BIOLOGY

Reach Out and Touch Someone

Cellular extensions called cytonemes may allow nonneuronal cells to communicate directly with each other over long distances.

Pernille Rørth

How do cells in the body communicate over long distances? Neurons do so through long cellular extensions—axons and dendrites—that establish direct contacts (synapses) with target cells. Other cells are thought to receive information through secreted signaling molecules that diffuse through a tissue. For example, cells that become the fingers of the hand receive patterning information from one side of the limb primordia, with the proximal cells receiving more signal than the distal ones and, as a consequence, taking on a different digit identity. On page 852 of this issue, Roy *et al*. (*1*) provide evidence that signal-receiving cells do not passively wait, but reach out and grab the signal by making direct contact with signal-sending cells (see the figure).

Patterning a field of cells by concentration-dependent signals from a localized source makes intuitive sense. Thus, the suggestion that long, thin cellular extensions, specialized filopodia called cytonemes, might be responsible for such patterning was considered somewhat unorthodox (*2*). Cytonemes were initially described in *Drosophila* cells that respond to Decapentaplegic (Dpp), a signaling molecule that patterns imaginal discs (flat, epithelial tissue from which adult structures develop). Subsequently it was discovered that individual cytonemes differ and display receptors appropriate for the signal they perceive (*3*). This and the present work mostly involved the study of *Drosophila* air sac cells. Like vascular cells in vertebrates, they make many long filopodia.

Roy *et al*. use the reconstitution of a split fluorescent molecule, one part attached to signaling cells and the rest to distant receiving cells, to show that these cells are in physical contact. After contact, endocytosis of activated receptors returns them to the body of the receiving cell. Mutations that perturb formation of cytonemes or proper cell-cell contacts ("synapses") interfere with signaling, suggesting that these long-distance cell contacts are important. Such contact-mediated signaling could convey spatial information from a source to a field of cells if there are more short cytonemes than long ones, or if the signal is attenuated with cytoneme length.

Institute of Molecular and Cell Biology, 61 Biopolis Drive, Singapore 138673. E-mail: prorth@imcb.a-star.edu.sg

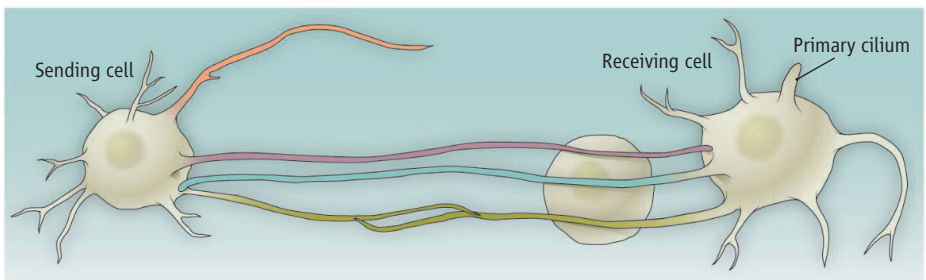

Membrane extensions in signaling. Filopodia-like cytonemes with different receptors or signaling molecules (different colors) are made by signal-receiving and -sending cells, and make direct cell-to-cell contacts.

Long, thin, actin-rich cellular membrane extensions classified broadly as filopodia are known from many contexts. "Tunneling nanotubes" directly connect distant cells in culture and allow mechanical and Ca^{2+}-based coupling directly or via gap junctions (*4*–*6*). And signal transfer decreases with nanotube length. Nanotubes transfer endocytic vesicles and F-actin, whether directly or by transcytosis. Thus, the parallel to endocytosis-dependent cytoneme signaling is striking.

Cytonemes have been implicated not just in receiving signals, but also in sending signals, as illustrated in two recent studies of the signaling molecule Hedgehog (Hh in *Drosophila* and Shh in vertebrates) (*7*, *8*). Careful genetics and quantitation in *Drosophila* (*8*) and sophisticated live imaging in chick embryos (*7*) provide evidence that the lipid-modified Hh/Shh proteins spread by traveling in, or on, cytonemes. The chick study also examined signal-receiving cells and found that filopodia from sending and receiving cells make direct contact (*7*). In light of the present study this is intriguing, but quantitation of such contacts and evidence for functional relevance are needed.

Intriguingly, Shh signaling is associated with another membrane-bound cellular extension in signal-receiving cells. In vertebrates, but not *Drosophila*, Shh signal transduction appears to occur at the primary cilium (*9*–*11*). The primary cilium is quite different from filopodia. It is a single, stable, microtubule-based structure. It is not known whether Shh-carrying filopodia contact the cilium to transfer signal; perhaps they are functionally independent specializations.

Knowing that both sending and receiving cells use cytonemes prompts consideration of what this mode of signaling contributes. Roy *et al*. argue, but do not strictly prove, that cytoneme-mediated contact is required for signaling. Cytonemes might find their target cells by chemotaxis, sensing the secreted molecules. Alternatively, cytonemes might initially grow in an unguided manner and selectively stabilize contacts with the appropriate signaling cell. Only quantitative live imaging can discriminate between these alternatives.

Long-range filopodia also play a role in membrane-tethered signaling interactions between Delta and Notch (*12*). Here, modeling and quantitative live imaging show that the dynamics of filopodia are required to refine patterning (*13*). Compartmentalization by cytonemes with only one type of signaling receptor might also allow highly sensitive signal detection, unaffected by other pathways.

Signaling by touch has several features not afforded by signaling at a distance using secreted molecules. Signaling events can include gap junctions and Ca^{2+}-based signals, as seen with nanotubes. The local membrane context can be sampled for the presence of the appropriate mechanical characteristics or adhesion molecules, for example, and this may direct signals only to specific recipient cells. And localized signaling may minimize signal loss. However, restricting signaling through a limited number of cytonemes also makes signaling more stochastic. The "private conversations" thus set up may not reach all intended recipients. Making the cytoneme contacts dynamic allows broader target sampling and, possibly, signal averaging over time. The stochastic differences between signals received may thus be reduced. But the one-on-one restricted signaling interactions may also be used actively, to make each cell-signaling contact unique.

CREDIT: P. HUEY/*SCIENCE*

Published by AAAS

Direct communication between adjacent cells underlies tissue organization. Communicating with a dispersed community of cells presents quite different challenges: Decisions must be made about which cells to communicate with, and how. Cytonemes, nanotubes, and other filopodia-like structures can be used for long-distance communication, but there is still limited information about their biological importance. The most informative experiments, like selective disruption of connections and detailed analysis of the consequences, are also the hardest to carry out. Direct communication allows private cell-to-cell conversations: Freely transmitting the signal makes it simpler to reach many cells. Employing a combination of these two signaling mechanisms may optimize strategies for decision-making in development. Even the nervous system, with its elaborate and sophisticated use of long-distance cell-cell connections, also uses dispersed signals to modulate general outputs such as mood and other emotions.

References

1. S. Roy, H. Huang, S. Liu, T. B. Kornberg, *Science* **343**, 124462 (2014); 10.1126/science.1244624.
2. F. A. Ramírez-Weber, T. B. Kornberg, *Cell* **97**, 599 (1999).
3. S. Roy, F. Hsiung, T. B. Kornberg, *Science* **332**, 354 (2011).
4. A. Rustom, R. Saffrich, I. Markovic, P. Walther, H. H. Gerdes, *Science* **303**, 1007 (2004).
5. S. C. Watkins, R. D. Salter, *Immunity* **23**, 309 (2005).
6. X. Wang, M. L. Veruki, N. V. Bukoreshtliev, E. Hartveit, H. H. Gerdes, *Proc. Natl. Acad. Sci. U.S.A.* **107**, 17194 (2010).
7. T. A. Sanders, E. Llagostera, M. Barna, *Nature* **497**, 628 (2013).
8. M. Bischoff *et al.*, *Nat. Cell Biol.* **15**, 1269 (2013).
9. D. Huangfu *et al.*, *Nature* **426**, 83 (2003).
10. K. C. Corbit *et al.*, *Nature* **437**, 1018 (2005).
11. R. Rohatgi, L. Milenkovic, M. P. Scott, *Science* **317**, 372 (2007).
12. C. de Joussineau *et al.*, *Nature* **426**, 555 (2003).
13. M. Cohen, M. Georgiou, N. L. Stevenson, M. Miodownik, B. Baum, *Dev. Cell* **19**, 78 (2010).

10.1126/science.1250885

STRUCTURAL BIOLOGY

Unraveling a Flavivirus Enigma

The structure of a flavirirus nonstructural protein provides mechanistic understanding for many of its functions.

Pei-Yong Shi

There is growing concern about the spread of flaviviruses, such as dengue virus and West Nile virus, to new geographic areas as they can cause major epidemics and represent global public health threats. Controlling these viruses requires a better molecular understanding of how they infect cells. Nonstructural protein 1 (NS1) is perhaps the most enigmatic flavivirus protein. During infection, NS1 exists in two distinct forms, travels to various compartments, decorates itself with different molecular disguises, and plays numerous roles in its infectious cycle and disease pathogenesis (*1*). How this protein manages all of this has been a puzzle since its discovery in 1970 (*2*). Crystallizing NS1 has daunted many researchers because of the heterogeneity of its glycosylation and association with lipids, but as reported on page 881 of this issue, Akey *et al.* (*3*) have accomplished this task. The unusual structural details revealed about NS1 may guide the design of compounds that inhibit viral replication and provide clues as to how it contributes to different stages of the virus life cycle and disease.

Flavivirus NS1 is a glycoprotein with a molecular mass of 46 to 55 kD, depending on its glycosylation status. The crystal structures of dengue virus NS1 (3 Å resolution) and West Nile virus NS1 (2.8 Å resolution) exhibit a similar hexameric arrangement of three dimers, confirming the hexameric structure (30 Å resolution) indicated by a cryoelectron-microscopy analysis (*4*). Each monomer displays an unusual fold consisting of three regions: a "β-roll" domain that dimerizes with that of another monomer; a "wing" domain that resembles a helicase domain; and a "β-ladder" domain that aligns with that of another NS1 molecule to form an extended β-sheet ladder. The ladder forms the plane of the NS1 dimer, with a hydrophobic side (exemplified by a "greasy finger" loop) that can associate with the membrane. The hydrophobic side of each dimer faces the interior of the hexamer. Remarkably, recombinant NS1, which does not possess any transmembrane domain, can convert large liposomes into smaller lipid-protein nanoparticles. This demonstrates that NS1 can directly modulate the lipid membrane without additional cellular proteins. Such lipid-modulation activity and its underlying structure could account for the myriad functions of NS1.

After flavivirus entry into a cell by endocytosis, the virus particle is released into the cytoplasm. Viral genomic RNA is translated into proteins and replicated, and virus assem-

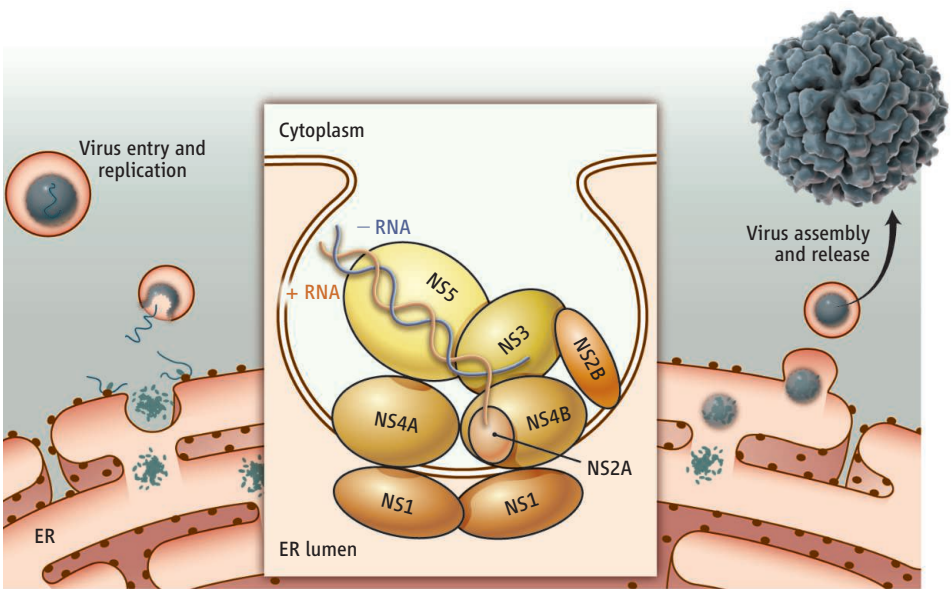

Assist before leaving. Flavivurus replicates at the ER surface in the infected cell. Viral NS1 protein forms dimers in the ER lumen, yet assist the replication complex on the opposite side of the membrane. Seven nonstructural proteins, together with host proteins (not shown), form the replication complex. Once immature viral particles bud into the secretory pathway, NS1 protein forms hexamers that are secreted as lipoproteins.

CREDIT: V. ALTOUNIAN/*SCIENCE*

Novartis Institute for Tropical Diseases, 10 Biopolis Road, 05-01 Chromos, Singapore 138670. E-mail: pei_yong.shi@novartis.com

bly occurs on the surface of the endoplasmic reticulum (ER). Viral particles bud into the ER and mature as they are transported through the secretory pathway for release from the cell.

NS1 protein is translated from viral RNA and translocated into the ER lumen, where it is glycosylated. NS1 dimers then form and associate with the luminal side of the ER membrane at a virus-induced vesicle packet (see the figure). Although dimeric NS1 is required for viral RNA synthesis, the replication complex resides on the cytoplasmic side of the ER membrane. Two factors could facilitate the recruitment of NS1 to the replication complex: the membrane-association of NS1, and the specific interactions between NS1 and viral transmembrane proteins NS4A and NS4B (*5*, *6*).

What happens after the NS1 dimer has facilitated viral replication? It is eventually released by the infected cell. A model proposes that the assembly of hexameric NS1 (*4*) is key to this process. Newly synthesized monomeric NS1 is water-soluble. As its concentration and glycosylation increase in the ER lumen, NS1 dimerizes, creating the hydrophobicity needed for its interaction with the membrane (*7*). Three NS1 dimers juxtapose on the lipid bilayer and pinch off the membrane, resulting in a water-soluble hexamer. Host lipids become trapped within the central channel of the hexamer, forming a lipoprotein particle. The particle is then transported and released from the cell through the secretory pathway.

In dengue virus–infected patients, the concentration of extracellular NS1 can reach 15 μg/ml in sera (*1*). NS1-based tests have been developed for rapid, point-of-care diagnosis. The concentration of serum NS1 correlates with the amount of the viral RNA present in the patient, and high amounts of circulating dengue virus NS1 early in illness correlate with severe disease outcome (*8*). Mounting evidence indicates that secreted NS1 modulates disease pathogenesis. Preincubation of hepatocytes with soluble NS1 enhances homologous dengue virus infection (*9*). Secreted NS1 interacts with host proteins, many of which are involved in the immune complement pathway (*10*, *11*); this may allow flaviviruses to evade the immune system. Secreted NS1 also is highly immunogenic. Some antibodies against NS1 are cross-reactive with cellular components; these auto-antibodies may contribute to platelet and endothelial cell damage, leading to vascular leakage, the hallmark of severe dengue hemorrhagic fever and dengue shock syndrome.

The critical roles of NS1 in flavivirus replication and pathogenesis implicate NS1 as an attractive antiviral target. A few tangible approaches can be envisioned. Cells expressing NS1 could be screened for inhibitors of NS1 dimerization and hexamerization, and libraries could be screened for compounds that block the ability of NS1 to convert liposomes into lipoprotein particles. The crystal structure will greatly facilitate structure-based rational design of antiviral compounds. In fact, inhibitors of cellular glucosidases that are required for NS1 glycosylation suppress flavivirus replication in cell culture and in a mouse model (*12*). Future studies should define how NS1 physically interacts with the replication complex and its specific role in RNA replication. The molecular details remain to be determined as to when, where, and how the conversion of NS1 monomer to dimer and then to hexamer is controlled. One question concerns the NS1 "wing" domain, whose folding is similar to that seen in two proteins [retinoic acid–inducible gene I (RIG-I) and melanoma differentiation–associated gene 5 (MDA5)] that function as viral sensors in the innate immune system. Does this somehow allow flaviviruses to evade the host immune response? Another intriguing question is why, within the family *Flaviviridae*, only members of the genus *Flavivirus* encode the NS1 protein; members of the other two genera, *Hepacivirus* and *Pestivirus*, do not contain a gene equivalent to NS1. The reason may be that most flaviviruses transfer between insects and mammals. If so, it raises the question of how flavivirus NS1 play distinct roles when replicating in different host cells. Perhaps more interesting is how the essential role of NS1 in flavivirus replication is compensated in hepacivirus and pestivirus. The answers to these questions will unravel more mysteries of this fascinating protein.

References

1. D. A. Muller, P. R. Young, *Antiviral Res.* **98**, 192 (2013).
2. W. E. Brandt, R. D. Cardiff, P. K. Russell, *J. Virol.* **6**, 500 (1970).
3. D. L. Akey *et al.*, *Science* **343**, 881 (2014); 10.1126/science.1247749.
4. I. Gutsche *et al.*, *Proc. Natl. Acad. Sci. U.S.A.* **108**, 8003 (2011).
5. B. D. Lindenbach, C. M. Rice, *J. Virol.* **73**, 4611 (1999).
6. S. Youn *et al.*, *J. Virol.* **86**, 7360 (2012).
7. G. Winkler *et al.*, V. Stollar, *Virology* **171**, 302 (1989).
8. D. H. Libraty *et al.*, *J. Infect. Dis.* **186**, 1165 (2002).
9. S. Alcon-LePoder *et al.*, *J. Virol.* **79**, 11403 (2005).
10. P. Avirutnan *et al.*, *J. Infect. Dis.* **193**, 1078 (2006).
11. K. M. Chung *et al.*, *Proc. Natl. Acad. Sci. U.S.A.* **103**, 19111 (2006).
12. A. P. S. Rathore *et al.*, *Antiviral Res.* **92**, 453 (2011).

10.1126/science.1251249

CHEMISTRY

Remote Control by Steric Effects

Mamoru Tobisu[1] and Naoto Chatani[2]

A rhodium-catalyzed reaction places a silicon substituent on the site farthest away from the largest group present on an aromatic ring.

The benzene ring is one of the most prevalent structural motifs found in organic compounds, and the development of efficient and selective methods for the synthesis of benzene derivatives has attracted the interest of organic chemists for more than a century. When introducing a new substituent onto substituted benzene derivatives, one critical issue is regioselectivity (i.e., which particular C-H bonds will react). One strategy for addressing this issue is to use bulky substituents on the ring—which often are added deliberately—to limit access of a reagent or a catalyst to adjacent C-H bonds, thus directing the reaction to other positions. On page 878 of this issue, Cheng and Hartwig (*1*) report that the steric bulk of the substituent can be used to achieve an unusually high selectivity among the C-H bonds that are located at more remote positions of the benzene ring.

The classical method for benzene functionalization is electrophilic aromatic substitution, in which the electronic nature of a substituent controls the regioselectivity for further substitution reactions. An electron-donating group such as methoxy ($–OCH_3$) results in the ortho and para positions being substituted, whereas an electron-withdrawing group such as nitro ($–NO_2$) delivers a

[1]Center for Atomic and Molecular Technologies, Graduate School of Engineering, Osaka University, Suita, Osaka 565-0871, Japan. [2]Department of Applied Chemistry, Faculty of Engineering, Osaka University, Suita, Osaka 565-0871, Japan. E-mail: tobisu@chem.eng.osaka-u.ac.jp; chatani@chem.eng.osaka-u.ac.jp

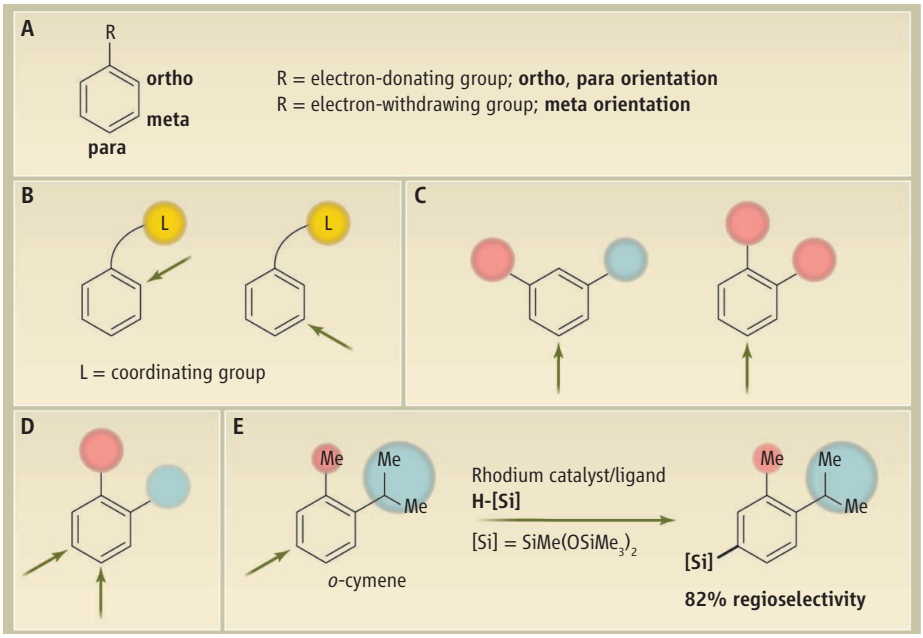

Regioselective functionalization of benzene derivatives. Several methods exist for controlling where substitution occurs on aromatic rings. (**A**) Control by the electronic nature of the substituent. (**B**) Control by a coordinating group. (**C**) Control by a steric effect; two classes of successful substrates are shown. (**D**) For unsymmetrically 1,2-disubstituted benzene derivatives, selectivity between the 4 and 5 positions is difficult to achieve. (**E**) The rhodium-catalyzed silylation of *o*-cymene developed by Cheng and Hartwig demonstrates control over regioselectivity by the remote steric effect. Me, methyl.

meta-substituted product (see the figure, panel A). Regioselectivity control by electronics is highly reliable and predictable, allowing for access to a range of di- or multisubstituted benzenes. Such electronic control can also be applied to some transition metal catalysis, in which aromatic substitution by an electrophilic metal complex determines the regioselectivity of the reaction.

However, arenes with substitution patterns that are incompatible with these rules can be difficult and the synthesis involves multiple steps. An approach that is complementary to electronic control involves the use of a coordinating group (see the figure, panel B). A coordinating group is a substituent with a heteroatom-containing functionality that can bind a metal-based reagent or catalyst and bring it into close proximity to the reaction center. An early example of this approach is directed ortho metallation, in which a strong base such as an organolithium reagent can regioselectively deprotonate the ortho hydrogen, ultimately leading to the formation of 1,2-disubstituted benzenes (*2*). Later on, this strategy was applied to transition metal catalysis (*3*, *4*).

The use of transition metal complexes instead of strong bases greatly increases the synthetic utility of this approach (*5*). In addition to high tolerance for functional groups already present on the ring, a mechanistic diversity for the C-H bond cleavage process results in the formation of a diverse range of metallacyclic intermediates that can be used for many types of transformations. Quite recently, Yu and co-workers devised well-designed coordinating groups for the selective functionalization of C-H bonds at the meta position (*6*).

The reactivity of aromatic C-H bonds can also be differentiated according to their acidity. However, a synthetically useful level of selectivity is achieved only in the case of polyfluorinated arene substrates (*7*). A more versatile strategy is to take advantage of steric effects, which guide aromatic functionalization reactions to proceed at the less hindered position. To date, the power of steric control is best appreciated in cases of two classes of substituted benzenes: 1,3-disubstituted and symmetrically 1,2-disubstituted benzenes (*7*). In these substrates, the substituents block the reaction at the ortho positions, with 1,3,5- or 1,2,4-trisubstituted benzenes being selectively produced (see the figure, panel C).

In contrast, the regioselective functionalization of unsymmetrically 1,2-disubstituted benzenes poses a greater challenge because the C-H bonds at positions 4 and 5 are remote from the substituents, and thus make it difficult to be discriminated only by sterics (see the figure, panel D). Cheng and Hartwig developed a remarkable catalyst system that can functionalize this class of substrates in a regioselective manner. For example, *o*-cymene, a benzene derivative bearing two different-sized alkyl groups at the 1 and 2 positions, incorporated a silicon functionality at the position para to a larger substituent with 82% selectivity when a rhodium-based catalyst was used (see the figure, panel E).

This selectivity value advances the state of the art; iridium-catalyzed borylation, a transformation synthetically equivalent to silylation, affords only a 42:58 mixture of regioisomers (*8*). The two substituents in *o*-cymene exert virtually no difference in the electronic state of the potential reaction sites. Thus, the selectivity of this reaction would be expected to result from the difference in the size of these substituents, but the potential reaction sites would normally be viewed as being too distant to be affected. The unusual sensitivity of this reaction to remote sterics can be attributed to the bulkiness of the ligand and the silicon reagent (*9*) and the use of rhodium (*10*).

The protocol of Cheng and Hartwig enhances the synthetic utility of C-H silylation by avoiding the need for harsh conditions and an excess of the arene substrates, as well as by using a stable yet easy-to-elaborate silicon functionality. This new silylation can be expected to replace iridium-catalyzed borylation as a principal method for use in the late-stage introduction of a reactive functionality into C-H bonds in complex molecules. Unresolved issues involve meta- and para-selective functionalization reactions of mono-substituted benzenes that do not depend on electronics. However, control through the use of a remote coordinating group (*6*) and remote steric effects discussed here holds considerable promise.

References

1. C. Cheng, J. F. Hartwig, *Science* **343**, 878 (2014).
2. V. Snieckus, *Chem. Rev.* **90**, 879 (1990).
3. T. W. Lyons, M. S. Sanford, *Chem. Rev.* **110**, 1147 (2010).
4. G. Rouquet, N. Chatani, *Angew. Chem. Int. Ed.* **52**, 11726 (2013).
5. S. Murai *et al.*, *Nature* **366**, 529 (1993).
6. D. Leow, G. Li, T.-S. Mei, J.-Q. Yu, *Nature* **486**, 518 (2012).
7. N. Kuhl, M. N. Hopkinson, J. Wencel-Delord, F. Glorius, *Angew. Chem. Int. Ed.* **51**, 10236 (2012).
8. I. A. I. Mkhalid, J. H. Barnard, T. B. Marder, J. M. Murphy, J. F. Hartwig, *Chem. Rev.* **110**, 890 (2010).
9. M. Murata, M. Fukuyama, J.-i. Wada, S. Watanabe, Y. Masuda, *Chem. Lett.* **36**, 910 (2007).
10. K. Ezbiansky *et al.*, *Organometallics* **17**, 1455 (1998).

10.1126/science.1250335

Cytoneme-Mediated Contact-Dependent Transport of the *Drosophila* Decapentaplegic Signaling Protein

Sougata Roy *et al.*

Science **343**, (2014);
DOI: 10.1126/science.1244624

Science (print ISSN 0036-8075; online ISSN 1095-9203) is published weekly, except the last week in December, by the American Association for the Advancement of Science, 1200 New York Avenue NW, Washington, DC 20005.

Cytoneme-Mediated Contact-Dependent Transport of the *Drosophila* Decapentaplegic Signaling Protein

Sougata Roy, Hai Huang, Songmei Liu, Thomas B. Kornberg*

READ THE FULL ARTICLE ONLINE
http://dx.doi.org/10.1126/science.1244624

Cite this article as S. Roy *et al.*, *Science* **343**, 1244624 (2014).
DOI: 10.1126/science.1244624

Introduction: In multicellular organisms, morphogen signaling proteins move from "signaling centers" where they are produced to target cells whose growth and patterning they regulate. Whereas much progress has been made identifying and characterizing signaling proteins such as the transforming growth factor–β family member Decapentaplegic (Dpp), which is produced in the *Drosophila* wing imaginal disc, the mechanisms that disperse signaling proteins remain controversial. We characterized Dpp signaling in a system in which cytonemes, a specialized type of filopodia implicated in long-distance signaling, could be imaged, and in which movement of signaling proteins and their receptors could be followed.

Methods: We expressed fluorescence-tagged forms of proteins that function in morphogen signaling to monitor Dpp in signal-producing cells, its receptor in signal-receiving cells, and proteins and cell structures that participate in trafficking of signaling proteins. Signaling was characterized in live, unfixed tissue as well as by immunohistochemistry, and under conditions of both gain- and loss-of-function genetics.

Results: Cells that received Dpp and activated Dpp signal transduction extended cytonemes that directly contacted Dpp-producing cells. The contacts were characterized by relative stability and membrane juxtaposition of less than 15 nm. Cytonemes that contained the Dpp receptor in motile puncta also contained Dpp taken up from Dpp-producing cells. In contrast, a different set of cytonemes that contacted fibroblast growth factor (FGF)–producing cells contained the FGF receptor but did not take up Dpp. The cytonemes were reduced in number and length in genetic loss-of-function conditions for *diaphanous*, which encodes a formin; for *neuroglian*, which encodes an L1-type cell adhesion molecule; and for *shibire*, which encodes a dynamin. Cytonemes were present in loss-of-function conditions for *capricious*, which encodes a leucine-rich repeat cell adhesion protein, but these cytonemes failed to contact Dpp-producing cells. Signaling was abrogated in all these conditions that created defective cytonemes, although the signal-producing cells were not compromised. The mutant conditions were not lethal to the affected cells, and the mutant cells retained competence to autocrine signaling.

Discussion: This work describes cytonemes that receive and transport signaling proteins from producing cells to target cells, and shows that cytoneme-mediated signal exchange is both contact-dependent and essential for Dpp signaling and normal development. Contact-mediated signal exchange and signaling are also the hallmarks of neurons—an analogy that extends to the functional requirements for the *diaphanous*, *neuroglian*, *shibire*, and *capricious* genes by both neurons and epithelial cells. Discoveries of cytonemes in many cell types and in many organisms suggest that contact-mediated signaling may be a general mechanism that is not unique to neurons.

FIGURES IN THE FULL ARTICLE

SUPPLEMENTARY MATERIALS

Figs. S1 to S3
Tables S1 to S5
Movie S1

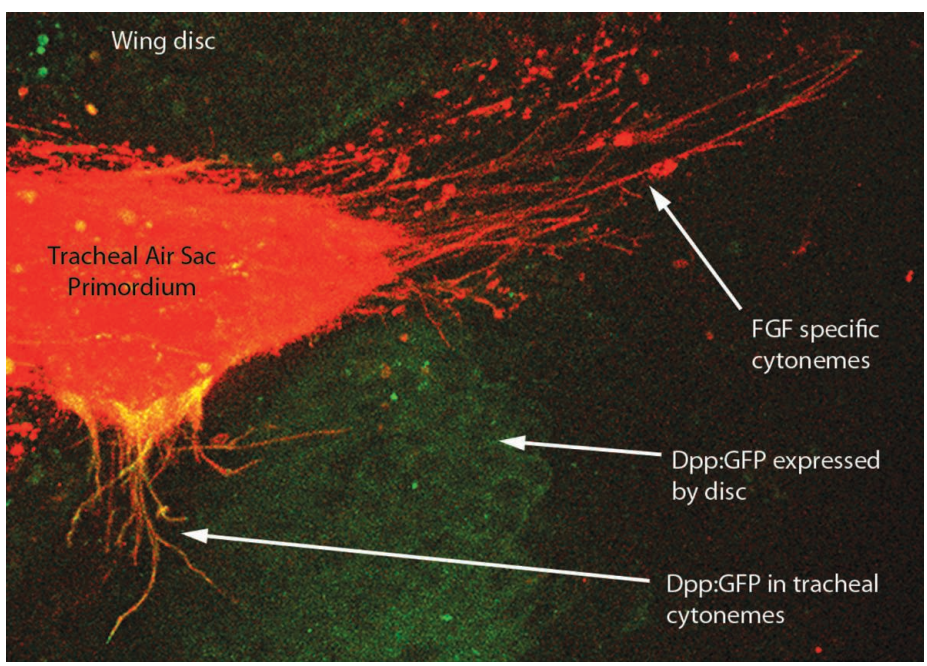

Cytonemes take up and transport morphogens. Micrograph showing a tracheal branch marked with mCherry overlying a wing disc expressing Dpp (tagged with green fluorescence). Cytonemes extend from the medial region of the branch to Dpp-expressing disc cells, and from the tip of the branch toward FGF-expressing disc cells. Dpp has been taken up and transported by the cytonemes that contact Dpp-expressing cells.

Cardiovascular Research Institute, University of California, San Francisco, CA 94158, USA.
*Corresponding author. E-mail: tkornberg@ucsf.edu

Cytoneme-Mediated Contact-Dependent Transport of the *Drosophila* Decapentaplegic Signaling Protein

Sougata Roy, Hai Huang, Songmei Liu, Thomas B. Kornberg*

Decapentaplegic (Dpp), a *Drosophila* morphogen signaling protein, transfers directly at synapses made at sites of contact between cells that produce Dpp and cytonemes that extend from recipient cells. The Dpp that cytonemes receive moves together with activated receptors toward the recipient cell body in motile puncta. Genetic loss-of-function conditions for *diaphanous*, *shibire*, *neuroglian*, and *capricious* perturbed cytonemes by reducing their number or only the synapses they make with cells they target, and reduced cytoneme-mediated transport of Dpp and Dpp signaling. These experiments provide direct evidence that cells use cytonemes to exchange signaling proteins, that cytoneme-based exchange is essential for signaling and normal development, and that morphogen distribution and signaling can be contact-dependent, requiring cytoneme synapses.

In many contexts during development, cell fate is determined by morphogen signaling proteins. The *Drosophila* wing imaginal disc, for instance, expresses the morphogen Decapentaplegic (Dpp), a transforming growth factor–β family member that regulates the fate, proliferation, and patterning of its cells [reviewed in (*1*, *2*)]. The disc expresses Dpp in a stripe of cells alongside the anterior/posterior (A/P) compartment border, and Dpp disperses across the disc to form exponential concentration gradients to either side that regulate target genes in adjacent cells in a concentration-dependent manner. Whereas the dispersion of Dpp across the disc and the functional importance of its concentration gradients are well established, the mechanism that moves Dpp from producing to target cells is not.

We tested the model that morphogens are transported along specialized signaling filopodia (cytonemes) that receive protein released at sites where producing and receiving cells contact each other (*3*). Cytonemes are on both the apical and the basal surfaces of wing disc cells. Apical cytonemes that orient toward Dpp-producing disc cells contain the Dpp receptor Thickveins (Tkv), and cytoneme shape, orientation, and distribution depend on the expression of Dpp (*3*–*5*). There are basal cytonemes that contain Hedgehog (Hh) and the Interference Hedgehog (Ihog) proteins (*6*, *7*). Hh is also present in short cytonemes that extend from Hh-producing cells in the female germline stem cell niche (*8*). These correlations are suggestive, but they do not establish that cytonemes mediate transfers of signaling proteins from producing to target cells or that such transfers, if they occur, are required for signaling.

Cardiovascular Research Institute, University of California, San Francisco, CA 94158, USA.

*Corresponding author. E-mail: tkornberg@ucsf.edu

The wing disc has associated trachea whose development depends in part on signaling from the disc (*9*). Larval trachea form an interconnected network of oxygen-carrying tubes; one, the transverse connective (TC) of Tr2 is bound to the wing disc (Fig. 1A). During the third larval instar (L3), Branchless [the fly fibroblast growth factor (FGF)] produced by a group of disc cells induces a new branch, the air sac primordium (ASP), to grow from the TC (*9*). The ASP is juxtaposed to the basal surface of the wing disc columnar epithelium; it is a monolayered epithelial tube. At the late L3 stage, the ASP has many cytonemes that extend toward the disc (Fig. 1B). Cells at the ASP tip extend long (≥30 μm) cytonemes that contain the FGF receptor (FGFR) Breathless and appear to touch FGF-producing disc cells. The presence and orientation of these cytonemes are dependent on FGF (*5*, *9*). The late L3 ASP also has shorter cytonemes that contain Tkv and that extend from its lateral flank toward Dpp-expressing disc cells (*5*).

In the wing disc, Dpp induces several changes in responding cells: induction of *Daughters against Dpp* (*Dad*) expression (*10*), increased phosphorylation of the Mothers against dpp protein (pMad) (*11*), and decreased *tkv* expression (*11*). Dpp signal transduction does not change expression of the other Dpp receptor subunit Punt (Put). Elevated *Dad* expression, increased pMad expression, and decreased *tkv* expression were observed in the ASP, presumably due to Dpp signaling, and their abundance indicates that Dpp signal transduction is probably higher in the lower layer cells that face the disc epithelium than in the cells that are further away in the upper layer (Fig. 1, C and D; fig. S1, A to D; and table S1). Put expression was uniform. Dpp expression was not detected in the TC or ASP (Fig. 1A and fig. S1E). These results show that Dpp signal transduction in the ASP inversely correlates with distance from Dpp-expressing cells in the wing disc.

Overexpressing dominant negative forms of Tkv or Put, or Dad (which negatively regulates Dpp signaling), in the trachea generated abnormally shaped ASPs and reduced Dpp signaling in the ASP (Fig. 1E; fig. S1, F to H; and tables S2 and S3). Expression of *dppRNAi* in the wing disc generated similar phenotypes and reduced Dpp signaling (Fig. 1F and table S3), indicating that the wing disc is the source of the Dpp that activates signal transduction in the ASP, and establishing that Dpp signaling from the disc is essential for normal ASP development.

ASP Cytonemes Receive Dpp from the Wing Disc

To investigate the basis for disc-dependent Dpp signaling in the ASP, we overexpressed an isoform of Dpp coupled to green fluorescent protein (Dpp:GFP) (*12*, *13*) in the disc *dpp* expression domain (*14*). GFP fluorescence was detected both in the Dpp-expressing disc cells and in the ASP. Amounts of Dpp:GFP in the ASP were highest in the medial region of the ASP nearest the Dpp-expressing disc cells and in the lower layer (Figs. 1D and 2A and table S1), showing that Dpp:GFP produced by the wing disc distributed to the ASP in a manner that correlates with amounts of Dpp signal transduction (Fig. 1C and fig. S1, A to D). To examine the subcellular localization of marked Dpp in the ASP, we expressed Dpp coupled to mCherry fluorescent protein (Dpp:Cherry) (*5*) in the disc *dpp* expression domain, and Dpp signaling was monitored in unfixed, "live" preparations with a transgene that expresses nuclear-localized GFP (nGFP) under *Dad* control. Dpp:Cherry puncta were observed in multiple optical sections of ASP cells with strongly marked GFP-positive nuclei (Fig. 2, B and B′); the presence of Dpp:Cherry puncta at apical positions (Fig. 2B″) indicated that Dpp:Cherry had likely been taken up from the disc by these ASP cells.

Whereas most tip cytonemes extended toward the region of the disc that expresses FGF (*5*, *9*), some TC and lateral cytonemes extended toward Dpp-expressing disc cells (Fig. 1B). Expression of Tkv:GFP marked puncta in these cytonemes (Fig. 2C). To determine whether activated Tkv was present in cytonemes, we overexpressed a variant of Tkv (TIPF) that fluoresces only in the phosphorylated state and that has been used to monitor receptor activation for Dpp or bone morphogenetic protein (BMP) signaling (*15*). ASP cytonemes with bright fluorescent puncta were present under conditions of TIPF overexpression (Fig. 2D). Expression of Tkv:Cherry and TIPF together in the TC and ASP generated puncta with both green (TIPF) and red (Tkv:Cherry) fluorescence, indicating that Tkv in these puncta had been activated (Fig. 2, E and E′). We propose that the presence of activated Tkv indicates that these cytonemes had received Dpp. The presence of

cytonemes with only red fluorescence suggests that not all the cytonemes had received Dpp.

To further validate and characterize Dpp reception, ASPs were marked with either CD8:Cherry (mCherry fused to the extracellular and transmembrane domains of the mouse lymphocyte protein CD8), Tkv:Cherry, or FGFR:Cherry, and Dpp:GFP was expressed in the disc *dpp* domain in a pulse during L3 (*14*). The ASP grows from the TC on the anterior side of the disc and extends posteriorly across the stripe of Dpp-expressing cells by late L3 (*9*) (Fig. 3A). At the "mid" or "late" stages, animals that expressed CD8:Cherry and Dpp:GFP had long ASP tip cytonemes marked with Cherry fluorescence that oriented toward FGF-expressing disc cells. These cytonemes had no apparent GFP fluorescence (Fig. 3B). Lateral ASP cytonemes that projected toward Dpp-expressing disc cells were also visible. These lateral cytonemes had both Cherry and GFP fluorescence (Fig. 3, B and B′), indicating that Dpp:GFP had been received by these cytonemes. Dpp:GFP in puncta "free" from either cells or cytonemes was not detected.

ASPs marked with Tkv:Cherry provided evidence that Dpp transport by cytonemes is associated with its receptor. Late-stage ASPs that expressed Tkv:Cherry had Dpp:GFP present in their medial region and in lateral cytonemes that extended from these cells, but there were few Tkv:Cherry-marked tip cytonemes, and Dpp:GFP was present in much lower amounts in the distal ASP cells (Fig. 3C). Some of the Dpp:GFPs present in the medial ASP cells were associated with Tkv puncta (Fig. 3C′). These images show that Dpp:GFP appears to move from the disc and are taken up by tracheal cells.

In mid-stage ASPs that expressed FGFR:Cherry and whose tip had not grown beyond the Dpp-expressing zone of the disc, FGFR:Cherry-marked tip cytonemes extended over Dpp-expressing disc cells toward the cells that expressed FGF (Fig. 3D). No Dpp:GFP puncta localized with the FGFR:Cherry-marked cytonemes. The absence of Dpp:GFP in the FGFR:Cherry-containing tip cytonemes is consistent with the localization of the FGFR and Tkv receptors to different cytonemes (*5*) and suggests that FGF and Dpp reception may be receptor-dependent and specific for cytonemes that contain FGFR or Tkv, respectively.

To better understand cytoneme-mediated movement of Dpp, we analyzed "early"- and mid-stage preparations that had Tkv:Cherry expressed in the trachea and Dpp:GFP expressed in the disc. Dpp source cells are distal to the ASP at these stages. Long, Tkv:Cherry-marked cytonemes extended toward Dpp-expressing disc cells (Fig. 3, E and F). These cytonemes contained motile puncta (movie S1). Some cytonemes had both Tkv:Cherry and Dpp:GFP fluorescence and had brightly fluorescent ends that localized with Dpp:GFP; these images suggest that these cytonemes contact Dpp-expressing disc cells. Not all cytonemes had both Tkv:Cherry and Dpp:GFP, suggesting that some, but not all, cytonemes had received Dpp:GFP. These images are consistent with the patterns of TIPF fluorescence (Fig. 2E). The presence of Dpp:GFP in tracheal cytonemes and the apparent contacts of cytonemes with Dpp-producing disc cells suggest that the Dpp:GFP may move from the disc to the tracheal cells by direct transfer at sites of cytoneme contact.

Cytonemes Synapse with Wing Disc Cells

The cytoneme model of signaling protein dispersion posits that distant cells contact directly despite their physical separation. To probe the apparent contacts at higher resolution, we adapted the GRASP (GFP Reconstitution Across Synaptic Partner) technique, which was developed to image membrane contacts at neuronal synapses (*16*, *17*). We expressed CD4:GFP$^{1–10}$ (a fragment of GFP that includes 10 strands of the GFP β-barrel photocenter fused as an extracellular postscript to the transmembrane domain of the mouse lymphocyte protein CD4) and CD4:GFP^{11} (a fragment that includes the 11th strand of the GFP β-barrel). To image cytoneme contacts, the two parts of GFP were expressed separately in tracheal cells and in either FGF- or Dpp-expressing disc cells. These nonfluorescent GFP fragments generated fluorescence that localized specifically at the disc cells that expressed either FGF or Dpp (Fig. 4, A to C). Expression of mCherry-CAAX (CAAX is a plasma membrane–targeting motif) in the disc *dpp* domain revealed that GRASP fluorescence correlates with *dpp*-expressing cells (Fig. 4C). Fluorescence was separated from the ASP cells by up to 40 μm (Fig. 4, A and B), the approximate length of the longest cytonemes that projected from the ASP toward disc cells, indicating that ASP and disc cells synapse even when separated. GFP fluorescence was not observed in animals that expressed only one of the fragments.

To show that the GRASP fluorescence was associated with cytoneme contacts, cytonemes

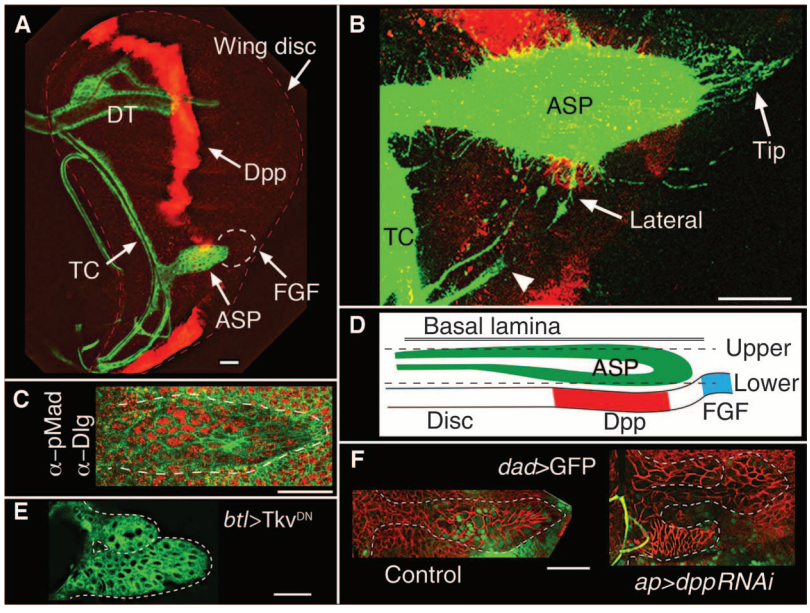

Fig. 1. Dpp produced in the wing disc signals to disc-associated tracheal cells. (**A**) Projection image of a third instar wing disc (outlined with dashed red line) showing disc-associated trachea (marked with green; membrane-tethered GFP) and Dpp-expressing disc cells (red, marked by antibody against LacZ that was expressed in the *dpp* domain). TC, DT (dorsal trunk), and ASP are labeled. Dotted circle indicates area of disc that expresses FGF. (**B**) Expression of CD8:RFP marks *dpp*-expressing disc cells (red); expression of CD8:GFP in trachea (*lexO*-CD8:GFP, *UAS*-CD8:RFP/+; *btl-LexA*/+; *dpp*-Gal4/+) marks cytonemes extending from ASP tip, from the lateral, medial region of the ASP, and from the TC (arrowhead), showing that some ASP and TC cytonemes orient toward Dpp-expressing cells. This plane of focus does not detect all *dpp*-expressing cells due to folds in the disc near the A/P organizer, but it did detect many *dpp*-expressing anterior cells that are in the plane of focus as "scattered" in the A compartment region between the ASP and TC. (**C**) Staining an ASP with antibody to pMAD (red) to show Dpp signaling in the medial region. Antibody to Dlg (discs large, green) marks cell outlines in ASP (bounded by white dashed line) and discs. (**D**) Cartoon of a sagittal ASP section depicting the position of the disc epithelium and basal lamina relative to the ASP in the late L3; dashed lines represent approximate locations of the upper and lower optical sections in all figures. (**E**) Overexpression of Tkv^{DN} in trachea (*btl*-Gal4) generated bifurcated, abnormally shaped ASPs. (**F**) *dppRNAi* expression in the dorsal compartment of the disc (*ap*-Gal4 *tub*-Gal80^{ts}) reduced *Dad* expression (*Dad*-nlsGFP, green) in disc-associated trachea (right panel) compared to control (*ap*-Gal4 *tub*-Gal80^{ts} *Dad*-nlsGFP) ASP (left panel); abnormal ASP growths are indicated by white dotted lines; cells are marked with α-Dlg staining (red); and both panels show lower layer of ASP. Orientation of discs in all figures: anterior, left; dorsal, down. Conditions of Gal80^{ts} inactivation for (E) and (F) are described in table S1 (*14*). Scale bars, 30 μm.

were marked independently of the GRASP GFP fragments by expression of mCherry-CAAX or Tkv:Cherry. Fluorescence of reconstituted GFP was mostly at or near cytoneme tips that contacted source cells (Fig. 4, A′ and B′). Tkv:Cherry fluorescence had a punctal distribution in these cytonemes and was also present at contact sites (Fig. 4B′). An estimate of the size of the CD4 domains (diameter, ~65 Å) (*18*, *19*) and of the linkers that join CD4 to the GFP fragments suggests that the apposition of a cytoneme tip with a target cell at a synapse is less than 20 nm. This distance is comparable to neuronal and immune synapses, and because GFP photocenter maturation is not instantaneous (*20*), the GRASP fluorescence indicates that cytonemes can make relatively stable contacts with target cells.

The proximity of the tubular ASP and the disc varies along the ASP proximodistal axis (1.5 to 10 μm), and the anatomies of the two epithelia are complex (Fig. 4, D and D″). The ASP cells that overlie Dpp-expressing disc cells are in close apposition, yet in this region, cytonemes emanated from both the ASP (Fig. 4E) and the disc (Fig. 4F). The ASP cytonemes in this region were short (≤10 μm); the disc cytonemes were as long as 30 μm, and many had bright bulbous tips at apparent points of contact with ASP cells. GRASP marked the contacts between the lower layer of the ASP and the disc (Fig. 4G), but did not resolve the relative contribution of the ASP and disc cytonemes.

In the wing pouch primordium of the wing disc, Dpp-dependent cytonemes on the apical cell surfaces orient toward the stripe of Dpp-expressing cells at the A/P developmental organizer and may ferry Dpp from the A/P organizer to cells as far away as the disc flanks (*3*–*5*). We applied GRASP to image contacts between the wing disc A/P organizer and flank cells by expressing the GFP fragments at the A/P organizer and in flank cells (Fig. 4H). In these discs, GFP fluorescence was observed in the region of the organizer (Fig. 4H′), in contrast to discs that expressed only one of the complementing fragments (Fig. 4H″). This pattern of GFP reconstitution suggests that cytonemes may extend from the cells at the disc flanks to synapse with cells of the A/P organizer.

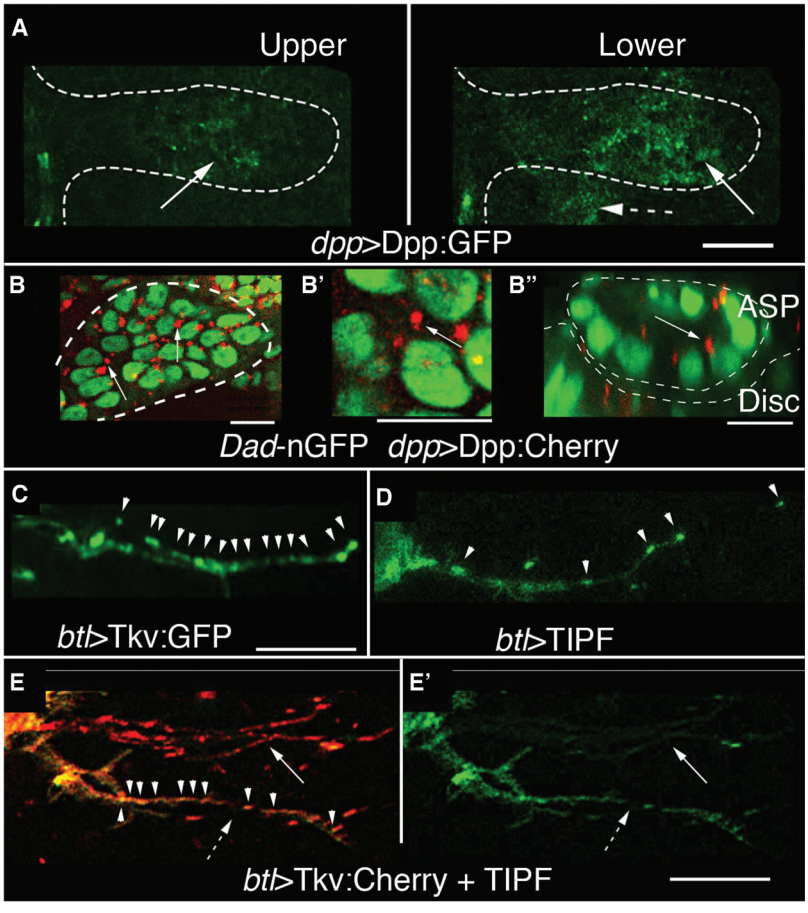

Fig. 2. The ASP takes up Dpp, and ASP cytonemes contain activated Tkv receptor. (**A**) Dpp:GFP expressed in the disc *dpp* domain (*dpp*-LexA *lexO*-Dpp:GFP, dashed arrow) is present (arrows) in the upper and lower ASP layers in this unfixed preparation. ASP is outlined by white dotted lines. (**B** to **B″**) Dpp:Cherry expressed in the disc *dpp* domain (*dpp*-Gal4/*UAS*-Dpp:Cherry, *Dad*-nGFP/*tub*-Gal80^{ts}) was detected as intracellular puncta (arrows) in ASP cells that also induce *Dad* expression. ASP outline is marked by white line [(B) and (B′), sagittal sections; (B″), transverse section]. (**C**) Expression of Tkv:GFP (*btl*-Gal4 *UAS*-Tkv:GFP) marks puncta (arrowheads) in ASP cytoneme. (**D**) Expression of TIPF (*btl*-Gal4 *UAS*-TIPF) marks puncta in ASP cytoneme. (**E** and **E′**) TIPF (green) and Tkv:Cherry fluorescence (*btl*-Gal4/*UAS*-Tkv:Cherry; *tub*-Gal80^{ts}/*UAS*-TIPF) colocalizes (arrowheads) in puncta in some, but not all, ASP cytonemes. Arrow, cytoneme with Tkv:Cherry only; dashed arrow, cytoneme with both TIPF and Tkv:Cherry; left panel, merge; right panel, TIPF only. Gal80^{ts} inactivation for (B) and (E) was for 6 to 8 hours in mid L3, followed by incubation at 25°C for 6 to 12 hours. Scale bars, 10 μm, except for (A), 30 μm.

Dpp Signaling in the ASP Requires Cytoneme-Mediated Transport

We identified four genes that are required for ASP morphogenesis and for cytoneme function: *diaphanous* (*dia*), *shibire* (*shi*), *neuroglian* (*nrg*), and *capricious* (*caps*). Mutant loss-of-function conditions were induced selectively in trachea during the L3 stage (*14*), and mutant ASPs were abnormal or duplicated at variable expressivity and penetrance (table S2 and fig. S1); we show and describe ASPs that were most normal in appearance. Wing discs in these experiments were not mutant, and wing disc development appeared normal.

The formin Dia is an actin nucleation factor (*21*) whose activated form localizes to the tips of filopodia (*22*). When Dia:GFP and activated Dia:GFP (*23*) were expressed in the ASP, Dia:GFP was mostly in the cell body and was present at low levels in cytonemes, but activated Dia:GFP was prominent in most cytonemes and localized to cytonemes tips (Fig. 5A). The distribution of activated Dia indicates that cytoneme tips may be sites of actin nucleation. To examine the role of Dia, we expressed *diaRNAi* in the ASP during the L3 stage. In >85% of the animals (n = 26), growth of the ASP was decreased and ASP morphogenesis was abnormal (for example, fig. S1J). The number of cytonemes was also decreased, and many of the cytonemes that extended from mutant ASPs were abnormally short and had blunt tips (Fig. 5, B to E), and Dpp signal transduction (*Dad*-GFP expression and pMad abundance) was decreased (Fig. 5, F and G, and table S3). We did not detect changes to cell shape, number of dividing cells, or number of dying cells in mutant ASPs (fig. S2, A and B). Thus, Dia appears to be required by the ASP to make cytonemes, and the defective cytonemes that are made in the absence of normal Dia function are incapable of mediating Dpp signaling from the disc.

We expressed a conditional mutant of *shibire* (fruit fly dynamin; *shi*^{ts1}) (*24*) together with CD8:GFP in the trachea and compared α-pMad staining as well as the number and length of cytonemes in ASPs that were isolated from larvae that had been incubated at either permissive (18°C) or restrictive (30°C) temperature (Fig. 5H). Dynamin is a multimer (*25*, *26*), and under nonpermissive conditions, the Shi^{ts1} protein functions as a dominant negative (*24*). Control larvae subjected to 3 hours at 30°C did not change the

number of "short" (<25 μm) or "long" (>25 μm) ASP cytonemes (~4.4 and ~4.9% reduction, respectively) or reduce amounts of pMad (~7%). However, shi^{ts1} larvae subjected to 30°C had decreased cytoneme numbers and pMad abundance (Fig. 5I and tables S3 and S4). The number of long cytonemes present after 30 min at 30°C was less than 10% of that in control experiments; numbers of short cytonemes also declined after 30 min at 30°C. Reductions in numbers of short cytonemes and amounts of pMad became more severe over time intervals of up to 3 hours. A 2-hour heat pulse and a 1-hour incubation at 20°C partially restored both long and short cytonemes (*14*), but the ASP morphology was not normal. Indeed, duplicated, abnormally shaped ASPs were produced when a 24-hour incubation at 20°C followed a 1-hour heat pulse (fig. S1I). Adults that developed at 20°C after a 2-hour heat pulse appeared to have normal morphology, and we did not examine the structure or function of their dorsal air sacs. Thus, Shi inactivation was not lethal in the cells of the ASP; the consequences of Shi inactivation on ASP development were partially reversible; and the effects on cytonemes preceded the reduction in signaling (as revealed by amounts of pMad).

To distinguish whether ASPs that are deficient for *dia* or *shi* expression failed to activate Dpp signal transduction because they did not receive Dpp from the wing disc or were incapable of initiating a response, we expressed Dpp:Cherry directly in ASPs with the *btl-Gal4* driver (*14*). Ectopic Dpp induced pMad in ASPs with reduced *dia* or Shi function (fig. S3, A and B). Thus, conditions that reduced *dia* expression or inactivated Shi did not abrogate the ability of ASP cells to respond to Dpp, and blocking cytoneme-mediated uptake of Dpp from the disc appears to be the most likely cause of the signaling deficits.

Cytonemes were also defective in loss-of-function conditions for *nrg* and *caps*, both of which encode putative cell adhesion transmembrane proteins. Nrg is an L1-type cell adhesion molecule implicated in the development and stability of neuronal synapses (*27*). Although fluorescence of an in-frame protein trap Nrg:GFP fusion protein was detected in the ASP, ASP cytonemes could not be resolved because of "background" expression in the wing disc. However, overexpression of Nrg:GFP in the ASP revealed that Nrg distributes in the ASP cytonemes and concentrates at the cytoneme tips (Fig. 5J). Expression of *nrgRNAi* reduced the number of both tip and lateral cytonemes (Fig. 5K and table S5), abrogated *Dad*-GFP expression and dpERK (diphospho–extracellular signal–regulated kinase) staining (Fig. 5, L and M), and caused growth of abnormal, duplicated ASP lobes (fig. S1K). Expression of *nrgRNAi* had no apparent effect on cell shape or the number or distribution of dividing or dying cells (fig. S2, C and D). Expression of Dpp:Cherry together with *nrgRNAi* in the ASP restored Dpp signaling (fig. S3C), indicating that *nrg*-deficient ASP cells can activate Dpp signal transduction.

We identified *caps* in an enhancer trap screen for genes that are expressed in the ASP (*14*) (fig. S2, E and F). Caps:GFP that was expressed in the trachea was detected in ASP cytonemes and concentrated at the tips (Fig. 6A). Caps and its paralog Tartan (Trn) have extracellular domains containing leucine-rich repeats (LRRs) and contribute partially redundant functions to the for-

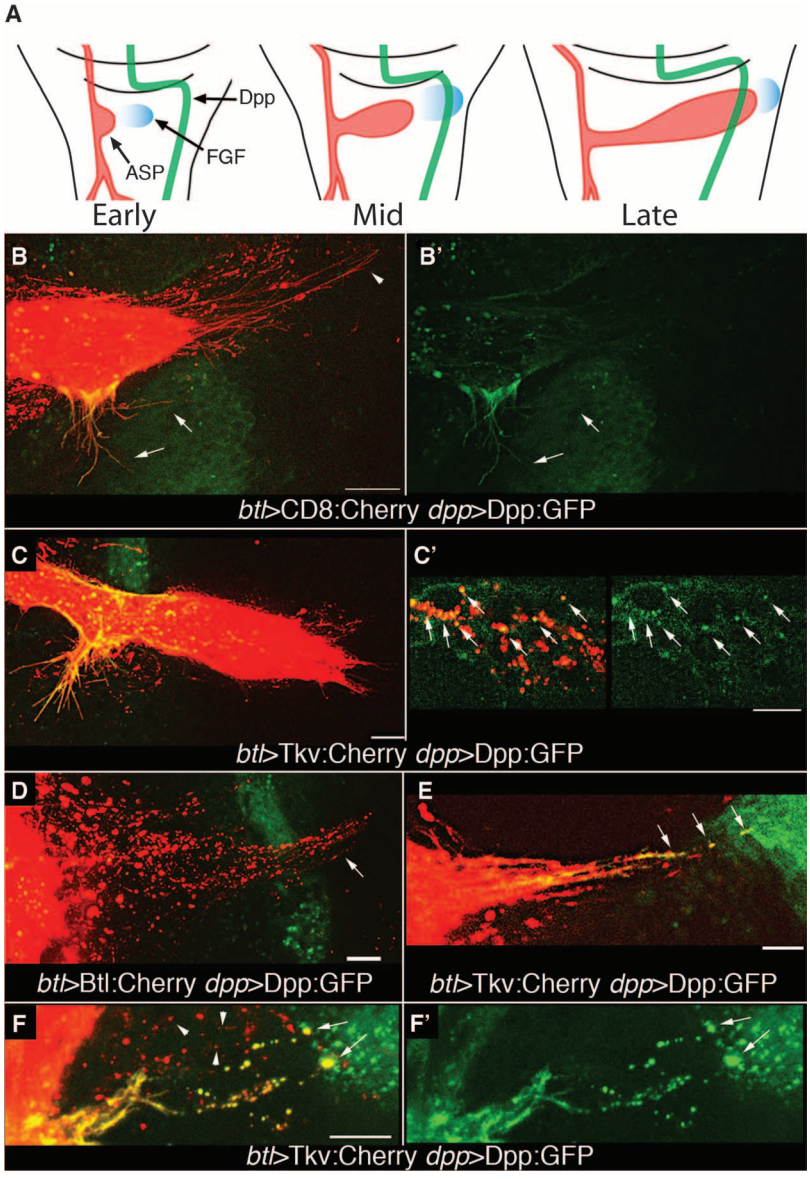

Fig. 3. Tkv-containing cytonemes transport Dpp. (**A**) Drawings of three third instar stages depict growth and development of the ASP (red) relative to wing disc cells expressing Dpp (green) and FGF (blue). (**B** and **B'**) Expression of CD8:Cherry in the ASP and Dpp:GFP in the *dpp* domain of the disc (*btl*-Gal4 *UAS*-CD8:Cherry *dpp*-LHG/*lexO*-Dpp:GFP) marks the ASP and ASP cytonemes (red) and *dpp*-expressing disc cells (green). GFP fluorescence is in the lateral ASP cytonemes (arrows) and in the lower medial region of ASP, but not in the tip of ASP cytonemes (arrowhead). Left panel, merge; right panel, GFP. (**C** and **C'**) Expression of Tkv:Cherry in the ASP and Dpp:GFP in the *dpp* domain of the disc (*btl*-Gal4/*UAS*-Tkv:Cherry; *dpp*-LHG/*lexO*-Dpp:GFP) marks the ASP and lateral ASP cytonemes (red), but few tip cytonemes; lateral Tkv-containing ASP cytonemes and the medial region of the ASP have received Dpp:GFP (green) (C). Dpp:GFP and Tkv:Cherry colocalize in puncta in ASP cells (C′, arrows). (**D**) FGFR:Cherry expressed in ASP and Dpp:GFP in the *dpp* domain of the disc (*btl*-Gal4/*UAS*-Btl:Cherry *dpp*-LHG/*lexO*-Dpp:GFP) marks puncta in the ASP tip cytonemes (arrow) that project beyond Dpp-expressing disc cells (green); no localization of FGFR:Cherry with Dpp:GFP was apparent in tip cytonemes. (**E**, **F**, and **F'**) Only cytonemes marked with Tkv:Cherry that appear to contact Dpp:GFP-expressing disc cells (*btl*-Gal4 *UAS*-Tkv:Cherry; *dpp*-LHG/*lexO*-Dpp:GFP) have GFP fluorescence in puncta and at their tips (arrows). Cytonemes that do not appear to make contact do not have GFP fluorescence at their tips or in their Tkv-containing puncta (F, arrowheads) lack GFP fluorescence. (F) merge; (F′) Dpp:GFP. Animals were raised at 18°C to minimize transgene expression and were incubated at 22° to 25°C for 12 to 16 hours before analysis. Scale bars, 10 μm.

mation of compartment boundaries of the wing disc (*28*). *caps* mutants do not mediate selection of synaptic partners normally (*29*–*32*), and Caps protein localizes at filopodia tips during partner recognition and synapse stabilization (*30*). We observed similar types of effects on ASP cytonemes.

Lack of *caps* function also led to abnormal ASP development. Expression of *capsRNAi*, *trnRNAi*, or a dominant negative Caps mutant ($Caps^{DN}$) that localizes similarly to wild-type Caps in synapses and decreases synaptic contacts (*30*, *32*) reduced Dpp signaling and yielded abnormal ASPs (*14*) (Fig. 6B; fig. S1, L to N; and tables S2 and S3). Phenotypes were more extreme in a heterozygous *caps trn* double-mutant background. Expression of $Caps^{DN}$ did not cause detectable changes to cell polarity, cell morphology, mitotic activity, or cell viability (fig. S2, G and H).

$Caps^{DN}$ reduced amounts of dpERK (Fig. 6C), indicating that *caps* function was also required for FGF signaling. Evidence that signal transduction per se was not abrogated in ASP cells that lack *caps* function was obtained by overexpressing FGF ubiquitously. Heat shock–induced expression of FGF or expression of Dpp:Cherry in the ASP increased amounts of dpERK or pMad, respectively, throughout the ASP, attenuating the effects of $Caps^{DN}$ (fig. S3D). These experiments show that Dpp and FGF proteins that are produced by the disc (Fig. 1) (*9*) require *caps* function in the ASP to activate signal transduction in ASP cells, and show that mutant ASP cells that cannot receive FGF and Dpp from the disc are competent for signal transduction.

The presence of Caps:GFP in the tips of cytonemes (Fig. 6A), the role of Caps at neuronal synapses (*30*), the fact that cytonemes make contact with Dpp-producing cells (Fig. 4, B, C, and G) and receive Dpp at apparent points of contact (Fig. 3, E and F), and the essential role of *caps* for Dpp signaling suggest that Caps may be required for cytonemes to establish functional contacts for Dpp exchange. However, the number and distribution of ASP cytonemes did not change under *caps* loss-of-function conditions (fig. S2I), indicating that the ASP cells do not require Caps to make cytonemes. In contrast, the contacts that ASP cytonemes made with Dpp-expressing disc cells required *caps*. We monitored these contacts with GRASP fluorescence: GFP fluorescence at the interface of Dpp-expressing disc cells and the lower layer of the ASP, and at cytoneme contacts of the lateral ASP and TC was reduced when $Caps^{DN}$ was expressed in the trachea (Figs. 1D; 4, C and D; and 6, D and E). In addition, $Caps^{DN}$ reduced uptake of Dpp:GFP from the disc (Fig. 6F), suggesting that although ASP cells make cytonemes in the absence of

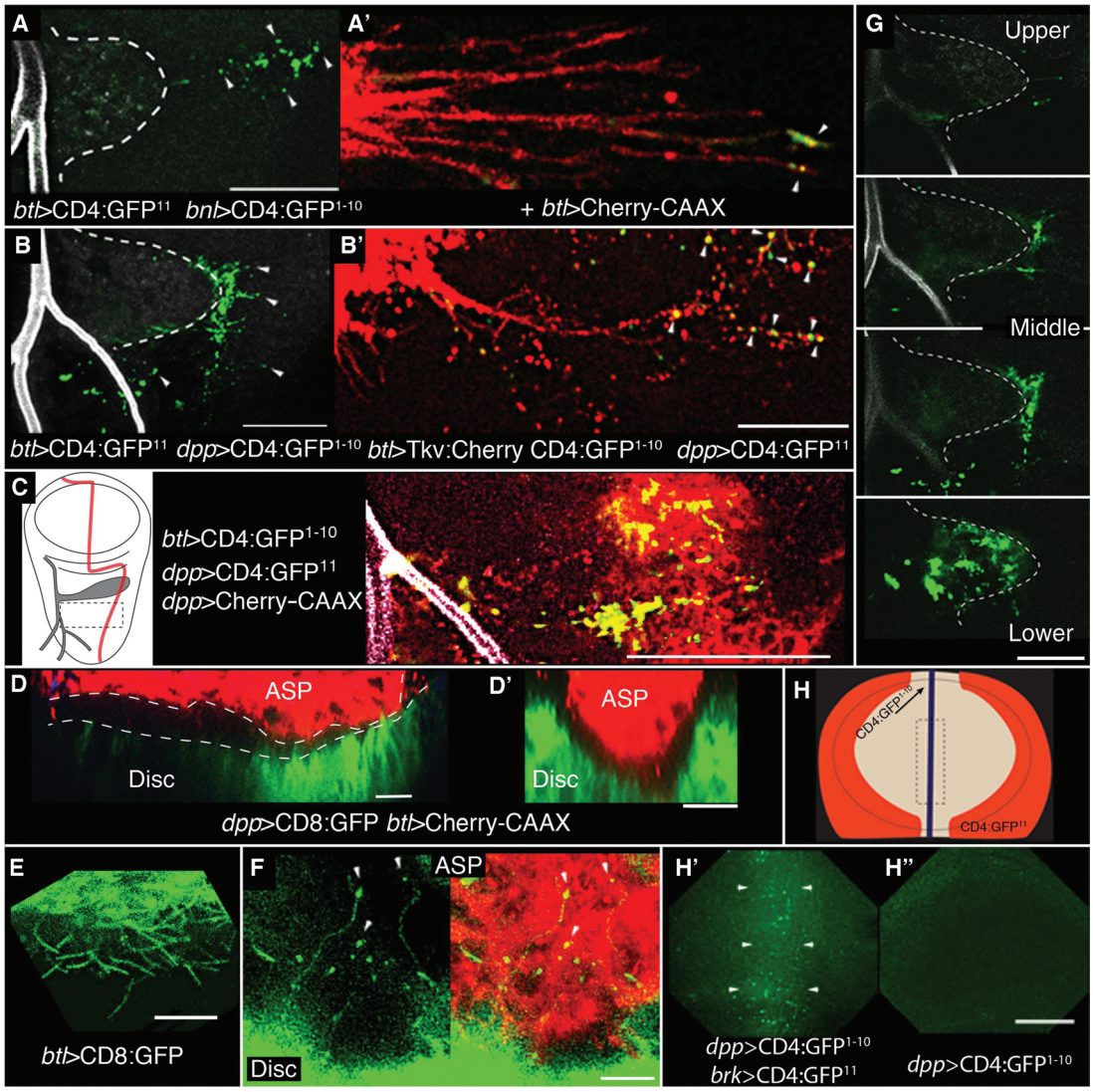

Fig. 4. Tracheal cytonemes contact Dpp- and FGF-expressing disc cells. (**A**, **A′**, **B**, and **B′**) Green fluorescence (arrowheads) from reconstituted GFP (GRASP) due to contact between ASP cytonemes and disc shown in projection images composed of several "upper" to mid optical sections. ASP (dashed white line), disc, and TC lumen were imaged at 405 nm for background fluorescence (gray). Normal *dpp* expression includes cells anterior to the stripe at the A/P compartment border (see Fig. 1, A and B). Marking cytonemes with Cherry-CAAX (A′) or Tkv:Cherry (B′) showed that GRASP fluorescence was cytoneme-associated (arrowheads). (**C**) Left panel: drawing of third instar wing disc depicting Dpp-expressing cells (red) and ASP and TC (gray). Right panel: region outlined by dashed lines in left panel for GRASP fluorescence (green) at the basal surface of *dpp*-expressing disc cells (red). (**D** and **D′**) Sagittal (D) and transverse (D′) sections in the mid-region of ASP show the spatial relationship of the ASP (red) lower layer to *dpp*-expressing disc cells (green, *dpp*-CD8:GFP; red, *btl*-Cherry-CAAX). (**E**) CD8:GFP expressed in the ASP marks cytonemes emanating from the lower aspect of the ASP; they orient toward the disc. (**F**) CD8:GFP expressed in the disc marks cytonemes that extend toward and appear to contact (arrowheads) ASP cells marked with Cherry:CAAX (*btl*-Cherry:CAAX *dpp*-CD8:GFP). (**G**) GFP reconstitution in four optical sections of (B) from the upper layer, from the two middle layers, and from the interface between lower layer and disc. (**H**) Drawing of the wing pouch region of a wing disc showing the stripe of *dpp* expression at the organizer (purple) and the flanking regions that express *brinker* (*brk*, orange). Box with dashed line indicates region imaged in (H′) and (H″). (**H′**) Reconstituted GFP (arrowheads) in the organizer region in disc with expression of the GFP fragments in the *brk* and *dpp* domains. (**H″**) Control with $CD4:GFP^{1–10}$ expression in the *dpp* domain only. Scale bars, 30 μm, except for (A′), (B′), (E), and (F), 10 μm.

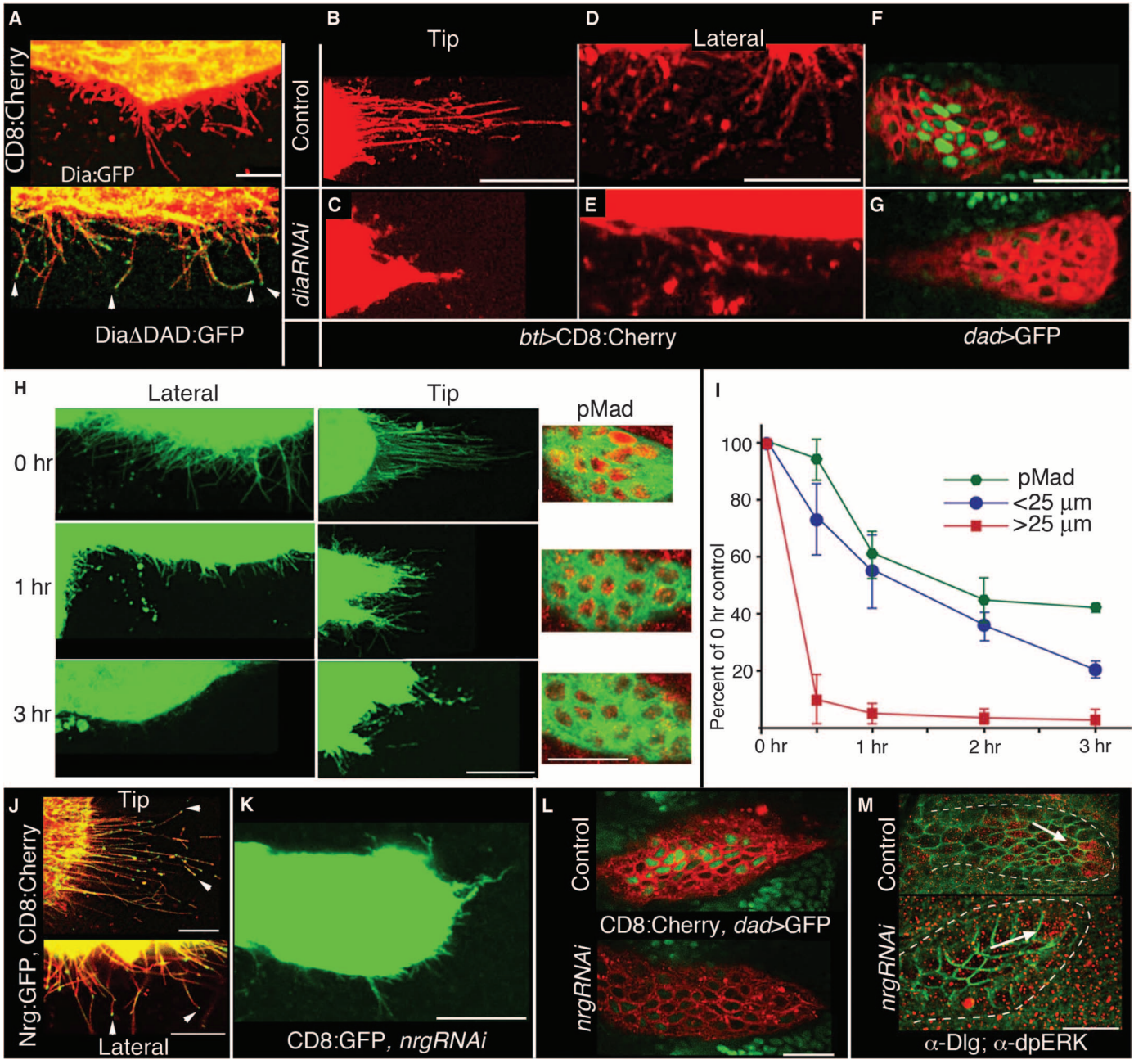

Fig. 5. ASP cytonemes require *dia* and Shi and *nrg*. (**A**) In the ASP, localization of Dia:GFP is predominantly in the cell bodies; activated Dia (DiaΔDad:GFP) localizes to cytoneme tips (*btl*-Gal4, *UAS*-CD8:Cherry/+; *tub*-Gal80^{ts}/*UAS*-Dia:GFP, or *UAS*-DiaΔDad:GFP). (**B** to **G**) Expression of *diaRNAi* shortened lateral and tip of ASP cytonemes (*btl*-Gal4, *UAS*-CD8:Cherry/*tub*-Gal80^{ts}; *Dad*-GFP/*UAS-diaRNAi*), and reduced expression of *Dad*-GFP. Control genotype: *btl*-Gal4, *UAS*-CD8:Cherry/*tub*-Gal80^{ts}; *Dad*-GFP/+. (**H** and **I**) Late third instar larvae that coexpressed *sh*^{ts1} and CD8:GFP (*btl*-Gal4, *UAS*-CD8:GFP, *UAS-shi*^{ts1}) were incubated at 30°C for the indicated times and after dissection; GFP fluorescence and α-pMad staining (red) were imaged in the lower layer of the ASPs (see Fig. 1C). The perimeter of each of the five ASPs was measured, cytonemes were counted (I) around the perimeter in about 35 to 40 optical sections, and the length of each cytoneme was measured. Graph (I) shows the average percentage change to the number of ASP cytonemes per micrometer perimeter in the length ranges of <25 μm (blue) and >25 μm (red). Amounts of pMad were determined by measuring the mean fluorescence intensity (555 nm) in four ASPs for each time point for a region of the lower ASP level that contained about 11 cells. (**J**) Nrg:GFP (*btl*-Gal4, *UAS*-CD8:Cherry/*UAS*-Nrg:GFP; *tub*-Gal80^{ts}) localizes to and concentrates at the tips (arrowheads) of ASP cytonemes. (**K**) Late third instar larvae that coexpressed *nrgRNAi* and CD8:GFP (*btl*-Gal4, *UAS*-CD8:GFP/*UAS-nrgRNAi*; *tub*-Gal80^{ts}/+). Lateral and tip cytonemes were stunted and reduced in number. (**L**) Expression of *Dad*-GFP was reduced in a lower ASP layer that expresses *nrgRNAi* (lower panel; *btl*-Gal4, *UAS*-CD8:Cherry/*UAS-nrgRNAi*; *Dad*-GFP/*tub*-Gal80^{ts}) compared to control (upper panel; *btl*-Gal4, *UAS*-CD8:Cherry/+; *Dad*-GFP/*tub*-Gal80^{ts}). (**M**) dpERK staining (arrows, red) is partially reduced in ASP that expresses *nrgRNAi* (lower panel, *btl*-Gal4/*UAS-nrgRNAi*; *tub*-Gal80^{ts}/+; upper panel, control *btl*-Gal4/*UAS-nrgRNAi*; *tub*-Gal80^{ts}/+); outline of ASP marked with dashed line and α-Dlg (green) outlines cells. Conditions for conditional inactivation are described in table S2 (*14*). Scale bars, 25 μm.

Caps function, Caps-deficient cytonemes that do not make stable synapses do not transfer Dpp from producing to recipient cells.

Discussion

This study revealed an essential role for cytoneme-based transport of signaling proteins in long-distance paracrine signaling. This mechanism involves contact-dependent transfer of signaling proteins from producing to responding cells, and although we studied signaling between two epithelial tissues in a *Drosophila* larva, evidence from other systems supports a general role for cytonemes in paracrine signaling.

Studies of cells in culture indicate that filopodia receive and transport signaling proteins that are taken up from culture medium. In experiments with human adenocarcinoma cells, uptake of epidermal growth factor (EGF) protein from the culture medium led to retrograde transport by filopodia along with activated EGF receptor (EGFR) and was sensitive to cytochalasin D, a disruptor of F-actin (*33*). Actin-based cytonemes that carry FGFR-rich puncta and that are dependent on the small GTPase (guanosine triphosphatase) RhoD are present in cultured mouse mesenchymal cells (*34*).

Some characteristics of Dpp signaling in the ASP are consistent with these cell culture experiments. Dpp that was taken up by an ASP cell was present in motile puncta that translocated along the ASP cell's cytoneme, and some puncta in the ASP cytonemes contained both Dpp and its receptor (Figs. 2, C and D; 3, C, E, and F; and 4B′). *Drosophila* cytonemes are actin-based (*3*). However, in contrast to cultured cells, signaling in the ASP did not appear to involve uptake of signaling proteins from the extracellular milieu, but was dependent on synaptic contact between the tip of a cytoneme that extended from a responding ASP cell and the cell body of a Dpp-expressing disc cell. This signaling mechanism appears to involve specific dynamic interactions between signaling and responding cells.

ASP cells express both the Tkv Dpp receptor and FGFR, and segregate these receptors to puncta in distinct cytonemes (*5*). At the early L3 stage, the ASP is small and does not extend across the disc, and both the Dpp- and FGF-expressing disc cells are distal to its tip. Both Tkv- and FGFR-containing cytonemes extended distally from the tip (*5*). The FGFR-containing cytonemes extended beyond the Dpp-expressing cells and did not take up Dpp (Fig. 3D). At later L3 stages, the ASP has grown across the disc, and although the FGF-expressing disc cells are distal to it, the Dpp-expressing disc cells lie under its medial region. In these ASPs, the Tkv-containing cytonemes emanated from the medial region and reached as much as 40 μm to pick up Dpp from disc cells (Fig. 3, B and C). Thus, in the ASP, spatially restricted Dpp signal transduction (Fig. 1, C and F) and uptake (Figs. 2A and 3, B and C) were associated with cytonemes whose orientation and composition appeared to be specific for Dpp.

The dynamism of this signaling system may be inferred from steady-state images. The distribution and orientation of cytonemes change if expression of signaling protein is compromised

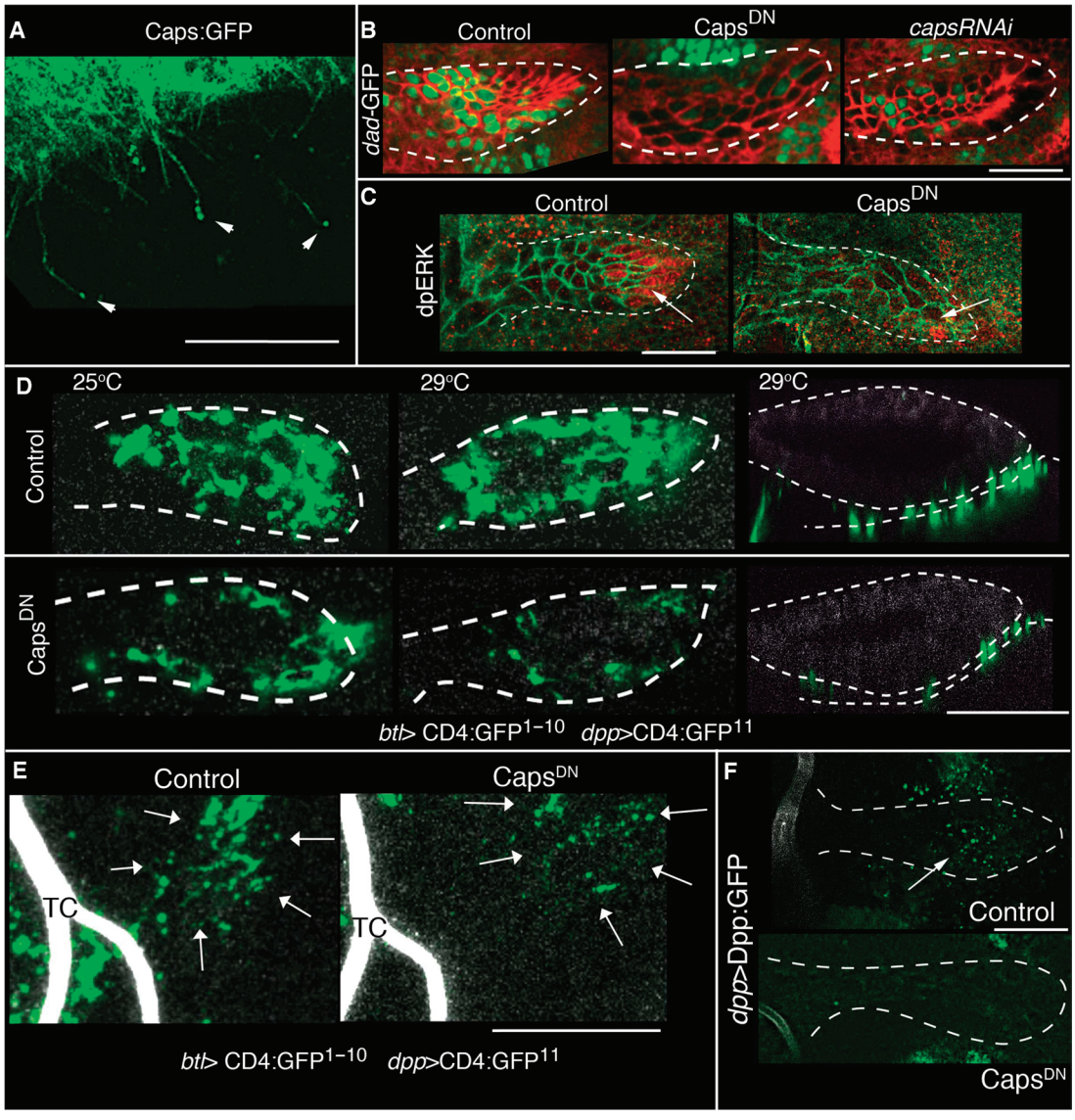

Fig. 6. ASP cytonemes require Caps. (**A**) Caps:GFP (*btl*-Gal4 *UAS*-Caps:GFP, *tub*-Gal80^{ts}) localizes to and concentrates at the tips (arrowheads) of cytonemes. Conditions for conditional inactivation are described in (*14*). (**B**) ASP expression (*btl*-Gal4) of Caps^{DN} (middle panel) and *capsRNAi* (right panel) reduced *Dad* expression in the ASP (*Dad*-nlsGFP; green); left panel, control. (**C**) ASP expression (*btl*-Gal4) of Caps^{DN} reduced dpERK staining (red) at the tip of ASP. Cells are marked with α-Dlg staining [red, (B); green, (C)]. (**D**) Sagittal optical sections at lower level of ASP (left and middle panels) and in coronal sections (right panels) showing that GRASP fluorescence is reduced by expression of Caps^{DN} (at 29°C); Caps^{DN} genotype includes two copies of *UAS*-Caps^{DN}. TC indicates the lumen of the transverse connective. (**E**) Caps^{DN} expression in the TC reduces GRASP fluorescence (arrows) associated with Dpp-expressing disc cells. Genotypes: same as (D). (**F**) Dpp:GFP uptake in ASP (arrow) in the presence (bottom panel) and absence (top panel) of Caps^{DN}. Genotypes: same as (D). In (D) to (F), ASP, disc, and TC are imaged for autofluorescence at 405 nm (gray). Scale bars, 30 μm, except for (A), 10 μm.

and if signaling protein is overexpressed in ectopic locations (*4*, *5*, *9*). These properties suggest that cytonemes are changeable and that their distributions reflect the relative positions of signal-producing and signal-receiving cells. The different distributions of Tkv-containing cytonemes in the temporal sequence described above are consistent with this idea and with a model of cytoneme impermanence. The observation that some ASP cytonemes contain Tkv, make contact with Dpp-producing cells, and take up Dpp, whereas other cytonemes contain Tkv but do not make contact with Dpp-producing cells or take up Dpp (Figs. 2E and 3F), may also suggest that cytoneme contacts may be transient.

Plasticity may be an important attribute of cytonemes that function in a developmental system such as the ASP, in which relations between producing and receiving cells change as the larva develops. Cytonemes may have the capacity to regulate release and uptake of signals and to direct signals to a preselected target. Regulated release may be implied by the absence of Dpp uptake and Dpp signal transduction in ASP mutant conditions that abolish synaptic contacts by ASP cytonemes. In these experiments, the signal-producing cells were not mutant, and the wing discs, which depend on Dpp signaling, developed normally, indicating that the signaling defect was specific to the ASP cells that made defective cytonemes. Because filopodia of cultured cells take up signaling proteins from culture medium and activate signal transduction (*33*), we may assume that ASP cytonemes are similarly capable of taking up signaling protein that their receptors encounter and that the inability of cytoneme-defective cells to take up Dpp or activate signal transduction may indicate that Dpp was not released in the absence of cytoneme contact.

There may be a functional analogy to neuronal signaling. Neurons make asymmetric extensions that send and receive signals, make specific contacts where signal release and uptake are regulated, and require the *diaphanous*, *neuroglian*, *shibire*, and *capricious* genes for contact-mediated signal exchange and signaling. In the developing *Drosophila* retina, Hh moves to the termini of retinal axons, where it signals to postsynaptic laminal neurons in the brain (*35*). Perhaps the strongest precedent is Wingless delivery at developing neuromuscular junctions in the *Drosophila* larva; in this case, Wingless moves to the postsynaptic cell after release in a vesicular form from the presynaptic neuron (*36*). Our studies have been limited to the cytonemes that are made by receiving cells, but in other contexts, cytonemes extend from cells that deliver signaling proteins, such as the Hh-containing cytonemes of the wing disc (*7*) and the cytonemes that extend from cap cells in the female germline stem cell niche (*8*) and that are associated with Notch and EGF signaling (*37*–*40*). Cytonemes that transport Hh across the chick limb bud from Hh-producing cells have also been described (*41*). The widespread presence of cytonemes in many cell types and in many contexts suggests that they may provide a general mechanism to move signaling proteins between nonneuronal cells at sites of direct contact.

Materials and Methods

Drosophila *Stocks*

Transgenes: *btl*-Gal4 (*9*), *ap*-Gal4 [Bloomington Stock Center (BSC)]; *dpp*-Gal4/*CyO*; *HS*-Bnl (*9*); *UAS*-Tkv:GFP (*4*); *UAS*-Dpp:Cherry, *UAS*-CD8:Cherry, *UAS*-CD8:GFP (*5*), *Dad*-nEGFP (III) (*42*), *UAS*-FGFR^{DN} (*43*); *dpp*-LHG/*TM6* (LexA-Gal4 activation domain fusion; III) (*44*), *dpp*-LHG (II; this study), *lexO*-Dpp:GFP/*TM6* and *brk*^{BM14}-LHG (*44*), *btl*-LHG (II and III) (this study), *lexO*-CD4:GFP^{11} (II), *UAS*-CD4:GFP$^{1-10}$ (III) (*17*), *UAS-dppRNAi* (BSC), *UAS-putRNAi* (BSC); *tub*-Gal80^{ts} (II and III; BSC), *UAS*-Dad (II) (BSC), *UAS*-Tkv^{QD}/*TM6B* [activated Tkv (*45*)], *UAS*-Tkv^{DN}, *UAS*-Put^{DN} [ΔGSK, dominant negative forms of Tkv and Put lacking GS and kinase domain (*46*)], *UAS*-TIPF (*15*), *UAS-capsRNAi* [BSC, Vienna Drosophila RNAi Center (VDRC)], *UAS-trnRNAi* [National Institute of Genetics (NIG), BSC], *UAS*-Caps^{DN} (*30*); *UAS*-CD4:GFP^{10} (II; this study), *UAS-diaRNAi* (BSC, NIG), *UAS-shi*^{ts1} (*24*), *lexO*-CherryCAAX [II and III (*44*)]; *UAS*-Dia:GFP (*47*) and *UAS*-DiaΔDad:GFP (*23*); *UAS-nrgRNAi* (II and III) (BSC); *10XUAS*-IVS-mCD8::RFP; *13XlexO*-mCD8::GFP (BSC); *UAS*-Nrg:GFP (II) (*27*).

Insertions and mutations: *Dad*^{j1E4}-LacZ/*TM3*, *tkv*^{k16713}-LacZ/*CyO*, *dpp*^{10638}-LacZ/*CyO*, *put*^{10460}-LacZ/*TM3* (BSC), and Nrg:GFP protein trap line (flytrap line G00305). Conditional inactivation of Dpp was in *dpp*^{4}/*dpp*^{56} L3 larvae for 18 hours at 29°C as described (*4*).

Overexpression

tub-Gal80^{ts} was present to limit expression to the L3 stage. Expression drivers were as follows: *ap*-Gal4 for *dppRNAi*; *btl*-Gal4 for Dad, Tkv^{DN}, Tkv^{QD}, Put^{DN}, *putRNAi*, Caps^{DN}, *capsRNAi*, *trnRNAi*, *diaRNAi*, Dia:GFP, DiaΔDad:GFP, *nrgRNAi*, and Nrg:GFP. Animals were reared at 18°C until L3 and were incubated at 29°C, as indicated in table S2, before dissection. For knockdown under heterozygous mutant background (table S2 and fig. S1M), Caps^{DN} and *capsRNAi* expression was driven by *btl*-Gal4 or by *dpp*>Gal4 in *caps*^{C28fs} *trn*$^{\Delta 17}$ and *caps*$^{65.2}$ *trn*^{S064117} double mutants. At 25°C, Caps^{DN} and *capsRNAi* overexpression is embryonic lethal in the Caps mutant background; animals were therefore reared at 20°C to the L3 stage and were incubated at 25°C for 1 day before dissection.

Ectopic Expression

For fig. S3, A to C, crosses were, for *dia*, *shi*, and *nrg*: *btl*-Gal4, *UAS*-CD8:GFP/+; *tub*-Gal80^{ts}/*UAS-dpp*:Cherry to either *UAS-diaRNAi*, *UAS-shi*^{ts}, or *UAS-nrgRNAi*. Control larvae expressed either *shi*^{ts}, *diaRNAi*, or *nrgRNAi*, but lacked *dpp*:Cherry; experimental larvae had *UAS-dpp*:Cherry. Animals were reared at 18°C to minimize the effects of Dpp overexpression. To express *diaRNAi*, L3 larvae were incubated at 25°C for 5 to 6 hours. Shi^{ts} larvae were treated similarly and were then shifted to 29°C for 1 hour. ASPs in the Shi^{ts} larvae did not grow normally because of temperature sensitivity of *shi*^{ts} at 25°C. *nrgRNAi* induction was for 14 to 18 hours at 29°C. Caps^{DN} larvae (*btl*-Gal4, *UAS*-CD8:GFP/*UAS*-Caps^{DN}; *UAS*-Caps^{DN}/*HS*-Bnl) were reared at 20°C until L3; heat shock induction of Bnl was for 30 min at 37°C followed by 3 hours of incubation at 20°C.

Dual Expression

LexA and Gal4: *10XUAS*-IVS-mCD8::RFP, *13XlexO*-mCD8::GFP flies (BSC) were crossed to *dpp*-Gal4/*SM5*; *btl*-LHG flies to mark Dpp-producing cells in wing disc with RFP (red fluorescent protein) and trachea with GFP. To express either Tkv:Cherry or FGFR:Cherry in trachea simultaneously with Dpp:GFP in the wing disc, *UAS*-Tkv:Cherry/*CyO-Weep*; *dpp*-LHG/*TM6* or *UAS*-FGFR:Cherry/*CyO-Weep*; *dpp*-LHG flies were crossed to *btl*-Gal4; *lexO*-Dpp:GFP/*TM6* flies. To minimize toxic effects, *btl*-Gal4/*UAS*-Tkv:Cherry (or FGFR:Cherry); *lexO*-Dpp:GFP/*dpp-LHG* animals were grown at 18°C until the L2 stage and were shifted to 20°C.

Enhancer Trap Screening

About 500 lines with randomly inserted enhancer trap transposons (gift from E. Heberlein) were screened for tracheal expression (*UAS*-GFP). A line with elevated expression in the ASP was identified; its Gal4 transposon was mapped by ends out sequencing to the first exon of *caps*. Wing disc GFP expression was similar to the expression of *caps* as indicated by in situ hybridization (*28*).

GFP Reconstitution

Genotype for reconstitution between Dpp signaling partners: *dpp*-Gal4/*lexO*-CD4:GFP^{11}; *btl*-LHG/*UAS*-CD4:GFP$^{1-10}$. Genotype for reconstitution between FGF signaling partners: *btl*-LHG/*lexO*-CD4:GFP^{11}; *bnl*-Gal4/*UAS*-CD4:GFP$^{1-10}$. For reconstitution in the wing disc: *dpp*-Gal4/*lexO*-CD4:GFP^{11}; *brk*-LexA/*UAS*-CD4:GFP$^{1-10}$. For reconstitution with marked cytonemes: *btl*-LHG, *lexO*-CherryCAAX/*lexO*-CD4:GFP^{11}; *bnl*-Gal4, *btl*-LHG/*UAS*-CD4:GFP^{10}. For reconstitution with in the presence of marked Tkv: *btl*-Gal4, *dpp*-LHG/*UAS*-Tkv:Cherry; *lexO*-CD4:GFP^{11}, *UAS*-CD4:GFP$^{1-10}$. For reconstitution with marked Dpp source: *btl*-Gal4, *dpp*-LHG/+; *lexO*-Cherry:CAAX/*UAS*-CD4:GFP$^{1-10}$, *lexO*-CD4:GFP^{11}. For reconstitution together with Caps^{DN} overexpression, *btl*-Gal4, *dpp*-lexA; *UAS*-CD4:GFP$^{1-10}$, *lexO*-CD4:GFP^{11} flies were crossed with either *w*$^{-}$(control) or *UAS*-Caps^{DN}. Larvae were reared in room temperature and shifted to 25° or 29°C for 1 day before assay.

shibire *Inactivation*

Larvae [*btl*>Gal4, *UAS*>CD8:GFP, *UAS*>*shi*^{ts1} (*24*)] were raised at 18°C before a single heat shock for 0.5, 1, 2, or 3 hours at 30°C. Larvae were dis-

sected and imaged for ASP cytonemes or were fixed for pMad staining. Rescue after heat shock was by returning larvae to 18°C before dissection and imaging. Control heat shock was with larvae expressing CD8:GFP in trachea (*btl*-Gal4 *UAS*-CD8:GFP) at 30°C for 0 and 3 hours. No significant change in numbers of cytonemes [either <25 μm (4.4 ± 4.7% reduction) or >25 μm (4.7 ± 7.6% increase)] was detected. Rescue after 30°C at 2 hours was at 20°C for 1 hour, followed by dissection and imaging. Increases in numbers of cytonemes [<25 μm (1.9× ± 0.4%, $P = 0.0471$) or >25 μm (11× ± 2.9%, $P = 0.0196$)] were evaluated by the unpaired *t* test.

Quantitation and Statistical Analyses

Cytonemes were counted and measured in z-section stacks of confocal images from five ASPs for each data point and were binned as <25 or >25 μm. Lengths represent measures from each tip along the connecting shaft to the point of its widening base either at the plasma membrane or at the lamellipodia-like protrusion. The size variation between ASPs was normalized by measuring the perimeter of each ASP and then calculating the number of cytonemes per unit length. Values in Fig. 5I are plotted as percentage of the 0-hour time point. pMad levels were quantified by measuring the mean intensity of 555-nm fluorescence in the cells of the lower layer of ASP, subtracting background fluorescence, and normalizing with respect to pMad fluorescence at the A/P border of the same wing disc. Values were plotted as percentage of the 0-hour time point. Statistical significance values were calculated with *t* test or analysis of variance (ANOVA) followed by Tukey honestly significant difference (HSD) test.

Molecular Cloning

btl>LHG: The P[B123] fragment upstream of the *btl* gene (*48*) was amplified from a genomic clone obtained from (*49*), with 5′ primer GGCTCGAGATAATCGCATTCTGACCTCGGTAAAC and 3′ primer GGTCTAGAGGATCGTACCCGTAATCCG, and the product was cloned in *pCASPER4*. The LexA:Gal4H-GAD portion was isolated from the *pDppattB-LHG* plasmid (*44*) and was inserted at the *pCASPER4* Not I site.

Tkv:Cherry: The Not I–Hind III fragment from a Tkv:GFP construct (*4*) was ligated to a mCherry fragment with 5′ Hind III and 3′ Kpn I sites in the presence of *pUAST* that had been digested with Not I and Kpn I. Primers for mCherry amplification: 5′ primer, GCAAGCTTATGGTGAGCAAGGGCGAGGAGG; 3′ primer, AGGTACCTTACTTGTACAGCTCGTCCATGCCGC. Tkv:Cherry and Tkv:GFP are similar in phenotype, activity, and localization in cytonemes.

In Situ Hybridization

RNA in situ hybridization was performed according to (*50*). Digoxigenin (DIG)–labeled antisense probe was generated by transcription from a T7 promoter joined to a 600–base pair fragment of *dpp* complementary DNA (cDNA) amplified with polymerase chain reaction primers: CAAGGAGGCGCTCATCAAG and TTGTAATACGACTCACTATAGGGAGACACCAGCAGTCCGTAGTTGC. Alkaline phosphatase–conjugated α-DIG antibody (Roche) was used to detect the DIG-labeled probe.

Immunohistochemistry

The following antisera were used: α-pMad [from E. Laufer and P. ten Dijke; at 1:2000 (*51*)]; α-dpERK (Sigma; 1:250) and α-apontic [from R. Schuh (*52*)]; and α-discs large (4F3; 1:50), α-DE-cadherin (DECAD2; 1:20), and anti–β-galactosidase (Developmental Studies Hybridoma Bank). dpERK staining was carried out as described (*9*) with antibody obtained from Cell Signaling Technology. Secondary antibodies were conjugated to Alexa Fluor 488, 555, or 647. To assay for cell lethality, α-cleaved caspase-3 (Asp^{175}; Cell Signaling Technology) was used as described (*53*). Cell proliferation was monitored with α-phosphohistone H3 antibody (Ser^{10}; Cell Signaling Technology).

Imaging Techniques

Wing discs were dissected and mounted as described (*5*), except that the second small coverslip was omitted. Images were made with a Leica TCS SPE or TCS SP2 confocal microscope with either 405, 488, 561, or 635 wavelength lasers and with LAS-AF software; or with a custom-built Zeiss spinning disc confocal with electron-multiplying charged-coupled device (EM-CCD) Hamamatsu camera (9100-13) and Volocity 5.5 software; or with a standard Zeiss AxioPlan 2 fluorescence microscope with sensicam CCD camera (Cooke Corporation) and SlideBook 4 acquisition software (Intelligent Imaging Innovations). Patterns of cytonemes were consistent in all three types of systems. Brightfield images were made on a Leica DMR microscope equipped with SPOT CCD camera (Diagnostics Instruments) and SPOT acquisition software. Final images were analyzed and processed with National Institutes of Health (NIH) ImageJ.

References and Notes

1. W. M. Gelbart, The *decapentaplegic* gene: A TGF-β homologue controlling pattern formation in *Drosophila*. *Development* **107** (suppl.), 65–74 (1989). pmid: 2699859
2. O. Wartlick *et al.*, Dynamics of Dpp signaling and proliferation control. *Science* **331**, 1154–1159 (2011). doi: 10.1126/science.1200037; pmid: 21385708
3. F. A. Ramírez-Weber, T. B. Kornberg, Cytonemes: Cellular processes that project to the principal signaling center in *Drosophila* imaginal discs. *Cell* **97**, 599–607 (1999). doi: 10.1016/S0092-8674(00)80771-0; pmid: 10367889
4. F. Hsiung, F. A. Ramirez-Weber, D. D. Iwaki, T. B. Kornberg, Dependence of *Drosophila* wing imaginal disc cytonemes on Decapentaplegic. *Nature* **437**, 560–563 (2005). doi: 10.1038/nature03951; pmid: 16177792
5. S. Roy, F. Hsiung, T. B. Kornberg, Specificity of *Drosophila* cytonemes for distinct signaling pathways. *Science* **332**, 354–358 (2011). doi: 10.1126/science.1198949; pmid: 21493861
6. A. Bilioni *et al.*, Balancing Hedgehog, a retention and release equilibrium given by Dally, Ihog, Boi and shifted/DmWif. *Dev. Biol.* **376**, 198–212 (2013). doi: 10.1016/j.ydbio.2012.12.013; pmid: 23276604
7. A. Callejo *et al.*, Dispatched mediates Hedgehog basolateral release to form the long-range morphogenetic gradient in the *Drosophila* wing disk epithelium. *Proc. Natl. Acad. Sci. U.S.A.* **108**, 12591–12598 (2011). doi: 10.1073/pnas.1106881108; pmid: 21690386
8. P. Rojas-Ríos, I. Guerrero, A. González-Reyes, Cytoneme-mediated delivery of Hedgehog regulates the expression of bone morphogenetic proteins to maintain germline stem cells in *Drosophila*. *PLOS Biol.* **10**, e1001298 (2012). doi: 10.1371/journal.pbio.1001298; pmid: 22509132
9. M. Sato, T. B. Kornberg, FGF is an essential mitogen and chemoattractant for the air sacs of the *Drosophila* tracheal system. *Dev. Cell* **3**, 195–207 (2002). doi: 10.1016/S1534-5807(02)00202-2; pmid: 12194851
10. K. Tsuneizumi *et al.*, *Daughters against dpp* modulates *dpp* organizing activity in *Drosophila* wing development. *Nature* **389**, 627–631 (1997). doi: 10.1038/39362; pmid: 9335506
11. H. Tanimoto, S. Itoh, P. ten Dijke, T. Tabata, Hedgehog creates a gradient of DPP activity in *Drosophila* wing imaginal discs. *Mol. Cell* **5**, 59–71 (2000). doi: 10.1016/S1097-2765(00)80403-7; pmid: 10678169
12. E. V. Entchev, A. Schwabedissen, M. González-Gaitán, Gradient formation of the TGF-β homolog Dpp. *Cell* **103**, 981–992 (2000). doi: 10.1016/S0092-8674(00)00200-2; pmid: 11136982
13. A. A. Teleman, S. M. Cohen, Dpp gradient formation in the *Drosophila* wing imaginal disc. *Cell* **103**, 971–980 (2000). doi: 10.1016/S0092-8674(00)00199-9; pmid: 11136981
14. See supplementary materials on *Science* Online.
15. M. Michel, I. Raabe, A. P. Kupinski, R. Pérez-Palencia, C. Bökel, Local BMP receptor activation at adherens junctions in the *Drosophila* germline stem cell niche. *Nat. Commun.* **2**, 415 (2011). doi: 10.1038/ncomms1426; pmid: 21811244
16. E. H. Feinberg *et al.*, GFP Reconstitution Across Synaptic Partners (GRASP) defines cell contacts and synapses in living nervous systems. *Neuron* **57**, 353–363 (2008). doi: 10.1016/j.neuron.2007.11.030; pmid: 18255029
17. M. D. Gordon, K. Scott, Motor control in a *Drosophila* taste circuit. *Neuron* **61**, 373–384 (2009). doi: 10.1016/j.neuron.2008.12.033; pmid: 19217375
18. S. E. Ryu *et al.*, Crystal structure of an HIV-binding recombinant fragment of human CD4. *Nature* **348**, 419–426 (1990). doi: 10.1038/348419a0; pmid: 2247146
19. J. H. Wang *et al.*, Atomic structure of a fragment of human CD4 containing two immunoglobulin-like domains. *Nature* **348**, 411–418 (1990). doi: 10.1038/348411a0; pmid: 1701030
20. S. Cabantous, T. C. Terwilliger, G. S. Waldo, Protein tagging and detection with engineered self-assembling fragments of green fluorescent protein. *Nat. Biotechnol.* **23**, 102–107 (2005). doi: 10.1038/nbt1044; pmid: 15580262
21. D. H. Castrillon, S. A. Wasserman, *diaphanous* is required for cytokinesis in *Drosophila* and shares domains of similarity with the products of the *limb deformity* gene. *Development* **120**, 3367–3377 (1994). pmid: 7821209
22. C. C. Homem, M. Peifer, Exploring the roles of diaphanous and enabled activity in shaping the balance between filopodia and lamellipodia. *Mol. Biol. Cell* **20**, 5138–5155 (2009). doi: 10.1091/mbc.E09-02-0144; pmid: 19846663
23. T. Rousso, A. M. Shewan, K. E. Mostov, E. D. Schejter, B.-Z. Shilo, Apical targeting of the formin Diaphanous in *Drosophila* tubular epithelia. *eLife* **2**, e00666 (2013). doi: 10.7554/eLife.00666; pmid: 23853710
24. T. Kitamoto, Conditional modification of behavior in *Drosophila* by targeted expression of a temperature-sensitive *shibire* allele in defined neurons. *J. Neurobiol.* **47**, 81–92 (2001). doi: 10.1002/neu.1018; pmid: 11291099
25. A. B. Muhlberg, D. E. Warnock, S. L. Schmid, Domain structure and intramolecular regulation of dynamin GTPase. *EMBO J.* **16**, 6676–6683 (1997). doi: 10.1093/emboj/16.22.6676; pmid: 9362482
26. J. E. Hinshaw, Dynamin spirals. *Curr. Opin. Struct. Biol.* **9**, 260–267 (1999). doi: 10.1016/S0959-440X(99)80036-0; pmid: 10322220

27. E. M. Enneking *et al*., Transsynaptic coordination of synaptic growth, function, and stability by the L1-type CAM Neuroglian. *PLOS Biol.* **11**, e1001537 (2013). doi: 10.1371/journal.pbio.1001537; pmid: 23610557
28. M. Milán, U. Weihe, L. Pérez, S. M. Cohen, The LRR proteins Capricious and Tartan mediate cell interactions during DV boundary formation in the *Drosophila* wing. *Cell* **106**, 785–794 (2001). doi: 10.1016/S0092-8674(01)00489-5; pmid: 11572783
29. W. Hong *et al*., Leucine-rich repeat transmembrane proteins instruct discrete dendrite targeting in an olfactory map. *Nat. Neurosci.* **12**, 1542–1550 (2009). doi: 10.1038/nn.2442; pmid: 19915565
30. H. Kohsaka, A. Nose, Target recognition at the tips of postsynaptic filopodia: Accumulation and function of Capricious. *Development* **136**, 1127–1135 (2009). doi: 10.1242/dev.027920; pmid: 19270171
31. E. Shishido, M. Takeichi, A. Nose, *Drosophila* synapse formation: Regulation by transmembrane protein with Leu-rich repeats, CAPRICIOUS. *Science* **280**, 2118–2121 (1998). doi: 10.1126/science.280.5372.2118; pmid: 9641918
32. H. Taniguchi, E. Shishido, M. Takeichi, A. Nose, Functional dissection of *Drosophila* capricious: Its novel roles in neuronal pathfinding and selective synapse formation. *J. Neurobiol.* **42**, 104–116 (2000). doi: 10.1002/(SICI)1097-4695(200001)42:1<104::AID-NEU10>3.0.CO;2-V; pmid: 10623905
33. D. S. Lidke, K. A. Lidke, B. Rieger, T. M. Jovin, D. J. Arndt-Jovin, Reaching out for signals: Filopodia sense EGF and respond by directed retrograde transport of activated receptors. *J. Cell Biol.* **170**, 619–626 (2005). doi: 10.1083/jcb.200503140; pmid: 16103229
34. K. Koizumi *et al*., RhoD activated by fibroblast growth factor induces cytoneme-like cellular protrusions through mDia3C. *Mol. Biol. Cell* **23**, 4647–4661 (2012). doi: 10.1091/mbc.E12-04-0315; pmid: 23034183
35. Z. Huang, S. Kunes, Hedgehog, transmitted along retinal axons, triggers neurogenesis in the developing visual centers of the Drosophila brain. *Cell* **86**, 411–422 (1996). doi: 10.1016/S0092-8674(00)80114-2; pmid: 8756723
36. C. Korkut *et al*., *Trans*-synaptic transmission of vesicular Wnt signals through Evi/Wntless. *Cell* **139**, 393–404 (2009). doi: 10.1016/j.cell.2009.07.051; pmid: 19837038
37. M. Cohen, M. Georgiou, N. L. Stevenson, M. Miodownik, B. Baum, Dynamic filopodia transmit intermittent Delta-Notch signaling to drive pattern refinement during lateral inhibition. *Dev. Cell* **19**, 78–89 (2010). doi: 10.1016/j.devcel.2010.06.006; pmid: 20643352
38. C. de Joussineau *et al*., Delta-promoted filopodia mediate long-range lateral inhibition in *Drosophila*. *Nature* **426**, 555–559 (2003). doi: 10.1038/nature02157; pmid: 14654840
39. O. Renaud, P. Simpson, *scabrous* modifies epithelial cell adhesion and extends the range of lateral signalling during development of the spaced bristle pattern in *Drosophila*. *Dev. Biol.* **240**, 361–376 (2001). doi: 10.1006/dbio.2001.0482; pmid: 11784069
40. Y. Peng, C. Han, J. D. Axelrod, Planar polarized protrusions break the symmetry of EGFR signaling during *Drosophila* bract cell fate induction. *Dev. Cell* **23**, 507–518 (2012). doi: 10.1016/j.devcel.2012.07.016; pmid: 22921201
41. T. A. Sanders, E. Llagostera, M. Barna, Specialized filopodia direct long-range transport of SHH during vertebrate tissue patterning. *Nature* **497**, 628–632 (2013). doi: 10.1038/nature12157; pmid: 23624372
42. N. Ninov *et al*., Dpp signaling directs cell motility and invasiveness during epithelial morphogenesis. *Curr. Biol.* **20**, 513–520 (2010). doi: 10.1016/j.cub.2010.01.063; pmid: 20226662
43. M. Reichman-Fried, B.-Z. Shilo, Breathless, a *Drosophila* FGF receptor homolog, is required for the onset of tracheal cell migration and tracheole formation. *Mech. Dev.* **52**, 265–273 (1995). doi: 10.1016/0925-4773(95)00407-R; pmid: 8541215
44. R. Yagi, F. Mayer, K. Basler, Refined LexA transactivators and their use in combination with the *Drosophila* Gal4 system. *Proc. Natl. Acad. Sci. U.S.A.* **107**, 16166–16171 (2010). doi: 10.1073/pnas.1005957107; pmid: 20805468
45. D. Nellen, R. Burke, G. Struhl, K. Basler, Direct and long-range action of a DPP morphogen gradient. *Cell* **85**, 357–368 (1996). doi: 10.1016/S0092-8674(00)81114-9; pmid: 8616891
46. T. E. Haerry, O. Khalsa, M. B. O'Connor, K. A. Wharton, Synergistic signaling by two BMP ligands through the SAX and TKV receptors controls wing growth and patterning in Drosophila. *Development* **125**, 3977–3987 (1998). pmid: 9735359
47. R. Massarwa, E. D. Schejter, B.-Z. Shilo, Apical secretion in epithelial tubes of the *Drosophila* embryo is directed by the Formin-family protein Diaphanous. *Dev. Cell* **16**, 877–888 (2009). doi: 10.1016/j.devcel.2009.04.010; pmid: 19531358
48. T. Ohshiro, Y. Emori, K. Saigo, Ligand-dependent activation of *breathless* FGF receptor gene in *Drosophila* developing trachea. *Mech. Dev.* **114**, 3–11 (2002). doi: 10.1016/S0925-4773(02)00042-4; pmid: 12175485
49. C. Ribeiro, A. Ebner, M. Affolter, In vivo imaging reveals different cellular functions for FGF and Dpp signaling in tracheal branching morphogenesis. *Dev. Cell* **2**, 677–683 (2002). doi: 10.1016/S1534-5807(02)00171-5; pmid: 12015974
50. A. Klebes, B. Biehs, F. Cifuentes, T. B. Kornberg, Expression profiling of *Drosophila* imaginal discs. *Genome Biol.* **3**, RESEARCH0038 (2002). doi: 10.1186/gb-2002-3-8-research0038; pmid: 12186645
51. U. Persson *et al*., The L45 loop in type I receptors for TGF-β family members is a critical determinant in specifying Smad isoform activation. *FEBS Lett.* **434**, 83–87 (1998). doi: 10.1016/S0014-5793(98)00954-5; pmid: 9738456
52. K. G. Eulenberg, R. Schuh, The tracheae defective gene encodes a bZIP protein that controls tracheal cell movement during Drosophila embryogenesis. *EMBO J.* **16**, 7156–7165 (1997). doi: 10.1093/emboj/16.23.7156; pmid: 9384592
53. A. Guha, L. Lin, T. B. Kornberg, Organ renewal and cell divisions by differentiated cells in *Drosophila*. *Proc. Natl. Acad. Sci. U.S.A.* **105**, 10832–10836 (2008). doi: 10.1073/pnas.0805111105; pmid: 18664581

Acknowledgments: We thank K. Basler, M. Affolter, K. Scott, E. Laufer, P. ten Dijke, T. Kitamoto, J. Pielage, C. Bökel, K. Wharton, A. Nose, L. Luo, M. Milan, B. Shilo, the BSC, and the Developmental Studies Hybridoma Bank for reagents; L. Lin and P. Rao for discussions; and M. Barna for access to the spinning disc confocal microscope. **Funding:** NIH K99HL114867 to S.R. and GM030637 to T.B.K.

Supplementary Materials

www.sciencemag.org/content/343/6173/1244624/suppl/DC1
Figs. S1 to S3
Tables S1 to S5
Movie S1

13 August 2013; accepted 13 December 2013
Published online 2 January 2014;
10.1126/science.1244624

Rhodium-Catalyzed Intermolecular C–H Silylation of Arenes with High Steric Regiocontrol

Chen Cheng and John F. Hartwig*

Regioselective C–H functionalization of arenes has widespread applications in synthetic chemistry. The regioselectivity of these reactions is often controlled by directing groups or steric hindrance ortho to a potential reaction site. Here, we report a catalytic intermolecular C–H silylation of unactivated arenes that manifests very high regioselectivity through steric effects of substituents meta to a potential site of reactivity. The silyl moiety can be further functionalized under mild conditions but is also inert toward many common organic transformations, rendering the silylarene products useful building blocks. The remote steric effect that we observe results from the steric properties of both the rhodium catalyst and the silane.

Methods for the selective functionalization of aromatic C–H bonds under mild, neutral conditions have synthetic applications in fields ranging from materials science to medicinal chemistry (*1*–*6*). Perhaps most important for the utility of C–H bond functionalization is the control of site selectivity. Regioselectivity in classical electrophilic aromatic substitution reactions is governed by the electronic properties of the substituents on the arene. In catalytic C–H functionalization of arenes, regiocontrol has been achieved in some cases by substituents on the arene that bind to the catalyst and direct the reaction to an *ortho*- (*2*) or *meta*-C–H bond (*7*–*9*). In other cases, such as in the widely used iridium-catalyzed borylation of arenes (*3*), the regioselectivity results from the steric properties of substituents ortho to a reacting C–H bond. However, reactions that occur with selectivity derived from the steric properties of groups distal to a potential site of reactivity on arenes have been challenging to develop. Groups in these positions are assumed to have minor steric effects on a reaction site, so much so that a classical method for probing the electronic effects of an aromatic ring on a chemical reaction is to introduce substituents meta or para to a site of reactivity.

The work described here focuses on the silylation of aromatic C-H bonds. The formation of arene-silicon bonds by C–H silylation would be a valuable route toward arylsilane monomers for silicone polymers and arylsilane intermediates in the synthesis of complex molecules (*10*, *11*). Compared to the borylation of C–H bonds, the silylation of C–H bonds would occur with a simpler and more accessible class of main group reagent, the arylsilane products would be more stable to many of the conditions of typical organic transformations, and the steric properties of the substituents at silicon could modulate the regioselectivities of the reaction.

For these reasons, much effort has been spent to develop protocols for the silylation of arenes, but the scope and efficiency of the reactions are limited. Intermolecular arene silylations with hydrosilanes have been conducted only at high temperatures (>100°C) or under photochemical conditions (*12*–*17*), with a large excess of arene relative to the silane. This stoichiometry is a limitation for synthetic applications because the arene is usually the more valuable reaction component. Furthermore, most silylation reactions have been conducted with trialkylsilanes (*12*, *16*, *18*), and the arylsilane products of these reactions have limited synthetic utility. To address this limitation, the silylation of arenes has been conducted with disilanes containing Si-F bonds, but these reactions also require high temperatures and excess arenes, and access to the disilane reagents requires multistep syntheses (*13*, *14*). Silylations of arenes assisted by directing groups has been reported more frequently, but these reactions are limited to functionalization ortho to the directing group (*19*–*27*).

Thus, practical silylations of arenes should be conducted with a readily available silane, under mild conditions, and with arenes as the limiting reagent. We report the combination of a rhodium catalyst, a simple hydrogen acceptor, and a readily available hydrosilane that generates arylsilanes in high yields with exceptional steric control, with arene as the limiting reagent, and with substituents on silicon that render the arylsilane products synthetically valuable. The arylsilane products undergo cross-coupling, oxidation, and halogenation; yet in the absence of fluoride

Table 1. Evaluation of the reaction conditions for the silylation of arenes.

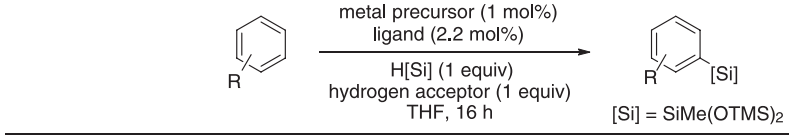

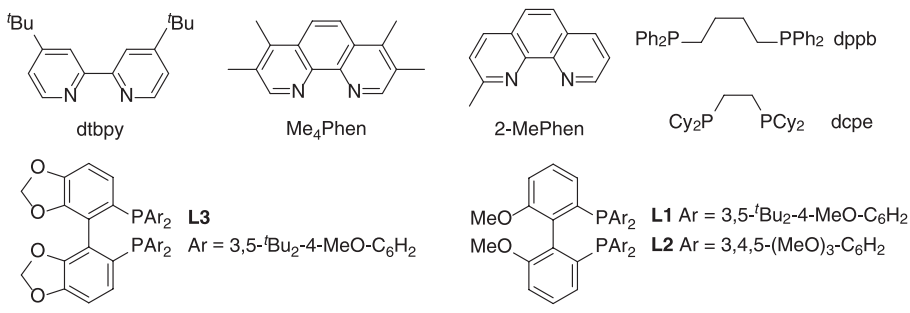

Entry	Arene	Metal precursor	Ligand	Acceptor	T (°C)	yield (%)*
1	Benzene	$[Ir(cod)OMe]_2$	dtbpy	None	80	8
2	Benzene	$[Ir(cod)OMe]_2$	Me_4Phen	None	80	11
3	Benzene	$[Ir(cod)OMe]_2$	2-MePhen	None	80	16
4	Benzene	$[Ir(cod)OMe]_2$	2-MePhen	Cyclohexene	80	29
5	Benzene	$[Rh(cod)Cl]_2$	dppb	Cyclohexene	80	0
6	Benzene	$[Rh(cod)Cl]_2$	dcpe	Cyclohexene	80	0
7	Benzene	$[Rh(cod)Cl]_2$	**L3**	Cyclohexene	80	68
8	1,3-Xylene	$[Rh(coe)_2OH]_2$	**L3**	Cyclohexene	50	64
9	1,3-Xylene	$[Rh(coe)_2OH]_2$	**L1**	Cyclohexene	50	68
10	1,3-Xylene	$[Rh(coe)_2OH]_2$	**L2**	Cyclohexene	50	75
11†	1,3-Xylene	$[Rh(coe)_2OH]_2$	**L2**	Cyclohexene	45	92‡

*Yields determined by gas chromatography (GC) analysis. Reaction run with two equivalents of silane and cyclohexene.
‡Yield determined by ^1H nuclear magnetic resonance (NMR) spectroscopy.

Department of Chemistry, University of California, Berkeley, CA 94720, USA.
*Corresponding author. E-mail: jhartwig@berkeley.edu

or strong bases as activators, the silyl moiety is stable toward many common organic transformations. These studies show the value of C–H bond silylation for synthetic applications, the importance of rhodium catalysts for this class of transformation, and the capacity of catalysts to achieve C–H bond functionalization with remote steric control.

Evaluation of Reaction Conditions and Catalysts

Based on our previous studies on the dehydrogenative silylation of alkenes (*28*), we investigated the reaction of benzene with $HSiMe(OTMS)_2$ (TMS is trimethylsilyl) (*29*) (Table 1 and table S1). We conducted these reactions with equimolar amounts of arene and silane in tetrahydrofuran (THF) at 80°C catalyzed by combinations of $[Ir(cod)OMe]_2$ (cod is 1,5-cyclooctadiene) and phenanthroline or bipyridine derivatives. These reactions afforded the corresponding silylbenzene in 8 to 16% yield (Table 1, entries 1 to 3). Given that the reactions occur with formal loss of hydrogen, we added 1 equivalent of cyclohexene as the hydrogen acceptor to the silylation reaction catalyzed by $[Ir(cod)OMe]_2$ and 2-methylphenanthroline. The reaction conducted with this hydrogen acceptor resulted in a higher, but modest, 29% yield of silylbenzene (Table 1, entry 4).

To identify a more active catalyst, we investigated combinations of metal complexes and ligands not typically used for intermolecular arene silylation or the related arene borylation (*3*, *13*, *14*). Specifically, we probed the reactivity of the combination of $[Rh(cod)Cl]_2$ and several phosphine ligands (*30*). Reactions run with simple bisphosphines, such as dppb [1,4-bis(diphenylphosphino)butane] or dcpe [1,2-bis(dicyclohexylphosphino)ethane], as the ligand gave no silylbenzene product (Table 1, entries 5 and 6). However, reactions run with DTBM-Segphos (**L3**) (DTBM is 3,5-^{t}Bu$_2$-4-MeO-C_6H_2) as the ligand and $[Rh(coe)_2OH]_2$ (coe is cyclooctene) as the rhodium source occurred with high selectivity for arene silylation over alkene hydrosilylation (*31*) at 50°C (Table 1, entry 8). (Also see fig. S1 for the results of reactions catalyzed by $[Rh(cod)Cl]_2$ and **L3** with other hydrogen acceptors.) We found that several classes of bisphosphines containing biaryl backbones afforded the product in good yields (fig. S2).

Regioselectivity of the Arene Silylation

The regioselectivity of the silylation of arenes results from a high level of steric control by substituents ortho and meta to the reacting C–H bond. Studies on regioselectivity were conducted with rhodium catalysts derived from 2,2′-biphenylphosphine derivatives **L1** and **L2** because reactions with these ligands afforded the product in the highest yields (Table 1, entries 9 and 10), and the two ligands possess different steric properties. Because the silane and cyclohexene are commercially available and inexpensive, we conducted the silylation reaction with 2 equivalents of the silane and cyclohexene to maximize the conversion of the arene (*32*) (Table 1, entry 11).

Under these conditions, the silylation of various 1,3-disubstituted arenes occurred at the mutually meta positions with >95:5 selectivities (Fig. 1) (*33*). Even the reaction with **6a** bearing a potentially ortho-directing amide group gave the 1,3,5-trisubstituted arene **6b** as the sole product. The reactions of symmetrically 1,2-disubstituted arenes gave the 1,2,4-trisubstituted arylsilanes with >99:1 selectivities. These regioselectivities parallel those of the iridium-catalyzed borylation of arenes, but with a more stable and less expensive reagent to form a linkage that undergoes transformations under conditions orthogonal to those of arylboronates (*3*, *4*). Similar to previous borylation (*34*) and silylation (*18*) reactions, the silylation of an indole derivative (**16a**) and of benzofuran (**17a**) occurred at the 2-position of the heteroarenes with ≥97:3 selectivities (*35*).

Selective functionalization of fluoroarenes can provide synthetically valuable intermediates, but high sterically derived selectivity is often difficult to achieve because of the small size of fluorine. For example, the regioselective reaction of 3-fluorotoluene (**18a**) at the position meta to both the fluorine and methyl group requires the catalyst to distinguish between the steric environment of

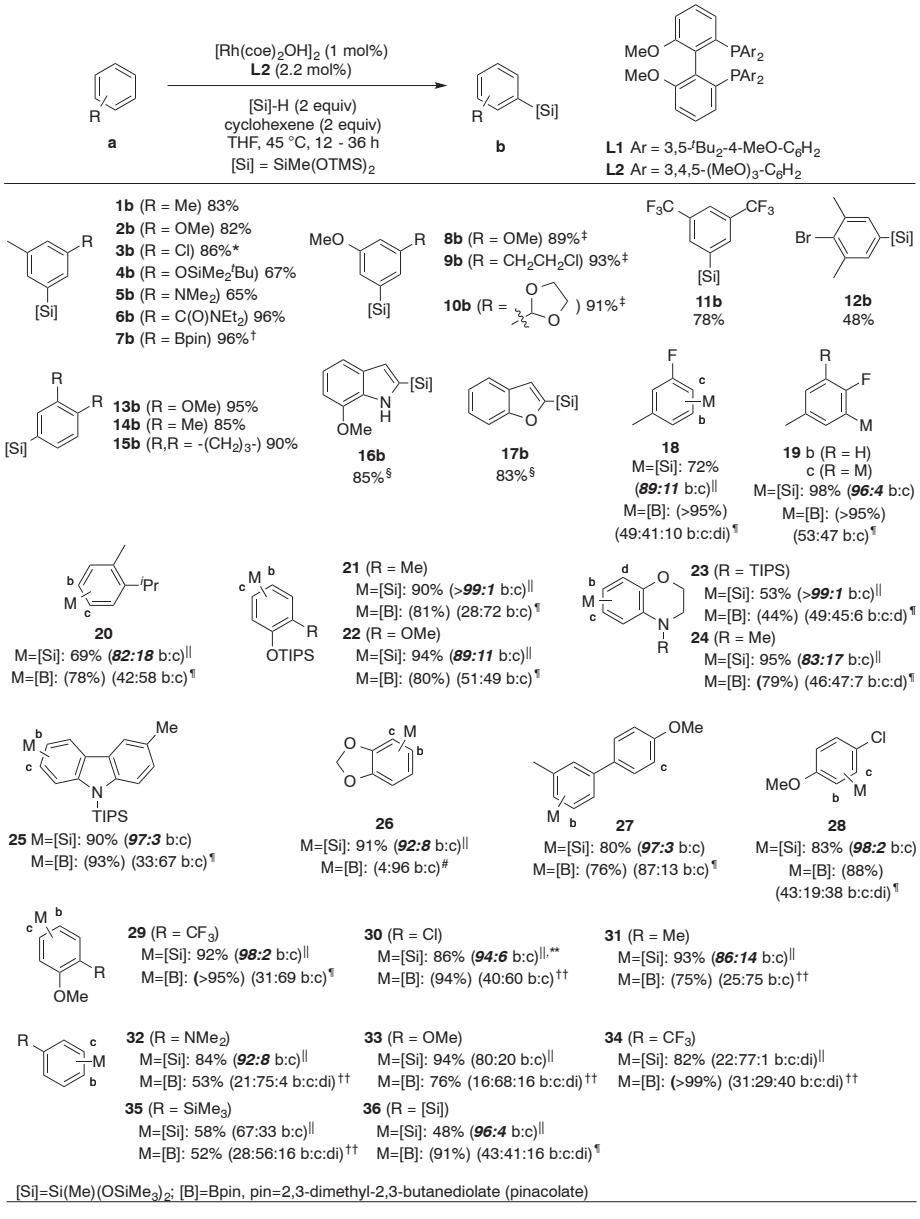

Fig. 1. The regioselective silylation of arenes. Reactions were conducted on a 0.3-mmol scale unless otherwise stated. Reported yields are for isolated materials. Yields in parentheses were determined by GC analysis for borylation reactions run on a 0.05-mmol scale. "di" denotes diborylation or disilylation products. *Dechloronated product was obtained in 4% yield. †Reaction run on a 2.0-mmol scale. ‡See (*33*). §See (*35*). ‖Silylation carried out with **L1** as the ligand. ¶Results of C–H borylation carried out following the literature procedure (*44*). #Results from (*38*). See (*39*). **Dechloronated product was obtained in 9% yield. ††Results of borylation of the substrates obtained from (*36*).

two C-H bonds ortho and meta to the fluorine atom. Silylation of **18a** occurred with an 89:11 selectivity favoring functionalization at the mutually meta position and without the formation of disilylation products. In contrast, the borylation of this substrate was unselective toward the C–H bonds ortho and meta to the fluorine (ortho:meta ~ 1:1).

The selective functionalization of unsymmetrically 1,2-disubstituted arenes is particularly challenging to achieve because the steric effects that control the site selectivity must be transmitted remotely. A catalytic system that addresses these problems must have exquisite sensitivity to steric differences at sites beyond the ortho positions. The borylation of arenes is only sensitive to substituents at the ortho positions. Therefore, the borylation of unsymmetrically 1,2-disubstituted arenes occurs with poor regioselectivity (*36*). A recently reported gold-catalyzed direct arylation occurs with high regioselectivity for unsymmetrically 1,2-disubstituted arenes (*37*). In this case, the regioselectivity is derived from the electronic properties of the substituents and is similar to that of electrophilic aromatic substitution.

The silylation of arenes reported here addresses the challenge of achieving site selectivity from remote steric effects. The following examples provide a comparison of the product distributions for the rhodium-catalyzed silylation and the iridium-catalyzed borylation of the same arenes (Fig. 1). In short, the silylation of arenes leads to products resulting from steric effects of substituents located meta to the site of reactivity. Higher regioselectivity was obtained from reactions run with ligand **L1** bearing more sterically demanding *tert*-butyl groups than with ligand **L2** bearing less sterically demanding methoxy groups.

The silylation of *o*-cymene (**20a**) containing one large and one small alkyl group illustrates the sensitivity of the reaction to the substituents meta to the potentially reactive C–H bonds. The reaction of **20a** with **L1** as the ligand occurred with a selectivity of 82:18 in favor of the product containing the silyl group para to the larger of the two alkyl groups. In contrast, the borylation of this substrate occurred roughly equally at the two C–H bonds located para to the methyl and isopropyl groups. A similar remote steric sensitivity is illustrated by the reaction of 2-tri(isopropyl) siloxyanisole (**22a**), containing two electronically similar oxygen-based substituents of different sizes. The reaction of this arene catalyzed by the complex containing **L1** as ligand occurred selectively para to the larger substituent to give the products in an 89:11 ratio. In contrast, the borylation of this substrate gave two products in a ratio of 51:49.

This sensitivity to the size of the meta substituent allows the size of a group on nitrogen in a heterocycle to modulate the regioselectivity of the C–H bond functionalization remotely. The silylation of *N*-TIPS (TIPS is tri(isopropyl)silyl) benzomorpholine (**23a**) containing a large substituent on nitrogen occurred at the C–H bond para to the nitrogen atom with >99:1 regioselectivity. In contrast, when the substituent on nitrogen is smaller, such as in *N*-methyl benzomorpholine (**24a**) the regioselectivity is lower (83:17). This effect of the *N*-TIPS group is also illustrated by the regioselective silylation of carbazole. The silylation of the *N*-TIPS-carbazole **25a** occurred with 97:3 selectivity for the position para to the *N*-TIPS group over the position meta to this group.

The silylation of benzodioxole (**26a**) is an example in which the steric effects override a propensity for metalation ortho to a substituent. The borylation of **26a** is reported to occur primarily at the ortho position because of the small size of the dioxole unit and the higher acidity of the C–H bonds ortho to the oxygen-based substituents than meta to these substituents (*38*, *39*). In contrast, the silylation of this arene gave the 1,2,4-substituted arylsilane as the predominant product from functionalization at the more sterically accessible C–H bond.

The rhodium-catalyzed silylation reaction can also selectively functionalize biaryls in which the two aryl groups have different steric properties. For example, the silylation of 4′-methoxy-3-methyl-1,1′-biphenyl (**27a**) occurred preferentially on one aryl ring with a selectivity of 97:3 because of the 1,4-substitution pattern of the other aryl ring. In comparison, the selectivity for the borylation of this substrate is lower (87:13).

The electronic properties of the substituents do have a secondary influence on the regioselectivities. Silylation occurs at the more electron-rich position of the arene. This electronic effect can be

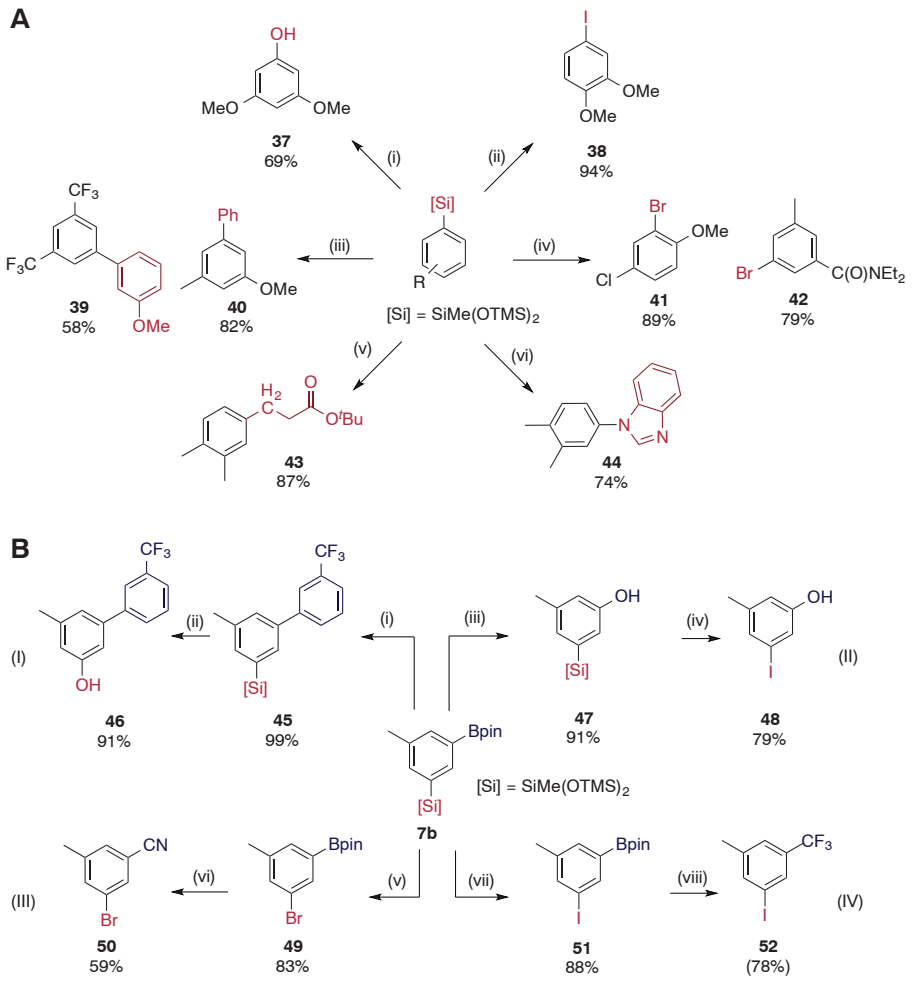

Fig. 2. Functionalization of the arylsilane products. Yields reported are for isolated materials. (**A**) Silyl substitution. Reaction conditions: (i) tetrabutylammonium fluoride (TBAF) [4 equivalents (equiv)], H_2O_2 (20 equiv), $KHCO_3$ (5 equiv), THF, MeOH, 23°C, 18 hours; (ii) ICl (1.1 equiv), CH_2Cl_2, 23°C, 3 hours; (iii) PhBr or 3-iodoanisole (0.7 to 1.5 equiv), KOTMS (3 equiv), $Pd(OAc)_2$ (0.05 equiv), dcpe (0.055 equiv), THF or toluene, 65 to 100°C, 5 to 14 hours; (iv) Br_2 (1.5 to 8 equiv), CH_2Cl_2, 23°C, 1 to 24 hours; (v) *tert*-butyl acrylate (0.5 equiv), $[Rh(cod)Cl]_2$ (0.02 equiv), TBAF (3 equiv), THF, H_2O, 100°C, 14 hours; (vi) benzimidazole (0.5 equiv), $Cu(OAc)_2$ (0.6 equiv), TBAF (1 equiv), dimethylformamide (DMF), 23°C, 36 hours. (**B**) Orthogonality of silyl and boronate substituents. Reaction conditions: (i) $Pd(dppf)Cl_2$ (0.04 equiv), 3-CF_3-C_6H_4Br (1.5 equiv), K_2CO_3 (3 equiv), THF, H_2O, 70°C, 12 hours; (ii) TBAF (4 equiv), H_2O_2 (20 equiv), $KHCO_3$ (5 equiv), THF, MeOH, 23°C, 18 hours; (iii) NaOH (2 equiv), H_2O_2 (2 equiv), THF, H_2O, 23°C, 3 hours; (iv) ICl (1.1 equiv), CH_2Cl_2, 23°C, 3 hours; (v) Br_2 (2 equiv), CH_2Cl_2, 0°C, 1 hour; (vi) $Cu(NO_3)_2 \cdot 3H_2O$ (2 equiv), $Zn(CN)_2$ (3 equiv), CsF (1 equiv), MeOH, H_2O, 100°C, 6 hours; (vii) ICl (1.2 equiv), CH_2Cl_2, 0°C, 1 hour; (viii) (Phenanthroline)$Cu(CF_3)$ (1.2 equiv), KF (1 equiv), air, DMF, 50°C, 16 hours, yield determined by ^{19}F NMR spectroscopy analysis.

gleaned from the reactions of 4-chloroanisole (**28a**) and some 1,2-disubstituted arenes (**29** to **31**). Reaction of **28a** occurred with a selectivity of 98:2 favoring silylation ortho to the methoxy group, whereas borylation of this substrate occurred at the two positions in a ratio of 2:1 (*40*). Because a methoxy group (cyclohexane A value = 0.55 to 0.75) is usually considered to be slightly larger than a chlorine (A value = 0.53 to 0.64) (*41*), we attribute the regioselectivity of the silylation of **28a** to the electronic activation of the 2-position by the methoxy group. Likewise, silylation of a series of 2-substituted anisoles (**29** to **31**) catalyzed by the rhodium complex containing **L1** predominantly occurred para to the methoxy substituent.

The reactions of monosubstituted arenes are less selective than those of disubstituted arenes, but they reveal the combination of electronic and steric effects on the silylation reaction (**32** to **34**). The silylation of *N,N*-dimethylaminobenzene (**32**) occurred predominantly at the more electron-rich para position (para:meta = 92:8; statistical ratio = 1:2), and the silylation of trifluoromethylbenzene (**34**) occurred preferentially at the less electron-deficient meta positions (para:meta = 22:78), indicating that silylation is favored at the C–H bond on the more electron-rich position of the ring. Disilylation occurred to a minimum extent, even during the reaction with **34**. One might expect to observe the product from silylation at both C–H bonds meta to the CF_3 group, but the large size of the $SiMe(OTMS)_2$ group hinders silylation at a position meta to it. Consistent with this assertion, the silylation of $PhSiMe(OTMS)_2$ (**36**) formed the disilylbenzene product with a para-to-meta ratio of 96:4.

Derivatization of the Silylarene Products

The silyl-substituted arenes generated from this catalytic process underwent a series of transformations made possible by the presence of the Si–O bonds (Fig. 2A). For example, the silylarenes underwent cross-coupling with aryl halides to form biaryls and oxidation to form phenols. These silylarenes also underwent bromination and iodination, and these halogenation reactions were more facile and were conducted with simpler reagents than the copper-mediated halogenation of arylboronates (*42*). In addition, rhodium-catalyzed 1,4-addition of silylarenes to acrylates and copper-mediated amination with benzimidazole occurred with good yields.

The arylsilanes and arylboronate esters react under conditions that are orthogonal to each other, and the difference between these conditions enables the sequential diversification of polysubstituted arenes. With a silyl-substituted arylboronate ester (**7b**), oxidation, cross-coupling, and halogenation can be conducted at the site of the C–Si or C–B bond depending on the conditions and reagents chosen (Fig. 2B). For example, cross-coupling was conducted at the C–B bond before oxidation at the C–Si bond by using a weak base for the coupling process (sequence I). The C–B bond underwent oxidation with a basic solution of hydrogen peroxide before halogenation at the C–Si bond (sequence II). Furthermore, the halogenations at the C–Si bond were conducted in the presence of the C–B bond before oxidative functionalizations at the C–B bond (sequences III and IV).

The methyl- and siloxy-substituted silyl group is stable to a range of classical organic transformations (Fig. 3). For example, an aldehyde unit underwent alkylation, reduction, Wittig alkenylation, aldol addition, and Takai alkenylation without affecting the silyl group. The C–Si bond is also stable to the conditions of a catalytic Heck reaction, a Sonogashira coupling (see fig. S3), olefin cross metathesis, and cross-coupling and oxidation of arylboronate esters (Fig. 2B). These reactions encompass a large fraction of the transformations conducted by medicinal and process chemists in the preparation of complex molecules (*43*). Thus, the silyl group can be installed by C–H bond functionalization and transformed at a later stage of a synthesis.

Preliminary Mechanistic Insights

Although the detailed reaction mechanism and the nature of the active catalyst remain under investigation, several observations about the reaction rates provide mechanistic insights. First, the reaction of equimolar amounts of toluene and toluene-d_8 with 1 equivalent of silane and hydrogen acceptor occurred with an isotope effect of 5.1. However, when toluene and toluene-d_8 were allowed to react in separate vessels, the kinetic isotope effect from the initial reaction rates was only 1.3. Second, a competition experiment between bis(trifluoromethyl)benzene (**11a**) and 1,3-xylene (**1a**) gave products in a ratio of 2.9:1 favoring

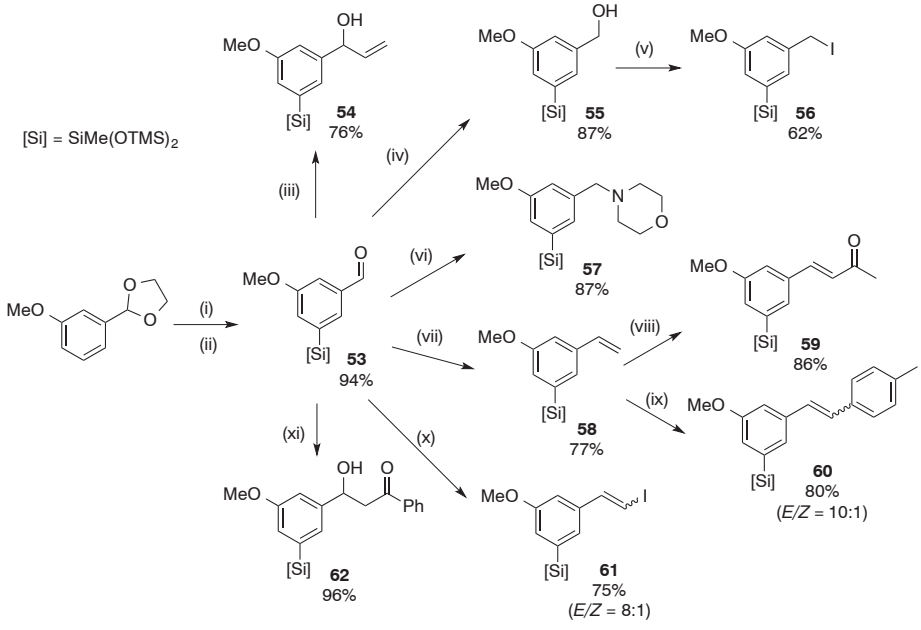

Fig. 3. Silylarenes as useful building blocks. Yields reported are for isolated material. Reaction conditions: (i) $[Rh(coe)_2OH]_2$ (0.01 equiv), **L2** (0.022 equiv), $HSiMe(OTMS)_2$ (2 equiv), cyclohexene (2 equiv), THF, 45°C, 36 hours; (ii) $Pd(MeCN)_2Cl_2$ (0.06 equiv), acetone, 23°C, 16 hours; (iii) vinylmagnesium bromide (1.2 equiv), THF, 0°C, 0.5 hours; (iv) $NaBH_4$ (3 equiv), THF, MeOH, 0→23°C, 2 hours; (v) Ph_3P (1.5 equiv), I_2 (1.5 equiv), imidazole (2 equiv), THF, 23°C, 2 hours; (vi) morpholine (1.2 equiv), $NaHB(OAc)_3$ (1.5 equiv), 1,2-dichloroethane, 23°C, 20 hours; (vii) ^{n}BuLi (1.1 equiv), Ph_3PMeI (1.3 equiv), THF, 0→23°C, 4 hours; (viii) Hoveyda-Grubbs catalyst second generation (0.09 equiv), methyl vinyl ketone (6 equiv), CH_2Cl_2, 45°C, 24 hours; (ix) $Pd(OAc)_2$ (0.03 equiv), 4-bromotoluene (2 equiv), triethanolamine, THF, 100°C, 16 hours; (x) CHI_3 (2 equiv), $CrCl_2$ (6 equiv), dioxane, THF, 23°C, 2 hours; (xi) acetophenone (1.2 equiv), $MgBr_2$ (1.2 equiv), $(iPr)_2NEt$ (1.3 equiv), CH_2Cl_2, 23°C, 2 hours.

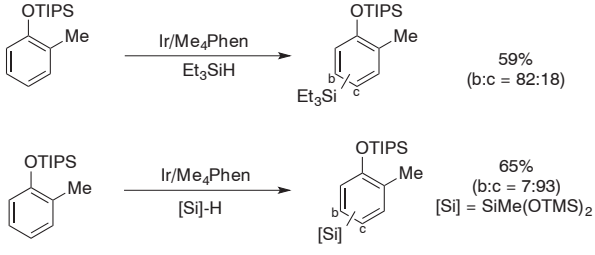

Fig. 4. Comparison of Et_3SiH and $HSiMe(OTMS)_2$ in the iridium-catalyzed silylation of 21a. Conversions of the silane and the regioselectivities were determined by GC analysis. Reaction conditions: (top) $[Ir(cod)OMe]_2$ (0.01 equiv), 3,4,7,8-tetramethyl-1,10-phenanthroline (0.022 equiv), Et_3SiH (1 equiv), norbornene (1.1 equiv), arene (5 equiv), THF, 100°C, 16 hours; (bottom) $[Ir(cod)OMe]_2$ (0.01 equiv), 3,4,7,8-tetramethyl-1,10-phenanthroline (0.022 equiv), $HSiMe(OTMS)_2$ (1 equiv), arene (5 equiv), THF, 100°C, 16 hours.

functionalization of the more electron-deficient arene, whereas the ratio of the initial rates of separate reactions was only 1.2:1 (**11a:1a**). These results suggest that cleavage of the aryl C-H bond is not the overall turnover-limiting step of the silylation of toluene and that the cleavage of the aryl C-H bond of toluene is irreversible.

The regioselectivities of the silylation reactions appear to arise from the steric bulk of both the ligand and the silane. The absence of reactivity with other silanes in the rhodium-catalyzed C–H silylation has prevented a direct comparison of the selectivity of reactions of $HSiMe(OTMS)_2$ with that of other silanes. However, results from the analogous iridium-catalyzed silylations provide evidence for the influence of the silane on the selectivity. The reaction of 5 equivalents of 2-tri(isopropyl)siloxytoluene (**21a**) with Et_3SiH generated the major product in which the silyl group is installed meta to the larger OTIPS group at the less electron-rich position of the arene (82:18 major:minor isomers) (Fig. 4). However, the reaction of 5 equivalents of **21a** with $HSiMe(OTMS)_2$ gave predominantly the product in which the silyl group is installed para to the larger group (7:93 minor:major isomers). We ascribe this change in selectivity to the unfavorable placement of the bulky $SiMe(OTMS)_2$ group meta to the OTIPS group on the arene in the latter transformation.

Conclusions

The intermolecular, rhodium-catalyzed silylation of arenes that we report here occurs under mild conditions, with arene as the limiting reagent and with regioselectivities that complement or surpass those of other arene functionalizations. Several factors lead to the selectivity and synthetic utility of the silylation reaction. First, the silicon reagent is sterically demanding. Assuming the intermediate that cleaves the aryl C–H bond contains a silyl group on the metal, the size of the silane reagent, along with the size of the ancillary ligands, control the degree of regioselectivity. Second, two of the substituents on the silane are bound to silicon through oxygen, and a silicon-heteroatom bond is typically required for many of the transformations of arylsilanes at the C–Si bond. The origin of the remote selectivity remains to be defined. However, our results suggest that a wide scope of functionalization reactions with remote regiocontrol should be achievable through judicious choice of ancillary ligands and reagents with appropriate steric bulk.

References and Notes

1. K. Godula, D. Sames, *Science* **312**, 67–72 (2006).
2. T. W. Lyons, M. S. Sanford, *Chem. Rev.* **110**, 1147–1169 (2010).
3. I. A. I. Mkhalid, J. H. Barnard, T. B. Marder, J. M. Murphy, J. F. Hartwig, *Chem. Rev.* **110**, 890–931 (2010).
4. J. F. Hartwig, *Acc. Chem. Res.* **45**, 864–873 (2012).
5. D. Alberico, M. E. Scott, M. Lautens, *Chem. Rev.* **107**, 174–238 (2007).
6. G. P. McGlacken, L. M. Bateman, *Chem. Soc. Rev.* **38**, 2447–2464 (2009).
7. R. J. Phipps, M. J. Gaunt, *Science* **323**, 1593–1597 (2009).
8. N. Hofmann, L. Ackermann, *J. Am. Chem. Soc.* **135**, 5877–5884 (2013).
9. D. Leow, G. Li, T.-S. Mei, J.-Q. Yu, *Nature* **486**, 518–522 (2012).
10. I. Fleming, J. Dunoguès, R. Smithers, in *Organic Reactions,* A. S. Kende, Ed. (John Wiley & Sons, 1989), vol. 2, pp. 57–193.
11. T.-Y. Luh, S.-T. Liu, in *The Chemistry of Organic Silicon Compounds,* Y. A. Z. Rappoport, Ed. (Wiley, vol. 2, Chichester, 2003), pp. 1793–1868.
12. K. Ezbiansky *et al*., *Organometallics* **17**, 1455–1457 (1998).
13. T. Ishiyama, K. Sato, Y. Nishio, N. Miyaura, *Angew. Chem. Int. Ed.* **42**, 5346–5348 (2003).
14. T. Saiki, Y. Nishio, T. Ishiyama, N. Miyaura, *Organometallics* **25**, 6068–6073 (2006).
15. M. Murata, N. Fukuyama, J.-i. Wada, S. Watanabe, Y. Masuda, *Chem. Lett.* **36**, 910–911 (2007).
16. T. Sakakura, Y. Tokunaga, T. Sodeyama, M. Tanaka, *Chem. Lett.* **16**, 2375–2378 (1987).
17. M. Ishikawa, S. Okazaki, A. Naka, H. Sakamoto, *Organometallics* **11**, 4135–4139 (1992).
18. B. Lu, J. R. Falck, *Angew. Chem. Int. Ed.* **47**, 7508–7510 (2008).
19. H. Ihara, M. Suginome, *J. Am. Chem. Soc.* **131**, 7502–7503 (2009).
20. F. Kakiuchi, K. Igi, M. Matsumoto, N. Chatani, S. Murai, *Chem. Lett.* **30**, 422–423 (2001).
21. J. Oyamada, M. Nishiura, Z. Hou, *Angew. Chem. Int. Ed.* **50**, 10720–10723 (2011).
22. N. A. Williams, Y. Uchimaru, M. Tanaka, *J. Chem. Soc. Chem. Commun.* (11): 1129–1130 (1995).
23. T. Ureshino, T. Yoshida, Y. Kuninobu, K. Takai, *J. Am. Chem. Soc.* **132**, 14324–14326 (2010).
24. Y. Kuninobu, T. Nakahara, H. Takeshima, K. Takai, *Org. Lett.* **15**, 426–428 (2013).
25. E. M. Simmons, J. F. Hartwig, *J. Am. Chem. Soc.* **132**, 17092–17095 (2010).
26. E. M. Simmons, J. F. Hartwig, *Nature* **483**, 70–73 (2012).
27. G. Choi, H. Tsurugi, K. Mashima, *J. Am. Chem. Soc.* **135**, 13149–13161 (2013).
28. C. Cheng, E. M. Simmons, J. F. Hartwig, *Angew. Chem. Int. Ed.* **52**, 8984–8989 (2013).
29. $HSiMe(OTMS)_2$ is commercially available.
30. For applications of phosphine-ligated rhodium catalysts in intramolecular silylation reactions, see (*23*, *24*).
31. Silylcyclohexane [GC–mass spectrometry; mass/charge ratio = 289.1; $M\text{-}CH_3$], from hydrosilylation of the hydrogen acceptor, cyclohexene, is the only major side product.
32. The side reaction, cyclohexene hydrosilylation, consumes both the silane and cyclohexene.
33. For reactions with **8a**, **9a**, and **10a**, the selectivities of silylation meta and ortho to the methoxy groups are 95.4:4.6, 97.0:3.0, and 97.4:2.6, respectively, as determined by GC analysis. The selectivities for all other 1,3-disubstituted arenes are >99:1.
34. T. Ishiyama, Y. Nobuta, J. F. Hartwig, N. Miyaura, *Chem. Commun.* **23**, 2924–2925 (2003).
35. For silylations of **16a** and **17a**, the selectivities for reactions at the 2-positions over all other positions are 98:2 and 97:3, respectively.
36. H. Tajuddin *et al*., *Chem. Sci.* **3**, 3505–3515 (2012).
37. L. T. Ball, G. C. Lloyd-Jones, C. A. Russell, *Science* **337**, 1644–1648 (2012).
38. B. A. Vanchura 2nd *et al*., *Chem. Commun. (Camb.)* **46**, 7724–7726 (2010).
39. Borylation of benzodioxole following the procedure in (*44*) afforded a mixture of meta, ortho, and diborylation products (92% yield) in a ratio of 6:33:61. This difference from (*38*) is likely due to the difference in the amount of the diboron reagent used.
40. Two constitutional isomers of the borylation product, along with a diborylation product, were obtained in a ratio of 43:18:39 following the literature procedure (*44*).
41. E. L. Eliel, S. H. Wilen, L. N. Mander, *Stereochemistry of Organic Compounds* (Wiley, New York, 1994).
42. J. M. Murphy, X. Liao, J. F. Hartwig, *J. Am. Chem. Soc.* **129**, 15434–15435 (2007).
43. S. D. Roughley, A. M. Jordan, *J. Med. Chem.* **54**, 3451–3479 (2011).
44. C. W. Liskey, X. Liao, J. F. Hartwig, *J. Am. Chem. Soc.* **132**, 11389–11391 (2010).

Acknowledgments: We thank the NSF (CHE-1213409) for financial support, Johnson-Matthey for a gift of $[Ir(cod)OMe]_2$, and T. W. Wilson for helpful discussions. A provisional patent application on this work has been submitted.

Supplementary Materials

www.sciencemag.org/content/343/6173/853/suppl/DC1
Materials and Methods
Figs. S1 to S3
Table S1
References (*45*–*58*)

4 November 2013; accepted 14 January 2014
10.1126/science.1248042

Dendritic Inhibition in the Hippocampus Supports Fear Learning

Matthew Lovett-Barron,[1,2]* Patrick Kaifosh,[1,2]* Mazen A. Kheirbek,[2,3] Nathan Danielson,[1,2] Jeffrey D. Zaremba,[1,2] Thomas R. Reardon,[1,2] Gergely F. Turi,[2] René Hen,[1,2,3] Boris V. Zemelman,[4] Attila Losonczy[1,2,5]†

Fear memories guide adaptive behavior in contexts associated with aversive events. The hippocampus forms a neural representation of the context that predicts aversive events. Representations of context incorporate multisensory features of the environment, but must somehow exclude sensory features of the aversive event itself. We investigated this selectivity using cell type–specific imaging and inactivation in hippocampal area CA1 of behaving mice. Aversive stimuli activated CA1 dendrite-targeting interneurons via cholinergic input, leading to inhibition of pyramidal cell distal dendrites receiving aversive sensory excitation from the entorhinal cortex. Inactivating dendrite-targeting interneurons during aversive stimuli increased CA1 pyramidal cell population responses and prevented fear learning. We propose subcortical activation of dendritic inhibition as a mechanism for exclusion of aversive stimuli from hippocampal contextual representations during fear learning.

Aversive stimuli cause animals to associate their environmental context with these experiences, allowing for adaptive defensive behaviors during future exposure to the context. This process of contextual fear conditioning (CFC) is dependent upon the brain

performing two functions in series: first developing a unified representation of the multisensory environmental context (the conditioned stimulus, CS), then associating this CS with the aversive event (unconditioned stimulus, US) for memory storage (*1*–*5*). The CS is encoded by the dorsal hippocampus, whose outputs are subsequently associated with the US through synaptic plasticity in the amygdala (*6*–*10*). The hippocampus must incorporate multisensory features of the environment into a representation of context but, paradoxically, must exclude sensory features during the moment of conditioning, when the primary sensory attribute is the US. The sensory features of the US may disrupt conditioning (*11*). Although the cellular and circuit mechanisms of fear learning and sensory convergence have been extensively studied in the amygdala (*3*, *5*, *12*), much less is known about how the neural circuitry of the hippocampus contributes to fear conditioning.

The primary output neurons of the hippocampus, pyramidal cells (PCs) in area CA1, are driven to spike by proximal dendritic excitation from CA3 and distal dendritic excitation from the entorhinal cortex (*13*). Whereas CA3 stores a unified representation of the multisensory context (*14*), the entorhinal cortex conveys information pertaining to the discrete sensory attributes of the context (*15*). At the cellular level, nonlinear interactions between inputs from CA3 and entorhinal cortex in the dendrites of PCs can result in burst-spiking output and plasticity (*16*–*18*). PCs can carry behaviorally relevant information in the timing of single spikes (*19*), spike rate (*13*), and spike bursts (*20*), but information conveyed with just bursts of spikes is sufficient for hippocampal encoding of context during fear learning (*21*). Distinct CA1 PC firing patterns are under the control of specialized local inhibitory interneurons (*22*, *23*). Whereas spike timing is regulated by parvalbumin-expressing (Pvalb$^+$) interneurons that inhibit the perisomatic region of PCs, burst spiking is regulated by somatostatin-expressing (Som$^+$) interneurons that inhibit PC dendrites (*24*–*26*). This functional dissociation suggests that CA1 Som$^+$ interneurons may play an important role in CFC. However, the activity of specific interneurons during CFC and their causal influence remain unknown.

To facilitate neural recording from multiple genetically and anatomically defined circuit elements in CA1 during CFC with two-photon Ca^{2+} imaging, we developed a variation of CFC for head-fixed mice (hf-CFC). We combined Ca^{2+} imaging with cell-type–specific inactivation tech-

[1]Doctoral Program in Neurobiology and Behavior, Columbia University, New York, NY, USA. [2]Department of Neuroscience, Columbia University, New York, NY, USA. [3]Division of Integrative Neuroscience, New York State Psychiatric Institute, New York, NY, USA. [4]Center for Learning and Memory, University of Texas, Austin, TX, USA. [5]Kavli Institute for Brain Science, Columbia University, New York, NY, USA.

*These authors contributed equally to this work
†Corresponding author. E-mail: al2856@columbia.edu

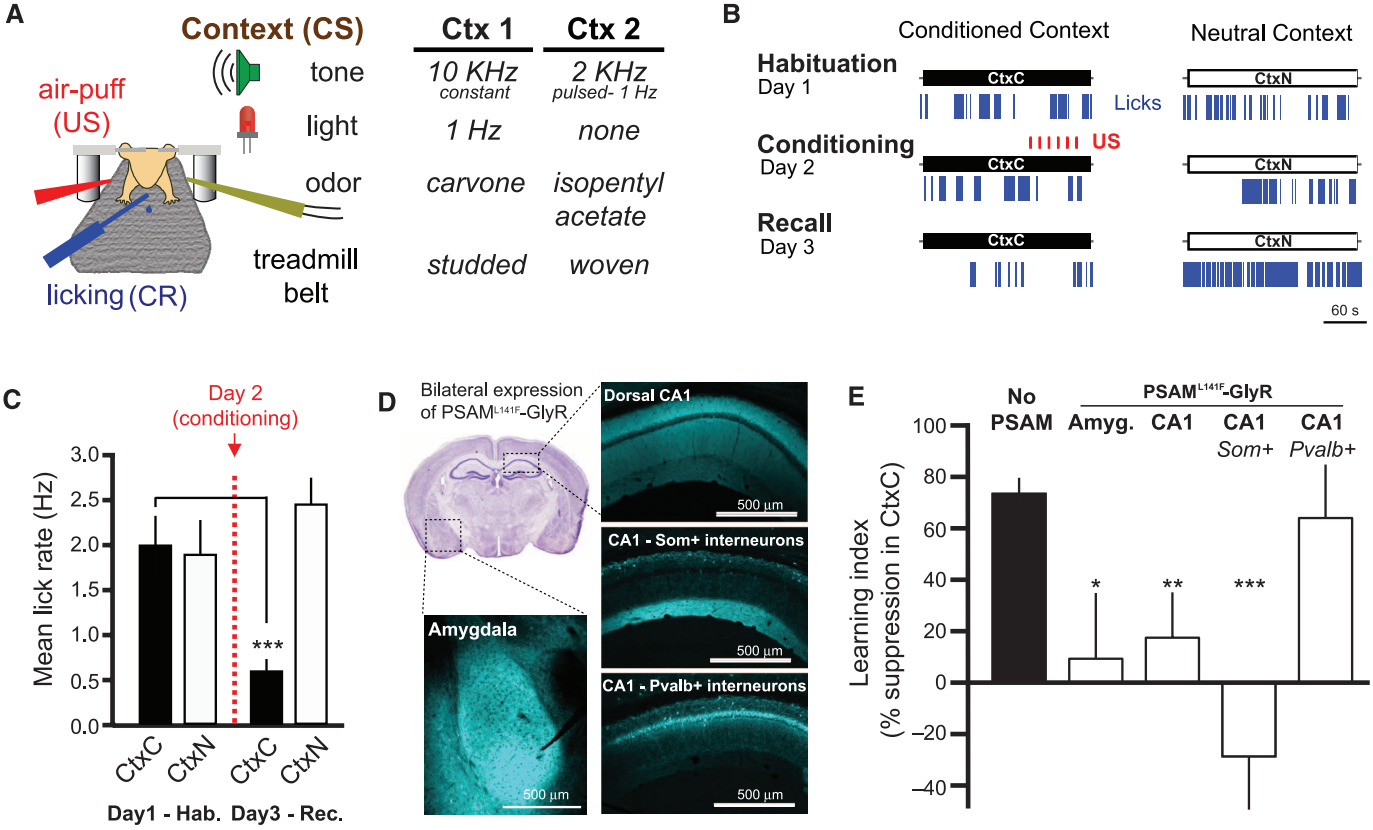

Fig. 1. Som$^+$ interneurons in CA1 are required for learning hf-CFC. (**A**) Schematic of hf-CFC task. A head-fixed mouse on a treadmill is exposed to contexts (CS) defined by distinct sets of multisensory stimuli. We used air puffs as the US and suppression of water-licking as a measure of learned fear (CR). The two distinct contexts used in this study are described at right. (**B**) Behavioral data from an example mouse over the hf-CFC paradigm. Conditioned (CtxC) and neutral (CtxN) contexts are each presented once a day, and lick rate is assessed during the 3-min context. (**C**) Summary data for 19 mice [two-way analysis of variance (ANOVA), context x session, $F_{(1,19)} = 9.34$, $P < 0.01$]. Mice showed a selective decrease in mean lick rate between habituation and recall in CtxC but not CtxN (paired sign tests). (**D**) Viral expression of PSAM^{L141F}-GlyR in the amygdala or dorsal CA1, revealed by α-bungarotoxin-Alexa647 immunostaining. All injections were bilateral; for simplicity, only one hemisphere is shown. Image at top left is from the Allen Brain Atlas. (**E**) Summary data for mice injected with PSEM^{89} systemically 15 min before the conditioning session in CtxC (day 2 of hf-CFC paradigm). Learning is assessed by the percentage of lick-rate decrease in the CtxC recall session (day 3) relative to the mean lick rate in all sessions. Mice expressing PSAM^{L141F}-GlyR in amygdala cells (Amyg., $n = 6$ mice), dorsal CA1 cells (CA1, $n = 5$ mice), or CA1 Som$^+$ interneurons (CA1-Som$^+$, $n = 8$ mice) showed impaired learning compared with mice not expressing PSAM^{L141F}-GlyR (No PSAM, $n = 11$ mice), whereas mice expressing PSAM^{L141F}-GlyR in CA1 Pvalb$^+$ interneurons (CA1-Pvalb$^+$, $n = 4$ mice) did not. Comparisons are Mann-Whitney U tests. Error bars, mean ± SEM. *$P < 0.05$; **$P < 0.01$; ***$P < 0.001$.

niques in head-fixed and freely moving mice to investigate the contribution of CA1 neural circuitry to fear learning.

CFC for Head-Fixed Mice

Conditioned fear in rodents is typically measured in terms of freezing upon re-exposure to the context where the subject experienced an aversive stimulus (*3*, *5*). However, using freezing as a conditioned response (CR) is problematic in head-fixed mice. Instead, we measured learned fear using conditioned suppression of water licking (*27*, *28*), an established measure of fear that translates well to head-fixed preparations. We trained water-restricted mice to lick for small water rewards while head-fixed on a treadmill (*29*), then exposed them to two multisensory contexts (sets of auditory, visual, olfactory, and tactile cues) over three consecutive days and monitored their rate of licking (Fig. 1A and fig. S1A) (see Materials and Methods). On the second day, we paired the air-puff US with one of the contexts and assessed lick rate in both contexts the following day. We found that US pairing caused a decrease in the rate of licking in the conditioned context (CtxC) but not the neutral (CtxN) (Fig. 1, B and C, and fig. S1, B to E).

We used pharmacogenetic neuronal inactivation to test the necessity of the hippocampus and amygdala for the encoding of hf-CFC. We targeted bilateral injections of recombinant adeno-associated virus [rAAV(*Synapsin-PSAM^{L141F}-GlyR*)] to express the ligand-gated Cl^- channel PSAM^{L141F}-GlyR in either dorsal hippocampal area CA1 or the amygdala in wild-type mice (Fig. 1D). Neurons expressing PSAM^{L141F}-GlyR are inactivated for ~15 to 20 min upon systemic administration of its ligand PSEM^{89} (60 mg per kg of weight, intraperitoneally) (*30*). We administered PSEM^{89} to mice before conditioning in CtxC, and tested their memory 24 hours later without the drug by assessing lick suppression in CtxC recall compared with mean licking across all sessions. In agreement with conventional freely moving CFC results (*6*, *7*, *31*, *32*), we found that inactivating neurons in dorsal CA1 or the amygdala prevented contextual fear learning (Fig. 1E).

Som$^+$ Interneurons Are Required for CFC

To determine the relevance of CA1 inhibitory circuits for the acquisition of hf-CFC, we asked whether acute inactivation of γ–aminobutyric acid-releasing (GABAergic) interneuron subclasses in CA1 would alter learning. We injected rAAV (*Synapsin-PSAM^{L141F}-GlyR*)^{cre} bilaterally into CA1 of *Som-cre* or *Pvalb-cre* mice to express PSAM^{L141F}-GlyR selectively in either Som$^+$ dendrite-targeting

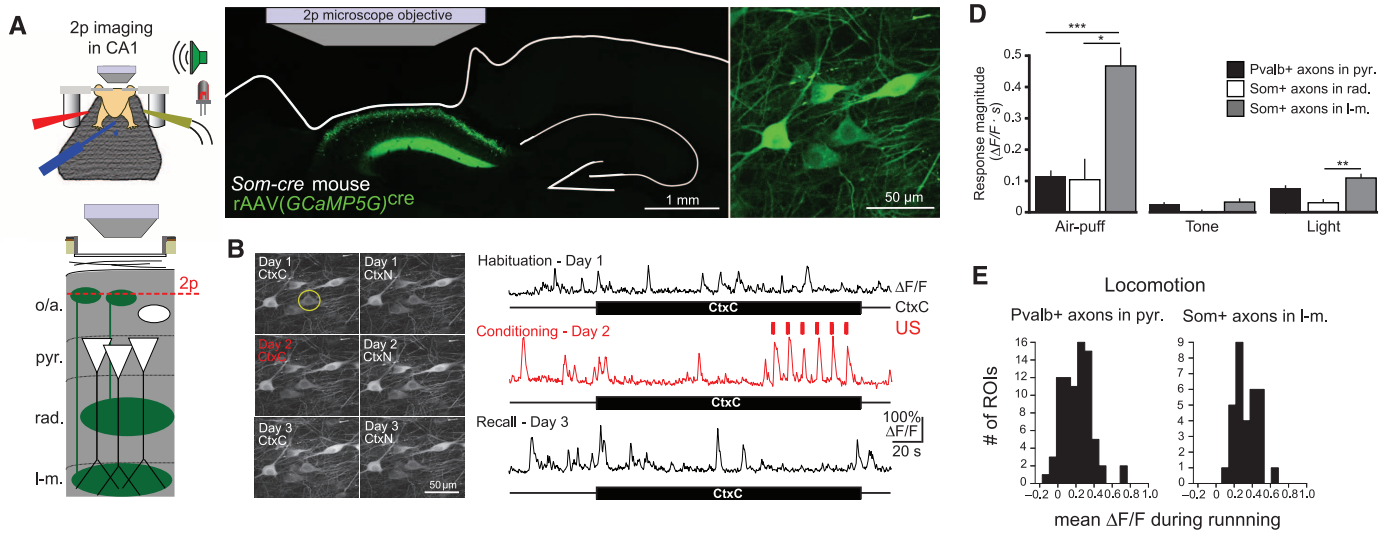

Fig. 2. Som$^+$ interneurons targeting stratum lacunosum-moleculare are activated by the US. (**A**) (Top left) Schematic of hf-CFC during two-photon (2p) imaging from hippocampal neurons. (Bottom left) Schematic of recording configuration, with 2p imaging from Som$^+$ interneurons in the oriens/alveus layers of CA1 in vivo (o/a, strata oriens/alveus; pyr., stratum pyramidale; rad., stratum radiatum; l-m., stratum lacunosum-moleculare). (Right) Confocal image of coronal section from mouse expressing GCaMP5G in Som$^+$ interneurons in dorsal CA1. The 2p microscope objective and landmarks showing the outline of the brain, including the removed cortex and the contralateral hippocampus, are illustrated. An in vivo 2p image of GCaMP-expressing Som$^+$ interneurons is shown at far right. (**B**) (Left) 2p images of the same field of view from (A) for the six hf-CFC sessions over the course of 3 days. Images are time averages of 2000 motion-corrected imaging frames collected for each imaging session. (Right) $\Delta F/F$ traces from an example Som$^+$ CA1 interneuron (circled at left) over the three daily exposures to CtxC. (**C**) (Left) Schematic of recording configuration, with in vivo 2p imaging from Som$^+$ axons in radiatum or lacunosum-moleculare layers of CA1, Pvalb$^+$ axons in the pyramidale layer. (Middle) Expression of GCaMP5G in layer-specific axonal projections, revealed by confocal images of coronal sections and in vivo 2p images of each layer. (Right) Example trial-averaged responses (five trials each presented in pseudorandom order) of layer-specific whole-field fluorescence responses to discrete 200-ms sensory stimuli and locomotion (mean with shaded SD). (**D**) Summary data for sensory stimulation experiments shown in (C). Responses are quantified as the mean integral of whole-field $\Delta F/F$ over the 3 s after the stimulus. [two-way ANOVA, axon-type x stimulus type, $F_{(4,84)} = 16.9$, $P < 0.001$; post hoc Mann-Whitney U tests]. Error bars, mean ± SEM. *$P < 0.05$; **$P < 0.01$; ***$P < 0.001$. (**E**) Summary data for whole-field $\Delta F/F$ responses to treadmill-running. Pvalb$^+$ axons in pyramidale exhibit locomotion responses similar to Som$^+$ axons in lacunosum-moleculare (Mann-Whitney U test, $P = 0.101$).

interneurons or Pvalb$^+$ perisomatic-targeting interneurons, respectively (*25*) (Fig. 1D and fig. S2). Systemic PSEM^{89} administration during conditioning prevented learning in mice expressing PSAM^{L141F}-GlyR in CA1 Som$^+$ interneurons, but not in mice expressing PSAM^{L141F}-GlyR in CA1 Pvalb$^+$ interneurons (Fig. 1E).

We repeated our inactivation experiments in conventional CFC experiments with freely-moving mice, with a foot-shock US and freezing as the CR. Inactivating CA1 Som$^+$ interneurons during conditioning prevented recall 24 hours later without the drug, while inactivating Pvalb$^+$ interneurons had no effect (fig. S3, A and B). Inactivating Som$^+$ interneurons or Pvalb$^+$ interneurons did not alter perception of the US, as hippocampal-independent auditory cued conditioning was left intact (fig. S3C). Inactivating Som$^+$ neurons did not simply alter CS perception, as inactivation during both conditioning and recall also prevented learning (fig. S4). The absence of a role for Pvalb$^+$ interneurons in CFC was not due to insufficient neuronal inactivation. In agreement with previous findings (*33*), this manipulation reduced performance in a spatial working memory task (fig. S5).

The US Activates Som$^+$ Interneurons

We used two-photon Ca^{2+} imaging to record the activity of CA1 Som$^+$ interneurons over the course of hf-CFC. We unilaterally injected rAAV(*Synapsin-GCaMP5G*)^{cre} into dorsal CA1 of *Som-cre* mice to express the genetically encoded Ca^{2+} indicator GCaMP5G (*34*) in the somata, dendrites, and axons of Som$^+$ interneurons (Fig. 2A). To visualize CA1 neurons in vivo, we used established surgical techniques (*29*, *35*) to implant a chronic imaging window superficial to dorsal CA1. After recovery, water restriction, and habituation to head-restraint, we engaged mice in the hf-CFC task while imaging Ca^{2+}-evoked GCaMP5G fluorescence transients from Som$^+$ interneuron somata in the oriens and alveus layers of CA1. We returned to the same field of view for each of the six sessions of hf-CFC (Fig. 2B) and processed fluorescence time-series data using established methods for motion-correction and signal processing (*29*, *36*). Strikingly, Som$^+$ interneurons displayed increased activity in response to the US during hf-CFC (example neuron in Fig. 2B).

To investigate the dynamics of stimulus-evoked GABAergic signaling in more detail, we imaged CA1 inhibitory neurons during the pseudorandom presentation of discrete sensory stimuli from the hf-CFC task: light flashes and tones, which were elements of the CS, or air-puffs, which served as the US. To image a greater variety of interneurons simultaneously, we injected cre-independent rAAV(*Synapsin-GCaMP5G*) into CA1 of *Som-cre* mice crossed with a tdTomato reporter line, which allowed us to simultaneously image sensory responses of Som$^+$ and Som$^-$ interneurons (fig. S6A). Air puffs activated most Som$^+$ interneurons (fig. S6B), whereas a smaller proportion of Som$^-$ and Pvalb$^+$ interneurons had comparable responses (fig. S6C).

Not all Som$^+$ interneurons were activated by the air puff, which could reflect a difference between bistratified cells and oriens-lacunosum-moleculare (OLM) cells, both of which are labeled in *Som-cre* mice (*25*). The axons of bistratified cells arborize in stratum oriens and radiatum, whereas those of OLM cells arborize in stratum lacunosum-moleculare (*22*, *23*). These two inhibitory projections contact the dendritic compartments of CA1 PCs that receive input from CA3 and the entorhinal cortex, respectively, suggesting potentially distinct functions. To isolate the relative contributions of these two inhibitory pathways to US-evoked signaling, we labeled Som$^+$ neurons with GCaMP5G in *Som-cre* mice and focused our imaging plane on the axons of bistratified cells in radiatum, or the axons of OLM cells in lacunosum-moleculare (Fig. 2C).

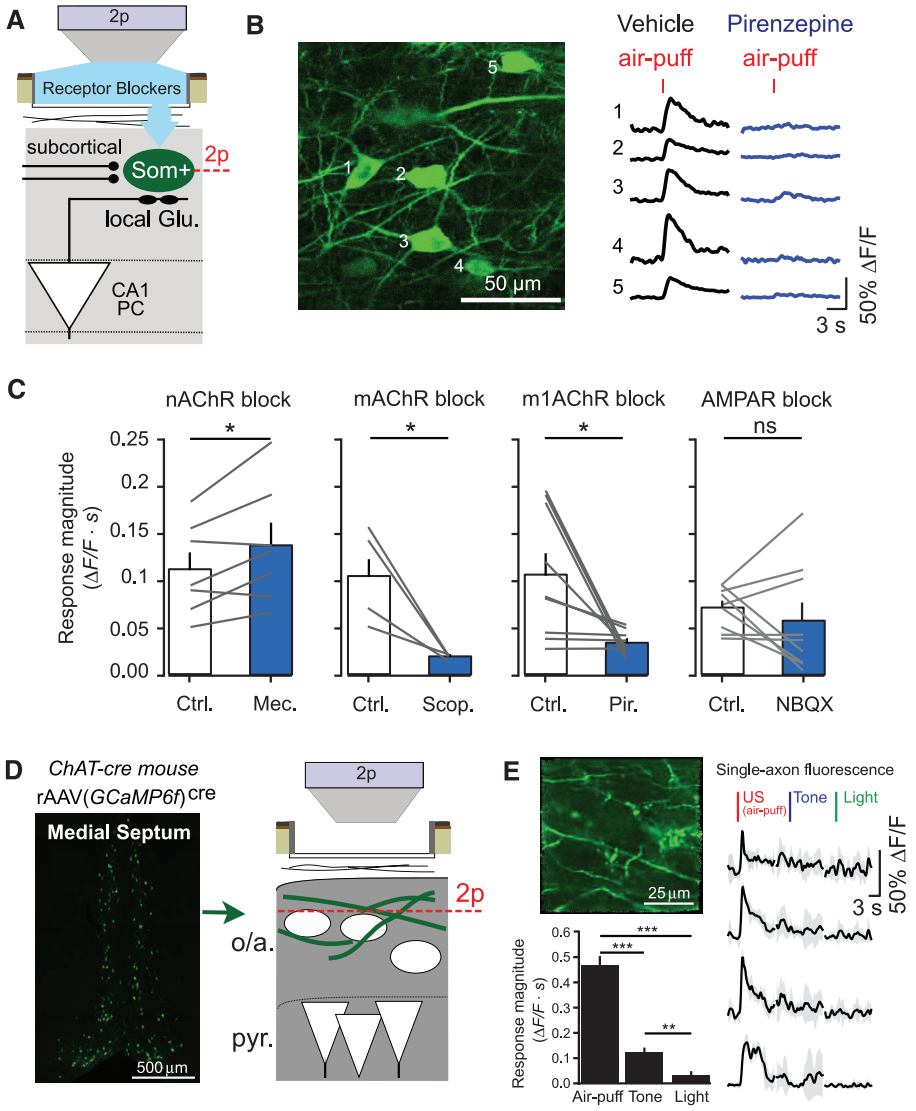

Fig. 3. Cholinergic inputs from the medial septum drive CA1 Som$^+$ interneurons during the US. (**A**) Schematic of recording configuration, with 2p imaging from Som$^+$ interneurons in the oriens and alveus layers of CA1, and local pharmacological manipulations through an aperture in the imaging window. (**B**) Example in vivo 2p image of GCaMP-expressing Som$^+$ interneurons and their fluorescence responses to air puffs in vehicle (cortex buffer) and in the presence of 1 mM pirenzepine. (**C**) Summary data for local pharmacological manipulations. Each point is the mean response of all Som$^+$ interneurons within a field of view (FOV) to air puffs (5 trials each) in vehicle (Ctrl.) and upon drug application (nAChR block, 7 FOVs in 5 mice; mAChR block, 4 FOVs in 3 mice; m1AChR block, 9 FOVs in 5 mice; AMPAR block, 9 FOVs in 4 mice). Comparisons are paired *t* tests between drug conditions. (**D**) (Left) Coronal confocal image of GCaMP6f$^+$/ChAT$^+$ neurons in the medial septum of a *ChAT-cre* mouse. (Right) Schematic of recording configuration, with 2p imaging from ChAT$^+$ axons in the oriens and alveus layers of CA1. (**E**) (Top left) Example in vivo 2p image of GCaMP6f-expressing ChAT$^+$ axons in CA1. (Right) Mean responses of individual axons to sensory stimuli. (Bottom left) Summary data from ChAT$^+$ axons averaged within each FOV (sign tests; $n = 20$ FOVs in 2 mice). Error bars, mean ± SEM. $^*P < 0.05$; $^{**}P < 0.01$; $^{***}P < 0.001$; ns, nonsignificant.

Whole-field recording from the dense Som$^+$ axonal termination in lacunosum-moleculare revealed a fast, high-amplitude increase in fluorescence in response to the air puff but not the tone or light (Fig. 2D). In contrast, the lower density axons in radiatum revealed little response to these stimuli. We also expressed GCaMP5G in *Pvalb-cre* mice to record from Pvalb$^+$ basket cell axons in stratum pyramidale. These high-density axons had much smaller responses to the US (Fig. 2, C and D) but responded robustly to treadmill running (Fig. 2E).

Acetylcholine Drives Som$^+$ Interneurons

To drive fast-onset responses to the US, Som$^+$ interneurons in CA1 must receive a time-locked source of US-driven excitation. However, most excitatory inputs to OLM cells are synapses from CA1 PCs (*23*), and PCs do not encode the US (*5*, *10*) or robustly respond to it (fig. S6C) (*37*–*40*). Alternatively, Som$^+$ interneurons could be excited by extrahippocampal sources such as subcortical neuromodulatory inputs. Indeed, OLM cells in CA1 can be depolarized through both nicotinic and muscarinic acetylcholine receptors (*41*, *42*), and lesions of cholinergic inputs from the medial septum are known to prevent the suppressive effects of aversive stimuli on CA1 spiking activity (*38*, *43*–*45*). Additionally, neocortical interneurons have been demonstrated to respond to aversive stimuli through cholinergic input (*46*).

To probe the source of US-evoked activation of Som$^+$ interneurons, we modified our imaging window to allow for local pharmacological manipulation of the imaged neural tissue (fig. S7A) (*29*). We applied antagonists of neuromodulatory receptors through the imaging window, which passively diffused into CA1; there, we imaged GCaMP5G-expressing Som$^+$ interneuron responses to stimuli before and after drug administration (Fig. 3, A and B). Blockade of the nicotinic acetylcholine receptor (nAChR) did not decrease Som$^+$ interneuron responses to air puffs (1 mM mecamylamine) (Fig. 3C) but instead modestly increased responses. However, blockade of the muscarinic acetylcholine receptor (mAChR) significantly reduced air-puff responses in Som$^+$ interneurons (1 mM scopolamine) (Fig. 3C). We recapitulated this result with more selective blockade of type 1 mAChRs (1 mM pirenzepine; Fig. 3, B and C), which reduced air-puff–evoked Som$^+$ interneuron responses in a dose-dependent manner (fig. S7B). Metabotropic receptors like mAChRs generally act on slower time scales, but studies in brain slices have demonstrated that muscarinic input can evoke fast-onset depolarization and spiking of CA1 OLM cells (*41*, *47*). mAChRs in dorsal hippocampus are required for encoding CFC (*48*), and our results suggest a possible circuit mechanism that contributes to this requirement. This effect was not a consequence of reduced disynaptic drive from m1AChR-responsive PCs (*49*), because m1AChR block did not substantially alter air-puff–evoked activity in the minority of responding PCs (fig. S7C), and responses of Som$^+$ interneurons were not substantially changed by blockade of glutamatergic AMPA receptors (20 μM 2,3-Dioxo-6-nitro-1,2,3,4-tetrahydrobenzo[*f*]quinoxaline-7-sulfonamide) (Fig. 3C).

Cholinergic input to the hippocampus arises from projection neurons in the medial septum (*50*), a region required for CFC (*51*). To directly record the activity of these projections, we injected rAAV(*ef1α-DIO-GCaMP6f*)^{cre} into the medial septum (MS) of *ChAT-cre* mice to express the sensitive Ca^{2+} indicator GCaMP6f (*52*) in cholinergic projection neurons. We imaged cholinergic (ChAT$^+$) axons in the oriens and alveus layers of CA1 during sensory stimulation (Fig. 3D and fig. S8). ChAT$^+$ axons responded robustly to air puffs, with smaller responses to tones and very little response to light flashes (Fig. 3E). ChAT$^+$ axon responses were independent of air-puff duration, similar to Som$^+$ axons in lacunosum-moleculare (fig. S9) but differing from the graded responses of septohippocampal GABAergic projections (*29*).

Coaligned Dendritic Inhibition and Excitation

The distal tuft dendrites of PCs receive excitatory input from the entorhinal cortex, raising the possibility that the inhibition we observe is counteracting US-evoked excitation to these dendrites. The entorhinal cortex provides sensory information to CA1 (*15*), including projections from the lateral entorhinal cortex (LEC) (*53*) and nonspatial neurons of the medial entorhinal cortex (MEC) (*54*) that synapse with CA1 PC distal dendrites. In contrast, the proximal dendrites of PCs receive input from CA3 believed to carry stored contextual representations rather than sensory information (*14*). To directly record from these excitatory inputs, we injected rAAV(*Synapsin-GCaMP6f*) into CA3, LEC, or MEC and imaged axonal activity in ipsilateral CA1 layers oriens/radiatum (CA3 axons) or lacunosum-moleculare (LEC and MEC axons) (Fig. 4A and fig. S10, A and B). Sensory inputs, particularly aversive air puffs, evoked stronger signals from LEC and MEC axonal boutons compared with CA3 axonal boutons, reflected by changes in whole-field fluorescence (Fig. 4, B and C). These data indicate that US-driven inhibition of PC distal tuft dendrites in stratum lacunosum-moleculare is coaligned with

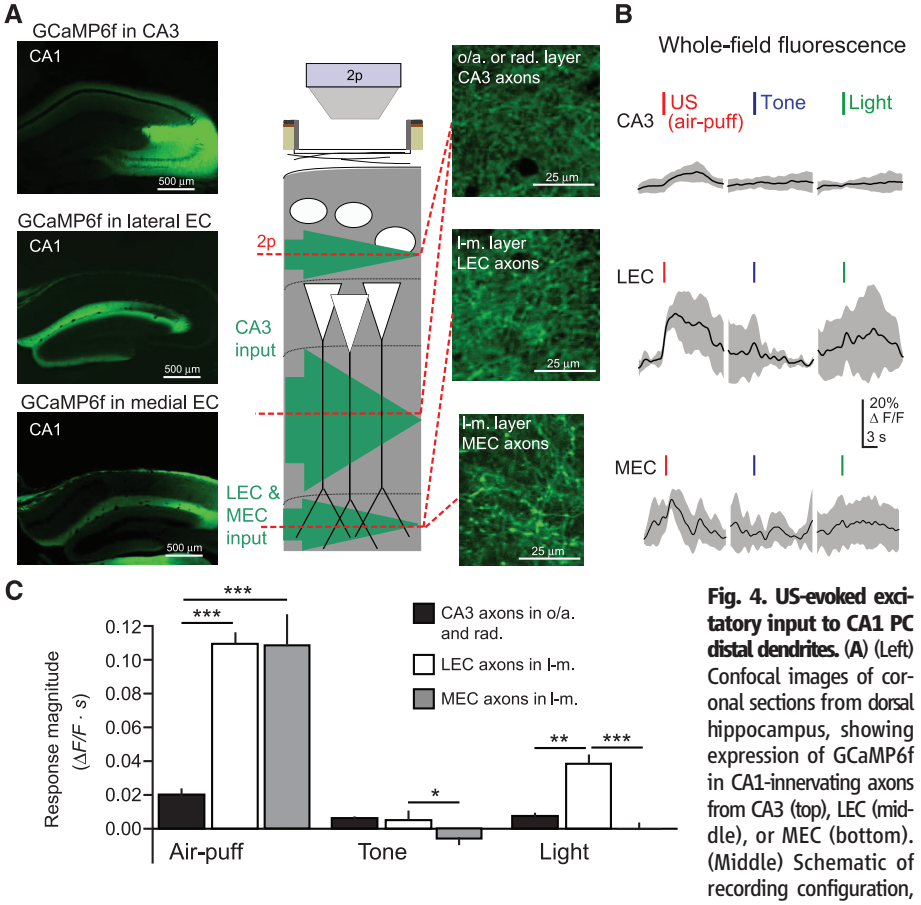

Fig. 4. US-evoked excitatory input to CA1 PC distal dendrites. (A) (Left) Confocal images of coronal sections from dorsal hippocampus, showing expression of GCaMP6f in CA1-innervating axons from CA3 (top), LEC (middle), or MEC (bottom). (Middle) Schematic of recording configuration, with 2p imaging from excitatory axons in the oriens/radiatum layers (CA3 projections) or lacunosum-moleculare layer (LEC or MEC projections) of CA1. (Right) Example in vivo 2p images of GCaMP6f-expressing axons in CA1 (CA3, top; LEC, middle; MEC, bottom). **(B)** Example mean whole-field fluorescence traces from CA3, LEC, and MEC axons [examples in (A)], in response to discrete sensory stimuli (mean with shaded SD). **(C)** Summary data for sensory stimulation experiments. Responses are quantified as the mean integral of $\Delta F/F$ over the 3 s after the stimulus (two-way ANOVA, axon type x stimulus type, $F_{(4,84)} = 10.7$, $P < 0.001$; post hoc Mann-Whitney U tests). Error bars, mean ± SEM. *$P < 0.05$; **$P < 0.01$; ***$P < 0.001$.

excitatory input, which could effectively limit dendritic depolarization (*55*). Compartmentalized inhibition can also prevent propagation of excitation from distal to proximal dendrites (*16*–*18*), potentially preserving responses of PCs to sparse excitation from CA3 axons (fig. S10C). Similar US-driven signals may occur in other excitatory inputs to lacunosum-moleculare, such as the thalamic reuniens nucleus.

Consequences for Hippocampal Output and Learning

Ultimately, any dysfunction in hippocampal encoding of context is likely reflected in changes to the primary hippocampal output neurons: CA1 PCs. Som$^+$ interneurons appear poised to inhibit excitation during the US and are required for CFC, but the response of PCs in their absence is unknown. To probe the consequences of inactivating Som$^+$ interneurons for US-evoked PC population activity, we simultaneously imaged air-puff responses of ~150 to 200 PCs while inactivating Som$^+$ interneurons. We injected rAAV(*Synapsin-PSAM^{L141F}-GlyR*)^{cre} and rAAV(*Synapsin-GCaMP6f*) into CA1 of *Som-cre* mice, and imaged air-puff–evoked responses of PC populations in pyramidale before and during Som$^+$ interneuron inactivation with local application of PSEM^{89} through the hippocampal imaging window (Fig. 5A). Although systemic PSEM^{89} reduced air-puff–evoked Ca^{2+} activity in Som$^+$/PSAM^{L141F}GlyR$^+$ interneurons (fig. S11), we applied PSEM^{89} locally to the imaging window to extend the duration of neuronal inactivation. We imaged PC populations during control conditions and PSEM^{89} application, identifying neurons with significant air-puff–evoked Ca^{2+} transients (fig. S12) (*36*). Inactivating Som$^+$ interneurons significantly increased the number of PCs activated by the air puff within a field of view (Fig. 5, B and C) and significantly increased the duration of Ca^{2+} transients in PCs that responded to the US in both control and PSEM^{89} conditions (Fig. 5, B and C). Extended transient duration likely corresponds to the longer spike bursts previously reported from electrophysiological measurements of CA1 PCs upon inactivating Som$^+$ interneurons (*25*, *26*). These effects were not observed in control mice that did not express PSAM^{L141F}-GlyR (fig. S13A). Nonspecific reduction in inhibition with $GABA_AR$ blocker bicuculine substantially increased the number of PCs responding to the air puff and their duration (fig. S13B), suggesting that other inhibitory synapses in CA1 also contribute to the control of PC population activity during aversive sensory events.

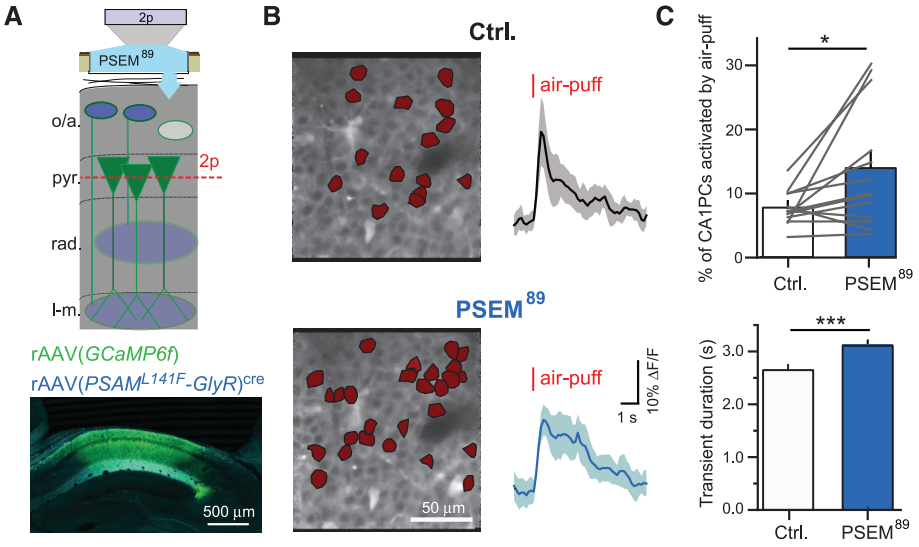

Fig. 5. Effects of inactivating CA1 Som$^+$ interneurons on US-evoked PC population activity. (**A**) (Top) Schematic of recording configuration, with 2p imaging from CA1 PC populations in the pyramidale layer of CA1 and local pharmacologenetic manipulation of PSAM^{L141F}-GlyR–expressing Som$^+$ interneurons through an aperture in the imaging window. (Bottom) Confocal image of coronal CA1 sections, with GCaMP6f expression in all neurons (green) and PSAM^{L141F}-GlyR expression in Som$^+$ interneurons, revealed by α-BTX immunostaining (blue). (**B**) (Left) Corrected time-average images of example recordings in pyr. of a mouse expressing PSAM^{L141F}-GlyR in Som$^+$ interneurons. PCs with significant US responses are marked in red. (Right) Mean $\Delta F/F$ responses of cells active in both control and PSEM^{89} conditions from left (shading is SD). (**C**) Summary data for multiple FOVs between drug conditions. (Top) Mean percentage of significantly active CA1 PCs (ctrl, 7.6 ± 0.7%; PSEM^{89}, 13.7 ± 2.5%; n = 13 FOVs; paired t test). (Bottom) Mean duration of significant transients in cells active in both drug conditions (ctrl, 2.64 ± 0.09 s; PSEM^{89}, 3.09 ± 0.09 s; n = 96 cells; paired t test). Error bars, mean ± SEM. *P < 0.05; ***P < 0.001.

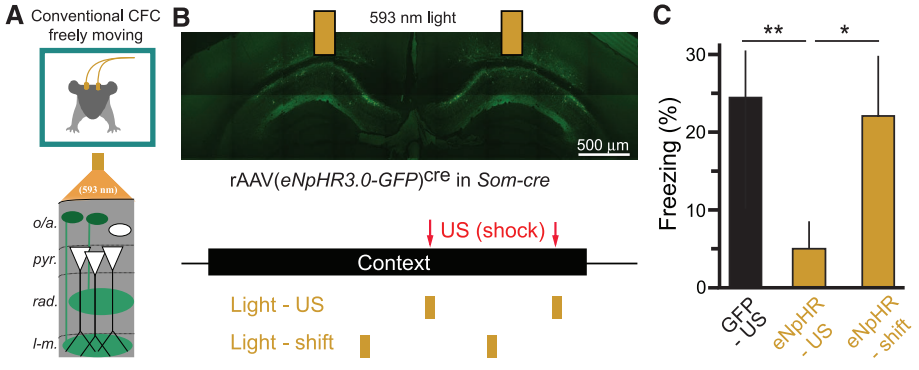

Fig. 6. Inactivating CA1 Som$^+$ interneurons during the US alone is sufficient to prevent CFC. (**A**) Schematic of optogenetic experiments in freely moving mice. Bilateral optic fibers deliver 593-nm light to inhibit eNpHR3.0-eGFP–expressing Som$^+$ interneurons in CA1 during CFC in freely moving mice. (**B**) (Top) Confocal image of eNpHR3.0-eGFP–expressing Som$^+$ interneurons in dorsal CA1 and indication of optic fiber positions. (Bottom) Experimental protocol. Mice are exposed to a context for 3 min, with two footshocks (2 s, 1 mA) 118 s and 178 s into the context. Two pulses of 593-nm light (6 s) were delivered through bilateral optical fibers starting at 116 s and 176 s (Light-US group) or 86 s and 146 s (Light-shift group). (**C**) Summary data for optogenetic stimulation experiments. GFP-US, n = 6 mice; eNpHR-US, n = 8 mice; eNpHR-shift, n = 6 mice; one-way ANOVA, $F_{(2,19)} = 3.87$, $P < 0.05$; comparisons are unpaired t tests. Error bars, mean ± SEM. *P < 0.05; **P < 0.01.

Our imaging data suggest that Som$^+$ interneurons are required for CFC because of their activation during the US. To test this hypothesis directly in a conventional CFC task, we used optogenetic methods in freely moving mice to inactivate Som$^+$ interneurons selectively during the footshock US (Fig. 6A). We expressed the light-gated Cl^- pump halorhodopsin (*56*) in Som$^+$ interneurons by injecting rAAV(*Synapsin-eNpHR3.0-eGFP*)^{cre} bilaterally into dorsal CA1 of *Som-cre* mice (fig. S14A) and implanting optic fibers over the injection sites. We used a CFC paradigm with two footshocks, which were each accompanied by coincident illumination of dorsal CA1 with 593-nm light (Fig. 6B), which suppressed spiking of Som$^+$/eNpHR3.0$^+$ neurons (fig. S14b). Inactivating Som$^+$ interneurons during the US significantly reduced conditioned freezing 24 hours later compared with controls injected with rAAV(*Synapsin-eGFP*)^{cre} (Fig. 6, B and C). Importantly, shifting the optical suppression of Som$^+$ interneurons

to 30 s before each US did not reduce freezing (Fig. 6, B and C).

Discussion

Classical fear conditioning implies a separation of CS and US prior to their association in the amygdala (*3*–*5*). In the case of cued fear conditioning (e.g., tone and shock), the brain achieves CS-US segregation by separate anatomical pathways for auditory and aversive somatosensory inputs (*57*, *58*). Standard models of CFC also assume that the hippocampus does not receive information about the US; rather, the hippocampus encodes the CS alone, whose outputs to the amygdala can be paired with the US for associative conditioning (fig. S15, A and B). However, here we observe a direct cortical excitatory input to CA1 during the US via the entorhinal cortex, indicating an anatomical overlap between sensory information for CS and US before the amygdala (*59*, *60*). This US may impede contextual conditioning (*11*). We suggest an alternative conceptual model for CFC that addresses the problem of sensory convergence in the hippocampus. In this model, subcortical neuromodulatory input drives CA1 Som^+ interneurons to selectively inhibit integration of the excitatory input pathway carrying US information to CA1. These data suggest a circuit mechanism for previously reported suppression of CA1 activity upon aversive stimulation (*37*–*40*). Compartmentalized inhibition suppresses integration of excitatory input in PC distal dendrites, which reduces US-evoked CA1 PC activity and can help limit interference of the US with CS encoding. This circuit can ensure that hippocampal output reliably encodes the CS during learning, so that memories stored downstream in the amygdala can be reactivated by exposure to the CS alone (fig. S15, C and D).

Inactivating Som^+ interneurons both increases CA1 PC activity and prevents learning. Impairments in memory storage could therefore result from a disruption of the hippocampal ensemble identity or population sparsity. The downstream mechanisms by which associative fear memories are impaired by CA1 Som^+ interneuron inactivation can be addressed by studying CS-US convergence and plasticity in the amygdala. Som^+ interneurons may also influence processing in the entorhinal cortex and medial septum through long-range inhibition (*61*). Furthermore, it remains to be determined whether US-driven excitation to CA1 contributes to long-term changes in CA1 PC activity after fear conditioning, such as place-cell remapping (*62*).

Our data suggest that inhibitory circuits can inhibit selected dendritic compartments to favor integration of one excitatory input pathway (proximal) over another (distal). GABA release localized to lacunosum-moleculare could accomplish this input segregation by inhibiting localized dendritic electrogenesis, which is required for propagating entorhinal excitatory inputs to drive output spikes and for inducing plasticity (*16*–*18*). This mechanism may also be present in sensory neocortex, where aversive footshocks activate cholinergic input to drive layer 1 interneurons in primary auditory and visual cortex (*46*). Layer 1 interneurons inhibit the apical tuft dendrites of layer 5 PCs, the primary output cell of the neocortex, at the site of multimodal association in layer 1 (*55*). Therefore the same mechanism we describe in CA1 could protect layer 5 PCs in primary sensory cortex from interference by the US, so that their outputs to the amygdala are driven by inputs to their basal dendrites reflecting local sensory processing, rather than inputs to tuft dendrites reflecting cross-modal influences.

These results suggest that dendrite-targeting Som^+ interneurons provide US-evoked inhibition that is required for successful contextual fear learning. These interneurons are central to a mechanism by which the hippocampus processes contextual sensory inputs as a CS while excluding the sensory features of the US. Selective inhibitory control over integration of excitatory input pathways could be a general strategy for nervous systems to achieve separate processing channels in anatomically overlapping circuits, a process that could be flexibly controlled by a multitude of inhibitory interneuron types (*22*, *23*) and neuromodulatory systems (*63*).

References and Notes

1. M. S. Fanselow, *Learn. Motiv.* **17**, 16–39 (1986).
2. M. S. Fanselow, *Anim. Learn. Behav.* **18**, 264–270 (1990).
3. S. Maren, *Annu. Rev. Neurosci.* **24**, 897–931 (2001).
4. J. W. Rudy, N. C. Huff, P. Matus-Amat, *Neurosci. Biobehav. Rev.* **28**, 675–685 (2004).
5. M. S. Fanselow, A. M. Poulos, *Annu. Rev. Psychol.* **56**, 207–234 (2005).
6. J. J. Kim, M. S. Fanselow, *Science* **256**, 675–677 (1992).
7. R. G. Phillips, J. E. LeDoux, *Behav. Neurosci.* **106**, 274–285 (1992).
8. S. L. Young, D. L. Bohenek, M. S. Fanselow, *Behav. Neurosci.* **108**, 19–29 (1994).
9. S. Maren, M. S. Fanselow, *J. Neurosci.* **15**, 7548–7564 (1995).
10. P. W. Frankland *et al.*, *Hippocampus* **14**, 557–569 (2004).
11. M. S. Fanselow, J. P. DeCola, S. L. Young, *J. Exp. Psychol. Anim. Behav. Process.* **19**, 121–137 (1993).
12. P. Sah, E. S. Faber, M. Lopez De Armentia, J. Power, *Physiol. Rev.* **83**, 803–834 (2003).
13. O. J. Ahmed, M. R. Mehta, *Trends Neurosci.* **32**, 329–338 (2009).
14. R. P. Kesner, *Learn. Mem.* **14**, 771–781 (2007).
15. S. Maren, M. S. Fanselow, *Neurobiol. Learn. Mem.* **67**, 142–149 (1997).
16. N. L. Golding, N. P. Staff, N. Spruston, *Nature* **418**, 326–331 (2002).
17. J. T. Dudman, D. Tsay, S. A. Siegelbaum, *Neuron* **56**, 866–879 (2007).
18. H. Takahashi, J. C. Magee, *Neuron* **62**, 102–111 (2009).
19. M. W. Jones, M. A. Wilson, *PLOS Biol.* **3**, e402 (2005).
20. K. D. Harris, H. Hirase, X. Leinekugel, D. A. Henze G. Buzsáki, *Neuron* **32**, 141–149 (2001).
21. W. Xu *et al.*, *Neuron* **73**, 990–1001 (2012).
22. T. F. Freund, G. Buzsáki, *Hippocampus* **6**, 347–470 (1996).
23. T. Klausberger, P. Somogyi, *Science* **321**, 53–57 (2008).
24. A. Losonczy, B. V. Zemelman, A. Vaziri, J. C. Magee, *Nat. Neurosci.* **13**, 967–972 (2010).
25. M. Lovett-Barron *et al.*, *Nat. Neurosci.* **15**, 423–430, S1–S3 (2012).
26. S. Royer *et al.*, *Nat. Neurosci.* **15**, 769–775 (2012).
27. W. J. Mahoney, J. J. B. Ayres, *Anim. Learn. Behav.* **4**, 357–362 (1976).
28. M. E. Bouton, R. C. Bolles, *Anim. Learn. Behav.* **8**, 429–434 (1980).
29. P. Kaifosh, M. Lovett-Barron, G. F. Turi, T. R. Reardon, A. Losonczy, *Nat. Neurosci.* **16**, 1182–1184 (2013).
30. C. J. Magnus *et al.*, *Science* **333**, 1292–1296 (2011).
31. S. G. Anagnostaras, G. D. Gale, M. S. Fanselow, *Hippocampus* **11**, 8–17 (2001).
32. I. Goshen *et al.*, *Cell* **147**, 678–689 (2011).
33. A. J. Murray *et al.*, *Nat. Neurosci.* **14**, 297–299 (2011).
34. J. Akerboom *et al.*, *J. Neurosci.* **32**, 13819–13840 (2012).
35. D. A. Dombeck, C. D. Harvey, L. Tian, L. L. Looger, D. W. Tank, *Nat. Neurosci.* **13**, 1433–1440 (2010).
36. D. A. Dombeck, A. N. Khabbaz, F. Collman, T. L. Adelman, D. W. Tank, *Neuron* **56**, 43–57 (2007).
37. O. Herreras, J. M. Solís, M. D. Muñoz, R. Martín del Río, J. Lerma, *Brain Res.* **461**, 290–302 (1988).
38. S. Khanna, *Neuroscience* **77**, 713–721 (1997).
39. M. Funahashi, Y. F. He, T. Sugimoto, R. Matsuo, *Brain Res.* **827**, 215–220 (1999).
40. O. S. Vinogradova, *Hippocampus* **11**, 578–598 (2001).
41. J. J. Lawrence, J. M. Statland, Z. M. Grinspan, C. J. McBain, *J. Physiol.* **570**, 595–610 (2006).
42. R. N. Leão *et al.*, *Nat. Neurosci.* **15**, 1524–1530 (2012).
43. S. W. Miller, P. M. Groves, *Physiol. Behav.* **18**, 141–146 (1977).
44. O. Herreras, J. M. Solís, A. S. Herranz, R. M. del Río, J. Lerma, *Brain Res.* **461**, 303–313 (1988).
45. F. Zheng, S. Khanna, *Neuroscience* **103**, 985–998 (2001).
46. J. J. Letzkus *et al.*, *Nature* **480**, 331–335 (2011).
47. H. Widmer, L. Ferrigan, C. H. Davies, S. R. Cobb, *Hippocampus* **16**, 617–628 (2006).
48. G. D. Gale, S. G. Anagnostaras, M. S. Fanselow, *Hippocampus* **11**, 371–376 (2001).
49. S. Dasari, A. T. Gulledge, *J. Neurophysiol.* **105**, 779–792 (2011).
50. M. E. Hasselmo, *Curr. Opin. Neurobiol.* **16**, 710–715 (2006).
51. L. Calandreau, R. Jaffard, A. Desmedt, *Learn. Mem.* **14**, 422–429 (2007).
52. T.-W. Chen *et al.*, *Nature* **499**, 295–300 (2013).
53. E. L. Hargreaves, G. Rao, I. Lee, J. J. Knierim, *Science* **308**, 1792–1794 (2005).
54. S. J. Zhang *et al.*, *Science* **340**, 1232627 (2013).
55. L. Palmer, M. Murayama, M. Larkum, *Frontiers in Neural Circuits* **6**, 26 (2012).
56. F. Zhang *et al.*, *Nature* **446**, 633–639 (2007).
57. L. M. Romanski, J. E. LeDoux, *Cereb. Cortex* **3**, 515–532 (1993).
58. E. Lanuza, K. Nader, J. E. Ledoux, *Neuroscience* **125**, 305–315 (2004).
59. J. Brankačk, G. Buzsáki, *Brain Res.* **378**, 303–314 (1986).
60. R. D. Burwell, D. G. Amaral, *J. Comp. Neurol.* **398**, 179–205 (1998).
61. S. Melzer *et al.*, *Science* **335**, 1506–1510 (2012).
62. M. A. Moita, S. Rosis, Y. Zhou, J. E. LeDoux, H. T. Blair, *J. Neurosci.* **24**, 7015–7023 (2004).
63. C. I. Bargmann, *Bioessays* **34**, 458–465 (2012)
Supplementary References.

Acknowledgments: We thank S. Sternson and P. Lee for proving PSEM^{89}, A. Castro for programming assistance, E. Balough and M. Cloidt for scoring freezing, R. Field for preparing brain slices, J. Tsai for assistance with histology, T. Machado for assistance with *ChAT-cre* mice, W. Fischler for assistance with odor stimuli, and C. Lacefield for assistance with behavioral apparatus. M.L.-B. was supported by an Canadian Natural Sciences and Engineering Research Council postgraduate scholarship. P.K. is an Howard Hughes Medical Institute International Predoctoral Fellow. M.A.K. is supported by NIMH K01MH099371, the Sackler Institute, and a NARSAD Young Investigator Award. R.H. is supported by NIH R37 MH068542, NIA R01 AG043688, New York State Stem Cell Science, and the Hope for Depression Research Foundation. B.V.Z. is supported by the Human Frontier Science Program. A.L. is supported by the Searle Scholars Program, the Human Frontier Science Program, and the McKnight Memory and Cognitive Disorders Award.

Supplementary Materials

www.sciencemag.org/content/343/6173/857/suppl/DC1
Materials and Methods
Figs. S1 to S15
References (*64*–*66*)

22 October 2013; accepted 23 January 2014
10.1126/science.1247485

Discovery of a Three-Dimensional Topological Dirac Semimetal, Na_3Bi

Z. K. Liu,[1*] B. Zhou,[2,3*] Y. Zhang,[3] Z. J. Wang,[4] H. M. Weng,[4,5] D. Prabhakaran,[2] S.-K. Mo,[3] Z. X. Shen,[1] Z. Fang,[4,5] X. Dai,[4,5] Z. Hussain,[3] Y. L. Chen[2,6]†

Three-dimensional (3D) topological Dirac semimetals (TDSs) represent an unusual state of quantum matter that can be viewed as "3D graphene." In contrast to 2D Dirac fermions in graphene or on the surface of 3D topological insulators, TDSs possess 3D Dirac fermions in the bulk. By investigating the electronic structure of Na_3Bi with angle-resolved photoemission spectroscopy, we detected 3D Dirac fermions with linear dispersions along all momentum directions. Furthermore, we demonstrated the robustness of 3D Dirac fermions in Na_3Bi against in situ surface doping. Our results establish Na_3Bi as a model system for 3D TDSs, which can serve as an ideal platform for the systematic study of quantum phase transitions between rich topological quantum states.

The discoveries of graphene and topological insulators (TIs) have inspired enormous efforts in the search for materials with similar electronic and topological properties (*1*–*4*). Graphene, a single sheet of carbon atoms, hosts two-dimensional (2D) Dirac fermions in its electronic structure (*1*, *2*, *5*); TIs are materials with a bulk energy gap but gapless surface states formed by an odd number of Dirac fermions with helical spin texture (*3*, *4*, *6*–*8*). In the course of this search, the following questions arose: Does a 3D counterpart of graphene exist? Can materials other than insulators possess unusual topology in their electronic structures?

In a class of materials called the topological Dirac semimetals, both of these questions are answered in the affirmative. There, the bulk conduction and valence bands touch only at discrete (Dirac) points and disperse linearly along all (three) momentum directions, forming bulk (3D) Dirac fermions—a natural 3D counterpart of graphene. Although a similar electronic structure was discussed more than seven decades ago (*9*), its topological classification was only appreciated recently (*10*–*15*), leading to the theoretical proposal of topological Dirac semimetals (TDSs) (*12*–*16*).

The distinct electronic structure of a TDS not only makes it possible to realize some exciting phenomena and applications of graphene (*17*) in 3D materials—it also gives rise to many unusual properties, such as the giant diamagnetism that diverges logarithmically when the Fermi energy (E_F) approaches the 3D Dirac point (*16*, *18*, *19*); quantum magnetoresistance showing linear field dependence in the bulk (*20*, *21*); characteristic Landau level structures under a strong magnetic

[1]Stanford Institute for Materials and Energy Sciences, SLAC National Accelerator Laboratory, 2575 Sand Hill Road, Menlo Park, CA 94025, USA. [2]Physics Department, Clarendon Laboratory, University of Oxford, Parks Road, OX1 3PU, UK. [3]Advanced Light Source, Lawrence Berkeley National Laboratory, Berkeley, CA 94720, USA. [4]Beijing National Laboratory for Condensed Matter Physics and Institute of Physics, Chinese Academy of Sciences, Beijing 100190, China. [5]Collaborative Innovation Center of Quantum Matter, Beijing, China. [6]Diamond Light Source and Rutherford Appleton Laboratory, Didcot, UK.

*These authors contributed equally to this work.
†Corresponding author. E-mail: yulin.chen@physics.ox.ac.uk

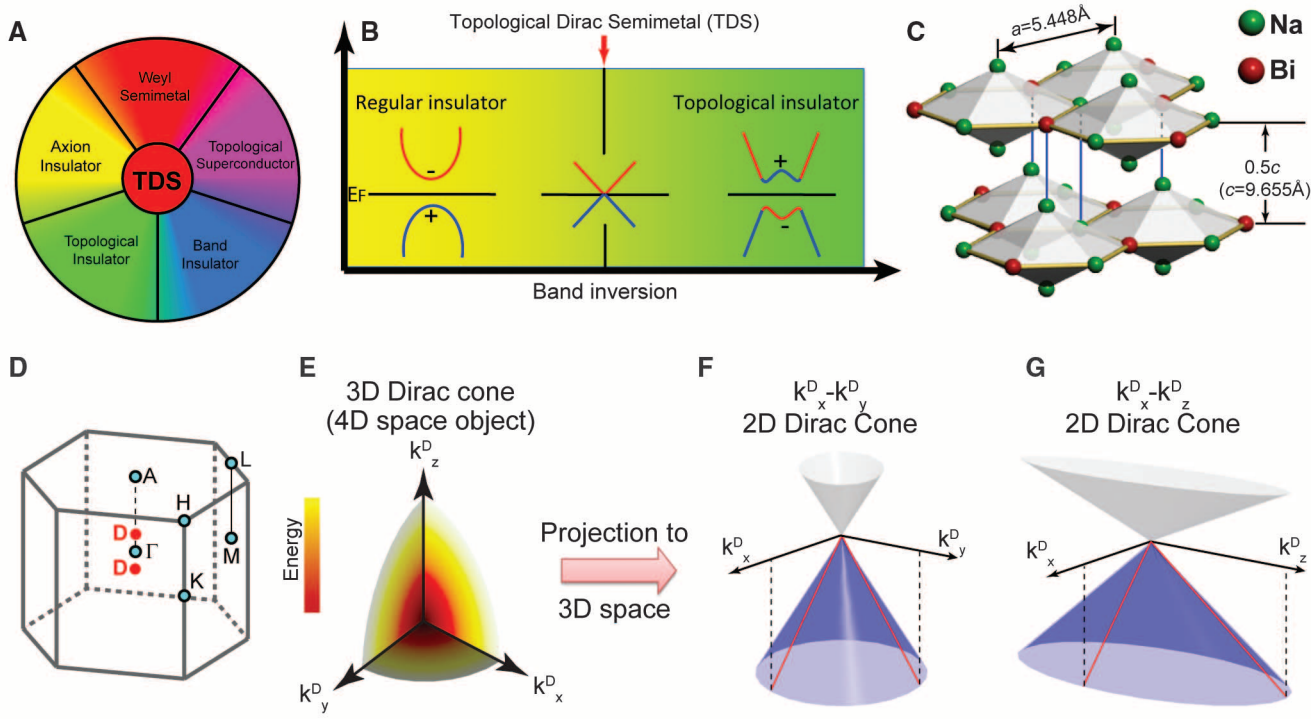

Fig. 1. Basic characteristics of the TDS. (**A**) The TDS state neighbors various unusual states. (**B**) The TDS state may be realized at the quantum critical point in the topological quantum phase transition from a normal insulator to a topological insulator. The "+" and "−" signs denote the even and odd parity of the bands at the time-reversal invariant point, respectively. (**C**) Crystal structure and (**D**) the BZ of Na_3Bi. Cyan dots indicate the high-symmetry points of the BZ, and red dots highlight the 3D Dirac point positions. (**E**) Visualization of a 3D Dirac fermion dispersion ($E = V_x \cdot k^D_x + V_y \cdot k^D_y + V_z \cdot k^D_z$); the color scale represents energy. (**F** and **G**) Projection of the 3D Dirac fermion onto (k^D_x, k^D_y, E) and (k^D_x, k^D_z, E) spaces (see text). Red lines outline the linear dispersions along k^D_x, k^D_y, and k^D_z directions.

field; and oscillating quantum spin Hall effect in quantum well structures (*15*, *22*). The 3D Dirac fermion in a TDS is composed of two overlapping Weyl fermions (chiral massless particles previously studied extensively in high-energy physics—e.g., as a description of neutrinos) (*23*) that can be separated in the momentum space if time-reversal or inversion symmetry is broken. This would result in a topological Weyl semimetal, another novel topological quantum state that shows a distinct Fermi-arcs geometry (*12*, *24*), exhibiting the pressure-induced anomalous Hall effect (*25*) and quantized anomalous Hall effect in quantum well structures (*24*).

In addition to these unusual properties, the TDS is the neighbor state to various quantum states (Fig. 1, A and B) (*12*–*16*, *26*) ranging from regular band insulators to topological superconductors. This versatility makes the TDS an ideal parent compound for the realization of other novel states, as well as a platform for the systematic study of topological quantum phase transitions.

The physical realization of the TDS is, however, challenging. In principle, it may be realized through topological phase transitions, such as tuning chemical composition or spin-orbital coupling strength to the quantum critical point through a normal insulator–topological insulator transition (Fig. 1B). Recently, it was realized that the crystal symmetry can protect and stabilize 3D Dirac points in several stoichiometric compounds such as β-cristobalite BiO_2 (*14*) and A_3Bi (where A is Na, K, or Rb) family of compounds (*15*). Because of the metastable nature of β-cristobalite BiO_2, we chose to study Na_3Bi.

We performed angle-resolved photoemission spectroscopy (ARPES) measurements to investigate the electronic structures of Na_3Bi (001) single crystals. [Further details of the sample preparation and ARPES experiments are available in (*27*).] The crystal structure of Na_3Bi (Fig. 1C) is composed of stacked …Na–(Na/Bi)–Na… triple-layer groups, with the adjacent triple layers rotated by 60° with respect to each other. The 3D Brillouin zone (BZ) of Na_3Bi is illustrated in Fig. 1D, with high-symmetry points indicated. According to recent ab initio calculations (*15*), a pair of 3D Dirac fermions is located near the Γ point in each BZ (labeled as "D" in Fig. 1D), with linear dispersion along k_x, k_y, and k_z directions. Because a 3D Dirac fermion is a surface in 4D space ($E = V_x \cdot k_x^D + V_y \cdot k_y^D + V_z \cdot k_z^D$, where V_x, V_y, and V_z are the Fermi velocities along x, y, and z directions, respectively; and $k^D{}_x$, $k^D{}_y$, and $k^D{}_z$ represent the momentum measured from the Dirac point), in Fig. 1E, we visualize it by using $k^D{}_x$, $k^D{}_y$, and $k^D{}_z$ as variables and colors to represent E (the fourth dimension). The projections of the 3D Dirac fermion onto two 2D momentum planes are shown in Fig. 1, F and G. The figures reflect the calculated small in-plane and large out-of-plane anisotropy ($V_x \approx V_y = 3.74 \times 10^5$ m/s, $V_z = 2.89 \times 10^4$ m/s).

The overall electronic structure from ARPES measurements is summarized in Fig. 2. The characteristic peaks of Na and Bi elements are evident in the core-level spectra (Fig. 2A); the band dispersions (Fig. 2B) agree well with our ab initio calculations, represented by solid lines [details of the calculations are in (*27*)]. The electronic structure at the Dirac point is illustrated in Fig. 2C, showing a cone shape with linear dispersions [details on selecting k_z positions and identifying Dirac points in momentum space are in (*27*)]. This Dirac cone dispersion results in a pointlike Fermi surface (FS) at $\bar{\Gamma}$ in the projected 2D BZ (Fig. 2D). Moreover, the constant-energy contours of the Dirac cone at different binding energies (Fig. 2E) demonstrate the small in-plane anisotropy.

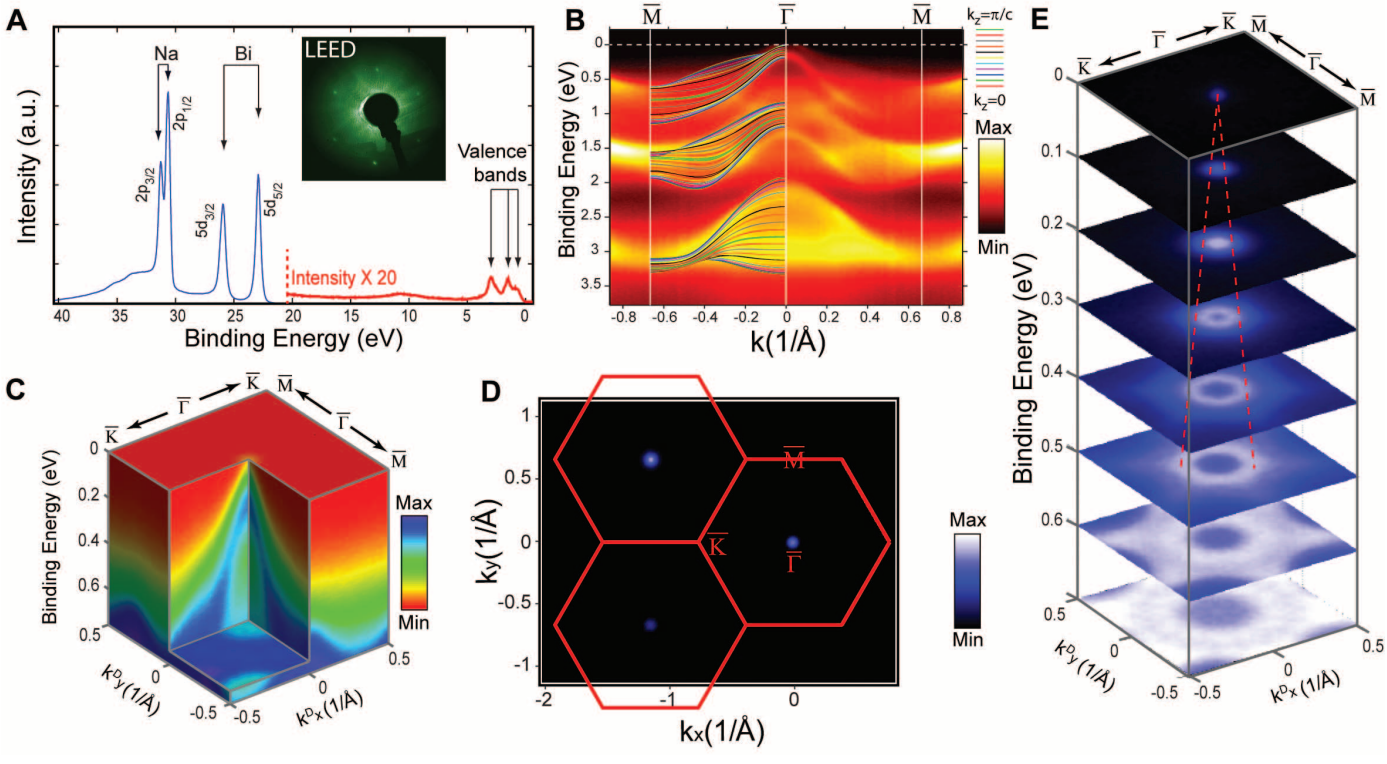

Fig. 2. Electronic structure of Na_3Bi. (**A**) Core-level photoemission spectrum shows strong characteristic Na 2p and Bi 5d doublet peaks (blue curve). Features at low binding energy (E_B < 21 eV) were magnified 20 times to enhance the details (red curve). Inset: Low-energy electron diffraction (LEED) pattern shows the hexagonal structure of Na_3Bi (001) surface. (**B**) Comparison of the valence band spectra between ARPES measurement (background) and ab initio calculations (solid lines) along the $\bar{M} - \bar{\Gamma} - \bar{M}$ direction. The color of the lines represents different k_z dispersions in the calculation. (**C**) A 3D intensity plot of the photoemission spectra at the Dirac point, showing cone-shape dispersion. (**D**) Broad FS map from ARPES measurements that covers three BZs. The red hexagons represent the surface BZ, and the uneven intensity of the FS points of different BZs results from the matrix element effect. (**E**) Stacking plot of constant-energy contours at different binding energies shows Dirac cone band structure. Red dotted lines are guides to the eye that indicate the dispersions and intersect at the Dirac point.

To demonstrate the 3D nature of the Dirac cone in Na_3Bi, it is necessary to show that the band dispersion is also linear along k_z (as well as k_x and k_y), which was achieved by performing photon-energy–dependent ARPES measurements (*27*, *28*). By assembling the measurements under a broad range of photon energies (*27*), we obtained the band structures of Na_3Bi throughout the 3D BZ. Figure 3A illustrates the complete FS of Na_3Bi in a 3D BZ, showing a pair of pointlike FSs in the vicinity of Γ at $k_x = k_y = 0$ and $k_{z\pm} = \pm 0.095$/Å or $\pm 0.29\pi/c$ (where c is the z-direction lattice constant), which agrees well with our ab initio calculations that predict two Dirac points at $k_{z\pm} = \pm 0.26\pi/c$ (*15*). In Fig. 3A (ii), which shows the data for a Na-deficient sample surface, an additional cylindrical FS appears and vertically crosses the whole 3D BZ (and thus is dispersionless along k_z). This feature originates from the surface states (*27*, *28*) that emerge due to the loss of the surface Na atoms, which easily migrate away during the experiment (*27*).

As well as studying the 3D FS, we investigate the band dispersion along all three k directions. Similar to Fig. 2C, Fig. 3B illustrates the 3D electronic structure along the k^D_y-k^D_z direction, showing a clearly elongated (along the k^D_z direction) Dirac cone (corresponding to a much smaller V_z; see Fig. 3, B and C). Furthermore, we study the detailed dispersions along each momentum direction (see schematics in Fig. 3, D to F): For a 3D Dirac fermion, ARPES measurements along any k direction should yield either

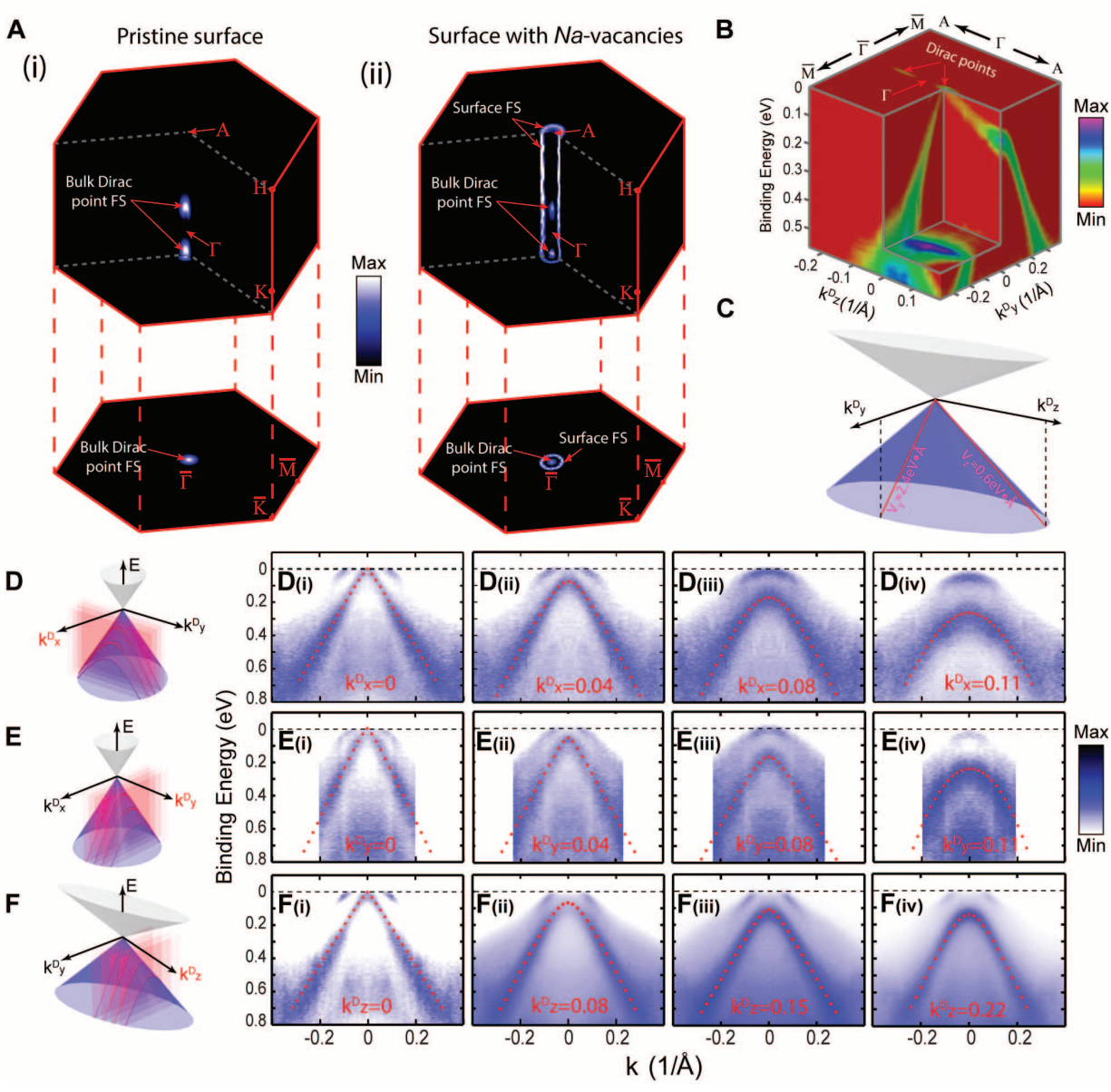

Fig. 3. Dispersion of the 3D Dirac fermion along all three momentum directions. (**A**) FS map across the whole 3D BZ (top panel) and its projection to the surface BZ (bottom panel) on (i) pristine and (ii) Na-deficient surfaces. An additional FS appears in panel (ii) [see text and (*27*) for details]. (**B**) A 3D intensity plot of the photoemission spectra (along the k^D_y-k^D_z direction) shows the elongated (along the k^D_z direction) cone-shape dispersion, indicating the large anisotropy between the k_y and the k_z direction. (**C**) The schematic of the k^D_y-k^D_z Dirac cone reconstructed from the experimental fit parameters: V_y = 2.4 eV•Å, and V_z = 0.6 eV•Å (*27*). (**D** to **F**) Schematics show the dispersions (red curves) that slice through the 3D Dirac cones at different (k^D_x, k^D_y, or k^D_z) momentum locations, showing either a linear or a hyperbolic shape. The Dirac velocity parameters obtained from our experiments are V_x = 2.8 eV•Å, V_y = 2.4 eV•Å, and V_z = 0.6 eV•Å (*27*). (D) (i to iv) Measured dispersion at k^D_x = 0, 0.04, 0.08, and 0.11 Å^{-1}, respectively. Red dotted lines show the fitted dispersions that agree well with the experiments [see text and (*27*)]. (E) (i to iv) Experiment and fitted dispersions at k^D_y = 0, 0.04, 0.08, and 0.11 Å^{-1}, respectively. (F) (i to iv) Experiment and fitted dispersions at k^D_z = 0, 0.08, 0.15, and 0.22 Å^{-1}, respectively.

linear or hyperbolic dispersions depending on whether the measurement cuts through the Dirac point. This is different from the usual parabolic dispersions of massive electrons.

In Fig. 3, D to F (i to iv), we use four examples along each k direction to show typical ARPES dispersions on Na_3Bi [for additional measurements and analysis, see (*27*)]. Along each k direction, the dispersion evolves from a linear [Fig. 3, D to F (i)] to a hyperbolic [Fig. 3, D to F (ii to iv)] shape, as expected. Notably, to fit all of the ARPES measurements [including those in (*27*)] requires only one set of 3D Dirac cone parameters (V_x = 2.75 eV·Å or 4.17 × 10^5 m/s, V_y = 2.39 eV·Å or 3.63 × 10^5 m/s, and V_z = 0.6 eV·Å or 0.95 × 10^5 m/s). This excellent agreement proves that the bulk band structure of Na_3Bi forms 3D Dirac cones, with a large anisotropy along the k_z direction ($V_z \approx 0.25\ V_x$; see Fig. 3C).

To test the robustness of 3D Dirac fermion in Na_3Bi, we modified the sample surface (by in situ evaporating K atoms; see Fig. 4, A and B) and monitored the band dispersions' evolution with the increase in surface impurities. In addition, the K doping can compensate the charge loss caused by the surface Na-atom loss discussed above [and in (*27*)]. Indeed, we could even overcompensate the charge loss with sufficient doping and observed the upper part of the Dirac cone beyond the Dirac point (Fig. 4C). With the increase in K doping, the E_F shifts upward (Fig. 4, D to F), whereas the surface-state band disappears (Fig. 4, E and F), owing to the deterioration of the sample surface by randomly deposited K atoms. By contrast, the bulk Dirac cone (both the linear dispersion and the Dirac point) persists despite such surface deterioration (Fig. 4, E and F), supporting the notion that the Dirac fermion is protected by the bulk crystal symmetry (which is preserved during surface K doping).

The TDS Na_3Bi realizes a 3D counterpart of graphene, opening the door to exploring other 3D TDSs, some of which may realize various exciting applications of graphene in 3D materials. Furthermore, the extremely long Fermi wavelength (which diverges at the Dirac points) of the bulk conducting electrons in a TDS can greatly enhance the Ruderman-Kittel-Kasuya-Yosida interaction, making it possible to realize ferromagnetic states by unusually dilute magnetic doping [similar to the Dirac surface states in a topological insulator (*29*)]—which could make the TDS an ideal platform for spintronics applications.

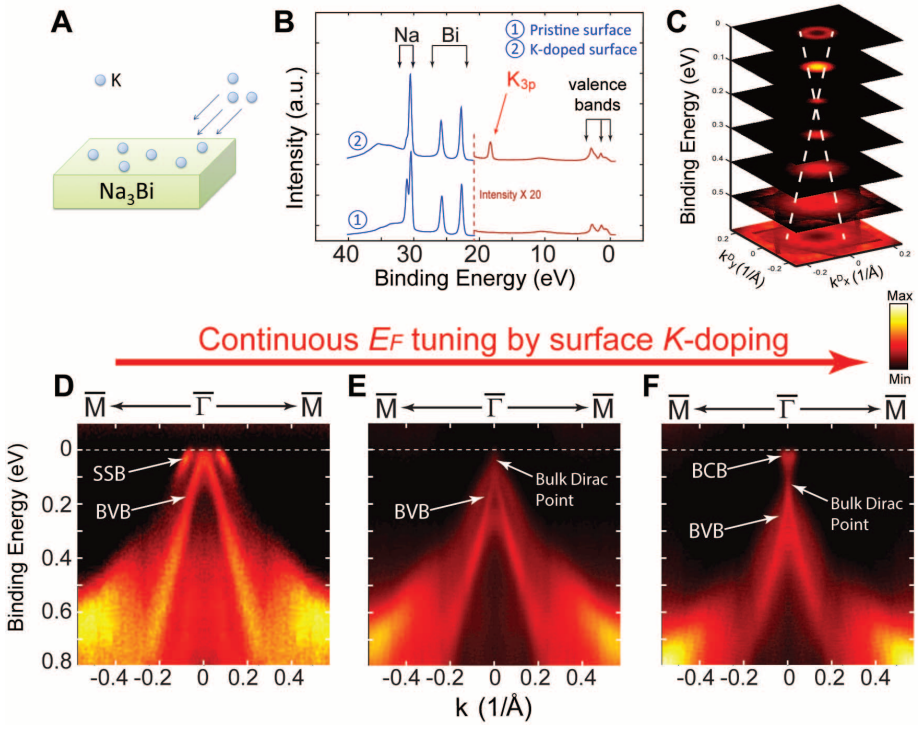

Fig. 4. Bulk Dirac fermion stability and E_F tuning by surface doping. (**A**) Illustration of the in situ surface K doping. (**B**) Core-level photoemission spectra before and after the K doping show the K_{3p} core-level peak (which can be used to monitor the dosage level). (**C**) Stacking plot of constant-energy contours shows the upper Dirac cone after the in situ K doping. White dashed lines are guides to the eye that trace the Dirac dispersions. (**D** to **F**) ARPES intensity plots show the rise in E_F with K dosage: (D) before in situ K doping; (E) at a level of K doping required to bring E_F to the bulk Dirac point; and (F) after further K doping drives the system into n-type. The surface state band (SSB) in (D) is destroyed by the K doping and thus does not appear in (E) and (F). BCB, bulk conduction band; BVB, bulk valence band.

References and Notes

1. A. K. Geim, K. S. Novoselov, *Nat. Mater.* **6**, 183–191 (2007).
2. A. H. Castro Neto, F. Guinea, N. M. R. Peres, K. S. Novoselov, A. K. Geim, *Rev. Mod. Phys.* **81**, 109–162 (2009).
3. M. Z. Hasan, C. L. Kane, *Rev. Mod. Phys.* **82**, 3045–3067 (2010).
4. X.-L. Qi, S.-C. Zhang, *Rev. Mod. Phys.* **83**, 1057–1110 (2011).
5. K. S. Novoselov *et al.*, *Science* **306**, 666–669 (2004).
6. C. L. Kane, E. J. Mele, *Phys. Rev. Lett.* **95**, 226801 (2005).
7. L. Fu, C. L. Kane, E. J. Mele, *Phys. Rev. Lett.* **98**, 106803 (2007).
8. J. E. Moore, *Nature* **464**, 194–198 (2010).
9. C. Herring, *Phys. Rev.* **52**, 365–373 (1937).
10. S. Murakami, *New J. Phys.* **9**, 356 (2007).
11. G. E. Volovik, in *Quantum Analogues: From Phase Transitions to Black Holes and Cosmology*, W. Unruh, R. Schützhold, Eds., Lecture Notes in Physics (Springer, Berlin, Heidelberg, 2007), vol. 718, pp. 31–73.
12. X. Wan, A. M. Turner, A. Vishwanath, S. Y. Savrasov, *Phys. Rev. B* **83**, 205101 (2011).
13. A. A. Burkov, L. Balents, *Phys. Rev. Lett.* **107**, 127205 (2011).
14. S. M. Young *et al.*, *Phys. Rev. Lett.* **108**, 140405 (2012).
15. Z. Wang *et al.*, *Phys. Rev. B* **85**, 195320 (2012).
16. P. Goswami, S. Chakravarty, *Phys. Rev. Lett.* **107**, 196803 (2011).
17. A. K. Geim, *Science* **324**, 1530–1534 (2009).
18. M. Koshino, T. Ando, *Phys. Rev. B* **81**, 195431 (2010).
19. E. Röber, K. Hackstein, H. Coufal, S. Sotier, *Phys. Status Solidi B* **93**, K99–K102 (1979).
20. A. A. Abrikosov, *Phys. Rev. B* **58**, 2788–2794 (1998).
21. W. Zhang *et al.*, *Phys. Rev. Lett.* **106**, 156808 (2011).
22. C.-X. Liu *et al.*, *Phys. Rev. B* **81**, 041307 (2010).
23. G. E. Volovik, *The Universe in a Helium Droplet* (Clarendon, Oxford, 2003).
24. G. Xu, H. Weng, Z. Wang, X. Dai, Z. Fang, *Phys. Rev. Lett.* **107**, 186806 (2011).
25. K.-Y. Yang, Y.-M. Lu, Y. Ran, *Phys. Rev. B* **84**, 075129 (2011).
26. F. R. Klinkhamer, G. E. Volovik, *Int. J. Mod. Phys. A* **20**, 2795–2812 (2005).
27. Materials and methods are available as supporting materials on *Science* Online.
28. Y. Chen, *Front. Phys* **7**, 175–192 (2012).
29. Q. Liu, C.-X. Liu, C. Xu, X.-L. Qi, S.-C. Zhang, *Phys. Rev. Lett.* **102**, 156603 (2009).

Acknowledgments: We thank X. L. Qi and Z. Wang for insightful discussions, S. Clarke and J. Wright for help in sample synthesis, and P. Han and R. Yang for help with data analysis. Y.L.C. and B.Z. acknowledge support from the Engineering and Physical Sciences Research Council (UK) grant EP/K04074X/1 and a Defense Advanced Research Projects Agency (USA) MESO project (no. N66001-11-1-4105). Z.K.L. and Z.X.S. acknowledge support by the U.S. Department of Energy, Office of Science, Materials Sciences and Engineering Division. Z.F., X.D., and H.M.W. acknowledge support by the NSF of China, the National Basic Research Program of China, and the International Science and Technology Cooperation Program of China. The experiments were performed, and data were collected, at Beamline 10.0.1 of the Advanced Light Source, Lawrence Berkeley National Laboratory, USA.

Supplementary Materials

www.sciencemag.org/content/343/6173/864/suppl/DC1
Materials and Methods
Figs. S1 to S8
References (*30–38*)

23 August 2013; accepted 2 January 2014
Published online 16 January 2014;
10.1126/science.1245085

Artificial Muscles from Fishing Line and Sewing Thread

Carter S. Haines,[1] Márcio D. Lima,[1] Na Li,[1] Geoffrey M. Spinks,[2] Javad Foroughi,[2] John D. W. Madden,[3] Shi Hyeong Kim,[4] Shaoli Fang,[1] Mônica Jung de Andrade,[1] Fatma Göktepe,[5] Özer Göktepe,[5] Seyed M. Mirvakili,[3] Sina Naficy,[2] Xavier Lepró,[1] Jiyoung Oh,[1] Mikhail E. Kozlov,[1] Seon Jeong Kim,[4] Xiuru Xu,[1,6] Benjamin J. Swedlove,[1] Gordon G. Wallace,[2] Ray H. Baughman[1]*

The high cost of powerful, large-stroke, high-stress artificial muscles has combined with performance limitations such as low cycle life, hysteresis, and low efficiency to restrict applications. We demonstrated that inexpensive high-strength polymer fibers used for fishing line and sewing thread can be easily transformed by twist insertion to provide fast, scalable, nonhysteretic, long-life tensile and torsional muscles. Extreme twisting produces coiled muscles that can contract by 49%, lift loads over 100 times heavier than can human muscle of the same length and weight, and generate 5.3 kilowatts of mechanical work per kilogram of muscle weight, similar to that produced by a jet engine. Woven textiles that change porosity in response to temperature and actuating window shutters that could help conserve energy were also demonstrated. Large-stroke tensile actuation was theoretically and experimentally shown to result from torsional actuation.

Artificial muscle fibers are needed for diverse applications, ranging from humanoid robots, prosthetic limbs, and exoskeletons to comfort-adjusting clothing and miniature actuators for microfluidic "laboratories on a chip." However, performance, scalability, and cost problems have restricted their deployment. Electrothermally driven shape-memory metal wires can contract fast and deliver large strokes under heavy loads, but are expensive and hysteretic, which makes them difficult to control (*1*, *2*). Thermally powered shape-memory polymers have low work capacity unless they are fiber-reinforced (*3, 4*), and giant-work-capacity polymer/carbon nanotube (CNT) composite fibers must be redrawn between cycles (*5*). High-performance hybrid CNT muscles (*6*), in which a guest (such as paraffin wax) is infiltrated into a twist-spun carbon nanotube yarn, are expensive because of the cost of CNT yarn. Electrochemically driven fibers of organic conducting polymers can provide large strokes but have limited cyclability and cycle rate and require an electrolyte, counter-electrode, and containment system, which adds to system weight and cost (*7*–*9*). Polymeric electric field–driven electrostrictive rubbers and relaxor ferroelectrics (*10*–*12*) are attractive because of their large strokes and high efficiencies but would be difficult to deploy as muscle-like fibers because of the high required electric fields.

The present goal is to convert inexpensive (~$5/kg) high-strength polymer fibers into artificial muscles that match or exceed the performance of mammalian skeletal muscle to deliver millions of reversible contractions and over 20% tensile stroke, while rapidly lifting heavy loads. These muscles should provide hysteresis-free actuation to enable convenient control, be scalable in force-lifting capability without decreasing stroke or gravimetric work capabilities, and be weavable into textiles that actuate to accomplish amplified mechanical work or change textile porosity.

We started from low-cost high-strength fibers, most often those used as fishing line or sewing thread (table S1). Commercially produced polyethylene and nylon fibers are important muscle precursors, because they combine reversible–fiber-direction thermal contraction, large volumetric thermal expansion, and large anisotropy in thermally induced dimension changes to provide enhanced muscle stroke.

These precursor fibers are composed of flexible polymer chains that are highly oriented in the fiber direction. Although crystalline regions of highly drawn polymers, such as polyethylene and nylon, can have small negative thermal expansion coefficients (*13*), fiber-direction–aligned polymer chains in neighboring noncrystalline regions are less conformationally constrained, so they can provide large reversible contractions as they access conformational entropy when heated (*14*, *15*) (fig. S1). The resulting thermal contraction of nylon 6,6 fibers (Fig. 1A) can be as large as 4% (Fig. 2A and fig. S2A), which is similar to that of commercial NiTi shape-memory wires.

As with CNT yarn muscles (*6*, *16*), twist is inserted into these polymer fibers to make them

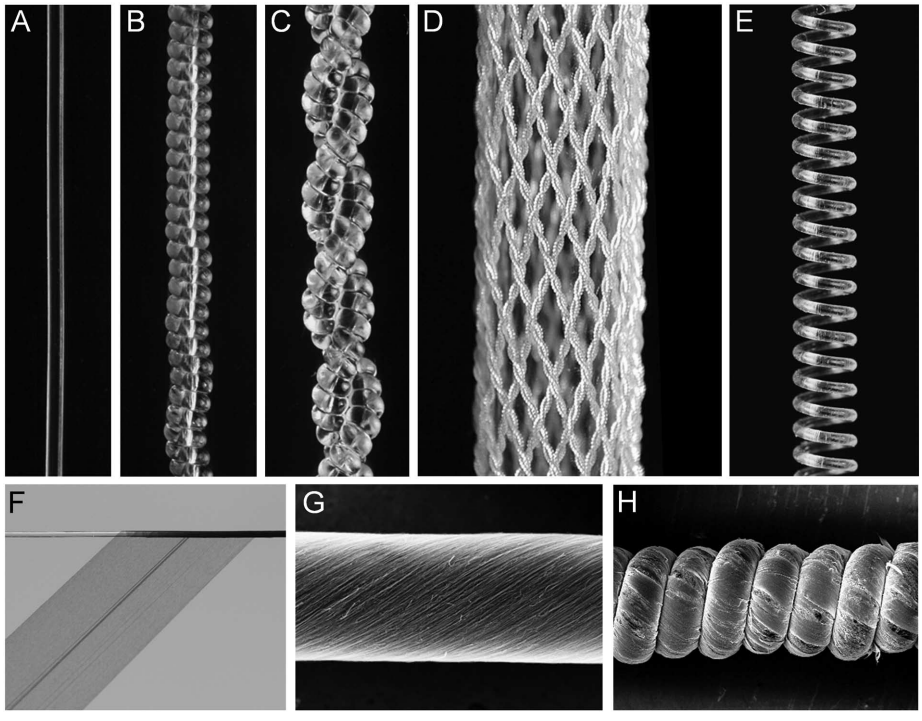

Fig. 1. Muscle and precursor structures using nylon 6,6 monofilament sewing thread. Optical images of (**A**) a nontwisted 300-μm-diameter fiber; (**B**) the fiber of (A) after coiling by twist insertion; (**C**) a two-ply muscle formed from the coil in (B); (**D**) a braid formed from 32 two-ply, coiled, 102-μm-diameter fibers produced as in (C); (**E**) a 1.55-mm-diameter coil formed by inserting twist in the fiber of (A), coiling it around a mandrel, and then thermally annealing the structure; and (**F**) helically wrapping the fiber of (A) with a forest-drawn CNT sheet and scanning electron microscope images of a CNT-wrapped, 76-μm-diameter nylon 6,6 monofilament (**G**) before and (**H**) after coiling by twist insertion.

[1]The Alan G. MacDiarmid NanoTech Institute, University of Texas at Dallas, Richardson, TX 75083, USA. [2]Intelligent Polymer Research Institute, ARC Centre of Excellence for Electromaterials Science, University of Wollongong, Wollongong, New South Wales 2522, Australia. [3]Department of Electrical and Computer Engineering and Advanced Material and Process Engineering Laboratory, University of British Columbia, Vancouver, British Columbia V6T 1Z4, Canada. [4]Center for Bio-Artificial Muscle and Department of Biomedical Engineering, Hanyang University, Seoul 133-791, South Korea. [5]Department of Textile Engineering, Çorlu Engineering Faculty, Namık Kemal University, Çorlu-Tekirdağ, Turkey. [6]Alan G. MacDiarmid Institute, Jilin University, Changchun 130012, China.

*Corresponding author. E-mail: ray.baughman@utdallas.edu

chiral, which enables them to function as torsional muscles. Most importantly, we greatly amplified tensile stroke by inserting such a large amount of twist that some twist converted to fiber coiling (movie S1), called writhe (*17*, *18*). By completely coiling the fibers (Fig. 1B), tensile contractions (Fig. 2A) exceeding the maximum in vivo stroke of human skeletal muscles (~20%) (*19*) were obtained. This coiling is more compact than that used to amplify the stroke of shape-memory metal wires, thereby providing contraction against higher applied stress (19 MPa for nylon) than reported for NiTi coils (~1.6 MPa) (*1*), in which stress is obtained by normalization to the nonactuated coil's cross-sectional area. The spring index (*C*), the ratio of mean coil diameter to the fiber diameter, for such polymer muscles will typically be less than 1.7, whereas for NiTi coils this ratio exceeds 3.0.

The weight applied during coiling is important and is adjustable over a narrow range for a given fiber: Too little weight and the fiber snarls during twist insertion; too much weight and the fiber breaks. For example, the load during coiling can be varied between 10 and 35 MPa for a 127-μm-diameter nylon 6,6 sewing thread, yielding coils with spring indices between 1.7 and 1.1, respectively. Immediately after coiling, adjacent coils are in contact, limiting contraction during actuation, and must be separated by increasing load or reducing twist.

Coils formed by twist insertion maintain some twist liveliness, meaning that they can untwist, especially when under load. This problem can be avoided by preventing end rotation during actuation, by thermal annealing to set the structure, or by forming torque-balanced structures. Figure 1C depicts a coiled polymer muscle that has been torque-balanced by plying (in the *Z* direction) two S-twisted fibers. Thereby stabilized, the plied, highly coiled muscles can be woven into textiles or braids (Fig. 1D).

Coiled muscles can also be made by wrapping highly twisted fibers around a mandrel and then stabilizing the coils by thermal annealing (Fig. 1E). This process enables the formation of larger-diameter coils than by direct, unconfined (i.e., mandrel-free) twist insertion. Although such structures have reduced load capacity, they can contract more before adjacent coils contact, thereby achieving larger stroke. The relative directions and amounts of twist in the fibers and the coils can be varied using this method. When the chirality of fiber twist matches the coil's chirality, the muscle contracts during heating. However, when these chiralities are opposite, the coiled polymer muscle expands during heating (movie S2). We hereafter refer to such coils as homochiral and heterochiral, respectively.

Thermomechanical analysis (TMA) results for fiber thermal expansion before and after coiling are shown in Fig. 2A for four polymer fibers (Table 1 and table S1). Unless otherwise indicated, tensile stress and modulus are calculated as nominal values by normalizing applied force to the diameter of the initial nontwisted fiber, because coil and fiber diameter are difficult to measure accurately during isotonic (constant applied force) measurements, where coil diameter varies during large-stroke actuation. Gravimetric capabilities were used to provide performance comparisons between natural and artificial muscles.

The reversible thermal contraction of nylon 6,6 monofilament between 20° and 240°C increased from 4 to 34% as a result of coiling (Fig. 2A and fig. S2). Polyethylene's lower melting temperature limited contraction to less than 0.3% for the noncoiled fiber and 16% for the coiled muscle between 20° and 130°C. However, the higher modulus and strength of coiled polyethylene

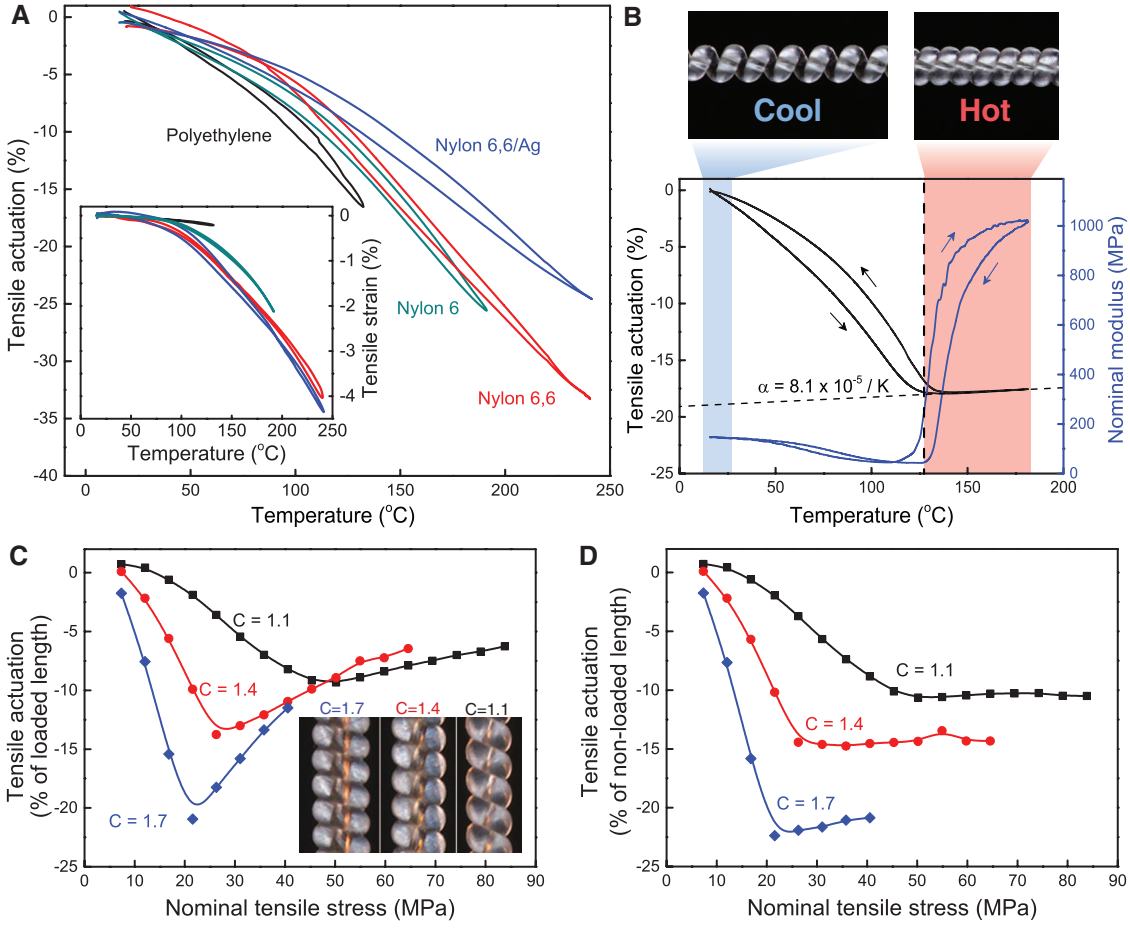

Fig. 2. Thermomechanical analysis of various muscles. (**A**) Comparison of the negative thermal expansion of braided polyethylene, nylon 6 monofilament, nylon 6,6 monofilament, and silver-coated nylon 6,6 multifilament fibers before twisting (inset) and after coiling by twist insertion. (**B**) Tensile stroke and nominal modulus versus temperature for a coiled, 300-μm-diameter nylon 6,6 monofilament muscle under 7.5 MPa static and 0.5 MPa dynamic load. During contraction, neighboring coils come into complete contact at ~130°C, which dramatically increases nominal elastic modulus and causes the thermal expansion coefficient to become positive. Optical micrographs (top) are shown of the coils before and after contact. (**C**) Tensile stroke versus load, as a percent of the loaded muscle length, for a 127-μm-diameter nylon 6,6 monofilament fiber that was coiled by twist insertion under loads of 10, 16, and 35 MPa, which resulted in spring indices of 1.7, 1.4, and 1.1, respectively. Optical images of the coils are inset. (**D**) The results of (C) when normalized to the initial nonloaded muscle length, indicating that the absolute displacement during actuation remains nearly constant at loads above those at which coils contact.

fibers (a nearly 10 times higher nominal modulus than for coiled nylon, fig. S8) are especially useful for muscles that lift heavy loads and provide increased energy efficiency.

When adjacent coils contact, due to insufficient applied load or excessive twist, the muscle-direction thermal expansion becomes positive, as in Fig. 2B. Under low tensile load (7.5 MPa), upon coil contact at ~130°C, the nylon 6,6 muscle expands at a rate comparable to the fiber's radial thermal expansion. After inter-coil contact, the coiled structure stiffens with increasing temperature, producing a 24-fold increase in nominal tensile modulus (Fig. 2B). Such large temperature-controlled changes in compliance may be useful for humanoid robots, in which actions such as catching a ball require both tensile actuation and tunable stiffness.

The tensile stroke and load-carrying capabilities of coiled muscles can be varied by adjusting the coil spring index, which is inversely related to spring stiffness (*1*). Figure 2C plots the load dependence of tensile stroke for coils having spring indices of 1.1, 1.4, and 1.7, produced by coiling under stresses of 10, 16, and 35 MPa, respectively. For each muscle, maximum stroke was realized for the lowest applied load (called the optimal load) that prevented inter-coil contact over the temperature range used (20° to 120°C). For the largest diameter coil (C = 1.7), this maximum stroke (21%) occurred for an optimal load of 22 MPa. When the polymer muscle was tightly coiled (C = 1.1), the maximum stroke decreased to 9.3%, but the optimal load increased to 50 MPa. Large-diameter mandrel-formed coils can yield even larger strokes, such as the 49% contraction provided at 1 MPa for a nylon 6 fiber having C = 5.5 (movie S2).

When coils are noncontacting, absolute stroke and stroke normalized to the nonloaded muscle length do not substantially depend on applied load (Fig. 2D), even though stroke normalized to loaded initial muscle length decreases with increasing load (Fig. 2C) because of muscle lengthening. Hence, the work done during contraction increases up to loads where the muscle breaks. The maximum specific work during contraction was 2.48 kJ/kg for the C = 1.1 nylon 6,6 muscle of Fig. 2C (*1*), which is 64 times that for natural muscle (*19*). The average mechanical output power during contraction (27.1 kW/kg) was 84 times the peak output of mammalian skeletal muscles (0.323 kW/kg) (*1*, *20*). However, although natural muscles have a typical energy conversion efficiency of 20%, the maximum energy conversion efficiency during contraction was 1.08 and 1.32% for the coiled nylon and polyethylene fibers, respectively (*1*). These polymer muscle efficiencies are similar to those of commercial shape-memory metals, which can reach 1 or 2% (*21*).

Shape-memory NiTi muscles suffer from over 20°C hysteresis in stroke, complicating actuator control (*2*, *22*). Scanning at a slow 2°C/min rate, to reduce artificial hysteresis due to temperature measurement errors, reveals that coiled nylon 6,6 actuators exhibit little or no inherent hysteresis (less than 1.2°C, Fig. 3A). This substantial absence of hysteresis, combined with the far more linear temperature dependence than for the commercially important NiTi shape-memory wires, makes these coiled polymer fiber muscles well suited for robotics and prosthetics, where a continuous range of control is desired. Although very recent work has provided shape-memory metal wires exhibiting down to 2°C hysteresis, these muscles comprise ~56.5 weight % gold (*23*).

Although such muscles can be driven chemically, photonically, hydrothermally, or by ambient temperature changes (*1*), electrothermally driven muscles must contain an electrical heating element. This can be provided by helically wrapping the coiled muscle or precursor fiber with a CNT sheet (*24*) (Fig. 1F-1H), using commercial metal-coated sewing thread, or placing a conductor on the inside or outside of the coiled muscle fiber (such as wires woven into an actuating textile or placed interior to actuating fiber braids, movies S5 and S6).

A coiled nylon 6,6 muscle delivered over 1 million cycles during periodic actuation at 1 Hz (Fig. 3B), raising and lowering a 10-g weight producing 22 MPa of nominal stress. This actuation was powered by applying a 30 V/cm square-wave potential (normalized to coil length) at a 20% duty cycle. Although the coiled fiber did experience creep (inset of Fig. 3B), this creep was below 2% over the 1.2 million investigated cycles, stroke amplitude was negligibly affected, and the creep rate decreased with cycling.

Similar to other thermally or electrochemically driven artificial muscles, muscle cycle rate decreases with increasing fiber diameter. This response time is unimportant when harvesting energy from slowly varying ambient temperature changes or for clothing textiles that change porosity to provide wearer comfort, but it is critically important when maximizing average output power. Passive cooling offers an economical solution to increase cycle rate. For instance, when immersed in water, a two-ply, coiled, silver-plated, 180-μm-diameter nylon fiber can be electrothermally actuated at 5 Hz to produce ~10% stroke while lifting a 22-MPa load (movie S4). Similarly, in helium, a coiled, 26-μm-diameter CNT-wrapped, nylon 6,6 monofilament was capable of actuation at over 7.5 Hz (*1*).

Fast, high-force actuation can be driven hydrothermally. A coiled polymer muscle made from 860-μm-diameter nylon 6 fishing line (Fig. 4, A and B) was driven at 1 Hz by switching between cold (~25°C) and hot (95°C) water (movie S3), achieving 12% reversible actuation under a 0.5-kg load (8.4 MPa). Even though nylon muscles absorb water (*25*), 1500 reversible actuation cycles were observed.

Polyethylene fiber muscles, which do not absorb water, can similarly be driven hydrothermally if a surfactant (dishwashing soap) is added to facilitate polymer wetting. A coiled polyethylene muscle was prepared by twisting an 800-μm-diameter bundle of four polyethylene fishing lines. Containing the muscle in a flexible silicone tube to allow fast water flow provided 4.5% contraction at 2 Hz while lifting a 7.2 kg (140 MPa) load (movie S3). The mechanical work output during contraction (2.63 kJ/kg), normalized to the total cycle time, was 5.26 kW/kg (7.1 horsepower/kg), which is over 100 times that of a human biceps muscle (*26*) and roughly the same as for a modern jet engine (*27*).

Polymer fibers that are twisted, but not coiled, are capable of producing surprisingly large amounts of mechanical work as torsional actuators. Constant-torque torsional actuation measurements were performed (using the apparatus of fig. S5) on an 860-μm-diameter, 5.5-cm-long, twisted nylon 6 fiber. When heated from 20° to 160°C, this muscle lifted a 1-kg load by 7 mm by rotating a 2.8-mm-diameter axle by 286°, thereby providing 2.1 kJ/kg of mechanical work (Fig. 3D). This work during rotation is similar to the 2.48 kJ/kg provided during tensile actuation of a coiled nylon 6,6 muscle.

Why do two-end–tethered, fully coiled homochiral polymer fibers thermally contract during heating, independent of whether the nontwisted fibers have a positive or negative axial thermal expansion coefficient (fig. S2), and why is such thermal contraction so large? The answers are found in the ability of twisted fibers to generate giant torque by reversibly untwisting when heated, as shown in Fig. 3C.

Until just before coiling, initially parallel polymer chains are twisted into helices that have a bias angle relative to the fiber direction of approximately

$$\alpha_f = \tan^{-1}(2\pi rT) \qquad (1)$$

where r is the radial distance from the fiber center and T is the amount of twist inserted per initial fiber length.

Table 1. Summary of the polymer fibers found to be most useful for actuation as coiled tensile muscles, and the parameters used to fully coil them. The tensile actuation results are given in Fig. 2A.

Material	Diameter (μm)	Load during coiling (MPa)	Twist to coil (turns/m)
Nylon 6 monofilament fishing line	270	17	1430
Nylon 6,6 monofilament sewing thread	127	16	3020
Nylon 6,6 silver-plated multifilament sewing thread	180	14	2430
Polyethylene braided fishing line	130	37	2270

After twisting, both length contraction of these helically configured polymer chains and fiber diameter expansion will cause fiber untwist (*1*). To enable physical understanding, consider the case where these effects are artificially decoupled, so that polymer chain length contracts while the fiber diameter is kept constant, or fiber diameter increases while the polymer chain length is kept constant. Both cases result in fiber untwist. Although thermal untwist can occur in any fiber whose radial expansion exceeds its axial expansion, polymers such as nylon are ideal because negative

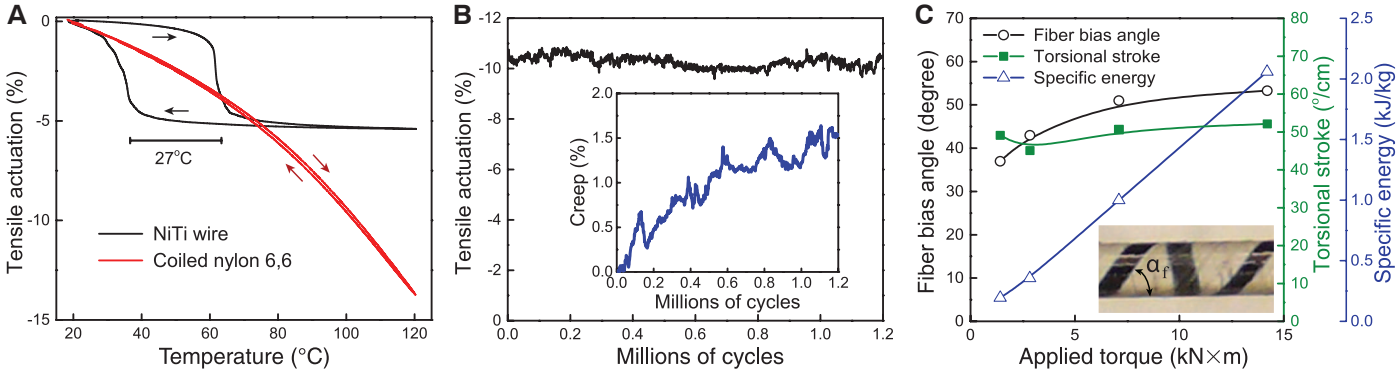

Fig. 3. Performance of torsional and tensile artificial muscles. (**A**) Comparison of hysteresis for a 152-μm-diameter NiTi wire muscle and a coiled, 127-μm-diameter nylon 6,6 monofilament muscle, measured using a 2°C/min scan rate. Less than 1.2°C of hysteresis is observed for the nylon muscle versus the 27°C hysteresis for the NiTi muscle. (**B**) Tensile actuation versus cycle for a coiled, 76-μm-diameter, nylon 6,6 monofilament wrapped in a CNT sheet and driven electrothermally at 1 Hz under a 22-MPa load (each point averages 1000 cycles). The inset provides creep as a function of cycle. (**C**) The optically measured fiber bias angle induced by an applied torque and the torsional stroke and work during thermal actuation (between 20° and 160°C) as a function of this applied torque for a noncoiled torsional muscle made from 860-μm-diameter nylon 6 fishing line (*1*). The inset photograph was used to optically determine the fiber bias angle by measuring the displacement of a black line from its initial orientation parallel to the fiber axis.

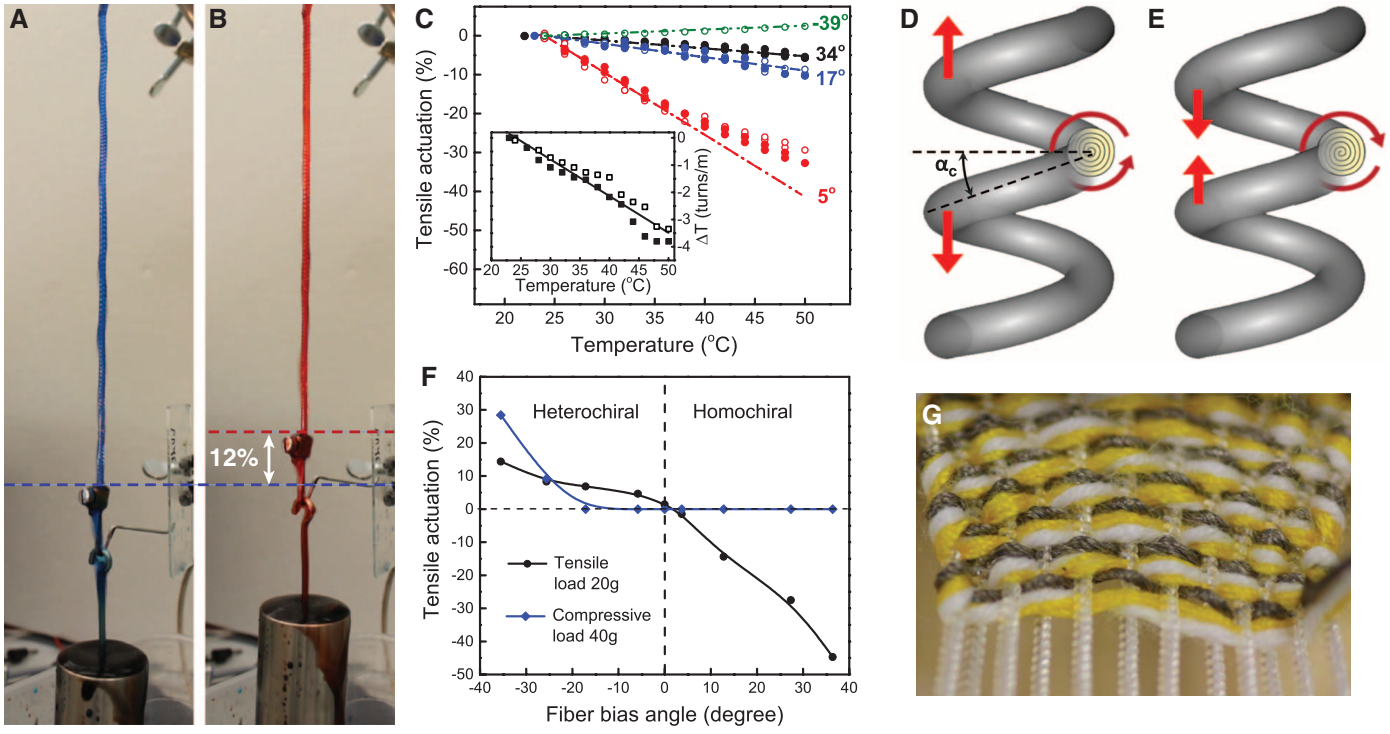

Fig. 4. Mechanism and applications for coiled polymer muscles. Hydrothermal actuation of a coiled 860-μm-diameter nylon 6 fishing line lifting a 500-g load by 12% when switched at 0.2 Hz between (**A**) ~25°C water (dyed blue) and (**B**) 95°C water (dyed red). (**C**) Calculated temperature dependence of tensile actuation (dashed lines) compared to experimental results (using an applied stress of 2.2 MPa, solid symbols, and 3.1 MPa, open symbols, respectively) for twisted 450-μm-diameter, nylon 6 monofilament fibers that are mandrel-wrapped to the indicated initial coil bias angles (*1*). Contracting and expanding coils were homochiral and heterochiral, respectively. From Eq. 3, fiber untwist during heating was calculated for the coiled fiber with a 17° bias angle to provide the data in the inset, which was then used to predict tensile actuation for the other coiled fibers. (**D** and **E**) Schematic illustration of the mechanism by which torsional fiber actuation drives large-stroke tensile actuation for (D) heterochiral and (E) homochiral coiled fibers. (**F**) Measured tensile actuation versus fiber bias angle for coiled, 860-μm-diameter nylon 6 muscles actuated between 25° and 95°C. These results show, for highly twisted fibers, that the homochiral muscles thermally contract when coils are noncontacting, and the heterochiral muscles expand. (**G**) An actuating textile woven from conventional polyester, cotton, and silver-plated nylon (to drive electrothermal actuation) yarn in the weft direction and coiled nylon monofilament muscle fibers in the warp direction.

axial expansion and positive radial expansion additively contribute to untwist.

This thermally induced fiber untwist (ΔT, measured in turns per initial fiber length) generates the torsional actuation observed for twisted fibers and drives the length change for coiled fibers by requiring coil bias angle to change from α_c to α_c', as described by the spring mechanics equation (*28*)

$$\Delta T = \frac{\sin(\alpha_c')\cos(\alpha_c')}{\pi D'} - \frac{\sin(\alpha_c)\cos(\alpha_c)}{\pi D} \quad (2)$$

where D and D' are the coil diameters, taken through the fiber centerline before and after heating, and the coil bias angle α_c is the angle between the fiber and the coil's cross-section. For a coil of N turns and length L made from a fiber of length l: $\sin(\alpha_c) = L/l$ and $\cos(\alpha_c) = \pi ND/l$. Using these relationships and assuming negligible change in fiber length l (fig. S4), stretching a coil clamped to prevent end rotation creates a change in fiber twist of

$$\Delta T = \frac{N\Delta L}{l^2} \quad (3)$$

From this equation, we can predict the giant contractions and expansions in coil length resulting from fiber untwist during heating [Fig. 4C and table S2 (*1*)]. This twist-driven coil actuation mechanism is best demonstrated using mandrel-formed coils. Upon heating of a homochiral muscle, the fiber generates an untwisting torque that pulls coils together, providing work by contracting in length (Fig. 4E). Conversely, when oppositely twisted and coiled to form a heterochiral muscle, fiber untwist during heating increases coil length (Fig. 4D). This relationship is depicted in Fig. 4F, which shows, for highly twisted fibers, that the strokes for homochiral and heterochiral coils are maximized when using tensile and compressive loads, respectively. For compressive loads, the homochiral muscle stroke is near zero because adjacent coils are in contact. By preventing inter-coil contact, thermally driven fiber untwist can cause giant muscle contraction (>45%, Fig. 4F and movie S2).

Retention of muscle stroke and specific work capacity as fiber diameter changes by orders of magnitude is important for the diverse family of targeted applications, ranging from microscopic actuators for microfluidic circuits to those for giant-force-capacity exoskeletons and morphing air vehicles. Present experimental results for twist-insertion–coiled nylon 6 (150- to 2.45-mm-diameter fibers coiled under 16 MPa of nominal stress) provided nearly constant percent stroke and specific energy during contraction against 32 MPa of nominal stress (fig. S9, *1*), despite spanning a 267-fold range in cross-sectional area and a 325-fold range in load rating for precursor fishing lines (0.91 to 295 kg).

This near-invariance of actuator performance with fiber diameter implies near-perfect scaling of structure and therefore of properties. Indeed, we find to good approximation that the twist insertion per muscle length needed to initiate and complete coiling is inversely proportional to precursor fiber diameter (fig. S10B). This means that the fiber bias angle is nearly scale-invariant, and the number of coils per fiber length inversely depends on fiber diameter. Hence, images of twist-insertion–coiled fibers having vastly different diameters look much the same when scaled by adjusting magnification to have the same diameter (fig. S10A).

The performance of coiled muscle fibers suggests many possible applications, such as for window shutters that noiselessly open and close to conserve energy (movie S8). Additionally, spools of both conductive and nonconductive nylon are cheaply obtainable, used in clothing, and easily processed into high-stroke artificial muscles. These advantages encourage incorporating coiled fiber muscles in actuating textiles and braids.

Figure 1D shows a braid produced from 32 two-ply coils of 102-μm-diameter nylon fiber. This braid was used as a sleeve over a glass tube containing a nichrome heating element. Upon heating to 120°C, the braid delivered 16.4% stroke while lifting a 630-g load (movie S6). During contraction, the structure of the braid changed (fig. S10), decreasing the braid helix angle from 66.2° to 62.1°, corresponding to a 20.6% drop in pore area. Figure 4G shows a textile woven from coiled nylon muscles, conductive silver-plated fibers for electrothermal heating, and polyester and cotton fibers. Twelve muscle fibers were deployed in parallel to lift 3 kg (movie S5), while providing increased cycle rate capabilities by dissipating heat over a much larger area than for a single large-diameter muscle of similar strength.

Textiles and braids that change porosity in response to temperature can potentially be used for clothing that increases wearer comfort or protects emergency responders from intense heat. For instance, movie S7 demonstrates a braid with a coiled nylon muscle inserted in the center. When heated electrically, the muscle contracts, increasing the diameter of the braid, and thereby opening its pores. The braid bias angle and muscle chirality can be selected so that pores either open or close during heating. Using novel textile weaves, comfort-adjusting clothing might be created by combining polymer muscles having large thermal contractions (up to 1.2%/°C, Fig. 4C) with those that thermally expand, to thereby amplify textile porosity changes.

References and Notes

1. Materials and methods are available as supplementary materials on *Science* Online.
2. J. Cui *et al*., *Nat. Mater.* **5**, 286–290 (2006).
3. H. Koerner, G. Price, N. A. Pearce, M. Alexander, R. A. Vaia, *Nat. Mater.* **3**, 115–120 (2004).
4. J. Leng, X. Lan, Y. Liu, S. Du, *Prog. Mater. Sci.* **56**, 1077–1135 (2011).
5. P. Miaudet *et al*., *Science* **318**, 1294–1296 (2007).
6. M. D. Lima *et al*., *Science* **338**, 928–932 (2012).
7. R. H. Baughman, *Synth. Met.* **78**, 339–353 (1996).
8. E. Smela, *Adv. Mater.* **15**, 481–494 (2003).
9. J. L. Tangorra *et al*., *Bioinspir. Biomim.* **2**, S6–S17 (2007).
10. R. Pelrine, R. Kornbluh, Q. Pei, J. Joseph, *Science* **287**, 836–839 (2000).
11. F. Carpi, S. Bauer, D. De Rossi, *Science* **330**, 1759–1761 (2010).
12. Z. Cheng, Q. Zhang, *MRS Bull.* **33**, 183–187 (2008).
13. Y. Kobayashi, A. Keller, *Polymer (Guildf.)* **11**, 114–117 (1970).
14. C. L. Choy, F. C. Chen, K. Young, *J. Polym. Sci. Polym. Phys. Ed.* **19**, 335–352 (1981).
15. L. R. G. Treloar, *Rubber Elasticity* (Oxford Univ. Press, Oxford, 1975).
16. J. Foroughi *et al*., *Science* **334**, 494–497 (2011).
17. F. B. Fuller, *Proc. Natl. Acad. Sci. U.S.A.* **68**, 815–819 (1971).
18. G. H. M. van der Heijden, J. M. T. Thompson, *Nonlinear Dyn.* **21**, 71–99 (2000).
19. J. D. W. Madden *et al*., *IEEE J. Oceanic Eng.* **29**, 706–728 (2004).
20. R. K. Josephson, *Annu. Rev. Physiol.* **55**, 527–546 (1993).
21. J. E. Huber, N. A. Fleck, M. F. Ashby, *Proc. R. Soc. London A* **453**, 2185–2205 (1997).
22. D. Grant, V. Hayward, *IEEE Control Sys.* **17**, 80–88 (1997).
23. Y. Song, X. Chen, V. Dabade, T. W. Shield, R. D. James, *Nature* **502**, 85–88 (2013).
24. M. Zhang *et al*., *Science* **309**, 1215–1219 (2005).
25. Y. Kojima *et al*., *J. Appl. Polym. Sci.* **49**, 1259–1264 (1993).
26. J. M. Hollerbach, I. W. Hunter, J. Ballantyne, in *The Robotics Review* (MIT Press, Cambridge, MA, 1992), vol. 2, pp. 299–342.
27. W. F. Phillips, *Mechanics of Flight* (Wiley, 2004).
28. A. E. Love, in *The Mathematical Theory of Elasticity* (Dover Publications, New York, 1944), pp. 414–417.

Acknowledgments: We thank C. Mozayan, D. B. Hagenasr, Y. Zhang, D. A. Tolly, D. E. Wait, and P. E. Javidnia for assistance with sample preparation and measurements. Support is largely from Air Force Office of Scientific Research grant FA9550-12-1-0211, with additional support from Air Force grants AOARD-10-4067 and AOARD-13-4119, Office of Naval Research MURI grant N00014-08-1-0654, Robert A. Welch Foundation grant AT-0029, the Creative Research Initiative Center for Bio-Artificial Muscle, the Korea–U.S. Air Force Cooperation Program grant 2012-00074 (Korea), Centre of Excellence funding from the Australian Research Council and the Australian National Fabrication Facility, China National 973 Project (nos. 2007CB936203 and S2009061009), NSF China (no. 51003036), and a Natural Sciences and Engineering Research Council of Canada Discovery grant. Correspondence and requests for materials should be addressed to ray.baughman@utdallas.edu. A provisional patent application (61784247) and an international patent application (PCT/US2013/053227) have been filed by N. Li *et al*. on "Coiled and non-coiled twisted nanofiber yarn and polymer fiber torsional and tensile muscles."

Supplementary Materials

www.sciencemag.org/content/343/6173/868/suppl/DC1
Materials and Methods
Supplementary Text
Figs. S1 to S13
Tables S1 and S2
References (*29*–*31*)
Movies S1 to S8

7 October 2013; accepted 23 January 2014
10.1126/science.1246906

"Nonswellable" Hydrogel Without Mechanical Hysteresis

Hiroyuki Kamata,[1] Yuki Akagi,[1] Yuko Kayasuga-Kariya,[1] Ung-il Chung,[1,2,3] Takamasa Sakai[1]*

Hydrogels are three-dimensional polymer networks that contain a large amount of water inside. Certain hydrogels can be injected in solution and transformed into the gel state with the required shape. Despite their potential biomedical applications, the use of hydrogels has been severely limited because all the conventional hydrogels inevitably "swell" under physiological conditions, which drastically degrades their mechanical properties. We report the synthesis of injectable "nonswellable" hydrogels from hydrophilic and thermoresponsive polymers, in which two independently occurring effects (swelling and shrinking) oppose each other. The hydrogels can endure a compressive stress up to 60 megapascals and can be stretched more than sevenfold without hysteresis. Our results demonstrate that the suppression of swelling helps retain the mechanical properties of hydrogels under physiological conditions.

Hydrogels are used as scaffolds for tissue engineering (*1*), temporary supports for cells (*2*), and vehicles for drug delivery systems (*3*). Although specially engineered hydrogels are known to exhibit excellent physical properties (*4*–*7*), they may have limited applicability because conventional hydrogels "swell" as a result of the difference in osmotic pressure. Swelling drastically weakens the mechanical toughness. Further, in the case of hydrogels that exhibit hysteresis while being deformed, the equilibrium between osmotic and elastic energies is inevitably lost when the polymer network is partly (or even temporarily) broken. This occurrence consequently leads to swelling (*8*), and a continual mechanical load eventually destroys the hydrogels. This phenomenon commonly occurs in engineered gels made of natural components (*9*–*11*); self-healing gels (*12*–*16*), which are based on noncovalent cross-links; and exceptionally tough double-network gels (*4*, *8*), which use sacrificial bonds.

Our strategy to achieve a robust hydrogel that can operate under physiological conditions is based on the control of swelling by means of the introduction of thermoresponsive segments—which collapse above a certain critical temperature (T_c) because of predomination of hydrophobic interactions (*17*)—into the polymer network. We designed and fabricated hydrogels composed of tetra-armed hydrophilic and thermoresponsive polymer units (Fig. 1). The cross-linking reaction is based on the mutually reactive functional end-groups (active ester and amino end-groups). Here, the molar amount of active ester end-groups always equals to that of amino end-groups. We can prepare hydrogels with the required shape simply by mixing aqueous solutions of the polymer units, and the resultant hydrogels contain a high amount of water (89.8 to 90.4%) in the as-prepared state. No organic solvent, catalyst, or ultraviolet radiation is involved in the preparation step. The gelation time after injection can be controlled from seconds to hours (fig. S1), which allows for a range of potential applications. The swelling behavior can be controlled through a selection of the proper ratio of polymer units without losing the ideal network structure (Fig. 1D). The homogeneous network structure contributes to the high deformability (*7*). Furthermore, because the polymer network is made of covalent cross-links and has no special energy dissipation mechanism, the hydrogels do not undergo hysteresis during the deformation process.

The swelling behavior is regulated by the thermoresponsive segment ratio (r); for example, when $r = 0$, the hydrogel is composed only of hydrophilic segments (Fig. 1D, left). An alternating structure is formed when $r = 0.5$ (Fig. 1D, right). The swelling ratio (Q) of hydrogels with different r values is shown in Fig. 2A. All the hydrogels, which were prepared at 10°C, swelled in an aqueous environment at 10°C ($Q \approx 300\%$). However, the hydrogels drastically changed their volume around their T_c (~25°C, irrespective of r). This control over swelling at a fixed T_c cannot be achieved with conventional thermoresponsive hydrogels that are fabricated by a random copolymerization of hydrophilic and thermoresponsive monomer; T_c increases with an increase in the amount of hydrophilic monomer and can exceed 37°C (*18*). Based on the volume change, the water content also decreased; the degree of water release depended on r (Fig. 2C). In the same manner as conventional hydrogels, the swelling ratio for $r = 0$ is greater than 100% over the whole temperature range, indicating that the hydrogel swells and alters its original shape in an aqueous environment. Although the hydrogel with $r = 0.4$ also swelled at 10°C, the hydrogel re-

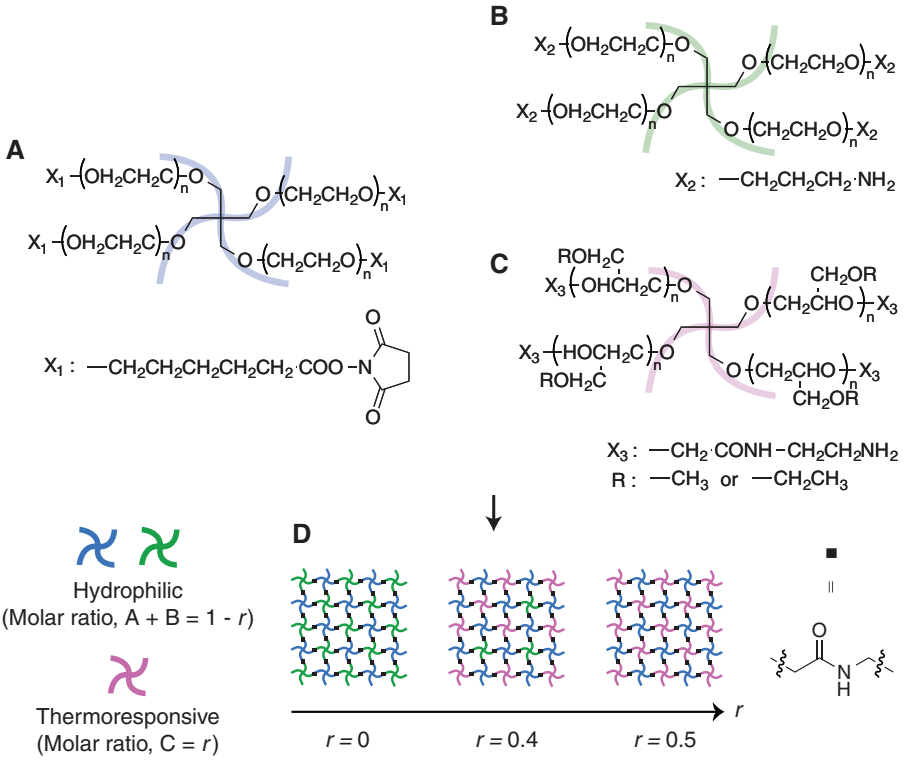

Fig. 1. Schematic of the hydrogel system. (**A**) Tetra-armed poly(ethylene glycol) with active ester end-groups. (**B**) Tetra-armed poly(ethylene glycol) with amino end-groups. (**C**) Tetra-armed poly(ethyl glycidyl ether-*co*-methyl glycidyl ether) with amino end-groups. (**D**) Polymer network composed of hydrophilic (blue) and thermoresponsive (pink) polymer units, where r represents the thermoresponsive segment ratio. Solid square indicates junction amide bonds.

[1]Department of Bioengineering, School of Engineering, University of Tokyo, 7-3-1 Hongo, Bunkyo-ku, Tokyo 113-8656, Japan. [2]Center for Disease Biology and Integrative Medicine, Division of Clinical Biotechnology, School of Medicine, University of Tokyo, 7-3-1 Hongo, Bunkyo-ku, Tokyo 113-0033, Japan. [3]Division of Tissue Engineering, University of Tokyo Hospital, 7-3-1 Hongo, Bunkyo-ku, Tokyo 113-0033, Japan.

*Corresponding author. E-mail: sakai@tetrapod.t.u-tokyo.ac.jp

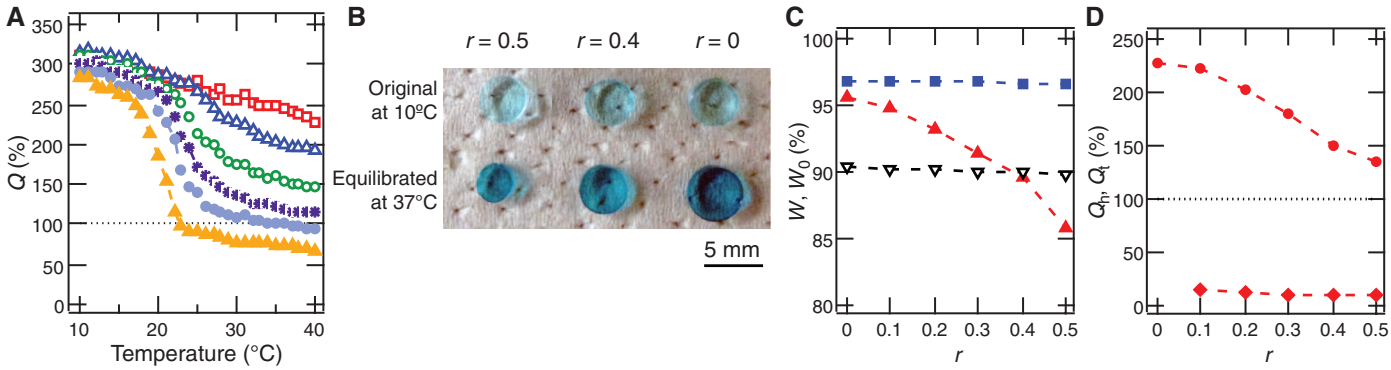

Fig. 2. Swelling behavior of the hydrogels in D-PBS. (**A**) Q as a function of temperature. The symbols represent r; r = 0 (open square), 0.1 (open triangle), 0.2 (open circle), 0.3 (asterisk), 0.4 (solid circle), and 0.5 (solid triangle). $Q = V/V_0 \times 100$, where V is the volume of the samples in the equilibrium-swollen state at each temperature and V_0 is the initial volume of the samples. The dotted line is a guide to the eye for 100%. (**B**) Photos of hydrogels that exhibit different swelling degrees depending on r; as-prepared samples at 10°C (top) and samples equilibrated in D-PBS at 37°C (bottom). The transparent hydrogels were colored only for visibility. (**C**) Equilibrium water content (W) of hydrogels at 10°C (solid squares) and 40°C (solid triangles). Initial water content (W_0) of the as-prepared samples (open inverted triangles). $W = (V - V_p)/V \times 100$, where V_p is the total volume of polymers. (**D**) The swelling ratios in the hydrophilic (Q_h, solid circles) and thermoresponsieve (Q_t, solid diamonds) segments at 40°C. $Q_h = V_h/V_{h\_0} \times 100$, where V_h is the volume of the hydrophilic segment in the equilibrium-swollen state at 40°C and V_{h_0} is the initial volume of the hydrophilic segment. $Q_t = V_t/V_{t\_0} \times 100$, where V_t is the volume of the thermoresponsive segment in the equilibrium-swollen state at 40°C and V_{t_0} is the initial volume of the thermoresponsive segment. The dotted line is a guide to the eye for 100%.

covered its original shape at ~37°C ($Q \approx 100\%$) (Fig. 2A). The hydrogels with $r = 0.4$ still retain a high amount of water at 37°C [equilibrium water content (W) ≈ 90%] (Fig. 2C). Further, unlike other conventional hydrogels with similar compositions that often induce turbidity (*19*–*21*), our hydrogels retain their transparency even above T_c, irrespective of r (Fig. 2B), which suggests that the hydrogels have a homogeneous network structure.

Because of the polymer network structure, the hydrogels exhibit an anomalous water allotment between hydrophilic and thermoresponsive segments. We estimated the swelling ratios of the thermoresponsive (Q_t) and swollen phases (Q_h), assuming that the water content of the thermoresponsive segments at 40°C (W_t) is an intrinsic value for each chemical compound ($W_t \approx 12\%$) (supplementary text). Although the hydrophilic segments are highly hydrated even at 40°C ($Q_h > 135\%$), the swelling ratio decreased with an increase in r (Fig. 2D). When the two segments independently hold water molecules, Q_h should be constant irrespective of r. This r-dependent swelling ratio suggests that the water molecules in the hydrophilic segments are also expelled by the shrinkage of the thermoresponsive segments.

The mechanical properties of hydrogels are strongly affected by their degree of swelling. To examine the general effect of swelling, we performed elongation tests with different r values after the hydrogels reached their equilibrium-swollen state in Dulbecco's phosphate-buffered saline (D-PBS) at 37°C. The representative stress-elongation curves showed that the maximum elongation ratio (λ_{max}) diminished with a decrease in r (Fig. 3A). This decrease in λ_{max} can be explained by the following definition: λ_{max} of polymer gels is defined as the ratio of two lengths of network strands—the fully stretched and initial states (*22*). Because swelling prestretches the network strands of the initial state, λ_{max} inevitably decreases.

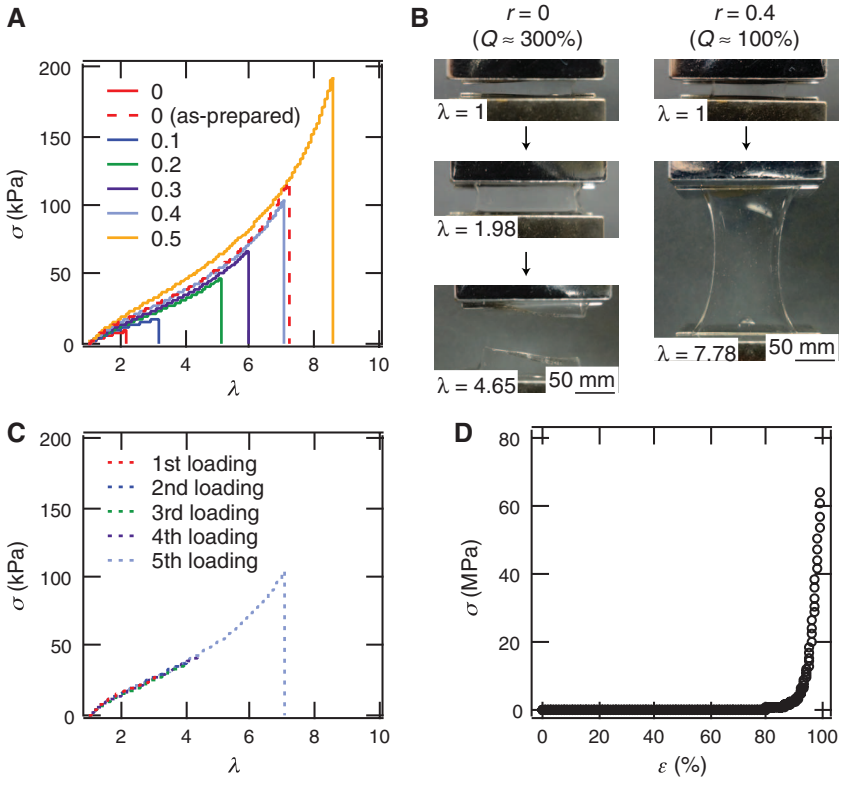

Fig. 3. Mechanical properties of hydrogels equilibrated in D-PBS at 37°C. (**A**) Representative stress–elongation curves. The colors represent r. Only for r = 0 (as-prepared), the samples were measured immediately after taken from the mold. (**B**) Photos of hydrogels (r = 0 and 0.4) during elongation tests. (**C**) Stress–elongation curves of hydrogel (r = 0.4). (**D**) The results of a compression test (r = 0.4). ε represents strain.

The hydrogel with $r = 0.4$, in which the swelling is suppressed, showed improved mechanical properties. Although a conventional hydrogel ($r = 0$) in the equilibrium-swollen state was easily torn off before the hydrogel was stretched threefold, the hydrogel with $r = 0.4$ did not rupture even after being stretched more than sevenfold (Fig. 3B). In addition, the "nonswellable" hy-

drogel showed practically no hysteresis, at least when stretched less than fourfold, which indicates that the elongation did not break the covalent bonds of the polymer network (Fig. 3C). This reversible feature is prominent when compared with the hydrogels that exhibit hysteresis during deformation, which essentially fail to tolerate a continual mechanical load. In contrast to such hydrogels, our hydrogels showed no swelling or weakening in aqueous media even after a repetitive mechanical overload. The nonswellable hydrogel endured a compressive stress of up to 60 MPa even though the hydrogel was in its equilibrium-swollen state (Fig. 3D), which is comparable with so-called "tough hydrogels" previously reported (*4*–*7*), whereas the swollen hydrogel ($r = 0$) fractured at a strain of ~80%, showing a maximum stress of ~0.4 MPa.

The properties of the hydrogels can thus be tuned through the selection of r, which will give specific values for extensibility, breakage strength, or elasticity. The hydrogels can be further adjusted via the introduction of other functional polymer units. For example, the hydrogels can be used as biodegradable materials for certain applications by introducing a cleavable polymer unit (fig. S2). The degradation profiles of the modified hydrogels are simply regulated by the amount of cleavable polymer units (fig. S3); hydrogels with a higher amount of cleavable linkages are subject to faster degradation. Our results demonstrate that the swelling suppression of hydrogels may help maintain their initial shape and retain their mechanical properties under physiological conditions.

References and Notes

1. K. Y. Lee, D. J. Mooney, *Chem. Rev.* **101**, 1869–1880 (2001).
2. G. D. Nicodemus, S. J. Bryant, *Tissue Eng. Part B Rev.* **14**, 149–165 (2008).
3. A. S. Hoffman, *Adv. Drug Deliv. Rev.* **54**, 3–12 (2002).
4. J. P. Gong, Y. Katsuyama, T. Kurokawa, Y. Osada, *Adv. Mater.* **15**, 1155–1158 (2003).
5. K. Haraguchi, T. Takehisa, *Adv. Mater.* **14**, 1120 (2002).
6. Y. Okumura, K. Ito, *Adv. Mater.* **13**, 485–487 (2001).
7. T. Sakai *et al*., *Macromolecules* **41**, 5379–5384 (2008).
8. T. Nakajima, T. Kurokawa, S. Ahmed, W. L. Wu, J. P. Gong, *Soft Matter* **9**, 1955 (2013).
9. P. A. Janmey *et al*., *J. Biol. Chem.* **269**, 32503–32513 (1994).
10. S. M. Mithieux, J. E. J. Rasko, A. S. Weiss, *Biomaterials* **25**, 4921–4927 (2004).
11. C. Storm, J. J. Pastore, F. C. MacKintosh, T. C. Lubensky, P. A. Janmey, *Nature* **435**, 191–194 (2005).
12. E. A. Appel, J. del Barrio, X. J. Loh, O. A. Scherman, *Chem. Soc. Rev.* **41**, 6195–6214 (2012).
13. K. Haraguchi, K. Uyama, H. Tanimoto, *Macromol. Rapid Commun.* **32**, 1253–1258 (2011).
14. A. Phadke *et al*., *Proc. Natl. Acad. Sci. U.S.A.* **109**, 4383–4388 (2012).
15. J. Y. Sun *et al*., *Nature* **489**, 133–136 (2012).
16. Q. Wang *et al*., *Nature* **463**, 339–343 (2010).
17. M. Heskins, J. E. Guillet, *J. Macromol. Sci. A Chem.* **2**, 1441 (1968).
18. J. E. Chung, M. Yokoyama, T. Aoyagi, Y. Sakurai, T. Okano, *J. Control. Release* **53**, 119–130 (1998).
19. J. Cui, M. A. Lackey, G. N. Tew, A. J. Crosby, *Macromolecules* **45**, 6104–6110 (2012).
20. J. Li *et al*., *Biomaterials* **27**, 4132–4140 (2006).
21. S. Reinicke *et al*., *Soft Matter* **5**, 2648 (2009).
22. S. P. Obukhov, M. Rubinstein, R. H. Colby, *Macromolecules* **27**, 3191–3198 (1994).

Acknowledgments: This work was supported by the Japan Society for the Promotion of Science (JSPS) through the Grants-in-Aid for Scientific Research, the Center for Medical System Innovation (CMSI), the Graduate Program for Leaders in Life Innovation (GPLLI), the International Core Research Center for Nanobio, Core-to-Core Program, A. Advanced Research Networks, and the Funding Program for World-Leading Innovative R&D on Science and Technology (FIRST program); the Ministry of Education, Culture, Sports, Science, and Technology in Japan (MEXT) through the Center for NanoBio Integration (CNBI) and Grants-in-Aid for Scientific Research from MEXT (23700555 to T.S. and 24240069 to U.C.); the Japan Science and Technology Agency (JST) through the S-innovation program and COI STREAM.

Supplementary Materials

www.sciencemag.org/content/343/6173/873/suppl/DC1
Materials and Methods
Schemes S1 to S4
Figs. S1 to S3

29 October 2013; accepted 23 January 2014
10.1126/science.1247811

The Robustness and Evolvability of Transcription Factor Binding Sites

Joshua L. Payne[1,2] and Andreas Wagner[1,2,3]*

Robustness, the maintenance of a character in the presence of genetic change, can help preserve adaptive traits but also may hinder evolvability, the ability to bring forth novel adaptations. We used genotype networks to analyze the binding site repertoires of 193 transcription factors from mice and yeast, providing empirical evidence that robustness and evolvability need not be conflicting properties. Network vertices represent binding sites where two sites are connected if they differ in a single nucleotide. We show that the binding sites of larger genotype networks are not only more robust, but the sequences adjacent to such networks can also bind more transcription factors, thus demonstrating that robustness can facilitate evolvability.

Changes in gene expression via mutations in cis-regulatory regions can explain much of life's diversity (*1*). Of particular importance are mutations in the specific sequences that determine transcription factor (TF) binding sites and coordinate gene expression in both space and time. Such mutations may change the identity of the cognate TF or alter the affinity with which a site is bound (*2*). This may, in turn, change the structure or logic of the transcriptional regulatory circuits in which these sites are embedded (*3*) and lead to adaptations in the form of novel gene expression patterns (*4*). Such adaptations may eventually lead to evolutionary innovations, such as new pigmentation patterns (*5*) or body structures (*6*).

Transcription factor binding sites are typically between 6 and 10 nucleotides long, which may reflect a tradeoff between the specificity of a site and its robustness to mutation (*7*). TF binding sites can be degenerate, with some TFs binding hundreds of different sequences, whereas others bind merely dozens (*8*). It is not known how this degeneracy contributes to the mutational robustness of TF binding sites, nor to their evolvability, which is defined as the ability to bind different TFs after mutation.

Many recent studies have attempted to elucidate the robustness and evolvability of living systems [reviewed in (*9*)]. These studies tend to use computation to map genotypes to phenotypes, facilitating the systematic characterization of vast genotype spaces. Several of these modeling efforts suggest that genotype networks [neutral networks (*10*)] are responsible for the robustness and evolvability of living systems. A genotype network is a set of genotypes that have the same phenotype, where two genotypes are connected by an edge if they differ by a single mutation. Large genotype networks confer robustness because genetic perturbations are unlikely to drive a genotype off the network (*11*), and these networks confer evolvability because they extend throughout genotype space, providing mutational access to a diversity of genotypes that have different phenotypes (*12*).

Although for most biological systems it is currently not possible to experimentally determine an exhaustive genotype-to-phenotype map, recent advances in microarray technologies (*13*, *14*) have made such a mapping possible for TF binding sites. We used protein binding microarray data to characterize the genotype networks of TF binding sites for 104 mouse (*8*) and 89 yeast (*15*) TFs (*16*). For each TF, we used the enrichment score (*E*-score)—a proxy for binding affinity (*8*, *13*)—of each of the 32,896 possible contiguous binding sites (eight nucleotides in length) to categorize a site as bound or unbound (fig. S1) (*16*). We then assessed the genotype networks for the robustness and evolvability of individual TF binding sites and of the complete binding repertoires of TFs (Fig. 1). For example, the mouse TF Foxa2 (Fig. 1A), a key regulator of developmental processes (*17*), is presented as a representative

[1]University of Zurich, Institute of Evolutionary Biology and Environmental Studies, Zurich, Switzerland. [2]Swiss Institute of Bioinformatics, Lausanne, Switzerland. [3]The Santa Fe Institute, Santa Fe, NM 87501, USA.

*Corresponding author. E-mail: andreas.wagner@ieu.uzh.ch

of the TFs we consider (database S1 and fig. S2) and is used to illustrate how sites are connected in the genotype network (Fig. 1B) and how mutation can change a site's cognate TFs (Fig. 1C). Where possible, we complement our analysis with in vivo binding data generated by genome-wide chromatin immunoprecipitation followed by DNA sequencing.

For 99% of the TFs (103 of 104 in mice and 87 of 89 in yeast), the majority of bound sites were part of a single connected genotype network, which we refer to as the dominant genotype network. Moreover, for 60% of the TFs (65 of 104 in mice and 51 of 89 in yeast), the dominant genotype network comprised all of the bound sites (e.g., Foxa2) (Fig. 1 and database S1). We also observed that the number of disconnected genotype networks per TF decreased as the number of bound sites increased (fig. S3), indicating that decreasing TF specificity promotes genotype network connectivity. The basic structural properties of these genotype networks did not differ between mouse and yeast TFs (fig. S4), but were significantly different from what was expected under a null model [Permutation test, $P_{null} < 0.005$ (*16*) (fig. S5)] and exhibited variation both within and among DNA binding domain structural classes (fig. S6 and database S1).

We quantified the robustness of each of a TF's binding sites as the site's number of neighbors in the genotype network, divided by its number of possible neighbors (*16*). Because the timing, location, and level of gene expression are important for many biological functions, their disruption through mutations in TF binding sites can be deleterious. Thus, the mutational robustness of a TF binding site can be an important factor in the resilience of gene expression to genetic change. On average, a Foxa2 binding site (Fig. 2A) can tolerate 37% of possible mutations [significantly more than expected under the null model (*16*); Permutation test, $P_{null} < 0.005$] but exhibits substantial variation around this average and ranges from binding sites that can only tolerate 3% of all possible single mutations to those that can tolerate the majority of such mutations (72%). For all other TFs, average mutational robustness ranged from 7 to 48% (Fig. 2B). We additionally found that mutational robustness and binding affinity were positively correlated (fig. S7) (*18*) and that high-affinity sites were often enriched in vivo (fig. S7A) (*18*), both genome-wide (table S1) and within putative enhancers (table S2), suggesting that in vivo binding sites are often mutationally robust.

Many of the morphological differences between closely related organisms are caused by mutations in cis-regulatory regions (*4*, *6*, *19*–*21*). These mutations often comprise only one or a few base pair changes that may result in the gain or loss of one or more TF binding sites. To assess how mutations in the binding sites of specific TFs may bring about novel regulation, we measured a binding site's evolvability as the proportion of TFs in our data set that bind the sequences that lie within a single mutation of the binding site, but are not themselves part of the TF's genotype network (Figs. 1C and 2, C and D). Whereas such mutations are likely often deleterious, they also have the potential to generate novel gene expression patterns that may be adaptive. The estimate of evolvability for all binding sites of Foxa2 demonstrates that every site is within a single mutation of at least one sequence that binds a TF other than Foxa2, as expected under the null model (Permutation test, $P_{null} = 1$). This suggests that the binding preferences of the TFs considered here are so highly intertwined that any sequence, whether or not it is part of a large genotype network, will neighbor at least one sequence that binds another TF. On average, the sites bound by Foxa2 were separated by a single mutation from sequences that bind 26% of the other 103 mouse TFs (Permutation test, $P_{null} = 0.069$). Similar observations hold for all of the mouse and yeast TFs that we considered (Fig. 2D and database S1).

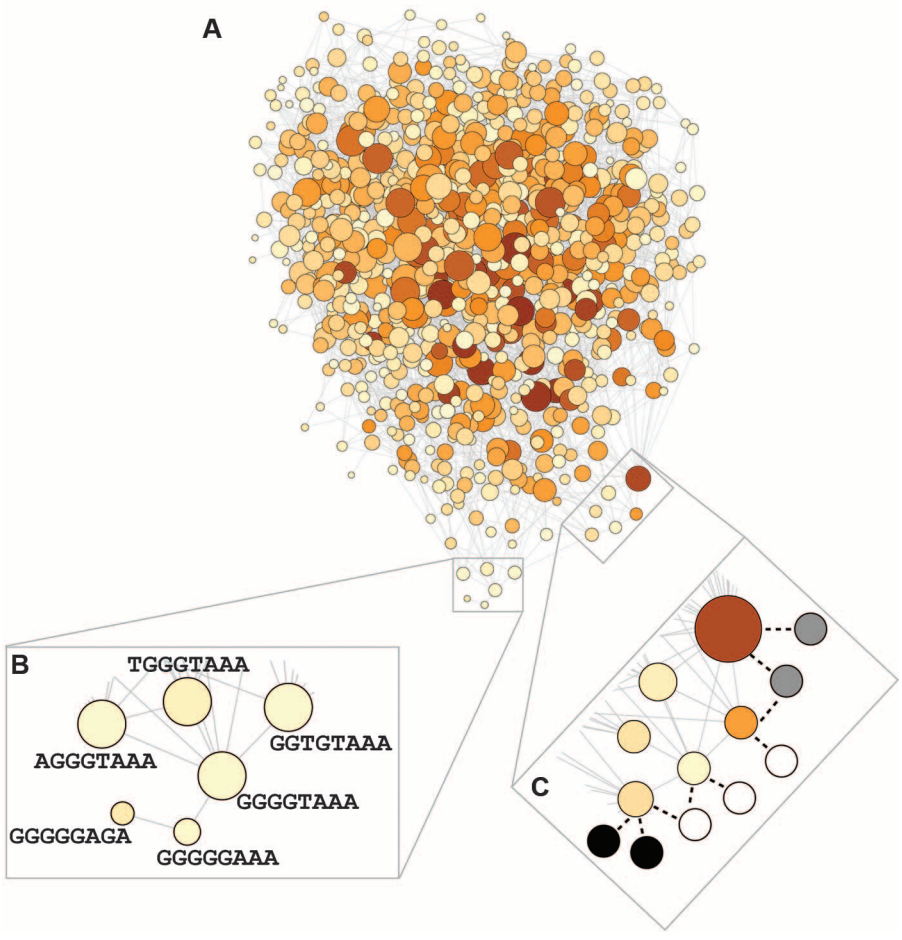

Fig. 1. Genotype networks of TF binding sites. (**A**) Genotype network for the mouse TF Foxa2. Each vertex represents a DNA sequence bound by a TF (false discovery rate $Q < 0.001$), its color captures binding affinity (darker = higher), and its size indicates the number of neighboring binding sites (bigger = more neighbors). The latter is proportional to mutational robustness (see text). (**B**) Vertices are neighbors and are connected by an edge if they represent sites that are separated by a single small mutation. We consider two kinds of such mutations, namely point mutations and indels that shift an entire, contiguous binding site by a single base (*16*). (**C**) Some mutations transform a DNA sequence that is on the genotype network into one that is not (black dotted lines). In these cases, the mutant sequence may bind another TF (hypothetical new cognate TFs indicated by black, white, and gray circles).

Theoretical studies suggest that both robustness and evolvability are facilitated by the existence of large genotype networks (*9*). We provide empirical evidence for this theory through the measurement of repertoire robustness, defined as the average mutational robustness of each binding site in the repertoire (see Fig. 2B), and repertoire evolvability, defined as the proportion of TFs in our data set that bind sequences within a single mutation of any binding site in the repertoire. These measurements show that large genotype networks confer repertoire robustness (Fig. 3A) (Spearman's correlation coefficient $r = 0.90$, $P < 1.0 \times 10^{-50}$) and repertoire evolvability (Fig. 3B) (Spearman's $r = 0.65$, $P = 1.84 \times 10^{-24}$). Although repertoire robustness increased gradually with genotype network size and was significantly higher than expected for all TFs (Permutation test, $P_{null} < 0.005$), repertoire evolvability increased more abruptly and was significantly higher than

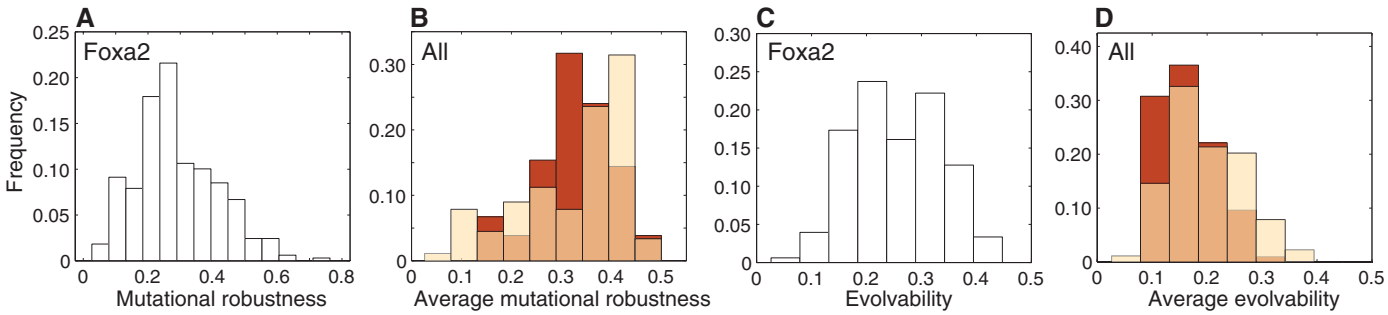

Fig. 2. The mutational robustness and evolvability of TF binding sites. (**A**) Distribution of mutational robustness for all sites bound by Foxa2. (**B**) Distribution of the average mutational robustness across all sites bound by each of the 104 mouse (dark red) and 89 yeast (light beige) TFs. An intermediate shade indicates that the bars are overlapping. (**C**) Distribution of evolvability for all sites bound by Foxa2. (**D**) Distribution of the average evolvability across all sites bound by each of the mouse and yeast TFs.

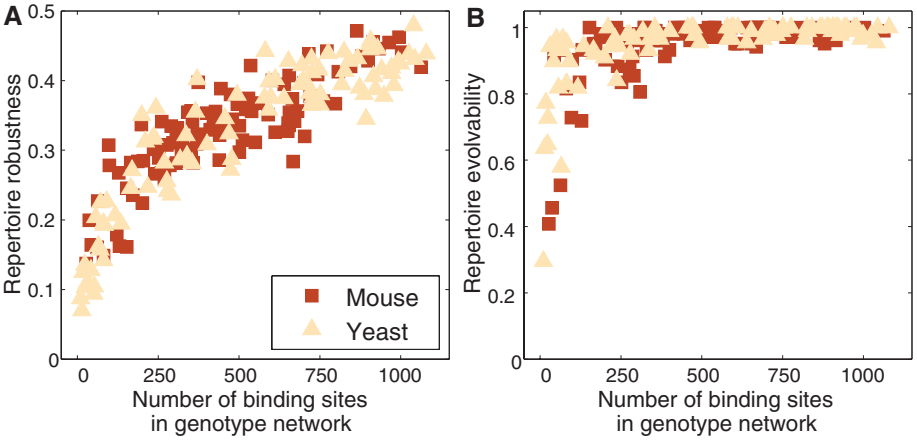

Fig. 3. Large genotype networks confer repertoire robustness and evolvability. Repertoire (**A**) robustness and (**B**) evolvability are shown as a function of the number of TF binding sites in the dominant genotype network for all 104 mouse and 89 yeast TFs.

expected for 91% of TFs, as compared with the null model (Permutation test, $P_{null} < 0.005$ for 96 of 104 in mouse and 80 of 89 in yeast) (database S1), such that even small genotype networks had high evolvability. This stems from the diversity of TFs that bind the sequences one mutation away from any two sites (fig. S8) (*18*). We also found that the binding sites of TFs with large genotype networks were more likely to arise de novo in DNA sequences (fig. S9) (*18*). These results show that whereas a tradeoff may exist between robustness and evolvability at the level of an individual binding site (*18*), the organization of these sites as a connected genotype network facilitates a synergistic relation between robustness and evolvability at the level of the binding repertoire. These results are insensitive to the threshold used to define a site as bound (figs. S10 to S12) (*18*), as well as to an alternative evolvability measure that considers only TFs with differing DNA binding domains (fig. S13) (*18*).

On the basis of in vitro and in vivo measurements of TF-DNA interactions, our observations imply that it is almost always possible to transform one bound site into any other via a series of small mutations that preserve TF binding. This suggests that the mutational robustness of TF binding sites can be fine-tuned via mutation. The broad distributions of binding site robustness and evolvability are consistent with in vivo studies of TF binding sites, which have reported that the number of point mutations with a regulatory effect can vary greatly among sites (*2*, *22*), and with comparative studies of binding site turnover in closely related species (*19*–*21*). Our analysis of TF binding repertoires indicate that decreased TF specificity yields large connected genotype networks that confer robustness and evolvability to the binding sites they harbor. Although our findings have several caveats (*18*), they are in line with studies of genotype networks in biological systems, including the existence of a large dominant genotype network (*10*), the tradeoff between robustness and evolvability for individual genotypes (*23*), and the observation that large genotype networks confer robustness and evolvability (*12*). As high-throughput technologies continue to advance, it may become possible to exhaustively study not only TF binding sites, but also entire regulatory circuits (*24*), paving the way for a more complete understanding of the robustness and evolvability of living systems.

References and Notes

1. G. A. Wray, *Nat. Rev. Genet.* **8**, 206–216 (2007).
2. J. C. Kwasnieski, I. Mogno, C. A. Myers, J. C. Corbo, B. A. Cohen, *Proc. Natl. Acad. Sci. U.S.A.* **109**, 19498–19503 (2012).
3. C. C. Guet, M. B. Elowitz, W. Hsing, S. Leibler, *Science* **296**, 1466–1470 (2002).
4. B. B. Tuch, D. J. Galgoczy, A. D. Hernday, H. Li, A. D. Johnson, *PLOS Biol.* **6**, e38 (2008).
5. N. Gompel, B. Prud'homme, P. J. Wittkopp, V. A. Kassner, S. B. Carroll, *Nature* **433**, 481–487 (2005).
6. I. Guerreiro *et al.*, *Proc. Natl. Acad. Sci. U.S.A.* **110**, 10682–10686 (2013).
7. A. J. Stewart, S. Hannenhalli, J. B. Plotkin, *Genetics* **192**, 973–985 (2012).
8. G. Badis *et al.*, *Science* **324**, 1720–1723 (2009).
9. A. Wagner, *Proc. Biol. Sci.* **279**, 1249–1258 (2012).
10. P. Schuster, W. Fontana, P. F. Stadler, I. L. Hofacker, *Proc. Biol. Sci.* **255**, 279–284 (1994).
11. J. Cotterell, J. Sharpe, *Mol. Syst. Biol.* **6**, 425 (2010).
12. S. Ciliberti, O. C. Martin, A. Wagner, *Proc. Natl. Acad. Sci. U.S.A.* **104**, 13591–13596 (2007).
13. M. F. Berger *et al.*, *Nat. Biotechnol.* **24**, 1429–1435 (2006).
14. S. J. Maerkl, S. R. Quake, *Science* **315**, 233–237 (2007).
15. C. Zhu *et al.*, *Genome Res.* **19**, 556–566 (2009).
16. Materials and methods are available as supplementary materials on *Science* Online.
17. C. Kimura-Yoshida *et al.*, *Proc. Natl. Acad. Sci. U.S.A.* **104**, 5919–5924 (2007).
18. See supplementary text on *Science* Online.
19. J. Ihmels *et al.*, *Science* **309**, 938–940 (2005).
20. M. Z. Ludwig, C. Bergman, N. H. Patel, M. Kreitman, *Nature* **403**, 564–567 (2000).
21. D. Schmidt *et al.*, *Science* **328**, 1036–1040 (2010).
22. R. P. Patwardhan *et al.*, *Nat. Biotechnol.* **30**, 265–270 (2012).
23. A. Wagner, *Proc. Biol. Sci.* **275**, 91–100 (2008).
24. Y. Schaerli, M. Isalan, *Mol. Biosyst.* **9**, 1559–1567 (2013).

Acknowledgments: We thank A. Barve, D. Pechenick, J. Aguilar-Rodríguez, K. Sprouffske, and D. Urbach for discussions. J.L.P. acknowledges support from the International Research Fellowship Program of the NSF. A.W. acknowledges support through Swiss National Science Foundation grant 315230-129708 and the University Priority Research Program in Evolutionary Biology at the University of Zurich. Database S1 is available as supplementary material on *Science* Online.

Supplementary Materials

www.sciencemag.org/content/343/6173/875/suppl/DC1
Materials and Methods
Supplementary Text
Figs. S1 to S15
Tables S1 and S2
References (*25*–*71*)
Database S1

27 November 2013; accepted 23 January 2014
10.1126/science.1249046

Structural Insights into Ubiquinone Biosynthesis in Membranes

Wei Cheng[1] and Weikai Li[1]*

Biosynthesis of ubiquinones requires the intramembrane UbiA enzyme, an archetypal member of a superfamily of prenyltransferases that generates lipophilic aromatic compounds. Mutations in eukaryotic superfamily members have been linked to cardiovascular degeneration and Parkinson's disease. To understand how quinones are produced within membranes, we report the crystal structures of an archaeal UbiA in its apo and substrate-bound states at 3.3 and 3.6 angstrom resolution, respectively. The structures reveal nine transmembrane helices and an extramembrane cap domain that surround a large central cavity containing the active site. To facilitate the catalysis inside membranes, UbiA has an unusual active site that opens laterally to the lipid bilayer. Our studies illuminate general mechanisms for substrate recognition and catalysis in the UbiA superfamily and rationalize disease-related mutations in humans.

The UbiA superfamily of intramembrane prenyltranferases catalyzes a key step in the synthesis of ubiquinones, menaquinones, chlorophylls, hemes, and vitamin E, which are released into membranes to serve as electron and proton carriers for cellular respiration and photosynthesis and as antioxidants to reduce cell damage. The UbiA superfamily (fig. S1) includes the UbiA and MenA enzymes in bacteria and archaea; chlorophyll synthases and homogentisate prenyltransferases in photosynthetic organisms; and *para*-hydroxybenzoate polyprenyltransferase (COQ2) (*1*) and UBIAD1 (*2*) enzymes that play important physiological roles in eukaryotes (*3*). COQ2 is involved in the biosynthesis of ubiquinones, which function as electron carriers for the mitochondria respiration. The UBIAD1 enzyme is involved in maintaining vascular homeostasis (*4*), preventing oxidative damage in cardiovascular tissues (*5*), and sustaining mitochondrial function (*6*).

Members in the UbiA superfamily share considerable sequence similarity (fig. S2) and catalyze a common reaction of fusing a phytyl or isoprenyl chain to an aromatic ring. As the prototype of the superfamily, the UbiA enzyme catalyzes the condensation of isoprenylpyrophosphate (IPP) with the aromatic *p*-hydroxybenzoate (PHB). UbiA cleaves the pyrophosphate from the IPP substrate to generate a carbocation intermediate at the end of the isoprenyl chain, which reacts at the meta-position of the aromatic PHB substrate to form a C–C bond (Fig. 1A). Although the prenylation of PHB is regiospecific, UbiA promiscuously recognizes IPPs of various chain lengths to generate the ubiquinones CoQ_6 to CoQ_{10} in different species (*7*–*9*). Short-chain substrates such as geranylpyrophosphate (GPP) can be used by UbiA in vitro (*10*, *11*). UbiA is a transmembrane protein that contains two conserved Asp-rich motifs (fig. S2) and requires magnesium for catalysis (*10*). UbiA may be evolutionarily related to trans-prenyltransferases that catalyze the elongation of isoprenyl chains (*12*) but shares no sequence similarity with soluble aromatic prenyltransferases that synthesize secondary metabolites (*3*). Unlike these soluble enzymes, UbiA recognizes long isoprenyl chains and releases a prenylated quinone product directly into the membrane. Structural knowledge of UbiA is essential to understand how prenyl transfer is catalyzed within lipid bilayers.

Here, we report the 3.3 Å crystal structure of a UbiA homolog from *Aeropyrum pernix* (ApUbiA). The overall structure of ApUbiA contains nine transmembrane helices (TMs) that are arranged counterclockwise in a U shape with a large central cavity (Fig. 1B and fig. S3). When viewed from the cytoplasmic side, the central cavity is surrounded by TM1, TM2, and TM9 at the front and TM5 and TM6 from the back. The C-terminal extensions of TM2, TM4, and TM6 are kinked to create a short extramembrane helix followed

[1]Department of Biochemistry and Molecular Biophysics, Washington University School of Medicine, St. Louis, MO 63110, USA.

*Corresponding author. E-mail: liw@biochem.wustl.edu

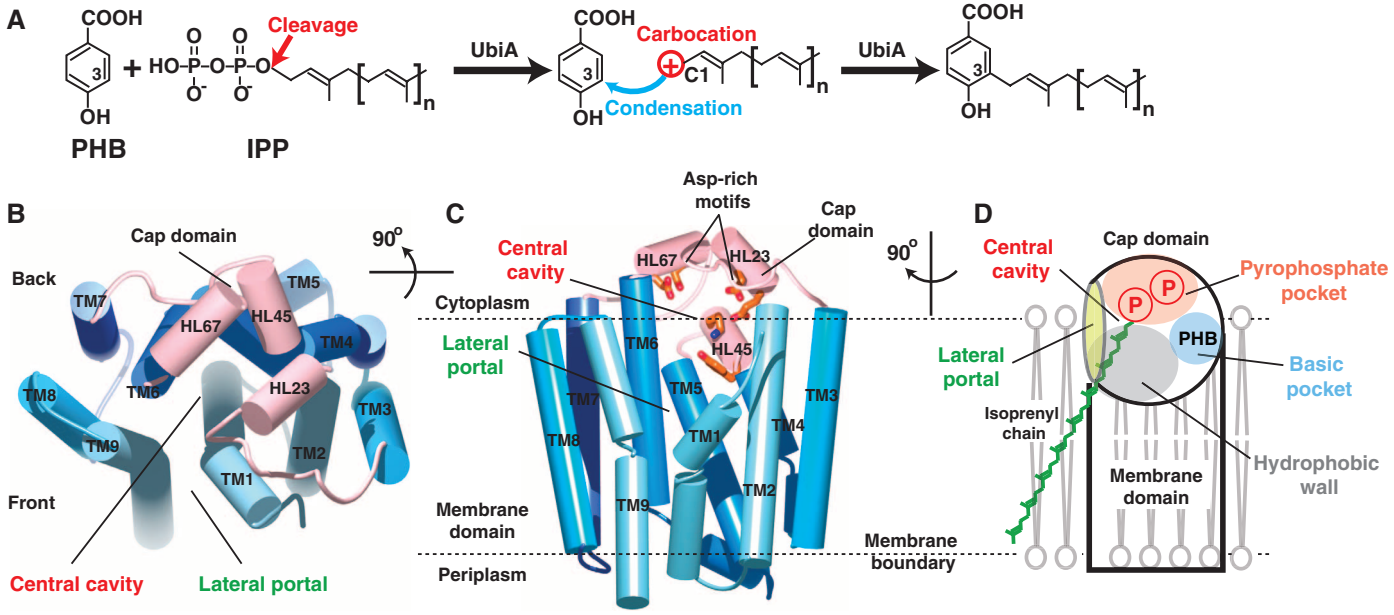

Fig. 1. Scheme of UbiA catalysis and structure of ApUbiA. (**A**) UbiA catalysis. Cleavage of the pyrophosphate group from the IPP substrate generates a carbocation intermediate, which reacts at the meta-position of the PHB substrate to complete the condensation reaction. (**B**) Apo structure of ApUbiA viewed from the cytoplasmic side. The cap domain is shown in pink, and the TMs are shown in different blue colors. (**C**) A side view of the same structure. Conserved residues in the central cavity are shown in orange. (**D**) Cartoon representation of the structure, which has a unique lateral portal that opens to membrane. The large central cavity contains a polar pocket (pink) for pyrophosphate binding, a hydrophobic wall (gray) for the binding of isoprenyl chains, and a small basic pocket (blue) for PHB binding (see fig. S5).

by a C-terminal loop. These helix/loop regions are termed HL2-3, HL4-5, and HL6-7, respectively, and they form a cap over the central cavity of the transmembrane domain. HL2-3 and HL6-7 each contain an Asp-rich motif, $D_{54}XXXD_{58}$ and $D_{182}XXXD_{186}$ (D, Asp; X, any amino acid), respectively (*13*, *14*), and HL4-5 harbors another conserved motif, $Y_{115}XXXK_{119}$ (fig. S2) (Y, Tyr; K, Lys). All these conserved residues protrude into the central cavity (Fig. 1C), where they are likely involved in substrate binding or catalysis. One side of the central cavity has an opening that we term the lateral portal that is largely buried in the membrane (Fig. 1C). The lateral portal is delineated by TM1 and TM9, both of which are kinked helices with a proline in the middle. The central cavity has a hydrophobic portion leading to the lateral portal (fig. S5) that could accommodate the isoprenyl chain of the IPP substrate (Fig. 1D).

To capture a substrate-bound state, we soaked ApUbiA crystals in a mixture of PHB; Mg; and an uncleavable IPP analog, geranyl thiolopyrophosphate (GSPP). This 3.6 Å structure shows GSPP binding in the central cavity (Fig. 2A and fig. S3C). A cluster of conserved residues around GSPP implies the formation of an extensive interaction network that recognizes the pyrophosphate group of GSPP. Because Mg^{2+} ions are required to mediate the interaction between Asp residues and the pyrophosphate group (*10*, *15*), we modeled (*16*) two Mg into the electron density (Fig. 2A): Mg1 may bridge the O1 atom of the pyrophosphate to Asp^{54} and Asp^{58}, and Mg2 may bridge the O2 atom to Asp^{182} and Asp^{186} through a water. Asp^{54} and Asp^{182} seem to have an additional role of positioning the side chains of Arg^{67} and Arg^{63}, respectively. These two arginine residues, together with Tyr^{115} and Lys^{119}, may in turn interact with other oxygens of the pyrophosphate group.

Comparison of the electron density maps (Fig. 2B) in the apo and substrate-bound states

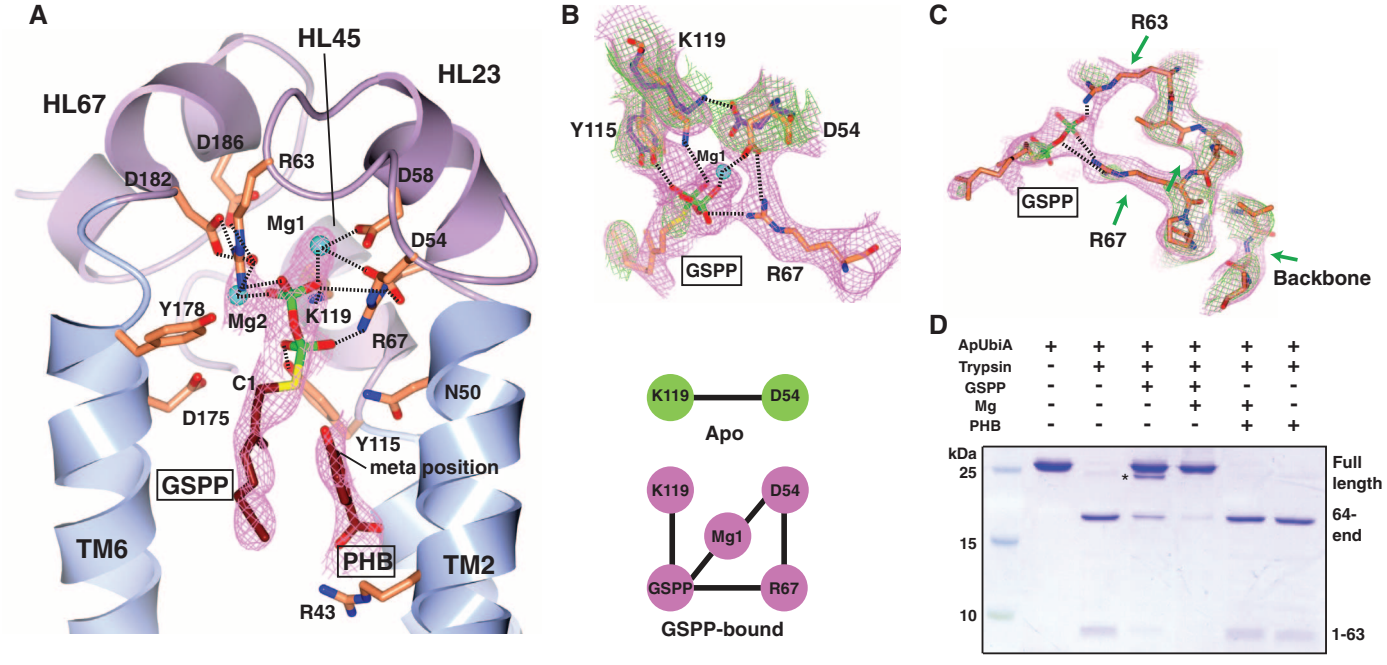

Fig. 2. Substrate binding of ApUbiA. (**A**) The ApUbiA structure in complex with the substrates. The B-factor–sharpened experimental map (in purple) is contoured at 1σ. Because of the limited resolution, the interactions (dashed lines) between individual atoms are putative. N, Asn; R, Arg. (**B**) Conformational changes induced by GSPP binding. (Top) The experimental maps (1σ) of the apo (green) and GSPP-bound (purple) structures suggest the change of interactions. (Bottom) A cartoon shows that an interaction network is established upon GSPP binding. (**C**) Comparison of the loop region near Arg^{63} and Arg^{67} [same maps as in (B)]. The green arrows indicate a few disordered regions in the apo structure. (**D**) Trypsin digestion of the ApUbiA protein in presence of GSPP, PHB, and Mg. The primary digestion site is at Arg^{63}, and a minor digestion site (asterisk) is in a linker region of the N-terminal His tag.

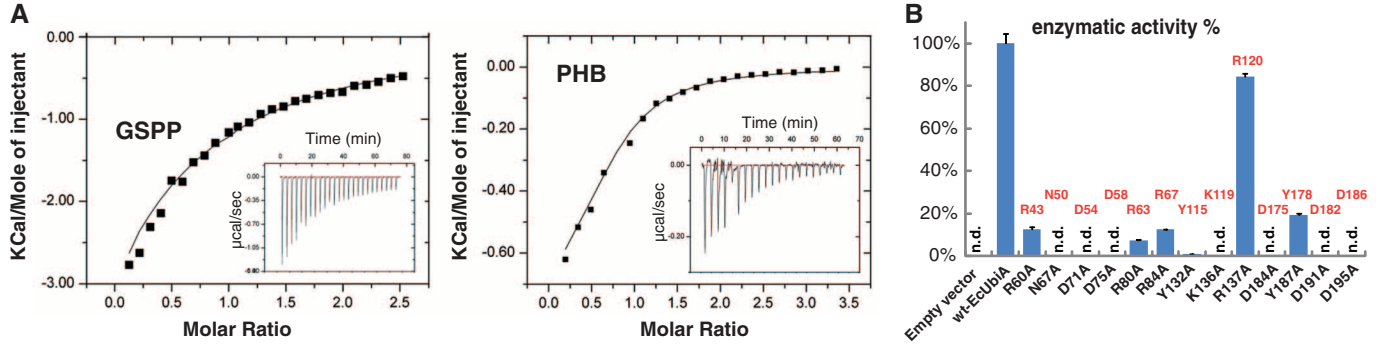

Fig. 3. Binding and activity assays of UbiA enzymes. (**A**) ITC measurements of the GSPP (left) and PHB (right) binding to ApUbiA in presence of Mg. (Insets) The original titration traces. (**B**) Prenyltransferase activities of EcUbiA mutants. Conserved residues at the central cavity are mutated (n.d., not detected; error bars, SEM of duplicated assays; wt, wild type). Corresponding residues in the ApUbiA structure (Fig. 2A) are labeled in red. R137 is a positive control that is not at the active site in our structure yet was predicted important in an in silico model (*19*).

suggests that binding of GSPP induces conformational changes in several active-site residues. The interaction between Lys^{119} and Asp^{54} in the apo structure is "unlocked," and a new interaction network is established, with Lys^{119} recognizing the pyrophosphate and Asp^{54} interacting with Arg^{67}. Moreover, the loop region containing Arg^{63} and Arg^{67} becomes ordered (Fig. 2C), consistent with protection of this loop region from trypsin digestion when GSPP binds in a Mg-dependent manner (Fig. 2D). GSPP binding seems to only induce local changes in the active site of ApUbiA, whereas the overall architecture is retained (fig. S4A).

The large central cavity of UbiA contains a small basic pocket near the GSPP binding site (Fig. 1D and fig. S5). The electron density contained in this pocket is suggestive of PHB binding (fig. S5). With PHB modeled so that its carboxyl group contacts Arg^{43} (Fig. 2A and fig. S5), the meta-position of PHB can be close to the C1 atom of the IPP, consistent with C–C bond formation during the condensation reaction.

The residues lining the central cavity are highly conserved in the superfamily (fig. S2) and are essential for ApUbiA's binding of GSPP and PHB in vitro. Binding constants of wild-type ApUbiA for GSPP and PHB were determined by isothermal titration calorimetry (ITC) to be about 0.3 and 0.1 mM, respectively (Fig. 3A). These ApUbiA affinities are comparable to the Michaelis constant (K_M) values of GPP (0.255 mM) and PHB (0.188 mM) for the condensation reaction catalyzed by *Escherichia coli* UbiA (*10*). Consistent with the structure (Fig. 2A), Ala mutations of residues that bind GSPP significantly lowered its binding affinity for ApUbiA (fig. S6). In addition, Arg^{43}→Ala^{43} (Arg43Ala) and Asn50Ala mutations in the small basic pocket interfered with PHB binding (fig. S7).

To identify residues essential for UbiA catalysis, we went on to test the enzymatic activities of mutant UbiA enzymes. We were unable to establish an activity assay for the hyperthermophilic ApUbiA at elevated temperature (*16*), probably because this enzyme was expressed in *E. coli* membranes (*17*, *18*). Therefore, our subsequent enzymatic assays used *E. coli* UbiA (EcUbiA), a model enzyme (*10*, *14*) that shares 52% sequence similarity to ApUbiA and has all the conserved active-site residues (fig. S2). Among the residues that bound GSPP in the ApUbiA structure (Fig. 2A), several single mutations abolished EcUbiA catalysis (Fig. 3B). As a more stringent test for activity, most of these EcUbiA mutants failed to rescue the growth defect of a quinone-deficient strain of *E. coli* (fig. S8). The Asp residues in the two DXXXD motifs are essential, likely because they chelate the Mg^{2+} ions required for UbiA catalysis (*10*, *15*). In addition, the Asn67Ala and Asp184Ala mutations but not Tyr187Ala completely abolished the activity. These residues correspond to those (Asn^{50}, Asp^{175}, and Tyr^{178} in ApUbiA) close to the C1 atom of GSPP (Fig. 2A) and therefore are candidates for stabilizing the carbocation intermediate. For those mutants with partial activity (Fig. 3B), we were able to investigate the enzyme kinetics. We found that the Arg60Ala mutation increased the K_M of PHB to about 3 mM (10 times that of the wild-type enzyme), whereas mutating residues involved in pyrophosphate binding did not generate this dramatic effect (fig. S9). The Arg^{60} residue in EcUbiA corresponds to Arg^{43} in the ApUbiA structure (Fig. 2A), which is predicted to bind PHB's carboxyl group. Because Arg60Ala did not completely abolish the EcUbiA activity, the PHB binding could involve other residues around the basic pocket.

Previous models postulated that one of the Asp-rich motifs binds to PHB (*13*, *14*, *19*), but the ApUbiA structure suggests that both Asp motifs in UbiA are likely to engage the pyrophosphate group of IPP through Mg-dependent interactions (Fig. 2A). As for trans-prenyltransferases (*12*), the Mg^{2+} ions may trigger the ionization of the carbocation (*20*), which could be stabilized by nearby residues such as Asn^{67} or Asp^{184} in EcUbiA (Figs. 2A and 3B). Although the active site of UbiA opens laterally to the bilayer, the highly reactive carbocation intermediate would be protected from water by the surrounding lipids (Fig. 1D). In contrast to previous models (*13*, *14*, *19*), PHB is probably bound in a basic pocket (fig. S5) adjacent to the carbocation. Consistent with this proposal, mutating residues in the basic pocket affects PHB binding (figs. S7 and S9). Our results for EcUbiA and ApUbiA are also consistent with the enzymatic characterization of LePGT1, a UbiA homolog in plants. LePGT1 mutations corresponding to Arg43Ala and Asn50Ala (Fig. 2A and fig. S5) increased the K_M for PHB by 10- and 50-fold, respectively (*13*). At this binding site, the covalent bond formation between the meta-position of PHB and the C1 atom of IPP may proceed without a substantial conformational change.

Ubiquinones incorporate long-chain, highly lipophilic tails of 6 to 10 isoprenyl units (*7*–*9*). The promiscuous use of long-chain IPP substrates by UbiA can now be explained by structural comparisons (Fig. 4). UbiA is an all–α-helical structure that is completely different from the α/β barrel structure of soluble aromatic prenyltransferases (*21*–*24*). However, the membrane-bound UbiA shares some structural features with a soluble trans-prenyltransferase (Fig. 4A), farnesyl pyrophosphate synthase (*20*) (FPPS), that catalyzes isoprenyl chain elongation and adopts a typical isoprenyl synthase fold (*12*, *20*, *25*) with three layers of helices. It appears that part of the allylic binding pocket in FPPS corresponds to the PHB binding pocket of UbiA (Fig. 4B). Conversely, the IPP substrate in UbiA is positioned similarly to the homoallylic substrate in FPPS and also extended to the pyrophosphate pocket of FPPS's allylic substrate. Unlike FPPS, which has two defined chambers for substrate binding (Fig. 4B), the absence of the third layer of helices in UbiA (Fig. 4A) leaves an unrestricted opening (the lateral portal) to the central cavity. Without a defined chamber

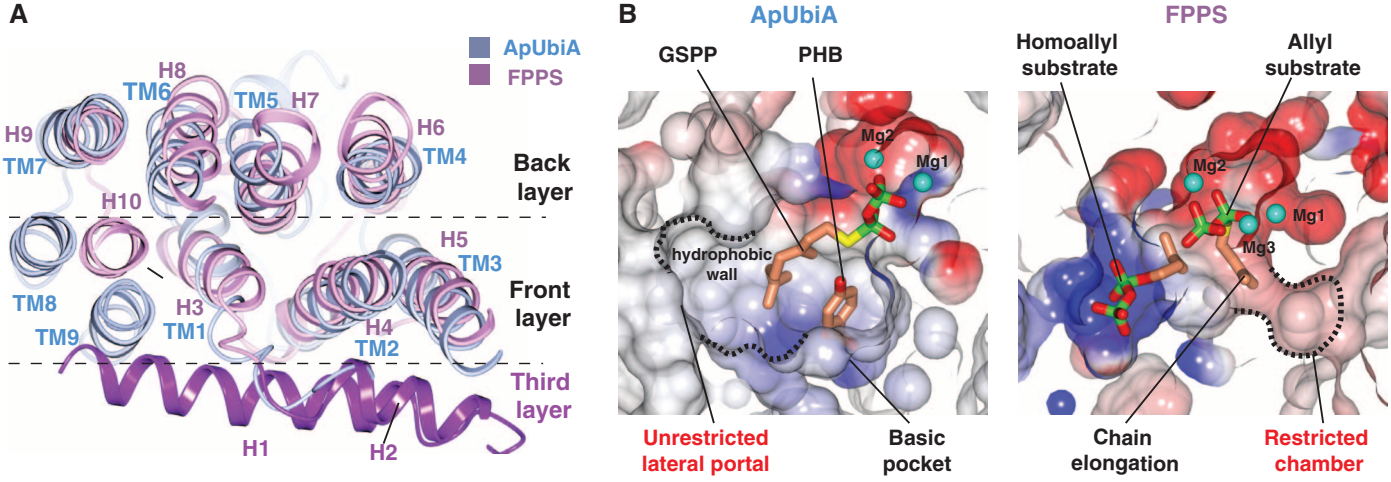

Fig. 4. Structural comparison of ApUbiA and a soluble trans-prenyltransferase. The FPPS [PDB code 1RQI (*20*)] structure is a top DALI (*29*) hit of the ApUbiA structure. (**A**) The superimposed structures of ApUbiA (blue) and FPPS (purple). (**B**) Electrostatic representation of the binding pockets in UbiA (left) and FPPS (right). The two pockets are generated from superimposed structures and shown in the same orientation.

to restrict the chain length, UbiA can promiscuously recognize a variety of long-chain IPP substrates and generate the precursors of CoQ_6 to CoQ_{10} in different species (*7*–*9*). During the condensation reaction, these long isoprenyl chains may extend through the lateral portal and directly contact lipid molecules (Fig. 1D). Thus, the lateral portal can facilitate the binding of long-chain IPP substrates, and the prenylated products can be directly released into membranes through this portal. This is a strategy that intramembrane enzymes can use to catalyze reactions in lipid bilayers.

Mutations in eukaryotic COQ2 and UBIAD1 have been linked to various diseases (*4*–*6*, *26*–*28*). Several of these mutations correspond to conserved residues (fig. S2) located in the active site of ApUbiA (Fig. 2A). We have shown that mutating these residues in EcUbiA lowers enzymatic activity (Fig. 3B) or substrate binding affinity (figs. S6 and S7) and therefore is likely to have similar effects in the human enzymes (fig. S10).

The structures of ApUbiA reveal mechanisms of substrate recognition and catalysis that are likely generally applicable to all superfamily members catalyzing the synthesis of lipid-soluble aromatic compounds. Our studies build a framework to understand other important UbiA superfamily members and to design chemoenzymatic synthesis of new aromatic compounds (*11*, *14*).

References and Notes

1. M. Forsgren *et al.*, *Biochem. J.* **382**, 519–526 (2004).
2. K. Nakagawa *et al.*, *Nature* **468**, 117–121 (2010).
3. T. Bonitz, V. Alva, O. Saleh, A. N. Lupas, L. Heide, *PLOS ONE* **6**, e27336 (2011).
4. J. M. Hegarty, H. Yang, N. C. N. Chi, *Development* **140**, 1713–1719 (2013).
5. V. Mugoni *et al.*, *Cell* **152**, 504–518 (2013).
6. M. Vos *et al.*, *Science* **336**, 1306–1310 (2012).
7. K. Suzuki *et al.*, *Biosci. Biotechnol. Biochem.* **58**, 1814–1819 (1994).
8. E. Swiezewska, G. Dallner, B. Andersson, L. Ernster, *J. Biol. Chem.* **268**, 1494–1499 (1993).
9. A. Kalén, E. L. Appelkvist, T. Chojnacki, G. Dallner, *J. Biol. Chem.* **265**, 1158–1164 (1990).
10. M. Melzer, L. Heide, *Biochim. Biophys. Acta* **1212**, 93–102 (1994).
11. L. Wessjohann, B. Sontag, *Angew. Chem. Int. Ed. Engl.* **35**, 1697–1699 (1996).
12. F. H. Wallrapp *et al.*, *Proc. Natl. Acad. Sci. U.S.A.* **110**, E1196–E1202 (2013).
13. K. Ohara, A. Muroya, N. Fukushima, K. Yazaki, *Biochem. J.* **421**, 231–241 (2009).
14. L. Bräuer, W. Brandt, D. Schulze, S. Zakharova, L. Wessjohann, *ChemBioChem* **9**, 982–992 (2008).
15. I. G. Young, R. A. Leppik, J. A. Hamilton, F. Gibson, *J. Bacteriol.* **110**, 18–25 (1972).
16. Material and methods are available as supplementary materials on *Science* Online.
17. D. Yernool, O. Boudker, Y. Jin, E. Gouaux, *Nature* **431**, 811–818 (2004).
18. M. Jormakka *et al.*, *Nat. Struct. Mol. Biol.* **15**, 730–737 (2008).
19. L. Bräuer, W. Brandt, L. A. Wessjohann, *J. Mol. Model.* **10**, 317–327 (2004).
20. D. J. Hosfield *et al.*, *J. Biol. Chem.* **279**, 8526–8529 (2004).
21. T. Kuzuyama, J. P. Noel, S. B. Richard, *Nature* **435**, 983–987 (2005).
22. U. Metzger, S. Keller, C. E. M. Stevenson, L. Heide, D. M. Lawson, *J. Mol. Biol.* **404**, 611–626 (2010).
23. U. Metzger *et al.*, *Proc. Natl. Acad. Sci. U.S.A.* **106**, 14309–14314 (2009).
24. Y. Yang, Y. Miao, B. Wang, G. Cui, K. M. Merz Jr., *Biochemistry* **51**, 2606–2618 (2012).
25. B. A. Kellogg, C. D. Poulter, *Curr. Opin. Chem. Biol.* **1**, 570–578 (1997).
26. J. S. Weiss *et al.*, *Invest. Ophthalmol. Vis. Sci.* **48**, 5007–5012 (2007).
27. M. L. Nickerson *et al.*, *PLOS ONE* **5**, e10760 (2010).
28. W. J. Fredericks *et al.*, *J. Cell. Biochem.* **114**, 2170–2187 (2013).
29. L. Holm, P. Rosenström, *Nucleic Acids Res.* **38**, W545–W549 (2010).

Acknowledgments: We thank the staff at Advanced Photon Source beamline ID-24C (GM103403) for support with data collection; T. Lohman and A. Kozlov for assistance with ITC experiments; J. Janetka and Z. Han for aid with the HPLC analysis; J. Wang, F. Murphy, and J. Schuermann for help with structure analysis; S. Chen for mass spectrometry analysis of protein samples; N. Ke and J. Beckwith for generating the quinone-deficient strains; R. Zhang for help with the figures; and D. Fremont, J. Chai, T. Lohman, and T. Ellenberger for critical reading of the manuscript. W.L. is supported by a R00 grant 5R00HL097083 from the National Heart, Lung, and Blood Institute and a scholar award from the American Society of Hematology. The structure factors and coordinates were deposited in the Protein Data Bank (PDB accession code 4OD4 for the apo structure and accession code 4OD5 for the substrate-bound structure). The authors declare no conflicts of interest.

Supplementary Materials

www.sciencemag.org/content/343/6173/878/suppl/DC1
Materials and Methods
Figs. S1 to S10
Table S1
References (*30*–*42*)

3 October 2013; accepted 22 January 2014
10.1126/science.1246774

Flavivirus NS1 Structures Reveal Surfaces for Associations with Membranes and the Immune System

David L. Akey,[1]* W. Clay Brown,[1]* Somnath Dutta,[1] Jamie Konwerski,[1] Joyce Jose,[2] Thomas J. Jurkiw,[1] James DelProposto,[1] Craig M. Ogata,[3] Georgios Skiniotis,[1,4] Richard J. Kuhn,[2,5] Janet L. Smith[1,4]†

Flaviviruses, the human pathogens responsible for dengue fever, West Nile fever, tick-borne encephalitis, and yellow fever, are endemic in tropical and temperate parts of the world. The flavivirus nonstructural protein 1 (NS1) functions in genome replication as an intracellular dimer and in immune system evasion as a secreted hexamer. We report crystal structures for full-length, glycosylated NS1 from West Nile and dengue viruses. The NS1 hexamer in crystal structures is similar to a solution hexamer visualized by single-particle electron microscopy. Recombinant NS1 binds to lipid bilayers and remodels large liposomes into lipoprotein nanoparticles. The NS1 structures reveal distinct domains for membrane association of the dimer and interactions with the immune system and are a basis for elucidating the molecular mechanism of NS1 function.

Flaviviruses have a positive-sense RNA genome that encodes a single viral polyprotein. The polyprotein is inserted into the endoplasmic reticulum (ER) membrane through several signal sequences and processed by viral and host proteases into three structural and seven nonstructural proteins (NS1, NS2A, NS2B, NS3, NS4A, NS4B, and NS5) (*1*). Six of the nonstructural proteins (NS2A to NS5) form a replication complex on the cytoplasmic side of the ER membrane, where the NS3 and NS5 enzymes function at a scaffold created by the other four transmembrane proteins. The remaining protein, the conserved glycosylated NS1, is associated with lipids, both early in infection, where intracellular dimeric NS1 localizes on the ER membrane at the site of viral RNA replication, and late in infection, where secreted hexameric NS1 lipoprotein particles interact with components of the complement-mediated immune system (*2*, *3*). NS1 is essential for replication of the flavivirus genome (*4*–*8*), possibly through interactions with transmembrane proteins NS4A and NS4B (*5*, *9*). Electron microscopy (EM) studies of secreted NS1 (sNS1) identified a symmetric barrel-shaped hexamer that carries a cargo of ~70 lipid molecules (*10*, *11*). NS1 interacts with multiple components of both the innate and adaptive immune systems (*12*–*14*), is involved in immune system evasion and pathogenesis (*12*–*15*), and is the major antigenic marker of viral infection (*16*). Although the role of NS1 in multiple stages of the virus life cycle is well established, little is known of the molecular mechanisms of its various functions. The lack of sequence identity to any protein of known structure and the difficulty of producing pure, stable proteins have hindered progress in understanding the roles and mechanisms of NS1.

[1]Life Sciences Institute, University of Michigan, Ann Arbor, MI 48109, USA. [2]Department of Biological Sciences, Purdue University, West Lafayette, IN 47907, USA. [3]GM/CA @ APS, Advanced Photon Source, Argonne National Laboratory, Argonne, IL 60439, USA. [4]Department of Biological Chemistry, University of Michigan, Ann Arbor, MI 48109, USA. [5]Bindley Bioscience Center, Purdue University, West Lafayette, IN 47907, USA.

*These authors contributed equally to this work.
†Corresponding author. E-mail: janetsmith@umich.edu

An understanding of NS1 structure will help to sort out these contradictory results and will facilitate more efficient vaccine development.

We used a baculovirus expression system to produce recombinant, full-length, glycosylated West Nile virus (WNV) and dengue virus type 2 (DEN2) NS1 in insect cells (see supplementary materials and methods). Despite the presence of a secretion signal in the expression construct, nearly all NS1 was retained by cells and partitioned with the membrane fraction. Soluble NS1 was released by mild detergent treatment of the membrane fraction and appeared as a dimer by gel filtration chromatography, in agreement with direct visualization of particles by negative-stain EM (fig. S1, A and B). Multiple chromatography steps without detergent shifted the oligomeric state to a hexamer, presumably due to removal of bound detergent (fig. S1, C and D). WNV NS1 crystallized in two forms and DEN2 NS1 in one form. We used high-multiplicity (~100-fold) data acquired from 18 crystals of form 1 (table S1 and fig. S2, A and B) to solve the WNV NS1 dimer structure from the anomalous scattering of the native sulfur atoms (12 Cys and 5 Met residues per subunit). The 12 cysteines form six disulfide bonds within the NS1 monomer. Three asparagines are glycosylated (Asn^{130}, Asn^{175}, and Asn^{207}), each with clear electron density for one to five sugar residues (fig. S2C). The structure is complete for all amino acids, with the exception of one internal loop (amino acids 108 to 128). Identical dimer structures occur in WNV and DEN2 NS1 (0.58 Å root mean square deviation of 576 Cα atoms).

The NS1 dimer is constructed around an extended central β-sheet domain (Fig. 1, A and B, and fig. S3). Each monomer has three domains. A small "β-roll" dimerization domain (amino acids 1 to 29) is a mini domain-swap structure of two β hairpins, each stabilized by a disulfide linkage (Cys^{4}-Cys^{15}). The β hairpins extend across the dimer axis and intertwine to form a four-stranded β sheet that curves into a roll-like structure (Fig. 1A, blue, and fig. S2, D and E). The second domain (amino acids 30 to 180) of each monomer protrudes from the central β domain like a wing (Fig. 1A, yellow). Each "wing" domain contains two glycosylation sites (Asn^{130} and Asn^{175}), an internal disulfide (Cys^{55}-Cys^{143}), and two discreet subdomains. An α/β subdomain (amino acids 38 to 151) comprises a four-stranded β sheet, two α helices, and a disordered distal tip [amino acids 108 to 128 (Fig. 1A, dotted line)]. A discontinuous connector subdomain (amino acids 30 to 37 and 152 to 180) packs against the β roll (Fig. 1A, orange) and also links the wing to the central β-sheet domain through a disulfide (Cys^{179}-Cys^{223}). The predominant structural feature of NS1 is the third domain, a continuous β sheet that extends along the length of the dimer with its 18 β strands arranged like the rungs of a ladder (Fig. 1A, red). This core "β-ladder" domain is formed by the C-terminal half of NS1 (amino acids 181 to 352), in an arrangement where each monomer contributes nine rungs to the antiparallel β ladder. In a

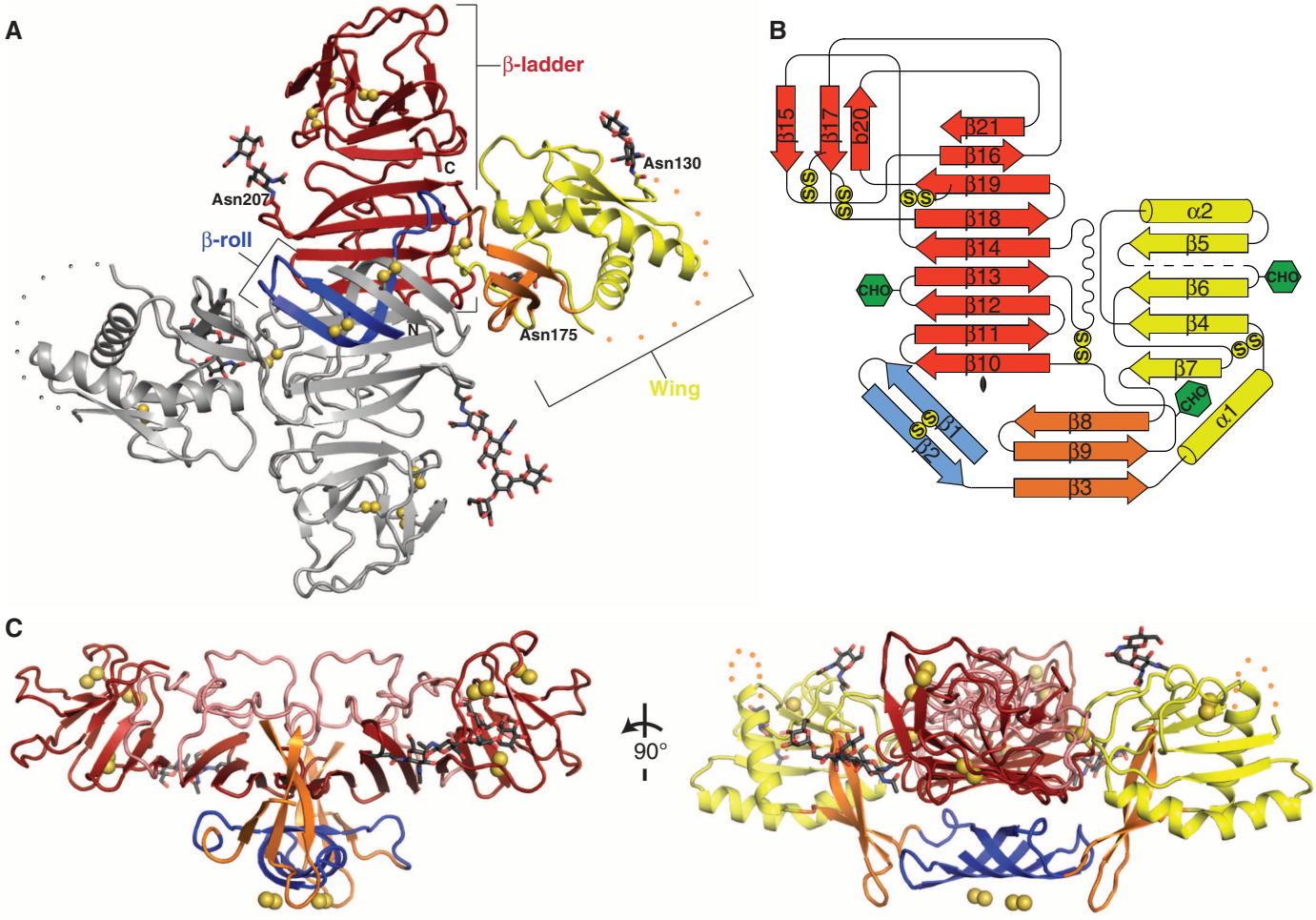

Fig. 1. NS1 dimer structure. (**A**) NS1 dimer with one subunit in gray and the other colored by domain (blue, β roll; yellow, wing with orange connector subdomain; red, central β ladder). Disulfides are shown as yellow spheres and N-linked glycosylation sites as black sticks. A 20-residue disordered region is indicated with dotted lines. C, C terminus; N, N terminus. (**B**) Topology diagram for NS1 monomer [colored in blue, yellow, orange, and red as in (A)]. Glycosylation sites are indicated with green hexagons and disulfides with yellow circles. (**C**) Perpendicular views of NS1 from the edge (left) and the end (right) of the β ladder. The β roll (blue) and β-connector subdomain (orange) of the wing form a protrusion on one face of the β ladder with the spaghetti loop (pink) and glycosylation sites on the other face. The wing domain is omitted from the left image for clarity.

simple (+1) topology, the first five β-strand rungs of each monomer begin at the dimer interface and proceed sequentially toward the end of the ladder (Fig. 1B). Most of the interstrand loops are short, with the notable exception of a long "spaghetti loop" between β13 and β14 (amino acids 219 to 272) that lacks secondary structure but is ordered by 57 hydrogen bonds (Fig. 1C, pink). A conserved tip region (fig. S3) at each end of the β-ladder domain (amino acids 278 to 352) contains four strands of the central β ladder, a small three-stranded β sheet, and three disulfides.

The overall dimensions of the NS1 dimer are 90 Å along the length of the β ladder, 90 Å in width from wingtip to wingtip, and 40 Å in the third dimension (Fig. 1A). The β ladder defines a plane through the NS1 dimer with the β-roll domain on one side (Fig. 1C). On the other side of the plane are the spaghetti loop, the glycosylation sites, the wing-domain disordered loop, and the C terminus, which, before proteolytic cleavage, is fused to the >20-residue lumen-side N terminus of viral protein NS2A.

The β roll and connector subdomain of the wing create a protrusion with a markedly hydrophobic surface on one face of the dimer (Figs. 1C and 2A). Extra electron densities at this surface were evident in the earliest maps and were fit as parts of three detergent molecules after all regions of the polypeptide had been assigned (fig. S2, D and E). The hydrophobic character of the β-roll–connector protrusion is conserved (figs. S3 and S4). Furthermore, a dipeptide (Arg^{10}-Gln^{11}) implicated in interaction with the transmembrane protein NS4B (*9*) is located at the periphery of the hydrophobic surface in a loop of the β roll (fig. S2E). Thus, the hydrophobic protrusion is a strong candidate for dimeric NS1 interaction with the ER membrane and with the replication complex through transmembrane proteins NS4A and NS4B, where NS1 plays a poorly defined but essential role in viral replication.

We investigated the ability of recombinant WNV NS1 to interact with membranes by incubating purified protein with liposomes and imaging the mixture by negative-stain EM. Upon exposure to NS1, the large heterogeneous liposomes were not only coated with NS1, presumably in its dimeric form, but also converted into much smaller lipid-protein nanoparticles (Fig. 2B and fig. S5). This unexpected ability to interact with and remodel membranes may have implications for the role of NS1 in organizing replication complexes or in conversion from a membrane-associated dimer in the ER lumen to a secreted proteolipid hexamer.

A "greasy-finger" loop on the connector subdomain forms a prominent part of the hydrophobic protrusion and is mobile, as it is disordered in the DEN2 NS1 structure. Mutations to this conserved region (Gly^{159}-Phe-Gly-Val^{162}) were deleterious to virus replication, as measured by plaque assay (table S2). Substitution of charged amino acids in DEN2 NS1 [Phe^{160}→Asp^{160} (F160D) and V162D; V, Val] or the double substitution G159A and F160A (G, Gly; A, Ala) resulted in no detectable plaques. A single substitution (F160A) impaired virus viability and RNA synthesis (fig. S6). Purified NS1 variants with these substitutions remodeled liposomes similarly to the wild type (fig. S6D), suggesting that the observed phenotype is due to loss of effective interactions with transmembrane proteins of the replication complex.

Intracellular NS1 is thought to be predominantly dimeric, whereas secreted NS1 is a soluble, hexameric proteolipid particle (*3*, *10*, *11*). Lipid-free recombinant NS1 occurred in both dimeric and hexameric forms in solution (fig. S1), but in all three crystal structures, NS1 exists in a hexameric arrangement of three dimers (Fig. 3A). The three β rolls face the interior of the hexamer, whereas the outer surface contains the spaghetti loops, glycosylation sites, and disordered wing-domain loop. The DEN2 NS1 dimer and those in WNV NS1 crystal form 2 are arranged as loose, open hexamers with full D3 symmetry and dimensions ~80 Å along the central threefold axis and ~110 Å in diameter (Fig. 3A, left and center panels), whereas the WNV NS1 form 1 hexamer is splayed open at one end and lacks full hexameric symmetry (Fig. 3A, right panel). The inner-facing hydrophobic protrusions create a conserved hydrophobic interior hexamer surface of diameter ~20 Å (Fig. 3B and figs. S3 and S4). We compared the D3 hexamers in crystal structures with EM images of the NS1 hexamer in solution (Fig. 3C). Two-dimensional EM class averages of NS1 embedded in negative stain reveal particle projections that are markedly similar to reprojections of the hexamer assemblies observed in crystal structures of DEN2 NS1 and in WNV NS1 form 2. The symmetric hexamers in our crystal structures and the EM images, although without lipids, have overall dimensions similar to those of lipid-bound sNS1 secreted from virus-infected cells (*10*, *11*). Given the hydrophobic interior of the crystallized hexamer, we conclude that the secreted lipid-NS1 particle is organized similarly, with β rolls facing inward and the spaghetti loop, glycosylation sites, and disordered loop facing outward.

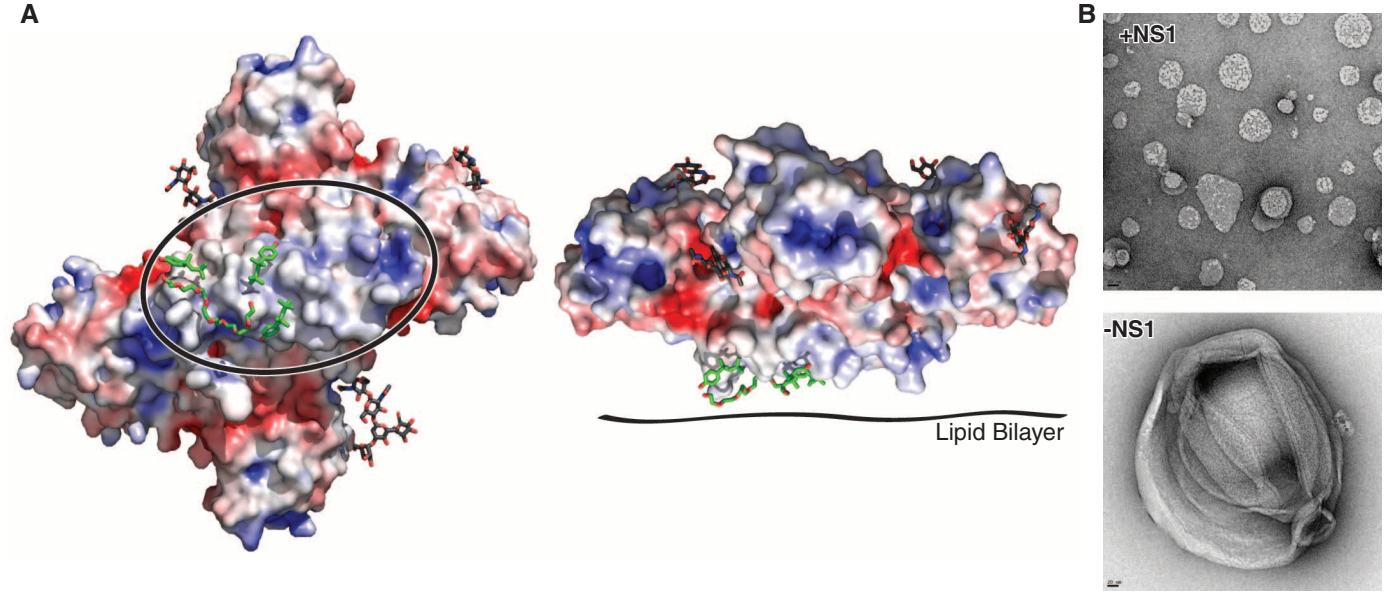

Fig. 2. Hydrophobic protrusion for membrane interaction. (**A**) NS1 electrostatic surface potential at pH 6.5 colored from electropositive (blue; +5 kT) to electronegative (red; −5 kT) with bound detergent (green sticks) and glycosylation sites (black sticks). (Left) View is as in Fig. 1A, with the β roll circled and facing the reader; (right) view is as in the right panel of Fig. 1C. (**B**) Effect of WNV NS1 on liposome structure. The negative-stain EM images show how NS1 treatment remodels liposomes (10% cholesterol, 90% phosphatidyl choline) into nanoparticles, leaving almost no free NS1 when mixed in a 585:1 ratio of lipid:NS1 hexamer. (Control images are shown in fig. S5.)

Secreted NS1 is a diagnostic marker for flavivirus infection in serum (*17*), where immune system proteins encounter the sNS1 hexamer as a proteolipid particle. We identified 108 NS1 linear epitopes elicited in response to immune stimulation by virus or full-length NS1 (*18*) and mapped these onto the hexamer structure (Fig. 4A). The epitopes localize to a few hotspots, including the wing domain, the C-terminal tip of

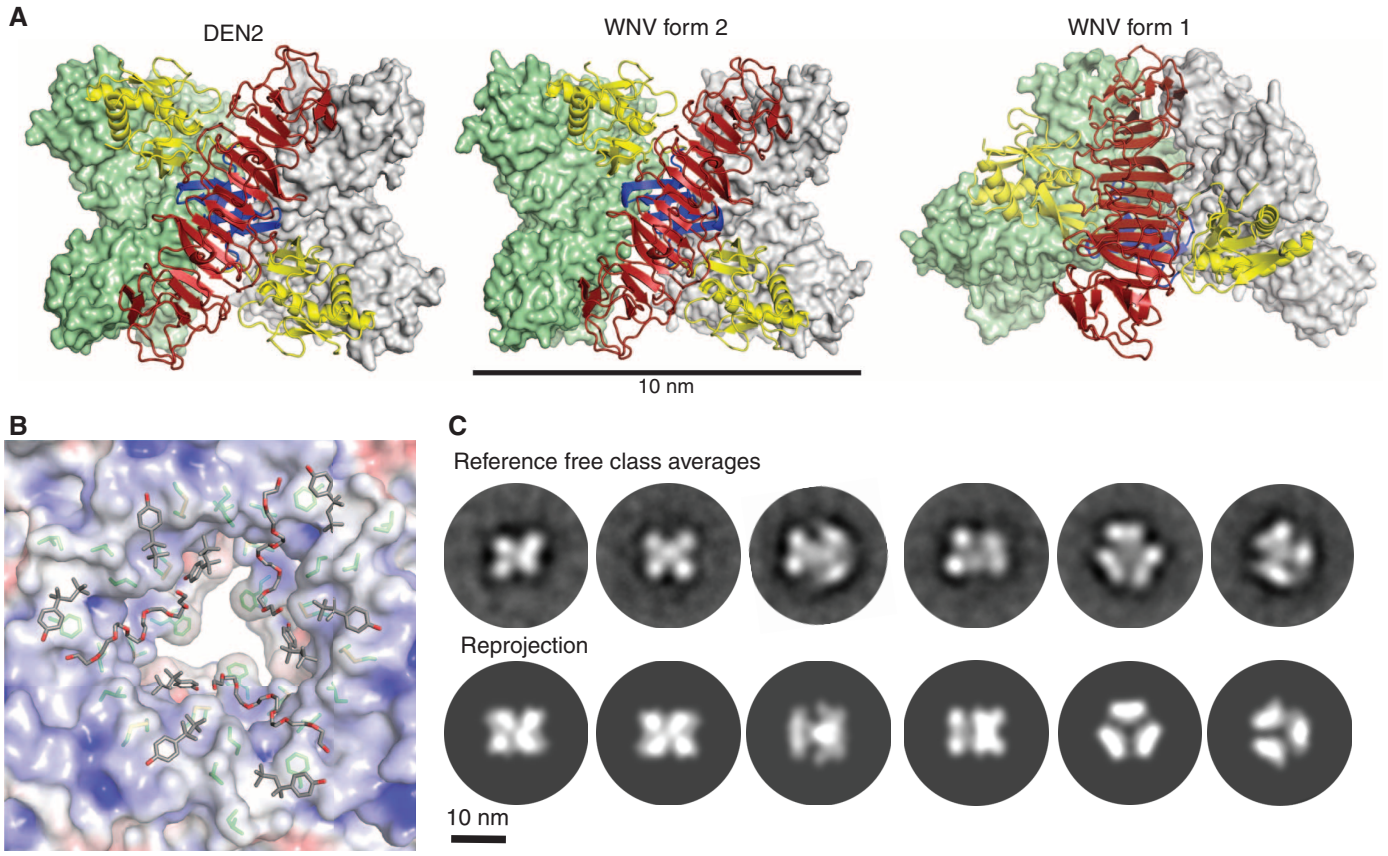

Fig. 3. NS1 hexamer association. (**A**) NS1 hexamers: the symmetric hexamers in DEN2 NS1 (left) and WNV NS1 form 2 (center) and the splayed hexamer in WNV NS1 crystal form 1 (right). Molecular surfaces are green and white for two dimers. The third, frontmost dimer has a red β ladder, a blue β roll, and yellow wings. The β roll is entirely inside the hexamer. (**B**) Association of hydrophobic protrusions at the center of the NS1 hexamer: The electrostatic surface potential illustrates the hydrophobicity of the surfaces. Conserved side chains that form this surface are shown as green sticks. Fragments of the detergent molecules (Triton X-100, Acros) bound to the hydrophobic surface are shown as gray sticks. For clarity, the splayed WNV NS1 form 1 is viewed from the open end. (**C**) Comparison of WNV NS1 hexamers in solution with the symmetric NS1 hexamer in crystals. Two-dimensional class averages (top row) are very similar to reprojections calculated from the WNV NS1 hexamer in crystal form 2 (bottom row).

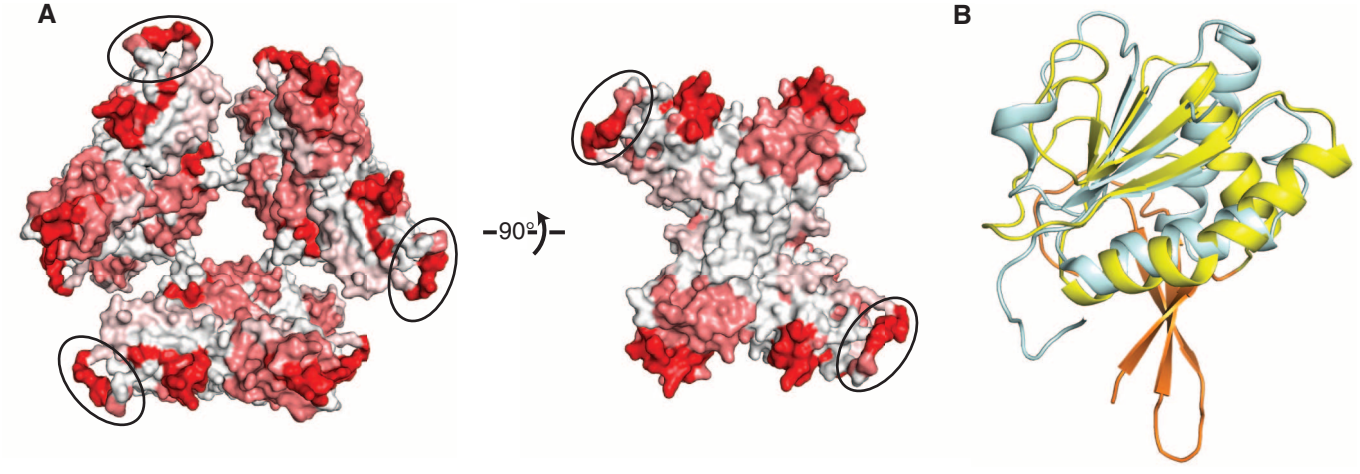

Fig. 4. NS1 and the immune system. (**A**) Linear epitopes to NS1 mapped on the structure. The molecular surface of hexameric NS1 is colored from white to red based on the frequency of 108 NS1-mapped epitopes (www.iedb.org). The disordered loop at the periphery of the wing domain, modeled as polyalanine and circled, is a frequent epitope. (**B**) Similarity of the NS1 wing α/β subdomain to the RIG-I family of innate immune proteins. An SF2 helicase domain of RIG-I [blue; PDB accession code 3TBK (*25*)] is superimposed on the WNV NS1 wing domain (yellow). Orange, connector subdomain.

the β ladder, and the β roll. The most frequently identified epitopes are the most accessible parts of the NS1 hexamer: the wing-domain disordered loop and the C-terminal tip of the β ladder. The wing-domain epitopes are concentrated at a highly conserved Gly-Trp-Lys-Ala-Trp-Gly peptide (amino acids 114 to 119) (fig. S3), with invariant tryptophans and conserved lysine. The hydrophobic protrusion is another frequently identified epitope, implying that the inside of the hexameric proteolipid is accessible to the immune recognition system at some point, either before hexamer formation or by hexamer dissociation. Antibodies to NS1 have been implicated in immune pathogenesis in dengue virus (*19*–*23*), and antibodies with cross-reactivity to human proteins have been mapped to the conserved wing peptide (*23*) and to the conserved tip of the β ladder (*19*).

Production of interferons and cytokines by the innate immune system is an important host defense against flaviviruses, particularly through the pattern-recognition receptors retinoic acid–inducible gene I (RIG-I), melanoma differentiation antigen 5 (MDA5), and Toll-like receptor 3 (*2*, *24*). The α/β subdomain of the NS1 wing resembles a helicase domain of RIG-I (*25*) and MDA5 (*26*) (Fig. 4B). These cytoplasmic helicase domains recognize pathogenic RNAs and trigger the antiviral response. As viral mimicry of host proteins is a well-established method to thwart the immune system, it is tempting to propose such a role for the NS1 wing domain. However, the NS1 wing-domain surface analogous to the RIG-I and MDA5 RNA binding surface is negatively charged and in contact with the central β-ladder domain. Moreover, NS1 is not known to localize to the cytoplasm where RIG-I or MDA5 detect RNA. Thus, this intriguing similarity to RIG-I and MDA5 adds yet another enigma to the NS1 story.

References and Notes

1. B. D. Lindenbach, C. M. Rice, *Adv. Virus Res.* **59**, 23–61 (2003).
2. M. S. Suthar, M. S. Diamond, M. Gale Jr., *Nat. Rev. Microbiol.* **11**, 115–128 (2013).
3. D. A. Muller, P. R. Young, *Antiviral Res.* **98**, 192–208 (2013).
4. A. A. Khromykh, P. L. Sedlak, E. G. Westaway, *J. Virol.* **74**, 3253–3263 (2000).
5. B. D. Lindenbach, C. M. Rice, *J. Virol.* **73**, 4611–4621 (1999).
6. E. G. Westaway, J. M. Mackenzie, M. T. Kenney, M. K. Jones, A. A. Khromykh, *J. Virol.* **71**, 6650–6661 (1997).
7. B. D. Lindenbach, C. M. Rice, *J. Virol.* **71**, 9608–9617 (1997).
8. J. M. Mackenzie, M. K. Jones, P. R. Young, *Virology* **220**, 232–240 (1996).
9. S. Youn *et al.*, *J. Virol.* **86**, 7360–7371 (2012).
10. I. Gutsche *et al.*, *Proc. Natl. Acad. Sci. U.S.A.* **108**, 8003–8008 (2011).
11. D. A. Muller *et al.*, *J. Gen. Virol.* **93**, 771–779 (2012).
12. P. Avirutnan *et al.*, *J. Immunol.* **187**, 424–433 (2011).
13. P. Avirutnan *et al.*, *J. Exp. Med.* **207**, 793–806 (2010).
14. K. M. Chung *et al.*, *Proc. Natl. Acad. Sci. U.S.A.* **103**, 19111–19116 (2006).
15. V. D. Krishna, M. Rangappa, V. Satchidanandam, *J. Virol.* **83**, 4766–4777 (2009).
16. P. R. Young, P. A. Hilditch, C. Bletchly, W. Halloran, *J. Clin. Microbiol.* **38**, 1053–1057 (2000).
17. S. Alcon-LePoder *et al.*, *Novartis Found. Symp.* **277**, 233–247, discussion 247–253 (2006).
18. R. Vita *et al.*, *Nucleic Acids Res.* **38** (suppl. 1), D854–D862 (2010).
19. H. J. Cheng *et al.*, *Exp. Biol. Med.* **234**, 63–73 (2009).
20. A. K. Falconar, *Arch. Virol.* **142**, 897–916 (1997).
21. A. K. Falconar, *Clin. Vaccine Immunol.* **15**, 549–561 (2008).
22. E. A. Henchal, L. S. Henchal, J. J. Schlesinger, *J. Gen. Virol.* **69**, 2101–2107 (1988).
23. I. J. Liu, C. Y. Chiu, Y. C. Chen, H. C. Wu, *J. Biol. Chem.* **286**, 9726–9736 (2011).
24. J. R. Wilson, P. F. de Sessions, M. A. Leon, F. Scholle, *J. Virol.* **82**, 8262–8271 (2008).
25. F. Civril *et al.*, *EMBO Rep.* **12**, 1127–1134 (2011).
26. C. Motz *et al.*, *Science* **339**, 690–693 (2013).

Acknowledgments: We thank D. Raymond for characterization of initial crystals, G. Dodge for assistance with protein purification and crystallization, and A. Dosey for assistance with EM. This work was supported by a grant from the NIH (P01AI055672) to R.J.K. and J.L.S., the Martha L. Ludwig Professorship of Protein Structure and Function to J.L.S., the Pew Scholar Program in Biomedical Sciences to G.S., and a Perrigo Undergraduate Summer Fellowship to T.J.J. Beamlines of GM/CA @ APS were supported by the National Institute of General Medical Sciences ("GM," Y1-GM-1104) and the National Cancer Institute ("CA," Y1-CO-1020). Atomic coordinates and structure factor files have been deposited in the RCSB Protein Data Bank (PDB) under the accession codes 4O6B for DEN2 NS1, 4O6C for WNV NS1 crystal form 2, and 4O6D for WNV NS1 crystal form 1. J.L.S., D.L.A., W.C.B., and R.J.K. are inventors on a patent application filed by The University of Michigan in collaboration with Purdue University on four uses of the NS1 three-dimensional structure (development of flavivirus vaccines, antiviral drugs, antibody diagnostics, or liposome-based NS1-membrane interaction assays) and on the method of production of recombinant NS1.

Supplementary Materials

www.sciencemag.org/content/343/6173/881/suppl/DC1
Materials and Methods
Figs. S1 to S6
Tables S1 and S2
References (*27*–*43*)

28 October 2013; accepted 17 January 2014
Published online 6 February 2014;
10.1126/science.1247749

Growth Factors Engineered for Super-Affinity to the Extracellular Matrix Enhance Tissue Healing

Mikaël M. Martino,[1,2]* Priscilla S. Briquez,[1]* Esra Güç,[1] Federico Tortelli,[1] Witold W. Kilarski,[1] Stephanie Metzger,[1] Jeffrey J. Rice,[1,3] Gisela A. Kuhn,[4] Ralph Müller,[4] Melody A. Swartz,[1,5,6] Jeffrey A. Hubbell[1,6]†

Growth factors (GFs) are critical in tissue repair, but their translation to clinical use has been modest. Physiologically, GF interactions with extracellular matrix (ECM) components facilitate localized and spatially regulated signaling; therefore, we reasoned that the lack of ECM binding in their clinically used forms could underlie the limited translation. We discovered that a domain in placenta growth factor-2 (PlGF-$2_{123-144}$) binds exceptionally strongly and promiscuously to ECM proteins. By fusing this domain to the GFs vascular endothelial growth factor–A, platelet-derived growth factor–BB, and bone morphogenetic protein–2, we generated engineered GF variants with super-affinity to the ECM. These ECM super-affinity GFs induced repair in rodent models of chronic wounds and bone defects that was greatly enhanced as compared to treatment with the wild-type GFs, demonstrating that this approach may be useful in several regenerative medicine applications.

Tissue repair is strongly regulated by a number of growth factors (GFs), including vascular endothelial growth factor (VEGF), which triggers angiogenesis crucial for the repair of most tissues (*1*); bone morphogenetic protein–2 (BMP-2), which induces the formation of new bone (*2*); and platelet-derived growth factor–BB (PDGF-BB), which is critical for the formation of granulation tissue and recruitment of stem cells (*3*). These and other GFs have been explored therapeutically, yet their translation to clinical use in regenerative medicine has been limited (*4*), probably in part because of their use at supraphysiological levels, as well as issues related to safety and cost effectiveness (*2*, *5*–*9*).

Physiologically, the partitioning, availability, and signaling of GFs are orchestrated by their binding to the extracellular matrix (ECM) (*10*, *11*). We recently characterized high-affinity GF binding sites in fibronectin (*12*), fibrinogen (*13*), and tenascin C (*14*), and we showed that ECM binding and co-ligation with integrins can modulate the

[1]Institute of Bioengineering, School of Life Sciences and School of Engineering, Ecole Polytechnique Fédérale de Lausanne, CH-1015 Lausanne, Switzerland. [2]World Premier International Immunology Frontier Research Center, Osaka University, Suita, Osaka 565-0871, Japan. [3]Department of Chemical Engineering, Tennessee Technological University, Cookeville, TN, USA. [4]Institute for Biomechanics, ETH Zurich, CH-8093 Zurich, Switzerland. [5]Swiss Institute for Experimental Cancer Research, School of Life Sciences, Ecole Polytechnique Fédérale de Lausanne, CH-1015 Lausanne, Switzerland. [6]Institute of Chemical Sciences and Engineering, School of Basic Sciences, Ecole Polytechnique Fédérale de Lausanne, CH-1015 Lausanne, Switzerland.

*These authors contributed equally to this work.
†Corresponding author. E-mail: jeffrey.hubbell@epfl.ch

signaling of multiple GFs (*15*).We took a GF protein engineering approach to enhance ECM binding, reasoning that engineering second-generation GF variants may enhance their activity and provide a simple delivery system to address these issues.

We began by screening 25 molecules from the VEGF/PDGF, transforming growth factor–β (TGF-β), fibroblast growth factor (FGF), and neurotrophin GF families for binding to six key ECM proteins: fibronectin, vitronectin, tenascin C, osteopontin, fibrinogen, and collagen I. As we previously reported, many GFs are able to bind fibronectin (*12*), fibrinogen (*13*), and tenascin C (*14*); here we also show that numerous GFs are also able to bind vitronectin, and osteopontin (Fig. 1). Most displayed poor binding to collagen I, which is not surprising given that no GF binding site has yet been reported. Among all the GFs screened, PlGF-2 displayed the strongest binding to all of the ECM proteins tested (Fig. 1). To the contrary, PlGF-1 did not display any binding. PlGF-2 and PlGF-1 are splice variants, with PlGF-2 but not PlGF-1 containing a heparin-binding (*16*) sequence (RRPKGRGKRRREKQRPTDCHL, PlGF-$2_{123\text{-}144}$) near the C terminus (fig. S1A). By fusing this sequence to the model nonbinding protein glutathione-sulfotransferase (GST), we revealed that this domain is responsible for the binding characteristics of PlGF-2 to the tested ECM proteins (fig. S1, B and C); a scrambled PlGF-$2_{123\text{-}144}$ sequence fused to GST did not show any specific binding (fig. S1B).

Based on the knowledge of the high affinity and promiscuous ECM protein-binding domain within PlGF-2, we used rational protein engineering to incorporate PlGF-$2_{123\text{-}144}$ into GFs that bear clinical translation limitations (*5*–*9*), namely VEGF-A, PDGF-BB, and BMP-2. Because VEGF-A and PlGF are structurally related, the alignment of VEGF-A165, VEGF-A121, and PlGF-2 sequences (fig. S2A) suggested substitution of the heparin-binding domain of VEGF-A165 with PlGF-$2_{123\text{-}144}$ to generate the engineered putative super-affinity variant VEGF-A/PlGF-$2_{123\text{-}144}$. We fused PlGF-$2_{123\text{-}144}$ to the C terminus of PDGF-BB to obtain PDGF-BB/PlGF-$2_{123\text{-}144}$, and we similarly generated BMP-2/PlGF-$2_{123\text{-}144*}$, fusing a version of PlGF-$2_{123\text{-}144}$ with a substitution of cysteine-142 by serine (PlGF-$2_{123\text{-}144*}$), because the presence of the cysteine impaired production of the fusion protein (fig. S2B).

Insertion of PlGF-$2_{123\text{-}144}$ into GFs did not alter their ability to activate their receptors, as determined by phosphorylation of VEGFR-2 in endothelial cells (ECs) and phosphorylation of PDGFR-β or induction of alkaline phosphatase in mesenchymal stem cells (fig. S3). Insertion of the PlGF-$2_{123\text{-}144}$ domain conferred super-affinity for ECM proteins and heparan sulfate, as determined by measurement of binding affinity [dissociation constant (K_D) value] (Table 1). K_D values of the PlGF-$2_{123\text{-}144}$–fused GFs for ECM proteins were driven to similar values as those displayed by PlGF-2, resulting in 2- to 100-fold elevations in affinity as compared to the wild type, depending on the particular GF (Table 1 and figs. S4 and S5). Moreover, PlGF-$2_{123\text{-}144}$–fused GFs could be strongly retained in a fibrin matrix mimicking a clot (fig. S6), and they could be released by the protease plasmin, in addition to association-dissociation kinetics (fig. S7).

After having verified that the engineered GFs could bind to and be retained by ECM molecules in vivo (fig. S8), we tested whether delivering GFs in the context of the strong association of the PlGF-$2_{123\text{-}144}$–fused domain with endogenous ECM would significantly enhance their capacity to induce tissue healing at doses where wild-type GFs are usually not effective. As a first model, we used skin wound healing in the diabetic *db*/*db* mouse, which is a well-established and relevant experimental model of impaired wound healing (*17*). Taking advantage of the synergistic and combinatorial effect between VEGF-A165 and PDGF-BB (*18*), we reasoned that VEGF-A165 would induce EC recruitment, whereas vessel stabilization by smooth muscle cells (SMCs) and pericytes as well as granulocyte recruitment would be driven by PDGF-BB (*15*). Because 20 μg per wound of VEGF-A165 or 10 μg per wound of PDGF-BB applied topically for five consecutive days were known to promote wound healing in the *db*/*db* mouse (*19*, *20*), we treated full-thickness back-skin wounds with a roughly 40- to 250-fold lower dose of GFs (200 ng each of PDGF-BB and VEGF-A, combined) delivered once in a fibrin matrix or simply applied topically three to four times. Low doses of wild-type PDGF-BB and VEGF-A did not significantly enhance wound healing as compared to untreated or fibrin alone–treated wounds, as indicated by either extent of wound closure (indicated by re-epithelialization) (Fig. 2, A and F) or amount of granulation tissue (Fig. 2, B and G). In contrast, wounds treated with PlGF-$2_{123\text{-}144}$–fused PDGF-BB and VEGF-A led to significantly faster wound

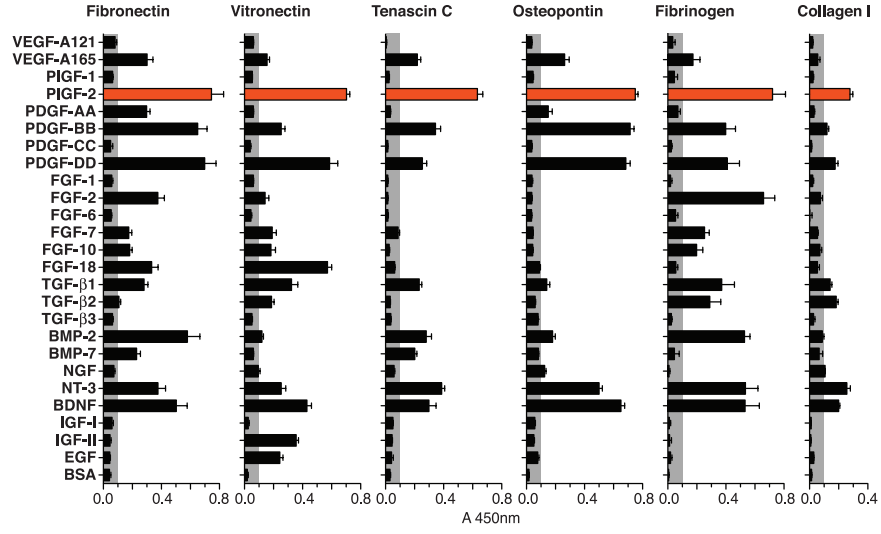

Fig. 1. GF binding to ECM proteins, measured by enzyme-linked immunosorbent assay. A signal over 0.1 (gray box) was considered to be significant. PlGF-2 strongly bound all ECM proteins tested (red bars). Bovine serum albumin was used as a control. $n \geq 3$ experiments, mean ± SEM.

Table 1. Affinity (K_D is shown) of wild-type versus PlGF-$2_{123\text{-}144}$–fused GFs for ECM proteins and heparan sulfate (HS). n = 3 enzyme-linked immunosorbent assays, mean ± SEM.

K_D (nM)	Fibronectin	Vitronectin	Osteopontin	Tenascin C	Fibrinogen	Collagen I	HS
VEGF-A	97.2 ± 10.4	70.9 ± 11.3	115.3 ± 15.7	71.0 ± 8.4	301.5 ± 73.0	> 500	60.9 ± 9.7
VEGF-A/PlGF-$2_{123\text{-}144}$	11.2 ± 3.3	2.8 ± 0.3	18.0 ± 1.2	26.4 ± 13.2	5.8 ± 0.6	123.9 ± 16.1	5.9 ± 0.5
PDGF-BB	11.6 ± 1.4	10.5 ± 1.0	19.0 ± 2.8	20.3 ± 2.2	250.4 ± 57.6	> 500	42.3 ± 6.3
PDGF-BB/PlGF-$2_{123\text{-}144}$	4.5 ± 0.3	1.2 ± 0.1	6.3 ± 0.6	3.3 ± 0.5	3.2 ± 0.2	96.3 ± 13.4	4.8 ± 0.4
BMP-2	19.2 ± 2.3	94.7 ± 12.8	25.5 ± 2.1	47.8 ± 4.2	47.1 ± 4.5	> 500	17.1 ± 1.9
BMP-2/PlGF-$2_{123\text{-}144*}$	5.2 ± 0.4	2.4 ± 0.2	6.9 ± 0.7	11.2 ± 1.1	2.0 ± 0.1	101.7 ± 17.9	4.8 ± 0.3
PlGF-2	7.2 ± 1.1	2.0 ± 0.2	10.1 ± 1.0	13.1 ± 1.4	4.5 ± 0.6	126.4 ± 15.7	4.6 ± 0.4

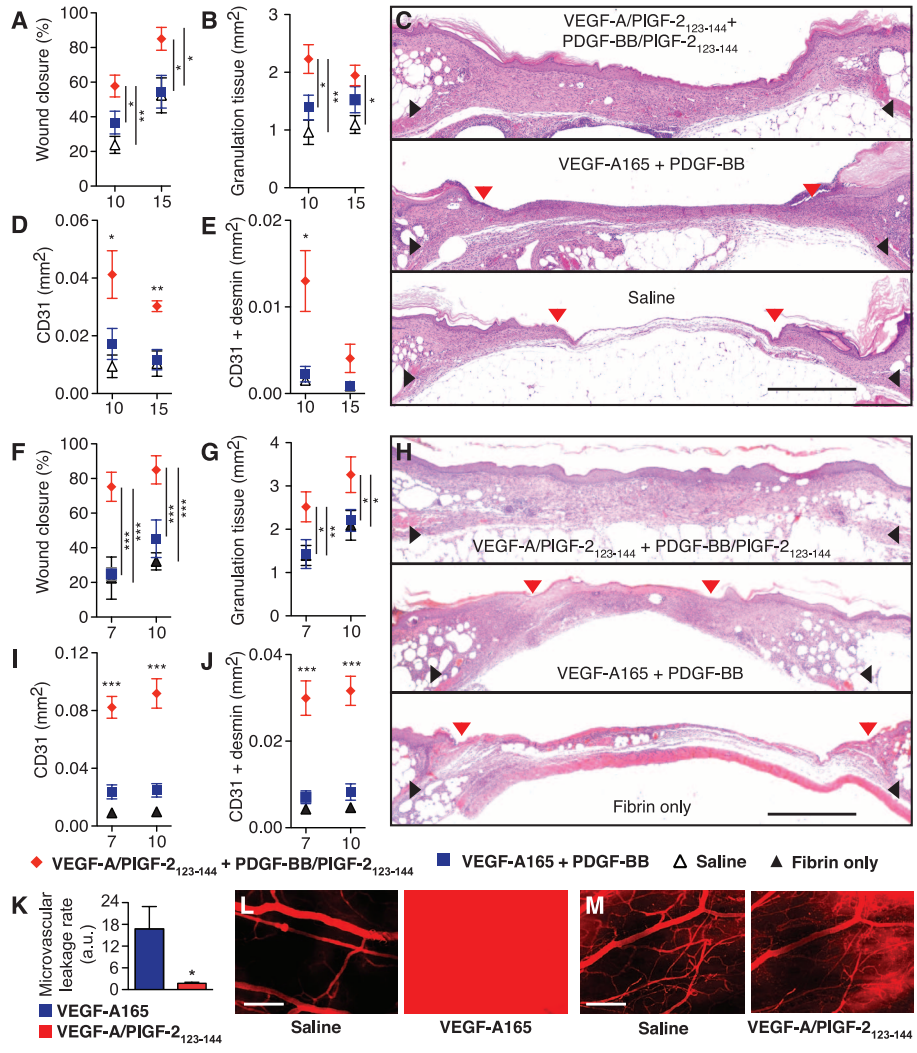

Fig. 2. VEGF-A/PlGF-$2_{123-144}$ and PDGF-BB/PlGF-$2_{123-144}$ induce greater skin wound healing and angiogenesis than wild-type VEGF-A and PDGF-BB. (**A** to **J**) Low doses of VEGF-A/PlGF-$2_{123-144}$ and PDGF-BB/PlGF-$2_{123-144}$ promoted skin wound healing in diabetic mice, whereas wild-type GFs did not. Full-thickness back-skin wounds (6 mm in diameter) were treated with GFs (200 ng of each, combined) delivered either topically three to four times or in a fibrin matrix once. After 10 and 15 days [topical groups, (A) and (B)], or 7 and 10 days [fibrin groups, (F) and (G)], wound closure and granulation tissue formation were evaluated by histology. $n \geq 8$ wounds per group per time point, mean ± SEM. Analysis of variance (ANOVA) with Bonferroni post hoc test for pairwise comparisons; $^{*}P < 0.05$, $^{**}P < 0.01$, $^{***}P < 0.001$. (C) and (H) Representative histology at 10 days for the fibrin groups and at 15 days for the topical groups (hematoxylin and eosin staining). Black arrows indicate wound edges; red arrows indicate tips of the healing epithelium tongue. Scale bar, 1 mm. (D), (E), (I), and (J) Quantification of the angiogenesis within the granulation tissue. After 10 and 15 days [topical groups, (D) and (E)], or 7 and 10 days [fibrin groups, (I) and (J)], wound tissues were stained for ECs ($CD31^{+}$ cells) and SMCs ($desmin^{+}$ cells); dual staining indicates stable vascular morphology. $n \geq 4$ wounds per group per time point, mean ± SEM. For statistics: ANOVA with Bonferroni post hoc test for pairwise comparisons; $^{*}P < 0.05$, $^{**}P < 0.01$, $^{***}P < 0.001$. (**K** to **M**) VEGF-A/PlGF-$2_{123-144}$ induces much less vascular permeability than the same dose of wild-type VEGF-A165 (500 ng). (K) The graphs show measurement of vascular permeability in the mouse ear skin. $n = 8$ ears, mean ± SEM. Mann-Whitney test; $^{*}P < 0.05$. (L) and (M) Representative images of the mouse ear skin vasculature 25 min after VEGF-A application. Induced permeability is visualized by the red-labeled dextran leaking from the vessels. Scale bar, 0.2 mm.

closure and more granulation tissue, both topically (Fig. 2, A to C) and in fibrin (Fig. 2, F to H). Because angiogenesis is a crucial step in sustaining newly formed granulation tissue (*21*), we compared how angiogenesis differed between the treatments. Immunohistological analysis for CD31 (highly expressed by ECs) and desmin (expressed by SMCs) revealed that angiogenesis within the granulation tissues was much more pronounced when PlGF-$2_{123-144}$–fused GFs were delivered (Fig. 2, D, E, I, and J; and figs. S9 to S11). In light of these results, EC response to VEGF-A/PlGF-$2_{123-144}$ may be different from that to the wild-type forms in vivo, because VEGF-A binding to the ECM critically controls angiogenesis via modulation of VEGF-A signaling kinetics (*22*).

We also explored whether our approach could resolve a major problem that has arisen in translating VEGF-A to clinical use. VEGF-A has been shown to rapidly induce vascular permeability, which leads to systemic hypotension and edema; this phenomenon has been the dose-limiting toxic response in peripheral and cardiovascular applications (*5*) and presents serious issues in regenerative medicine. Because VEGF-A/PlGF-$2_{123-144}$ displays an enhanced capacity to bind endogenous ECM, we explored whether VEGF-A/PlGF-$2_{123-144}$ might induce less vascular permeability. In a model of dextran extravasation from vessels in the skin of the mouse ear (*23*), the rate of leakage due to application of VEGF-A/PlGF-$2_{123-144}$ was only 10% of that induced by application of wild-type VEGF-A165 (Fig. 2, K to M, fig. S12, and movies

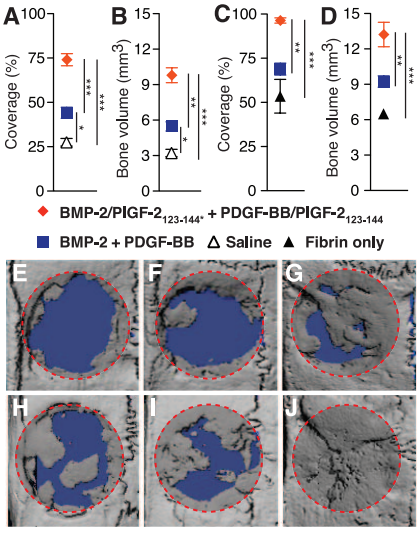

Fig. 3. Delivering PDGF-BB/PlGF-$2_{123-144}$ and BMP-2/PlGF-$2_{123-144}$* induces greater bone regeneration than wild-type PDGF-BB and BMP-2 Critical-size calvarial defects (6 mm in diameter) were treated with GFs delivered topically to the dura (1 μg of each GF, combined) or in a fibrin matrix (200 ng of each GF, combined). (**A** to **D**) Four weeks after treatment, bone repair was measured by μCT as bone volume and coverage of the defect [(A) and (B) show topical groups; (C) and (D) show fibrin groups]. (**E** to **J**) Representative calvarial reconstructions. (E) Saline vehicle; (F) BMP-2 + PDGF-BB; (G) BMP-2/PlGF-$2_{123-144}$* + PDGF-BB/PlGF-$2_{123-144}$; (H) fibrin only; (I) fibrin with BMP-2 + PDGF-BB; (J) fibrin with BMP-2/PlGF-$2_{123-144}$* + PDGF-BB/PlGF-$2_{123-144}$. The defect area is shaded with a red dotted outline. $n = 6$ defects per condition, mean ± SEM. ANOVA with Bonferroni post hoc test for pairwise comparisons; $^{**}P < 0.01$, $^{***}P < 0.001$.

S1 to S4), even though they showed equivalent activities regarding phosphorylation of VEGFR-2 (fig. S3A). This effect was shown not to depend on binding to the co-receptor neuropilin-1 (figs. S2C, S3A, and S12). The engineering of VEGF-A to tightly bind the ECM appears to decouple angiogenesis from hyperpermeability, potentially solving a major problem with VEGF-A's clinical translation.

In the context of bone repair, we tested whether PlGF-$2_{123\text{-}144}$–fused BMP-2 and PDGF-BB could drive bone regeneration at low doses. Again, taking advantage of a hypothetic combinatorial effect between GFs (*2*, *3*), we reasoned that PDGF-BB could induce progenitor cell recruitment, whereas the differentiation to bone tissue would be driven by BMP-2 (*15*). As a relevant model to illustrate translational potential, we used the critical-size calvarial defect in the rat (*24*). Because delivering micrograms of wild-type BMP-2 is usually barely sufficient to repair such calvarial defects (*25*), we tested a combination of BMP-2/PlGF-$2_{123\text{-}144}$* and PDGF-BB/PlGF-$2_{123\text{-}144}$ (200 ng of each) delivered in a fibrin matrix or delivered topically to the dura before surgical skin closure at a somewhat higher dose (1 μg of each, combined). After 4 weeks, bone healing—characterized by bone tissue deposition and coverage of the defects—was analyzed with microcomputed tomography (μCT). Delivery of wild-type GFs alone or within fibrin slightly increased bone healing when compared to the healing of defects without treatment or treated with fibrin only (Fig. 3, A to D, F, and I). In contrast, treatment with PlGF-$2_{123\text{-}144}$–fused GFs led to a marked increase of bone tissue deposition as to wild-type GF (Fig. 3, A to D, G, and J), yielding coverage at 96% when delivered in fibrin and at 74% when simply administered on the dura. The improved tissue regeneration with PlGF-$2_{123\text{-}144}$–fused GFs most likely involves elevated recruitment of progenitor cells, because we could detect more mesenchymal stem cells/pericytes in the defects treated with PlGF-$2_{123\text{-}144}$–fused GFs than in those treated with wild-type GFs (fig. S13).

In conclusion, we found that PlGF-2, through PlGF-$2_{123\text{-}144}$, displays extraordinarily strong and promiscuous binding to the ECM. When this domain was conferred to other GFs, we could dramatically improve their efficacy and reduce their dosing in preclinical models of skin and bone repair. We further show that a critical limitation of VEGF-A, its induction of vascular hyperpermeability, may be ameliorated through this protein engineering concept. Because localized GF delivery and dose reduction are critical for optimal efficacy and clinical safety, this simple and broadly applicable approach to engineering second-generation ECM super-affinity GFs may be useful in a number of applications in regenerative medicine.

References and Notes

1. S. P. Herbert, D. Y. Stainier, *Nat. Rev. Mol. Cell Biol.* **12**, 551–564 (2011).
2. K. W. Lo, B. D. Ulery, K. M. Ashe, C. T. Laurencin, *Adv. Drug Deliv. Rev.* **64**, 1277–1291 (2012).
3. A. L. Ponte *et al.*, *Stem Cells* **25**, 1737–1745 (2007).
4. J. J. Rice *et al.*, *Adv Healthc Mater* **2**, 57–71 (2013).
5. M. Simons, J. A. Ware, *Nat. Rev. Drug Discov.* **2**, 863–871 (2003).
6. E. J. Woo, *Spine J.* **12**, 894–899 (2012).
7. L. A. Solchaga, C. K. Hee, S. Roach, L. B. Snel, *J. Tissue Eng.* **3**, 2041731412442668 (2012).
8. "Panel Executive Summary for P050036 Medtronic's AMPLIFY™ rhBMP-2 Matrix" (U. S. Food and Drug Administration, Silver Spring, MD, 2010).
9. "Safety warning on becaplermin in Regranex®" (U. S. Food and Drug Administration, Silver Spring, MD, 2008).
10. L. Macri, D. Silverstein, R. A. Clark, *Adv. Drug Deliv. Rev.* **59**, 1366–1381 (2007).
11. G. S. Schultz, J. M. Davidson, R. S. Kirsner, P. Bornstein, I. M. Herman, *Wound Repair Regen.* **19**, 134–148 (2011).
12. M. M. Martino, J. A. Hubbell, *FASEB J.* **24**, 4711–4721 (2010).
13. M. M. Martino, P. S. Briquez, A. Ranga, M. P. Lutolf, J. A. Hubbell, *Proc. Natl. Acad. Sci. U.S.A.* **110**, 4563–4568 (2013).
14. L. De Laporte, J. J. Rice, F. Tortelli, J. A. Hubbell, *PLOS ONE* **8**, e62076 (2013).
15. M. M. Martino *et al.*, *Sci. Transl. Med.* **3**, 100ra89 (2011).
16. S. De Falco, *Exp. Mol. Med.* **44**, 1–9 (2012).
17. S. R. Sullivan *et al.*, *Plast. Reconstr. Surg.* **113**, 953–960 (2004).
18. T. P. Richardson, M. C. Peters, A. B. Ennett, D. J. Mooney, *Nat. Biotechnol.* **19**, 1029–1034 (2001).
19. R. K. Chan *et al.*, *J. Burn Care Res.* **27**, 202–205 (2006).
20. R. D. Galiano *et al.*, *Am. J. Pathol.* **164**, 1935–1947 (2004).
21. G. C. Gurtner, S. Werner, Y. Barrandon, M. T. Longaker, *Nature* **453**, 314–321 (2008).
22. N. Ferrara, *Mol. Biol. Cell* **21**, 687–690 (2010).
23. W. W. Kilarski *et al.*, *PLOS ONE* **8**, e57135 (2013).
24. P. P. Spicer *et al.*, *Nat. Protoc.* **7**, 1918–1929 (2012).
25. H. G. Schmoekel *et al.*, *Biotechnol. Bioeng.* **89**, 253–262 (2005).

Acknowledgments: The Protein Expression, Proteomics, and Histology Core Facilities of the Ecole Polytechnique Fédérale de Lausanne and M. Pasquier, X. Quaglia, and C. Dessibourg provided technical assistance. Funding was from the European Community's Seventh Framework Programme in the project Angioscaff, the Swiss National Science Foundation, and the Fondation Bertarelli. J.A.H., M.M.M., and P.S.B. are named as inventors on a patent application filed by the Ecole Polytechnique Fédérale de Lausanne that covers the technology described in this paper.

Supplementary Materials

www.sciencemag.org/content/343/6173/885/suppl/DC1
Materials and Methods
Figs. S1 to S13
Table S1
References (*26*–*35*)
Movies S1 to S4

25 October 2013; accepted 28 January 2014
10.1126/science.1247663

Action Monitoring and Medial Frontal Cortex: Leading Role of Supplementary Motor Area

Francesca Bonini,[1,2,3,4]* Boris Burle,[1,3] Catherine Liégeois-Chauvel,[1,2] Jean Régis,[1,2,4] Patrick Chauvel,[1,2,4] Franck Vidal[1,3]

The capacity to evaluate the outcomes of our actions is fundamental for adapting and optimizing behavior and depends on an action-monitoring system that assesses ongoing actions and detects errors. The neuronal network underlying this executive function, classically attributed to the rostral cingulate zone, is poorly characterized in humans, owing to the limited number of direct neurophysiological data. Using intracerebral recordings, we show that the leading role is played by the supplementary motor area (SMA), which rapidly evaluates successful and erroneous actions. The rostral part of medial prefrontal cortex, driven by the SMA, was activated later and exclusively in the case of errors. This suggests a hierarchical organization of the different frontal regions involved in implementation of action monitoring and error processing.

Imagine a tennis player when serving. If the ball lands out, the subsequent serve is more likely to succeed. The required behavioral adjustments are subordinated to an error-identification process. Even during a successful first serve, the player may have tossed the ball too high, requiring a prompt adjustment of serving action. Such remedial actions rely on the existence of an action-monitoring system in charge of evaluating ongoing activities to adjust them and improve subsequent actions.

Studies in monkeys and humans have demonstrated the critical role of the medial frontal cortex (MFC) in such an evaluative process (*1*–*3*). A particular subregion within the MFC, the rostral cingulate zone (RCZ) (*4*), is often considered the crucial node in this control network (*1*).

We investigated the anatomical substrate of action monitoring in humans in more detail using intracerebral electroencephalography (iEEG). Five subjects (*5*), undergoing presurgical evaluation of their epilepsy with iEEG, performed a Simon task (*6*). In this conflict task, different classes of behaviorally relevant responses can be distinguished by means of electromyography (EMG):

[1]Aix-Marseille Université, 13385, Marseille, France. [2]INSERM, Institut de Neurosciences des Systèmes UMR 1106, 13385, Marseille, France. [3]CNRS, Laboratoire de Neurosciences Cognitives, UMR 7291, 13331, Marseille, France. [4]APHM (Assistance Publique–Hôpitaux de Marseille), Pôle de Neurosciences Cliniques, Timone Hospital, 13005, Marseille, France.

*Corresponding author. E-mail: francesca.bonini@univ-amu.fr

correct responses, overt errors, and covert errors (*7*) (Fig. 1 and supplementary materials). If we consider our initial analogy of the tennis player, overt errors represent a missed serve, whereas covert errors [often termed partial errors (*8*)] represent the ongoing serve's successful adjustment.

Local field potentials (LFPs) were recorded from 562 contacts on 42 electrodes positioned predominantly in the frontal cortex (Fig. 2 and table S1). LFPs were averaged time-locked to subjects' responses (as recorded by the EMG of the responding muscle; see Fig. 1B), so as to evaluate action-monitoring activity (behavioral results are presented in the supplementary materials and fig. S1).

Error-evoked LFPs were observed exclusively in the medial part of the frontal lobe. One set of electrodes clustered caudally, whereas other electrodes were more dispersed rostrally (Fig. 2, colored dots, and table S2).

In the caudal cluster, all subjects presented a sharp LFP, peaking between 100 and 190 ms after EMG activation. The largest LFPs occurred after overt errors; smaller LFPs appeared after covert errors; and even smaller, but clearly still present, LFPs occurred after correct responses (Fig. 2 and table S3). This pattern replicates previous scalp EEG data (*9*–*11*). Inspection of individual electrode placement showed that none of these active electrodes were positioned within the RCZ, but all were clearly located within the SMA—namely, above the calloso-marginal fissure and immediately posterior to the vertical commissure anterior (VCA) boundary (Fig. 2).

Although intracerebral electrodes are sensitive to current within only a small volume of cerebral tissue, it is possible that the recorded activity may have been volume-conducted from a remote generator outside the SMA. However, supplementary results (note S2 and figs. S2 and S3) exclude this possibility.

Other electrodes disclosing performance-sensitive activity were located more rostrally, in the medial prefrontal region—namely, in pregenual anterior cingulate cortex (pACC; i.e., in the anterior division of the RCZ) in patient 3 and in orbito-medial prefrontal cortex (OMPFC) in patients 3 and 5 (Fig. 3, B and D, and table S2). The activation profile of those more rostral electrodes differed from that of the caudal cluster in three ways (Fig. 3, A and C, fig. S8, and table S3): (i) The prefrontal activity was delayed and had a longer duration, with a caudo-rostral latency gradient; (ii) it was specific to errors (overt and covert); and (iii) it was more widespread than the activity within the SMA, as demonstrated by recordings from electrodes' lateral contacts.

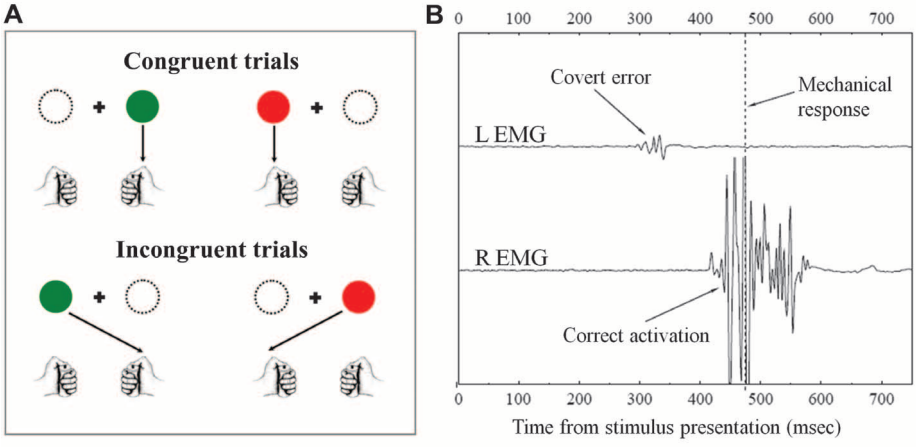

Fig. 1. Experimental procedure. (**A**) The Simon task is a between-hand choice reaction time task that induces errors: Subjects had to respond with a left or right thumb key-press as a function of the color of a target stimulus. The target could be presented on the same side as the response to be given (congruent trials), or on the opposite side (incongruent trials). (**B**) Covert errors (often called partial errors) are characterized by a small subthreshold EMG burst on the incorrect side preceding the correct response.

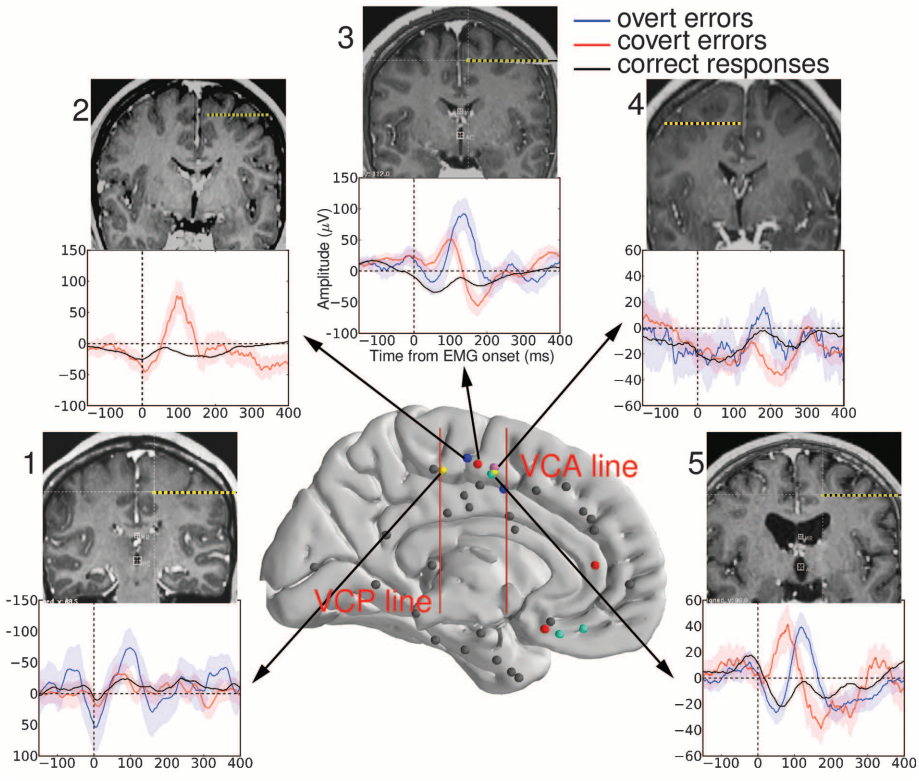

Fig. 2. Overview of EMG-locked LFPs and of all recording sites in the medial wall. A total of 562 contacts from 42 electrodes were included in the analysis, 34 of which were implanted up against the medial wall. The anatomical location of these 34 electrodes' internal contacts, converted into normalized MNI (Montreal Neurological Institute) brain space to allow comparison across subjects, is shown on a three-dimensional MNI standard brain in its medial aspect. The two red vertical bars represent the VCA (vertical commissure anterior) line and the VCP (vertical commissure posterior) line. A cluster of performance-sensitive electrodes (colored dots) is located in the SMA (caudal cluster, behind the VCA line), while other electrodes are more widespread in the rostral part of the medial prefrontal cortex (electrodes anterior to VCA). For each participant, averaged EMG-locked LFPs recorded from the SMA are displayed: The largest LFP occurs after overt errors (blue); a smaller LFP appears after covert errors (red); and an even smaller LFP occurs after correct responses (black). Colored bands represent between-trials confidence intervals set to 0.05. For each subject, an individual MRI and computed tomography (CT) fusion is provided, showing, in coronal view, the trajectory of the performance-sensitive electrode. All these electrodes were clearly located above the calloso-marginal fissure and behind the VCA line (that is, in the SMA).

We further investigated the relation between rostral and caudal activity using trial-by-trial analysis (fig. S4 and note S3). Single-trial LFPs recorded in the SMA and in the medial prefrontal regions were significantly and positively correlated both in terms of latencies [$\rho = 0.8$, $P < 0.01$ between SMA and pACC on patient 3, and $\rho = 0.35$, $P < 0.05$ between SMA and OMPFC on patient 5 (*12*)] and, less strongly, amplitudes ($\rho = 0.63$, $P < 0.01$ and $\rho = 0.28$, $P < 0.1$, for patient 3 and 5 respectively; fig. S5). Medial prefrontal activity appeared to be contingent upon activity in the SMA because it was always preceded by SMA activity, and importantly, it was never present when SMA activity was absent. By contrast, SMA activity can and occasionally did occur without the subsequent prefrontal activity. This suggests a strong connection and potential hierarchy between these two regions in error processing. Such a connection is not necessarily direct and might be mediated by a third structure.

To further describe the functional importance of the SMA activity, we focused on covert errors. These trials are a prototypical case of efficient ongoing action control because the incorrect activation is interrupted and corrected (by the opposite "corrective" response). We therefore searched for a functional link between SMA activity and error correction (fig. S6 and note S4).

We correlated the latencies of LFPs and EMG activity in three patients for whom covert-error LFPs were detectable in the SMA on a trial-by-trial basis. The offset of EMG bursts linked to incorrect responses, representing response interruption, strongly correlated with the peak of the SMA LFP ($\rho = 0.63$ $P < 0.01$), whereas the onset of EMG bursts linked to corrective responses strongly correlated with the end of the SMA LFP ($\rho = 0.7$, $P < 0.01$) (fig. S7 and note S4).

In covert errors, SMA activity began with the first incorrect muscular activation, culminated when this incorrect action was inhibited, decreased, and finally extinguished when the subsequent corrective response was issued. This correlation, consistent with previous scalp EEG data (*13*), suggests that the SMA intervenes in action monitoring by emitting a performance-modulated "default" signal that possibly acts as an alert or a warning signal. Each time a behaviorally relevant response is produced, this default signal is emitted. For correct responses, it is rapidly subdued, giving rise to a small LFP. For covert errors, the warning signal keeps rising but begins to decrease once the incorrect action is inhibited and terminates with the activation of the corrective response. A slightly later suppression and correction would result in a prolonged alarm; that is, a longer and larger LFP. For overt errors, this alarm reaches its highest level, corresponding to the highest LFP's amplitude. We thus hypothesize that this alarm, when crossing a given threshold, hints at the need to enhance cognitive control.

This study shows that action monitoring is largely carried out by the SMA. This is consistent with limited data reported in humans (*11*, *14*–*18*) and in monkeys (*19*, *20*). However, much of the current literature indicates that human primate and nonprimate RCZ is sensitive to action outcome (*14*, *15*, *17*, *18*, *21*–*25*).

Even though the precise role of the RCZ vis à vis the SMA should be further evaluated with more extensive sampling, our data allow discussion of the apparent inconsistency in the literature from a new perspective. Functional magnetic resonance imaging (fMRI) data (contrasting errors minus correct responses) mainly show RCZ activity (*1*). By comparison, we showed a caudo-rostral latency gradient in medial frontal areas. On this basis one may expect RCZ to be active only for erroneous action, shortly after SMA, but the extent to which RCZ activity depends on SMA remains an open question. However, our results suggest a schema of how this cognitive control function operates, and of its underlying cortical network. We propose that this network, encompassing caudal and rostral parts of the MFC, is hierarchically organized to implement action control: medial prefrontal cortex, including the anterior RCZ, is engaged in the case of erroneous actions and thus, as usually assumed, is implicated in error processing following a caudo-rostral gradient. The role of the most rostral activities remains to be elucidated, but it could be related to the estimated (negative) value of errors (*26*). However, this process seems to be embedded in an action-monitoring process, which is carried out by the SMA. The SMA is therefore a core node in performance monitoring, whose function consists of continuously assessing ongoing actions and, in the case of errors only, recruiting the medial prefrontal cortex.

Action monitoring and error processing are thus two crucial stages of executive control in humans, allowing for efficient behavioral adjustment and optimization of performance. The involvement of the SMA in action monitoring appears functionally grounded, because the SMA is widely considered to be implicated in movement initiation and inhibition (*27*), response selection, and motor planning (*28*). The present study reveals a new function for SMA: the early evaluation of the outcome of actions that it has contributed to initiating.

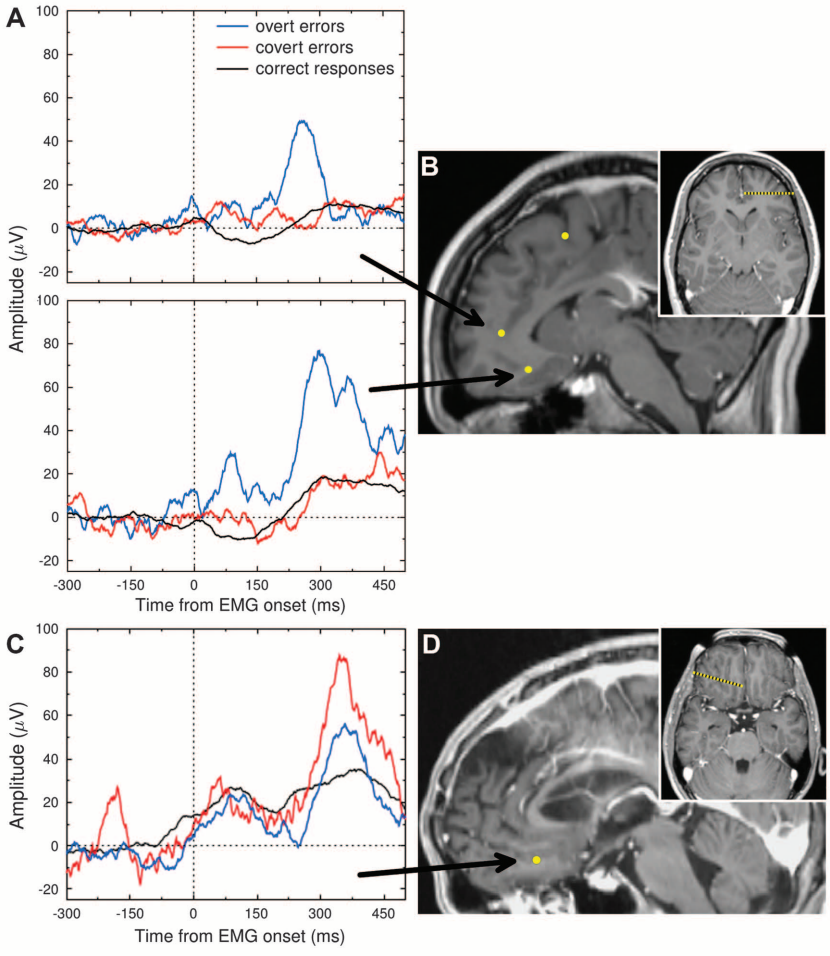

Fig. 3. Medial prefrontal LFPs evoked by erroneous activations. (**A**) Averaged LFPs evoked by overt errors peaking at 260 ms in pACC (top) and at 295 ms in OMPFC (bottom) in subject 3. (**B**) Individual reconstruction of subject 3's prefrontal electrodes based on an MRI-CT fusion scan in axial and sagittal view (note also the overlying electrode placed in the SMA). (**C**) Averaged LFPs peaking at 355 ms evoked by covert and overt errors in subject 5. (**D**) Individual reconstruction of subject 5's prefrontal electrode based on an MRI-CT fusion scan in axial and sagittal view.

References and Notes

1. K. R. Ridderinkhof, M. Ullsperger, E. A. Crone, S. Nieuwenhuis, *Science* **306**, 443–447 (2004).
2. V. van Veen, C. S. Carter, *J. Cogn. Neurosci.* **14**, 593–602 (2002).
3. M. M. Botvinick, J. D. Cohen, C. S. Carter, *Trends Cogn. Sci.* **8**, 539–546 (2004).
4. N. Picard, P. L. Strick, *Cereb. Cortex* **6**, 342–353 (1996).
5. A sixth subject was not included (see note S1).
6. J. R. Simon, in *Stimulus-Response Compatibility: An Integrated Perspective* (R. W. Proctor, T. G. Reeve, Eds. (North-Holland, Amsterdam, 1990), pp. 31–86.
7. H. G. Smid, G. Mulder, L. J. Mulder, *Acta Psychol. (Amst.)* **74**, 169–201 (1990).
8. M. G. Coles, M. K. Scheffers, L. Fournier, *Acta Psychol. (Amst.)* **90**, 129–144 (1995).
9. F. Vidal, T. Hasbroucq, J. Grapperon, M. Bonnet, *Biol. Psychol.* **51**, 109–128 (2000).
10. M. Falkenstein, J. Hoormann, S. Christ, J. Hohnsbein, *Biol. Psychol.* **51**, 87–107 (2000).
11. C. Roger, C. G. Bénar, F. Vidal, T. Hasbroucq, B. Burle, *Neuroimage* **51**, 391–403 (2010).
12. Although the averaged activity in OMPFC in patient 3 was larger than activity in pACC, its signal/noise ratio was too low to reliably detect single-trial activity on a sufficient number of trials for analysis.
13. B. Burle, C. Roger, S. Allain, F. Vidal, T. Hasbroucq, *J. Cogn. Neurosci.* **20**, 1637–1655 (2008).
14. H. Garavan, T. J. Ross, K. Murphy, R. A. P. Roche, E. A. Stein, *Neuroimage* **17**, 1820–1829 (2002).
15. P. Luu, D. M. Tucker, D. Derryberry, M. Reed, C. Poulsen, *Psychol. Sci.* **14**, 47–53 (2003).
16. M. J. Herrmann, J. Römmler, A. C. Ehlis, A. Heidrich, A. J. Fallgatter, *Brain Res. Cogn. Brain Res.* **20**, 294–299 (2004).
17. K. D. Fitzgerald *et al.*, *Biol. Psychiatry* **57**, 287–294 (2005).
18. E. R. A. de Bruijn, F. P. de Lange, D. Y. von Cramon, M. Ullsperger, *J. Neurosci.* **29**, 12183–12186 (2009).
19. V. Stuphorn, T. L. Taylor, J. D. Schall, *Nature* **408**, 857–860 (2000).
20. K. W. Scangos, R. Aronberg, V. Stuphorn, *J. Neurophysiol.* **109**, 1928–1939 (2013).
21. K. A. Kiehl, P. F. Liddle, J. B. Hopfinger, *Psychophysiology* **37**, 216–223 (2000).
22. S. Debener *et al.*, *J. Neurosci.* **25**, 11730–11737 (2005).
23. E. E. Emeric *et al.*, *J. Neurophysiol.* **99**, 759–772 (2008).
24. S. Hoffmann, M. Falkenstein, *Hum. Brain Mapp.* **31**, 1305–1315 (2010).
25. T. E. Ham *et al.*, *Cereb. Cortex* **23**, 703–713 (2013).
26. N. Kolling, T. E. J. Behrens, R. B. Mars, M. F. S. Rushworth, *Science* **336**, 95–98 (2012).
27. P. Y. Chauvel, M. Rey, P. Buser, J. Bancaud, *Adv. Neurol.* **70**, 199–209 (1996).
28. P. Nachev, C. Kennard, M. Husain, *Nat. Rev. Neurosci.* **9**, 856–869 (2008).

Acknowledgments: We thank P. Marquis for technical help in acquiring intracerebral recordings; D. Schön for critical discussion and reading the manuscript; and R. Hewett, M. Woodman, and J. Coull for English revision. B.B. was supported by the European Research Council under the European Community's Seventh Framework Program (FP7/2007-2013 Grant Agreement no. 241077). F.B. was supported by the Ecole Doctorale Science de la Vie et de la Santé, Aix-Marseille Université. F.V. and B.B. designed the study. F.B. administered the Simon task and obtained intracerebral recordings. J.R. performed the surgical procedure and provided coordinates of intracerebral electrodes. F.B. analyzed data. B.B. and F.B. performed statistical analysis. F.V., B.B., F.B., P.C., and C.L.-C. interpreted data and discussed results. F.B. and F.V. wrote the manuscript. All authors commented on and edited the manuscript. The authors declare no conflict of interest.

Supplementary Materials

www.sciencemag.org/content/343/6173/888/suppl/DC1
Materials and Methods
Supplementary Text
Figs. S1 to S8
Tables S1 to S3
References (*29*–*36*)

21 October 2013; accepted 24 January 2014
10.1126/science.1247412

Grid-Layout and Theta-Modulation of Layer 2 Pyramidal Neurons in Medial Entorhinal Cortex

Saikat Ray,* Robert Naumann,* Andrea Burgalossi,*† Qiusong Tang,* Helene Schmidt,* Michael Brecht‡

Little is known about how microcircuits are organized in layer 2 of the medial entorhinal cortex. We visualized principal cell microcircuits and determined cellular theta-rhythmicity in freely moving rats. Non–dentate-projecting, calbindin-positive pyramidal cells bundled dendrites together and formed patches arranged in a hexagonal grid aligned to layer 1 axons, parasubiculum, and cholinergic inputs. Calbindin-negative, dentate-gyrus–projecting stellate cells were distributed across layer 2 but avoided centers of calbindin-positive patches. Cholinergic drive sustained theta-rhythmicity, which was twofold stronger in pyramidal than in stellate neurons. Theta-rhythmicity was cell-type–specific but not distributed as expected from cell-intrinsic properties. Layer 2 divides into a weakly theta-locked stellate cell lattice and spatiotemporally highly organized pyramidal grid. It needs to be assessed how these two distinct principal cell networks contribute to grid cell activity.

Temporal (*1*–*3*) and spatial (*4*) discharge patterns in layer 2 of the medial entorhinal cortex (MEC) are related through phase precession (*5*) and the correlation of gridness (hexagonal regularity) and theta-rhythmicity (*2*). Layer 2 principal neurons divide into pyramidal and stellate cells, the latter of which have been suggested to shape entorhinal theta (*6*, *7*) and grid activity (*8*) by their intrinsic properties. Progress in understanding entorhinal microcircuits has been limited because most though not all data (*9*–*11*) stem from extracellular recordings of unidentified cells. Such recordings have characterized diverse functional cell types (*12*–*14*) in layer 2. Clustering of grid cells (*15*) points to spatial organization. It is not clear, however, how functionally defined cell types correspond to stellate and pyramidal cells (*7*, *16*), which differ in conductances, immunoreactivity, projections, and inhibitory inputs (*6*, *17*–*20*). We combined juxtacellular labeling with principal cell identification (*20*) to visualize microcircuits in the MEC (Fig. 1A).

Calbindin immunoreactivity (*20*) identifies a relatively homogeneous pyramidal neuron population in MEC layer 2. Parasagittal sections stained for calbindin (Fig. 1B) showed that calbindin-positive (calbindin$^+$) pyramidal cells were arranged in patches (*21*). Apical dendrites of calbindin$^+$ pyramidal cells bundled together in layer 1 to form tent-like structures over the patches (Fig. 1B). The patchy structure is well defined at the layer 1/2 border, whereas a "salt-and-pepper" appearance of calbindin$^+$ and calbindin$^-$ cells is observed deeper in layer 2 (fig. S1). Patches contained 187 ± 70 cells (111 ± 42, ~60% calbindin$^+$; 76 ± 28, ~40% calbindin$^-$ cells; counts of 19 patches from four brains). We double-stained tangential sections for calbindin (green) and the neuronal marker NeuN (red) to visualize patches in the cortical plane. Calbindin$^+$ (green/yellow) patches covered the MEC except for a 400- to 500-μm-wide patch-free medial stripe adjacent to the parasubiculum (Fig. 1C). Clustering was not observed in calbindin$^-$ neurons (red) (Fig. 1C). We noted a striking hexagonal organization of calbindin$^+$ patches (Fig. 1, C and D) and characterized this organization by means of three techniques. (i) We used two-dimensional spatial autocorrelation analysis (*4*), which captures spatially recurring features and revealed a hexagonal regularity (Fig. 1E). (ii) We modified grid scores (*12*) to quantify hexagonality also in elliptically distorted hexagons (*22*), distortions that result from tissue curvature and anisotropic shrinkage. Grid scores range from –2 to +2, with values >0 indicating hexagonality. The example in Fig. 1D had a grid score of 1.18, suggesting a high degree of hexagonality. (iii) We assessed the probability of hexagonal patch arrangements given preserved local structure (*14*) by means of a shuffling procedure. We found that the strongest Fourier component of the sample

Bernstein Center for Computational Neuroscience, Humboldt University of Berlin, Philippstrasse 13 Haus 6, 10115 Berlin, Germany.

*These authors contributed equally to this work.
†Present address: Werner Reichardt Centre for Integrative Neuroscience, Otfried-Müller-strasse 25, 72076 Tübingen, Germany.
‡Corresponding author. E-mail: michael.brecht@bccn-berlin.de

(Fig. 1D) exceeded that of the 99th percentile of shuffled data, suggesting that such hexagonality is unlikely to arise by chance.

We retrogradely labeled neurons from ipsilateral dentate gyrus (Fig. 2A) using biotinylated dextran amine (BDA) (Fig. 2B) or cholera toxin B (Fig. 2C) to investigate the arrangement of layer 2 principal cells with identified projection patterns and immunoreactivity (*20*). Although most retrogradely labeled neurons were stellate cells (*16*, *23*), a small fraction had pyramidal morphologies, but these neurons appeared larger than calbindin$^+$ pyramidal cells (Fig. 2B). Calbindin$^+$ neurons did not project to the dentate gyrus (only 1 double-labeled out of 313 neurons in Fig. 2, C to E) (*20*). Calbindin$^+$ patches were hexagonally arranged (Fig. 2, C, D, and F), whereas dentate-gyrus–projecting neurons (red) were uniformly distributed (Fig. 2, E and G). Reconstructions of calbindin$^+$ and calbindin$^-$ cells labeled in vivo confirmed their pyramidal and stellate morphologies, respectively. Calbindin$^+$ dendrites were largely confined to patches, whereas calbindin$^-$ stellates cells had three times larger dendritic trees (7.6 versus 2.6 mm average total length, $P < 0.03$), which extended unrelated to patches (Fig. 2, H and I). Differentiating layer 2 neurons by calbindin and reelin immunoreactivity confirmed patchy hexagonality of calbindin$^+$ cells and scattered distribution of reelin$^+$ cells without overlap between these neurons (fig. S2) (*20*).

To investigate the organization of calbindin$^+$ patches across the MEC, we prepared flattened whole-mount preparations. Patches had similar arrangements throughout the dorsoventral extent of the MEC (fig. S3). At the layer 1/2 border, we consistently observed hexagonal arrangements in well-stained specimens. We quantified patch size and spacing in 10 largely complete MEC whole-mounts. Patch density was similar throughout the MEC, whereas patch diameter slightly increased toward ventral (fig. S3). We estimated 69 ± 17 patches across the entire MEC ($n = 10$ hemispheres). Calbindin patches stained also positive for cytochrome-oxidase activity (*9*). However, the two staining patterns were not the same because calbindin patches were more sharply delineated than were spots revealed by cytochrome-oxidase activity, and cytochrome-oxidase staining revealed many more patches than did calbindin staining in the MEC (*9*). Moreover, the staining patterns did not correspond at all in the parasubiculum.

Calbindin$^+$ patches shared a roughly 60° symmetry of their axes (Fig. 3A). One axis runs parallel to the dorsoventral axis of the parasubiculum (Fig. 3, A and B). Lines fitted through the dorsoventral axis of the parasubiculum, and the most medial column of calbindin$^+$ patches had the same orientation (Fig. 3B). A second consistent axis was tilted ~60° relative to the dorsoventral axis. This calbindin$^+$ patch axis curved ventrally at more lateral positions and aligned with the orientation of overlaying layer 1 myelinated axons (Fig. 3, C to F). Thus, the line connecting diagonally neighboring calbindin patches (revealed by spatial autocorrelation) (Fig. 3, D and E) aligned with the orientation of layer 1 axons (Fig. 3F). We quantified the orientation of axonal segments by a polar plot shown in Fig. 3G and confirmed that layer 1 axons share one main orientation in the MEC (*9*, *24*, *25*).

MEC function and grid cell activity (*26*, *27*) depend on medial septum inputs (*28*, *29*) and cholinergic transmission (*30*). We observed a patchy pattern of acetylcholinesterase labeling at the layer 1/2 border (Fig. 3H), which colocalized with the cores of calbindin$^+$ patches (Fig. 3, H to J). Axonal terminals positive for the vesicular acetylcholine transporter (VAChT) were closely apposed to calbindin$^+$ cells, and their density was twofold larger in calbindin$^+$ patches than between patches (fig. S4). We also stained for m1 muscarinic receptors and observed a diffuse labeling without colocalization of these receptors to VAChT puncta.

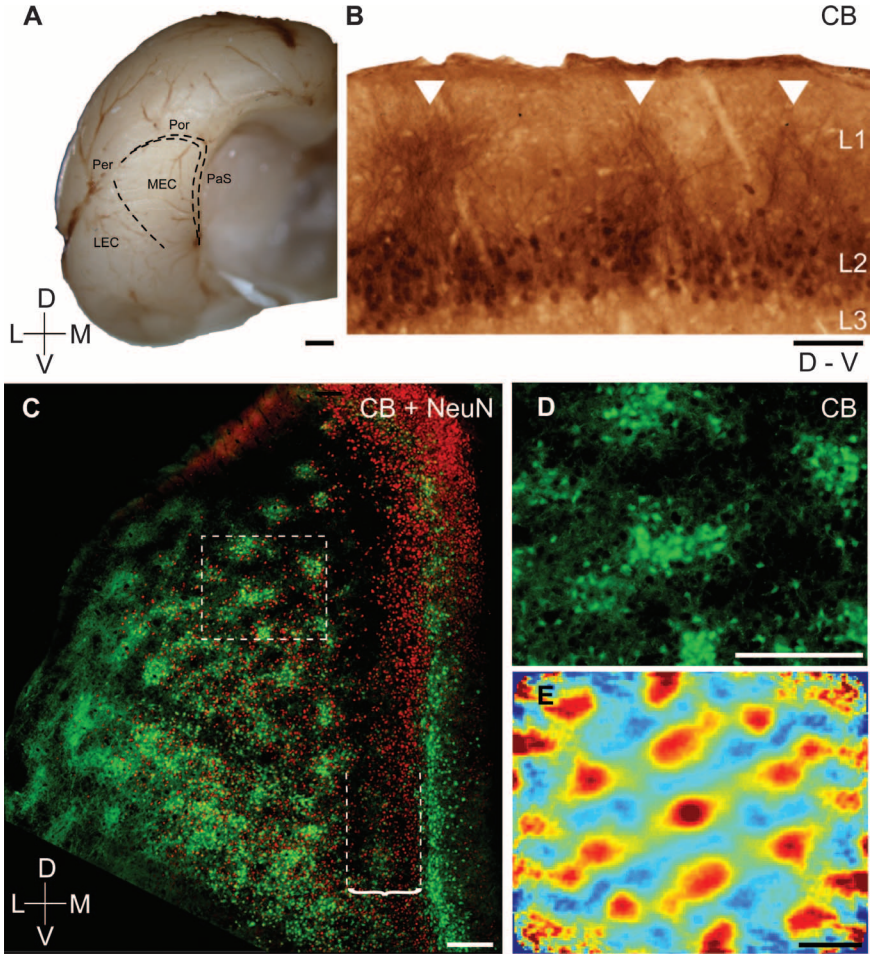

Fig. 1. Grid-like arrangement of calbindin$^+$ pyramidal cells in the MEC. (**A**) Posterior view of a rat cortical hemisphere. LEC, lateral entorhinal cortex; PaS, parasubiculum; Per, perirhinal cortex; Por, postrhinal cortex. (**B**) Calbindin-immunoreactivity (brown precipitate) in a parasaggital section reveals patches with apical dendrites of calbindin$^+$ pyramidal cells forming tents (white arrows) in layer 1. (**C**) Tangential section showing all neurons (red, NeuN-antibody) and patches of calbindin$^+$ neurons (green). Bracket, dashed lines indicate the patch-free stripe of MEC. (**D**) Inset from (C). (**E**) Two-dimensional spatial autocorrelation of (D) revealing a hexagonal spatial organization of calbindin$^+$ patches. Color scale, −0.5 (blue) through 0 (green) to 0.5 (red); grid score is 1.18. Scale bars, (A) 1 mm; (B) 100 μm; (C) to (E) 250 μm. D, dorsal; L, lateral; M, medial; V, ventral.

Moreover, we analyzed the apposition and distribution of presynaptic VAChT puncta relative to dendrites of in vivo filled calbindin$^+$ and calbindin$^-$ layer 2 cells by means of confocal microscopy. VAChT puncta were much more abundant around calbindin$^+$ than calbindin$^-$ layer 2 cells, but proximity histograms of VAChT puncta and dendrites did not indicate a direct targeting of calbindin$^+$ cell dendrites by cholinergic synapses (fig. S4). Both the m1 receptor labeling and our dendrite-VAChT puncta colocalization analysis are in line with a volumetric action of acetylcholine in the MEC (*31*–*33*).

Last, we assessed in freely moving animals how activity of identified neurons related to the entorhinal theta-rhythm. We recorded 31 layer 2 neurons in rats trained to explore open fields and classified them by morphology and immunoreactivity. Calbindin$^+$ neurons ($n = 12$) were pyramidal cells, whereas calbindin$^-$ neurons ($n = 19$) had stellate morphologies. Firing rates were not different (calbindin$^+$ = 2.1 ± 1.1 Hz; calbindin$^-$ = 2.3 ± 1.5 Hz; $P > 0.5$, Mann-Whitney test). We found, however, that calbindin$^+$ neurons (Fig. 4, A to C) showed stronger theta-rhythmicity of spiking than that of calbindin$^-$ cells ($P < 0.01$, unpaired t test) (Fig. 4, D to G). Theta-rhythmicity was associated

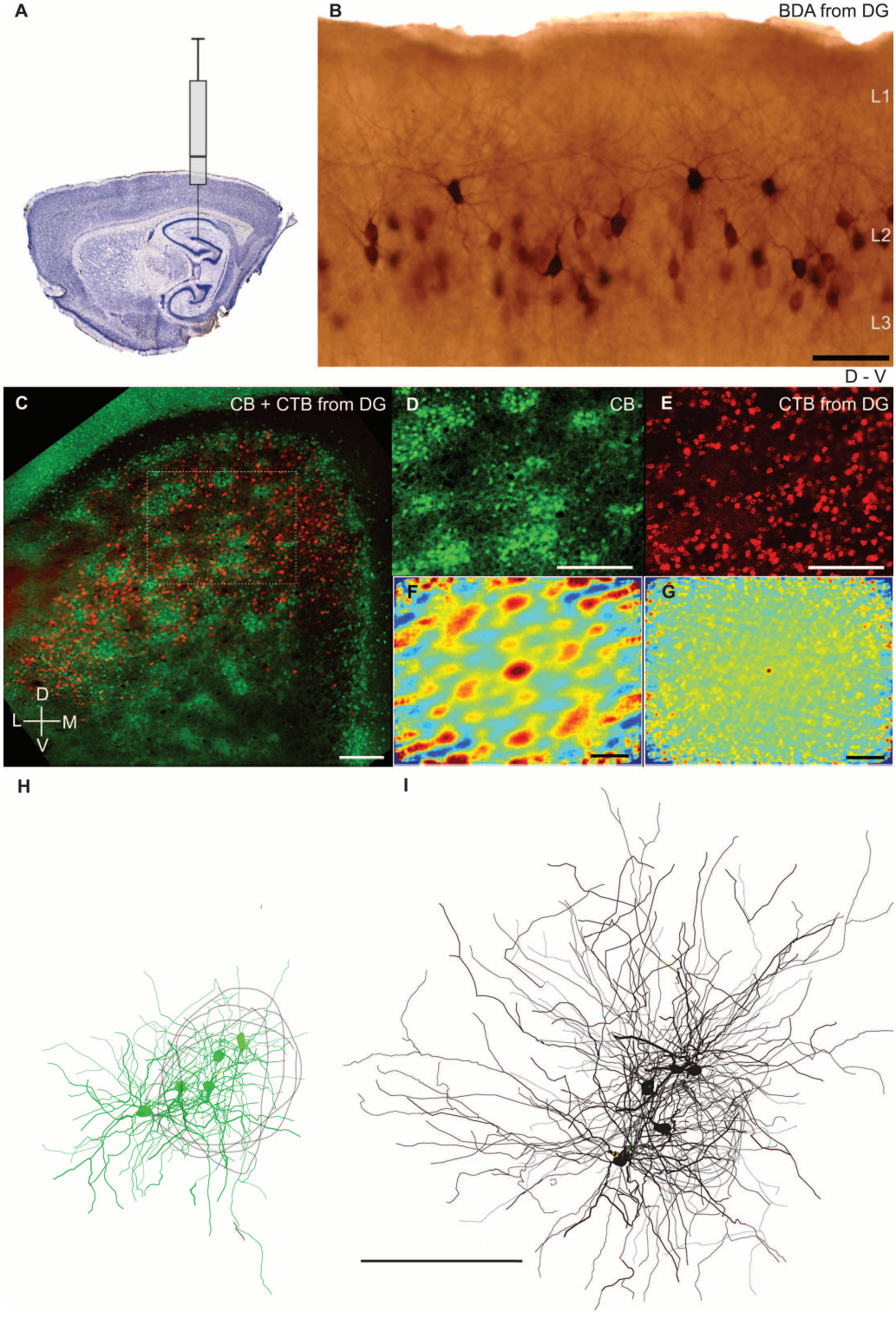

Fig. 2. Calbindin$^+$ pyramidal but not dentate-projecting stellate neurons form patches. (**A**) Schematic of retrograde labeling from dentate gyrus. (**B**) Such retrograde labeling (BDA, brown) stains neurons (most with stellate morphologies) in a parasaggital MEC section. (**C**) Tangential MEC section showing calbindin$^+$ neurons (green) and retrogradely labeled neurons (red) after dentate-gyrus–cholera–toxin-B injection. (**D** and **E**) Insets from (C). (**F**) Two-dimensional spatial autocorrelation of (D) reveals regular organization of calbindin$^+$ patches; grid score is 0.32. The strongest Fourier component of the sample exceeded that of the 99th percentile of shuffled data confirming hexagonality. (**G**) Two-dimensional spatial autocorrelation of (E) reveals no spatial organization; grid score is −0.03. (**H** and **I**) Superimposed reconstructions of dendritic morphologies of 5 calbindin$^+$ pyramidal (green) and 5 calbindin$^-$ stellate neurons (black) in the tangential plane. Morphologies were "patch-centered" aligned according to orientation and the center of the nearest calbindin$^+$ patch (gray outlines). Scale bars, (B) 100 μm; (C) to (E) and (G) to (I) 250 μm. D, dorsal; L, lateral; M, medial; V, ventral.

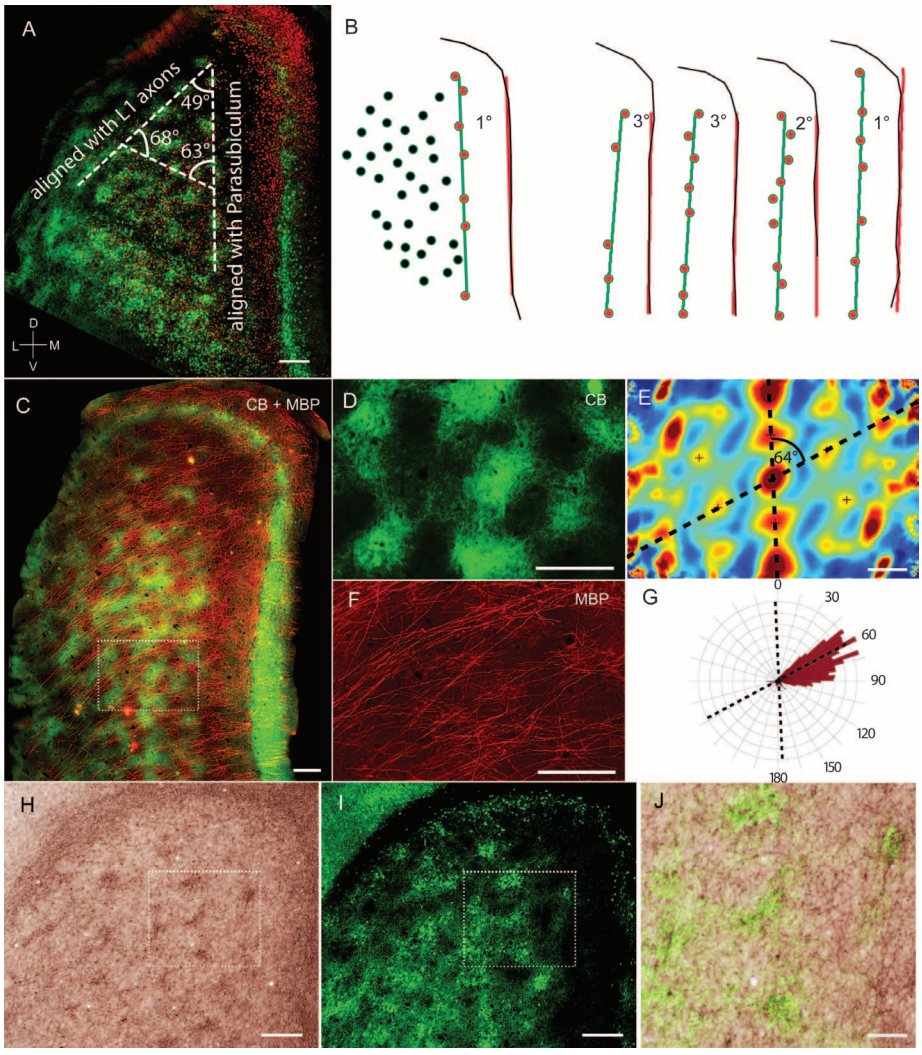

Fig. 3. Alignment of the calbindin grid to parasubiculum, layer 1 axons, and cholinergic markers. (**A**) Section from Fig. 1C. Dashed white lines indicate axes of the calbindin$^+$ grid (angles are indicated). Axes aligned with parasubiculum (B) and layer 1 axons [(C) to (G)]. (**B**) (Left) Schematic of calbindin patches and parasubiculum from (A). The orange line fits the dorsoventral axis of the parasubiculum, and the green line fits the most medial column of patches (red); the angle between these lines is indicated. (Right) Fitted lines and their relative angles for four other brains. (**C**) Tangential section processed for calbindin (green) and myelin basic protein (red). (**D**) Inset from (C). (**E**) Two-dimensional spatial autocorrelation of (D). Dashed black lines indicate grid axes. (**F**) Inset from (C). (**G**) Axonal segments in (F) were manually traced from left to right, and we computed a polar plot (red) of the orientations of the axonal segments. The orientations of axonal segments aligned with one axis of the grid of calbindin patches [superimposed dashed lines from (E)]. (**H**) Tangential section stained for acetylcholinesterase activity. (**I**) Section from (H) costained for calbindin. (**J**) Overlay of (H) and (I) shows overlap between acetylcholinesterase and calbindin staining. Scale bars, (A), (C) to (F), (H), and (I) 250 μm; (J) 100 μm. D, dorsal; L, lateral; M, medial; V, ventral.

with locomotion of the animal (fig. S5). A similar twofold difference in theta-rhythmicity between calbindin$^+$ (n = 14) and calbindin$^-$ (n = 20) cells was observed under urethane-ketamine anesthesia (P = 0.0003, Mann-Whitney test) (Fig. 4H), which preserves cortico-hippocampal theta-rhythmicity (*3*, *34*). Pharmacological blockade of cholinergic transmission suppressed theta-rhythmicity in both calbindin$^+$ and calbindin$^-$ cells (Fig. 4I). Specifically, we observed that cholinergic blockade led to a loss of the distinct peak at theta-frequency in the power spectra of spike discharges (fig. S6). Cells also differed in their phase-locking to entorhinal field potential theta: Calbindin$^+$ cells were more strongly phase-locked (average Rayleigh vector length = 0.54 versus 0.22 in calbindin$^-$ cells; P < 0.0012, Mann-Whitney test) and fired near the trough of the theta-oscillation, whereas locking was weaker and more variable in calbindin$^-$ cells (Fig. 4J).

What is the cellular basis of theta-rhythmicity in MEC layer 2? Stellate cells have been prime candidates for theta discharges in layer 2 (*6*, *7*) because intrinsic conductances make them resonate at theta-frequency (*35*, *36*). We found, however, that calbindin$^+$ pyramidal cells showed twofold stronger theta-rhythmicity and theta-phase-locking than calbindin$^-$ stellate neurons. The stronger theta-rhythmicity of calbindin$^+$ pyramidal neurons, which have weaker sag-currents (*7*, *20*), is opposite from what had been predicted on the basis of intrinsic properties (*8*, *37*). Hence, layer 2 theta-modulation is cell-type–specific but not distributed as expected from cell-intrinsic resonance properties. This finding agrees with other evidence that questioned the causal relationship between intrinsic properties and theta-rhythmicity in vivo (*10*, *37*, *38*). The membrane properties of calbindin$^+$ neurons are not tuned to the generation of theta-rhythmicity (*20*). Their strongly rhythmic discharges suggest that calbindin$^+$ neurons might correspond to a subset of cells with strong membrane potential theta-oscillations (*11*), which—in the absence of cell-intrinsic mechanisms—probably arise from synaptic interactions. Cholinergic innervation and effects of cholinergic blockade suggest cholinergic drive sustains theta-rhythmicity of calbindin$^+$ cells.

We were not yet able to assess spatial modulation in a sufficient number of identified neurons to directly relate our results to grid cell function. The limited available evidence suggests that grid cells are recruited from a heterogeneous neuronal population in layer 2 (*10*, *11*, *39*), possibly indicating weak structure-function relationships (*40*). Yet, we observed similarities between calbindin$^+$ neurons and grid cells: Calbindin$^+$ patches receive cholinergic inputs, which are required for grid cell activity according to preliminary data (*30*); calbindin$^+$ cells have strong theta-rhythmicity, a feature that correlates with grid cell discharge (*2*); and, like grid cells, calbindin$^+$ cells are clustered.

We have hypothesized that calbindin$^+$ neurons form a "grid-cell-grid" (*41*)—that their hexagonal arrangement might be an isomorphism to hexagonal grid cell activity, much like isomorphic cortical representations of body parts in tactile specialists (*42*, *43*). However, hexagonality often results from spacing constraints and hence might be unrelated to grid cell activity. Determining the spatial modulation patterns of identified entorhinal neurons will help clarifying whether and how the calbindin$^+$ grid is related to grid cell activity.

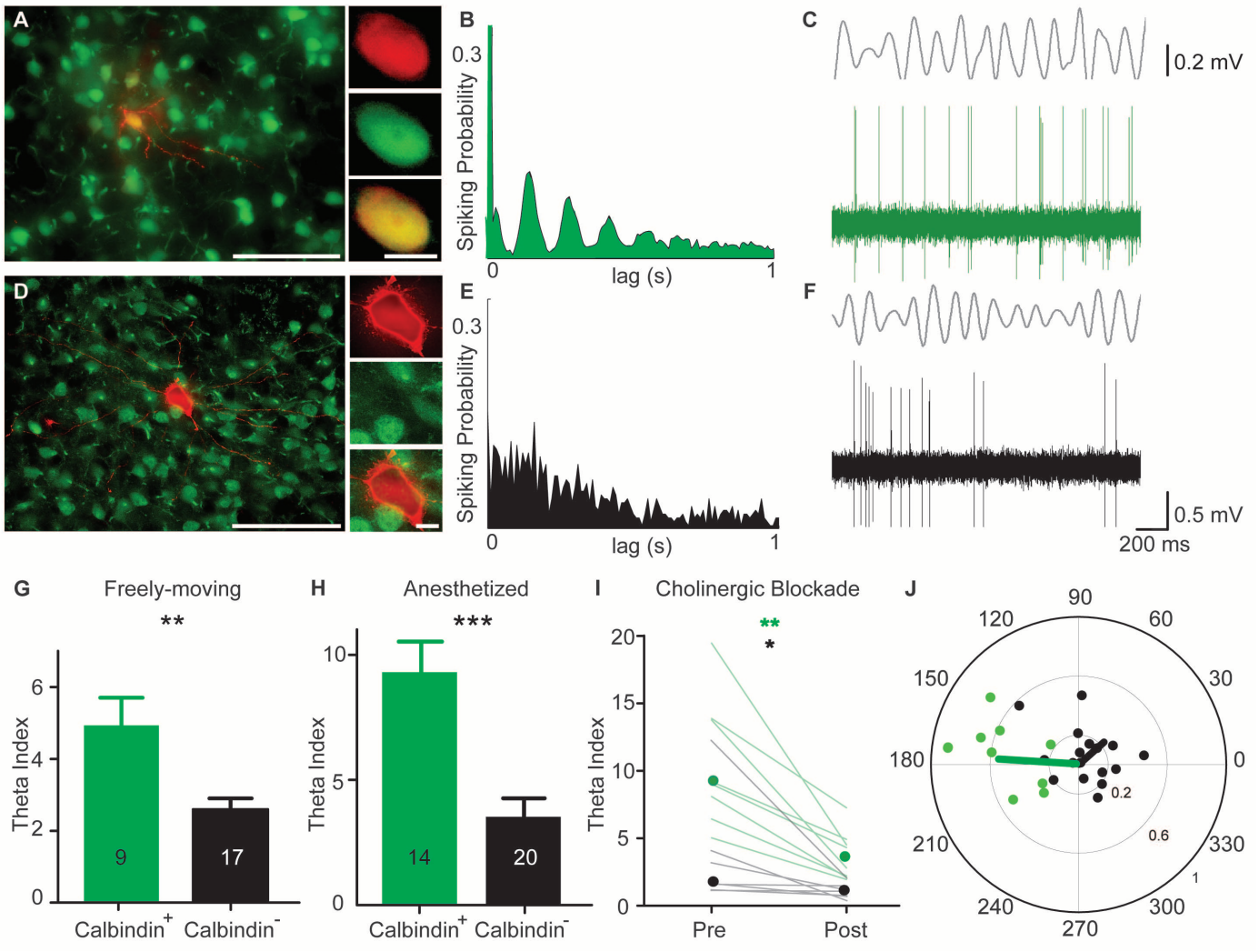

Fig. 4. Theta-modulation of calbindin$^+$ positive and calbindin$^-$ cells. (**A**) (Left) Micrograph (tangential section) of a calbindin$^+$ neuron recorded in a freely moving animal. Green, calbindin; red, neurobiotin. (Right) Soma in red, green channel, and overlay. (**B**) Autocorrelogram of spike discharges for the calbindin$^+$ neuron shown in (A). (**C**) Filtered (4 to 12 Hz) local field potential (top) and spiking pattern (bottom) of the neuron shown in (A). (**D** to **F**) Same as (A) to (C) but for a calbindin$^-$ neuron. (**G**) Strength of theta-rhythmicity in calbindin$^+$ and calbindin$^-$ neurons in freely moving animals. Numbers are *n* of neurons. Error bars indicate SEM. (**H**) Same as (G) but for recordings under urethane-ketamine anesthesia (*34*). (**I**) Theta-rhythmicity in calbindin$^+$ neurons (green, $n = 8$) and calbindin$^-$ neurons (black, $n = 7$) under anesthesia before and after systemic cholinergic blockade with scopolamine (Wilcoxon signed rank test, $P = 0.0078$ for calbindin$^+$, $P = 0.0156$ for calbindin$^-$ cells). Dots indicate medians. (**J**) Polar plot of preferred theta-phase (theta-peak = 0°) and modulation strength (Rayleigh vector, 0 to 1, proportional to eccentricity) for calbindin$^+$ (green) and calbindin$^-$ (black); dots indicate single cells, and lines indicate averages. Scale bars, (A) and (D) 100 μm (left), 10 μm (right).

References and Notes

1. K. Mizuseki, A. Sirota, E. Pastalkova, G. Buzsáki, *Neuron* **64**, 267–280 (2009).
2. C. N. Boccara *et al.*, *Nat. Neurosci.* **13**, 987–994 (2010).
3. P. Quilichini, A. Sirota, G. Buzsáki, *J. Neurosci.* **30**, 11128–11142 (2010).
4. T. Hafting, M. Fyhn, S. Molden, M.-B. Moser, E. I. Moser, *Nature* **436**, 801–806 (2005).
5. T. Hafting, M. Fyhn, T. Bonnevie, M.-B. Moser, E. I. Moser, *Nature* **453**, 1248–1252 (2008).
6. A. Alonso, R. R. Llinás, *Nature* **342**, 175–177 (1989).
7. A. Alonso, R. Klink, *J. Neurophysiol.* **70**, 128–143 (1993).
8. M. E. Hasselmo, L. M. Giocomo, E. A. Zilli, *Hippocampus* **17**, 1252–1271 (2007).
9. A. Burgalossi *et al.*, *Neuron* **70**, 773–786 (2011).
10. C. Schmidt-Hieber, M. Häusser, *Nat. Neurosci.* **16**, 325–331 (2013).
11. C. Domnisoru, A. A. Kinkhabwala, D. W. Tank, *Nature* **495**, 199–204 (2013).
12. F. Sargolini *et al.*, *Science* **312**, 758–762 (2006).
13. T. Solstad, C. N. Boccara, E. Kropff, M.-B. Moser, E. I. Moser, *Science* **322**, 1865–1868 (2008).
14. J. Krupic, N. Burgess, J. O'Keefe, *Science* **337**, 853–857 (2012).
15. H. Stensola *et al.*, *Nature* **492**, 72–78 (2012).
16. P. Germroth, W. K. Schwerdtfeger, E. H. Buhl, *Neuroscience* **30**, 683–691 (1989).
17. K. Lingenhöhl, D. M. Finch, *Exp. Brain Res.* **84**, 57–74 (1991).
18. R. Klink, A. Alonso, *J. Neurophysiol.* **77**, 1813–1828 (1997).
19. C. B. Canto, M. P. Witter, *Hippocampus* **22**, 1277–1299 (2012).
20. C. Varga, S. Y. Lee, I. Soltesz, *Nat. Neurosci.* **13**, 822–824 (2010).
21. Y. Fujimaru, T. Kosaka, *Neurosci. Res.* **24**, 329–343 (1996).
22. C. Barry, L. L. Ginzberg, J. O'Keefe, N. Burgess, *Proc. Natl. Acad. Sci. U.S.A.* **109**, 17687–17692 (2012).
23. N. Tamamaki, Y. Nojyo, *Hippocampus* **3**, 471–480 (1993).
24. T. W. Blackstad, *J. Comp. Neurol.* **105**, 417–537 (1956).
25. M. P. Witter, H. J. Groenewegen, F. H. Lopes da Silva, A. H. Lohman, *Prog. Neurobiol.* **33**, 161–253 (1989).
26. C. Barry, J. G. Heys, M. E. Hasselmo, *Front. Neural Circuits* **6**, 5 (2012).
27. J. G. Heys, N. W. Schultheiss, C. F. Shay, Y. Tsuno, M. E. Hasselmo, *Behav. Neurosci.* **6**, 32 (2012).
28. J. Koenig, A. N. Linder, J. K. Leutgeb, S. Leutgeb, *Science* **332**, 592–595 (2011).
29. M. P. Brandon *et al.*, *Science* **332**, 595–599 (2011).
30. E. L. Newman, M. E. Hasselmo, Society for Neuroscience Annual Meeting Abstract No. 730.07 (2011).

31. M. E. Hasselmo, J. McGaughy, *Prog. Brain Res.* **145**, 207–231 (2004).
32. L. F. Agnati *et al*., *Acta Physiol. (Oxf.)* **187**, 329–344 (2006).
33. L. M. Teles-Grilo Ruivo, J. R. Mellor, *Front. Synaptic Neurosci.* **5**, 2 (2013).
34. T. Klausberger *et al*., *Nature* **421**, 844–848 (2003).
35. D. L. F. Garden, P. D. Dodson, C. O'Donnell, M. D. White, M. F. Nolan, *Neuron* **60**, 875–889 (2008).
36. L. M. Giocomo, M. E. Hasselmo, *J. Neurosci.* **28**, 9414–9425 (2008).
37. F. R. Fernandez, J. A. White, *J. Neurosci.* **28**, 3790–3803 (2008).
38. L. M. Giocomo *et al*., *Cell* **147**, 1159–1170 (2011).
39. S. J. Zhang *et al*., *Science* **340**, 1232627 (2013).
40. D. C. Rowland, M.-B. Moser, *Curr. Opin. Neurobiol.* **24**, 22–27 (2014).
41. M. Brecht *et al*., *Philos. Trans. R. Soc. London B Biol. Sci.* **369**, 20120521 (2013).
42. T. A. Woolsey, H. Van der Loos, *Brain Res.* **17**, 205–242 (1970).
43. K. C. Catania, R. G. Northcutt, J. H. Kaas, P. D. Beck, *Nature* **364**, 493 (1993).

Acknowledgments: This work was supported by Humboldt Universität zu Berlin, Bernstein Center for Computational Neuroscience Berlin [German Federal Ministry of Education and Research (BMBF), Förderkennzeichen 01GQ1001A], NeuroCure, the Neuro-Behavior European Research Council grant, and the Gottfried Wilhelm Leibniz Prize of the Deutsche Forschungsgemeinschaft. We thank C. Ebbesen, M. von Heimendahl, R. Rao, J. Steger, J. Tukker, U. Schneeweiß, P. Turko, and I. Vida.

Supplementary Materials
www.sciencemag.org/content/343/6173/891/suppl/DC1
Materials and Methods
Figs. S1 to S6
References (*44*–*57*)

10 July 2013; accepted 19 December 2013
Published online 23 January 2014;
10.1126/science.1243028

Island Cells Control Temporal Association Memory

Takashi Kitamura,[1]* Michele Pignatelli,[1]* Junghyup Suh,[1] Keigo Kohara,[1] Atsushi Yoshiki,[2] Kuniya Abe,[2] Susumu Tonegawa[1,3]†

Episodic memory requires associations of temporally discontiguous events. In the entorhinal-hippocampal network, temporal associations are driven by a direct pathway from layer III of the medial entorhinal cortex (MECIII) to the hippocampal CA1 region. However, the identification of neural circuits that regulate this association has remained unknown. In layer II of entorhinal cortex (ECII), we report clusters of excitatory neurons called island cells, which appear in a curvilinear matrix of bulblike structures, directly project to CA1, and activate interneurons that target the distal dendrites of CA1 pyramidal neurons. Island cells suppress the excitatory MECIII input through the feed-forward inhibition to control the strength and duration of temporal association in trace fear memory. Together, the two EC inputs compose a control circuit for temporal association memory.

Episodic memory consists of associations of objects, space, and time (*1*). In humans and animals, the entorhinal cortex (EC)–hippocampal (HPC) network plays an essential role in episodic memory (*2*), with medial EC (MEC) and lateral EC (LEC) inputs into HPC providing spatial and object information, respectively (*3*). Neural circuits have been identified in the EC-HPC network that mediate space and object associations (*4*–*6*). In contrast, the neural circuits for time-related aspects of episodic memory are only beginning to be studied (*7*, *8*). Direct inputs from MEC layer III (MECIII) cells to CA1 pyramidal cells drive the temporal association of discontiguous events (*9*). Like most cognitive and motor phenomena, temporal association memory must be regulated for optimal adaptive benefit, yet nearly nothing is known about the underlying mechanisms of this regulation. We investigated this issue by mapping and characterizing an unsuspected neuronal circuit within the EC-HPC network and examining the effect of its optogenetic manipulations on a temporal association memory.

A retrograde tracer, cholera toxin subunit B (CTB), was injected into the dentate gyrus (DG) of C57BL6 mice (Fig. 1A). Although a majority of cells in EC layer II (ECII) were CTB-positive, a large proportion was CTB-negative and clustered in a series of about 130-μm-diameter bulblike structures (Fig. 1, B and C). Hereafter, we refer to these CTB-negative cells as ECII island (ECIIi) cells. ECIIi cells are mostly pyramidal (Fig. 1F and fig. S1) and express Wfs1 (*10*) and calbindinD-28K (*11*) (Fig. 1, B to D and F). CTB-positive cells were identified as previously well known DG-projecting stellate cells (*12*, *13*) (Fig. 1G and figs. S1 and S2) that express reelin (*14*) but not Wfs1 or calbindinD-28K (Fig. 1E). Hereafter, we refer to these CTB-positive cells as ECII ocean (ECIIo) cells. ECIIi cells are excitatory (Fig. 1F and figs. S1 and S2) and present in both MEC and LEC (fig. S2), but they are distinct from ECIIo cells not only by their morphology and molecular markers but also by their intrinsic electrophysiological properties (*15*, *16*) (fig. S1).

We created a Cre transgenic mouse line by using the Wfs1 promoter (fig. S3). When the Cre-dependent adeno-associated virus encoding double-floxed inverted open reading frame with enhanced yellow fluorescent protein under control of elongation factor 1 α promoter (AAV9-EF1α-DIO-eYFP) was injected into the superficial layers of the EC (Fig. 1H), eYFP expression was restricted to Wfs1- and calbindinD-28K–positive ECIIi cells (Fig. 1, I and J, and fig. S4). These ECIIi cells appeared in a curvilinear matrix of bulblike structures in tangential MEC sections (Fig. 1K). We injected the AAV_9-EF1α-DIO-ChR2-eYFP virus (where ChR2 indicates channelrhodopsin-2) (*17*) into the EC of Wfs1-Cre mice (Fig. 1L). ECIIi cells projected primarily to the CA1 region via the temporoammonic pathway (Fig. 1M). Additional weaker projections were detected in the subiculum, parasubiculum, and contralateral CA1 and EC (Fig. 1M and fig. S5). Wfs1- and calbindinD-28K–positive ECIIi cells are also present in rat and project to the CA1 region (fig. S6).

In the CA1 region, ECIIi axons specifically innervated the border between the stratum radiatum (SR) and stratum lacunosum-moleculare (SLM) (Fig. 2A), terminating sharply at the proximal end of CA1, and did not enter into CA2 (Fig. 2A), which was marked with regulator of G protein signaling 14 (RGS14) (*18*). ECIIi axons were strongly myelinated (fig. S7) (*19*) and preferentially innervate the stratum lacunosum (SL) (Fig. 2B). In contrast, MECIII axons innervate the stratum moleculare (SM) immediately adjacent to the SL (Fig. 2C). Experiments conducted with a ChR2eYFP transgenic mouse line under control of vesicular γ-aminobutyric acid (GABA) transporter promoter (VGAT-ChR2eYFP) (*20*) and immunohistochemistry of glutamate decarboxylase 67 (GAD67) suggested that the primary target of the ECIIi cells are GABA-releasing interneurons in the SL (SL-INs) (Fig. 2, D to F) (*21*). Presynaptic terminal analysis showed ECIIi cells are glutamatergic (Fig. 2G and fig. S8). Low expression of PSD-95 in the SL suggested that innervations of ECIIi axons onto CA1 pyramidal cell dendrites in the SL are relatively infrequent (fig. S9).

Optogenetic stimulation of ChR2-expressing ECIIi axons during in vitro patch-clamp recordings of SL-INs revealed reliable excitatory postsynaptic currents (EPSCs, average amplitude of 54 ± 7 pA, average onset of 2.05 ± 0.07 ms, $n = 40$) in 87% of SL-INs ($n = 53$; Fig. 2, H to J, and fig. S10), which were sensitive to ionotropic glutamate receptor antagonists (fig. S11). In current mode, repetitive photostimulation was sufficient to trigger action potentials in SL-INs ($n = 14$ out of 40; Fig. 2, K and Q). Under similar stimulation conditions, CA1 pyramidal cells showed small EPSCs (average amplitude of 19 ± 5 pA, average onset of 3.11 ± 0.08 ms, $n = 29$) in 70% of them ($n = 50$; Fig. 2, L to N, and fig. S11), suggesting a weaker impact of ECIIi cells to CA1 pyramidal cells than to SL-INs

[1]RIKEN-MIT Center for Neural Circuit Genetics at the Picower Institute for Learning and Memory, Department of Biology and Department of Brain and Cognitive Sciences, Massachusetts Institute of Technology (MIT), Cambridge, MA 02139, USA. [2]RIKEN BioResource Center, 3-1-1 Koyadai, Ibaraki 305-0074, Japan. [3]Howard Hughes Medical Institute at MIT, Cambridge, MA 02139, USA.

*These authors contributed equally to this work.
†Corresponding author. E-mail: tonegawa@mit.edu

(Fig. 2P). In current mode, repetitive photostimulation never triggered action potentials in CA1 pyramidal cells (n = 35). However, somatic depolarization to –55 mV revealed strong inhibitory potentials (IPSPs) in 30% of CA1 pyramidal cells (n = 50, Fig. 2O) in response to optogenetic stimulation of ECIIi axons, which was abolished by bath application of GABA receptor antagonists (Fig. 2R). These data demonstrate a previously unknown feedforward inhibitory circuit controlled by ECIIi cells (Fig. 2S).

Input selectivity to SL-INs was investigated by replacing the Wfs1-Cre transgenic mice with the MECIII cell–specific pOxr1-Cre mice (*9*) or the CA3 cell–specific KA1-Cre transgenic mice (*5*) (Fig. 3, A to C). SL-INs were preferentially innervated by ECIIi cells (Fig. 3, D to G, and supplementary statistics).

The SL-INs exert an inhibitory effect on the apical dendrite of CA1 pyramidal cells (*22*). To investigate whether the ECIIi-SL-INs circuit has the ability to inhibit MECIII inputs to CA1 pyramidal cells, we injected the AAV_9-EF1α-DIO-ChR2-eYFP virus into the EC of pOxr1-Cre mice. We then simultaneously recorded connected pairs of SL-INs and CA1 pyramidal cells (Fig. 3H) to test whether SL-INs activity was sufficient to inhibit MECIII input. We found 8 connected pairs out of 260 tested pairs ($P_{connection}$ = 0.03, average unitary EPSP (uEPSP) amplitude of –0.18 ± 0.09 mV, average uIPSP onset of 1.45 ± 0.2 ms, Fig. 3I). A confocal microscopic analysis suggested an average of 2 ± 0.3 putative synaptic contacts between SL-INs axons and CA1 pyramidal cell's apical dendrites (Fig. 3H inset and fig. S12). By eliciting a brief burst in SL-INs, we observed IPSPs in all the connected CA1 pyramidal cells (Fig. 3J). Optogenetic stimulation of MECIII axons elicited EPSPs in CA1 pyramidal cells (Fig. 3K). However, pairing optogenetic and SL-IN stimulations significantly reduced the amplitude of EPSP to 60% of the response evoked by MECIII axonal stimulation alone (average amplitude of MEC stimulation only was 1.6 ± 0.4 mV; for pairing MEC and SL-INs, 0.9 ± 0.4 mV; n = 8, Fig. 3, K and L). The lack of significant difference between the average IPSP amplitude and the inhibited component of the response suggested a reduction mediated mainly by linear subtraction (Wilcoxon signed-rank P = 0.5).

We then sought the functional importance of ECIIi–SL-IN circuit-mediated inhibition of MECIII input to CA1 at the behavioral level. For this purpose, we injected bilaterally AAV_9-CBA-DIO-ArchT-eGFP (*23*) into the EC of pOxr1-Cre mice. Unilateral shining of green light to a CA1 area of these mice with an optic fiber implanted to this area (*24*) (Fig. 4A and fig. S13) inhibited the ArchT-expressing MECIII axons resulting in a reduction of the multiunit activity of CA1 pyramidal cells in vivo (58% reduction, Fig. 4B). We subjected mice to trace fear conditioning (TFC) while delivering green light bilaterally to the CA1 areas during the entire training period (i.e., three rounds of tone, trace, and shock periods). Mice expressing ArchT, but not control mice expressing the fluorescence marker only (i.e., tdTomato), exhibited severe freezing deficits during both training and testing sessions (Fig. 4, C and D) but not in response to the context (fig. S15). The remaining freezing observed during the tone period of the testing session is likely due to nonassociative learning (fig. S14).

We injected bilaterally AAV_9-EF1α-DIO-ChR2-eYFP into the EC of Wfs1-Cre mice. Unilateral shining of blue light to a CA1 area resulted in reduced multiunit activity of CA1 pyramidal cells in vivo (46% reduction, Fig. 4B), strongly supporting the feed-forward inhibition of CA1 activity

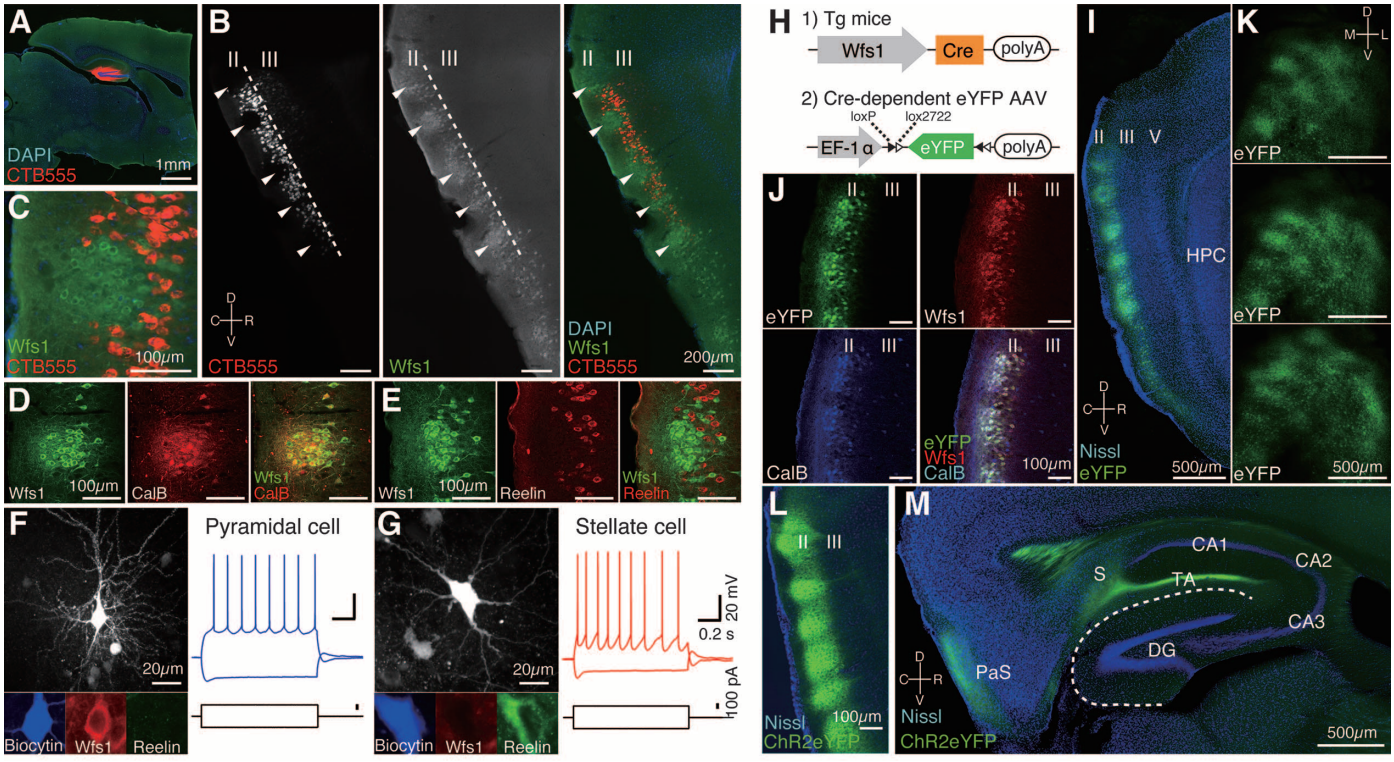

Fig. 1. Characterizations of island cells and generation of Wfs1-Cre transgenic mice. (**A**) Injection sites of CTB (red) in DG. (**B**) Parasagittal sections of MEC visualized with CTB-labeled cell bodies (red) and immunostained with anti-Wfs1 (green). Arrowheads indicate Wfs1-positive and CTB-negative ECIIi cells. (**C**) Magnified image from (B). (**D**) Parasagittal sections of EC immunostained with anti-Wfs1 (green) and anti–calbindin D-28K (red). (**E**) Parasagittal sections of EC immunostained with anti-Wfs1 (green) and anti-reelin (red). Wfs1-positive cells do not express reelin. (**F** and **G**) Examples of biocytin-stained Wfs1-positive pyramidal cell (F) and reelin-positive stellate cell (G) and electrophysiological responses to positive or negative current step injections. (**H**) Transgenic mouse combined with AAV injection. (**I** and **J**) Parasagittal sections of Wfs1-Cre mouse injected with AAV_9-EF1α-DIO-eYFP (green) and immunostained with anti-Wfs1 (red) and anti–calbindinD-28K (blue). (**K**) Tangential MEC sequential caudorostral sections of a Wfs1-Cre mouse injected with AAV_9-EF1α-DIO-eYFP. (**L** and **M**) Parasagittal sections of a Wfs1-Cre mouse injected with AAV_9-EF1α-DIO-ChR2-eYFP: injection site (EC) (L) and hippocampal innervations (M). The dotted line indicates the hippocampal fissure. TA, temporoammonic pathway; PaS, parasubiculum; S, subiculum, D, dorsal; V, ventral; R, rostral; C, caudal; L, lateral; M, medial.

by the ECIIi-INs pathway, which was demonstrated also by the in vitro study (Fig. 2O). In TFC, these mice exhibited severe freezing deficits during both training (Fig. 4E) and testing (Fig. 4F) sessions compared with the three control groups when blue-light pulses were delivered bilaterally to the CA1 areas during the entire training period. The freezing deficits were particularly large during the post-tone periods of the testing session. In contrast, the ChR2 light-on group froze as much as the control groups in response to the training context (fig. S15). When light of the same intensity and duration was delivered to the ChR2 group before (82 s before) the training period, there was no light effect on freezing (fig. S16). The delivery of blue-light pulses during the entire training period had no effect on freezing when mice were subjected to delayed fear conditioning (DFC) in which trace was omitted (Fig. 4, G and H), indicating that deficits observed in TFC (Fig. 4, E and F) are not due to an inability to encode the conditioned stimulus (CS) or unconditioned stimulus (US). A direct stimulation of SL-INs in VGAT-ChR2-eYFP transgenic mice by blue light during the training period caused freezing deficits in TFC but not in response to the context (fig. S17).

We restricted the stimulation to the trace plus foot shock period (Tr-S group) or to the tone period (To group). The light-on Tr-S group showed severe freezing deficits during both training and post-tone periods of testing sessions (Fig. 4, I and J). The patterns of freezing deficits of the light-on Tr-S group and the light-on ChR2 group were com-

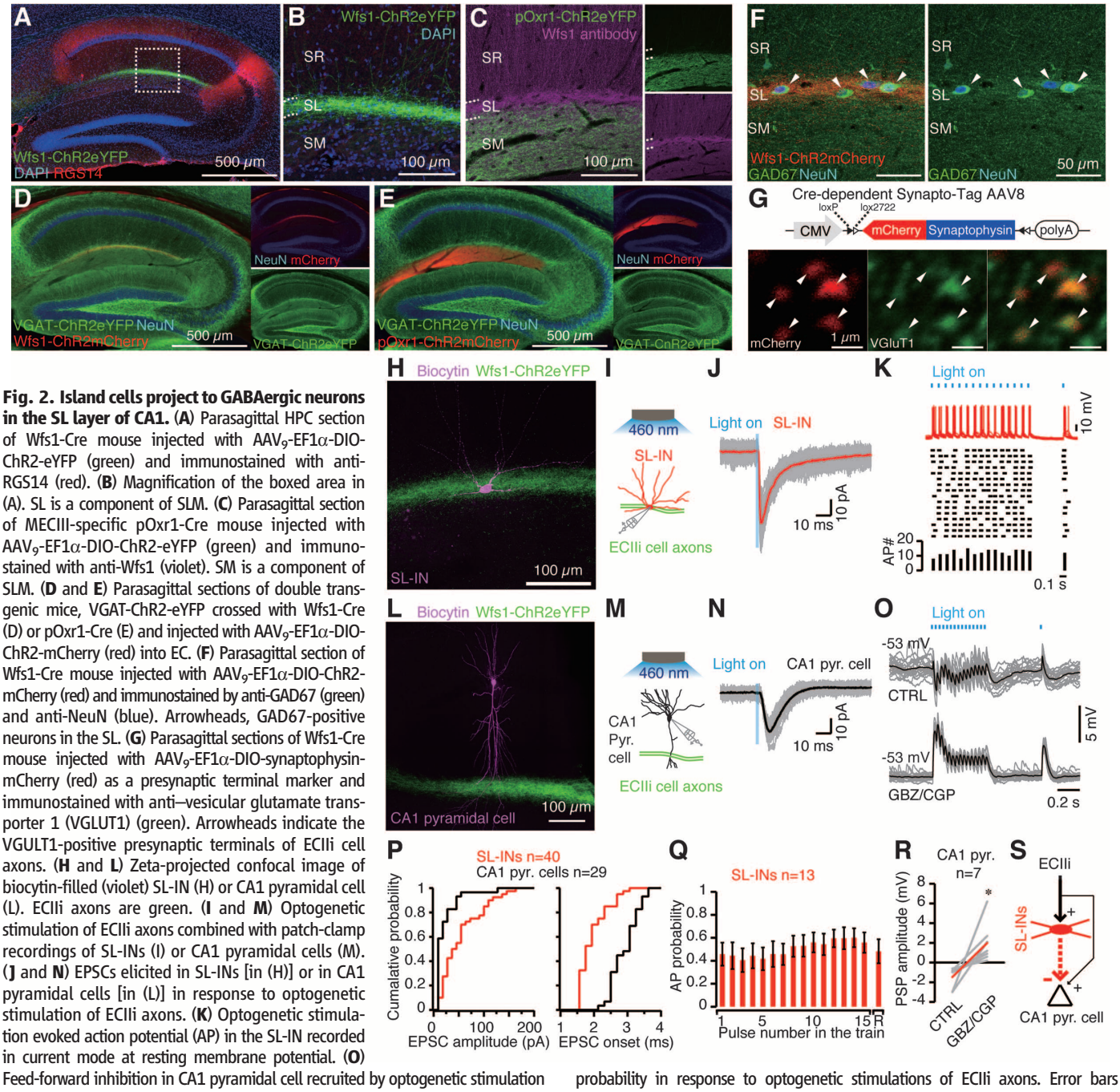

Fig. 2. Island cells project to GABAergic neurons in the SL layer of CA1. (**A**) Parasagittal HPC section of Wfs1-Cre mouse injected with AAV$_9$-EF1α-DIO-ChR2-eYFP (green) and immunostained with anti-RGS14 (red). (**B**) Magnification of the boxed area in (A). SL is a component of SLM. (**C**) Parasagittal section of MECIII-specific pOxr1-Cre mouse injected with AAV$_9$-EF1α-DIO-ChR2-eYFP (green) and immunostained with anti-Wfs1 (violet). SM is a component of SLM. (**D** and **E**) Parasagittal sections of double transgenic mice, VGAT-ChR2-eYFP crossed with Wfs1-Cre (D) or pOxr1-Cre (E) and injected with AAV$_9$-EF1α-DIO-ChR2-mCherry (red) into EC. (**F**) Parasagittal section of Wfs1-Cre mouse injected with AAV$_9$-EF1α-DIO-ChR2-mCherry (red) and immunostained by anti-GAD67 (green) and anti-NeuN (blue). Arrowheads, GAD67-positive neurons in the SL. (**G**) Parasagittal sections of Wfs1-Cre mouse injected with AAV$_9$-EF1α-DIO-synaptophysin-mCherry (red) as a presynaptic terminal marker and immunostained with anti–vesicular glutamate transporter 1 (VGLUT1) (green). Arrowheads indicate the VGULT1-positive presynaptic terminals of ECIIi cell axons. (**H** and **L**) Zeta-projected confocal image of biocytin-filled (violet) SL-IN (H) or CA1 pyramidal cell (L). ECIIi axons are green. (**I** and **M**) Optogenetic stimulation of ECIIi axons combined with patch-clamp recordings of SL-INs (I) or CA1 pyramidal cells (M). (**J** and **N**) EPSCs elicited in SL-INs [in (H)] or in CA1 pyramidal cells [in (L)] in response to optogenetic stimulation of ECIIi axons. (**K**) Optogenetic stimulation evoked action potential (AP) in the SL-IN recorded in current mode at resting membrane potential. (**O**) Feed-forward inhibition in CA1 pyramidal cell recruited by optogenetic stimulation of ECIIi axons. Individual traces in gray, average in black. (**P**) Kinetic of the EPSCs elicited by optogenetic stimulation of ECIIi axons. EPSCs recorded in SL-INs displayed larger amplitude [Kolmogorov-Smirnov (KS) statistic < 0.001] and faster onset (KS < 0.001) than EPSCs recorded in pyramidal cells. (**Q**) SL-INs' average AP probability in response to optogenetic stimulations of ECIIi axons. Error bars indicate SEM. (**R**) Feed-forward inhibition recruited in CA1 pyramidal cells is abolished by bath application of GABA receptor antagonists (Wilcoxon signed-rank $P < 0.05$, $n = 7$). See example in (O). (**S**) Schematic of the feed-forward inhibition. Thickness of the lines indicates connection strength.

parable during both training and testing sessions. The light-on To group did not show any significant freezing deficits during either the training or the testing session (Fig. 4, I and J).

We subjected eArch3.0eYFP-expressing (eArch group) (*17*) and eYFP only–expressing (eYFP group) Wfs1-Cre mice to in vivo recordings. The stimulation of the eArch3.0-positive ECIIi axons in the CA1 area with green light increased the multiunit activity of CA1 pyramidal cells (30% enhancement, Fig. 4B). We subjected them to TFC with green light delivered bilaterally during the entire training period. During the training session, the eArch group showed as much freezing as the control eYFP group (Fig. 4K). However, during the testing session, the eArch group displayed significantly enhanced freezing during the post-tone periods that lasted about 1 min longer compared with the control eYFP group (Fig. 4L), but freezing was unaltered in response to the context (fig. S15). Maximal levels of freezing were unaltered during training and testing sessions, although this could be due to a ceiling effect of the training protocol. Indeed, when the strength of the foot shocks was lowered, the maximal levels and the post-tone duration of freezing were greater in the eArch group compared with the control eYFP group during both training and testing sessions (Fig. 4, M and N). We injected AAV_9-EF1α-DIO-ChR2-mCherry into the EC of pOxr1-Cre mice. The blue-light pulse stimulation to the CA1 area increased the multiunit activity of CA1 pyramidal cells in vivo (31% enhancement, Fig. 4B). We subjected ChR2mCherry-expressing (ChR2 group) and mCherry only–expressing (mCherry group) pOxr1-Cre mice to TFC with the lower shock intensity with blue-light stimulations during the trace period. During the testing session, the ChR2 group displayed significantly enhanced freezing amplitudes and post-tone freezing duration compared with the control mCherry group (Fig. 4, O and P).

The interplay of synaptic excitation and inhibition contributes to the regulation of perception, memory, and motor behavior (*25*). A major challenge in neuroscience is to define this interplay at the levels of specific neuronal circuits and the specific cell types participating in them. We identified and characterized a neural circuit in the EC-HPC network that regulates temporal association memory, an essential component of episodic memory.

Previous studies determined that about one-third of ECII excitatory cells are made of pyramidal cells (*15*, *16*, *26*), but their projections to

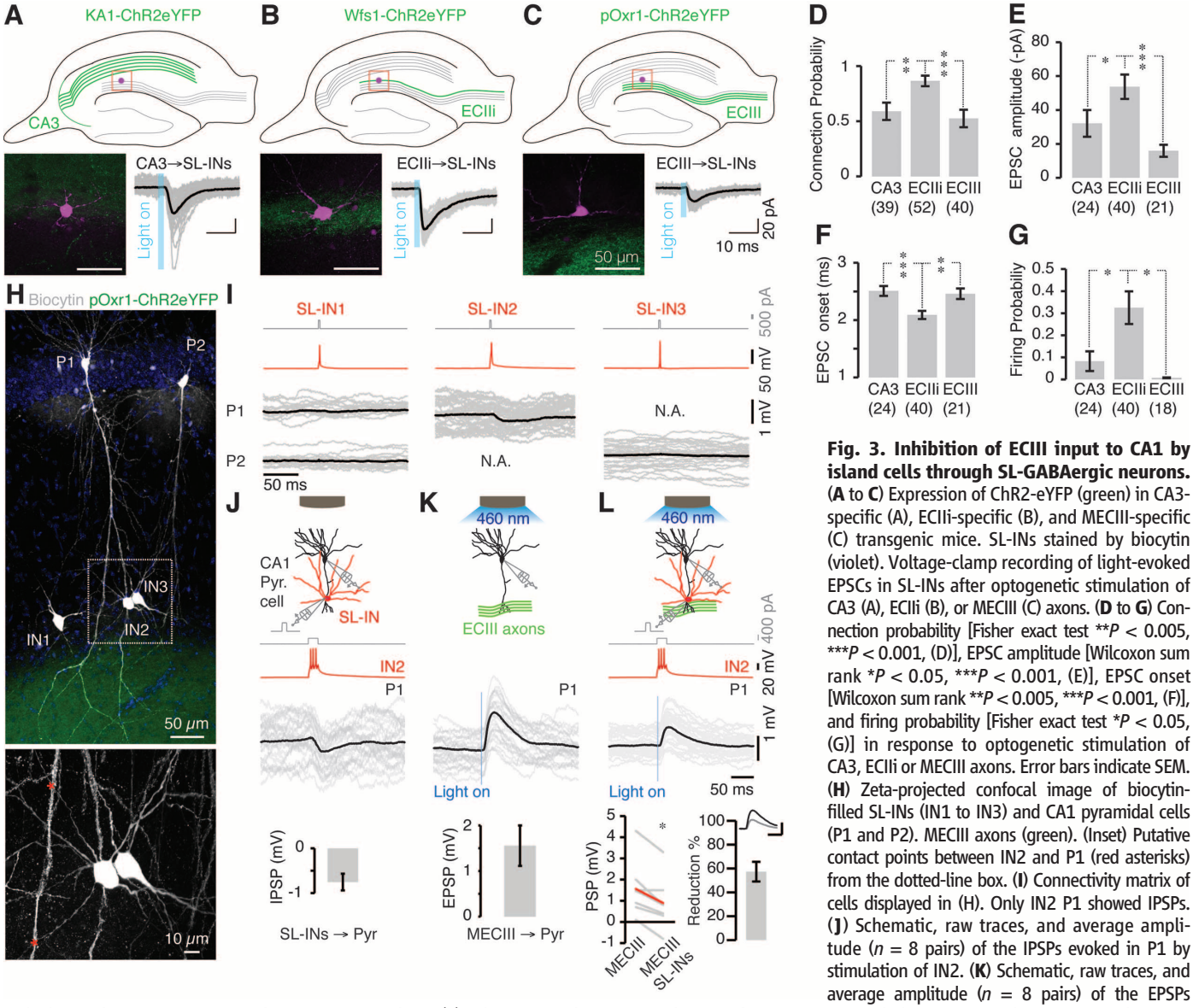

Fig. 3. Inhibition of ECIII input to CA1 by island cells through SL-GABAergic neurons. (**A** to **C**) Expression of ChR2-eYFP (green) in CA3-specific (A), ECIIi-specific (B), and MECIII-specific (C) transgenic mice. SL-INs stained by biocytin (violet). Voltage-clamp recording of light-evoked EPSCs in SL-INs after optogenetic stimulation of CA3 (A), ECIIi (B), or MECIII (C) axons. (**D** to **G**) Connection probability [Fisher exact test $^{**}P < 0.005$, $^{***}P < 0.001$, (D)], EPSC amplitude [Wilcoxon sum rank $^{*}P < 0.05$, $^{***}P < 0.001$, (E)], EPSC onset [Wilcoxon sum rank $^{**}P < 0.005$, $^{***}P < 0.001$, (F)], and firing probability [Fisher exact test $^{*}P < 0.05$, (G)] in response to optogenetic stimulation of CA3, ECIIi or MECIII axons. Error bars indicate SEM. (**H**) Zeta-projected confocal image of biocytin-filled SL-INs (IN1 to IN3) and CA1 pyramidal cells (P1 and P2). MECIII axons (green). (Inset) Putative contact points between IN2 and P1 (red asterisks) from the dotted-line box. (**I**) Connectivity matrix of cells displayed in (H). Only IN2 P1 showed IPSPs. (**J**) Schematic, raw traces, and average amplitude (n = 8 pairs) of the IPSPs evoked in P1 by stimulation of IN2. (**K**) Schematic, raw traces, and average amplitude (n = 8 pairs) of the EPSPs evoked in P1 by optogenetic stimulation of MECIII fibers. (**L**) Schematic and raw traces showing the response recorded in P1 to simultaneous stimulation of MECIII axons and IN2. Note the reduction elicited by the simultaneous stimulation when compared with optogenetic stimulation of MECIII axons only (Wilcoxon signed-rank $^{*}P < 0.05$, n = 8 pairs, average in red).

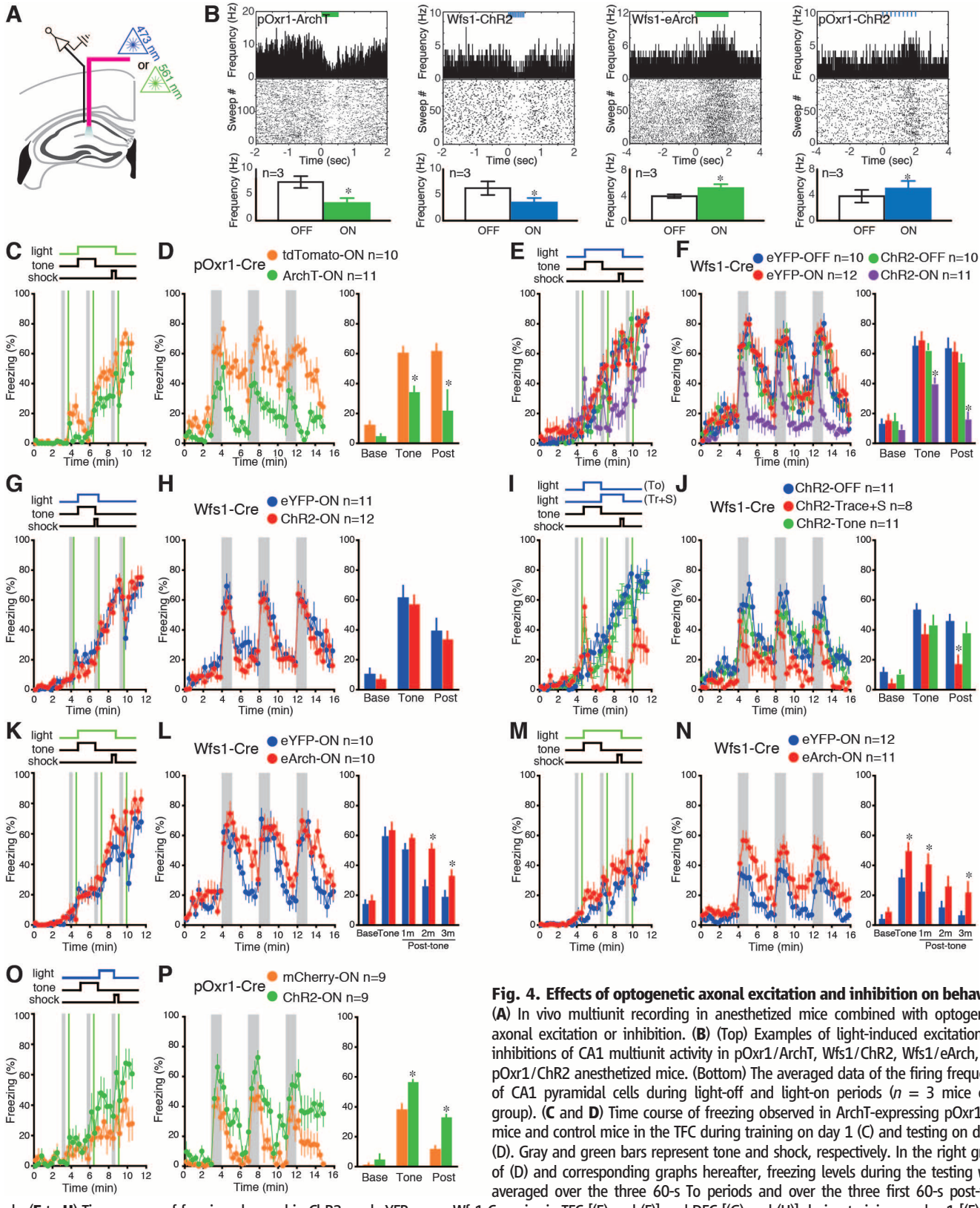

Fig. 4. Effects of optogenetic axonal excitation and inhibition on behavior. (**A**) In vivo multiunit recording in anesthetized mice combined with optogenetic axonal excitation or inhibition. (**B**) (Top) Examples of light-induced excitations or inhibitions of CA1 multiunit activity in pOxr1/ArchT, Wfs1/ChR2, Wfs1/eArch, and pOxr1/ChR2 anesthetized mice. (Bottom) The averaged data of the firing frequency of CA1 pyramidal cells during light-off and light-on periods (n = 3 mice each group). (**C** and **D**) Time course of freezing observed in ArchT-expressing pOxr1-Cre mice and control mice in the TFC during training on day 1 (C) and testing on day 2 (D). Gray and green bars represent tone and shock, respectively. In the right graph of (D) and corresponding graphs hereafter, freezing levels during the testing were averaged over the three 60-s To periods and over the three first 60-s post-tone periods. (**E** to **H**) Time courses of freezing observed in ChR2- and eYFP-group Wfs1-Cre mice in TFC [(E) and (F)] and DFC [(G) and (H)] during training on day 1 [(E) and (G)] and testing on day 2 [(F) and (H)]. In (G), blue light was delivered during training periods (22 s). (**I** and **J**) Blue light was delivered during To (20 s) or Tr-S (22 s) periods. Time courses of freezing observed in ChR2-expressing Wfs1-Cre mice in TFC during training on day 1 (I) or testing on day 2 (J). (**K** to **N**) Time courses of freezing observed in eArch- and eYFP-group Wfs1-Cre mice in TFC [(K) and (L)] and weak TFC [(M) and (N)] during training on day 1 [(K) and (M)] and testing on day 2 [(L) and (N)]. Right graphs of (L) and (N) show freezing levels during testing on day 2 averaged over the first, second, and third 60-s post-tone periods. (**O** and **P**) Time courses of freezing observed in ChR2- and mCherry-group pOxr1-Cre mice in weak TFC during training on day 1 (O) and testing on day 2 (P). *$P < 0.05$.

SL-INs in CA1 have been unknown. The modularity of ECII neurons has been reported previously. The patchlike structures identified by anti–calbindinD-28K (*11*) and the "islets" detected by the expression of Wfs1 mRNA (*10*) probably correspond to our ECIIi cells. However, projections of these subpopulations of ECII cells into HPC have not been reported previously. Cytochrome oxidase (CO) staining revealed patches of axonal terminals in ECII that are derived from metabolically active cells (*27*, *28*). These CO-positive patches are larger than ECIIi cells and contain both calbindinD-28K–positive ECIIi cells (fig. S6) and stellate cells (*28*).

The strategic location of SL-INs, the primary target of ECIIi cells, immediately adjacent to the inner side of the SM layer where MECIII cells synapse to the distal dendrites of CA1 pyramidal cells enables ECIIi cells to suppress MECIII input by feed-forward inhibition. Our findings are consistent with previous studies pointing to the existence of a feed-forward inhibitory circuit arising from direct entorhinal inputs into CA1 (*29*, *30*). However, these earlier studies used electrical stimulation of SLM axons and hence could not distinguish ECIII and ECIIi axons that run in the SM and SL, respectively. SL-INs are connected by gap junctions (*31*). Thus, activation of ECIIi axons can evoke a depolarizing response broadly among SL-INs, which propagates through gap junctions, amplifying the effect of ECIIi cell inputs.

Our behavioral data allow for two conclusions. First, the fact that behavioral freezing in TFC was optogenetically impaired by either inhibition of MECIII input or activation of ECIIi input provides evidence for inhibition of the former input by the latter through feedforward inhibition. This conclusion is reinforced by the enhanced freezing level and the prolonged post-tone freezing period induced by eArch-mediated inactivation of the ECIIi axons. Thus, the freezing response can be regulated bidirectionally by the relative strength of MECIII and ECIIi inputs to CA1. Our data suggest that this regulatory system controls the strength of a temporal association memory as well as the duration of the expression of this memory after the recall cues cease. Such a regulation is crucial for optimal adaptive benefit; too strong an association of a particular pair of events may interfere with associations of other useful pairs, whereas too weak an association for a given pair of events will not result in an effective memory. Additionally, the ECIIi-INs pathway input can provide a specific pattern of temporal windows within which MECIII input can drive the associations.

Second, our observation that the freezing deficit was caused by the inhibition of MECIII input by the ECIIi-CA1 pathway during the Tr-S period but not during the To period indicates that the trace is not stored in CA1 and that post-tone MECIII input is crucial for the formation of temporal association memory. We propose that the source of this input could be persistent activity triggered in MECIII by the tone (*9*, *32*, *33*). Such activity will be transmitted to CA1 pyramidal cells and then to the basolateral amygdala via the EC layer V (*34*) as a CS (i.e., tone signal) coincident with the US (i.e., shock signal) to generate a fear memory engram via Hebbian synapses in the basolateral amygdala (*35*). The tone-triggered persistent activity in ECIII may also be instrumental for the prolonged post-tone freezing during recall of the temporal association memory.

Although our study has demonstrated that the feed-forward inhibition of MECIII input to CA1 pyramidal cells by the ECIIi–SL-INs pathway serves as an important mechanism for the control of temporal association memory, other circuits and/or mechanisms may also contribute to this process. For instance, a recent study described long-range projections of entorhinal interneurons into HPC interneurons, including SL-INs (*36*). This circuit could also participate in the regulation of temporal association memory by countering the effect of the ECIIi–SL-INs circuit. Another possibility is that SL-INs may contribute to the regulation of temporal association memory by rhythmic dendritic inhibition of CA1 pyramidal cells through their rhythmic activation (*22*).

CA1 pyramidal cells receive a multitude of other excitatory and inhibitory inputs (*26*) including the Schaffer collateral (SC) input from CA3 that originates from ECIIo cells. The in vitro interaction of ECIII and CA3 inputs on the activity and synaptic plasticity of CA1 pyramidal cells have been reported (*37*), but the inhibition of SC input does not seem to have a substantial effect on the TFC performance (*9*). Although the role of the direct pathway, ECIIi-CA1 pyramidal cells, has not been yet elucidated, we hypothesize that the indirect pathway from ECIIo to CA1 via the trisynaptic circuit primarily processes context and space, whereas the direct pathways from MECIII and ECIIi-SL-INs are responsible for temporal properties of episodic memory.

References and Notes

1. E. Tulving, *Annu. Rev. Psychol.* **53**, 1–25 (2002).
2. H. Eichenbaum, *Nat. Rev. Neurosci.* **1**, 41–50 (2000).
3. E. L. Hargreaves, G. Rao, I. Lee, J. J. Knierim, *Science* **308**, 1792–1794 (2005).
4. D. Marr, *Philos. Trans. R. Soc. London Ser. B* **262**, 23–81 (1971).
5. K. Nakazawa *et al*., *Science* **297**, 211–218 (2002).
6. T. J. McHugh *et al*., *Science* **317**, 94–99 (2007).
7. G. V. Wallenstein, M. E. Hasselmo, H. Eichenbaum, *Trends Neurosci.* **21**, 317–323 (1998).
8. C. J. MacDonald, K. Q. Lepage, U. T. Eden, H. Eichenbaum, *Neuron* **71**, 737–749 (2011).
9. J. Suh, A. J. Rivest, T. Nakashiba, T. Tominaga, S. Tonegawa, *Science* **334**, 1415–1420 (2011).
10. J. Kawano *et al*., *Neurosci. Res.* **64**, 213–230 (2009).
11. Y. Fujimaru, T. Kosaka, *Neurosci. Res.* **24**, 329–343 (1996).
12. N. Tamamaki, Y. Nojyo, *Hippocampus* **3**, 471–480 (1993).
13. J. J. Couey *et al*., *Nat. Neurosci.* **16**, 318–324 (2013).
14. C. Varga, S. Y. Lee, I. Soltesz, *Nat. Neurosci.* **13**, 822–824 (2010).
15. A. Alonso, R. Klink, *J. Neurophysiol.* **70**, 128–143 (1993).
16. R. Klink, A. Alonso, *Hippocampus* **7**, 571–583 (1997).
17. J. Mattis *et al*., *Nat. Methods* **9**, 159–172 (2012).
18. S. E. Lee *et al*., *Proc. Natl. Acad. Sci. U.S.A.* **107**, 16994–16998 (2010).
19. A. Hjorth-Simonsen, J. Zimmer, *J. Comp. Neurol.* **161**, 57–70 (1975).
20. S. Zhao *et al*., *Nat. Methods* **8**, 745–752 (2011).
21. T. F. Freund, G. Buzsáki, *Hippocampus* **6**, 347–470 (1996).
22. S. Bertrand, J. C. Lacaille, *J. Physiol.* **532**, 369–384 (2001).
23. X. Han *et al*., *Front Syst Neurosci* **5**, 18 (2011).
24. O. Yizhar, L. E. Fenno, T. J. Davidson, M. Mogri, K. Deisseroth, *Neuron* **71**, 9–34 (2011).
25. J. S. Isaacson, M. Scanziani, *Neuron* **72**, 231–243 (2011).
26. P. Andersen, R. Morris, D. Amaral, T. Bliss, J. O'Keefe, *The Hippocampus Book* (Oxford Univ. Press, New York, 2007).
27. R. F. Hevner, M. T. Wong-Riley, *J. Comp. Neurol.* **326**, 451–469 (1992).
28. A. Burgalossi *et al*., *Neuron* **70**, 773–786 (2011).
29. R. M. Empson, U. Heinemann, *J. Physiol.* **484**, 707–720 (1995).
30. H. Dvorak-Carbone, E. M. Schuman, *J. Neurophysiol.* **82**, 3213–3222 (1999).
31. C. J. Price *et al*., *J. Neurosci.* **25**, 6775–6786 (2005).
32. A. V. Egorov, B. N. Hamam, E. Fransén, M. E. Hasselmo, A. A. Alonso, *Nature* **420**, 173–178 (2002).
33. T. T. Hahn, J. M. McFarland, S. Berberich, B. Sakmann, M. R. Mehta, *Nat. Neurosci.* **15**, 1531–1538 (2012).
34. O. P. Ottersen, *J. Comp. Neurol.* **205**, 30–48 (1982).
35. M. Fendt, M. S. Fanselow, *Neurosci. Biobehav. Rev.* **23**, 743–760 (1999).
36. S. Melzer *et al*., *Science* **335**, 1506–1510 (2012).
37. M. Remondes, E. M. Schuman, *Nature* **416**, 736–740 (2002).

Acknowledgments: We thank K. Deisseroth (ChR2 and eArch3.0 construct) and E. Boyden (ArchT construct) for providing the plasmids; R. Neve for generating the AAV-DIO-synaptophysin-mCherry; J. Martin, C. Ragion, N. Nayyar, M. Serock, L. Sultzman, M. Ragion, L. Smith, and A. Rivest for experimental help; J. Young, C. Yokoyama, T. Ryan, R. Redondo, X. Liu, and K. Mulroy for comments; and the members of Tonegawa lab for support. This work was supported by the RIKEN Brain Science Institute.

Supplementary Materials

www.sciencemag.org/content/343/6173/896/suppl/DC1
Materials and Methods
Figs. S1 to S17
References

13 August 2013; accepted 18 December 2013
Published online 23 January 2014;
10.1126/science.1244634

Gordon Research Conferences

frontiers of science

2014 "Session II" Meetings will be held between June and August in New England in the United States, and internationally in Italy, Spain, and Hong Kong, China. A list of preliminary programs appears on the following 24 pages. For detailed programs, fees, site/travel information and online application, visit our web site at **www.grc.org**.

Colonies formed by primary human breast epithelial cells expressing the polycomb complex protein Bmi-1. Immunoflourescent staining shows epithelial cells expressing Keratin 18 (red) and Keratin 14 (green). DAPI (blue) stains the nuclei. Courtesy of Stephan Duss and Mohamed Bentires-Alj (Friedrich Miescher Institute for Biomedical Research). Submitted by Mohamed Bentires-Alj, Chair, Mammary Gland Biology GRC. The Mammary Gland Biology GRC will take place June 8-13, 2014 at the Renaissance Tuscany Il Ciocco Resort, Lucca (Barga), Italy.

2014 "Session II" Preliminary Programs

The list of meetings, topics and speakers begins below (discussion leaders, where known, are noted in italics).

*Note: **Gordon Research Seminars (GRS)** are listed in green boxes below their associated Gordon Research Conference, where applicable. Gordon Research Seminars are 2-day meetings that precede an associated GRC, designed for graduate students, post-docs, and other young scientists to present and exchange new data and cutting edge ideas.*

ADVANCED MATERIALS FOR SUSTAINABLE INFRASTRUCTURE DEVELOPMENT

NEW!

Advanced Materials for Sustainable Energy Efficient Buildings
Aug 3-8, 2014
The Hong Kong University of Science and Technology, Hong Kong, China
Chair: Zongjin Li
Vice Chair: Christopher Leung

- **The Scientific Base for Advanced Building Materials at Nanometer Scale** (*S P. Shah* / Karen Scrivener / Baoshan Wang)
- **Nanomechanical Properties of Advanced Materials** (*Ian Richardson* / M.S. Konsta-Gdoutos / Guang Ye / Zhihui Sun)
- **Micromechanics** (*Adnan Ibrahimbegovic* / Henrik Stang / Jiri Nemecek)
- **Heat Insulation Properties of Advanced Materials** (*Daniel Quenard* / Dong Zhang / Yunping Xi)
- **Self Cleaning, Air-Purifying and Low CO_2 Advanced Materials** (*H.J.H. (Jos) Brouwers* / King Lun Yeung / L.E. Yu)
- **Mechanical Properties of Advanced Materials** (*David Lange* / Nemy Banthia / Yamei Zhang / Xiangming Zhou)
- **Durability of Advanced Materials** (*Odd E. Ggjorv* / Pedro Castro Borges / Xinyu Jin)
- **Dimension Stability of Advanced Materials** (*Kamal H. Khayat* / Herbert Zheng / Jun Zhang / Sokhwan Choi)
- **The Application of Advanced Materials** (*Changwen Miao* / Jinguang Teng / Hands Reinhardt)

ATOMIC & MOLECULAR INTERACTIONS

Energy Conversion Processes and Chemical Reactions in Clusters, Solution, Surfaces, Interfaces, and Biological Systems
Jul 13-18, 2014
Stonehill College, Easton, MA
Chair: Sharon Hammes-Schiffer
Vice Chair: Gilbert M. Nathanson

- **Combustion and Renewable Energy** (*Bruce Kay* / Emily Carter / David Chandler / Donald Truhlar)
- **Radicals and Hydrated Electrons** (*Hanna Reissler* / David Bartels / Pavel Jungwirth / Bern Kohler / David Manolopoulos)
- **Dynamics and Reactions in the Condensed Phase** (*Lyudmila Slipchenko* / Chris Cheatum / Michael Fayer / John Herbert)
- **Interactions and Dynamics in Clusters and Molecules** (*Arthur Suits* / Mark Johnson / Anne McCoy / Bill McCurdy / Dan Neumark)
- **Photochemistry and Nonadiabatic Dynamics** (*Spirodoula Matsikis* / Greg Engel / Nancy Levinger / Joseph Subotnik)
- **Interactions and Reactions at Surfaces and Interfaces** (*Rich Loomis* / Anastassia Alexandrova / Giulia Galli / Tim Minton / Hrvoje Petek)
- **Interactions and Reactions in Clusters and Molecules** (*Millard Alexander* / Bob Continetti / Michael Duncan / Krishnan Raghavachari)
- **Photochemistry in Biology and Nanoparticles** (*Todd Martinez* / Christine Aikens / Victor Batista / Leif Hammarstrom / Emily Weiss)
- **Interactions and Dynamics in Biological Systems** (*Marsha Lester* / David Nesbitt / George Schatz / Tim Zwier)

GRS ATOMIC & MOLECULAR INTERACTIONS

Chemical Reactions and Energy Conversion Processes
Jul 12-13, 2014
Chair: Julia H. Lehman
Associate Chair: Bernadette M. Broderick

AUDITORY SYSTEM

Encoding Hearing: From Genes to Behavior
Jul 13-18, 2014
Bates College, Lewiston, ME
Chair: Ruth Anne Eatock
Vice Chair: Stephen G. Lomber

- **Hearing on Different Scales** (Catherine Carr / Jeffrey Holt / Josh McDermott)
- **Making the Inner Ear Work** (Michael Deans / Caroline Wichmann / Ulrich Müller / Carolina Abdala / Bob Carlyon)
- **Plasticity in Adult Hearing** (Mitch Sutter / Larry Roberts / Rich Mooney)
- **Encoding Speech and Song** (Jan Schnupp / Laurel Carney / Frédéric Theunissen / Jonathan Simon)
- **Rocking and Rolling in the Inner Ear** (Dolores Bozovic / Walter Marcotti / Mark Rutherford)
- **Regulating Mechanoelectrical Signals** (Ping Chen / Ebenezer Yamoah / Bechara Kachar / Peter Heil / Dan Tollin)
- **Encoding Self-Motion** (Joe Trapani / Soroush Sadeghi / David Dickman)

- **Encoding Sound Location**
  (Phil Joris / Larry Trussell / Rachel Wilson / Bill Spain / Chris Stecker)
- **Breaking and Making Hearing**
  (Sharon Kujawa / Adrian K.C. Lee / Stefan Heller)

AUDITORY SYSTEM
Encoding Hearing: From Genes to Behavior
Jul 12-13, 2014
Chair: Sean J. Slee
Associate Chair: Catherine Weisz

BACTERIAL CELL SURFACES
Building, Splitting, and Traversing the Cell Surface
Jun 22-27, 2014
Mount Snow Resort, West Dover, VT
Chairs: Yves V. Brun & Lotte Sogaard-Andersen
Vice Chairs: Zemer Gitai & Mariana G. Pinho

- **Cell Wall Biogenesis**
  (Waldemar Vollmer / Andrea Dessen / Matthias Horn)
- **Surface Polymers, Exopolysaccharides and Their Secretion**
  (Nicola R. Stanley-Wall / Lynette Cegelski / P. Lynne Howell / Stephen Trent)
- **Cell Compartmentalization and Protein Localization**
  (Irmgard Sinning / Martin Thanbichler / Nora Ausmees)
- **Motility, Surface Structures and Contact-Dependent Intercellular Activities**
  (John Mekalanos / Dan Kearns / Lori Burrows / David Low)
- **Protein Secretion**
  (Olivera Francetic / Arnold Driessen / Ben Berks)
- **Cell Division and Morphogenesis**
  (Tanneke den Blaauwen / Martin Loose / Jeff Errington / Jie Xiao)
- **Envelope Stress Responses**
  (Carol Gross / Kirsten Jung / Angelika Gründling)
- **Inner and Outer Membrane Biogenesis**
  (Ian Henderson / Ross Dalbey / Tom Silhavy / Susan Buchanan)
- **Transport Across the Cell Envelope**
  (Natalie Strynadka / Colin Kleanthous / Chris Whitfield)

BARRIERS OF THE CNS
Expanding the Understanding of CNS Barriers in Health and Disease
Jun 15-20, 2014
Colby-Sawyer College, New London, NH
Chair: Margareta Hammarlund-Udenaes
Vice Chair: Robert G. Thorne

- **Keynote Session: Keys to Crossing the Blood-Brain Barrier**
  (*Margareta Hammarlund-Udenaes* / Joan N. Abbott / Gert Fricker)
- **Structure and Function of the CNS Barriers**
  (*Stefan Liebner* / Christer Betsholtz / Paula Dore-Duffy / Elisabetta Dejana / Francesca Bosetti)
- **Delivery Strategies to Improve Treatment of CNS Diseases**
  (*Weihong Pan, David E. Smith* / Danica Stanimirovic / Joy Yu Zuchero / Elisa Konofagou)
- **Barriers in Disease**
  (*Helga de Vries, Lester R. Drewes* / Britta Engelhardt / Zena Vexler / Alexandre Prat)
- **Barriers and Fluids of the Brain**
  (*Nathalie Strazielle, Robert Thorne* / Charles Nicholson / Ling Wei / Martha E O'Donnell / Adam Chodobski)
- **Model Systems of CNS Barriers**
  (*Paul Lockman, Maria A. Deli* / Michael Taylor / Roland J. Bainton / Lara Ogunshola / Eric Shusta)
- **Imaging of Brain Barrier Function**
  (*Quentin Smith, Li Di* / Joel S. Pachter / Jeffrey Iliff / Oliver Langer / Katerina Akassoglou)
- **Transporters and Signaling at the Brain Barriers**
  (*David S. Miller, Reina Bendayan* / Margaret S. Bynoe / Masanori Tachikawa / Bjoern Bauer / Irena Loryan)
- **Translational Understanding of Barrier Function and Disease**
  (*William F. Elmquist, Tetsuya Terasaki* / Elizabeth C.M. de Lange / Christopher Shaffer / Mark Schmidt)

BARRIERS OF THE CNS
The Neurovascular Unit: Partners for Life
Jun 14-15, 2014
Chair: Kavi Devraj

BIOANALYTICAL SENSORS
Twenty First Century Technologies for Probing Biological Systems
Jun 22-27, 2014
Salve Regina University, Newport, RI
Chairs: Susan Lunte & Paul S. Cremer
Vice Chairs: Elizabeth Hall & Andre A. Adams

- **Keynote Session: 'Nano-Flares' for the Analysis of Circulating Cancer Cells / The Biocompatibility of Implanted Biosensors**
  (*Paul Cremer* / Chad Mirkin / Buddy Ratner)
- **Biochemical/Biomedical Applications of Microfluidics**
  (*Takehiko Kitamori* / Hubert Girault / Aaron Wheeler / Amy Herr)
- ***In Vivo* Sensing and Analysis**
  (*R. Scott Martin* / Andy Ewing / Julie Stenken / Mark Schoenfisch)
- **Mass Spectrometry Based Sensing**
  (*Andre Adams* / Lingjun Li / Richard Caprioli / Milan Mrksich / Amanda Hummon)
- **Sensing at Interfaces**
  (*Zeev Rosenzweig* / Rick Van Duyne / Rob Corn / Craig Aspinwall)
- **Nanomaterial Platforms**
  (*Lisa Hall* / Shana O. Kelley / Yi Lu / Tosh Chilkoti / Susan Daniel)
- **Optical Sensors**
  (*Steve Soper* / Duncan Graham / Bob Dunn / Darryl Bornhop)
- **New Analytical Separation Platforms**
  (*Emmanuel Carrilho* / Mary Wirth / Lisa Holland / Frank Gomez / Scott Phillips)
- **Young Investigator Presentations**
  (*Susan Lunte* / Chris Easley / Tiffany Matthews / Michael Heien)

BIOANALYTICAL SENSORS
Sensor Development & Field Applications
Jun 21-22, 2014
Chair: John T. Connelly
Associate Chair: Kristina L. Roskos

BIOCATALYSIS
Changing Paradigms in Catalysis
Jul 6-11, 2014
Bryant University, Smithfield, RI
Chairs: Joelle N. Pelletier & Oliver May
Vice Chairs: John M. Woodley & Gjalt W. Huisman

- **Keynote Session: Enyzme Engineering - From Fundamentals to Applications**
  (*Joelle Pelletier* / Frances H. Arnold)
- **Synthetic Biology**
  (*Claudia Schmidt-Dannert* / Rebecca Goss / Elmar Heinzle)
- **The Impact of Disruptive Technologies on Biocatalysis**
  (Andreas Schmid / Toby Richardson)
- **Fundamental Science in Biocatalysis**
  (*David Berkowitz* / Dorothy Kern / José Manuel Sanchez-Ruiz / Jürgen Pleiss)
- **Advancing Science Through Flagship Programs**
  (*Oliver May* / Robert Lortie / Anton Glieder / David Berkovitz)
- **Novel Chemistry and Enzymes**
  (*Gjalt Huisman* / Isabel Arends / Harald Gröger)
- **Food, Feed and Materials Applications**
  (*Anton Glieder* / Adrienne Huston Davenport / Georg Gübitz)
- **Fine Chemical and Pharma Applications**
  (*Jeffrey C. Moore* / Zhanglin Lin / Matthew Truppo / Robert DiCosimo)
- **Enzyme Engineering**
  (*Nicholas J. Turner* / Oscar Alvizo / Daniela Grabs)

BIOCATALYSIS
Changing Paradigms in Catalysis
Jul 5-6, 2014
Chair: Maria T. Gundersen
Associate Chair: Maximilian Ebert

BIOELECTROCHEMISTRY
Cellular and Organismal Responses to Endogenous and Exogenous Fields
Jul 6-11, 2014
University of New England, Biddeford, ME
Chair: David A. Dean
Vice Chair: Marie-Pierre Rols

- **Role of Electric Fields in Development and Aberrant Growth**
  (*Danny Adams* / Mike Levin / Mustafa Djamgoz)
- **Effects of Voltage Gradients and Endogenous Fields on Wound Healing and Cell Migration**
  (*Ann Rajneicek* / Min Zhao / Cindi Morshead)
- **Field Sensing**
  (Petra Bolte / David Robert / Sarah Stamper)
- **Responses of Intracellular Components to Electric Fields**
  (*Frank Hart* / Robert Gatenby / Nicholas Minc / William Ristenpart)
- **Nanopores**
  (Mounir Tarek / Marija Drndic)
- **Pore-Inducing Methods for Gene Transfer**
  (*Pernille Hojman* / Frank Gunn-Moore / Mark Jaroszeski / Shawna Shirley)
- **Mechanisms of Electroporation**
  (*Damijan Miklavcic* / Rafi Korenstein / Rumiana Dimova)
- **Plasma and Internal Membrane Electroporation**
  (*Raphael Davalos* / Jim Weaver / Boris Rubinsky)
- **Electroporation-Mediated Gene Delivery - New Concepts**
  (*Marie-Pierre Rols* / Richard Heller / Maja Cemezar)

BIOELECTROCHEMISTRY
Towards Understanding and Mastering the Effects of Endogenous and Exogenous Electric Fields on Biological Cells
Jul 5-6, 2014
Chair: Aude Silve
Associate Chair: Bostjan Markelc

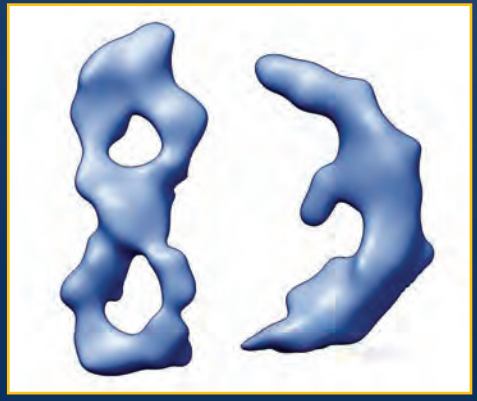

Supercoiled 336 bp DNA minicircles spell out "83" to commemorate the 83rd year of the Gordon Research Conferences. Courtesy of Rossitza N. Irobalieva, Jonathan M. Fogg, Daniel J. Catanese, Jr., Anna Barker, Michael F. Schmid, Wah Chiu, and Lynn Zechiedrich (Baylor College of Medicine). Submitted by Anthony Maxwell, Chair, DNA Topoisomerases in Biology & Medicine GRC.

BIOGENIC HYDROCARBONS & THE ATMOSPHERE

Interactions in a Changing World
Jun 29 - Jul 4, 2014
Melia Golf Vichy Catalan Business & Convention Center, Girona - Costa Brava, Spain
Chairs: Allison L. Steiner & Janne Rinne
Vice Chairs: Todd N. Rosenstiel & Thomas Karl

- **Global Change and Biogenic Hydrocarbons: From Global to Cellular**
  (*Russ Monson* / Ranga Myneni / Ian Galbally)
- **Biogenic Hydrocarbon Response to Biotic and Abiotic Stresses**
  (*Sue Owen* / Jonathan Gershenzon / Dorothea Tholl / Maaria Rosenkranz)
- **Changing Plant Functions Under Global Change**
  (*Josep Penuales* / Joanna Joiner / Ulo Niinemets)
- **Biogenic Hydrocarbons and Changing Ecosystems**
  (*Silvano Fares* / Peter Curtis / Gannet Haller / Riika Rinnan)
- **Biogenic Hydrocarbons and Changing Land Use**
  (*Kirsti Ashworth* / Evan DeLucia / Martin Graus)
- **Aerosol Formation from Biogenic Hydrocarbons in a Changing Climate**
  (*Marianne Glasius* / Scot Martin / Nadine Unger / Michael Boy)
- **Young Investigator Presentations**
  (*Todd Rosenstiel, Thomas Karl*)
- **The Oxidation of Biogenic Hydrocarbons in a Changing Atmosphere**
  (*Jose Fuentes* / Delphine Farmer / May Fu / Thomas Mentel)
- **Synthesis: Biogenic Hydrocarbons from the Old to the New World**
  (*Christine Wiedinmyer* / Almut Arneth / Alex Guenther)

BIOINSPIRED MATERIALS

Exploiting Biological Concepts and Strategies in Functional Synthetic Materials
Jun 22-27, 2014
Sunday River Resort, Newry, ME
Chair: Phillip B. Messersmith
Vice Chair: Timothy J. Deming

- **Glycomimetics**
  (Laura Kiessling / Katharina Ribbeck)
- **Peptide Mimetics**
  (Sam Stupp / Dennis Discher / Shaoyi Jiang)
- **Immunomaterials**
  (*Evan Scott* / Jeff Hubbell / Joel Collier)
- **Mechanics of Biological Materials and Mineralized/ Hybrid Materials**
  (*LaShanda Korley* / Lara Estroff / Daniel Morse / Markus Buehler)
- **DNA Assemblies**
  (*Jennifer Cha* / Chad Mirkin / Hanadi Sleiman)
- **Polypeptides, Engineered Proteins and Protein Assemblies**
  (Jianjun Cheng / Ashutosh Chilkoti / Roman Jerala)
- **Peptides and Polymers at Interfaces**
  (*Aaron Lau* / Rajesh Naik / Haeshin Lee)
- **Bioinspired Synthetic Polymers**
  (*Phil Messersmith* / Zhibin Guan / Kazuhiko Ishihara)
- **Catechols / Catecholamines / Polyphenols**
  (*Niels Holten-Andersen* / Aranzazu del Campo / Frank Caruso)

GFS BIOINSPIRED MATERIALS

Better Materials via Biological Blueprints
Jun 21-22, 2014
Chair: Hyun Ok Ham
Associate Chair: Benjamin D. Almquist

BIOINTERFACE SCIENCE

Engineered Biomolecular Interfaces
Jun 15-20, 2014
Renaissance Tuscany Il Ciocco Resort, Lucca (Barga), Italy
Chair: Stefan Zauscher
Vice Chair: Atul N. Parikh

- **Biointerface Design Challenges for Synthetic Cellular Interfaces**
  (*Christine Keating* / Jeff Brinker / Madan Rao)
- **Synthetic Cells and Interfaces**
  (*Sebastien Leccomandeaux* / Dan Hammer / Wolfgang Meier / Jan v.Hest)
- **Cell-Material Interface**
  (*Jeff Karp* / Chris Chen / Molly Stevens)
- **Progress in Nanopores: Diagnostics and Information Exchange**
  (Cees Dekker / Hagan Bailey / Aleksei Aksimentiev)
- **Engineering "Smart" Biointerfaces**
  (*Chris Bettinger* / Joanna Aizenberg / Noo Li Jeon)
- **Progress in Biosurface Imaging**
  (*Peter Jönsson* / Jürgen Plitzko / Stefan Hell / Mary Kraft)
- **Wiring Up Biology**
  (*Caroline Ajo-Franklin* / Charles Lieber)
- **New Biointerfacial Diagnostics and Design**
  (*Scott Phillips* / Ashutosh Chilkoti / Jay Groves / Carsten Werner)
- **Perspectives**
  (*Atul Parikh* / Luigi Luisi)

GFS BIOINTERFACE SCIENCE

Towards Constructing the Biological Interface
Jun 14-15, 2014
Chair: Julie-Anne Gandier
Associate Chair: Christian Zafiu

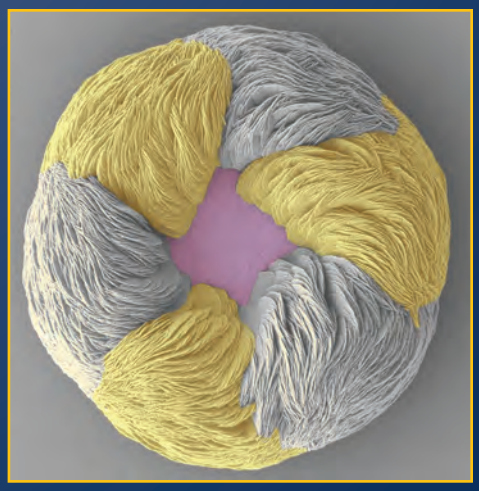

Pseudocolored image of coiled and aligned vaterite tablets (calcium carbonate mineral) organized hierarchically into discoidal chiral suprastructures as formed by the chiral activity of a small biomolecule. Courtesy of Wenge Jiang and Marc McKee. Submitted by Marc McKee, Chair, Biomineralization GRC.

BIOMINERALIZATION

Where Geology Meets Biology: The Inorganic-Organic Interface
Aug 17-22, 2014
Colby-Sawyer College, New London, NH
Chair: Marc D. McKee
Vice Chair: Nico A.J.M. Sommerdijk

- **Biomineral Nucleation and Growth**
  (R. Lee Penn / Pupa Gilbert / Fiona Meldrum)
- **Intracellular Biomineralization**
  (Nils Kroger / Colin Brownlee / Arash Komeili)
- **Biomineralization in Marine Invertebrates**
  (Dorrit Jacob / Paul Falkowski / Sylvie Tambutte)
- **Regulation of Biomineralization in Marine Invertebrates**
  (Bernard Degnan / Frederic Marin / Giuseppe Falini)
- **Protein/Peptide Structural Biology Regulating Biomineralization**
  (Peter Tompa / Graeme Hunter / John Evans)
- **Computational Simulations of Biomineralization Processes**
  (Jeffrey Gray / Nita Sahai / John Harding)
- **Transgenic Mouse Models for Understanding Normal and Pathologic Biomineralization**
  (James Simmer / Beate Lanske / Monzur Murshed)
- **Mineralized Material Properties and Bioinspired Materials**
  (Philipp Thurner / Peter Fratzl / Wolfgang Tremel)
- **Co-Evolution of the Geo- and Biospheres**
  (Linda Kah / Robert Hazen [keynote])

GFS BIOMINERALIZATION

A Multidisciplinary Science at the Interface of Biology, Medicine and Engineering
Aug 16-17, 2014
Chair: Sergio Bertazzo
Associate Chair: Betty Hoac

BIOORGANIC CHEMISTRY

Global Challenges in the 21st Century
Jun 8-13, 2014
Proctor Academy, Andover, NH
Chairs: Michael D. Burkart & Stacie Canan
Vice Chairs: Michelle Arkin & Violeta L. Marin

- **Modern Approaches to Antibacterials**
  (*Paramjit Arora* / Deb Hung / Clif Barry / Natalie Strynadka)
- **The Diversity of Natural Products**
  (*Bill Wuest* / Chaitan Khosla / Carole Bewley)
- **Carbohydrates in Life and Medicine**
  (*Amanda Hargrove* / Ben Davis / Linda Hsieh-Wilson)
- **Lessons from Protein Structure/Function**
  (*George Zheng* / Jamie Williams / Seok-Yong Lee)
- **Challenges of Non-Traditional Drug Discovery**
  (*Eli Wallace* / Eric Rubin / Charlie Mowbray)
- **Innovation in Drug Discovery**
  (*Jim Kiefer, Nick Skelton* / Siegfried Reich / Peter Senter)
- **New Targets for Therapeutic Development**
  (*Jay Schneekloth* / Andreas Gosberg / Byron DeLaBarre / Dewey McCafferty)
- **Approaches to Molecular Diagnostics**
  (*Krishna Kumar* / Craig Lindsley / Scott Phillips)
- **Global Health**
  (*Jerry Zeldis* / Jeremy Burrows / Carl Nathan / Dave Matthews)

BIOPOLYMERS

Mechanisms of Biomolecular Interactions: From Physical Principles to Biological Insights
Jun 1-6, 2014
Salve Regina University, Newport, RI
Chair: Ivet Bahar
Vice Chair: Harald Schwalbe

- **Keynote Session: Biomolecular Machinery, Signaling and Regulation**
  (*Harald Schwalbe* / John Kuriyan / Andrej Sali)
- **Biomolecular Complex Formation, Oligomerization and Assembly**
  (*Shoshana Wodak* / Gidon Schreiber / Holger Stark / Sarah Woodson)
- **Structural Dynamics of Membrane Proteins: From Single Molecules to Cell Interactions**
  (*Benoit Roux* / Tamir Gonen)
- **Membrane Transport: Structures, Dynamics and Mechanisms**
  (*Gary Rudnick* / Lucy Forrest / Olga Boudker)
- **Allosteric Modulation of Function by Substrate / Ligand Binding**
  (Poul Nissen / Stephen Blacklow)
- **Protein-Drug Interactions: From Molecular Docking to Systems Pharmacology**
  (*Andy McCammon* / Brian Shoichet)

- **Detection of Conformational Changes and Mechanisms of Function**
  (*Robert Jernigan* / Robert Sauer / Yann Chemla)
- **Design and Evolution**
  (Tanja Kortemme / Sarah Teichmann / Nikolay Dokholyan)
- **Misfolding and Aggregation**
  (*Teresa Head-Gordon* / John Straub / Patricia Clark)

CARDIAC REGULATORY MECHANISMS
Bridging the Gap Between Cardiac Pathological Discovery and Clinical Application
Jun 8-13, 2014
Colby-Sawyer College, New London, NH
Chairs: Mark E. Anderson & Walter J. Koch
Vice Chairs: Bjorn C. Knollmann & Barbara Casadei

- **New Technologies and Methods to Aid in Cardiac Studies**
  (*Steve Houser, PeiPei Ping* / Dietmar Kappes / Heping "Peace" Cheng / Don Bers)
- **iPS Cells: A Window on Human Myocardial Biology and Disease**
  (*Rongli Liao, Ju Chen* / Thomas Eschenhagen / Sean Wu / Andre Terzic / Nikhil Munshi)
- **Right Heart Failure, Pulmonary Hypertension and Diastolic Heart Failure**
  (*David Kass, Wen Chen* / Evangelos D. Michelakis / Joseph Metzger / LongShen Song)
- **Mitochondrial Ca^{2+} and Ion Channels**
  (*Tom Shannon, Jon Lederer* / Robert Dirksen / Brian O'Rourke / Madesh Muniswamy / Shey-Shing Sheu)
- **Novel Roles and Regulation of microRNAs in the Heart**
  (*Joseph Hill, Thomas Force* / Chad Grueter / Don Menick / Stefanie Dimmeler / Yibin Wang)
- **Mitochondrial Metabolism in Physiology and Disease**
  (*Robert Balaban, Jun Sadoshima* / Rong Tian / Dale Abel / Asa Gustafsson / Gerald Dorn)
- **What is New and Exciting in Ca^{2+} and Ion Channels?**
  (*Karin Sipido, David Eisner* / Jeff Molkentin / Mukash Jain / Bjorn Knollman)
- **Novel Signaling Pathways in Heart Disease**
  (*Barbara Casadei, Pete Mohler* / Maria Kontaridis / Joan Heller Brown / Tish Murphy / Burns Blaxall)
- **iPSCs for Modeling Inherited Cardiomyopathies**
  (*Mark Sussman* / Joseph Wu)

GRS CARDIAC REGULATORY MECHANISMS
New Approaches to Cardiac Research
Jun 7-8, 2014
Chair: Shirin Doroudgar
Associate Chair: Jerry Curran

CATALYSIS
From Art to Science
Jun 22-27, 2014
Colby-Sawyer College, New London, NH
Chair: John R. Regalbuto
Vice Chair: Christopher L. Marshall

- **Keynote Session: Science in Catalyst Development**
  (*Jeff Bricker* / David Thompsett)
- **Understanding and Designing Oxides and Carbon**
  (*Juliette Blanchard* / Lisa Pfefferle / Mayfair Kung / Umit Ozkan)
- **Metal Nanoparticle Thermodynamics**
  (*Mike Wong* / Laurence Marks / Oana Malis)
- **Rational Synthesis of Supported Metal Nanoparticles**
  (*Petra de Jongh* / John Monnier / Catherine Louis / Mike Reynolds)
- **Computations for Mechanistic Understanding and Catalyst Design**
  (*Mike Janik* / Dion Vlachos / Randall Meyer)
- **State of the Art Characterization Methods**
  (*Ilke Arslan* / Jeff Miller / Renu Sharma / Maureen Bricker)
- **The Art of Surface Science**
  (*Rob Rioux* / Donna Chen / Martin Sterrer)
- **Understanding Catalytic Reactivity**
  (*Carsten Sievers* / Eduardo Wolf / Friederike Jentoft / Jane Cheng)
- **Keynote Session: Continuing the Transformation of Catalysis Art into Science**
  (*Harold Kung* / Krijn de Jong)

CELL BIOLOGY OF THE NEURON
Mechanistic Insight into Neuronal Development, Plasticity, Disease and Regeneration
Jun 22-27, 2014
Waterville Valley Resort, Waterville Valley, NH
Chairs: Graeme W. Davis & Nils Brose
Vice Chairs: Thomas L. Schwarz & Claudia Bagni

- **Keynote Session: Genetics and Genomics, from Neuron to Behavior**
  (*Graeme Davis* / Catherine DuLac / Yuh-Nung)
- **Developmental Mechanisms**
  (*Esther Stoeckli* / Madeline Lancaster / Xiaowei Zhuang / Esther Stoeckli / Beth Stevens)
- **Protein Trafficking**
  (*Erika Holzbaur* / Volker Haucke / Robert Edwards / Erika Holzbaur)
- **Neurotransmitter Release**
  (*Christian Rosenmund* / Takeshi Sakaba / Christian Rosenmund / Erik Jorgensen / Matthijs Verhagen)
- **Cellular Physiology**
  (*Tim Ryan* / Tom Schwarz / Ryohei Yasuda / Tim Ryan)
- **Neural Plasticity**
  (*Gina Turrigiano* / Lu Chen / Susumu Tomita / Gina Turrigiano / Kelsey Martin)
- **Models of Disease**
  (*Claudia Bagni* / Claudia Bagni / Mike Ehlers / Anirvan Ghosh)
- **Degeneration and Regeneration**
  (*Yishi Jin* / Barris Bingol / Aaron Gitler / Mark Freeman / Yishi Jin)
- **Glia / Keynote Session: The Synaptic Vesicle Fusion Machine**
  (*Nils Brose* / Klaus Nave / Tom Sudhoff)

CELL DEATH
Cell Death Mechanisms at the Interface of Health and Disease
Jun 8-13, 2014
Mount Snow Resort, West Dover, VT
Chair: Eric H. Baehrecke
Vice Chair: Henning Walczak

- **Keynote Session: Repurposing the Death Machine / Interplay Between Regulators of Apoptosis and Necroptosis**
  (*Doug Green* / John Abrams / Vishva Dixit)
- **Cell Signaling, Survival and Death**
  (*Joan Brugge* / Hao Wu / Sally Kornbluth / Seamus Martin)
- **Mitochondria and Cell Death**
  (*Sally Kornbluth* / Marie Hardwick / Andreas Strasser)
- **Apoptotic Linchpins**
  (*Domagoj Vucic* / Pascal Meier / Marion MacFarlane / Guy Salvesen)
- **Clearance of Dying Cells**
  (*John Abrams* / Kodi Ravichandran / Francesca Peri / Will Wood / Shige Nagata)
- **Cell Survival and Death in Cancer**
  (*Huseyin Mehmet* / Kevin Ryan / Joan Brugge / Ricky Johnstone / Gerry Melino / Anthony Letai)
- **Cell Survival and Death in the Nervous System**
  (*Marie Hardwick* / Richard Youle / Beth Stevens / Marc Freeman)
- **Non-Apoptotic Death Pathways**
  (*Guy Salvesen* / Junying Yuan / Michael Overholtzer / Sudan He / Zhirong Shen / Christine Watson)
- **Programmed Necrosis and Inflammation**
  (*Junying Yuan* / Francis Chan / John Silke / Doug Green)

CELL POLARITY SIGNALING
NEW!
Cell Polarity
Jun 1-6, 2014
Bentley University, Waltham, MA
Chair: Linda Van Aelst
Vice Chair: Ian G. Macara

- **Stem Cells**
  (*Margaret Fuller* / Juergen Knoblich / Fiona Watt)
- **Cell Polarity in Development**
  (*Monica Gotta* / Fumio Motegi/ Buzz Baum / David Bilder)
- **Mechanisms of Polarization**
  (*Crislyn D'Souza-Schorey* / Barry Thompson / Alan Hall / Orion Weiner)
- **Polarity, EMT, and Cancer**
  (*Zena Werb* / Senthil Muthuswamy / Tsukasa Shibue / Valerie Weaver)
- **Neuronal Polarity**
  (*Mary E. Hatten* / Silvia Cappello / Frank Polleux)
- **RNA Localization, Differential Inheritance of DNA and Centrosomes, Aging**
  (*Matthew Gibson* / Fabrice Caudron / Songhai Shi / Anne Ephrussi)
- **Vesicle Traffic and Cell Polarization**
  (*Ulrich Tepass* / Keith Mostov / Enrique Rodriguez-Boulan)
- **Planar Cell Polarity and Tissue Morphogenesis**
  (*Yohanns Bellaiche* / Jennifer Zallen / Aron Jaffe / Lila Solnica-Krezel)
- **Polarity and the Primary Cilium**
  (*Tim Stearns* / Benjamin Margolis / Peter Jackson)

CELLULAR & MOLECULAR FUNGAL BIOLOGY
Fungal Biology from the Integrated Perspective of Molecular Mechanisms, Systems and Evolution
Jun 15-20, 2014
Holderness School, Holderness, NH
Chairs: Jennifer Lodge & James B. Anderson
Vice Chairs: Amy S. Gladfelter & Natalia N. Requena

- **Secretion and Growth**
  (Alexandra Brand / Meritxell Riquelme / Barbara Valent / Arturo Casadevall)
- **Genome Dynamics and Expression**
  (*Brendan Cormack* / Jason Slot / Mark Farman / Judy Berman / Nicolas Corradi)
- **Fungi in Plant, Animal, and Environmental Microbiomes**
  (*Christina Cuomo* / Betsy Arnold / Betsy Arnold / Georgina May)
- **Sensing, Signaling, and Development (in Host-Pathogen Interactions)**
  (*Joe Heitman* / Rosa Ruiz-Vazquez / Leah Cowen / Xiaorong Lin / Luis Corrochano / Gregory Jedd)
- **Late-Breaking Topics**
  (*Amy Gladfelter, Natalia Raquena*)
- **Systems Biology**
  (*Maitreya Dunham* / Jennifer Loros / Audrey Gasch / Christian Landry / Al Brown / Rachel Brem / Charlie Boone)
- **Fungal Degradation of Plant Macromolecules and Bioenergy**
  (*Dan Cullen* / Jonathan Walton / Bernard Henrissat / Louise Glass / Emma Master)
- **Organismal Interactions**
  (*Brett Tyler* / Shiv Kale / Wenbo Ma / Claire Veneault / David Hughes / Elaine Bignell)
- **Evolutionary and Population Genomics**
  (*Antonis Rokas* / John Taylor / Tim James / Chris Hittinger / Eva Stukenbrock)

CENTROMERE BIOLOGY
NEW!
The Genomics and Epigenomics of Centromere Function and Dysfunction
Jul 27 - Aug 1, 2014
Bentley University, Waltham, MA
Chair: Rachel J. O'Neill
Vice Chair: Beth A. Sullivan

- **Keynote Session: Centromere Genomics**
  (*Michael Freitag* / Jiming Jiang / Karen Hayden-Miga / Hiroshi Masumoto / Steve Henikoff [keynote])

- **Centromere Organization and Dynamics**
  (*Don Cleveland* / Gary Karpen / Lars Jansen / Barbara Mellone / Dan Foltz)
- **Cenp-A Nucleosomes and Centromere Structure**
  (*Gary Karpen* / Ben Black / Don Cleveland)
- **Coordination of Essential Centromeric Domains**
  (*Lars Jansen* / Kristen Scott / Robin Allshire / Bill Sullivan / Kaustuv Sanyal)
- **Building the Centromere/Kinetochore**
  (*Arshad Desai* / Kerry Bloom / Munira Basrai / Ian Cheeseman)
- **Synthetic, *De Novo* and Ectopic Centromeres**
  (*Bill Earnshaw* / Tatsuo Fukagawa / Vladimir Larionov / Jim Birchler / Aaron Straight)
- **Centromeres, Transcription and RNAs**
  (*Patrick Heun* / Arshad Desai / Kelly Dawe / Yamini Dalal)
- **Centromeres: Comparative Studies and Evolution**
  (*Karen Hayden-Miga* / Mario Rocchi / Lucia Carbone / Michael Freitag / Harmit Malik)
- **Variant Centromeres**
  (*Ben Black* / Patrick Heun / Judy Berman / Bill Earnshaw)

CERAMICS, SOLID STATE STUDIES IN
Challenges Around Transport and Reactivity in Ceramics
Jul 20-25, 2014
Mount Holyoke College, South Hadley, MA
Chair: Monika Backhaus-Ricoult
Vice Chair: Michael J. Hoffmann

- **Keynote Session: Defects, Transport and Reactivity in Constrained Ceramics or Electrochemical Devices**
  (*Carol Handwerker* / Joachim Maier / Sossina Haile)
- **Structure, Defects and Transport at Grain Boundaries, Interfaces and Surfaces**
  (*Greg Rohrer* / Roger de Souza / Patrick Cantwell / Dominique Chatain)
- **Ceramics Under Large and/or Coupled Driving Forces**
  (Igor Lubomirsky)
- **Charge Transfer and Transport in Ceramics for Capacitive or Memristive Storage**
  (Jennifer Rupp / Bruce S. Dunn / Yury Gogotsi)
- **Carrier and Phonon Transport in Thermoelectric Materials**
  (*Dmitri Kossakovski* / Gang Chen / Anke Weidenkaff)
- **Assessment of Exchange Processes by *In-Situ* Studies and/or Modeling**
  (*Mogens Mogensen* / Venkat Visnarathan / Bilge Yildiz / Sergei Kalinin)
- **H-conduction in Ceramics and Energy-Related Devices**
  (*Sangtae Kim* / John Irvine / Saiful Islam)
- **Exchange Processes and Transport in Li- and Na-Batteries and Their Challenges**
  (*Linda Nazair* / Jürgen Janek / Nancy Dudney / Ryoji Kanno / Edwin Garcia)
- **Keynote Session: Semiconductor Physics of α-Al_2O_3 - Defect Chemistry and Fermi Level**
  (*Monika Backhaus* / Arthur Heuer)

CHEMOTACTIC CYTOKINES
Positioning Cells in Immunity and Disease
Jul 27 - Aug 1, 2014
Mount Snow Resort, West Dover, VT
Chair: Andrew D. Luster
Vice Chair: Tracy M. Handel

- **Keynote Session: Dissecting Immune Cell Navigation Control Using Systems Methods and *In Vivo* Imaging**
  (*Andrew Luster* / Ron Germain)
- **Chemokine Gradient Sensing**
  (*Ronen Alon* / Michael Sixt / Carol Parent / Holger Knaut / Darren Gilmour)
- **Chemokines in Innate Immunity**
  (*Ann Richmond* / G. Scott Worthen / Steffen Jung / Reinhold Forster)
- **Chemokines in Adaptive Immunity**
  (*Joshua Farber* / Federica Sallusto / Frances Lund / Adrian Erlebacher / Dan Littman)
- **Regulation of Chemokine Function**
  (*Tracy Handel* / Gerry Graham / Antal Rot / Benjamin Doranz)
- **Chemokines in Inflammatory Diseases**
  (*Amanda Proudfoot* / Tom Schall / Jose-Carlos Gutierrez-Ramos / Ziad Mallat / Wolfgang Wenniger)
- **Chemokines in Infectious Diseases**
  (*Phil Murphy* / Akiko Iwasaki / Stefan Kaufmann / Thomas Gebhardt)
- **Chemokines in Cancer**
  (*Alberto Mantovani* / Fran Balkwill / Mihaela Skobe / Naofomi Mukaido / Bodduluri Haribabu)
- **Chemokines in CNS Function and Disease**
  (*Sergio Lira* / Richard Ransohoff / Robyn Klein / Marie-Eve Tremblay)

GRS **CHEMOTACTIC CYTOKINES**
New Frontiers in Chemokine Research
Jul 26-27, 2014
Chair: Joanna R. Groom
Associate Chair: Clive S. McKimmie

CHROMATIN STRUCTURE & FUNCTION
Regulation of Chromatin Assembly and Genome Functions
Jun 8-13, 2014
Bentley University, Waltham, MA
Chair: Shiv Grewal
Vice Chair: Wendy Bickmore

- **Nucleosomes and Chromatin Dynamics**
  (*Geeta Narlikar* / Genevieve Almouzni / Steve Henikoff / Dinshaw Patel / Karolin Lugar)
- **Chromatin Remodeling**
  (*Anja Groth, Bob Kingston* / Carl Wu / Craig Peterson / Frank Pugh / Brad Cairns / Geeta Narlikar)
- **Chromatin Modifications**
  (*Barbara Meyer, Steve Henikoff* / David Allis / Jerry Workman / Ali Shilatifard / Steve Buratowski)
- **Chromatin-Mediated Gene Regulation**
  (*Genevieve Almouzni, Ali Shilatifard* / Bob Kingston / Danny Reinberg / Shelley Berger / Jurg Muller)
- **Specialized Chromatin Domains**
  (*Susan Gasser, Brad Cairns* / Barbara Meyer / Yasushi Hiraoka / Julie Cooper / Robin Allshire)
- **RNA-Mediated Shaping of Chromatin and Heterochromatin Assembly**
  (*Julie Cooper, Steve Jacobsen* / Howard Chang / Jeanie Lee / Julius Brennecke)
- **DNA Methylation, Chromatin and Development**
  (*Jeanie Lee, Howard Chang* / Steve Jacobsen / Eric Selker / Kristian Helin / Ken Zaret)
- **Chromatin Changes During DNA Replication and Repair**
  (*Karolin Lugar, Brad Cairns* / Toshi Tsukiyama / Iestyn Whitehouse / Anja Groth)
- **Chromosome Architecture**
  (*Wendy Bickmore, Toshi Tsukiyama* / Nick Gilbert / Bing Ren / Bas van Steensel / Susan Gasser)

CO_2 ASSIMILATION IN PLANTS: GENOME TO BIOME
Gaining Insights from Evolution to Mitigate a Challenging Future
Jun 8-13, 2014
Waterville Valley Resort, Waterville Valley, NH
Chairs: David T. Hanson & Christoph Peterhaensel
Vice Chairs: Stephen P. Long & Martha Ludwig

- **Photosynthesis and Atmospheric Change**
  (*Stephen Long* / Graham Farquhar / Carl Bernacchi)
- **Real-World Dynamics of Photosynthesis**
  (*Dayle McDermitt* / Jeremy Harbinson / Ulo Niinemets / Alistair Rogers / Danielle Way)
- **Control of Carbon Metabolism**
  (*Thomas Sharkey* / Stephanie Arrivault / Guillaume Tcherkez)
- **Environmental and Structural Control of Rubisco Activity**
  (*Manajit Hayer-Hartl* / Elizabete Carmo-Silva / George Espie / Rebekka Wachter / Spencer Whitney)
- **Engineering Photosynthesis for Food and Fuel Security**
  (*Stephen Schrader* / Thomas Brutnell / Christine Raines)
- **Balancing More Carbon with Less Water**
  (*Ichiro Terashima* / Asaph Cousins / David Granot / Yu Tanaka / Robert Teskey / Nerea Ubierna)
- **Photosynthate, Where Does It Go?**
  (*Robert Turgeon* / Abhijit Karve / Michael Knoblauch / Sanna Sevanto)
- **Evolution and Harnessing of CCMs for Higher Yield**
  (*Tammy Sage* / Murray Badger / Anne Borland / Pascal-Antoine Christin / Peter Westhoff)
- **CO_2 Assimilation Through Time**
  (*Martha Ludwig* / Jennifer McElwain / David Beerling [keynote])

GRS **CO_2 ASSIMILATION IN PLANTS: GENOME TO BIOME**
Integrating Processes in Photosynthesis
Jun 7-8, 2014
Chair: Sarah Covshoff
Associate Chair: Justin McGrath

COLLOIDAL SEMICONDUCTOR NANOCRYSTALS
NEW!
From Fundamental Physics to Functional Materials
Jul 20-25, 2014
Bryant University, Smithfield, RI
Chair: Emily A. Weiss
Vice Chair: Delia J. Milliron

- **Keynote Session: The Versatility of Quantum Dots**
  (*David Watson* / Moungi Bawendi / Edward Sargent)
- **Bio-Applications and Biocompatibility**
  (*Xiaohu Gao* / Sandra Rosenthal / Vincent Rotello / Vicki Colvin / Igor Medintz / Jessica Winter)
- **Self-Assembled Systems and Materials**
  (*Kevin Ryan* / J. Alexander Liddle / Thomas Basché / Y. Charles Cao)
- **Photophysics and Blinking**
  (*Vanessa Huxter* / Jennifer Hollingsworth / Pat Kambhampati / Stephen Leone / Dan Oron / Marcus Jones)
- **Synthesis and Surface Characterization**
  (*Christopher Murray* / Liberato Manna / Zeger Hens / Jonathan Owen)
- **Energy Conversion and Charge Transport**
  (*Will Tisdale* / Alexander Eychmüller / Gordana Dukovic / Seth Coe-Sullivan / Mark Lusk / Justin Johnson)
- **Magnetically Active Systems**
  (*Ken Knappenberger* / Dong Hee Son / Xiaosong Li / Geoffrey Strouse)
- **Non-Traditional Materials and Properties**
  (*Janet McDonald* / Geoff Ozin / Seokwoo Jeon / Brian Korgel / Liang-shi Li / Andrea Tao)
- **Keynote Session: Structure-Function Relationships**
  (*Horst Weller* / Mark Green / Richard Robinson / A. Paul Alivisatos)

COMPLEX ADAPTIVE MATTER
NEW!
Towards a Unifying Perspective of Emergent Complexity
Jul 13-18, 2014
The Chinese University of Hong Kong, Hong Kong, China
Chair: Robert H. Austin
Vice Chair: Leihan Tang

- **Keynote Session: How Can Information Control Matter?**
  (Nigel Goldenfeld / Sriram Ramaswamy)
- **Origins of Complexity: The Ur-Cell**
  (Paul Chaikin / Krastan Blageov)
- **The Emergence of Complexity in Biology**
  (Chao Tang / Mukund Thattai)
- **Making Active Matter Adaptive**
  (Peter Hoffmann)
- **Bacteria as Adaptive Computers**
  (Yuhai Tu / Erwin Frey)
- **The Emergence of Computation in Biological Systems**
  (Bill Bialek)
- **Re-Thinking the Emergence of Diseases**
  (Ping Ao / Michael Demm)

- **The Emergence of Death**
  (Hao Li / Szymon Kaczanowski)
- **Keynote Session: Physical Principles of Complexity in Biology**
  (Eshel Ben-Jacob / Paul Davies)

COMPUTATIONAL CHEMISTRY

Accuracy and Sampling Across Quantum Chemistry and Molecular Modeling
Jul 20-25, 2014
Mount Snow Resort, West Dover, VT
Chair: Jay W. Ponder
Vice Chair: Adrian J. Mulholland

- **Keynote Session: The Future of Molecular Simulation & Quantum Chemistry**
  (William Jorgensen / Peter Gill)
- **Accurate Free Energy Calculations**
  (*Pengyu Ren* / J.C. Gumbart / Wei Yang / Carol Post)
- **NMR-Related Calculations**
  (*David Case* / Teresa Carlomagno / Robert Best / Douglas Turner)
- **Modeling Biomolecule-Membrane Interactions**
  (*Benoit Roux* / Alan Grossfield / Yi Wang / Carmen Domene)
- **Status of DFT & Other Low-Cost Wavefunction Methods**
  (*Gustavo Scuseria* / Eric Neuscamman / Donald Truhlar / Stefan Grimme)
- **Modeling of Protein pKa Values**
  (*Nathan Baker* / Jens Nielsen / Charles Brooks III)
- **Community-Assisted Distributed Computing**
  (*Vijay Pande* / Rhiju Das / Gianni De Fabritiis)
- **Methods for Treatment of Transition Metals**
  (*Clark Landis* / Angela Wilson / Robert Deeth / Laura Gagliardi)
- **Coarse-Grained & Multi-Scale Modeling**
  (*Gregory Voth* / Cecilia Clementi / Siewert-Jan Marrink / Christian Holm)

GRS COMPUTATIONAL CHEMISTRY

Enhancing Prediction and Design of Physical Systems Through Computational Chemistry
Jul 19-20, 2014
Chair: Deborah A. Penchoff
Associate Chair: Nicholas Leioatts

CONDUCTIVITY & MAGNETISM IN MOLECULAR MATERIALS

NEW!

Understanding and Controlling Emergent Properties
Aug 3-8, 2014
Bates College, Lewiston, ME
Chair: John Schlueter
Vice Chair: James S. Brooks

- **Modeling Molecular Systems**
  (*Roser Valenti* / Judith Howard / Jesper Bendix)
- **Molecule-Based Conductors**
  (*Lahcene Ouahab* / Hatsumi Mori / Jens Mueller / Takako Konoike)
- **Nanostructures**
  (*Concepcio Rovira* / Carmen Herrmann / Petro Maksymovych)
- **Magnetic Coordination Polymers**
  (*Steve Hill* / Jamie Manson / Paul Goddard / Tom Lancaster)
- **Organic Radicals**
  (*Richard Oakley* / Kunio Awaga / Steve Winter)
- **Photo-Induced Effects**
  (*Janice Musfeldt* / Corine Mathoniere / Isabelle Malfant / Lapo Bogani)
- **Charge Order**
  (*Stuart Brown* / Shinichori Iwai / Peter Lundenheimer)
- **Superconductivity**
  (*Steve Blundell* / Erio Tosatti / Tadashi Kawamoto)
- **Spin Liquids**
  (*Kazushi Kanoda* / Ben Powell / Satoshi Yamashita)

CORRELATED ELECTRON SYSTEMS

Textures, Topology, and Strong Interactions
Jun 22-27, 2014
Mount Holyoke College, South Hadley, MA
Chairs: N Peter Armitage & Joerg Schmalian
Vice Chairs: Peter M. Abbamonte & Joel E. Moore

- **Heavy Fermions Meet Topology**
  (*Piers Coleman* / Victor Galitski / Jing Xia / Satoru Nakatsuji)
- **Correlations in Strong Spin-Orbit Coupled Systems**
  (*Yong-Baek Kim* / Leon Balents / Roser Valenti / Radu Coldea / Hide Takagi)
- **Correlations at Oxide Interfaces**
  (*Alexander Brinkman* / Jochen Mannhart / Kathryn Moler / Shahal Ilani)
- **Non-Equilibrium Quantum Matter**
  (*Joe Orenstein* / Andrea Cavalleri / Gil Refael / Brian DeMarco / Nuh Gedik)
- **New Approaches to Understanding Mott-Ioffe-Regel Limit Violation**
  (*Nigel Hussey* / Dmitri Basov / Gabi Kotliar / Sean Hartnoll)
- **New Approaches to New Materials**
  (*Hai-Hu Wen* / Tyrel McQueen / Kyle Shen / Rebecca Flint / Hari Manoharan)
- **Is the Cuprate Pseudogap a Broken Symmetry State?**
  (*Sudip Chakarvarty* / Philippe Bourges / Andrew J. Millis / Aharon Kapitulnik)
- **Nematic States in Correlated Systems**
  (*Andrey Chubukov* / Subir Sachdev / Steve Kivelson / Ian Fisher / Yuji Matsuda)
- **Skyrmions in Correlated Materials**
  (*Naoto Nagaosa* / Christian Pfeiderer / Naoya Kanazawa / Achim Rosch)

GRS CORRELATED ELECTRON SYSTEMS

Correlated Electrons *In Extremo*: Frustration, Topology, and Ultrafast Dynamics
Jun 21-22, 2014
Chair: Matthew S. Foster

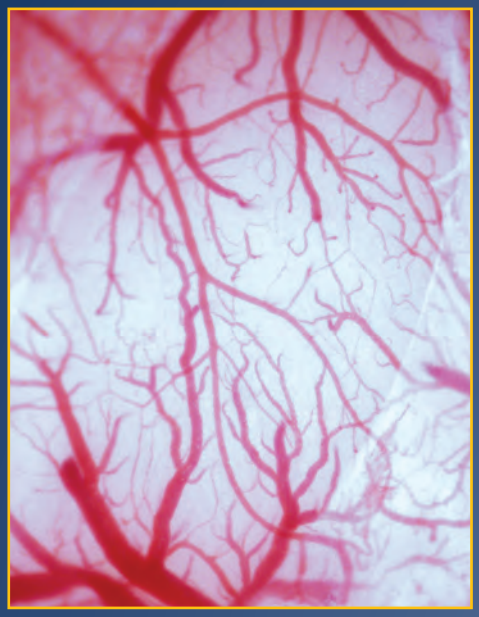

Image obtained through an open cranial window in an anesthetized, adult rat showing the numerous blood vessels overlying the somatosensory cortex of the brain. After penetrating the brain's surface, arteries and arterioles divide and ramify extensively, giving rise to the brain's capillary network where blood-borne chemicals are screened and selectively shielded from brain entry by specialized central nervous system (CNS) barriers. Courtesy of D.J. Wolak and R.G. Thorne (University of Wisconsin-Madison). Submitted by Margareta Hammarlund-Udenaes, Chair, Barriers of the CNS GRC.

CORROSION - AQUEOUS

Tools and Techniques for Corrosion Assessment
Jul 13-18, 2014
Colby-Sawyer College, New London, NH
Chair: Narasi Sridhar
Vice Chair: Sannakaisa Virtanen

- **Smart Coatings**
  (*Rudy Buchheit* / Michael Rohwerder / Mario Ferreira)
- **Environmentally Assisted Cracking - Test Techniques and Predictive Methods**
  (*Ramgopal Thodla* / Peter Andresen / Stefan Ritter / Richard Gangloff)
- **Localized Corrosion - Mechanisms and Techniques**
  (*Nick Birbilis* / Geraint Williams / Ricardo Carranza / Gareth Hinds)
- ***In-Situ*/*Ex-Situ* Analytical Techniques**
  (*Jamie Noël* / Alison Davenport / Philippe Marcus / Benedetto Bozzini)
- **Localized Corrosion in CO_2 and H_2S Environments**
  (*Roger Newman* / David Williams / Andre Anderko / Anne Neville)
- **Biochemical Interactions at Electrodes**
  (*Brenda Little* / Damien Feron / César Torres / Jason Lee)
- **Infrastructure**
  (*Yves Van Ingelgem* / Alberto Sagüés)
- **Atomic-Scale Measurement and Modeling**
  (Michael Francis / Santanu Chaudhuri)
- **How Do We Reduce Corrosion Risks?**
  (*Sannakaisa Virtanen* / Roger Staehle / John Beavers / Richard Woollam)

GRS CORROSION - AQUEOUS

Tools and Techniques for Corrosion Assessment
Jul 12-13, 2014
Chair: Yves Van Ingelgem
Associate Chair: Robert M. Asmussen

CRYSTAL ENGINEERING

Form Meets Function
Jun 1-6, 2014
Waterville Valley Resort, Waterville Valley, NH
Chairs: Christer Aakeroy & Mike J. Zaworotko
Vice Chair: Adam Matzger

- **From Structure to Function in Molecular Solids**
  (*Eric Bosch* / Fraser Stoddart / Jerry Atwood)
- **Intermolecular Interactions; Theory and Practice**
  (*Bill Pennington* / Chris Hunter / T.N. Guru Row / Giuseppe Resnati)
- **Coordination Polymers**
  (*Ian Williams* / M.W. Hosseini / Davide Proserpio)
- **Assembly of Cocrystals and Other Multicomponent Molecular Solids**
  (*Andrew Bond* / Duncan Bruce / Len MacGillivray / Tong-Bu Lu)
- **Metal Organic Frameworks: Separation and Storage**
  (*Tomislav Friščic* / Mohamed Eddaoudi / M.P. Suh)
- **Metal Organic Frameworks: Reactivity and Catalysis**
  (*Hemamala Karunadasa* / Neil Champness / J.J. Vittal)
- **Nucleation and Crystal Growth**
  (*Jen Swift* / Allan Myerson / Mike Ward / Nicola Pinna)
- **Crystallographic Databases, Crystal Structure Prediction and Polymorphism**
  (*Aurora Cruz-Cabeza* / Neil Feeder / Tonglei Li)
- **Pharmaceutical Aspects of Crystal Engineering**
  (*Susan Reutzel-Edens* / Scott Childs / Eric Munson / Jane Li)

GRS CRYSTAL ENGINEERING

Mechanochemistry and Solid-State Reactivity: State of the Art
May 31 - Jun 1, 2014
Chair: Dejan-Kresimir Bucar

CYCLIC NUCLEOTIDE PHOSPHODIESTERASES

Signaling Regulation in the Pathogenesis and Treatment of Disease
Jun 1-6, 2014
Mount Holyoke College, South Hadley, MA
Chairs: Manuela Zaccolo & Nickolas J. Brandon
Vice Chairs: Rodolphe P. Fischmeister & David Kass

- **Keynote Session: A Novel Paradigm in cAMP Signal Transduction - GPCR Signaling from Endosomes** (M. von Zastrow)
- **CNS - Movement Disorders** (*Jim O'Donnell* / Jim Surmeier / Chris Schmidt / Tony West / Francesca Fusco)
- **CNS - Cognition** (*Arjan Blokland* / Jos Prickaerts / Robbert Havekes / Holger Rosenbrock / Arjan Blokland)
- **Cyclic Nucleotide Signalling and Cardiac Disease** (*Don Maurice* / David Kass / Don Bers / John Scott / Julia Gorelik / Kjetil Tasken)
- **Regulation of cAMP Signalling in the Cardiovascular System** (*Rodolphe Fischmeister* / Veronique Leblais / Tanya Mayadas / Delphine Mika)
- **PDE Inhibitors in On-Going Clinical Trials** (*Miles Houslay* / Peter Schafer / Domenico Spina / Larry Wennogle / Kurt Jarnagin)
- **Phosphodiesterases and Gene Defects** (*Marco Conti* / Caroline Silve / Eamonn Sheridan)
- **Phosphodiesterases and Cancer** (*Adam Lerner* / Rajkumar Savai / Jun Yang / Nicholas Dumaz / George Baillie)
- **PDE: New Avenues to Drug Design** (*Frank Menniti* / Rick Cote / Patsy Babbitt / Jay Pandit)

GRS CYCLIC NUCLEOTIDE PHOSPHODIESTERASES

Novel Paradigms in Cyclic Nucleotide Signaling
May 31 - Jun 1, 2014
Chair: Lindsay Wilson
Associate Chair: Nadiia Rozmaritsa

DEFECTS IN SEMICONDUCTORS

Power, Efficiency, and Functionality
Aug 3-8, 2014
Bentley University, Waltham, MA
Chair: Christian M. Wetzel
Vice Chair: Martin Brandt

- **Organic Semiconductors** (Bob Street / Alan J. Drew)
- **Graphene and Like Materials** (Mildred Dresselhaus / Ian Sharp)
- **Oxides, Functional, and Semiconducting** (Darrell Schlom / Ed Seebauer / Wladek Walukiewicz / Keith McKenna / Bruno Meyer)
- **Wide Bandgap Nitride for Efficiency** (Akira Uedono / Volkmar Dierolf / Benjamin Hourahine / Anelia Kakanakova / Andrew Armstrong / Rachel Oliver)
- **Silicon Carbide for Power** (Bengt Svensson / Izabela Szlufarska / Pat Lenahan)
- **Elemental and Compound Semiconductor for Cost** (Joerg Weber / Robert Kudrawiec / Nick Cowern / Uwe Gerstmann)
- **Magnetics for Functionality** (Alberta Bonanni / Hannes Raebiger)
- **Direct Defect Imaging** (Sven Rogge / K.V. Lakshmi)
- **Materials for Photovoltaics** (Steve Ringel / Minjoo Lee / Yanfa Yan)

GRS DEFECTS IN SEMICONDUCTORS

From Fundamental Concepts to Practical Implications
Aug 2-3, 2014
Chair: Audrius Alkauskas
Associate Chair: Mark T. Durniak

DIFFRACTION METHODS IN STRUCTURAL BIOLOGY

Faster, Smaller, Better: Novel Technologies for Diffraction Experiments in Molecular Biology and Drug Discovery
Jul 27 - Aug 1, 2014
Bates College, Lewiston, ME
Chair: Anastassis Perrakis
Vice Chair: Edward Snell

- **Structures for Understanding Cell Biology** (*Ana Gonzales* / John Kuriyan / Randy Read)
- **X-Ray Free Electron Lasers on the Move** (*Ilme Schlichting* / Henry Chapman / Graeme Winter / Aina Cohen)
- **New Instruments and Ideas for Diffraction Experiments** (*Thomas Schneider* / Gwyndaf Evans / Bob Fischetti / Flora Meilleur)
- **Growing Crystals for the New Generation Experiments** (*Janet Newman* / John Hunt / Michael Duszenko / Jose Antonio Marquez)
- **From Diffraction Data to Density Maps** (*Paul Adams* / Clemens Vonrhein / Airlie McCoy / Brent Nannenga)
- **From Density Maps to Structural Models** (*Zbyszek Dauter* / Tom Terwilliger / Garib Murshudov / Gerard Kleywegt / Paul Emsley)
- **Scattering Methods** (*Dmitri Svergun* / Peter Zwart / Michael Hammel / Lois Pollack)
- **New Cool Methods and Hot New Structures** (*Elspeth Garman*)
- **Structural Biology Accelerating Drug Development** (*Lisa Keefe* / Gary Gilliland / Aydnan Achour / Giovanna Scapin)

GRS DIFFRACTION METHODS IN STRUCTURAL BIOLOGY

Towards Integrative Structural Biology
Jul 26-27, 2014
Chair: Jeffrey J. Headd
Associate Chair: Maike Bublitz

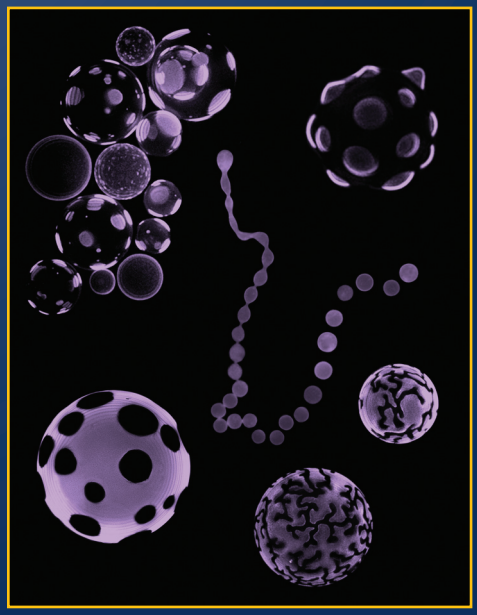

Active, flexible, and dynamic interfaces of vesicular compartments exhibit dramatic transformations in shape, topology, and domain organization in single populations in response to subtle ambient-phase perturbations as revealed by fluorescence microscopy. The physical mechanisms underlying these shape changes reflect an interplay between membrane elasticity, pressure differential across the vesicular compartments, and changes in tension at the membrane surface. Courtesy of Kamila Oglęcka, Rachel Kraut, Bo Liedberg, and Atul N. Parikh. Submitted by Stefan Zauscher, Chair, Biointerface Science GRC.

DNA TOPOISOMERASES IN BIOLOGY & MEDICINE

NEW!

From Molecular Structure to Drug Targeting
Aug 10-15, 2014
Sunday River Resort, Newry, ME
Chair: Anthony Maxwell
Vice Chair: Mary-Ann Bjornsti

- **Keynote Session: The Scope and Diversity of DNA Topoisomerases** (*Tao Hsieh* / James Champoux / Patrick Forterre)
- **DNA Topology** (*Andrzej Stasiak* / David Levens / Lynn Zechiedrich / Sarah Harris)
- **Topoisomerase Structure and Mechanism** (*Stewart Shuman* / James Berger / Alfonso Mondragon)
- **Nano-Manipulation of DNA Topoisomerases** (*Nynke Dekker* / Zev Bryant / Dagmar Klostermeier / Keir Neuman)
- **Topoisomerases as Targets for Anti-Bacterial Agents** (*Ben Bax* / Yuk-Ching Tse-Dinh / Mark Fisher)
- **DNA Topoisomerases in Cancer Chemotherapy** (*Yves Pommier* / Renate Griffith / Nei-Li Chan / Neil Osheroff)
- **DNA Topoisomerases and Human Health** (*Mary-Ann Bjornsti* / Scott Kaufman / Ed Yeh)
- **DNA Topoisomerases and DNA Damage** (*John Nitiss* / Keith Caldecott / Alessandro Vindigni / Sue Jinks-Robertson)
- **Topoisomerases and Genomic Stability** (*Hannah Klein* / Scott Keeney / Rodney Rothstein)

DRUG CARRIERS IN MEDICINE & BIOLOGY

Leveraging Mechanism and Chemical Design for Improved Therapeutic Effect
Aug 17-22, 2014
Waterville Valley Resort, Waterville Valley, NH
Chairs: Heather D. Maynard & Paul A. Burke
Vice Chairs: Paula T. Hammond & Jan E. Schnitzer

- **Drug Carriers - Transforming Medicine Now and in the Future** (*Phil Low* / Jim Baker / Krystof Bankiewicz)
- **Trafficking Mechanisms, Intracellular Uptake & Transport of Drug Carriers** (*Ruth Duncan* / Marino Zerial / Kirsten Sandvig / Gerald Wong / Warren Chan)
- **Nanoengineered Systems for Targeted Cancer Therapy** (*Sasha Kabanov* / Dane Wittrup / Kit Lam / Jesus Gonzalez)
- **Vaccine Carriers, Mucosal Barriers and Immunotherapy** (*Vlad Muzykantov* / David Mooney / Melody Schwartz / Darrell Irvine / Dan Peer)
- **Engineered Protein Delivery Systems and Protein Materials** (*Pat Stayton* / Steven Schwendeman / Matt Francis / Omolola Eniola Adefeso)
- **Emerging Polymeric Systems** (*Joe DeSimone* / Karen Wooley / Molly Stevens / Frank Caruso / Maria Vicent)
- **Late-Breaking Topics / Young Investigator Presentations** (*Jan Schnitzer, Paula Hammond*)
- **Targeted Systems for Imaging & Theranostic Applications / RNA Delivery for Therapeutic and Vaccine Applications** (*Theresa Reineke* / Ick Chan Kwon / Michelle Bradbury / Laura Sepp-Lorenzino / Andrew Geall)
- **Ocular Delivery** (*Patrick Hughes* / Tejal Desai / David Schaffer / Uday Kompella)

GRS DRUG CARRIERS IN MEDICINE & BIOLOGY

Molecular and Cellular Engineering Advances in Drug Targeting
Aug 16-17, 2014
Chair: Jonathan T. Sockolosky
Associate Chair: Caitlin Decker

DRUG METABOLISM
Integrating Drug Metabolism Sciences: From Enzymology to Systems Biology
Jul 6-11, 2014
Holderness School, Holderness, NH
Chair: Kenneth R. Korzekwa
Vice Chair: Michael A. Zientek

- **Keynote Session: Integrating Knowledge to Predict Drug Disposition and Toxicity - Is a Broader Perspective Needed?** (*Ken Korzekwa* / Kim Brouwer)
- **Drug Transporters: Approaches Toward an Increased Understanding of Their Roles in Drug Development** (*Xiaoyan Chu* / Swati Nagar / Hiroshi Kusuhara / Steven H Wright / Maciej Zamek-Gliszczynski)
- **Cell Biology and Physiology of the Liver** (*Gus Rosania* / Susanne Keiding / Gus Rosania)
- ***In Vivo* to Biomimetic Systems for the Study of Cytochrome P450: Simple and Complex Systems Compliment Each Other** (*Jeff Jones* / Jeff Jones / Roland Wolf / Emily Scott)
- **New Technologies** (*Aaron Moss* / Richard Caprioli/ Norm Dovichi / Aaron Moss)
- **Translational Modelling - From Protein to the Whole Body Pharmacokinetics** (*Aleksandra Galetin* / Aleksandra Galetin / Kazuya Maeda/ Jörg König / Jash Unadkat)
- **Young Investigator Presentations** (*Henry Strobel*)
- **Expanding Our View: Systems Biology of Drug Metabolism** (*Melissa Kemp* / Melissa Kemp / Lang Li / Ian Blair)
- **Do Small Molecule ADME Studies Translate to Large Molecules?** (*Donald Tweedie* / Dan Rock / Andy Boswell)

DRUG RESISTANCE
An Interdisciplinary Approach to Tackling Drug Resistance Across Disease States
Jul 13-18, 2014
Sunday River Resort, Newry, ME
Chairs: Amy C. Anderson & Marie-Pierre De Bethune
Vice Chairs: Manuel A. Navia & Sally Blower

- **A Global Perspective on the Drug Resistance Problem** (Pradipsinh Rathod / Jean Patel)
- **Evolution of Drug Resistance** (*Peg Riley* / Gerard Wright / Alan Perelson / Celia Schiffer)
- **Understanding and Overcoming Chronic Resistance** (Kim Lewis / Sreenath Sharma)
- **Designing Drugs to Overcome Resistance** (*Lynn Silver* / Erin Duffy / Min Jiang / Robert Bonomo)
- **Emerging Resistance** (*Michael Nailor, Jeffrey Aeschlimann* / Evan Snitkin / Daniel Zurawski)
- **The Evolution of New Drug-Resistant Populations** (*Manuel Navia* / Michael Pfaller / Carlos Borroto Nordelo / Jeffrey Scott)
- ***In Vitro*/*In Vivo* Modeling of Resistance** (*Jared Silverman* / David Hooper / Jennifer Leeds)
- **Genomic Profiling in Drug Resistance** (David Rogers / Edison Liu)
- **Resistance at the Molecular Level** (*Norton Peet* / Jennifer McKimm-Breschkin / John Manchester)

DRUG SAFETY
NEW!
Bridging the Divide Between Pre-Clinical and Clinical Drug Safety
Jun 1-6, 2014
Stonehill College, Easton, MA
Chair: David E. Watson
Vice Chairs: Thomas Schroeter & Michael Forstner

- **Keynote Session: Bioengineering Systems Analysis of Drug Reactions** (Doug Lauffenburger)
- **Chemical Biology: Merging Computational Chemistry and Systems Biology** (*Stephen Burley* / Jeremy Jenkins/ Michael Keiser/ Jeffrey Sutherland)
- **Use of Stem Cells as Models for Drug Toxicity** (*Kyle Kolaja* / Matt Peters/ Ed LeClyuse)
- **Tissue Architecture: Development of 3D Cell-Culture Models to Predict Organ Toxicities** (*Tony Bahinski* / Kit Parker / Uwe Marx)
- **Translational Safety - What Value are Non-Clinical Models?** (*David Jacobson-Kram* / James L. Stevens / Jill Steidl / Thomas Hartung)
- **Clinical Drug Toxicity** (*Ruth Roberts* / Richard Knight / Scott Henry)
- **Novel Biomarkers of Drug Toxicity** (*Warren Glaab*)
- **Pharmacovigilance: Drug Toxicity Issues Post-Launch** (Andrew John Bate / Israel Guttierez)
- **Keynote Session: Drug Safety, Human Genetics, and Tailored Therapeutics - The Path Ahead** (*Magnus Ingelman-Sundberg* / Stephen Evans)

ELECTRODEPOSITION
Electrochemical Materials Synthesis and Applications
Jul 27 - Aug 1, 2014
University of New England, Biddeford, ME
Chair: Kyoung-Shin Choi
Vice Chair: Olaf Magnussen

- **Keynote Session: New Avenues for Electrodeposition** (*Thomas Moffat* / Daniel Mandler / Wolfgang Schmickler)
- **Electrocatalysis** (*Giovanni Zangari* / Thomas Jaramillo / Jay Switzer / Andy Gewirth)
- **In-Depth Understanding of Electrodeposition** (*Elizabeth Podlaha-Murphy* / Philippe Allongue / Bridget Murphy)
- **Solar Energy Conversion** (*Stephan Maldonado* / Daniel Esposito / Raj Rajeshwar / Kevin Sivula)
- **Nucleation and Growth of Metals** (*Alan West* / Rohan Akolkar / John Stickney)
- **Electrodeposition for Energy Storage Application** (*Daniel Abraham* / Sherley Meng / Sang Bok Lee / Nikhilendra Singh)
- **Late-Breaking Topics** (*Olaf Magnussen*)
- **Nanostructures and Contacts** (*Daniel Schwartz* / Reginald Penner / Karen Kavanagh / Partik Schmuki)
- **Novel Use of Electrodeposition** (*Stanko Brankovic* / Mircea Dincă / Mike Zach)

ELECTRON DONOR-ACCEPTOR INTERACTIONS
Understanding and Manipulating Electron and Energy Transfer Processes
Aug 3-8, 2014
Salve Regina University, Newport, RI
Chairs: David H. Waldeck & C. Michael Elliott
Vice Chairs: Natia L. Frank & Dirk M. Guldi

- **Molecular Junctions** (*Latha Venkataraman* / David Cahen / Mark Ratner / Thomas Wandlowski)
- **Magnetic and Spin Effects** (*Lin Chen* / Christoph Boehm / Ron Naaman / Ulrich Steiner)
- **Proteins and Electron Transfer** (*David Beratan* / Marcus Elstner / Dmitry Matyushov / Antoni Vlcek / Christophe Leger)
- **Electron and Energy Transfer in Metal Redox Systems** (*Claudia Turro* / Catalina Achim / James McCusker / David McMillin)
- **Dye-Sensitized Solar Cells** (*Elena Gallopini* / Curtis Berlinguette / Juan Bisquert / Joseph Hupp)
- **New Strategies for Solar Energy Conversion** (*Arthur Nozik* / Marc Baldo / Felix Castellano / Victor Klimov / Matthew Law)
- **Coupled Electron Transfer Processes** (*Geoffrey Hutchison* / Etsuko Fujita / Thomas Miller / Daniel Nocera)
- **Electron and Energy Transfer in Nanoscale Systems** (*Gerald Meyer* / Yan Liu / Thuc-Quyen Nguyen / Gary Rumbles / Cherie Kagan)
- **Keynote Session: New Frontiers in Electron Donor-Acceptor Interactions** (*Ana Moore* / Michael Wasielewski)

GRS **ELECTRON DONOR-ACCEPTOR INTERACTIONS**
Electron Transfer Events for Energy Conversion and Storage
Aug 2-3, 2014
Chair: Yang Wang
Associate Chair: Megan S. Lazorski

ENDOTHELIAL CELL PHENOTYPES IN HEALTH & DISEASE
Endothelial Pathogenic Pathways: Challenges and Opportunities for Translation
Jul 6-11, 2014
Melia Golf Vichy Catalan Business & Convention Center, Girona - Costa Brava, Spain
Chair: S. Ananth Karumanchi
Vice Chair: Victoria L. Bautch

- **Keynote Session: Targeting Vascular Metabolism - Principles and Strategies** (Peter Carmeliet)
- **Gas and Lipids in Vasculature** (*Asif Ahmed* / Tim Hla / Bill Sessa / Dipak Panigraphy / Rui Wang)
- **Vascular Permeability in Health and in Disease** (*Samir Parikh* / Asrar Malik / Susan Quaggin / Samir Parikh)
- **Novel Endothelial Signaling Pathways** (*Christiana Ruhrberg* / John Greenwood / Guillermo Garcia-Cardena / Christiana Ruhrberg / Ralf Adams)
- **Building and Maintaining Blood Vessels** (*Merv Yoder* / Mike Simons / Eli Keshet / Merv Yoder)
- **The Endothelium in Cardiovascular Diseases** (Zoltan Arany / Joey Granger / Yuri Millner / Ed Conway)
- **Ocular Vasculopathies: Molecular Mechanisms and Targeted Therapies** (*Jayakrishna Ambati* / Jayakrishna Ambati / Richard Lang / Lois Smith / Bala Ambati)
- **Angiogenesis in Tumor Biology** (*Laura Benjamin* / Laura Benjamin / Gabrielle Bergers / Kari Alitalo)
- **Keynote Session: Targeting Vascular Morphogenesis and Maturation** (*Victoria Bautch* / David Cheresh / Elisabetta Dejana)

GRS **ENDOTHELIAL CELL PHENOTYPES IN HEALTH & DISEASE**
Basic and Translational Aspects of Endothelial Cell Biology
Jul 5-6, 2014
Chair: John C. Chappell

ENERGETIC MATERIALS
Forward Thinking: New Approaches, Concepts, and Paradigms Towards Understanding and Predicting EM Response
Jun 15-20, 2014
Sunday River Resort, Newry, ME
Chair: Leanna M.G. Minier
Vice Chair: Nick Glumac

- **Science Underlying EM Ignition and Initiation: Critical Physical and Chemical Phenomena** (*Eric Welle* / Margo Greenfield / Ryan Wixom)
- **Engineering Next-Generation EM: Synthesis, Morphological Control and New Techniques** (*Michael Hiskey* / Alan De Hope)

- **Chemical Reactions Controlled by Organized Complexity - Seeking New Fundamental Concepts** (*Richard Behrens* / Michael Lindsay)
- **Advancing Measurements of Dynamic & Reactive EM Phenomena for Discovery & Model Validation** (*Colin Pulham* / Joseph Hooper / Keith Nelson / Joe Zaug)
- **Identifying and Characterizing Critical Material/ Physical Properties Underlying EM Performance (Safety, Sensitivity, Reliability, Behavior)** (*Jim Parker* / Darla Thompson / Scott Jackson)
- **Detonation Theory & Modeling: Advances in Modeling Physics Across Multiple Scales** (*Jennifer Jordan* / Ralph Chamberlain / Min Zhou / Matei Radulescu)
- **Advances in Theoretical and Computational Techniques for Predicting EM Properties Behavior** (*Al Stern* / Betsy Rice / Jean-Bernard Maillet)
- **Combustion Theory, Phenomena, and Modeling: Building Our Understanding of Physics Across Scales** (*Clifford Bedford* / Lori Groven / Dave Adams)
- **Overview of Needs in EM R&D for Global Issues** (*Ruth Doherty* / Jimmie Oxley)

GFS ENERGETIC MATERIALS
The Influence of Microstructure on Performance
Jun 14-15, 2014
Chair: Paul Specht
Associate Chair: Michael Clemenson

ENVIRONMENTAL SCIENCES: WATER
Environmental Sciences in a Human-Impacted World
Jun 22-27, 2014
Holderness School, Holderness, NH
Chair: Paul G. Tratnyek
Vice Chair: Allison MacKay

- **Human-Altered Landscapes** (*Diane McKnight* / Peter Groffman / George Hornberger)
- **Biogeochemistry of Marine Systems** (*Bettina Voelker* / Colleen Hansel / Dagmar Woebkin / George Luther III)
- **Unconventional Contaminants** (Karen Lavendar / Thomas Bucheli)
- **Analytical Tools for Probing Environmental Processes** (*Howard Fairbrother* / Sam Arey / André Simpson / Peter Vikesland)
- **Drinking Water Quality** (*Bill Cooper* / Charlie Werth / Tamar Kohn)
- **Interfacial Processes** (Catherine Peters / David Richardson)
- **Environmental Epigenetics** (*Carlos Sonnenschein* / Bruce Blumberg / Janine LaSalle)
- **Science-Based Decisions** (*Bill Arnold* / Ed Kolodziej / Werner Brack / Janet Hering)
- **Communicating Important Environmental Science**

GFS ENVIRONMENTAL SCIENCES: WATER
Science Ahead of the Game: Linking Fundamental Science to Applied Problems
Jun 21-22, 2014
Chair: Jennifer Guelfo
Associate Chair: Peter A. Maraccini

ENZYMES, COENZYMES & METABOLIC PATHWAYS
Enzymic Catalysis in Health and Disease
Jul 13-18, 2014
Waterville Valley Resort, Waterville Valley, NH
Chairs: Paul R. Thompson & Walter L. Fast
Vice Chairs: Giovanni Gadda & Mark S. Hixon

- **Phosphorylation and Disease** (John Kozarich / Kevin Dalby / Jin Zhang)
- **Metalloenzyme Mechanisms** (Marty Bollinger / Amy Rosenzweig / Peter Tipton)
- **Enzymes and Metabolism in Cancer** (Stefan Gross / Linda Hsieh-Wilson)
- **Chromatin Modifying Enzymes** (Philip Cole / Robert Copeland / Carol Fierke / Chris Schofield)
- **Nucleic Acid Enzymology** (Chuan He / Kenneth Johnson / Ron Raines)
- **Mechanisms and Inhibitor Development** (Jim Wells / Irene Lee / Lizbeth Hedstrom)
- **Mechanisms of Antibiotic Resistance** (Gerry Wright / Suzanne Walker / John Blanchard)
- **Natural Product Biosynthesis** (Jon Thorson / Helen Blackwell)
- **Frontiers of Enzymology** (Vern Schramm / Don Hilvert)

FLOW & TRANSPORT IN PERMEABLE MEDIA
Understanding Micro-Scale Physics, and Translation to Larger Scales
Jul 6-11, 2014
Bates College, Lewiston, ME
Chair: Hamdi A. Tchelepi
Vice Chair: Rainer Helmig

- **Recovery from Unconventional Resources** (Tadeusz Patzek / Gunter Siddiqi)
- **Subsurface Characterization and Flow Modeling** (Inga Berre / Olaf Cirpka)
- **Pore-Scale Reaction Dynamics** (Martin Blunt / Amir Raoof)
- **Modeling Reactive Transport in Large-Scale Systems** (Ilenia Battiato / Alexandre Tartakovsky / Carl Steefl)
- **Uncertainty Quantification** (Jef Caers / Alberto Guadagnini)
- **Coupled Flow Dynamics** (Jerome Neufeld / Jan Vanderborght / Philip Binning)
- **Moving Across Scales: Pore-to-Continuum Representations** (Mohammad Piri / Matthew Balhoff)
- **Pore-Scale Representation and Modeling** (Daniel Tartakovsky / Masha Prodanovic / Dorthe Wildenschild)
- **Flow and Transport in Bio-Systems** (Kent-Andre Mardal / Dominik Obrist)

GFS FLOW & TRANSPORT IN PERMEABLE MEDIA
Fluid-Solid Coupling in Permeable Media
Jul 5-6, 2014
Chair: Christopher W. MacMinn
Associate Chair: Xiaochen Wang

FRAGILE X AND AUTISM-RELATED DISORDERS
Progress and Struggles in Translating Scientific Advances into Human Therapy
Jun 1-6, 2014
Mount Snow Resort, West Dover, VT
Chair: Jennifer C. Darnell
Vice Chair: Michael R. Tranfaglia

- **Keynote Session: Insights from Fragile X Syndrome, the Leading Single Gene Cause of Autism** (David L. Nelson)
- **The Molecular Basis of Autism and Fragile X Syndrome: Key Players at the DNA, RNA and Protein Level** (*David L. Nelson* / Brian O'Roak / Steven Warren / Neelroop Parikshak / Joel Richter)
- **The Cellular Basis of Cognition and Behavior** (*Len Kaczmarek* / Carlos Portera-Cailliau / Peter Kind / Kimberly M. Huber)
- **Challenges in Translating Results from Models to Human Therapy** (Michael Tranfaglia / Elizabeth Berry-Kravis / David Hessl / Christopher McDougle)
- **Clinical Trials of Targeted Treatments** (*Elizabeth Berry-Kravis* / Paul Wang / Jeffrey Neul)
- **Models for FXS and Autism and Their Application** (Jacqueline Crawley / Xinyu Zhao / Flora Vaccarino)
- **Synaptic Plasticity and Circuits** (*Peter Kind* / Vitaly Klyachko / Pavel Osten / Andrés Ozaita)
- **New Approaches and Therapy** (*Michael Tranfaglia* / Gül Dölen / Emily Osterweil / Mark Zylka)
- **Dysregulated Protein Expression and Neurologic Disease** (*Joel Richter* / Eric Klann / Damon Page / Mustafa Sahin / Cristina Alberini)

GFS FRAGILE X AND AUTISM-RELATED DISORDERS
Engineering the Building Blocks of Translational Research
May 31 - Jun 1, 2014
Chair: Aditi Bhattacharya

FUEL CELLS
Technological Progress and New Scientific Insights
Aug 3-8, 2014
Bryant University, Smithfield, RI
Chairs: Peter N. Pintauro & Elena R. Savinova
Vice Chairs: Adam Z. Weber & Plamen Atanassov

- **Electric Vehicles: Will Fuel Cells Regain Market Shares from Battery Vehicles?** (*Harry Hoster* / Byung Ki Ahn / Tobias Brunner / Lance Atkins)
- **Catalysis** (*Peter Strasser* / Hiroyuki Uchida / Jonah Erlebacher / Ulrike Kramm)
- **Meso-Scale Architectures for Fuel Cell Electrodes and MEAs** (*Steven Holdcroft* / Di-Jia Liu / Stephen Marsh / Shawn Litster)
- **Multi-Scale Modeling** (*Yu Morimoto* / Ryosuke Jinnouchi / Michael Eikerling / Andrei Kulikovsky)
- **Membranes** (*Wen Liu* / Deborah Jones / Kirt Page / Klaus-Dieter Kreuer)
- **Alkaline Fuel Cells** (*Shimshon Gottesfeld* / Michael Hickner / Takenori Isomura / Miles Page)
- **MEA Durability** (*Hubert Gasteiger* / Vijay Ramani / Karren More)
- **Regenerative Fuel Cells and Flow Batteries** (*Trung Nguyen* / Karen Waldrip / Jun Liu / Maria Skyllas-Kazacos)
- **Keynote Session: Global Energy Perspective** (*Elena Savinova, Peter Pintauro* / Nate Lewis)

GFS FUEL CELLS
From Fundamentals to Practical Applications
Aug 2-3, 2014
Chair: Cenk Gumeci
Associate Chair: Ashley M. Maes

GENOMIC INSTABILITY
NEW!
Mechanisms That Cause DNA Damage and Related Diseases
Jul 6-11, 2014
The Hong Kong University of Science and Technology, Hong Kong, China
Chairs: Bik K. Tye & Marco Foiani
Vice Chair: Robert S. Weiss

- **Genome Maintenance During Development** (*Laura Landweber* / Fred Alt / K. Herrup)
- **DNA Damage Checkpoints** (*Karlene Cimprich* / Jiri Bartek / Michael Huen / M. Smolka)
- **Chromosome Segregation and Aneuploidy** (*Barbara Meyer* / Tatsuya Hirano / U. Surana)
- **Replication Fork Conflict and Epigenetic Inheritance** (*Rob Martienssen* / Jade Wang / Zhiguo Zhang / Anindya Dutta)
- **Replication Stress, Fidelity and Mutagenesis** (*Wei Yang* / Dana Branzei / Tom Kunkel)
- **Chromatin Dynamics and Genome Maintenance** (*Anja Groth* / Jessica Downs / Susan Gasser / Y. Qi)

- **DNA Recombination and Repair**
  (*Stephen West* / Jun Huang / Akira Shinohara)
- **Genomic Instability-Induced Cancer and Aging**
  (*Takehiko Kobayashi* / Jan Hoeijmakers / Andre Nussenzweig / Jun Wang)
- **DNA Repair Pathways as Therapeutic Targets**
  (*Alan Ashworth* / Thomas Helleday / Jos Jonkers)

GRANULAR & GRANULAR-FLUID FLOW
Fundamental Challenges and Applications of Particulate Systems
Jul 20-25, 2014
Stonehill College, Easton, MA
Chair: Bulbul Chakraborty
Vice Chairs: Douglas J. Durian & Matthias Schroeter

- **Large Scale Phenomena in Nature**
  (Carlos Santamarina / Derek Richardson)
- **Shear Jamming and Dilatancy**
  (*Robert P. Behringer* / Jie Ren / Dapeng Bi / Brian Tighe)
- **Avalanches and Plasticity**
  (Takahiro Hatano / Chris Marone / Jean Carlson)
- **Granular Physics in the Pharmaceutical Industry**
  (*Rahul Bharadwaj* / Adam Procopio / Jon Hilden)
- **Jamming of Frictionless Grains**
  (David Egolf / Atsushi Ikeda)
- **Self-Propelled Particles**
  (Aparna Baskaran / Nitin Kumar)
- **Gravity-Driven Flow**
  (Iker Zuriguel / Naryanan Menon)
- **Bulk Material Processing**
  (John Carson / Martin Schilling)
- **Dense Athermal Suspensions**
  (Jeff Morris / Eric Brown)

GFS GRANULAR & GRANULAR-FLUID FLOW
Fundamental Challenges and Applications of Particulate Systems
Jul 19-20, 2014
Chair: Dapeng Bi
Associate Chair: Theodore A. Brzinski

GRAPHITIC CARBON MATERIALS, CHEMISTRY AND PHYSICS OF
From Fundamentals to Opportunities and Challenges
Jun 15-20, 2014
Bates College, Lewiston, ME
Chairs: Liang-Shi Li & Antonio Castro Neto
Vice Chairs: Feng Wang & Michael S. Strano

- **Opportunities and Challenges in Graphitic Carbon Materials: Fundamental Science and Applications**
  (*Antonio Castro Neto* / James Hone / Jian-Min Zuo)
- **Chemistry of Graphene Allotropes: Synthesis**
  (*Michael Strano* / Klaus Müllen / Nancy Goroff / Jing Kong)
- **Electronic Properties of Graphene Allotropes**
  (*Herb Fertig* / Eva Andrei / Alessandra Lanzara)
- **Young Investigator Presentations**
  (*William Dichtel* / Pablo Jarillo-Heerrero / Byung Hee Hong / Zhigang Jiang)
- **Characterization of Graphitic Carbon Materials**
  (*Feng Wang* / Andrea C. Ferrari / Nikolai Zhitenev)
- **Chemistry of Graphene Allotropes: Functionalization**
  (*Michael Arnold* / Marina Petrukina / Bruce Hinds / Alex Star)
- **Carbon Materials: Applications and Sustainability**
  (*Liang-shi Li* / Paul E. Sheehan / Sheng Dai)
- **Novel Physics in Graphene Allotropes**
  (*Godfrey Gumbs* / Allan MacDonald / Leonid Levitov / Jie Shan)
- **Graphitic Materials in Biology and Medicine**
  (*Dal-Hee Min* / Robert Hurt / Zhuang Liu)

GFS GRAPHITIC CARBON MATERIALS, CHEMISTRY AND PHYSICS OF
From Fundamentals to Applications
Jun 14-15, 2014
Chair: Qiqi Li

GREEN CHEMISTRY
Industrial Successes and Challenges
Jul 27 - Aug 1, 2014
The Chinese University of Hong Kong, Hong Kong, China
Chairs: Kenneth Seddon & Mark A. Harmer
Vice Chairs: William J. Kruper & Elsje (Alessandra) Quadrelli

- **Keynote Session: On Being Green - Can Flow Chemistry Help?**
  (*István Horváth* / Steve Ley)
- **Oil and Gas Industry**
  (*Martin Atkins* / Xinhe Bao / Zhang Tao / Ross Gilmore)
- **Biomass Processing**
  (*Peter C. Pawlicki* / Roger Sheldon / Mark Davis / Tom Foust)
- **Polymer Industry**
  (*Qun Sun* / Carlos Afonso / Akira Isogai / Amar Mohanty / Amy Landis)
- **Comestibles**
  (*Jennifer Holgren*)
- **Pharma**
  (*David Constable* / Janet Scott / Chao-Jun Li / Nicholas Turner)
- **Education and Communication**
  (*Mary Kirchhoff* / Alan Alda / Reinhilde Veugelers)
- **Green Energy**
  (*Peter Wasserscheid* / Andreas Jess / Suojiang Zhang / Oliver Kappe)
- **Global Green Challenges**
  (*Suojiang Zhang* / Ah-Hyung (Alissa) Park)

GFS GREEN CHEMISTRY
Applications for a Sustainable Future
Jul 26-27, 2014
Chair: Magdalena B. Foreiter

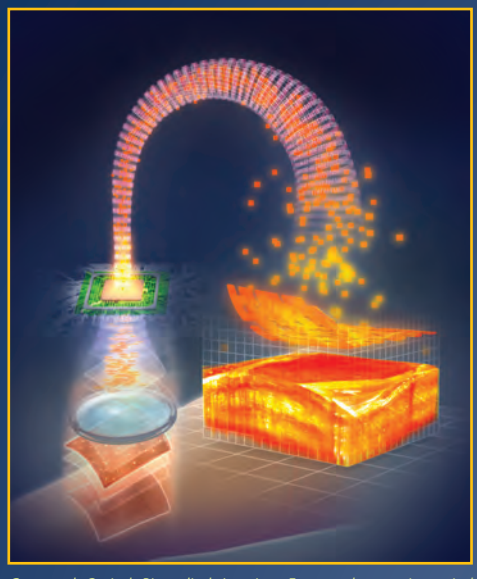

Computed Optical Biomedical Imaging. Future advances in optical biomedical imaging will leverage the convergence of novel optical hardware and sophisticated software algorithms to computationally shape wavefronts, correct aberrations, and reconstruct images. Submitted by Stephen Boppart, Co-Chair, Lasers in Medicine & Biology GRC.

HEMOSTASIS
Emerging Concepts in Hemostasis Research
Jul 27 - Aug 1, 2014
Waterville Valley Resort, Waterville Valley, NH
Chair: Andrew S. Weyrich
Vice Chairs: James H. Morrissey & Jorge A. DiPaola

- **The Vessel Wall in Thrombosis and Coagulation**
  (*Karen Hoffmeister* / Jose Lopez / Karen Vanhoorelbeke)
- **Thrombosis and Coagulation During Infection**
  (*Jane Freedman* / Nigel Mackman / Craig Morrell / Mark Looney / Ed Pryzdial)
- **Platelets and Coagulation Factors in Development and Disease**
  (*Keith Neeves* / Mark Kahn / Katerina Akassoglou / David Gailani)
- **Crosstalk in the Vascular Milieu**
  (*Paul Bray* / Patrick Provost / Alan Mast / Stephanie Smith / Chuck Esmon)
- **Links Between Thrombosis, Coagulation, and Inflammation**
  (*Pete Lollar* / Eric Boilard / Alisa Wolberg / Xiaoping Du)
- **Coagulation and Platelets in Disease**
  (*Martha Sola-Visner* / Owen McCarty / David Corry / Jay Degen)
- **Late-Breaking Topics**
  (*Jorge DiPaola, Jim Morrissey*)
- **Defective Hemostasis**
  (*Paula Tracy* / Barry Coller / David Lillicrap / Paula Tracy / Beth Bouchard/ Sriram Krishnaswamy)
- **Keynote Session: The Impact of Mouse and Human Genetics on Thrombosis and Hemostasis**
  (*Jorge DiPaola* / David Ginsburg / Frits Rosendaal)

GFS HEMOSTASIS
Hemostasis, Inflammation & Infection: Mechanisms of Cooperation
Jul 26-27, 2014
Chair: Angela A. Aggrey
Associate Chair: Thomas V. Colace

HETEROCYCLIC COMPOUNDS
Contemporary Topics in Synthesis and Utility
Jun 15-20, 2014
Salve Regina University, Newport, RI
Chair: George S. Sheppard
Vice Chair: Tadeusz F. Molinski

- **Catalysis**
  (*Yi-Yin Ku* / Silas Cook / Dean Toste)
- **Synthesis of Heterocyclic Compounds**
  (*Sebastien Caille* / Steve Miller / Eric Fang / Tohru Fukuyama)
- **Synthetic Methods**
  (*Sarah Dolman* / Andre Beauchemin / Karl Scheidt)
- **Contemporary Problems**
  (*Tom von Geldern* / Martine Keenan / Brandon Ashfeld / James Mack / Joe Pont)
- **Target Directed Synthesis**
  (*Paul Lobben* / Joe Harrity / Jeff Kallemeyn / Alison Frontier)
- **Heterocyclic Compounds in Cancer Research**
  (*Chudi Ndubaku* / Katherine Seley-Radtke / Teddy Johnson / Jennifer Prescher / Jeff Johnston)
- **New Approaches to Heterocyclic Compounds**
  (*Michael Nee* / Anita Mattson / Jason Herr / Dawei Ma)
- **Biologically Active Heterocyclic Compounds**
  (*Stefan France* / Anna Mapp / Ivar McDonald / Christopher Grote / Greg Basarab / Dirk Trauner)
- **Synthesis of Heterocyclic Natural Products**
  (*Ramon Vargas* / Ryan Shenvi / Viresh Rawal)

HIGH PRESSURE, RESEARCH AT
Tuning Energy Density to Reveal or Control Properties of Extreme Matter
Jun 22-27, 2014
University of New England, Biddeford, ME
Chair: Gilbert Collins
Vice Chair: Shanti S. Deemyad

- **Carbon Based Matter (Diamonds to Life)**
  (*Rus Hemley* / Marco Merlini)
- **Young Investigator Presentations**
  (Tim Strobel / Marius Millot / Luke Schulenberger)
- **High Pressure Liquids and Melting**
  (*Sergei Stishov* / Federica Gorelli / Paul Asimow)
- **Earth and Planetary Science (Exploring the Microphysics of Planets)**
  (*David Stevenson* / Tom Duffy / Burkhard Militzer / Adam Burrows)
- **Late-Breaking Topics**
  (Andy Higgenbottom)

- **Novel Materials and Extreme Chemistry**
  (Eva Zurek / Chris Pickard / Leonid Dubrovinky / Alexandra Navrotsky)
- **Next Generation Sources Applied to High Pressure**
  (Damian Swift / Norimasu Osaki)
- **Dense Hydrogen and Other Light Elements**
  (*Neil Ashcroft* / Paul Loubeyre / Issac Silvera)
- **Future Directions in Extreme Compression Science**

HIGH PRESSURE, RESEARCH AT
Utilizing High Pressure Techniques to Elucidate the Behavior of Matter
Jun 21-22, 2014
Chair: Rachael T. Hazael
Associate Chair: Richard G. Kraus

HOST-PARASITE INTERACTIONS, BIOLOGY OF
Molecular Mechanisms of Pathogenesis and Treatment of Parasitic Diseases
Jun 8-13, 2014
Salve Regina University, Newport, RI
Chairs: Steve Hajduk & Dominique Soldati-Favre
Vice Chairs: Malcolm J. McConville & Kasturi Haldar

- **Epigenetics, Chromatin Remodeling and Gene Regulation**
  (*Luisa Miranda Figueiredo* / Jonathan Weitzman / Till Voss)
- **Metabolism and Sensing of Host Environment**
  (*Malcolm McConville* / Maria Mota / Upi Singh / Richard Grencis)
- **Organelles Biogenesis and Trafficking**
  (*Kasturi Haldar* / Boris Striepen / Andre Schneider)
- **Parasite Persistence and Differentiation**
  (*Kent Hill* / Rita Tewari / Matthias Marti / Maria Yazdanbakhsh)
- **Therapeutic Interventions/Drugs and Drug Resistances**
  (*Meg Philips* / Kip Guy / Marc Ouellette)
- **Host/Parasite Co-Evolution**
  (*L. Aravind* / Sven Gould)
- **Protein Structure and Vaccine Development**
  (*Simon Draper* / Gavin Wright / Martin Boulanger)
- **Invasion and Subversion of Host Functions**
  (*Isabelle Coppens* / Ali Hakimi / Volker Heussler / Christina Hull)
- **Host Immune Defenses and Parasite Evasion**
  (*Edward Pearce* / Annette MacLeod / Felix Yarovinsky / Thor Theander)

HUMAN SINGLE NUCLEOTIDE POLYMORPHISMS & DISEASE NEW!
Understanding the Genetic Origin of Human Diseases and Natural Differences
Aug 3-8, 2014
Stonehill College, Easton, MA
Chair: Emil Alexov
Vice Chair: Anna R. Panchenko

- **Functional Studies of Human Mutations**
  (*Emil Alexov, Anna Panchenko* / Joshua Akey / Susan Taylor)
- **Discriminating Disease-Causing and Harmless Mutations**
  (*Mauno Vihinen* / Tom Blundell / Shamil Sunyaev / Sean Mooney)
- **Characterizing Common Patterns of Human Genetic Variation**
  (*Pauline Ng* / Steve Sherry / Michael Hammer)
- **Regulatory SNPs and Disease**
  (*Laura Elnitski* / Thomas Hudson / Nicholas Schork / Nadav Ahituv)
- **Assessing the Effect of Missense Mutations on Protein Stability and Dynamics**
  (*Ruth Nussinov* / Roland L Dunbrack / Rita Casadio)
- **Missense Mutations and Protein-Protein Interactions**
  (*John Moult* / Barry Honig / Tanja Kortemme / Ozlem Keskin)
- **Identification of Core Pathways and Driver Genes in Cancer**
  (*Teresa Przytycka* / Gábor Balázsi / Stan Lipkowitz)
- **Prediction of Disease Related Genes from Mutation Patterns and Interaction Networks**
  (*Andrey Rzhetsky* / Roded Sharan / Mark Gerstein / Philip Jager)
- **Missense Mutations Causing Rare Diseases**
  (*Donna Martin* / Rachel Karchin / Charles Sanders)

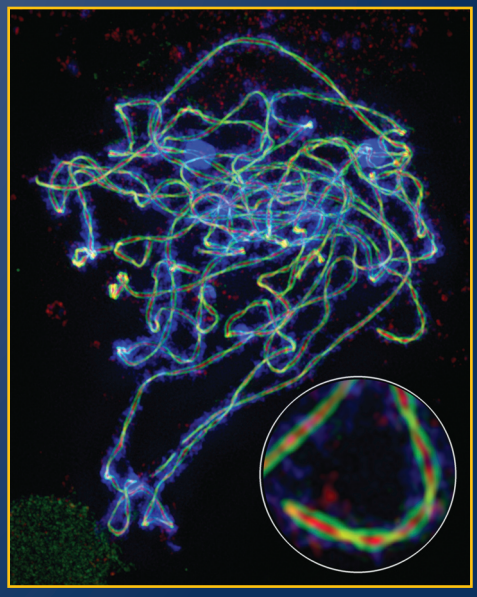

The synaptonemal complex of a maize male meiocyte at pachytene stage acquired by super-resolution Structured Illumination Microscopy. The tripartite structure with two lateral elements (green) and one central element (red) was detected by immunofluorescence and chromosomes were stained with DAPI (blue). Courtesy of Ding-Hua Lee and Chung-Ju Rachel Wang (Institute of Plant and Microbial Biology, Academia Sinica, Taiwan). Submitted by Gregory P. Copenhaver, Chair, Meiosis GRC.

HYBRID ELECTRONIC & PHOTONIC MATERIALS AND PHENOMENA NEW!
Understanding the Interplay Between Organic and Inorganic Materials
Jun 22-27, 2014
The Hong Kong University of Science and Technology, Hong Kong, China
Chairs: Michael Graetzel & Ben Zhong Tang
Vice Chairs: Tobin J. Marks & Henry Yan

- **Late-Breaking Results on Hybrid Material Systems**
  (*Tobin Marks* / Anders Hagfeldt / Guillermo Bazan)
- **Dye-Sensitized Solar Cells**
  (*Henry Yan* / Mohammad Nazeeruddin / Chen-Yu Yeh / Licheng Sun)
- **Hybrid Photovoltaic Phenomena**
  (*Anders Hagfeldt* / Henry Snaith / Nam Gyu Park)
- **Hybrid Electronic Devices and Phenomena**
  (*Qian Miao* / Zhenan Bao / He Tian / Henning Sirringhaus)
- **Organic/Inorganic Interface**
  (*Henning Sirringhaus* / William Gillin / Seth Marder)
- **Organic/Inorganic Hybrid Materials for Bio-Imaging/ Sensing**
  (*Christoph Chang* / Bin Liu / Deqing Zhang / Angela Belcher)
- **Hybrid Materials in Bio-Systems**
  (*Angela Belcher* / Vivian Yam / Christoph Chang)
- **Other Hybrid Electronics and Photonics**
  (*Licheng Sun* / Michael Wasielewski / Hong Lin / Milko Van der Boom)
- **Product Developments Related to Hybrid Materials**
  (*Henry Snaith* / Yan Liu)

IMAGE SCIENCE NEW!
Accelerating the Pace of System Design and Task-Based Evaluation
Jun 8-13, 2014
Stonehill College, Easton, MA
Chair: Kyle J. Myers
Vice Chair: Richard G. Paxman

- **Methodologies and Observers for Objective Assessment of Image Quality**
  (*Craig Abbey* / J. Chris Dainty / Harrison Barrett)
- **Use of Object Models and Priors in Imaging**
  (*Michael Insana* / Jim Duncan / Jeff Fessler / Alan Yuille)
- **Task-Based Design of Imaging Systems**
  (*Jannick Rolland* / Eric Frey / Eric Clarkson)
- **Imaging in Four or More Dimensions**
  (*Robert Guenther* / Tim Schulz / Richard Leahy / John Gore)
- **Extraction of Information from Multiple Time Points and Imaging Platforms**
  (*Joseph (Jody) A. O'Sullivan* / Christine de Mol / Paul Carson)
- **Adaptive Imaging**
  (*Jack Hoppin* / Matt Kupinski / Stefano Soatto / Olivier Guyon)
- **Compressive and Coded Sensing Systems**
  (*Ravi Athale* / Lawrence Carin / Amit Ashok)
- **Image Science in Astronomy**
  (*Peter Lawson* / Peter Tuthill / Laurent Pueyo / Matthew Kenworthy)
- **Unconventional Imaging**
  (*Ramesh Raskar* / Jim Fienup / David Brady)

IMMUNOCHEMISTRY & IMMUNOBIOLOGY
Re-Evaluating the Fundamentals of Immunology, Their Clinical Potentials, Their Meaningful Measures, and the Unmet Needs
Jun 1-6, 2014
Sunday River Resort, Newry, ME
Chair: Adrian Hayday
Vice Chair: Yasmine Belkaid

- **Immune Cell Development and Renewal**
  (*Cynthia Guidos* / Miriam Merad / Paul Frenette)
- **Regulation of Immune Cells and Systems**
  (*Gillian Griffiths* / Marc Jenkins / Ruslan Medzhitov / Art Weiss)
- **Immunology and Metabolism**
  (*Luke O'Neill* / Claudia Kemper / Erika Pearce)
- **Memory in Innate and Adaptive Cells**
  (*Federica Sallusto* / Sue Kaech / Lewis Lanier / Hans-Gustaf Ljunggren)
- **Immunity Within Tissues**
  (*Yasmine Belkain* / Dan Littman / Wendy Garrett)
- **Human Immunobiology**
  (*Rafi Ahmed* / Antonio Lanzavecchia / Mark Davis / Danny Douek / Alex Sigal / Zaza Ndhlovu)
- **Immunity in the Very Young**
  (*J.C. Zuniga-Pflucker* / T. Burt)
- **The Mechanisms of Cytokine Action**
  (*Fiona Powrie* / Hergen Spits / Charles Dinarello / Ajay Chawla)
- **Tumour Immunology**
  (*Padmanee Sharma* / Jim Allison)

IMMUNOCHEMISTRY & IMMUNOBIOLOGY
Harnessing Discovery for Breakthroughs in Human Health
May 31 - Jun 1, 2014
Chair: Anne G. Kasmar
Associate Chair: Livija Deban

Visit the Frontiers of Science. . . Go to a Gordon Conference! (www.grc.org)

IN VIVO MAGNETIC RESONANCE
From Molecules to Humans
Jul 27 - Aug 1, 2014
Proctor Academy, Andover, NH
Chair: Penny Gowland
Vice Chair: Jurgen K. Hennig

- **Hyperpolarization**
  (*David Gadian* / Simon Duckett / Robert Bartha)
- **Hardware at the Frontier**
  (*Dan Sodickson* / Michael Poole / Mark Ladd / Fa-Hsuan Lin)
- **MRI of Pain: From Bone to Brain**
  (*Juergen Hennig* / Shamillar Majumdar / Jonathan Brookes)
- **MR in Neuroscience / Late-Breaking Topics**
  (*Hanzhang Lu, Joel Garbow* / Shella Keilholz / Anna Devor)
- **MR in Multiple Sclerosis**
  (*Greg Stanisz* / Corree Laule / Claudia Wheeler Kingshott)
- **MR in Cardiovascular Disease**
  (*Xin Yu* / Michael Markl / Christopher Francois / Craig Malloy)
- **Molecular Engineering for Molecular Imaging**
  (*Louise van der Weerd* / Mikhail Shapiro / Anna Moore)
- **CEST Versus Spin Locking Versus MRS**
  (*Daniel Gochberg* / Xavier Golay / Tao Jin / Anke Henning)
- **Imaging Moving Targets**
  (*Oliver Speck* / Krishna Nayak / Colin Studholme)

INDUSTRIAL ECOLOGY
Transforming the Industrial Metabolism
Jun 1-6, 2014
Renaissance Tuscany Il Ciocco Resort, Lucca (Barga), Italy
Chair: Helga Weisz
Vice Chair: Heinz Schandl

- **Keynote Session: Industrial Metabolism in the Anthropocene**
  (Nebrosja Nakicenovic)
- **Toward an Industrial Ecology of Trade**
  (Joy Murray / Tommy Wiedmann / Peter-Paul Pichler)
- **Biomass Metabolism Under Climate Change**
- **Balancing Criticality, Dematerialization and Climate Mitigation**
  (Edgar Hertwich / Barbara Reck / Daniel Müller)
- **The Socio-Metabolic Implications of Time Use**
  (*Marina Fischer-Kowalski* / Angela Druckmann / Kyle W. Knight)
- **Resource Efficiency and Climate Mitigation in Cities**
  (James Keirstead / Chris Kennedy)
- **The Next Generation of Industrial Ecology**
  (*David Luke Oates, Sarah Russell Smith*)
- **Social Metabolism and Human Development**
  (Julia Steinberger)
- **Excellence and Relevance: Combining Science and Policy Advice**

INORGANIC CHEMISTRY
Enabling Tomorrow's Technologies
Jun 8-13, 2014
University of New England, Biddeford, ME
Chair: Keith J. Watson
Vice Chair: Francois P. Gabbai

- **Keynote Session: Copper-Oxygen Complexes as Models of Catalytic Intermediates**
  (*Keith Watson* / Bill Tolman)
- **Chemistry of Main Group Elements**
  (*Janet Braddock-Wilking* / Steve Westcott / Stefanie Dehnen / Louise Berben / Manfred Scheer)
- **Energy Applications**
  (*Seth Snyder* / Wenbin Lin / Tina Salguero / Qijie Guo)
- **Solid State Materials**
  (*Rick Finke* / Susannah Scott / Richard Brutchey / Susan Kauzlarich / Julia Chan)
- **Applied Inorganic Chemistry**
  (*Kim Johnson* / Kurt Hirsekorn / Monika Backhaus-Ricoult / Chuck Winter)
- **Catalysis**
  (*Cathy Tway* / Chris Goldsmith / Deryn Fogg / Janis Louie / Jonas Peters)
- **Coordination Chemistry**
  (*Christine Thomas* / Connie Lu / Jeremy Smith / Eric Schelter)
- **Nanotechnology**
  (*Brad Holliday* / Richard Brotzman / Mircea Dinca)
- **Perspectives**
  (*Francois Gabbai* / Clark Landis)

GRS INORGANIC CHEMISTRY
Highlighting Emerging Technologies Grounded in Fundamental Inorganic Research
Jun 7-8, 2014
Chair: Samantha J. Connelly
Associate Chair: Tracy L. Lohr

INTERMEDIATE FILAMENTS
Intermediate Filaments at the Crossroads Between Health and Disease
Jun 15-20, 2014
Mount Snow Resort, West Dover, VT
Chair: John E. Eriksson
Vice Chair: Karen M. Ridge

- **Keynote Session: Repurposing Intermediate Filaments - Interplay Between Structure, Signaling, Transcription, and Chromatin Organization**
  (*John Eriksson* / Jean-Pierre Julien / Pierre Coulombe)
- **At the Gates of Cell Stress and Disease**
  (Bishr Omary / Birgit Lane / Diana Toivola / Pavel Strnad)
- **Neuronal Degeneration**
  (Anthony Brown / Harish Pant / Milos Pekny)
- **Cellular Integration, Adhesion, and Migration**
  (Kathleen Green / Gerhard Viche)
- **Development of Cancer**
  (Thomas Magin / Karen Ridge / Sandrine Etienne-Manneville)
- **Mechanotransduction, Mechanosensing, and Tissue Stiffness**
  (*Ueli Aebi* / Harald Herrman / Sara Köster / Gaudenz Danuser / Jan Lammerding / Dennish Discher)
- **Signaling and Transcriptional Control**
  (*Ron Liem* / Harish Pant / Roland Foisner)
- **Cardiac and Muscular Control and Diseases**
  (Howard Worman / Brian Kennedy / Gisele Bonne / Gloria Conover / Yassemi Capetanaki)
- **Aging and Premature Aging Diseases**
  (Yosef Gruenbaum / Yixian Zheng / Maria Eriksson / Robert Goldman)

GRS INTERMEDIATE FILAMENTS
Intermediate Filaments at the Crossroads Between Health and Disease
Jun 14-15, 2014
Chair: Fang Cheng

INTRINSICALLY DISORDERED PROTEINS
Understanding Intrinsically Disordered Regions (IDRs) at Different Scales: From Single Molecules to Complex Systems
Jul 6-11, 2014
Stonehill College, Easton, MA
Chairs: M.Madan Babu & Gary W. Daughdrill
Vice Chairs: Richard W. Kriwacki & Monika Fuxreiter

- **Keynote Session: Structural Ensembles Link Genotype to Phenotype of IDRs**
  (*Richard Kriwacki* / Rohit Pappu / Ruth Nussinov)
- **Binding Motifs and PTMs in IDRs: From Transcription Regulation to Protein Degradation**
  (*Rob Russell* / Doug Barrick / Vishva Dixit / Michael Yaffe / John Scott / Ben Luisi / Mark Dodding)
- **Synthetic Biology and Therapeutic Applications of Disordered Peptide Motifs**
  (*George Rose* / John Dueber / Ashutosh Chilkoti / Christian Heinis / Volker Schellenberger)
- **Reversible Assemblies and Phase Transition Involving IDRs**
  (*Vladimir Uversky* / Stephen Michnick / Hao Wu / Clifford Brangwynne / Dirk Gorlich / L. Samelson / Gregory Jedd)
- **Functional and Non-Functional Protein Aggregation of IDRs**
  (*Anna Panchenko* / Anne Bertolotti / Simon Alberti / James Bardwell / Wilfried Weber)
- **Evolution, Regulation and Systems Biology of IDRs**
  (*Philip Kim* / Anthony Wright / Patrick Aloy / Gonzalo de Prat / Jacqui Matthews / Joerg Gsponer / Harvey McMahon)
- **Dynamics, Structural Ensembles and Allostery of IDRs**
  (*Ashok Deniz* / Jane Clark / Vince Hilser / Peter Wright / Iain McEwan)
- **State-of-the-Art Approaches to Investigate the Structures and Functions of IDRs**
  (*Ben Schuler* / Philip Selenko / Colin Kleanthus / Shin-Ichi Tate / Michal Sharon / Julian Gough / F. Marty Ytreberg)
- **Keynote Session: The Future of 'Unstructural' Biology**
  (*Monika Fuxreiter* / Peter Tompa / Keith Dunker)

GRS INTRINSICALLY DISORDERED PROTEINS
Fundamental Characteristics and Approaches to Understand the Biological Functions of IDPs
Jul 5-6, 2014
Chair: K. Aurelia Ball
Associate Chair: Charles Ravarani

ION CHANNELS
The Molecular Basis of Excitability and Disease
Jul 6-11, 2014
Mount Holyoke College, South Hadley, MA
Chair: Colin G. Nichols
Vice Chair: Emily R. Liman

- **New Channels**
  (*Carol Deutsch* / David Clapham / Bernd Fakler)
- **Trafficking and Regulators**
  (*Fred Sigworth* / Lily Jan)
- **New Partners**
  (*Bill Kobertz* / Stephen Long / Youxing Jiang)
- **Gating Mechanisms**
  (*William Zagotta* / Teresa Giraldez / Thomas DeCoursey)
- **Membranes and Toxins**
  (*Ehud Isacoff* / Eric Lingueglia / Heather Pinkett)
- **Drugs and Para(pharm)ernalia**
  (*Kenton Swartz* / Owen McManus / Cindy Czajkowski)
- **Channels in Specialized Places**
  (*Bertil Hille* / Ardem Patapoutian / Chris Lingle)
- **Engineering, Modification and New Methods**
  (*Gary Yellen* / Pancho Bezanilla / Katie Henzler-Wildman)
- **Channels and Disease**
  (*Cathy Morris* / Geoff Pitt / Fran Ashcroft)

GRS ION CHANNELS
Channel Structure, Function, Disease and Drugs
Jul 5-6, 2014
Chair: Randy Stockbridge
Associate Chair: Karthik Bodhinathan

IONIC LIQUIDS
Solvents, Materials, or Medicines?
NEW!
Aug 17-22, 2014
Sunday River Resort, Newry, ME
Chair: Robin D. Rogers
Vice Chair: Anja V. Mudring

- **From Molten Salts to Ionic Liquids**
  (*John Wilkes* / Austen Angell / Joan Brennecke)
- **The Ionic Liquid Landscape**
  (*Jim Davis* / Tom Welton / Luis Rebelo)
- **Theory and Modeling**
  (*Ed Maginn* / Claudio J. Margulis / Margarida Costa-Gomes)
- **Ionic Liquids Energy, Fuel, and Chemical Production**
  (*Ed Castner* / Blake Simmons / Peter Wasserscheid / Doug Gin)
- **Energetic and Nanoparticle Ionic Liquids**
  (*Sheng Dai* / Jean'ne Shreeve / Jairton DuPont)

- **Advanced Electrolytes**
  (*Paul Trulove* / Masa Watanabe / Jenny Pringle / Wesley Henderson)
- **Separations**
  (*Violina Cocalia* / João Coutinho / Mark Schiflett)
- **The Ionic Liquid Future**
  (*Thomas Schubert* / Gary Baker / Rico del Sesto)
- **Biotechnology and Pharmaceuticals**
  (*Rasmus Fehrmann* / Hiro Ohno / Doug MacFarlane)

IRON-SULFUR ENZYMES
Mechanisms and Applications in Energy, Environment and Medicine
Jun 15-20, 2014
Stonehill College, Easton, MA
Chair: Markus Ribbe
Vice Chair: Jonas C. Peters

- **The Great Iron Sulfur Clusters**
  (*Richard Holm* / Douglas Rees / Catherine Drennan)
- **Nitrogenase**
  (*Yilin Hu* / Brian Hales / Lance Seefeldt / Akif Tezcan / John Rittle)
- **Iron Sulfur Chemistry**
  (*Jonas Peters* / David Britt / Yasuhiro Ohki)
- **Hydrogenase**
  (*Chris Pickett* / Rolf Thauer / John Peters / Marc Fontacave / Oliver Lenz)
- **Iron/Sulfur Metabolism**
  (*Silke Leimkuehler* / Roland Lill / Mike Johnson / Tracey Rouault)
- **Radical SAM Enzymes**
  (*Joe Jarrett* / Squire Booker / Sean Elliot / Joan Broderick / Vahe Bandarian)
- **Non-Heme Iron Enzymes**
  (*Carsten Krebs* / Martin Bollinger Jr. / Holger Dobbek)
- **"Crosstalk" with Other Metals**
  (*Oliver Einsle* / Sabeeha Merchant / Florian Bittner / Amy Rosenzweig / Guenter Schwarz)
- **Looking Beyond Iron Sulfur Proteins**
  (*Liz Nolan* / Stephen Lippard)

LASERS IN MEDICINE & BIOLOGY
From Basic Science Discovery to Translational Applications
Jul 13-18, 2014
Holderness School, Holderness, NH
Chairs: Stephen A. Boppart & Arjen Amelink
Vice Chairs: Brett E. Bouma & Clare Elwell

- **Multimodal Deep-Tissue Imaging**
  (*Xavier Intes* / Simon Cherry / Wiendelt Steenbergen)
- **Optical Stimulation and Control of Biological Processes**
  (*Duco Jansen* / Hillel Chiel / Claus-Peter Richter / Ed Boyden)
- **Label-Free and Single-Molecule Microscopy**
  (*Paul French* / Ji-Xin Cheng / Warren Warren / Sua Myong)
- **Computed Optical Imaging, Modeling, and Processing**
  (*Tony Wilson* / John Schotland / Alwin Kienle / Jannick Rolland)
- **Advances in Optical Spectroscopy**
  (*Bruce Tromberg* / Chris Hoy / Dirk Faber / Paola Taroni)
- **Optical Diagnostics Using Polarized Light**
  (*Steve Jacques* / Alex Vitkin / Christoph K. Hitzenberger / Vadim Backman)
- **Image-Guided Surgery and Procedures**
  (*Laura Marcu* / David Sampson / Thomas Wang / Sylvain Gioux)
- **Diagnostics and Treatment Applications of Light for Global Health**
  (*Rox Anderson* / Tomasz Tkaczyk / Aydogan Ozcan / Dominic Robinson / Robert Redmond)
- **Non-Linear Optics and Imaging**
  (*Peter So* / Yaron Silberberg / Chris Xu / Marcos Dantos)

LIPOPROTEIN METABOLISM
Molecular Mechanisms in Physiology and Disease
Jun 15-20, 2014
Waterville Valley Resort, Waterville Valley, NH
Chairs: Robert V. Farese & Joachim J. Herz
Vice Chair: John S. Parks

- **Lipases**
  (*Rudolf Zechner* / Rudolf Zechner / Perry Bickel / Jorge Plutzsky)
- **Hepatic & Intestinal Lipid Metabolism**
  (*Jay Horton* / Jay Horton / Steve Kliewer / Carlos Fernandez-Hernando / Chih Hao Lee)
- **HDL & Reverse Cholesterol Transport**
  (*Peter Edwards* / Tom Vallim / Mark Brown / Marina Cuchel)
- **Lipoprotein Receptors and Vascular Wall**
  (*Joachim Herz* / Ira Tabas / Philipe Boucher / Phil Shaul / Andreas Niemeier)
- **CNS & Lipids**
  (*Cheryl Wellington* / Cheryl Wellington / David Holtzman / Emily Osterweil)
- **Intracellular Lipid Metabolism**
  (*Tobias Walther* / Tobias Walther / Peng Li / Anders Naar / Jin Ye)
- **Genetics of Lipid and Lipoprotein Metabolism**
  (*Dan Rader* / Jake Lusis / Alan Shuldiner / Karen Reue)
- **Therapeutics of Lipid and Cardiovascular Disease**
  (*Shirly Pinto* / Nancy Thornberry / Craig Hammond / Rosanne Crooke)
- **Keynote Session: Lipid and Lipoprotein Metabolism**
  (Helen Hobbs)

GRS LIPOPROTEIN METABOLISM
Advances in Cellular and Molecular Mechanisms of Lipoproteins
Jun 14-15, 2014
Chair: Hagai Tavori
Associate Chair: Humra Athar

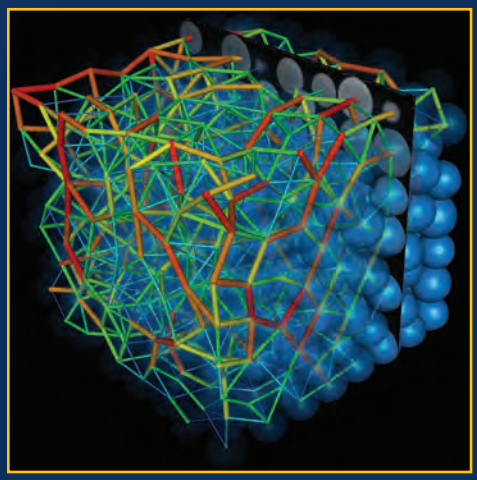

Forces in 3D in a granular material, obtained by optical tomography using refractive index matching. Force chains supporting the imposed load are tracked as the grain assembly is stressed. Courtesy of Joshua Dijksman, Nicolas Brodu and Robert P. Behringer (Duke University), and Felice Frankel (MIT). Supported by NASA, NSF and ARO. Submitted by Bulbul Chakraborty, Chair, Granular & Granular-Fluid Flow GRC

LYSOSOMES & ENDOCYTOSIS
Mechanisms of Endocytic Processes: From Molecules to Organisms, from Evolution to Patho-Physiology
Jun 15-20, 2014
Proctor Academy, Andover, NH
Chair: Beverly Wendland
Vice Chair: Roberto Weigert

- **Diabetes and Metabolism**
  (*Mara Duncan* / Tim McGraw / Jeffrey Pessin / Silvia Corvera)
- **Endocytic Mechanisms**
  (*Juan Bonifacino, Mary Munson* / Sandy Schmid / Maribel Geli / Scott Emr / Marko Kaksonen / David Owen)
- **Host-Pathogen Interactions**
  (*Mark Marsh* / Marcia Goldberg / Felix Randow / Janet Iwasa)
- **Signaling: Endocytic Trafficking in Cancer and Cellular Physiology**
  (*Christopher Burd, Linton Traub* / Alexander Sorkin / Johanna Ivaska / Avital Rodal / JoAnn Trejo / Robbie Loewith)
- **Endocytic Regulation in Neurons**
  (*Victor Faundez, Phyllis Hanson* / Tim Ryan / Pietro De Camilli / Rejji Kuruvilla / Mark Von Zastrow)
- **Autophagy, Endosomes and Lysosomes**
  (*Santiago Di Pietro, Graça Raposo* / Jim Hurley / Lois Weisman / Liz Conibear / Jonathan Weissman / Anjon Audhya)
- **Late-Breaking Topics / New Directions**
  (*Roberto Weigert, Frances Brodsky*)
- **Lessons from Evolutionary Conservation**
  (*Mickey Marks, Sandra Lemmon* / Mark Field / Maria Touz / Jenny Hirst / Maya Schuldiner / Gia Voeltz)
- **Keynote Session: Dynamics of Endocytosis**
  (*Beverly Wendland* / Tomas Kirchhausen)

GRS LYSOSOMES & ENDOCYTOSIS
Integration of Endocytic and Lysosomal Pathways in Health and Disease
Jun 14-15, 2014
Chair: Satdip Kaur
Associate Chair: Colin D.H. Ratcliffe

MAMMALIAN REPRODUCTION
NEW!
Translating Basic Science into Clinical Applications
Aug 10-15, 2014
Colby-Sawyer College, New London, NH
Chairs: John R. McCarrey & Francesco J. Demayo
Vice Chairs: Blanche Capel & Anne Croy

- **Fate Determination and Development of Reproductive Tissues**
  (*Blanche Capel* / Humphrey Yao / Erika Matunis / David Page)
- **Epigenetic Programming and Reproduction**
  (*Marisa Bartolomei* / Alex Meissner / Antoine Peters / Amander Clark)
- **Stem Cells and Reproduction**
  (*Haifan Lin* / Rene Rejo-Pera / Linda Giudice / Jon Oatley)
- **Environmental Effects on Reproductive Functions**
  (*Stuart Moss* / Sarah Kimmins / Patricia Hunt / Carmen Williams)
- **Pregnancy and Parturition**
  (*Anne Croy* / Adrian Erlebacher / Sing Sing Way / Mala Mahendroo)
- **Infertility and Contraception**
  (*Carlos Simon* / Marty Matzuk / Mellissa Mann / Patricia Morris)
- **Male Reproductive Tract**
  (*Dolores Lamb* / Carolina Jorgez / Sylvie Breton / Martin Cohn)
- **Genomics/Systems Biology Approaches to Reproduction**
  (*Tom Spencer* / Wolf Reik / Gunter Wagner / Douglas Lauffenburger)
- **Milestones in Reproductive Biology**
  (*Asgi Fazleabas, Koji Yoshinaga* / Azim Surani / Fuller Bazer / S.K. Dey)

MAMMARY GLAND BIOLOGY
Molecular and Cellular Basis of Breast Development and Cancer Progression
Jun 8-13, 2014
Renaissance Tuscany Il Ciocco Resort, Lucca (Barga), Italy
Chair: Mohamed Bentires-Alj
Vice Chairs: Caroline M. Alexander & Victoria Seewaldt

- **Keynote Session: Targeting PI3K in Breast Cancer**
  (*Mohamed Bentires-Alj* / Lewis Cantley)

- **The Mammary Gland Niche and Reprogramming** (*Cédric Blanpain* / Zena Werb / Pier Giuseppe Pelicci / Gil Smith)
- **Molecular and Cellular Basis of Breast Cancer Risk and Prevention** (*Victoria Seewaldt* / David Kleinberg / Coral Alfred Lamartiniere)
- **Breast Tumor Heterogeneity and Resistance to Therapy** (*Jos Jonkers* / Jeff Rosen / Jacco Van Rheenen / Matthew Smalley / Hege E. Gierckskiy Russnes)
- **Pubertal and Pregnancy Hormones** (*Rob Clarke* / Cathrin Brisken / Myles Brown)
- **Lactation and Involution** (*Caroline Alexander* / Katie Hinde / Russ Hovey / Pepper Schedin)
- **Tumor Dormancy** (*Eva Gonzalez Suarez* / Christoph Klein / Cyrus M. Ghajar)
- **Metastasis** (*Alana Welm* / Gerhard Christofori / Johanna A. Joyce / Nicola Aceto)
- **Keynote Session: Recurrence and Resistance** (Nancy Hynes)

MAMMARY GLAND BIOLOGY
Branching Toward New Horizons in Development and Disease
Jun 7-8, 2014
Chair: Lisa M. Arendt
Associate Chair: Irina S. Babina

MARINE MICROBES
Small Microbes, Big Data
Jun 22-27, 2014
Bentley University, Waltham, MA
Chair: Gabrielle Rocap
Vice Chair: Catherine Legrand

- **Keynote Session: Insights from Model Systems** (Sallie Chisholm)
- **Microbial Ecology One Cell at a Time** (Ramunas Stepanauskas / Ger van den Engh)
- **From Gene Functions to Ecosystem Function** (Chris Bowler)
- **Diversity: Prospecting the Rare Biosphere** (Linda Amaral Zettler / Mya Breitbart)
- **Life in Low Oxygen Zones** (Frank Stewart)
- **Viruses: Drivers of Diversity, Mortality and Information Transfer** (Debbie Lindell / Joshua Weitz)
- **Evolution: Impacts and Mechanisms of Horizontal Gene Transfer** (Tal Dagan)
- **Connecting Physiology to Biogeochemical Cycles** (Sonya Dyhrman / Kay Bidle)
- **Modeling Microbial Oceanography at the Global Scale** (Curtis Deutsch)

MARINE MICROBES
'Omic Enabled Ecophysiology of Marine Microbes
Jun 21-22, 2014
Chair: Jody J. Wright

MECHANISMS OF EPILEPSY & NEURONAL SYNCHRONIZATION
Dissecting Epilepsy from Genes to Circuits
Aug 17-22, 2014
Mount Snow Resort, West Dover, VT
Chairs: Jack M. Parent & Scott C. Baraban
Vice Chairs: Steve C. Danzer & Heinz W. Beck

- **Keynote Session: Epilepsy Research - Past Perspectives to Define the Future** (David Prince)
- **Ion Channel Defects in Intractable Epilepsies** (*Miriam Meisler* / Jennifer Kearney / William Catterall / Edward Cooper / Alfonso Represa)
- **Identification and Characterization of Epilepsy Mutations** (*Annapurna Poduri* / Heather Mefford / Michael Hammer / Diane O'Dowd / David Goldstein)
- **Development and Maldevelopment of the Central Nervous System** (*Peter Crino* / Joseph LoTurco / Xinyu Zhao / Christopher Walsh / Arnold Kriegstein)
- **Neuronal Microcircuits in Normal and Epileptic Brain** (*Mark Beenhakker* / J. Troy Littleton / Roger Traub / Rosa Cossart)
- **Stem Cells to the Rescue** (*Jennifer Hsieh* / Hongjun Song / Ricardo Dolmetsch / Lori Isom / Vania Broccoli)
- **Co-Morbidities of Network Dysfunction in Epilepsies and Related Disorders** (*Amy Brooks-Kayal* / Timothy Miller / Frances Jensen / Anne Anderson)
- **Novel Therapeutic Strategies: From Gene Therapy to Drug Interventions** (*Avtar Roopra* / Nicholas Poolos / David Henshall / Manisha Patel)
- **Balancing Inhibition and Excitation: Implications for Epileptogenesis** (*Jaideep Kapur* / Caroline Houser / Vijayalakshmi Santhakumar / Hillel Adesnik)

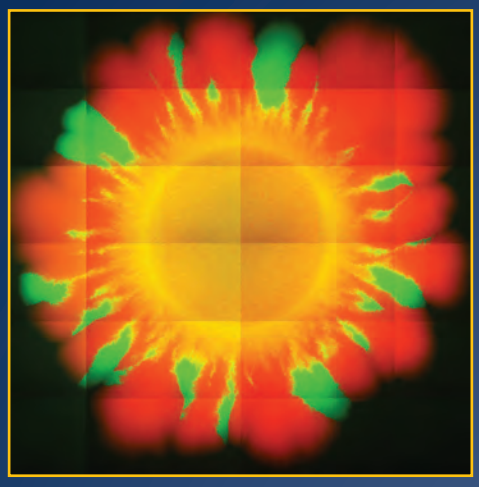

Two bacterial strains on an agar plate competing for common resources. Courtesy of Qiucen Zhang. Submitted by Robert H. Austin, Chair, Complex Adaptive Matter GRC.

MEDICINAL CHEMISTRY
The Leading Edge of Drug Discovery
Aug 3-8, 2014
Colby-Sawyer College, New London, NH
Chair: David P. Rotella
Vice Chair: Lori K. Gavrin

- **Disrupting Protein-Protein Interactions** (*Matthew Marx* / Bob Borzilleri / David Rees / Lew Pennington)
- **Taking Aim at Cancer: On Target Approaches** (*Gregory Ott* / Alexander Mazin / Jon Roffey / Chris Brain)
- **Drug Discovery Driven By Chemistry** (*Takashi Tsukamoto* / Jonathan Wilson / Paul Wender / Leonard Winneroski)
- **Advances in Neurodegeneration** (*Silvana Leit* / Celia Dominguez / Stephan Schiling / Jeffery Axten / Dario Doller)
- **Increasing the Chance of Clinical Success in Oncology** (*Silvina Garcia Rubio* / Olivier Michielin / John deGroot / Peter Dragovich)
- **Rare and Neglected Diseases** (*Bob Jacobs* / Wes Van Voorhis / David Barros-Aguirre / John McKew / Bob Marquis)
- **Being Image-Conscious: PET Ligands in Drug Discovery** (*Joanne Bronson* / Robert Mach / Eric Hostetler / David Donnelly)
- **Late-Breaking Topics** (*Christopher O'Donnell*)
- **Keynote Session: A Chemist's Foray into Translational Research - From Stem Cells to the Genetic Code** (*David Rotella* / Peter Schultz)

MEDICINAL CHEMISTRY
Explained and Applied
Aug 2-3, 2014
Chair: James R. Merritt

MEIOSIS
From Meiotic Entry to Gamete Production
Jun 1-6, 2014
Colby-Sawyer College, New London, NH
Chair: Gregory P. Copenhaver
Vice Chair: Neil Hunter

- **Initiating Recombination: How Recombination Starts** (*Francesca Cole* / Galina Petukhova / Maria Jasin / Scott Keeney / Bernard de Massy)
- **Mechanisms of Recombination: How Recombination Works** (*Rachel Wang* / Francesca Cole / Doug Bishop / Jeff Sekelsky / Gerry Smith / Rachel Wang)
- **Pairing, Synapsis and Cohesion: How Chromosomes Find One Another and Stay Together** (*Soni Lacefield* / Needhi Bhalla / Monica Colaiacovo / Denise Zickler / Sarit Smolikov)
- **Regulation of Recombination: How Recombination Frequency & Distribution are Controlled** (*Needhi Bhalla* / Paula Cohen / Neil Hunter / Raphael Mercier / Akira Shinohara / Kunihiro Ohta / Nancy Kleckner)
- **Checkpoints, Cell Cycle and Progression: How the Cell Enters, Executes and Exits Meiosis** (*Anne Villeneuve* / Nancy Hollingsworth / Abbey Dernberg / Soni Lacefield / Wolfgang Zachariae)
- **Chromosome Dynamics: How Chromosomes Move During Meiosis** (*Scott Hawley* / Hong Ma / Barbara Meyer / Dean Dawson / Iva Tolic-Norrelykke / Adele Marston / Hiro Ohkura)
- **Chromosome Segregation: How Chromosomes are Apportioned to Daughter Cells** (*Iva Tolić-Nørrelykke* / Anne Villeneuve / Yoshinori Watanabe / Arshad Desai / Scott Hawley)
- **Epigenetics, Expression & Regional Control: How Meiotic Processes are Regulated** (*Kirsten Bomblies* / Valerie Borde / Ian Henderson / Andreas Hochwagen / David Page)
- **Evolution and Natural Variation: How Meiosis Changes Across Time and in Populations** (*Ian Henderson* / Kirsten Bomblies / Nadia Singh / Joseph Loidl)

MEIOSIS
Molecular Foundations of Sexual Reproduction
May 31 - Jun 1, 2014
Chair: Sarah E. Zanders
Associate Chair: Nicole Crown

MEMBRANE TRANSPORT PROTEINS
Structure, Function, Physiology, and Targets in Disease
Jul 13-18, 2014
Mount Snow Resort, West Dover, VT
Chair: Poul Nissen
Vice Chair: Rajini Rao

- **Late-Breaking Topics in Membrane Transport Research** (*Hanne Poulsen* / Ernst Bamberg / Yifan Cheng)
- **Anion Transporters and Channels** (*Lydia Aguilar Bryan* / Joe Mindell / Lydia Aguilar Bryan / Criss Hartzell)
- **Ion Transporters: Sodium-Proton Exchangers** (*Rajini Rao* / Eric Morrow / David Drew / Daniel Fuster)
- **Ion Transporters: Sodium, Potassium, Chloride** (*Michael G. Palmgren* / Kai Kaila / Karin Lykke-Hartmann / David Goldstein)

- **Neurotransmitter Transporters: Structure, Function and Drugs**
  (*Baruch Kanner* / Eric Gouaux / Jonathan Javitch / Harald Sitte)
- **Neurotransmitter Transporters: Function and Disease**
  (*Ulrik Gether* / Robert Edwards / Aurellio Galli / Manju Kurian)
- **Transporters in Plants, Pathogens and Parasites**
  (*Enrico Martinoia* / Michael G. Palmgren / Enrico Martinoia / Kiaran Kirk)
- **Heavy-Metal, Peptide and Lipid Transporters**
  (*Svetlana Lutsenko* / Svetlana Lutsenko / Simon Newstead / Todd Graham)
- **Keynote Session: New Methods in Membrane Transport Research**
  (*Poul Nissen* / Ed Boyden / Dirk Trauner / Sonia Contera)

MEMBRANES: MATERIALS & PROCESSES
Making Engineering Membranes Alive
Jul 6-11, 2014
Colby-Sawyer College, New London, NH
Chairs: Bruce J. Hinds & Klaus-V Peinemann
Vice Chairs: Jamie Hestekin, Nancy K. Lape & Jeffrey R. McCutcheon

- **Keynote Session: Discoveries in the Sructures of Natural Protein Channels**
  (Tamir Gohen)
- **Advanced Fouling Recovery Systems**
  (*Mathias Ulbricht* / Vicky Chen / Menachem Elimelech / Zhongyi Jiang)
- **Active and Dynamic Engineering Membrane Systems**
  (*Thomas Schaefer* / Charles Martin / Susan Rempe)
- **Advanced Gas Separation and MOFs**
  (*Moises Carreon* / Hae-Kwon Jeong / Michael Tsapatsis / Zhiping Lai)
- **Fracking Challenges and Membrane Opportunities**
  (*Haiqing Lin* / Tim Merkel / Benny Freeman)
- **Advanced Water Purification**
  (*Dibakar Bhattacharyya* / Yoram Cohen / Rong Wang / Mark Wiesner)
- **Active Membrane Systems in Medicine and Pharmacy**
  (*Joerg Vienken* / Thomas Groth / Dimitrios Stamatialis)
- **Membrane Material Systems**
  (*Douglas Gin* / Ting Xu / Takashi Kato / Wolfgang Meier)
- **Innovation Membrane Process Systems**
  (*Peter Pfromm* / Ranil Wrickramasinghe / Ed Sanders)

GRS **MEMBRANES: MATERIALS & PROCESSES**
Electrons to Oceans: Membrane Innovation at Every Level
Jul 5-6, 2014
Chair: Heather C S. Chenette
Associate Chair: Michiel J.T. Raaijmakers

METALS IN MEDICINE
Defining the Future of Medicinal Inorganic Chemistry
Jun 22-27, 2014
Proctor Academy, Andover, NH
Chairs: Alan B. Packard & Michael J. Hannon
Vice Chairs: Katherine J. Franz & Nils Metzler-Nolte

- **Metallopharmaceuticals - Where We've Been and Where We're Going**
  (*Alan Packard, Michael Hannon* / Kenneth Raymond / Michael J. Abrams / Seth Cohen)
- **Radioactive Metals for Imaging and Therapy**
  (*Martin Brechbiel* / Tobias Ritter / William McBride / H.-J. Wester / Roy Larsen)
- **Pharmacology of Metal-Based Drugs**
  (*Trevor Hambley* / Tom Piccariello / Paula Jacobs / Des Richardson)
- **Inorganic Nanoparticles in Medicine**
  (*James Dabrowiak* / Wenbin Lin / Jeffrey Zink / Mostafa El-Sayed / Lawrence Tamarkin)
- **Nanoformulations**
  (*Debbie Crans* / Robert Strickley / Anne Vessières-Jaouen / Melissa Reynolds)
- **Metals and Magnets and Gold**
  (*Peter Caravan* / David Carmode / Dean Sherry / Kazuya Kikuchi / Marinella Massanti)
- **Fluorescent Metalloimaging Agents**
  (*Nils Metzler-Nolte* / Kenneth Kam-Wing Lo / Fijs van Leeuwen / Tia Keyes)
- **Non-Canonical DNA/RNA Recognition**
  (*Claudia Turro* / Jacqueline Barton / Janet Morrow / James Cowan / Marie-Paule Teulade-Fichou)
- **New Frontiers in Metallopharmaceuticals**
  (*Katherine Franz* / Steven Lippard)

MICROBIAL STRESS RESPONSE
Molecular Systems, and Community Responses
Jul 27 - Aug 1, 2014
Mount Holyoke College, South Hadley, MA
Chairs: Michael Ibba & Christine A. White-Ziegler
Vice Chairs: Eduardo A. Groisman & Dianne K. Newman

- **Responding to Stress as a Group**
  (*Joan Slonczewski* / Roberto Kolter / Caroline Harwood / Fitnat Yildiz)
- **Long-Term Adaptation to Stress**
  (*Alan Grossman* / Susan Rosenberg / Susan T. Lovett / Steven Finkel)
- **Shaping Microbial Communities**
  (Julia Vorholt / Gurol Suel / Eduardo Groisman)
- **Detecting and Responding to Stressful Environments**
  (*John Helmann* / Sigal Ben-Yehuda / Petra Levin / Kevin Devine / William Navarre)
- **Host-Microbe Interactions**
  (*Amy Cheng Vollmer* / Nancy Moran / Ned Ruby / Nina Salama)
- **Post-Transcriptional Stress Responses**
  (*Susan Gottesman* / Jörg Vogel / Marty Fedor / Tina Henkin / Peter Chien)
- **Cellular Networks**
  (*Tim Donohue* / Terry Hwa / Kathleen Marchal / Beth Lazazzera)
- **Microbial Barriers to Stress**
  (*Tricia Kiley* / Suzanne Walker / Kit Pogliano / Tom Bernhardt)
- **Toxins, Antitoxins and Antibiotics**
  (*Sarah Ades* / Chris Hayes / Mike Laub / Deborah Hung / Diarmaid Hughes)

GRS **MICROBIAL STRESS RESPONSE**
Microbial Stress Response/Cross-Disciplinary Studies of Microbes in Changing Environments
Jul 26-27, 2014
Chair: Julia Schwartzman
Associate Chair: Pete Chandrangsu

MICROBIAL TOXINS & PATHOGENICITY
Mechanisms that Govern Bacterial Disease
Jul 20-25, 2014
Waterville Valley Resort, Waterville Valley, NH
Chair: Michele S. Swanson
Vice Chair: Virginia L. Miller

- **Keynote Session: Microbial Toxins and Pathogenicity**
  (*Virginia Miller* / Victor Nizet / Jos van Strijp / Sarah Clark / Andrew Olive)
- **Mechanisms of Toxin Action and Strategies for Protection**
  (*Jimmy Ballard* / Brad Cookson / Liz Hartland / Rongsheng Jin / Drusilla Burns / Cheryl Quinn)
- **Cell Biology of Host Barriers to Infection**
  (*John Brumell* / David Mosser / Jost Enninga / Serge Mostowy)
- **Microbial Adaption Strategies**
  (*Vanessa Sperandio* / Matt Chapman / Rita Tamayo / Karen Ottemann / David Weiss / Andrew Camilli)
- **Infection Biology of the Gut Microbiota**
  (June Round / Vince Young / Cindy Sears)
- **Virulence Mechanisms**
  (*Jim Kaper* / J.-D. Sauer / Melanie Hamon / Joao Pedra / Tod Merkel / Darren Higgins)
- **The Battle for Nutrients**
  (*Chris Alteri* / Sabine Ehrt / Manuela Raffatellu / Anders Omsland)
- **Inflammatory Barriers to Infection**
  (*Lee-Ann Allen* / Ed Miao / Kate Fitzgerald / Ari Molofsky / Caroline Genco / Beth McCormick)
- **Microbiology of Infection Control**
  (*Eric Hewlett* / Man-Wah Tan / Julie Segre)

GRS **MICROBIAL TOXINS & PATHOGENICITY**
New Approaches to Understand the Host-Pathogen Dynamic
Jul 19-20, 2014
Chair: Andrew J. Olive
Associate Chair: Sarah E. Clark

MITOCHONDRIA & CHLOROPLASTS
Biology and Physiology of Energy Converting Organelles
Jul 6-11, 2014
Renaissance Tuscany Il Ciocco Resort, Lucca (Barga), Italy
Chair: Luca Scorrano
Vice Chair: Klaas J. Van Wijk

- **Organelle Biogenesis and Protein Sorting**
  (Hannes Hermann / Paul Jarvis / Thomas Langer)
- **Organellar Genes: From Maintenance to Expression**
  (*Helmut Kirkhoff* / Maureen Hanson / Aleksandra Filipovska / Ralph Bock / Ian Small)
- **Organelle Function**
  (Paolo Bernardi / Ildiko Szabo / Lixin Zhang)
- **Organellar Remodeling and Replication**
  (Helmut Kirkhoff / Mike Ryan / Konstanze Winklhofer / Laura Lackner)
- **Organelle Trafficking**
  (Gyuri Hajnoczky / Joe Kittler / Masamitsu Wada)
- **Organelle Interactions and Signaling**
  (Dean Dellapenna / Benoit Kornmann /Michel Havaux / Heidi Mcbride)
- **Organelle Metabolism and Cofactors**
  (Christian Frezza / Marinus Pilon / Atan Gross)
- **Organellar Proteolysis and Autophagy**
  (Hiroyuki Ishida / Stefan Hortensteiner / Helene Plun-Favreau / Gerald Dorn)
- **Organelle Dysfunction and Stress**
  (Sally Mackenzie / Anu Suomalainen / Andy Dillin)

MOLECULAR & CELLULAR NEUROBIOLOGY
Mechanisms of Neural Development, Circuit Assembly, Synaptic Plasticity and Neuropsychiatric Disorders
Jun 29 - Jul 4, 2014
The Hong Kong University of Science and Technology, Hong Kong, China
Chair: Eric J. Huang
Vice Chair: Yi E. Sun

- **Molecular Bases of Neurological Diseases / Keynote Presentation**
  (*John Trojanowski, Eric Huang* / Virginia Lee / Li-Huei Tsai / Ulrich Muller / Mu-Ming Poo [keynote])
- **Synapse Formation & Structures**
  (*Eunjun Kim* / Lily Jan / Minjie Zhang / Yang Dan)
- **Neural Development & Regeneration**
  (*John Ngai* / Yuh Nung Jan / Yimin Zou / David Rowitch)
- **Mechanism of Synaptic Plasticity**
  (*Louis Reichardt* / Peter Schieffele / Oliver Hobart)
- **Neurogenesis & Stem Cells**
  (*Yi Sun* / Arturo Alvarez-Buylla / Arnold Kriegstein / Jeff Macklis)
- **Neural Circuit Development**
  (*Shernaz Bamji* / Rachel Wong / Lu Chen / H. Robert Horvitz / Kazuo Emoto)
- **Circuit Assembly**
  (*Rong Yu* / Yi Zuo / Tomomi Shimogori / Hongjun Song / Lin Mei)
- **Neural Circuits & Behaviors**
  (*Yi Rao* / Nirao Shah / Baoji Xu / Lin Mei / Toru Takumi / Martha Constatine-Paton)

- **Mechanism of Neuronal Polarity & Regeneration / Keynote Presentation**
  (*Guo-li Ming, Eric Huang* / Cheng-Ting Cheng / Zhigang He / Joseph Lewcock / Scott Brady / Thomas Südhof [keynote])

GFS MOLECULAR & CELLULAR NEUROBIOLOGY
Exploring the Frontiers of Foundational and Translational Neuroscience
Jun 28-29, 2014
Chair: Sarah X. Luo
Associate Chair: Kwok-On Lai

MOLECULAR BASIS OF MICROBIAL ONE-CARBON METABOLISM
Probing the Biology: Chemistry Interface from Molecules to Ecosystems
Aug 10-15, 2014
Mount Holyoke College, South Hadley, MA
Chair: Thomas E. Hanson
Vice Chair: Stephane Vuilleumier

- **Applications of C1 Metabolism**
  (Frank Löffler / Caroline Plugge)
- **Chemical and Synthetic Biology: Towards New C1 Metabolisms**
  (*Tobias Erb* / Arren Bar-Even / Peter Dürre / Harry Beller / Joel Rosenthal)
- **Structure and Mechanism in Key C1 Enzymes and Complexes**
  (*Amy Rosenzweig* / Cheryl Kerfeld / Volker Müller / Masaharu Ishii)
- **C1 Metabolism in the Environment**
  (*Ronald Oremland* / Karen Lloyd / Kelly Wrighton / Françoise Bringel / Colin Murrell)
- **C1 Metabolism in Associations**
  (*Harold Drake* / Jörg Overmann / Andreas Brune / Victoria Orphan)
- **Regulation and Adaptation in C1 Microorganisms**
  (*Ludmila Chistoserdova* / F. Robert Tabita / John Leigh / Christopher Marx / Yasuyoshi Sakai)
- **Systems Biology of C1 Microorganisms**
  (*Daniel Segré* / Michael Rother / Lisa Stein / Nathan Price)
- **New C1 Reactions, Pathways and Organisms**
  (*Mike Jetten* / Katharina Ettwig / Samantha Joye / Dennis Bazylinski)
- **Metals in C1 Metabolism: Evolutionary and Functional Perspectives**
  (*Stephen Ragsdale* / Rolf Thauer / Wolfgang Nitschke / Jeremy Semrau)

GFS MOLECULAR BASIS OF MICROBIAL ONE-CARBON METABOLISM
From Single Molecules to Microbial Ecosystem Functioning
Aug 9-10, 2014
Chair: Cornelia Welte
Associate Chair: Dipti D. Nayak

MULTIFERROIC & MAGNETOELECTRIC MATERIALS NEW!
Designing for Multifunctionality
Aug 10-15, 2014
University of New England, Biddeford, ME
Chair: Janice L. Musfeldt
Vice Chair: Bernd Lorenz

- **New Materials and Devices**
  (*Ramamoorthy Ramesh* / Dipankar Das Sarma / Craig Fennie / Sayeef Salahuddin)
- **Domains**
  (*Sang-Wook Cheong* / Zhi-Xun Shen / Laurent Chapon / Caroline Ross / Ekhard Salje)
- **Non-Oxide Multiferroics**
  (*Naresh Dalal* / John Schlueter / Vivien Zapf / Thom Palstra)
- **Composites, Hybrids, Strain, and Light**
  (*Ichiro Takeuchi* / Ce-Wen Nan / Chang Bom Eom / Nian Sun / Tanusri Saha-Dasgupta)
- **Magnetoelectric Coupling in 5d Oxides**
  (*Daniel Khomskii* / Maxim Mostovoy / Gang Cao / Siddharth Saxena)
- **Nano- and Mesoscopic Magnetoelectrics**
  (*Evgeny Tsymbal* / Eugenio Coronado / Sarah Tolbert / Peter Fisher / Beatrice Noheda)
- **Magnetoelectric Coupling in Topological Insulators and on Surfaces**
  (*David Vanderbilt* / Xiaolin Wang / Silvia Picozzi / David Tanner / Umesh Waghmere)
- **Phase Transitions and Symmetry Considerations**
  (*Jens Kreisel* / Manfred Fiebig / Kee Hoon Kim / Randy Fishman / Jorge Iniguez)
- **Magnetically-Driven Multiferroics**
  (*Jaime Fernandez-Baca* / Tsuyoshi Kimura / Cristan Batista / Michel Kenzelmann)

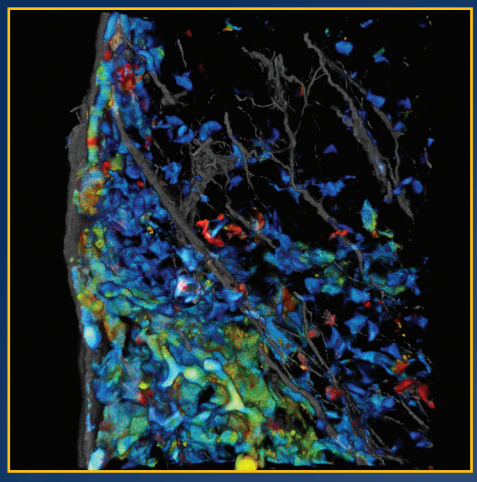

CXCL9 (red) and CXCL10 (blue) chemokine expression revealed in the draining lymph node of a dual CXCL9 and CXCL10 reporter mouse following subcutaneous immunization. In this 3D reconstruction, medullary sinus macrophages and dendritic cells are labeled green with a SIGNR1 antibody and collagen is visualized as grey by second harmonics. Courtesy of Matthew Woodruff and Michael Carroll. Submitted by Andrew Luster, Chair, Chemotactic Cytokines GRC.

MULTIPHOTON PROCESSES
Strong Field Processes and Frequency / Time Domain Frontiers
Jun 15-20, 2014
Bentley University, Waltham, MA
Chair: Barry C. Walker
Vice Chair: Johan Mauritsson

- **Keynote Session: Horizons in Multiphoton Science**
  (Paul Corkum)
- **New Ultrafast Laser Sources and Few Cycle Pulses**
  (Franz Kaertner / Robert Jones)
- **Multiphoton & Strong Field Processes in Molecular Systems**
  (Itzik Ben-Itzhak / Jian Wu / Francesca Calegari)
- **Multiphoton & Strong Field Processes in Complex Systems, Surfaces & Plasmas**
  (Pierre Agostini / Agnieszka Jaron-Becker)
- **Attosecond Pulse Generation, Spectroscopy and Characterization**
  (Zenghu Chang / Jon Marangos)
- **High-Frequency Multiphoton Processes and Multiphoton Processes at FEL Facilities**
  (Linda Young / Tenio Popmintchev / Robin Santra)
- **Ultrastrong Fields, High Energy Recollision Processes, and Strong Field Physics in the Long Wavelength Limit**
  (Christoph Keitel / Gerhard Paulus / Ursula Keller)
- **New Spectroscopy Techniques and Ultrafast Transient Absorption Spectroscopy**
  (Fabien Quere / Alexander Föhlisch / Kenneth Schafer / Steve Leone)
- **High-Harmonic Spectroscopy**
  (Jan Petter / David Villeneuve / Valerie Blanchet)

MUSCLE & MOLECULAR MOTORS
Resolving the Molecular Mechanisms of Contractile Biology
Jul 6-11, 2014
Mount Snow Resort, West Dover, VT
Chair: E. Michael Ostap
Vice Chair: Kathleen M. Trybus

- **Keynote Session: Molecular and Cellular Mechanisms of Contractility**
  (*Kathleen M. Trybus* / James R. Sellers / Erika L.F. Holzbaur)
- **Connecting Active Sites, AAAs, Levers, and Linkers with Translocation**
  (*Sharyn A. Endow* / Anne Houdusse / Stanley A. Burgess / Marcel Knossow / Andres E. Leschziner)
- **Structural Dynamics and Displacements**
  (*Shin'ichi Ishiwata* / Yale E. Goldman / David D. Thomas)
- **Building, Stabilizing, and Deconstructing Cytoskeletal Filaments**
  (*Roberto Dominguez* / Enrique M. De La Cruz / Edward H. Egelman / Melissa K. Gardner / Brad J. Nolen)
- **Force-Dependent Control of Cytoskeletal Motors**
  (*Claudia Veigel* / Marco Capitanio / Hiroyuki Iwamoto / Ahmet Yildiz)
- **Motors with Cargos, in Ensembles, and Emergent Behaviors**
  (*David M. Warshaw* / Michael R. Diehl / Kazuhiro Oiwa / Samara L. Reck-Peterson / Cecile Sykes)
- **Regulation and Control of Motor Activity**
  (*Samantha P. Harris* / Roger Craig / Thomas Surrey / Kristen J. Verhey)
- **Motors at Work in the Cell**
  (*Folma Buss* / Anna Akhmanova / John A. Hammer, 3rd / Roop Mallik / Margot E. Quinlan / Ronald S. Rock)
- **Motors in Health and Disease**
  (*H. Lee Sweeney* / Larry S. Goldstein / Steven S. Rosenfeld)

MUSCULOSKELETAL BIOLOGY & BIOENGINEERING
Identifying and Overcoming Barriers to Translation
Aug 3-8, 2014
Proctor Academy, Andover, NH
Chair: Christopher H. Evans
Vice Chair: Robert L. Mauck

- **The Research Translation Landscape**
  (*Peter Johnson* / Charles Vacanti / Kelly LaMarco / Cheryl Blanchard)
- **Getting Stem Cells into the Clinic**
  (*George Muschler* / Mahendra Rao / Malcolm Moos / George Muschler / Keith Wonnacott)
- **Ligament and Tendon**
  (*Lisa Larkin* / Lisa Larkin / Anthony Ratcliffe / Greg Altman)
- **Meniscus**
  (*Robert Mauck* / Suzanne Maher / Lawrence Bonassar)
- **Gene Therapy**
  (*Paul Robbins* / Jay Lieberman / Steven Ghivizzani / Henning Madry)
- **Bone**
  (*Edward Schwarz* / Joost D. de Bruijn / Sheldon Lin / Ivan Martin / Robert Guldberg)
- **Creating a Translational Research Environment**
  (*Cyril Frank* / Peter Johnson / Martin Stoddart / Andrew Carr)
- **Osteoarthriti**
  (*Linda Sandell* / Virginia Kraus / Sharmila Majundar / Frank Barry)
- **Keynote Session: Strategies and Requirements for Successful Research Translation**

GFS MUSCULOSKELETAL BIOLOGY & BIOENGINEERING
Bridging the Disciplines
Aug 2-3, 2014
Chair: Dana M. Cairns
Associate Chair: Matthew B. Fisher

MUTAGENESIS
Changes to the Genetic Landscape, from Single Nucleotides to Entire Genomes
Jun 15-20, 2014
Melia Golf Vichy Catalan Business & Convention Center, Girona - Costa Brava, Spain
Chair: Robert Lahue
Vice Chair: Simon Boulton

- **Keynote Session: From Molecular Mechanisms to Human Disease**
  (*Robert Lahue* / David Pellman / Karlene Cimprich)
- **RNA-Mediated Mutagenesis**
  (*Sue Jinks-Robertson* / Sue Jinks-Robertson / Hilde Nilsen / Andrew Jackson / Andres Aguilera)
- **Genomic and Chromosomal Alterations**
  (*Jessica Downs* / Jessica Downs / Shamil Sunyaev / Anton Gartner)
- **Decision Points: Repair or Mutate?**
  (*Simon Boulton* / Simon Boulton / Susan Lees-Miller / Kyungjae Myung / Bruce Demple)
- **DNA Polymerases and Translesion Synthesis**
  (*Wei Yang* / Wei Yang / Robert Fuchs / Roger Woodgate)
- **Challenges at the Replication Fork**
  (*Peter Burgers* / Peter Burgers / Virginia Zakian / Charles Swanton / Thomas Kunkel)
- **Editing and Repair**
  (*Ian Tomlinson* / Ian Tomlinson / Alison Gammie / Thomas Helleday)
- **DNA Structural Challenges**
  (*Nancy Maizels* / Nancy Maizels / Andre Nussenzweig / Christopher Pearson / Julian Sale)
- **Targeted Mutagenesis**
  (*Sergei Mirkin* / Sergei Mirkin / Myron Goodman / Christi Walter)

NANOSTRUCTURE FABRICATION
Nanostructures in Information Technology, Energy Conversion, and Nanoelectromechanical Systems
Jul 13-18, 2014
University of New England, Biddeford, ME
Chair: Charles T. Black
Vice Chair: James A. Liddle

- **Nanostructured Optoelectronic Materials and Devices**
  (*Charles Black* / Cherie Kagan / Henri Lezec)
- **Nanoelectromechanical Systems (NEMS)**
  (*Shalom Wind* / Daniel Lopez / Mandar Deshmukh)
- **Nanomagnetism**
  (Jordan Katine)
- **Polymer Self Assembly**
  (Caroline Ross / Ricardo Ruiz / Phil Hustad)
- **Directed Assembly of Complex Nanostructured Materials**
  (*Elena Shevchenko* / Oleg Gang)
- **Advanced Lithography**
- **Microelectronic Devices**
  (*Aaron Franklin* / Zhihong Chen / Heike Reil)
- **Quantum Computation**
  (*Mark Reed* / Dirk Englund / Mark Eriksson / Thomas Schenkel)
- **Selected Poster Presentations**
  (*J. Alex Liddle*)

NATURAL PRODUCTS
The Central Role of Natural Products in Biology and Chemistry
Jul 20-25, 2014
Proctor Academy, Andover, NH
Chair: Michael Calter
Vice Chair: Steven H. Olson

- **Methodology for Natural Product Synthesis**
  (Kay Brummond / Guangbin Dong / Robert Grubbs)
- **Biologically Active Molecules Through Synthesis and Isolation**
  (Rima Al-Anwar / Gerhard Bringmann / Tad Molinski)
- **Methods and Strategy for the Synthesis of Natural Products**
  (Sherry Chemler / Jonathan Ellman / Peter Wipf)
- **Clinical and Public Health Applications of Natural Products and Their Analogs**
  (Bruce Littlefield / Peter Seeberger / Craig Crews)
- **Synthesis and Biological Activity of Natural Products**
  (Gregory Dudley / Marissa Kozlowski / Rich Taylor)
- **Synthesis of Natural Products and Other Biologically Active Molecules**
  (Don Gauthier)
- **Methodology for Natural Product Synthesis**
  (Janis Louie / David MacMillan / John Montgomery)
- **Biosynthesis and Isolation of Natural Products**
  (Sarah O'Connor / Yi Tang)
- **Methods and Strategy for the Synthesis of Natural Products and Analogs**
  (Pavel Nagorny / Tomislav Rovis / Paul Wender)

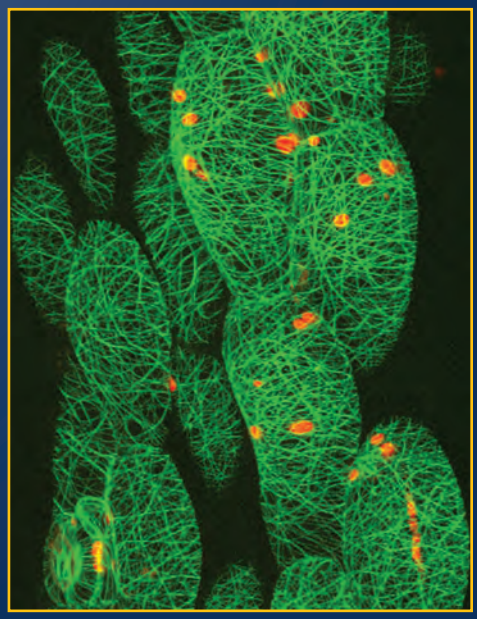

Confocal image of interphase cortical microtubule arrays in living Arabidopsis hypocotyl cells. Courtesy of Jessica Lucas and Sidney L. Shaw (Indiana University LMIC). Submitted by Fred Chang, Chair, Plant & Microbial Cytoskeleton GRC.

NEURAL DEVELOPMENT
From Stem Cells to Circuits
Aug 10-15, 2014
Salve Regina University, Newport, RI
Chair: Fiona Doetsch
Vice Chair: Marc R. Freeman

- **Keynote Session: Neural Stem Cells in Development and Evolution**
  (Arnold Kriegstein)
- **Neural Stem Cells**
  (Laure Bally-Cuif / Hongjun Song / Ryoichiro Kageyama / Juergen Knoblich / Laura Johnston / Violeta Silva-Vargas / Sean Megason)
- **Cellular Heterogeneity/Cell Fate Specification**
  (Chris Doe / Nicholas Spitzer / Uli Muller / David Rowitch)
- **Transcriptional and Epigenetic Control of Cell Fate**
  (Oliver Hobert / Jane Johnson / Dan Lim / Stavros Lomvardas / Alvaro Rada-Igelsias)
- **Wiring the Brain: Development of Axons and Dendrites**
  (Bing Ye / Sonia Garel / Beth Stevens / Yishi Jin)
- **Wiring the Brain: From Synaptogenesis to Circuitry**
  (Franck Polleux / Kelsey Martin / Julia Kaltschmidt / Silvia Arber / Won-Suk Chun / Kelly Monk)
- **CNS Periphery Interactions**
  (Chenghua Gu / Alex Gould / Stephen Noctor)
- **Brain Evolution and Regeneration**
  (Peter Reddien / Elly Tanaka)
- **Neurodevelopmental Disorders**
  (Azad Bonni / Alysson Muotri)

GRS **NEURAL DEVELOPMENT**
From Stem Cells to Circuits
Aug 9-10, 2014
Chair: Megan M. Corty

NEUROBIOLOGY OF BRAIN DISORDERS
Neurodegeneration and Aging-Related Disorders of the Nervous System
Jul 27 - Aug 1, 2014
Melia Golf Vichy Catalan Business & Convention Center, Girona - Costa Brava, Spain
Chair: Joachim J. Herz
Vice Chairs: Luciano D'Adamio & Bart Destrooper

- **Keynote Session: Epigenetic Protection of the Aging Brain; Presenilins in Synaptic Function and Disease**
  (*Joachim Herz* / Li-Huei Tsai / Jie Shen)
- **Aggregation and Protein Transmission Diseases**
  (*Eckard and Eva-Maria Mandelkow* / Richard Morimoto / Dieter Edbauer / Marc Diamond)
- **RNA-Mediated Mechanisms in Neurodegeneration**
  (*Orly Lazarov* / Rosa Rademakers / Ken Kosik / Kausik Si)
- **Mechanisms of Synaptic Function and Dysfunction**
  (*Bart de Strooper* / Thomas Südhof / Ottavio Arancio / Lisa Monteggia)
- **Aging and Network Changes**
  (*Pierluigi Nicotera* / Bill Seeley / Bill Jagust / Carol Barnes)
- **Lipid Metabolism and Lysosomal Dysfunction**
  (*Rafael Fernandez Chacon* / Silvana Franceschetti / David Holtzman / Cheryl Wellington / Yadong Huang)
- **Proteases and Processing**
  (*Carlos Saura* / Ana Maria Cuervo / Lucia Chavez-Guiterrez / Christian Haass)
- **Clinical and Translational Perspectives**
  (*Bruce Miller* / Monique Breteler / Adam Boxer / Mara Dierssen)
- **Keynote Session: Network Dysfunction During Aging and in Alzheimer's Disease**
  (*Luciano D'Adamio* / Lennart Mucke)

GRS **NEUROBIOLOGY OF BRAIN DISORDERS**
Neurodegeneration and Aging-Related Disorders of the Nervous System
Jul 26-27, 2014
Chair: Emilie Giaime
Associate Chair: Matthew Klein

NEUROBIOLOGY OF COGNITION
Circuits, Dynamics, Action and Perception
Jul 20-25, 2014
Sunday River Resort, Newry, ME
Chair: Charles E. Schroeder
Vice Chair: Tatiana Pasternak

- **Keynote Session: Brain Initiative**
  (*Xiao-Jing Wang* / John Maunsell / Larry Abbott)
- **Cognitive Circuitry: Connectivity**
  (*Carol Barnes* / Helen Barbas / Suzanne Haber / Murray Sherman / Jay Giedd / Olaf Sporns / Troy Hackett)
- **Motor Contributions to Cognition**
  (Nicholas Hatsopoulos / Mark Churchland / Bijan Pesaran / Richard Andersen)
- **Cognitive Circuitry: Coordination**
  (*Nancy Kopell* / Earl Miller / David Leopold / Marlene Cohen / Sabine Kastner / Donald Katz)
- **Music and Language**
  (David Poeppel / Lee Miller / Isabel Peretz / Aniruddh Patel)
- **Decision and Reward**
  (*Daeyeol Lee* / Michael Shadlen / Angela Yu / Yael Niv / Ben Hayden / Carl Olson / Valentin Wyart)
- **Social Cognition and Affective Behavior**
  (*Michael Platt* / Laurie Santos / Aina Puce / Daniela Schiller / Rebecca Saxe)
- **Attention**
  (*Robert DeSimone* / Alexander Thiele / Richard Krauzlis / Peter Lakatos / Tirin Moore / Marisa Carrasco / John Foxe)

- **Learning and Plasticity**
  (*Charles Gilbert* / Leonardo Cohen / John Krakauer / Takeo Watanabe / David Scheinberg)

GRS NEUROBIOLOGY OF COGNITION
From Computational Rules to the Neurobiology of Cognition
Jul 19-20, 2014
Chair: Lucia Melloni
Associate Chair: Ayelet N. Landau

NOBLE METAL NANOPARTICLES
Synthesis, Characterization, Modeling, and Applications
Jun 15-20, 2014
Mount Holyoke College, South Hadley, MA
Chair: Francesco Stellacci
Vice Chair: Catherine J. Murphy

- **Keynote Session: Emerging Trends**
  (*Francesco Stellacci* / Bartosz Grzybowski)
- **Plasmonics**
  (*Jennifer Dionne* / Alexander Govorov / Stephan Link / George Thomas)
- **Biological Applications**
  (*Shalini Gupta* / Chad Mirkin / Silke Krol / Teri Odom)
- **Advancements in Characterization**
  (*Lucia Pasquato* / Fabrizio Carbone / Paul Weiss / Thomas Wandlowsi)
- **Biology and Nanoparticles**
  (*Vincent Rotello* / Pierpaolo Pompa / Chunying Chen / Alfredo Aleksander Katz)
- **Assembly**
  (*Luis Liz-Marzan* / Andrea Tao / Rafal Klajn / Sharon Glotzer)
- **SERS**
  (*Cathy Murphy, Laura Fabris* / Christy Haynes / Prashant Jain / Enzo Di Fabrizio)
- **Emerging Fields**
  (*Cathy Murphy* / Xinhe Bao / Nanfeng Zheng)
- **Clusters**
  (*Osman Bakr* / Terry Bigioni / Chris Ackerson / Hannu Hakkinen)

GRS NOBLE METAL NANOPARTICLES
Synthesis, Characterization and Applications
Jun 14-15, 2014
Chair: Randy P. Carney
Associate Chair: Christopher J. DeSantis

NOTCH SIGNALING IN DEVELOPMENT, REGENERATION & DISEASE
Notch at the Interface of Health and Disease
Jul 20-25, 2014
Bates College, Lewiston, ME
Chair: Alain Israel
Vice Chairs: Warren Pear & Stephen Blacklow

- **Keynote Session: Wnt, Notch and Intestinal Stem Cells / Development of the Retina**
  (*Alain Israel* / Hans Clevers / Constance Cepko)
- **Mechanistic Aspects of Notch Regulation**
  (*Alain Israel* / François Schweisguth / Thomas Klein / Christel Brou / James Posakony / Gabrielle Boulianne / Raphael Kopan)
- **Stem Cells and Development: The Hematopoietic System**
  (*Lisa Minter* / Anna Bigas / Irwin Bernstein / Utpal Banerjee / Ryoichiro Kageyama)
- **Notch Signaling in Tissue Development**
  (*Irwin Bernstein* / Holger Gerhardt / Carl Blobel / Luisa Iruela-Arispe / Carmen Birchmeier / Stacey Rentschler / Jose Luis de la Pompa)
- **Immunology**
  (*Warren Pear* / Ivan Maillard / Iannis Aifantis / Juan-Carlos Zuniga-Pflücker / Freddy Radtke)
- **Cancer and Therapeutics**
  (*Jon Aster* / Jon Aster / Andrew Weng / Paolo Dotto / Adolfo Ferrando / Chris Siebel / Sean Egan / Anthony Capobianco / Gavin Thurston)
- **Late-Breaking Topics**
  (*Raphael Kopan*)
- **Structure and Transcription**
  (*Stephen Blacklow* / Rhett Kovall / Sarah Bray / Doug Barrick / Susan Lea)
- **Notch Regulation by Glycosylation**
  (*Stephen Blacklow* / Kenji Matsuno / Robert Haltiwanger / Pamela Stanley)

GRS NOTCH SIGNALING IN DEVELOPMENT, REGENERATION & DISEASE
From Molecular Mechanisms to Translational Research
Jul 19-20, 2014
Chair: Shinya Yamamoto
Associate Chair: Mustafa Turkoz

OCEAN GLOBAL CHANGE BIOLOGY NEW!
Interactive Effects of Multiple Global Change Variables
Jul 6-11, 2014
Waterville Valley Resort, Waterville Valley, NH
Chair: David A. Hutchins
Vice Chair: Philip Boyd

- **Lessons Learned from the Ocean Acidification Field**
  (*Jean-Pierre Gattuso* / Ulf Riebsell / Joan Kleypas / Jim Barry)
- **Feedbacks Between Ocean Acidification / Warming and Hypoxia**
  (*Shannon Meseck* / Brad Seibel / Lisa Levin / Wei-Jun Cai)
- **Paleo Proxies for Multiple Environmental Stressors**
  (*Adina Paytan* / Meixun Zhao / Baerbel Honish / Dani Schmidt)
- **Biogeochemical Consequences of Multi-Variable Global Change Processes**
  (*Andreas Andersson* / Uta Passow / Andreas Schmittner / Anne Cohen)
- **Acclimation / Plasticity and Adaptation**
  (*Gretchen Hofmann* / Sinead Collins / Steve Palumbi / Brian Helmuth)
- **Physiological and Genetic Responses to Interacting Anthropogenic Stressors**
  (*Doug Capone* / Elena Litchman / Andy Allen / Mak Saito / Kunshan Gao)
- **Ecosystem Modeling of Multiple Stressors**
  (*Scott Doney* / Al Tagliabue / Jorge Sarmiento / Stephanie Dutkiewicz)
- **Developing and Comparing Ocean Global Change Experimental Methods**
  (*Philip Boyd* / Bill Kirkwood / Christina McGraw / David Kline)
- **Temporal and Spatial Scales of Biological Responses to Environmental Change**
  (*Kevin Arrigo* / Matt Oliver / Mike Behrenfeld / Ricardo Letelier)

OCEANS & HUMAN HEALTH
Anthropogenic Impacts on Coastal Communities and Ecosystems
Jun 1-6, 2014
University of New England, Biddeford, ME
Chairs: Helena Solo-Gabriele & J. Evan Ward
Vice Chairs: Erin K. Lipp & Michael H. Depledge

- **Climate Change, Contaminants and OHH**
  (*Bob Bowen* / Kristie Ebi / Gary Stern)
- **Global Cycling of Legacy Contaminants Under Changing Climate Regimes**
  (*Rainer Lohmann* / Robert Mason / Carey Friedman / Celia Chen)
- **Technology at Extreme Scales: Modern Approaches to Understanding OHH**
  (*Fred Tyson* / Anders Goksøyr / Neel Aluru / Frank Muller-Karger)
- **Contaminants and Aquatic Food Webs: Potential Impacts on Ecosystem Services**
  (*Rebecca Klaper* / Karen Kidd / Marsha Black / Tamara Galloway)
- **Direct and Indirect Effects of Climate Change on Humans**
  (*Paul Snelgrove* / Keith Davidson / Patricia Yager / Tracey Goldstein)
- **Contaminants and Aquatic Food Webs: Transfer to Humans**
  (*Sylvain DeGuise* / Noelle Selin / Eric Dewailly / Jerome Ruzzin)
- **Contaminants and Aquatic Toxicology: Sentinel and Model Organisms**
  (*Ed Laws* / Richard Handy / Isaac Pessah)
- **Interface Between Natural and Anthropogenic Contaminants**
  (*Lihini Aluwihare* / Bradley Moore / Kathi Lefebvre / Rudolf Wu)
- **Moving Forward: Strategies for Improving OHH**
  (*Lora Fleming* / Niall McDonough / Jaymie R. Meliker / Laurie Chan)

GRS OCEANS & HUMAN HEALTH
Risks and Remedies from the Sea
May 31 - Jun 1, 2014
Chair: Matthew Phillips
Associate Chair: Jessica L. Joyner

ORGANIC GEOCHEMISTRY
Linking Past and Recent Systems and Processes
Aug 3-8, 2014
Holderness School, Holderness, NH
Chair: Erdem Idiz
Vice Chair: Ann Pearson

- **Integrated Perspectives in Organic Geochemistry**
  (*Darci Rush* / J. Sinninghe Damste / Lorenz Schwark)
- **Multiproxy Approaches to Paleoenvironmental Reconstruction: Bringing the Basin to the Core**
  (*Fang Lin* / Sze Ling Ho / Ron Hill / Alex Dickson / Julio Sepulveda)
- **Organic Carbon Burial and Preservation**
  (*Richard Pancost* / Sandra Arndt / Katja Meyer / Francois Gelin)
- **Macromolecules - Linking Kerogen to Biopolymers**
  (*Liz Kujawinski* / Vern Stasiuk / Amy McKenna / Brian Horsfield / Norbert Herkorn)
- **Isotopes: Beyond Carbon**
  (*Kate Freeman* / Alon Amrani / Clay Magill / Daniel Stolper)
- **Analytical Advances**
  (*Erik Tegelaar* / Cliff Walters / Lars Woermer / Ken Williford / Morgan Raven / Bob Burruss)
- **Gases on the Move / Dynamics of Hydrocarbon Gases**
  (*Michael Whiticar* / Jessica Whiteside / Barbara Tilley / Tom Darrah)
- **Biomarkers in Space and Time**
  (*John Volkman* / Kate French / Andrew Murray / Kliti Grice / Gordon Love)
- **Late-Breaking Topics**
  (*Ann Pearson* / Joe Chappell)

GRS ORGANIC GEOCHEMISTRY
New Advances for Organic Geochemists
Aug 2-3, 2014
Chair: Darci J. Rush

ORGANIC REACTIONS & PROCESSES
From Catalytic Processes to Chemical Biology
Jul 13-18, 2014
Bryant University, Smithfield, RI
Chairs: Doug E. Frantz & Joseph M. Fox
Vice Chairs: Jade D. Nelson & Jared L. Piper

- **Modern Catalytic Methods**
  (*Todd Nelson* / Mike Doyle / M. Christina White)
- **Industrial Process Development / New Avenues in Asymmetric Catalysis**
  (*Seble Wagaw, Don Watson* / Ben Sherry / Thomas Stevenson / Uttam Tambar / Karl Scheidt / Ohyun Kwon)
- **Complex Molecular Synthesis**
  (*Gojko Lilac* / Jeff Johnson / Richmond Sarpong)

- **Large Scale Organic Synthesis / Discovery of New Methodologies and Processes**
  (*Sonia Rodriquez, Stan McHardy* / Travis Remarchuk / Yi-Yin Ku / Greg Dudley / Silas Cook / Anita Mattson)
- **Efficient Strategies Towards Complex Molecules**
  (*Jenn Stockdill* / Vy Dong / Matthew Gaunt)
- **Process Research in Organic Synthesis**
  (*Kristin Price* / Chris Sfouggatkis / Adam Burrell / Eric Fang)
- **Novel Transition Metal Processes**
  (*Jeremy May* / Takashi Ooi / Tom Rovis)
- **Drug Discovery and Chemical Biology**
  (*Nikki Goodwin, Jared Piper* / Julia Cray / Marc Robillard)
- **Palladium Catalysis and Green Chemistry**
  (*Jade Nelson* / Matt Sigman / Mike Krische)

ORGANOMETALLIC CHEMISTRY
Advancing the Future Through Fundamental Discoveries
Jul 6-11, 2014
Salve Regina University, Newport, RI
Chair: Bernadette T. Donovan-Merkert
Vice Chair: Jerzy Klosin

- **Tools of the Trade**
  (*Jerzy Klosin* / Clark Landis / William Geiger)
- **Organic Transformations**
  (*Richard Fisher* / M. Christina White / Gojko Lalik / Patrick Walsh / Elizabeth Jarvo)
- **F and f-Block Chemistry**
  (*Nora Radu* / Tobias Ritter / Paula Diaconescu / James Boncella)
- **Energy and Sustainability**
  (*Clifford Kubiak* / Meike Niggemann / Monte Helm / Wesley Bernskoetter)
- **Ligand Platforms**
  (*John Walzer* / Connie Lu / Juan Casares / Thomas Clark)
- **Reactivity Across the Periodic Table**
  (*Russell Hughes* / Nilay Hazari / Todd Marder)
- **Mechanism and Theory**
  (*Karen Goldberg* / Jack Norton / Odile Eisenstein / Klaus Theopold)
- **Ligand Design and Reactivity**
  (*Kensha Clark* / John Arnold / Seth Brown / Jeremy Smith)
- **Organometallic Chemistry and the Future**
  (*Joseph Templeton* / Robert Bergman / Harry Gray)

GRS **ORGANOMETALLIC CHEMISTRY**
At the Interface Between Classical Organic and Inorganic Chemistry
Jul 5-6, 2014
Chair: Myles B. Herbert
Associate Chair: Mari S. Rosen

OSCILLATIONS & DYNAMIC INSTABILITIES IN CHEMICAL SYSTEMS
Self-Organization and Complexity
Jul 13-18, 2014
Melia Golf Vichy Catalan Business & Convention Center, Girona - Costa Brava, Spain
Chair: Dezso Horvath
Vice Chair: Annette F. Taylor

- **Electrochemical Systems**
  (*Istvan Kiss* / Katharina Krischer / Hamilton Varela)
- **Engineering Functional Materials**
  (*John Pojman* / Bartosz A. Grzybowski / Kohzo Ito / Katarina Novakovic)
- **Flow-Driven Complexity**
  (*Oliver Steinbock* / Anne De Wit / Stephen Morris)
- **Molecular Machines and Collective Behavior**
  (*Kenneth Showalter* / Carsten Beta / Tomohiko Yamaguchi)
- **Pattern Formation in Heterogeneous Systems**
  (*Irving Epstein* / Istvan Lagzi / Mark Tinsley / Daishin Ueyama)
- **Reactive Interfaces**
  (*Vilmos Gaspar*)
- **Self-Organization in Cellular Systems**
  (Marcus Dahlem / Annie Lemarchand / Stanislav Y. Shvartsman)
- **Systems Chemistry, Systems Biology**
  (Douglas Philp / Yannick Rondelez)
- **Late-Breaking Topics**
  (*Annette Taylor*)

GRS **OSCILLATIONS & DYNAMIC INSTABILITIES IN CHEMICAL SYSTEMS**
Self-Organization and Complexity
Jul 12-13, 2014
Chair: Laurence D. Rongy

PHOSPHORYLATION & G-PROTEIN MEDIATED SIGNALING NETWORKS
Regulation of Kinases and G Proteins in Normal, Pathological, and Synthetic Systems
Jun 15-20, 2014
University of New England, Biddeford, ME
Chair: Melanie H. Cobb
Vice Chair: Carmen W. Dessauer

- **Stem Cell Signaling**
  (Sylvain Meloche / Anne Brunet / Yukiko Gotoh)
- **Kinases and G Proteins in Development**
  (Swathi Arur / Joe Avruch / Stacy Ogden / Saikat Mukhopadhyay / Anton Bennett)
- **Kinases and G Proteins Controlled by Pathogens and Stress**
  (*Jessie English* / Neal Alto / Jean Wang / Roger Davis)
- **Target Discovery Through Networks and Proteomics**
  (*Dafna Bar-Sagi* / Dafna Bar-Sagi / Elliott Ross / Walter Kolch / Anne-Claude Gingras)
- **Biosynthetic Interactions with Kinases and G Proteins**
  (*Alexandra Newton* / Anabela Srebrow / Estele Jacinto / Alexandra Newton)
- **G Protein and Kinase Diversity and Control Mechanisms**
  (*Carmen Dessauer* / Carmen Dessauer / Gray Pearson / Carol Lange / David Robbins / Michael Reese)
- **Detection and Manipulation of Kinase and GPCR Signaling**
  (Jurgen Wess / Jin Zhang / Natalia Riobo / Piero Crespo)
- **Structures, Models, and Strategies**
  (*Natalie Ahn* / Stefan Knapp / Xuewu Zhang / Natalie Ahn / Ron Dror)
- **Keynote Session: Ras**
  (*Melanie Cobb* / Frank McCormick)

GRS **PHOSPHORYLATION & G-PROTEIN MEDIATED SIGNALING NETWORKS**
New Approaches to Characterizing Molecular Mechanisms of Disease
Jun 14-15, 2014
Chair: Aileen Klein
Associate Chair: Adam Coster

PHOTONUCLEAR REACTIONS
From Quarks to Nuclei
Aug 10-15, 2014
Holderness School, Holderness, NH
Chairs: Ronald A. Gilman & Lothar Tiator
Vice Chair: Alberto Accardi

- **Late-Breaking Topics**
  (*Ken Hicks* / Randolf Pohl / Buddhini Waidyawansa / Christine Aidala / Sevil Salur)
- **Long-Range Structure of Nucleons**
  (*Juergen Arends* / Michael Distler / Guy Ron / Michael Kohl / Marc Vanderhaeghen / Evangeline Downie / Phillipe Martel / Gerald Miller)
- **Low Energy Tests of the Standard Model**
  (*Xiaochao Zheng* / Angela Papa / Liping Gan / Liang Yang / Achim Denig / Raphael Dupre)
- **Quark and Spin Structure**
  (*Xiaodong Jiang* / Ami Rostomayan / Karl Slifer / Haiyan Gao / Paolo Pedroni / Julie Roche / Bernd Surrow)
- **Nuclear Structure**
  (*Bernd Krusche* / Concenttina Sfienti / Anne Sauerwein / Sonia Bacca / Douglas Higinbotham / Or Hen)
- **Hadron Structure**
  (*Reinhard Beck* / Ralf Gothe / Valentina Vegna / Masayuki Niiyama / Michael Ostrick / Annika Thiel / Andy Sandorfi / Irakli Keshelashvili)
- **Nuclear Structure at Short Range**
  (*William J. Briscoe* / Kawtar Hafidi / Valeria Muccifora / Eliezer Piasetzky / Misak Sargsian / Zein-Eddine Meziani)
- **Advances in Theory**
  (*Jan Ryckebusch* / Mikhail Gorshteyn / Ian Cloet / Ron Workman / Ulrich Mosel / Barbara Pasquini / Huey-Wen Lin / Ruben Flores)
- **Intersections and Future Possibilities**
  (*Paul E. Reimer* / Barbara Badelek / Victor Gehman / Charles Horowitz / Allison Lung)

PHOTOSYNTHESIS
From Evolution of Fundamental Mechanisms to Radical Re-Engineering
Aug 10-15, 2014
Mount Snow Resort, West Dover, VT
Chair: David Kramer
Vice Chair: Fabrice Rappaport

- **New Approaches and Radical Re-Engineering of Photosynthesis**
  (R. David Britt / Neil Hunter / Petra Fromme / John Golbeck / Marc Fontecave / Jim Allen)
- **Light Harvesting: Biophysical and Biochemical Mechanisms**
  (Greg Scholes / Diana Kirilovski)
- **Light Harvesting: Dynamics and Regulation**
  (Roberta Croce / Jun Minagawa)
- **Reaction Centers**
  (*Bill Rutherford* / Kevin Redding / Elisabet Romero / Haijun Liu)
- **Oxygen Evolution**
  (*Richard Debus* / Johannes Messinger / Nick Cox / Leonardo Guidoni)
- **The Electronic and Ionic Circuits of Photosynthesis: Electron Transfer**
  (Eva-Mari Aro / Mark Aurel Shoettler)
- **The Electronic and Ionic Circuits of Photosynthesis: Protons and Ions**
  (Giovani Finazzi / Cornelia Spetea-Wiklund / Helmut Kirchhoff)
- **Regulation and Integration of Photosynthesis with the Cell, Stress, NPQ, Nutrient Deficiency**
  (Arthur Grossman / Michael Hippler)
- **Evolution and Biodiversity of Photosynthesis**
  (Don Bryant / Eva Nowack / Benjamin Bailleul)

GRS **PHOTOSYNTHESIS**
Energy at the Interface: Photons to Chemical Bonds, and Back Again
Aug 9-10, 2014
Chair: Eliezer M. Schwarz

PHYSICS RESEARCH & EDUCATION
The Complex Intersection of Biology and Physics
Jun 8-13, 2014
Mount Holyoke College, South Hadley, MA
Chairs: Mel Sabella & Matthew J. Lang
Vice Chairs: Duncan Brown & Dean A. Zollman

- **Keynote Session: The Complex Intersection of Biology and Physics: Perspectives from Research and Education**
  (*Mike Klymkowsky* / Howard Berg / Edward "Joe" Redish)
- **Meeting the Needs of Life Science Students in Introductory Physics Through Course Transformation**
  (*Eric Brewe* / Catherine H. Crouch / Dawn C. Meredith / Robert C. Hilborn)
- **Single Cell and Molecular Techniques Involving Biological Motors at the Boundary of Biology and Physics**
  (*Mark Reeves* / Jonathon Howard / Wonmuk Hwang)

- **New Trends in Soft Condensed Matter Physics: Research and Education**
  (*Enrique M. De La Cruz* / David A. Weitz / Jennifer Ross / Edit Yerushalmi)
- **Novel Laboratory Activities for the Biophysics and Bio-Engineering Curriculum**
  (*Steven Vogel* / Steve Wasserman / Barbara Hughey)
- **Improving the Scientific Competencies and Attitudes of Biology and Pre-Med Students Through Multidisciplinary Reform**
  (*Kenneth Heller* / Todd Cooke / Ross Nehm / Kimberly D. Tanner)
- **Effective Use of the Textbook at the Intersection of Biology and Physics**
  (*Ruth Chabay* / Philip Nelson / Jané Kondev)
- **Understanding Current Health Needs and Novel Techniques in Biomedicine**
  (*Juan R. Burciaga* / Wolfgang Losert / Ralf Widenhorn / Manu O. Platt)
- **Involving Undergraduates in Cutting Edge Biophysics Research and its Implications for Instruction**
  (*Sean P. Robinson* / Ashley R. Carter / Carlos Castro)

PLANT & MICROBIAL CYTOSKELETON
Cell Morphogenesis and Division
Aug 10-15, 2014
Proctor Academy, Andover, NH
Chair: Fred Chang
Vice Chair: Magdalena Bezanilla

- **Keynote Session: Frontiers in Cell Morphogenesis**
  (*Fred Chang* / John Pringle / Grant Jensen / Jacque Dumais)
- **Cytoskeletal Building Blocks**
  (*Tom Pollard* / Joe Pogliano / David Kovar / Laurent Blanchoin / Marcel Janson)
- **Mitosis and Chromosomes**
  (*Geoff Wasteneys* / Wei Lih Lee / Agit Jokeglar / Rafael Daga)
- **Dividing the Cell**
  (*Harold Erikson* / Laurie Smith / Jian Qiu Wu / Petra Levin)
- **Selected Poster Presentations**
  (*Magdalena Bezanilla*)
- **Cellular Mechanics and Organization**
  (*KC Huang* / Zemer Gitai / Nicolas Minc / Otger Campas / Olivier Hamant)
- **Molecular Motors and Movement**
  (*Bruce Goode* / Gohta Goshima / Chad Pearson / Luis Vidali / Marko Kaksonen)
- **Shaping the Cell Wall**
  (*David Erhardt* / Doug Weibel / Ying Gu / Nassos Typas)
- **Breaking Symmetry**
  (*Laurie Smith* / Sophie Martin / Sid Shaw / Roland Wendlich-Soldner)

PLANT MOLECULAR BIOLOGY
Decision-Making Pathways, Networks, and Models in Plant Biology
Jul 20-25, 2014
Holderness School, Holderness, NH
Chair: Steven P. Briggs
Vice Chair: Mary Lou Guerinot

- **Keynote Session: Cross-Talk in Growth Regulatory Networks**
  (*Steve Briggs* / Dirk Inze)
- **Systems Biology**
  (Wolfgang Busch / Christine Queitsch)
- **Decoding Nutrients**
  (Rodrigo Gutierrez / Mary Lou Guerinot / Kiwamu Tanaka)
- **Growth and Development**
  (Katja Baerenfaller / Ginny Walbot / Philip Benfey)
- **Networks and Models**
  (Nelimma Sinha / Gloria Corruzzi)
- **Cross-Talk in Abiotic Stress Signaling**
  (Jose Dinneny / Julian Schroeder)
- **Cross-Talk in Biotic Stress Signaling**
  (Katie Dehesh / Heribert Hirt / Jane Glazebrook / Jean Greenberg)
- **Peptide Signaling**
  (Mike Sussman / David Jackson / Keiko Torii)
- **Epigenomics and Regulatory RNA**
  (Bob Schmitz)

GFS PLANT MOLECULAR BIOLOGY
Exploring High Throughput Data Sets
Jul 19-20, 2014
Chair: Ryan C. Sartor

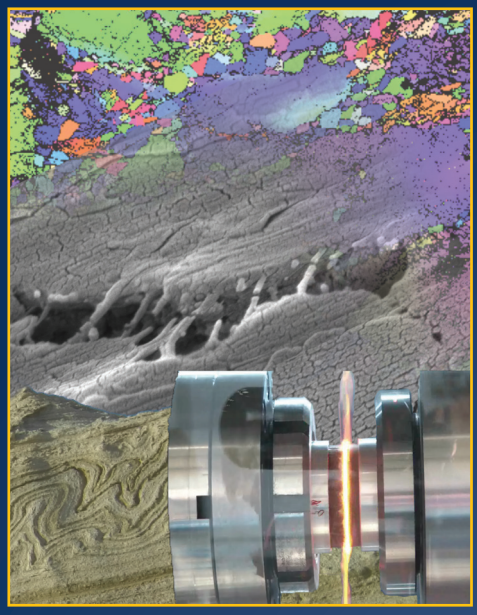

Photo mosaic of recrystallization microstructure in ice (top), super plastic calcite nano-fibers (middle), fluidization of sand bed due to earthquake (bottom left), and high-speed friction experiment (bottom right). Courtesy of Laurent G.J. Montesi, University of Maryland (mosaic creator); David Prior, Narayana Golding, and William B. Durham, MIT (ice); Bart Verberne and Christopher J. Spiers, Utrecht University (nano-fibers); Francois Renard, ISTerre, France (fluidization); Giulio Di Toro, INGV, Italy (high-speed friction). Submitted by Wen-lu Zhu, Chair, Rock Deformation GRC.

PLASMA PROCESSING SCIENCE
Many Scales, Many Applications, One Discipline
Jul 27 - Aug 1, 2014
Bryant University, Smithfield, RI
Chair: Jane P. Chang
Vice Chair: Achim Von Keudell

- **Will We Ever Control Plasmas?**
  (*Masaru Hori* / Miles Turner / Erik Wagenaars)
- **Plasma and Surface Chemistry at Extreme Scales**
  (*Mark Kushner* / Laurence Campbell / Eva Kovacevic / Erwin Kessels)
- **Plasmas and Nano-Materials**
  (*Vincent Donnelly* / Meyya Meyyappan / Uwe Kortshagen)
- **Dynamics of High Power Impulse Plasmas**
  (*Jón Tómas Guðmundsson* / Nils Brenning / Ante Hecimovic / James Bradley)
- **Plasma Modeling**
  (*Anthony Murphy* / Ute Ebert / Masaya Shigeta)
- **Plasma Medicine**
  (*Deborah O'Connell* / Theresa Freeman / Jan Benedikt / Jean-Michel Pouvesle)
- **Plasmas and Liquids**
  (*Luc Stafford* / Peter Bruggeman / Antoine Rousseau)
- **Demystifying Dielectric Barrier Discharges**
  (*Richard van de Sanden* / Fiorenza Fanelli / Ronny Brandenburg / David Go)
- **Plasmas for Energy Production and Storage**
  (*Yi-Kang Pu* / Eugen Stamate / Francisco Tabarés)

GFS PLASMA PROCESSING SCIENCE
Non-Equilibrium Plasma Diagnostics, Modeling, and Applications
Jul 26-27, 2014
Chair: Robert P. Geiger
Associate Chair: Natalie Shainsky

PLASMONICS
Manipulating Light-Matter Interaction at the Nanoscale
Jul 6-11, 2014
Sunday River Resort, Newry, ME
Chair: Mark L. Brongersma
Vice Chair: Harald W. Giessen

- **Recent Developments and Breakthroughs in Plasmonics**
  (*Albert Polman* / Peter Nordlander / Din Ping Tsai / Alexandra Boltasseva)
- **Fundamentals and Applications of Plasmonic Antennas**
  (*Mark Stockman* / Evelyn Hu / Xiang Zhang / Suljo Linic / Joachim Krenn)
- **New Materials for Plasmonics**
  (*Pieter Kik* / Otto L. Muskens / Thomas Taubner / Dmitry Basov)
- **Optical Antennas and Metasurfaces**
  (*Vlad Shalaev* / Philippe Lalanne / Olivier Martin / Federico Capasso / Sergey Bozhevolnyi)
- **Novel Fabrication and Characterization Techniques**
  (*Katherine Willets* / Teri Odom / Hao Yan / Jennifer Dionne)
- **Quantum, Singular, and Spin Effects in Plasmonics**
  (*Rashid Zia* / Asger Mortensen / Zubin Jacob / Harry Atwater / Erez Hasman)
- **Plasmonics in Biology and Sensing**
  (*Naomi Halas* / Hatice Altug / Romain Quidant / Gennady Shvets)
- **New Developments in Nanophotonic Devices**
  (*Uriel Levy* / Alain Dereux / Stefan Maier / Tobias Kippenberg / Jacob Khurgin)
- **Future Perspectives and Predictions**
  (*Harald Giessen* / Nader Engheta)

GFS PLASMONICS
Revolutions in Fundamental and Applied Control of Light at the Nanoscale
Jul 5-6, 2014
Chair: Patrick Landreman

POLYMER PHYSICS
New Developments in Polymer Dynamics, Crystallization, Self-Assembly, and Interface/Confinement Effects
Jul 13-18, 2014
Mount Holyoke College, South Hadley, MA
Chair: Sindee Simon
Vice Chairs: Jane E. Lipson, Scott T. Milner & Karen I. Winey

- **Polymers for Energy and Electronic Applications**
  (*Nitash Balsara* / Lynden Archer / Rachel Segalman)
- **Polymer Rheology and Entanglement Dynamics**
  (Dimitris Vlassopoulos / Hiroshi Watanabe / Bob Weiss)
- **Polymer Dynamics in Confinement**
  (*James Forrest* / Kari Dalnoki-Veress / Reiner Zorn)
- **Crystallization and Self-Assembly**
  (*Bryan Vogt* / Rufina Alamo / Chinedum Osuji / Richard Register)
- **Biomacromolecular Physics**
  (*Rajesh Khare* / Shekhar Garde / Arun Yethiraj)
- **The Next Generation of Polymer Physics**
  (*Connie Roth* / Harry Bermudez / Jodie Lutkenhaus / Cécile Monteux / Rodney Priestley / Robert Riggleman / Charles Schroeder)
- **Theory and Modeling of Polymer Dynamics**
  (*Kenneth Schweizer* / Jack Douglas / Marina Guenza)
- **Polymers at Interfaces and Surfaces**
  (Ramanan Krishnamoorti / Linda Schadler / Y. Elaine Zhu)
- **Self-Assembly of Supramolecular Assemblies and Block Copolymers**
  (*Ronald Hedden* / Stephen Cheng / Frank Bates)

POLYMER PHYSICS
At the Intersection Between Physics, Chemistry, and Engineering
Jul 12-13, 2014
Chair: Laura Gray
Associate Chair: Daniel R. King

POST-TRANSCRIPTIONAL GENE REGULATION
From Mechanism Stems Therapy
Jul 13-18, 2014
Salve Regina University, Newport, RI
Chair: Melissa Moore
Vice Chairs: Chris Burge & Peter Sarnow

- **Regulation of Translation**
  (Jonathan Weissman / Nahum Sonenberg / Peter Sarnow / Rachel Green)
- **Intracellular RNA Transport and Localization**
  (Robert Singer / Nancy Kedersha)
- **Biological Activity from Extracellular RNA**
  (Jan Lötvall / Anastasia Khvorova / Oliver Rando)
- **Pre-mRNA Processing**
  (Phillip Sharp / Tracy Johnson / Christine Guthrie / Yoshi Misui / Adrian Krainer / Brett Monia)
- **RNA and Congenital/Neurologic Disorders**
  (Gene Yeo / Stuart Peltz / Matthew Disney)
- **RNA/DNA Editing and Gene Silencing**
  (Kazuko Nishikura / Tao Pan / Hiten Madhani / Rachel Meyers)
- **Alternate 3'UTRs and mRNA Decay**
  (Christine Mayr / Lynne Maquat / Britt Glaunsinger / James Barsoum)
- **The Long and Short of Non-Coding RNAs**
  (Joan Steitz / Gideon Dreyfuss / Julia Salzman / Howard Chang / Mitch Guttmen)
- **Genomics and Evolution of RNA Biology**
  (Brent Graveley / Chris Burge / Ben Blencowe / Dan Herschlag)

POST-TRANSCRIPTIONAL GENE REGULATION
Controlling Gene Expression Through mRNA Regulation
Jul 12-13, 2014
Chair: Jason A. Somarelli
Associate Chair: Daneen Schaeffer

PROTEIN PROCESSING, TRAFFICKING & SECRETION
At the Crossroads of Understanding the Maturation and Transport of Proteins/Peptides and the Therapeutic Applications of Post-Translational Modulation
Jul 20-25, 2014
Colby-Sawyer College, New London, NH
Chair: John W. Creemers
Vice Chair: Paul H. Taghert

- **Folding, Quality Control and Activation in the Secretory Pathway**
  (*Peter Arvan* / Nabil Seidah [keynote] / Matthew Freeman / Feroz Papa / Randal Kaufman)
- **PCSK9: The Therapeutic Target for the Next Blockbuster Drug in Heart Disease?**
  (*Annik Prat* / Evan Stein / Thomas Legacé / Trond Leren / Rex Parker / Xiaowei Chen)
- **Granule Biogenesis and Secretion**
  (*Thomas Martin* / Chris Rhodes / Ronald Holz / Alan Attie / Aaron Turkewitz)
- **Proprotein Convertases in Homeostasis and Pathologies**
  (*Robert Day* / Iris Lindberg / Daniel Bassi / Torsten Steinmetzer / Geraldine Siegfried)
- **Trafficking Pathways, Sorting and Intercellular Communication**
  (*Robert Fuller* / Vivian Budnik / Wim Annaert / Indira Mysorekar / Tanja Kögel)
- **Posttranslational Modifications in the Secretory Pathway and Extracellular Matrix**
  (*Betty Eipper* / Vincent Tagliabracci / Hans-Ulrich Demuth / Maurine Linder / Tal Alani)
- **Golgi Apparatus Structure and Function**
  (*Gary Thomas* / Daniel Ungar / Masahiro Hosaka / Tsuyoshi Watanabe / Yanzhuang Wang)
- **NextGen and Omics Approaches to Study Posttranslational Modifications**
  (*Klaudia Brix* / Stephan Lichtenthaler / Marie Kveiborg / Martin Martin / Lloyd Fricker)
- **Processing and the Regulated Secretory Pathway**
  (*Majid Khatib* / Richard Mains / Peng Loh / Paul Taghert / Rina Rosin-Arbesfeld)

PROTEIN PROCESSING, TRAFFICKING & SECRETION
Insight into Molecular Mechanisms, Membrane Trafficking, Folding & ER Stress, Pathology and Therapeutic Applications
Jul 19-20, 2014
Chair: Jeroen Declercq

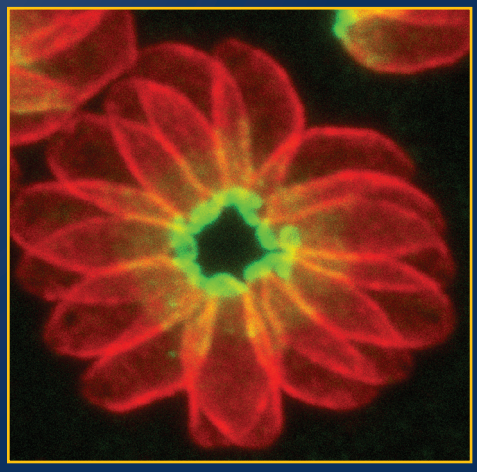

Toxoplasma gondii intracellular tachyzoites typically organised as a rosette. The glideosome refers to a large myosin motor based machinery that powers gliding motility. The MyoA motor is pellicular, ubiquitously conserved across the Apicomplexa phylum and labelled in red (GAP45), while the posterior and coccidian specific MyoC motor is shown in green. Courtesy of Karine Frenal and Dominique Soldati-Favre (Université de Genève). Submitted by Steve Hajduk & Dominique Soldati-Favre, Chairs, Biology of Host-Parasite Interactions GRC.

PROTEOGLYCANS
Diverse Regulators of Health and Disease
Jul 6-11, 2014
Proctor Academy, Andover, NH
Chair: Nicholas Shworak
Vice Chair: Jeremy E. Turnbull

- **Late-Breaking Topics**
  (*Kazuyuki Sugahara, Sarah Knox*)
- **The Rise and Fall of GAGs: Biosynthesis, Catabolism and Mucopolysaccharidoses**
  (*Lena Kjellén, Jian Liu*)
- **Advances in Synthesis, Structural Analysis, Interactions and Glycomics**
  (*Anthony Day*)
- **Regulation of Signaling and Development**
  (*Pascale Zimmermann, Matthew Hoffman* / John Couchman / Pascale Zimmermann)
- **Multiple Roles in Cancer**
  (*Renato Iozzo, Nikos Karamanos* / Mitchell Ho)
- **Insights into Neural, Muscular and Skeletal Diseases**
  (*Hideto Watanabe, Amanda Fosang*)
- **Modulation of Stem Cell Fate for Regenerative Medicine**
  (*Catherine Merry, Alison Nairn*)
- **Controlling the Cross Roads of Inflammation and Cardiovascular Disease**
  (*Vincent Hascall, Liliana Schaefer*)
- **Translational Glycanology: Diagnostics and Therapeutics**
  (*Shukti Chakravarti, Mauro Pavão* / Jake Reder)

PROTEOGLYCANS
The Rise of Proteoglycans in Mechanotransduction and Microenvironmental Signaling
Jul 5-6, 2014
Chair: Thomas E. Neill

PROTEOLYTIC ENZYMES & THEIR INHIBITORS
Dysfunction in Disease, Mechanism and Therapeutic Targeting
Jun 22-27, 2014
Renaissance Tuscany Il Ciocco Resort, Lucca (Barga), Italy
Chair: James C. Whisstock
Vice Chair: Johanna A. Joyce

- **The Cardiovascular System**
  (*James Huntington* / James Huntington / Stephanie Smith)
- **Cancer**
  (Chris Overall / Stig Linder / Johanna Joyce)
- **Infection**
  (*Sheena McGowan* / Jan Potempa / Piet Gros / Rob Pike / Denise Monack)
- **New Developments in Protease Targeted Therapeutics**
  (*Ian Smith, Bob Lazarus* / Matthew Bogyo / Ari Melnick / Henrik Østergaard / Ed Madison)
- **Inhibitors**
  (F. Xavier Gomis-Ruth / Cliff Luke / Martine Jandrot-Perrus)
- **Deubiquitination**
  (*Guy Salvesen* / Guy Salvesen / Vishva Dixit / Titia Sixma)
- **In the Membrane**
  (*Matthew Freeman* / Matthew Freeman / Taisuke Tomita / Joanne Lemieux)
- **Proteases and Inhibitors Reaching into the Extracellular Environment**
  (Klaudia Brix / Steve Weiss / Irit Sagi)
- **Late-Breaking Topics**
  (*Johanna Joyce*)

PROTEOLYTIC ENZYMES & THEIR INHIBITORS
Proteases: Making the Cut in Biological Processes and Diseases
Jun 21-22, 2014
Chair: Antoine H. Dufour
Associate Chair: Laura Edgington

QUANTUM SCIENCE
Simulation, Verification, and Control of Complex Quantum Many-Body Systems
Jul 27 - Aug 1, 2014
Stonehill College, Easton, MA
Chairs: David J. Wineland & Hans Briegel
Vice Chairs: Jun Ye & Frank Verstraete

- **Quantum Testing and Verification**
  (*Umesh Vazirani* / Philip Walther / Matthias Troyer)
- **Simulation with Atomic and Molecular Systems**
  (*Christopher Monroe* / Rainer Blatt / Debbie Jin / Immanuel Bloch)
- **New Directions for Quantum Simulation**
  (*Ana Maria Rey* / Uwe-Jens Wiese / Juan Ignacio Cirac)
- **New Interfaces Between Quantum Information and Condensed Matter**
  (*David Huse* / Jelena Klinovaja / Chris Laumann / Akimasa Miyake)
- **Quantum Metrology and Sensing**
  (*Vladan Vuletic* / Ania Bleszynski Jayich / Joerg Wrachtrup)
- **Cavity-QED, Real and Artificial Atoms**
  (*Rob Schoelkopf* / Jean-Michel Raimond / Andrew Houck / Jeff Thompson)
- **Photonics and Photon Interfaces**
  (*David Awschalom* / Jacqueline Bloch / Jeremy O'Brien)

- **Optomechanics, Hybrid Systems**
  (*Dan Stamper-Kurn* / Markus Aspelmeyer / John Teufel / Arno Rauschenbeutel)
- **Frontiers in Quantum Information Theory**
  (*Patrick Hayden* / Seth Lloyd / Renato Renner)

QUANTUM SCIENCE
Advances in Quantum Information Science
Jul 26-27, 2014
Chair: David Hayes

RADIATION CHEMISTRY
Radiation Driven Processes in Physics, Chemistry, Biology, and Industry
Jul 13-18, 2014
Proctor Academy, Andover, NH
Chair: Jay A. Laverne
Vice Chair: James F. Wishart

- **Challenges in the Nuclear Power Industry**
  (Dave Showsmith / Melissa Denecke)
- **Nanoparticles and Radiation**
  (Hynd Remita / Fred Currell / Sudipta Seal)
- **Young Investigator Presentations**
- **Low Energy Electron Radiolysis**
  (Elahe Alizadeh / Slywia Ptasinska / Bernd Winter)
- **Heavy Ion Therapy and Protection**
  (Karen Kirby / Gerard Baldacchino)
- **Track Structure and Modeling**
  (Zdenka Kuncic / Mathieu Karamitros)
- **Polymer and Composite Radiolysis**
  (Mohamad Al-Sheikhly / Marie Claude Clochard)
- **Fast Kinetics in Radiation Chemistry**
  (Yosuke Katsumura / Mehran Mostavi / Kenji Takahashi)
- **Radiolysis of Macromolecules**
  (Peter O'Neill / Krzysztof Bobrowski)

RADIATION CHEMISTRY
Radiation Driven Processes in Physics, Chemistry, Biology and Industry
Jul 12-13, 2014
Chair: Sarah C. Reiff

RARE CELLS IN CIRCULATION
NEW!
Circulating Tumor Cells and Metastasis
Aug 3-8, 2014
Mount Holyoke College, South Hadley, MA
Chair: Brian J. Kirby
Vice Chairs: Andrew D. Rhim & Howard I. Scher

- **Translating Circulating Tumor Cell (CTC) Capture Technologies for Widespread Clinical Use**
  (Shannon Stott / Leon Terstappen)
- **Dissemination and Self-Seeding: New Insights into the Role of Circulating Cells**
  (Max Wicha / Dario Marchetti)
- **What Do CTCs Tell Us About the Pre-Metastatic Niche?**
  (Thea Tlsty / Tony Hollingsworth)
- **Prognosis with CTCs: Getting Beyond Hazard Ratio and Kaplan-Meier**
  (*David Nanus* / Daniel Danila)
- **Can CTCs Be Used to Diagnose and Stage Cancer?**
  (*Stefanie Jeffrey* / Anriban Maitra)
- **Can CTCs and Progenitor Cells Inform Surgical and Medical Treatment?**
  (Linda Vahdat)
- **Mining Molecular Analyses of CTCs**
  (Jim Hicks)
- **Interaction of Chemotherapy with CTCs**
  (Stuart Martin)
- **EMT: Phenotypic Changes and its Effect on CTC Data and its Interpretation**
  (Jing Yang)

ROCK DEFORMATION
Evolving Rock Structure: From Grain-Scale to Planet-Scale
Aug 17-22, 2014
Proctor Academy, Andover, NH
Chair: Wenlu Zhu
Vice Chair: Francois Renard

- **Seismogenesis Along Subduction Megathrusts**
  (*Julia Morgan* / Rick Sibson / James Mori)
- **Fault Zone Structure and Earthquake Mechanics**
  (David Lockner / Thomas Mitchell / Heather Savage)
- **Coseismic Slip Behavior and Laboratory Earthquakes**
  (*Terry Tullis* / Ze'Ev Reches / Giulio Di Toro)
- **Transient Slip Behavior and Deep Earthquakes**
  (*Teng-Fong Wong* / Joan Gomberg / Chris Marone / Alexander Schubnel)
- **Spatiotemporal Characteristics of Earthquakes and Induced Seismicity**
  (Georg Dresen / William L. Ellsworth)
- **Brittle-Ductile Transition and Microstructure Evolution**
  (*Hans de Bresser* / Jessica Warren / Holger Stunitz / Florian Fusseis)
- **Storage and Transport Properties of Reservoir Rocks**
  (Chris Spiers / Tiziana Vanorio)
- **Ice Rheology and Microstructure**
  (*William Durham* / Sandra Piazolo / Alyssa Rhoden / Christine McCarthy)
- **Integration of Observations, Experiments and Modeling in Rock Deformation**
  (*Brian Evans* / Andrea Tommasi / Russ Ewy)

ROCK DEFORMATION
Deformation of Geological Materials in Multi-Scale and Multi-Phase Systems
Aug 16-17, 2014
Chair: Lars N. Hansen
Associate Chair: Christine McCarthy

SALT & WATER STRESS IN PLANTS
From Molecules to the Field
Aug 3-8, 2014
Sunday River Resort, Newry, ME
Chairs: Michael R. Blatt & Eduardo Blumwald
Vice Chairs: Julia Bailey-Serres & Erwin Grill

- **Plants at the Limit**
  (*Dorothea Bartels* / Jill Farrant / Simon Barak / Zvi Peleg / John Cushman)
- **Stress and Development**
  (*Kazuo Shinozaki* / Christa Testerink / Leslie Sieburth / Ken Birnbaum / Vassilis Fotopoulos / Songhu Wang / Nico Geldner)
- **The Genetics of Stress**
  (*Anna Amtmann* / Motoaki Seki / Elizabeth Weretilnyk / Francois Tardieu)
- **Signalling**
  (*Erwin Grill* / Christine Foyer / Doris Wagner / Ron Mittler / Sona Pandey / Takashi Ueda / Teun Munnik)
- **Transport Mechanisms and Stress Interactions**
  (*Heven Sze* / Enrico Martinoia / Nathalie Leonhardt / Rucha Karnik / Karin Schumacher)
- **Water and Homeostasis**
  (*Steve Tyerman* / Francois Chaumont / Tracy Lawson / Harkamal Walia)
- **Metabolic Interactions**
  (*Mel Oliver* / Joachim Kopka / Christoph Peterhansel / Barry Pogson / Paul Verslues)
- **Long Distance and Whole-Plant Functions**
  (*Julia Bailey-Serres* / Herve Cochard / Graham Farquhar / Ian Dodd / Josetter Masle / David Salt / Keith Mott)
- **Engineering for Water Efficiency and Stress Tolerance**
  (*Julian Schroeder* / Mark Tester / Roberto Gaxiola / Ju-Kon Kim / Raquel Chan)

SCIENCE & TECHNOLOGY POLICY
Systems Approaches to Research and Practice
Aug 10-15, 2014
Waterville Valley Resort, Waterville Valley, NH
Chairs: Jennifer Kuzma & Kaye Fealing
Vice Chair: Jason A. Delborne

- **Keynote Session: Systems Analysis for Engaged Scholarship**
  (*Dale Wahlstrom* / George Richardson / Kimberley Thompson)
- **STEM Funding & Innovation Systems: Interactions and Impacts**
  (*Joshua Rosenbloom* / Maryann Feldman / Alan Porter / Carolyn Nguyen / Ismael Rafols)
- **Intellectual Property and Ownership: System Effects on S&T and Society**
  (*Thomas Woodson* / Thomas Hemphill / Shobita Parthasarathy / Joel West)
- **S&T Risk Governance Systems: Challenges and Data Needs**
  (*Gary Marchant* / Alta Charo / Joanne Shatkin / Marc Saner / Igor Linkov)
- **Natural Resources: Socio-Ecological Systems and Policy**
  (*Daniel Sarewitz* / Anne Kapuscinski / Vince Tidwell / Krystyna Stave / Fred Gould)
- **Public and Policy Feedback: S&T Communication and Engagement**
  (*Michael Caccatoire* / Ann Bostrom / Daniel Kleinman / Cynthia Selin / David Berube)
- **Engineered and Technological Systems: Science, Policy and Ethics**
  (*Wendell Wallach* / Elizabeth Wilson / Daniel Hastings / Ann Johnson)
- **S&T System Diversity: Workforce, Education & Institutions**
  (*Al Teich* / Laurel Smith-Doerr / Jeff Warren / Deborah Stine)
- **Keynote Session: S&T Policy Systems Research - Building a Field**
  (*Michele Garfinkel* / Venky Narayanamurti / Caroline Wagner / Christopher Bosso / Granger Morgan)

SCIENCE & TECHNOLOGY POLICY
Systems Analysis from Research to Practice
Aug 9-10, 2014
Chair: Thomas Woodson

SCIENTIFIC METHODS IN CULTURAL HERITAGE RESEARCH
Challenges and Complexity in Characterization and Conservation
Jul 27 - Aug 1, 2014
Sunday River Resort, Newry, ME
Chairs: Francesca Casadio & Philippe Walter
Vice Chairs: Jennifer Mass & Tim Wess

- **Scientific Studies of Ancient and Historic Production: Putting Cultural Heritage Research in Context**
  (*Barbara Berrie* / Margaret W. Conkey / Ashok Roy)
- **Conservation: The Problem of Condition - Diagnosis and Treatment**
  (*Alison Murray* / Matija Strlic / Maria Luisa de Carvalho / Piero Baglioni)
- **Conservation: Modes of Alteration and Prevention**
  (*Paul Whitmore* / Jaap Boon / Jim Druzik)
- **Advanced Analytical Methods of Promise for Cultural Heritage Applications**
  (*Yeonhee Lee* / Sergei Kazarian / Ester Ferreira / Demian Ifa)
- **Biodeterioration**
  (*Mary Lou Florian* / Archana Vasanthakumar / Valme Jurado)
- **3D Transport Phenomena**
  (*Fenella France* / Katrien Keune / Philippe Dillmann / Christian Amatore)
- **Collagen-Based Materials: Characterization and Preservation**
  (*Matthew Collins* / Caroline Tokarski / Craig Kennedy)
- **Surface Phenomena**
  (*Silvia Centeno* / Patrick Ravines / Gianluca Valentini / C. Richard Johnson, Jr.)

- **Keynote Session: Scientific Research for Modern Art - Current Needs and Future Outlook**
  (*Heinz-Eberhard Mahnke* / Narayan Khandekar)

SCIENTIFIC METHODS IN CULTURAL HERITAGE RESEARCH
Molecular and Material Analysis for Art, Archaeometry and Conservation
Jul 26-27, 2014
Chair: Stephanie Zaleski

SIGNAL TRANSDUCTION BY ENGINEERED EXTRACELLULAR MATRICES

Enhancing Complexity in Cellular Microenvironments
Jul 6-11, 2014
Bentley University, Waltham, MA
Chair: Jason A. Burdick
Vice Chair: Linda G. Griffith

- **Keynote Session: Materials and Mechanics in Controlling Cell Behavior**
  (*Jason Burdick* / Kristi Anseth / Michael Sheetz)
- **Adhesion and Signaling**
  (*Andres Garcia* / Milan Mrksich / David Odde / Jean Schwarzbauer)
- **Cellular Mechanotransduction**
  (*Kristopher Kilian* / Sanjay Kumar / Craig Simmons / Robert Mauck)
- **Engineering Stem Cell Niches**
  (*Sharon Gerecht* / Fiona Watt / Joseph Wu / Nicola Elvassore)
- **Cell Migration**
  (*Doug DeSimone* / Denis Wirtz / Ken Yamada)
- **Engineering 3D Environments**
  (*Kristyn Masters* / Claudia Fischbach / Dror Seliktar / Kevin Healy)
- **Understanding Matrix Assembly**
  (*Rebecca Carrier* / Robert Mecham / Shyni Varghese)
- **Growth Factor and ECM Interactions**
  (*Linda Griffith* / Bill Murphy / Jeff Hubbell / Jennifer Cochran)
- **Engineering Tissue Function**
  (*Ed Botchwey* / Gordana Vunjak-Novakovic / Jim Wells)

SIGNAL TRANSDUCTION BY ENGINEERED EXTRACELLULAR MATRICES
Studying and Directing Cellular Function Through Natural and Engineered Microenvironment
Jul 5-6, 2014
Chair: Brandon L. Blakely
Associate Chair: Jorge Valdez

SIGNALING BY ADHESION RECEPTORS

Spatial Relevance of Adhesion Signals
Jun 22-27, 2014
Bates College, Lewiston, ME
Chair: Martin J. Humphries
Vice Chair: Alpha S. Yap

- **Keynote Session: Ancestry of Adhesion - How Far Have We Come and What Is There Still to Learn?**
  (*Martin Humphries* / Jean Paul Thiery)
- **Spatial Control of Adhesion Signaling**
  (*Jim Norman* / Olivier Rossier / Tony Kanchanawong / Johanna Ivaska)
- **Cellular Niches and Tissue Architecture**
  (*Martin Schwartz* / Chris Chen / Cay Kielty / Fiona Watt)
- **Adhesion Control of Cell Division and Polarity**
  (*Senthil Muthuswamy* / Alpha Yap / Francis Barr / Torsten Wittmann)
- ***In Vivo* Models of Adhesion Signaling in Development**
  (*Fiona Watt* / Tony Koleske / Magdalena Zernicka-Goetz / Jen Zallen)
- **Tension Sensing and Signaling**
  (*Chris Chen* / Mark Smith / Martin Schwartz / Kun-Liang Guan)
- **Cytoskeletal Regulation**
  (*Johanna Ivaska* / Anna Akhmanova / Andrea McClatchey / James Nelson)
- **Mechanisms of Cell Migration**
  (*Margaret Frame* / Carl-Philipp Heisenberg / Kozo Kaibuchi / Dylan Burnette)
- **Tumor Cell Invasion and Adhesion Signaling Therapies**
  (*Alpha Yap* / Jim Norman / Senthil Muthuswamy / Margaret Frame)

SIGNALING BY ADHESION RECEPTORS
Adhesion Receptor Signaling in Health and Disease
Jun 21-22, 2014
Chair: Nina N. Brahme
Associate Chair: Guillaume Jacquemet

SINGLE MOLECULE APPROACHES TO BIOLOGY

Understanding Life at a Higher Resolution
Jul 13-18, 2014
Renaissance Tuscany Il Ciocco Resort, Lucca (Barga), Italy
Chairs: Hermann Gaub & Michelle Wang
Vice Chairs: Toshio Yanagida & David Rueda

- **Keynote Session: From Mechano-Sensing to Biopysics of Cancer**
  (*Michelle Wang* / Steve Kowalzykowski / Mike Sheetz)
- **Nanodevices**
  (*Hermann Gaub* / Steven Quake / Philip Tinnefeld / Klaus Schulten)
- **Super Resolution Microscopy**
  (W.E. Moerner / Stefan Hell / Petra Schwille)
- **Force & Function**
  (Julio Fernandez / Daniel Müller)
- **Molecular Devices**
  (Kazuhiko Kinoshita / Cees Dekker / Hagan Bayley)
- **Molecular Motors**
  (*David Rueda* / Claudia Veigel / Zev Bryant / Keir Neuman)
- **Chromatin Mechanics**
  (Stirling Churchman / Yujie Sun / John Marko / Antoine van Oijen)
- ***In-Vivo* Methods**
  (Taekjip Ha / Bianxia Cui / Jan Liphardt / Lu Bai)
- **Advanced Instrumentation**
  (*Toshio Yanagida* / Tom Perkins / Toshio Ando / Vincent Croquette)

SINGLE MOLECULE APPROACHES TO BIOLOGY
Biomolecules at the Boundary Condition
Jul 12-13, 2014
Chair: Michael A. Nash

SOLID STATE CHEMISTRY

Solid State Compounds and Materials for Emerging Technologies and Sustainable Energy Generation
Jul 27 - Aug 1, 2014
Colby-Sawyer College, New London, NH
Chair: Susan M. Kauzlarich
Vice Chair: Hans-Conrad Zur Loye

- **Energy Conversion Materials**
  (Stu Soled / Joe Sunstrom / Galen Stucky)
- **High Temperature Materials**
  (Barbara Albert / Takao Mori / Sabah Bux)
- **Multifunctional Correlated Oxides**
  (Matt Rosseinsky / Craig Fennie / John Greedan)
- **Functional Intermetallics**
  (Claudia Felser / Julia Chan / Tyrell McQueen)
- **Energy Storage Materials**
  (Alexandra Navrotsky / Ryoji Kanno / Bart Bartlett / Ashfia Huq)
- **Nanostructured Materials**
  (Sara Skrabalak / Pingyun Feng / Artem Abakumov / Jillian Buriak)
- **Energy Efficient Materials**
  (Anja-Verena Mudring / Jen Aitken / Pierre Ferdinand Poudeu / Catherine Oertel)
- **Multiferroic Materials**
  (Antoine Maignan / Nicola Spaldin)
- **New Functional Materials**
  (John Parise / Josh Goldberger)

STEREOCHEMISTRY

Modern Stereochemistry in Synthesis, Catalysis, and Chemical Biology
Jul 27 - Aug 1, 2014
Salve Regina University, Newport, RI
Chairs: Joel Hawkins & Helma Wennemers
Vice Chairs: Scott Denmark & John Ragan

- **Frontiers in Stereoselective Catalysis**
  (*Scott Denmark* / Andreas Pfaltz / Gregory Fu)
- **Bioinspired Stereochemistry - Total Synthesis and Discovery**
  (*Mark Noe* / Wilfred van der Donk / Michelle Chang / Milan Mrksich / Dirk Trauner)
- **Asymmetric Catalysis and Stereoselective Synthesis**
  (*Hans Peter Nestler* / Mikiko Sodeoka / Michael Martinelli / Hisashi Yamamoto)
- **Stereocontrol on an Industrial Scale**
  (*Edward Grabowski* / Michael Cassidy / Vittorio Farina / James Leighton / David Collum)
- **Stereochemistry at Interfaces**
  (*Christopher Welch* / Eric Anslyn / Joanna Aizenberg / M.G. Finn)
- **Stereoselective Catalysis - Experiment and Theory**
  (*Jon Lorenz* / Abigail Doyle / Takashi Ooi / Cristina Nevado / Ken Houk)
- **Asymmetric Catalysis**
  (*Chris Senanayake* / Sarah Reisman / Eric Jacobsen / Erick Carreira)
- **Medicinal Chemistry**
  (*Guido Koch* / William Roush / Michael Shultz / Konrad Bleicher / John Wood)
- **Chemical Biology**
  (*John Ragan* / Laura Kiessling / Ronald Breslow [keynote])

STRUCTURAL NANOMATERIALS

NEW!

Recent Advances in Understanding the Structures and Properties of Nanomaterials
Jul 20-25, 2014
The Chinese University of Hong Kong, Hong Kong, China
Chairs: Chain T. Liu & T. G. Nieh
Vice Chairs: Jian Lu & Christopher Schuh

- **Keynote Session: Advanced in Energy Systems and Structural Materials**
  (*Jian Lu, Hayden Chen* / Way Kuo / Subra Suresh)
- **Bulk Metallic Glasses with Heterogeneous Structures: Deformation & Plastic Flow**
  (*A. Inoue, Chuang Dong* / Lindsay Greer / W.H. Wang / K. Samwer)
- **Bulk Metallic Glasses with Heterogeneous Structures: Atomistic Modeling**
  (*Katherine Flores, Peter Liaw* / En Ma / Yong Yang)
- **Nanostructured Steels and Metallic Materials: Nanostructures Features**
  (*Z.P. Lu, Shigeharu Ukai* / Ke Lu / David Seidman / Dierk Raabe)
- **Nanostructured Steels and Metallic Materials: Phase Relationship and Stability**
  (*K.C. Chou, J.R. Yang* / Simon P. Ringer / J.C. Zhao)
- **Nanomposite Materials: Deformation of Multilayered Structures**
  (*Andrea Hodge, John Balk* / Chris Schuh / Cynthia Volkert / Amit Misra)
- **Nanocomposite Materials: Composite Materials**
  (*Xingjun Liu* / Jacob Huang / C.Y. Liu)
- **Characterization Tools and Deformation Mechanics of Nanostructural Materials: Nanostructural Characterization**
  (*E. P. George, Ian Baker, Tong-yi Zhang* / M.W. Chen / Mike Mills / Mike Miller)
- **Characterization Tools and Deformation Mechanics of Nanostructural Materials: Deformation Mechanics**
  (*Xun-li Wang, Alfonso Ngan* / Helena Swygenhoven / Julia Greer)

SYNAPTIC TRANSMISSION
Synapses in Networks
Aug 3-8, 2014
Waterville Valley Resort, Waterville Valley, NH
Chair: Peter Jonas
Vice Chair: Ege Kavalali

- **Synaptic Transmission: From Molecular Machines to Network Activity**
  (*Roger Nicoll* / Reinhard Jahn / Edvard Moser)
- **Exocytosis of Synaptic Vesicles**
  (*Ege Kavalali* / Robert Edwards / Nils Brose / Axel T. Brunger)
- **Presynaptic Terminals**
  (*Ralf Schneggenburger* / Ling-Gang Wu / Craig Jahr / Wade Regehr / David DiGregorio)
- **Synaptic Spines**
  (Zoltan Nusser / Thomas Oertner / Haruo Kasai / Katherine Roche)
- **Pre- and Postsynaptic Plasticity**
  (*Pablo E. Castillo* / Steven A. Siegelbaum / Yukiko Goda / Richard L. Huganir)
- **Synaptic Connectomics**
  (*Kristen M. Harris* / Hollis Cline / Moritz Helmstädter / Dmitri B. Chklovskii / Joshua Trachtenberg)
- **Synaptic Diseases**
  (*Richard Tsien* / Thomas C. Südhof / Robert C. Malenka / Maria Lindskog / Stephen J. Smith)
- **Synaptic Transmission in Microcircuits**
  (*Yang Dan* / Michael Häusser / Ivan Soltesz / Andreas Lüthi)
- **Networks and Network Models**
  (Yang Dan / Jozsef Csicsvari / Jeffrey C. Magee)

GFS SYNAPTIC TRANSMISSION
From Molecular Machines to Local Circuit Function
Aug 2-3, 2014
Chair: Thomas J. Younts
Associate Chair: James A. Daniel

TETRAPYRROLES, CHEMISTRY & BIOLOGY OF
Hemes, Chlorophylls, Bilins, Corrins (Vitamin B12) and Related Cofactors of Life
Jul 20-25, 2014
Salve Regina University, Newport, RI
Chair: Martin J. Warren
Vice Chair: John Phillips

- **Understanding Tetrapyrrole Structure / Function**
  (*Andrew Munro* / CS Raman / Nicole Frankenberg-Dinkel)
- **Making and Breaking Tetrapyrroles**
  (*Jennifer Dubois* / Bernhard Krautler / Michi Taga / Wolfgang Schoefberger / Angela Wilks)
- **Tetrapyrroles in Signalling and Sensing**
  (*Alison Smith* / Bob Kranz / Eric Skaar / Catherine Drennan)
- **Metals and Tetrapyrroles**
  (*Dieter Jahn* / Mark O'Brian / Harry Dailey / Wilhem Boland)
- **Evolution of the Cofactors of Life**
  (*Stuart Ferguson* / Clark Lagarias / Jonathan Lindsey)
- **Tetrapyrroles in Health and Disease**
  (*Celia Golding* / Jean-Charles Deybach / Helga Refsum / Tim Egan)
- **Delivery and Repair of Tetrapyrroles**
  (*Gloria Ferreira* / Iqbal Hamza / Peter Nixon)
- **Synthetic Biology with Tetrapyrroles**
  (*Matthew Terry* / Joseph Hupp / Ross Anderson / Emma Raven)
- **Paradigm Shifts**
  (*Mark Shepherd* / Masao Ikeda-Saito / Neil Hunter)

THIN FILM & SMALL SCALE MECHANICAL BEHAVIOR
Observations, Insights and Analyses: What's New in the World of Micro Mechanics
Jul 13-18, 2014
Bentley University, Waltham, MA
Chair: Neville R. Moody
Vice Chair: Erica T. Lilleodden

- **Deformation and Fracture Under Dynamic Loading**
  (*Mathias Goeken* / Chris Eberl / Ellen Cerreta)
- **Advances in Small Scale Testing**
  (*Johann Michler* / Karsten Durst / David Armstrong)
- **Plasticity and Fracture at Small Length Scales**
  (*Ruth Schwaiger* / Christoph Kirchlechner / William Clegg)
- **Multi-Scale Modeling of Mechanical Behavior in Small Structures**
  (Alex Hartmaier / Chris Weinberger)
- **Deformation in Thin Film Structures**
  (Jeff Kysar / Steve Bull / Christophe Coupeau)
- **Biomaterials, Soft Materials, and Gels**
  (*Michelle Oyen* / Vicky Nguyen / Virginia Ferguson)
- **Energy Materials, Nanostructured Materials, and Nanocomposites**
  (*Julia Greer* / Seung Min Han / Jörg Weissmüller)
- **Nanostructured Materials**
  (*Brad Boyce* / Nathan Mara / Gerhard Dehm / Jon M. Molina-Aldareguia)
- **Keynote Session: Global Energy Challenges - Trends in Transportation and Energy Storage Technologies**
  (Mark Verbrugge)

GFS THIN FILM & SMALL SCALE MECHANICAL BEHAVIOR
The World of Small: Old and New Challenges
Jul 12-13, 2014
Chair: Samantha K. Lawrence
Associate Chair: Julia Hapke

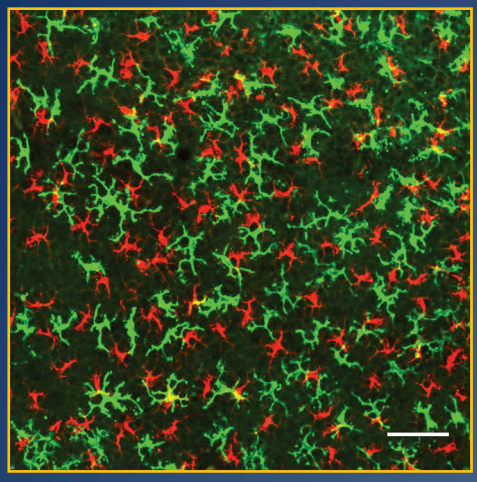

Dendritic Epidermal T cells and Langerhans Cells scaled: Confocal imaging of DETC and Langerhans cells (LC) in mouse epidermal sheets. V-gamma-5-FITC and MHC I-A/I-E-AlexaFluor647 antibodies were used to stain DETC (green) and LC (red), respectively. The images were acquired using Leica SP2 confocal microscope and 40x/NA1.25 objective, which captures a 375x375 µm field of view. Scale bar is 50 µm. Courtesy of Dmitry Ushakov (King's College London). Submitted by Adrian Hayday, Chair, Immunochemistry & Immunobiology GRC.

THIOL-BASED REDOX REGULATION & SIGNALING
From Redox Biology and Chemistry to Aging and Associated Diseases
Jul 20-25, 2014
Melia Golf Vichy Catalan Business & Convention Center, Girona - Costa Brava, Spain
Chair: Michel B. Toledano
Vice Chair: Cristina M. Furdui

- **Keynote Session: Redox Biology, a Pervading Discipline - From Stem Cells to Aging**
  (Thomas Nyström / Toren Finkel)
- **Redox Biology in Mitochondria**
  (Johannes Herrmann / Margaret Ashcroft / Jan Riemer / Mike Murphy)
- **Aging by ROS**
  (Mikael Molin / T. Keith Blackwell / Ursula Jakob / Gilles Charvin)
- **Redox Metabolism in the ER**
  (Roberto Sitia / Lloyd Ruddock / Carolyn Sevier / Maya Schuldiner)
- **Thiol-Based Redox Mechanisms**
  (Elena Hidalgo / Deborah Fass / Andreas Meyer / Anand Bachhawat)
- **Thiol and Methionine-Based Signaling in Physiology and Diseases**
  (Phil Eaton / Mark E. Anderson / Vadim Gladyshev / Jean-François Collet)
- **The Chemical Biology of Thiols, Iron and Sulfur**
  (Leslie Poole / Roland Lill / Xian Ming / Benjamin P. Tu)
- **Signaling by NO and H_2S**
  (Thomas Michel / John D. Hayes / Christine Winterbourn)
- **ROS and Redox Metabolism in Physiology and Pathology**
  (Navdeep Chandel / Richard Loeser / Miguel Soares)

GFS THIOL-BASED REDOX REGULATION & SIGNALING
Probing the Thiol Proteome
Jul 19-20, 2014
Chair: Maxwell A. Darch
Associate Chair: Alise Ponsero

THREE DIMENSIONAL ELECTRON MICROSCOPY
Technical Advances for a Rising Star in Structural Biology
Jun 22-27, 2014
Melia Golf Vichy Catalan Business & Convention Center, Girona - Costa Brava, Spain
Chair: Henning Stahlberg
Vice Chair: Eva Nogales

- **Keynote Session: Progress in Life Sciences and Materials Sciences in 3DEM**
  (*Henning Stahlberg* / Michael Rossmann / Paul Midgley)
- **Sample Preparation for Cryo-EM**
  (*Robert Glaeser* / Jürgen Plitzko / Thomas Braun / Rouslan Efremov / Ingeborg Schmidt-Krey)
- **Progress in Molecular and Cellular EM Through Instrumentation Advances**
  (*Werner Kühlbrandt* / Radostin Danev / Matthias Wolf)
- **Progress in Image Processing**
  (*Richard Henderson* / Carsten Sachse / Pawel Penczek / Hemant Tagare)
- **High Resolution**
  (*Stefan Raunser* / John Briggs / Janet Vonck / Jan Peter Abrahams / Maofu Liao)
- **Validation and Data Exchange**
  (Ardan Patwardhan)
- **New Approaches to Imaging**
  (Tamir Gonen / Grant Jensen / Dorit Hanein)
- **Selected Poster Presentations**
  (*Eva Nogales*)

TRANSGLUTAMINASES IN HUMAN DISEASE PROCESSES
Molecular Dissection of Human Diseases Pathogenesis
Jun 29 - Jul 4, 2014
Renaissance Tuscany Il Ciocco Resort, Lucca (Barga), Italy
Chair: Mauro Piacentini
Vice Chair: Timothy Johnson

- **Keynote Session: Inflammation and Cell Death Regulation**
  (Peter Vandenabeele)
- **Transglutaminases as Regulators of Cell Survival and Cell Death Modalities**
  (*Soichi Kojima* / Laszlo Fesus / In-Gyu Kim / Gail Johnson)
- **Transglutaminases in Oncogenesis and Metastasis Development**
  (*Simone Beninati* / Kevin D. Brown / Kapil Mehta / Daniela Matei)

- **Transglutaminases in Cardiovascular and Neurodegenerative Diseases**
  (*Rajiv Ratan* / Mauro Piacentini / Manuela Basso / M. Wilhelmus)
- **Transglutaminases as Regulators of Inflammatory Disease**
  (*Carlo Bergamini* / Shun Kawabata / Soo-Youl Kim / Luigi Maiuri)
- **Transglutaminases in Matrix Remodeling and Organ Fibrosis**
  (*Thimoty Johnson* / Elisabetta Verderio / Maria Nurminskaya)
- **Transglutaminases in Celiac Disease**
  (*Carla Esposito* / Katri Lindfors / Ludvig Sollid)
- **Approaches to Inhibit Transglutaminase Activity in Human Diseases and to Apply It to Biotechnology**
  (*Said Elaoui* / Fuchsbauer HL / Martin Griffin / Jeffrey Keillor / Chaitan Khosla)
- **Transglutaminases in the Skin**
  (*Eleonora Candi* / Richard Eckert / K. Hitomi)

TRIBOLOGY
Coupled Challenges at the Moving Interface
Jul 20-25, 2014
Bentley University, Waltham, MA
Chair: Roland Bennewitz
Vice Chair: Robert W. Carpick

- **Soft and Tough Materials**
  (*Kathryn Wahl* / Jian Ping Gong / David Burris)
- **Friction at the Nanoscale**
  (*Graham Cross* / Rachel Cannara / M. Clelia Righi / Martin Dienwiebel)
- **Confinement and Lubrication**
  (*Andrew Jackson* / Juliette Cayer-Barrioz / Daniele Dini)
- **Superlow Friction Materials**
  (*Nuria Espallargas* / Ali Erdemir / Jianbin Luo / Koshi Adachi)
- **The Onset of Sliding**
  (*Kenneth Holmberg* / Jay Fineberg / Eran Bouchbinder)
- **Modeling the Contact**
  (*Judith Harrison* / Michael Urbakh / Ashlie Martini / Mark O. Robbins)
- **Aqueous Lubrication**
  (*Seong H. Kim* / Elisabeth Charlaix / Izabela Szlufarska)
- **Friction in Complex Systems**
  (*Anand Jagota* / Hugh Spikes / Mark Rutland / Tetsuo Yamaguchi)
- **Keynote Session: Tribology and Soft Matter**
  (*Robert W. Carpick* / David Weitz)

GFS TRIBOLOGY
Challenges in an Interdisciplinary Field
Jul 19-20, 2014
Chair: Stefanie Hanke
Associate Chair: Xin Liu

UNIFYING ECOLOGY ACROSS SCALES
The Role of Nutrients, Metabolism, and Physiology
Jul 20-25, 2014
University of New England, Biddeford, ME
Chairs: Morgan Ernest & Michael J. Angilletta
Vice Chair: Richard M. Sibly

- **Developing Unified Theories of Ecology**
  (*Pablo Marquet* / Michael Sears / John Harte)
- **Macrophysiology Meets Macroecology**
  (*Lauren Buckley* / Piero Calosi / Amy Angert)
- **Biogeography of Environmental Tolerance**
  (*Jennifer Sunday* / Sarah Diamond / Hans Otto Portner)
- **Metabolic Adaptation to Changing Environments**
  (*Craig White* / Daniel Naya / Carla Sgro)
- **Mechanistic Basis of Macroecological Patterns**
  (*Brian Enquist* / Ethan White / Sally Keith)
- **Linking Organismal Traits to Community Dynamics**
  (*Elena Litchman* / Catherine Graham / Stephanie Dutkiewicz)
- **Using Stoichiometry to Link Organisms & Ecosystems**
  (*Susan Kilham* / Elizabeth Borer / Alan Townsend)
- **Predicting Diversity Across Scales**
  (*Brian McGill* / Maria Dornelas / Jessica Blois)
- **Integrating Ecological Processes at the Macroscale**
  (*James Brown* / Michael Kearney / James Brown)

GFS UNIFYING ECOLOGY ACROSS SCALES
Understanding Drivers of Biological Systems by Integrating Metabolism, Physiology, and Macroecology
Jul 19-20, 2014
Chair: Sarah R. Supp
Associate Chair: Sarah E. Diamond

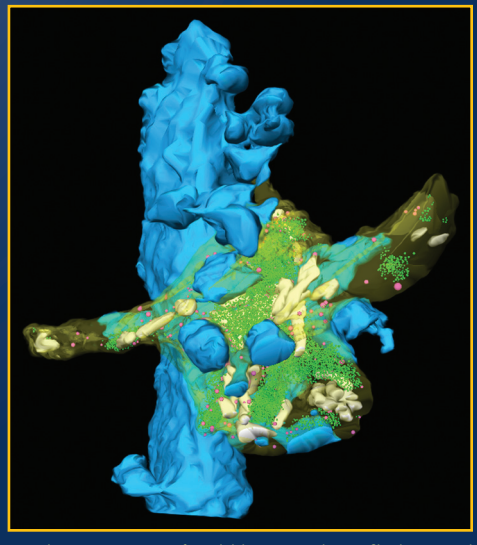

3D-volume reconstruction of an adult hippocampal mossy fiber bouton and its target structure, a dendritic segment of a CA3 pyramidal cell dendrite. Colour code: dendrite and spiny excrescences in blue, bouton in transparent yellow, mitochondria in white, synaptic vesicles in green and dense-core vesicles in magenta. Courtesy of Astrid Rollenhagen and Joachim Lübke; for details see Rollenhagen et al., J. Neurosci. 27: 10434-10444 (2007). Submitted by Peter Jonas, Chair, Synaptic Transmission GRC.

VIBRATIONAL SPECTROSCOPY
Watching Molecules at Work
Aug 3-8, 2014
University of New England, Biddeford, ME
Chairs: Arthur L. Utz & Mischa Bonn
Vice Chairs: Elsa C.Y. Yan & Victor S. Batista

- **Vibrational Dynamics in Energy Conversion and Catalysis**
  (*Mark Johnson* / Kramer Campen / Dana Dlott)
- **Vibrational Dynamics of Water**
  (Andrei Tokmakoff / Huib Bakker / Sander Woutersen)
- **Spatially Resolved Vibrational Spectroscopy**
  (*Andrew Orr-Ewing* / Richard VanDuyne / Maki Kawai)
- **Vibrational Motions in Chemical Reactions**
  (*Hua Guo* / David Nesbitt / David Moore / Rainer Beck / Bret Jackson)
- **Spectroscopic Probes of Structure and Dynamics**
  (*Carol Hirschmugl* / Lauren Webb / Yoshi Matsumoto)
- **Vibrations at Interfaces**
  (Ellen Backus / Dennis Hore / Hongfei Wang / Sylvie Roke)
- **Vibrational Spectroscopy in the Environment**
  (*Veronica Vaida* / Franz Geiger / Heather Allen)
- **Vibrational Dynamics in Biology**
  (Juli Gibbs-Davis / Nien-Hui Ge / Judy Kim / Martina Havenith)
- **Keynote Session: Vibrational Spectroscopy and Dynamics - Past, Present, and Future**
  (Casey Hines)

GFS VIBRATIONAL SPECTROSCOPY
Exploring Vibrational Motion and Interactions Through State-of-the-Art Techniques
Aug 2-3, 2014
Chair: Eric Dombrowski
Associate Chair: Dequan Xiao

WATER & AQUEOUS SOLUTIONS
Latest Experimental and Theoretical Advances in Water Research
Jul 27 - Aug 1, 2014
Holderness School, Holderness, NH
Chair: Douglas Tobias
Vice Chair: Nancy E. Levinger

- **Water Anomalies**
  (*Austen Angell* / Eugene Stanley / Gren Patey)
- **Aqueous Ionic Solvation**
  (*Christopher Mundy* / Kelly Gaffney / John Fulton / Evan Williams / A.J. Colussi)
- **Hydrophobic Solvation**
  (*Shekhar Garde* / Dor Ben-Amotz / John Weeks)
- **Chemistry at Aqueous Interfaces**
  (*Heather Allen* / Veronica Vaida / Francesco Paesani / James Donaldson / Thomas Kuhne)
- **Biomolecular Solvation Thermodynamics and Dynamics**
  (*Steven Corcelli* / Sihyun Ham / Alessandro Paciaroni)
- **Water Across the Phase Diagram**
  (*Valeria Molinero* / Thomas Loerting / Iwao Ohmine / Rachel Martin / Christophe Dellago)
- **Confined Water**
  (*Sapna Sarupria* / Giulia Galli / Daniela Russo)
- **Aqueous Solvation Dynamics**
  (*Damien Laage* / James Hynes / Stephen Bradforth / Minhaeng Cho / Peter Rossky)
- **Keynote Session: Water in Biology**
  (*Pavel Jungwirth* / Philip Ball)

GFS WATER & AQUEOUS SOLUTIONS
Water: Complex Traits of a Simple Molecule
Jul 26-27, 2014
Chair: Matthias Heyden
Associate Chair: Natasha H. Rhys

GRC

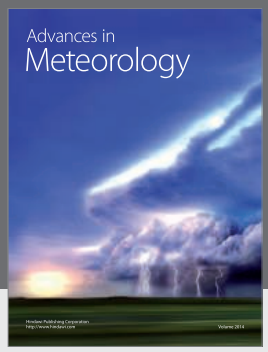

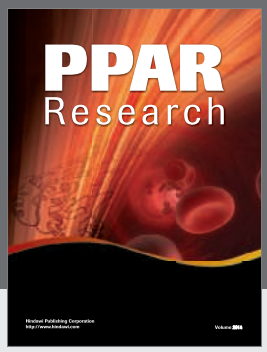

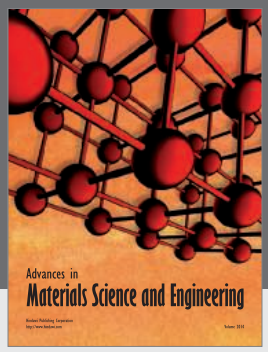

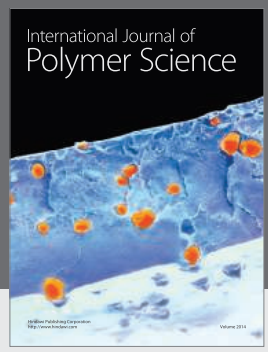

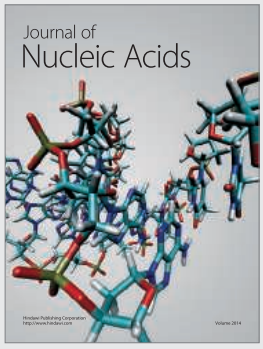

Hindawi

Submit your manuscripts at
http://www.hindawi.com

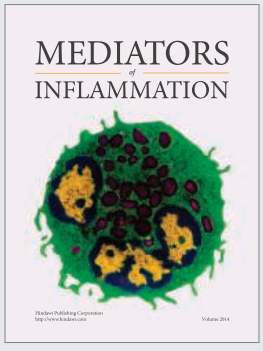

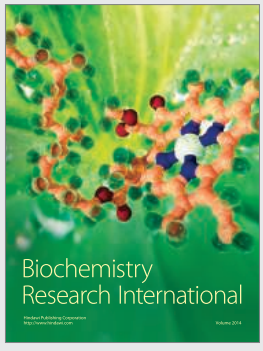

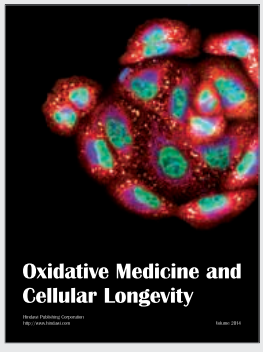

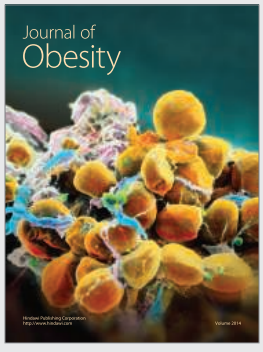

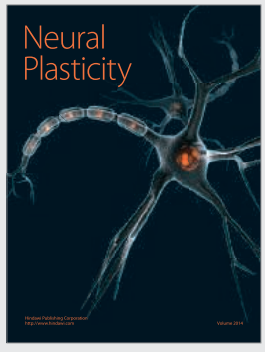

SCIENTIFIC CONFERENCES 2014:

Presenting the most significant research on cancer etiology, prevention, diagnosis, and treatment

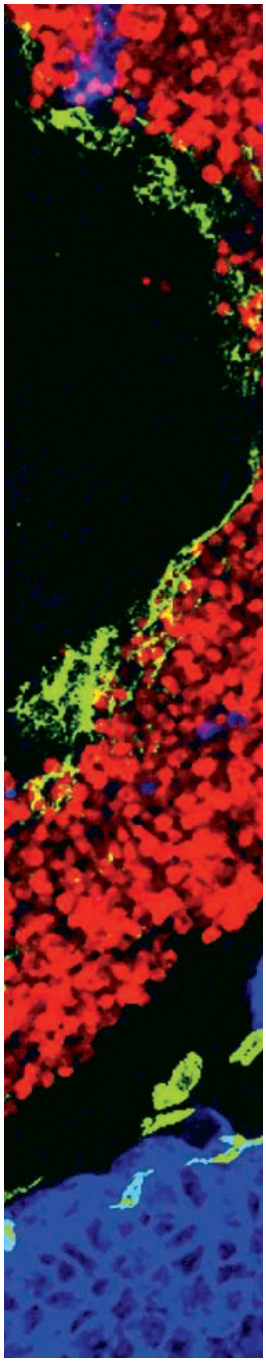

AACR Annual Meeting 2014
Chairperson: Scott W. Lowe
April 5-9, 2014
San Diego, CA

Pancreatic Cancer:
Innovations in Research and Treatment
Co-Chairpersons: Dafna Bar-Sagi, David A. Tuveson, Christine Iacobuzio-Donahue, Alec Kimmelman, and Andrew M. Lowy
May 18-21, 2014
New Orleans, LA

AACR Precision Medicine Series
Drug Sensitivity and Resistance:
Improving Cancer Therapy
Co-Chairpersons: Gideon Bollag, Elaine Mardis, Gordon Mills, and David Solit
June 18-21, 2014
Orlando, FL

Marsha Rivkin Center for Ovarian Cancer Research-AACR 10th Biennial Ovarian Cancer Research Symposium
Co-Chairpersons: Kathleen Cho, Sandra Orsulic, Mary L. "Nora" Disis, and Saul E. Rivkin
September 8-9, 2014
Seattle, WA

Targeting PI3K/mTOR Networks in Cancer
Co-Chairpersons: Lewis C. Cantley, Jose Baselga, Joan S. Brugge, Brendan D. Manning, and Malte Peters
September 14-17, 2014
Philadelphia, PA

Hematological Malignancies
Co-Chairpersons: Kenneth C. Anderson, Scott Armstrong, Riccardo Dalla-Favera, and Margaret Shipp
September 20-23, 2014
Philadelphia, PA

Advances in Melanoma:
From Biology to Therapy
Co-Chairpersons: Suzanne L. Topalian, Keith T. Flaherty, and Levi A. Garraway,
September 20–23, 2014
Philadelphia, PA

13th Annual International Conference on Frontiers in Cancer Prevention Research
Program Committee Chairperson: Phillip A. Dennis
September 28-October 1, 2014
New Orleans, LA

EORTC-NCI-AACR International Symposium on Molecular Targets and Cancer Therapeutics
Scientific Committee Co-Chairpersons: Jean-Charles Soria, Lee J. Helman, and Jeffrey A. Engelman
November 18-21, 2014
Barcelona, Spain

Tumor Immunology
Co-Chairpersons: Robert H. Vonderheide, Nina Bhardwaj, Stanley Riddell, and Cynthia L. Sears
December 1-4, 2014
Orlando, FL

www.AACR.org/2014Conferences

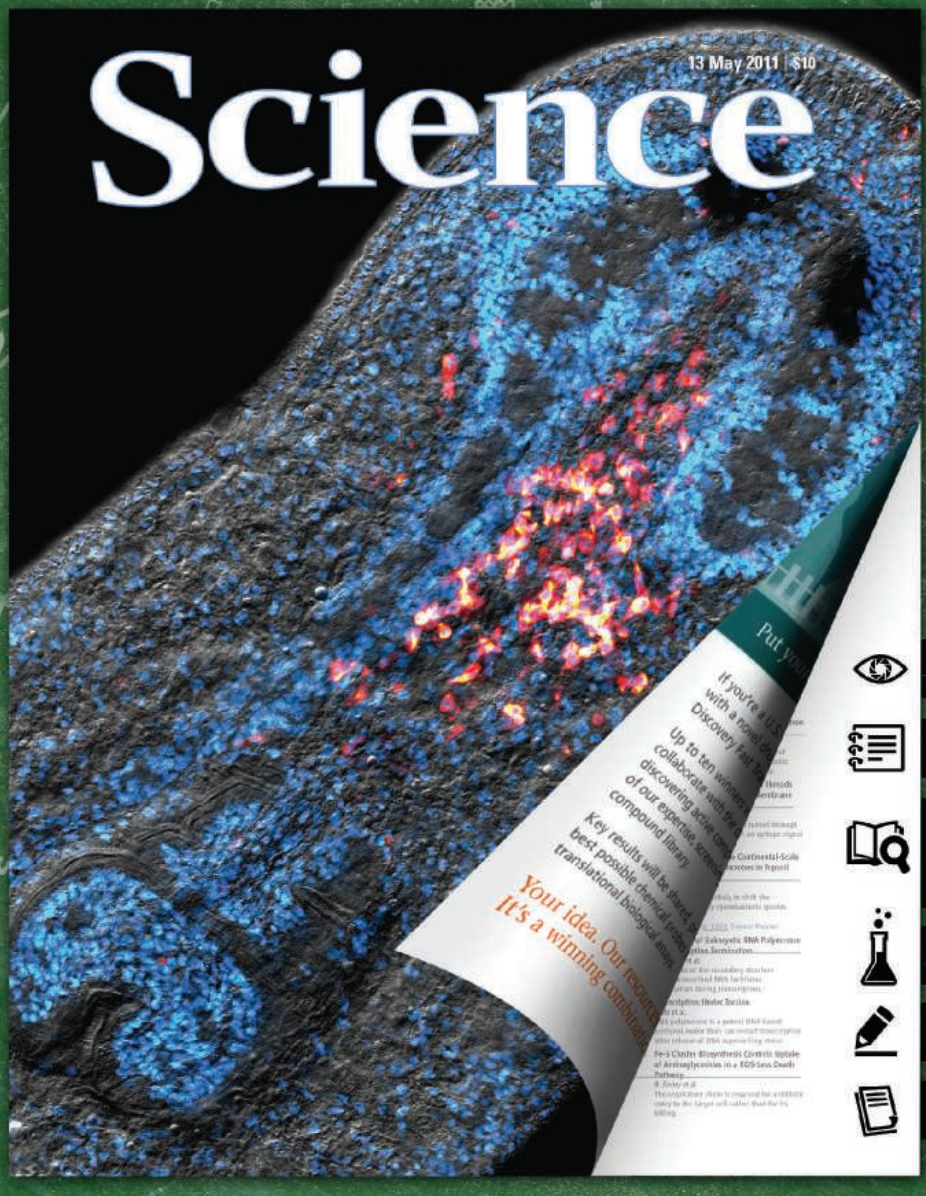

Science

Online tools to help your students analyze a professional research paper!

Tell me and I forget. Teach me and I remember. Involve me and I learn. -- Benjamin Franklin

Featuring over 6 research papers at any given time, *Science* in the Classroom is specifically designed to help young researchers understand the structure and workings of professional scientific research.

Learn for yourself how *Science* in the Classroom can help your students deepen their understanding of scientific research. **Visit scienceintheclassroom.org today.**

AAAS
ADVANCING SCIENCE, SERVING SOCIETY

Slow western

Fast western!

Novex®

Get the high-quality performance of traditional transfers in just 7 minutes

The new and improved iBlot® 2 Dry Blotting System offers:

- New touch screen
- Sturdier design
- Less consumable waste
- High transfer efficiency and uniformity on both PVDF and NC membranes

WESTERN WORKFLOW

SEPARATE TRANSFER DETECT

See the iBlot® 2 Gel Transfer Device at lifetechnologies.com/western

life technologies™

eppendorf & Science

PRIZE FOR NEURO BIOLOGY

2013 Winner
Dr. Michael Yartsev
CV Starr Research Fellow
Princeton Neuroscience Institute

Application Deadline
June 15, 2014

Call for Entries

Eppendorf & Science Prize for Neurobiology
The annual Eppendorf & Science Prize for Neurobiology, an international award, honors young scientists for their outstanding contributions to neurobiological research based on methods of molecular and cell biology.
The winner and finalists are selected by a committee of independent scientists, chaired by Science's Senior Editor, Dr. Peter Stern. To be eligible, you must be 35 years of age or younger.

You could be next to win this prize and to receive
> Prize money of US$25,000
> Publication of your work in Science
> Full support to attend the Prize Ceremony held in conjunction with the Annual Meeting of the Society for Neuroscience in the USA
> An invitation to visit Eppendorf in Hamburg, Germany

It's easy to apply!

Learn more at: www.eppendorf.com/prize

eppendorf

Science AAAS

For your career in science, there's only one **Science**

A career plan customized *for* you, *by* you.

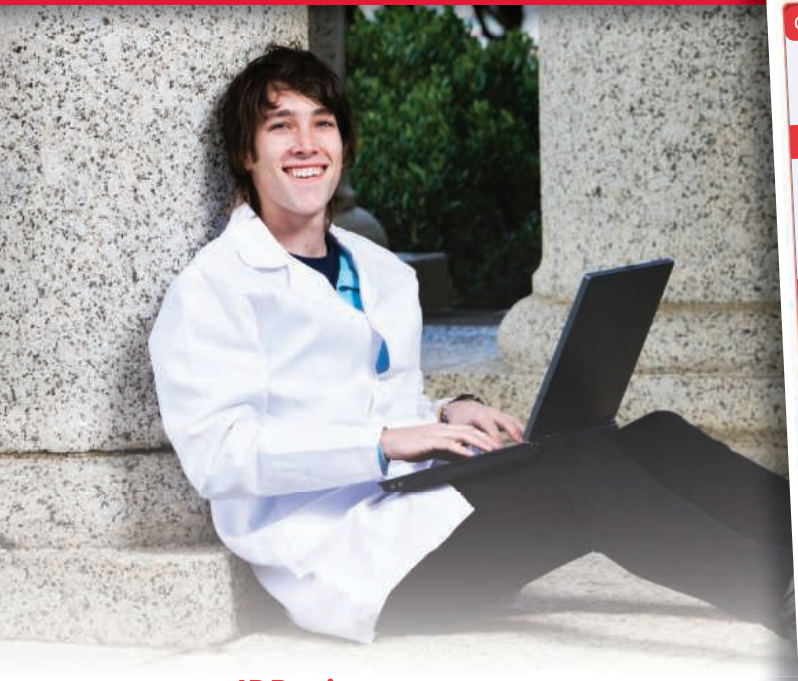

myIDP.sciencecareers.org

Recommended by leading professional societies and endorsed by the National Institutes of Health, an individual development plan will help you prepare for a successful and satisfying scientific career.

my IDP Science Careers

In collaboration with FASEB, UCSF, and the Medical College of Wisconsin and with support from the Burroughs Wellcome Fund, AAAS and *Science* Careers present the first and only online app that helps scientists prepare their very own individual development plan.

Visit the website and start planning today!
myIDP.sciencecareers.org

In partnership with:

advancing the life sciences 1912-2012 FASEB Federation of American Societies for Experimental Biology

UCSF University of California San Francisco

Medical College of Wisconsin

Burroughs Wellcome Fund

Miniaturizing Mass Spectrometry

Time was when mass spectrometry was the province of white-coated chemistry Ph.D.s with a secret language all their own. Terms like ion trap and post-source decay, mass-to-charge, and MALDI made the field inaccessible to others. Today, the technique has pushed beyond those narrow confines and entered the biology lab, where it underlies proteomics and biomarker research. But you can also find mass specs in airports and warehouses, and even at the bottom of the ocean. In many cases those instruments are being run not by specially trained researchers, but by TSA agents, soldiers, and first responders. Chalk that up to miniaturization. Researchers have finally figured out how to compress benchtop systems into portable, sometimes handheld gadgets. In so doing, they have created devices that empower not only themselves, but the wider world.
By Jeffrey M. Perkel

You can also find mass specs in airports and warehouses, and even at the bottom of the ocean.

Compact Mass Spectrometer

Peter Girguis is neither a mass spectrometrist nor a chemist. He's a microbial physiologist, and his interest is the biogeochemistry of the deep ocean.

"Our entire biosphere is run by microbes," Girguis, the John Loeb Professor of Natural Sciences at **Harvard University,** explains. "That's pretty much the bottom line."

But the vast majority of microbes cannot be cultured in the lab, making them refractory to standard analyses. Girguis tries to understand what these microbes do by studying their impact on the chemical composition of the ocean floor and correlating those data with gene expression analyses to figure out which microbes are doing what.

"That's where mass spectrometers are, I would argue, one of the single most advantageous tools, because with a single analyzer you can detect a wide array of compounds," says Girguis.

There's no denying the incredible power of mass spectrometry. Using these instruments researchers can tease apart proteins and peptides that differ by just a single chemical modification; they can scan complex biofluids and home in on the few molecules that make them different; and they can interrogate samples for hundreds of compounds at once.

But to perform that kind of research takes considerable expertise. And the instruments on which it is done, says R. Graham Cooks, the Henry Bohn Hass Professor of Chemistry at **Purdue University** and a leading light in the drive to miniaturize mass spectrometry, are almost always for laboratory use only.

Benchtop instruments "weigh several hundred pounds," Cooks says. They're expensive and power-hungry, coupled to gas lines and powerful vacuums, and often require front-end separation systems. On the analytical side, they produce incredibly detailed spectra that take specialized software to decipher. All of which makes it hard to get the technology into the hands of people who might benefit from it—physicians at the bedside, firefighters in a burning factory, and even food safety inspectors in a warehouse.

"The shrinking of mass spectrometers is really about doing in situ, on-site measurements," Cooks says. "And that calls for an instrument that is fully portable and … that can be moved around at will."

GO SMALL OR STAY HOME

In making mass specs smaller and friendlier, researchers empower a far wider circle of users to employ them. David Rafferty, president and chief technology officer at **1st Detect Corporation,** in Webster, Texas, likens the resulting democratization to the personal computer revolution. "Previously, only large institutions and large universities and companies had computers, but now with the advent of the personal computer it was made available to the masses, so to speak," Rafferty says. "We want to do the same thing with the mass spec."

Staffed heavily by expats from aerospace engineering, 1st Detect intends its MMS-1000 for industrial applications such as quality control and food safety testing, and, ultimately, homeland security. In contrast, **908 Devices** focuses its 3.75 lb, "high-pressure mass spectrometer" on first responders in the safety and security markets, says Chris Petty, the company's vice president of business development and marketing, while **Microsaic Systems,** based in Surrey, United Kingdom, targets its single-quad 4000 MiD at organic chemists in drug discovery.

Upcoming Features

Toxicology—March 14
Genomics—April 11
Microscopy—May 2

CREDITS: (CLOCKWISE, FROM TOP LEFT) PATENTED MICROSCALE ION TRAP TECHNOLOGY ENABLES OPERATION OF 908 DEVI CES' HANDHELD MASS SPEC PRODUCTS WITHOUT THE NEED FOR EXTREME VACUUM OR ADDITIONAL GAS SUPPLY; © SHUTTERSTOCK.COM/C.K.Ma/DABARTI CGI; BRUKER DALTONIK GMBH; (BACKGROUND MOLECULES) © SHUTTERSTOCK.COM/MILOS DIZAJN

The logical next step ... is to shrink that ion trap down to a size (and cost) that would make it a practical addition in operating rooms everywhere.

Girguis' need was more esoteric. His research calls for quantifying dissolved gases such as methane, hydrogen, and oxygen on and beneath the sea floor. It is, of course, possible to do that by installing a benchtop mass spec on a boat, collecting samples at depth, and analyzing them on deck. But a sample of water 1 km below the ocean can hold considerably more gas than it can on the sea surface, a function of the differences in pressure and temperature. "The solubility of methane at one atmosphere, 5°C, is about 2 mmol. The solubility of methane on the sea floor is much higher."

He realized he would need a mass spec he could use on site, and being "a bit of a gearhead," decided to build it himself.

Girguis got his first experience with high-pressure mass spectrometry as a graduate student at the University of California, Santa Barbara, when he was interested in the animals that colonize hydrothermal vents and their symbionts. He studied those in pressure vessels. Later, as a postdoc, he wanted to investigate the influence of microbes on the methane and hydrogen content of the ocean, but realized he needed a special instrument. How, though, to make a mass spec small enough and robust enough to operate underwater?

"The real serendipitous moment came when a couple of companies built small turbopumps," he says. (One of those companies, **Alcatel Vacuum,** was subsequently acquired by the other, **Pfeiffer Vacuum,** based in Germany.)

To build the mass spec itself, he worked with a mechanical engineer to package a commercial quadrupole mass analyzer from **Stanford Research Systems,** a Pfeiffer HiPace80 turbopump, and a custom gas extractor into a 25 cm x 90 cm cylinder. The result is the "in situ mass spectrometer" (ISMS), a 25 kg assembly that resembles a titanium-encased scuba tank, he says.

The extractor is a key element, Girguis says. Essentially a 10 μm thick Teflon membrane backed with a metal frit to provide structural support at high vacuum, this component degases the water being sampled by the mass spec, at up to 450 atmospheres of pressure. The resulting vapors are pulled into the instrument, ionized by electron ionization and mass analyzed, like a gas chromatography (GC)-coupled MS without the GC.

The ISMS has visited some enviable locales. Attached to either remotely operated vehicles or manned submersibles (like the Woods Hole Oceanographic Institute's *Alvin*), it has visited the Gulf of Mexico, hydrothermal vents off Washington state and the Azores (mid-Atlantic ridge in the North Atlantic), and the South Pacific. "I'm sure we've cleared over 100 dives at this point," Girguis says.

Using it, he has produced what he calls "geochemical maps" of dissolved gases at hydrothermal vents, collecting hundreds of data points both at different depths in the ocean sediment and across the floor. In one study, he discovered to his surprise that the charismatic deep-sea hydrothermal vents, sometimes called black smokers, often actually pump out less gas than do nearby "diffuse flows" on the ocean floor. "It just goes to show you that your eyes can deceive you," he says.

Girguis has published detailed plans and parts lists for the ISMS on his website, and anyone can build one. Total cost is about $15,000. But the housing is another matter. A simple polyvinyl chloride shell for relatively shallow dives (up to 50 m or so) might cost $1,000, but, "If you want titanium, to dive 4,000 m, you're going to have to shell out $20,000 for the housing alone."

HONEY, I SHRUNK THE SPEC!

Miniature mass specs have potential in other exotic locales, too. Rafferty says his company was approached by a museum looking to detect leakage of the preservative solution protecting an embalmed giant squid (though to date, no deal has been struck). Guido Verbeck, an associate professor at the **University of North Texas** who miniaturizes mass specs in his lab, envisions applications for his designs in homeland security and the military, such as being able to "toss" a mass spec into a burning industrial fire to have it report back what is burning, he says. "But you're going to destroy the device, so you have to make something that's cheap, small, [and] portable, with no moving parts."

As for Cooks, he targets the surgical suite. With colleague Nathalie Agar at Boston's **Brigham and Women's Hospital,** he already has demonstrated the feasibility of grading brain tumors using the lipid profiles they produce in a mass spectrometer (see "Mass Spec Imaging: From Bench to Bedside," scim.ag/1dCjmPx). But that experiment involved relatively simple benchtop instruments, Cooks says, **Bruker** and **Thermo Fisher Scientific** ion traps equipped with a **Prosolia** desorption electrospray ionization (DESI) source.

The logical next step, he says, is to shrink that ion trap down to a size (and cost) that would make it a practical addition in operating rooms everywhere.

As it turns out, one of the biggest challenges to shrinking a mass spectrometer is the vacuum, Cooks says. Mass specs function in a vacuum to eliminate background signal and avoid intermolecular collision events. But vacuum systems are large and heavy, and those parameters scale with the pressure differential needed. A Thermo Fisher Orbitrap requires three turbo pumps pulling some 900 L/sec in LC-MS modes to achieve a vacuum below 10^{-10} torr, according to a company representative.

Time-of-flight (TOF) mass analyzers also require high vacuum. As a result, most mini-mass specs are built from more forgiving mass analyzers, namely ion traps and quadrupoles—though at least two continued>

Featured Participants

1st Detect Corporation
www.1stdetect.com

908 Devices
www.908devices.com

Brigham and Women's Hospital
www.brighamandwomens.org

Bruker
www.bruker.com

Harvard University Department of Organismic and Evolutionary Biology
www.oeb.harvard.edu

Microsaic Systems
www.microsaic.com

Pfeiffer Vacuum
www.pfeiffer-vacuum.com

Prosolia
www.prosolia.com

Purdue University Department of Chemistry
www.chem.purdue.edu

Stanford Research Systems
www.thinksrs.com

Thermo Fisher Scientific
www.thermoscientific.com

Torion Technologies
torion.com

University of North Texas Department of Chemistry
chemistry.unt.edu

researchers have succeeded in miniaturizing a TOF, including Verbeck. Verbeck made a reflectron-based mini-TOF using a microelectromechanical system, or MEMS, technology, fashioning components out of boron-doped silicon wafers that he then assembled like old-fashioned tab-and-slot paper models. The analyzer measures just 2 cm x 5 cm, extending the ions' effective path length by moving ions back and forth for extended periods of time.

Cooks (with his associate at Purdue, Zheng Ouyang) built his miniature mass spectrometers using a linear (or quadrupole) ion trap, which operates at about 10^{-3} torr.

To produce that vacuum, he and Ouyang obtained the smallest commercial turbopump they could find, capable of about 10 L/sec. "You have to have a way of working with small vacuum pumps," he says. "This is the hardest part, the part that most people have stumbled over."

Such a pump is too small to allow continuous sample introduction, so the team built a discontinuous sample inlet system called DAPI (discontinuous atmospheric pressure introduction), which takes ions from the system's ionization source—in this case, a DESI wand—and holds them on one side of a pinch-valve, which opens periodically to introduce them into the mass analyzer en masse.

The result, Cooks says, is a fully self-contained device, the Mini-11, which weighs just 8.5 kg and yet contains a vacuum, pumps (a turbo pump and backing pump), ionization system, battery, electronics, and communications, in a single portable device. A backpack-mounted, 25 kg Mini-12 also exists, and Cooks has hinted that an even smaller device, perhaps powered by an iPhone, is in the works for at-home diagnostics.

Yet despite their small sizes, these devices are surprisingly powerful. The Mini-11 and -12 offer unit resolution mass spectra up to m/z 600, a range that makes it useful for studying metabolites, lipids, and other small molecules.

LITTLE MASS SPECS, BIG PROBLEMS

Besides the vacuum, miniaturizing a mass spec poses other difficulties, too. The central electrode of an ion trap, for instance, is traditionally curved—picture an aluminum can that is pinched in the middle. As it gets smaller, the shape becomes harder and harder to manufacture precisely, yielding imperfections that can negatively affect ion motion.

1st Detect circumvented that problem by swapping the traditional "hyperbolic" design for a more easily fabricated cylindrical device—basically a smooth hole bored into the electrode. "You can make it smaller more easily without having to follow that precise curve," Rafferty says.

Another problem, says Stephen Lammert, director of research and development at **Torion Technologies,** is that as traps get smaller, squeezing the same number of ions into them becomes harder and harder. "The grand challenge of miniaturizing mass spectrometers, and especially ion traps, is: How do you make the trap smaller without losing ion capacity?"

Torion's solution, embodied in its Tridion-9 mass spectrometer, is the toroidal ion trap, which transfers the trapping characteristics of a traditional trap into a doughnut-shaped volume that can hold up to 400 times more ions. "The toroidal ion trap we have in our instrument is one-fifth the radius of what would be considered a conventional laboratory ion trap, and yet it still has the ion capacity of the conventional trap because of the expanded geometric storage shape." It also uses 25 times lower voltage and 125 times less power overall.

For Verbeck, the primary challenge in making a smaller mass spec was electrical.

"We've gotten to the point where the devices are so small that [with] one wire next to another wire, there's cross-talk," he says. His team had to go back and redesign the electrical system, "making cleaner channels in between the conductive pads, and making them wider," among other things.

But perhaps the biggest issue when miniaturizing mass spectrometry devices is the tradeoff it requires in power and flexibility. Ion traps, for instance, are attractive candidates for miniaturization not only because they are so simple, but also because they have the built-in capacity for tandem mass spec analyses, enabling sophisticated structural analyses.

But a mass spectrometer intended for soldiers, firefighters, and physicians must be simple enough to be used by someone who knows nothing about such nuances and have the built-in intelligence to automatically switch into tandem mode as the data require.

Such a system must be efficient enough to run on a battery and yet accessible enough to mass-spec novices to hide the complexity of a mass spectrum behind a friendly interface. Be not a device that requires instructions from its user, but one that, as Rafferty puts it, can scan a sample and go "beep, pesticide."

That's not to say mini mass specs don't have a home in the lab. An inexpensive mass spectrometer that can fit inside a fume hood would be a welcome addition to any organic chemist's toolbox, and Microsaic Systems, at least, intends its 4000 MiD for exactly that purpose. But the most exciting applications for mini mass specs surely lie outside the lab.

"We don't even want the device to be called a mass spectrometer," Rafferty says of the MMS-1000. "We'd prefer to refer to it as a sensor or a chemical detector." And really, when you strip away all the bells and whistles, isn't that what a mass spec is?

Jeffrey M. Perkel is a freelance science writer based in Pocatello, Idaho.

DOI: 10.1126/science.opms.p1400082

IMMUNOHISTOCHEMISTRY WORKSTATION

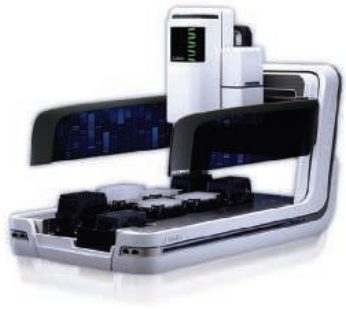

The Microlab Immunostain NIMBUS Workstation is designed for automated immunohistochemistry (IHC) and in situ hybridization (ISH) applications. This compact, automated, and cost-effective workstation accepts multiple slide configurations and staining kit brands for simple and error-free operations. Immunofluorescent staining is a laborious process that takes hours to complete and is subject to handling errors. However, labs now have a cost-effective alternative that significantly speeds the process, improves the chain of custody for samples processing and provides standardized, more quantifiably comparable results. The Immunostain NIMBUS Workstation reduces reagent use and removes operator-to-operator variability. It can process up to 24 slides at once and fully supports single-color and multicolor IHC and ISH kits. The NIMBUS workstation can also process slides for conventional light microscopy and comes with two washing options: automated pipetting or a tilt module. The demo method included with the Immunostain NIMBUS Workstation offers an easy-to-use software wizard.

Hamilton Company
For info: 800-648-5950 | www.hamiltonrobotics.com

CUSTOM PHOSPHO-SPECIFIC ANTIBODIES

A new custom phospho-specific antibody production service is now available that is both reliable and produces highly specific quality antisera. Phospho-specific antibodies are widely accepted for use in defining regulatory mechanisms that control cell functions such as activation of enzymes and receptors, cellular transcription, signal transduction, and cell signaling networks. Phospho-specific antibodies are affinity-purified rabbit polyclonal or monoclonal antibodies that are monospecific for a target protein that is phosphorylated on a specific tyrosine, threonine, or serine residue. The custom phospho-specific polyclonal antibody service includes synthesis of phosphorylated and nonphosphorylated peptides, conjugation to a carrier protein, immunization, and anti-sera production. All antibodies are then purified using a two-step immuno-affinity method. The purified phospho-specific antibody is fully characterized using both dot-blot and enzyme-linked immunosorbent assay techniques to ensure product of the highest consistency and quality. Hundreds of custom phospho specific antibodies have been successfully made by AMSBIO and supplied to leading international research groups.

AMS Biotechnology
For info: +44-(0)-1235-828200 | www.amsbio.com

ANTIBODY PRODUCTION SERVICES

Medix offers customized services for the in vitro generation of high-performance recombinant or monoclonal antibodies and Fab fragments for superior in vitro diagnostic (IVD) assays. With all antibodies produced to the strictest international quality standards (ISO 9001, ISO 13485, and FDA QSR) the services equip manufacturers with a competitive advantage, helping to increase sales revenue without the need to invest in costly production facilities and expertise. The advanced phage display recombinant production technology of the MedixMAB by Design service enables the targeting of a broader range of antigens than possible in vivo, including poorly immunoreactive and toxic compounds, with production available on a range of scales (milligrams to kilograms). As a rapid alternative to producing full length monoclonal antibodies, Fab fragments can be generated in just three months, and greatly enhance specificity and sensitivity of IVD assays in solid-phase applications. MedixMAB Manufacturing presents a cost-effective and flexible monoclonal antibody outsourcing option for IVD manufacturers.

Medix Biochemica
For info: +358-9-547-680 | www.medixbiochemica.com

HIGH THROUGHPUT CHIP ASSAY PLATE

The Chromatrap96 HT is an innovative 96-well chromatin immunoprecipitation (ChIP) assay plate is a new high throughput ChIP microplate based on the novel spin-column ChIP technology. It is essentially 96 separate Chromatrap spin-columns in one device designed to enable researchers to perform up to 96 ChIP experiments in parallel. Assays can be performed either by using a hand-held multichannel pipette or by using automated liquid handling robots. The optimized Chromatrap spin-columns protocol forms the basis of the approach to performing high throughput ChIP analysis in microplates. Each well has its own porous disc at the bottom in which protein A or protein G has been covalently attached. The functionalized discs have the same chemistry and stoichiometry as the spin columns so all of the reagent volumes and timings can be directly inferred from the spin-tube protocol. The microplate is supplied with a close fitting collection plate to recover the retained chromatins at the elution step.

Porvair Sciences
For info: +44-(0)-1372-824290 | www.porvair-sciences.com

PROTEIN AND PHOSPHOLIPID REMOVAL PLATE

The ISOLUTE PLD+ is a protein and phospholipid removal plate designed for the cleanup of blood-based matrix samples for analysis by liquid chromatography-tandem mass spectrometry (LC-MS)/MS. ISOLUTE PLD+ plates combine protein and phospholipid removal in a single product providing very effective and extremely simple sample cleanup for LC-MS/MS analysis. Utilizing our solvent crash/filter process, the plates also incorporate a phospholipid scavenging sorbent layer, which removes phospholipids from the sample during the filtration step. ISOLUTE PLD+ plates remove more than 99% of plasma proteins and phospholipids, the main causes of ion suppression. This leads to cleaner extracts and enables increased sensitivity and signal-to-noise for the detection of a broad range of analytes. Once purified, samples can be analyzed directly, or evaporated and reconstituted in a solvent that matches your analytical method requirements. ISOLUTE PLD+ plates can be processed using 96-well compatible positive pressure manifolds, vacuum manifolds, and most automated liquid handling systems.

Biotage
For info: 800-446-4752 | www.biotage.com

Electronically submit your new product description or product literature information! Go to **www.sciencemag.org/products/newproducts.dtl** for more information.

Newly offered instrumentation, apparatus, and laboratory materials of interest to researchers in all disciplines in academic, industrial, and governmental organizations are featured in this space. Emphasis is given to purpose, chief characteristics, and availability of products and materials. Endorsement by *Science* or AAAS of any products or materials mentioned is not implied. Additional information may be obtained from the manufacturer or supplier.

immunogenomics 2014

September 29 - October 1, 2014

HudsonAlpha Biotechnology Campus
Huntsville, Alabama, USA

Bringing together preeminent leaders and thinkers at the intersection of genomics and immunology

Our Keynote Speakers:

Christophe Benoist
Professor, Department of Microbiology and Immunobiology, *Harvard Medical School*

Mary Ellen Conley
Federal Express Chair of Excellence and Professor, Department of Pediatrics, *University of Tennessee, College of Medicine, Memphis*

Mark Davis
Investigator, Howard Hughes Medical Institute; Professor, Department of Microbiology and Immunology; Director, Institute for Immunity, Transplantation, and Infections, *Stanford University School of Medicine*

Register today at haig.aaas.org

presented by

HUDSONALPHA INSTITUTE FOR BIOTECHNOLOGY

Science AAAS

www.cellsignal.com/flowscience

Antibodies for Intracellular Flow Cytometry

from Cell Signaling Technology

WB | F | IHC | ChIP | IF | IP

In vertebrates, the Wnt/β-Catenin signaling pathway is important in early embryonic development and tumorigenesis. CST offers flow cytometry validated antibodies to multiple intracellular components in the Wnt/β-Catenin pathway.

- **Validated for intracellular proteins**
- **Highly specific and sensitive antibodies**
- **Lot-to-lot consistency**
- **Technical support from the CST scientists who produced and validated your antibody**

Request a Flow Cytometry Reference Wheel:
www.cellsignal.com/flowscience

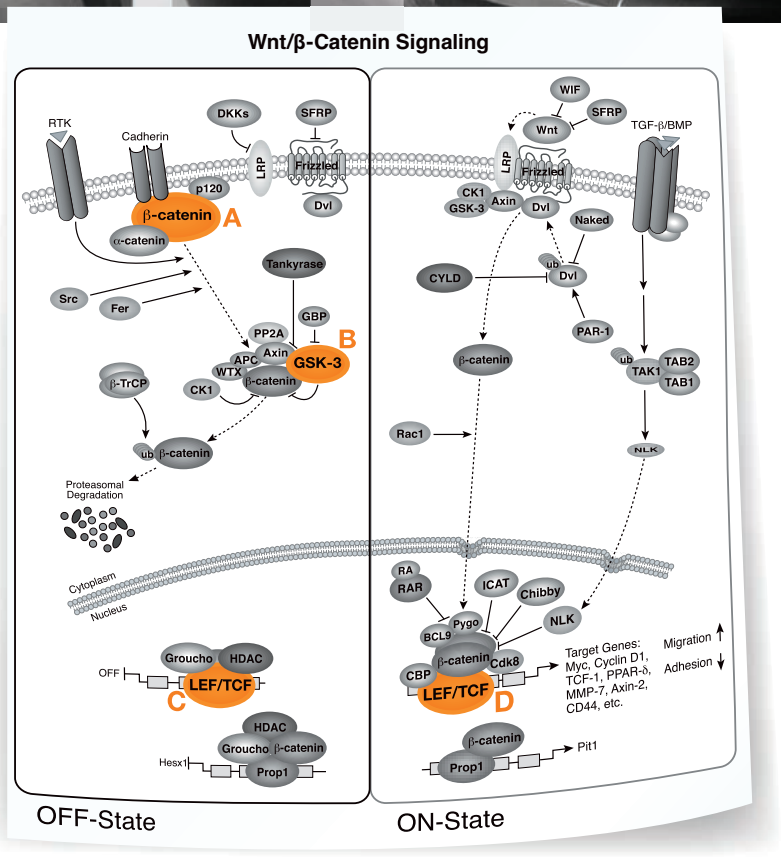

#4627 detects β-Catenin in HeLa (positive), but not NCI-H28 (negative) cells.

#8466 detects Ser9 phosphorylated GSK-3β in stimulated cells.

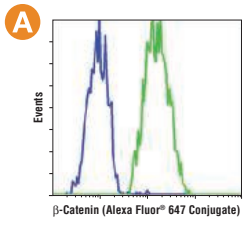

β-Catenin (L54E2) Mouse mAb (Alexa Fluor® 647 Conjugate) #4627: Analysis of NCI-H28 cells (blue) and HeLa cells (green).

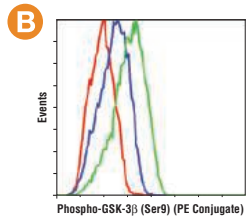

Phospho-GSK-3β (Ser9) (D85E12) XP® Rabbit mAb (PE Conjugate) #8466: Analysis of NIH/3T3 cells treated with hPDGF-BB #8912 and λ phosphatase (red), untreated (blue), or treated with hPDGF-BB #8912 only (green).

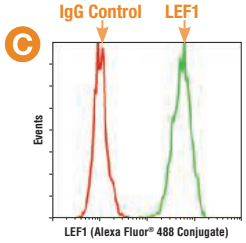

LEF1 (C12A5) Rabbit mAb (Alexa Fluor® 488 Conjugate) #8490: Analysis of Jurkat cells using LEF1 (C12A5) Rabbit mAb (Alexa Fluor® 488 Conjugate) (green) compared to Rabbit (DA1E) mAb IgG XP® Isotype Control (Alexa Fluor® 488 Conjugate) #2975 (red).

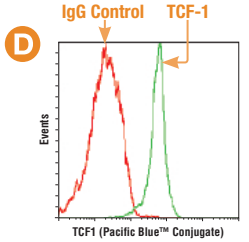

TCF1 (C63D9) Rabbit mAb (Pacific Blue™ Conjugate) #9066: Analysis of Jurkat cells using TCF1 (C63D9) Rabbit mAb (Pacific Blue™ Conjugate) (green) compared to Rabbit (DA1E) mAb IgG XP® Isotype Control (Pacific Blue™ Conjugate) #9078 (red).

14PADFLOWNONE_0094ENG_00

Cell Signaling TECHNOLOGY®

Science Careers Advertising

For full advertising details, go to ScienceCareers.org and click For Employers, or call one of our representatives.

Tracy Holmes
Worldwide Associate Director
Science Careers
Phone: +44 (0) 1223 326525

THE AMERICAS
E-mail: advertise@sciencecareers.org
Fax: 202-289-6742

Tina Burks
Phone: 202-326-6577

Marci Gallun
Phone: 202-326-6582

Online Job Posting Questions
Phone: 202-312-6375

EUROPE / INDIA / AUSTRALIA / NEW ZEALAND / REST OF WORLD
E-mail: ads@science-int.co.uk
Fax: +44 (0) 1223 326532

Axel Gesatzki
Phone: +44 (0)1223 326529

Sarah Lelarge
Phone: +44 (0) 1223 326527

Kelly Grace
Phone: +44 (0) 1223 326528

JAPAN
Yuri Kobayashi
Phone: +81-(0)90-9110-1719
E-mail: ykobayas@aaas.org

CHINA / KOREA / SINGAPORE / TAIWAN / THAILAND
Ruolei Wu
Phone: +86-1367-1015-294
E-mail: rwu@aaas.org

Science Careers
From the journal *Science* AAAS

ScienceCareers.org

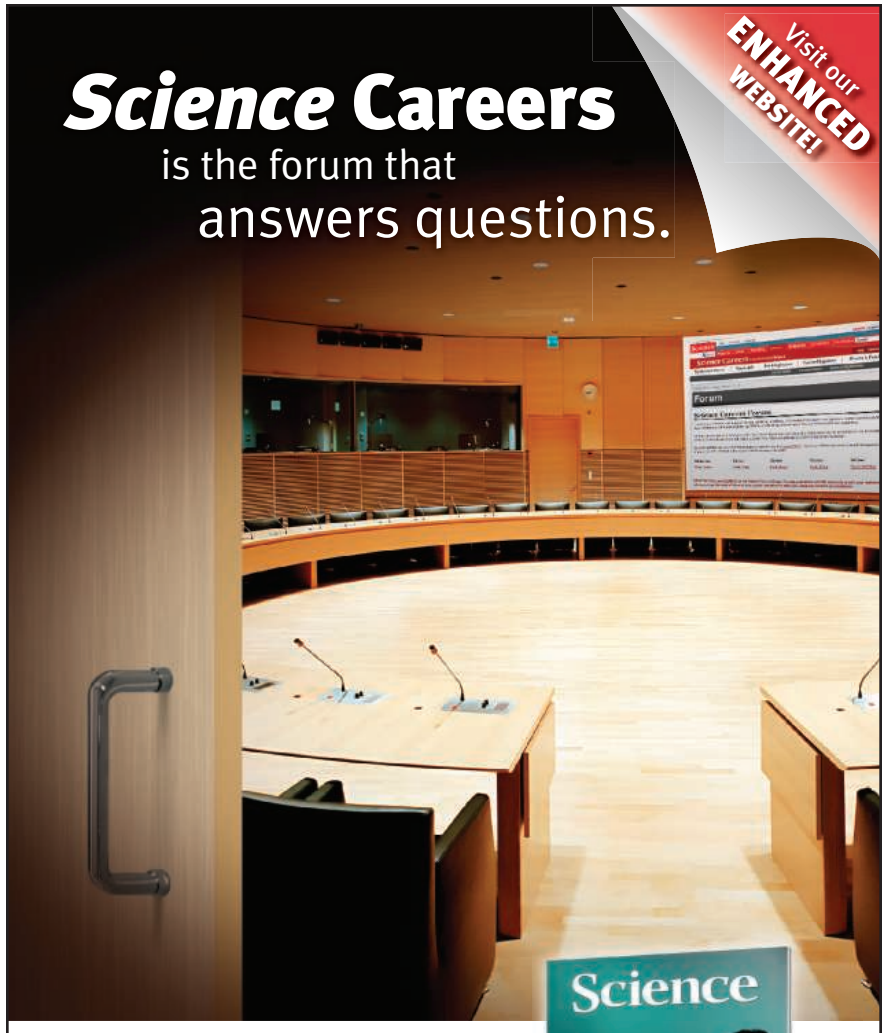

Science Careers is dedicated to opening new doors and answering questions on career topics that matter to you. We're the go-to career site for connecting with top employers, industry experts, and your peers. We're the source for the latest and most relevant career information across the globe.

With community feedback and a professional atmosphere, our careers forum allows you to connect with colleagues and associates to get the advice and guidance you seek.

***Science* Careers Forum:**

- » Relevant Career Topics
- » Advice and Answers
- » Community, Connections, and More!

Visit the forum and get your questions answered today!

Your Future Awaits.

Science Careers
From the journal *Science* AAAS
ScienceCareers.org

Imperial College London

MRC Centre for Molecular Bacteriology and Infection

Department of Life Sciences
MRC Centre for Molecular Bacteriology and Infection

Lectureship in Molecular Microbiology

Salary: Lecturer: £45,040 - £50,190 p.a.

The MRC Centre for Molecular Bacteriology and Infection (MRC-CMBI) is a major initiative at Imperial College London with a unique focus on the study of bacterial infection and immunity. We wish to appoint a Lecturer (equivalent in status to an Assistant Professor in the USA or a Group Leader in Europe) to direct a research programme in the area of bacterial pathogenesis and resistance, host-pathogen interactions and/or innate immune mechanisms. The successful candidate will have excellent opportunities to collaborate with the existing research groups within the MRC-CMBI (http://www.imperial.ac.uk/cmbi), the Department of Life Sciences (http://www3.imperial.ac.uk/ lifesciences) and within Imperial College London.

The Centre is located at the South Kensington Campus and benefits from world class research facilities as well as Postgraduate programmes. It is also supported by MRC-funded facilities and a dedicated PhD training programme.

You must have a PhD (or equivalent) in a relevant biological sciences field, together with a proven track record in conducting high quality, innovative and independent research, evidenced by high quality publications in peer reviewed journals. You will also be expected to demonstrate the ability to raise funding from a variety of sources and to direct a competitive independent research programme. Experience of teaching at Undergraduate and Postgraduate levels is also essential, and you must be able to communicate with, and inspire, students effectively as you will be expected to contribute to our Undergraduate and Postgraduate teaching programmes.

Applications should be made by submitting the completed Lecturer and Senior Lecturer (Clinical and Non-Clinical) (http://www3.imperial.ac.uk/employment/appformnotes2) application form and Recruitment monitoring form (http://www.imperial.ac.uk/workspace/employment/public/applicationformsirec/recruitment monitoring form.doc), along with any other relevant supporting documents such as your full CV, via e-mail to Ms Angela Kehoe, Senior HR Manager, Telephone: 00 44 (0) 20 7594 5653, e-mail: a.kehoe@imperial.ac.uk, **quoting reference number NS2014020AB**.

Informal enquiries may be made to Professor Alain Filloux, Professor of Molecular Microbiology, via e-mail: a.filloux@imperial.ac.uk.

Closing date: 1 April 2014.

Imperial Managers lead by example (http://bit.ly/163Lbh7).

Stonewall DIVERSITY CHAMPION

Athena SWAN Silver Award

Committed to equality and valuing diversity. We are also an Athena SWAN Silver Award winner, a Stonewall Diversity Champion and a two Ticks Employer.

JGI

JOINT GENOME INSTITUTE
DEPARTMENT OF ENERGY

Call for Large-Scale Genomics Proposals

The DOE Joint Genome Institute (DOE JGI) Community Science Program now invites **Letters of Intent** for genomic science projects that address questions of relevance to sustainable biofuel production, global carbon cycling, and biogeochemistry. Proposals will undergo a competitive review process for scientific and DOE mission relevance. Large-scale multi-investigator proposals are encouraged. The DOE JGI is a genomic science user facility, and will provide approved projects access, without charge, to an extensive portfolio of cutting-edge capabilities including:

- Genome sequencing and re-sequencing
- Single-cell and metagenome sequencing
- Transcriptome and epigenome profiling
- DNA synthesis
- Transposon mutagenesis
- Integrated platform for natural product pathway discovery and exploration
- Extensive data analysis pipelines
- … and more. **See http://bit.ly/Sci-CSP15**

Community Science Program Focus Areas

- **Functional Genomics and Microbiomes of Plants:** Study biofuel-relevant species including poplar, sorghum, *Brachypodium, Chlamydomonas,* soybean, foxtail millet, *Physcomitrella,* switchgrass, *Miscanthus* and Hall's panicgrass.
- **Functional Diversity of Microbes:** Use the DOE JGI's high-throughput (meta-)genome, (meta-)transcriptome, single-cell, DNA synthesis, transposon mutagenesis and epigenomic capabilities to study microbial activities relevant to the DOE mission.
- **Microbial Emission and Capture of Greenhouse Gases:** Study the role of terrestrial bacteria, archaea and fungi in global carbon and nitrogen cycles and develop genomic engineering-based mitigation strategies.
- **Discovery and Expression of Natural Product Pathways:** Use our new platform for metagenomics-driven discovery, DNA synthesis-enabled expression, and functional characterization to identify and explore energy- and environmentally relevant natural product pathways.

Full 2015 CSP Call for Proposals: http://bit.ly/Sci-CSP15

CSO0126

U.S. DEPARTMENT OF ENERGY
Office of Science

2014 *Science*/UCSF Career Event

March 21, 2014 • San Francisco, CA

UCSF Mission Bay Community Center • 10–4:45

A Day of Recruiting Opportunities and Career Workshops

***Science* Careers** and **UCSF** have joined forces to deliver an exciting event that includes five career workshops and a chance to meet face to face with recruiters. Two of the five workshops will focus on career opportunities in Asia.

► **Job seekers:** Visit the Mission Bay campus for a chance to get valuable advice from career experts and to meet with recruiters from some of the top scientific organizations. The combination of valuable career development content and exciting career opportunities makes this a "must-attend" event for scientists in the bay area. For more details and to register, visit **UCSF2014.ScienceCareers.org**

► **Employers:** Save time and money by meeting hundreds of scientists in person. If your organization would like to recruit at this event, please call 202 326-6577 for more information or e-mail **advertise@sciencecareers.org**

UCSF
University of California
San Francisco

Science Careers
From the journal *Science* AAAS
ScienceCareers.org